Enhancing Network-Level Pavement Macrotexture Assessment

Vincent Italo Bongioanni

Dissertation submitted to the faculty of the Virginia Polytechnic Institute and State University in partial fulfillment of the requirements for the degree of

Doctor of Philosophy
In
Civil Engineering

Gerardo W. Flintsch, Chair
Edgar de Leon Izeppi
Antonio A. Trani
John B. Ferris

27 March 2019
Blacksburg, VA

Keywords: macrotexture, friction, noise, outliers, dropouts, Accelerated Pavement Testing, Surface Properties, Agreement, Repeatability, calibration, accuracy, parameters

Enhancing Network-Level Pavement Macrotexture Assessment

Vincent Italo Bongioanni

ABSTRACT

Pavement macrotexture has been shown to influence a range of safety and comfort issues including wet weather friction, splash and spray, ambient and in-vehicle noise, tire wear, and rolling resistance. While devices and general guidance exist to measure macrotexture, the wide-scale collection and use of macrotexture is neither mandated nor is it typically employed in the United States. This work seeks to improve upon the methods used to calibrate, collect, pre-process, and distill macrotexture data into useful information that can be utilized by pavement managers. This is accomplished by 1. developing a methodology to evaluate and compare candidate data collection devices; 2. plans and procedures to evaluate the accuracy of high-speed network data collection devices with reference surfaces and measurements; 3. the development of a method to remove erroneous data from emerging 3-D macrotexture sensors; 4. development of a model to describe the change in macrotexture as a function of traffic; 5.finally, distillation of the final collected pavement surface profiles into parameters for the prediction of important pavement surface properties aforementioned. Various high-speed macrotexture measurement devices were shown to have good repeatability (between 0.06 to 0.09mm MPD) and interchangeability of single-spot laser devices was demonstrated via a limits of agreement analysis. The operational factors of speed and acceleration were shown to affect the resulting MPD of several devices and guidelines are given for vehicle speed and sensor exposure settings. Devices with single spot and line lasers were shown to reproduce reference waveforms on manufactured surfaces within predefined tolerances. A model was developed that predicts future macrotexture levels (as measured by RMS) for pavements prone to bleeding due to rich asphalt content. Finally, several previously published macrotexture parameters along with a suite of novel parameters were evaluated for their effectiveness in the prediction of wet weather friction and certain types of road noise. Many of the parameters evaluated outperformed the current metrics of MPD and RMS.

Enhancing Network-Level Pavement Macrotexture Assessment

Vincent Italo Bongioanni

GENERAL AUDIENCE ABSTRACT

A characteristic of the road's surface known as macrotexture has been shown to influence a range of safety and comfort issues including the resistance of a vehicle to hydroplane in wet weather, how much mist and splash is produced by vehicle tires in the rain, how much noise is produced by road vehicles and gas mileage. While devices and general guidance exist to measure macrotexture, the wide-scale collection and use of macrotexture is neither mandated nor is it typically employed in the United States. This work seeks to improve upon the methods used to collect, calibrate, pre-process, and distill macrotexture data into useful parameters that can be utilized by pavement managers. This is accomplished by developing a methodology to compare the output and accuracy of various candidate devices, a novel method to automatically remove erroneous data from 3-D data, development of a macrotexture degradation model, and development of several macrotexture indices that were shown to outperform the current standards. Various high-speed macrotexture measurement devices were shown to provide repeatable results and that they can be used interchangeably while others cannot. Factors such as speed and acceleration that vary during data collection in the real world were shown to affect the resulting macrotexture measurements of several devices and guidelines are given for the speed and sensor exposure settings. Several devices were shown to reproduce reference surfaces within predefined tolerance and vehicle and sensor characteristics. A model was developed that predicts future macrotexture levels (as represented by a statistical measure) for pavements that become smooth due to asphalt being squeezed to the surface. Finally, several previously published macrotexture parameters along with a suite of novel parameters were evaluated for their effectiveness in the prediction of available wet weather friction and certain types of road noise. Many of the parameters evaluated outperformed the most prevalent macrotexture metrics in used today.

ACKNOWLEDGEMENTS

First and foremost, this journey would not have had a well-chartered course and (relatively) smooth sailing without the stalwart guidance and leadership of my advisor, Dr. Gerardo Flintsch. You are a model for advisors around the world; keeping the needs of your advisees as a matter of primacy in your own life and providing truly effective and useful guidance, feedback, and correction for the good of the field.

Each of my committee members has had a profound and, I believe, lasting impact on my development as a scholar, scientist, and professional. Dr. Edgar de Leon Izeppi has a work ethic and commitment to his craft that knows no equal. Dr. Antonio Trani showed me there is usually a better way to do things than brute force and so to focus on the process with your mind before your fingertips write one line of code. Dr. John Ferris is a model of a world-renown expert in his field and showed me that, while we may come from different backgrounds, we are all in search of improving the extensive overlaps in our fields.

I'm indebted to the entire group at the Center for Sustainable Transportation Infrastructure of the Virginia Tech Transportation Institute, without whom I would not have pulled off the nationwide endeavor to collect enormous datasets for this work. Special thanks go to Billy Hobbs and Kenny Smith who supported me and helped reign-in my desires for more and more data and equipment.

Last but in no ways least, to my family. For my wife, Natalie, who has supported me through 14 years of marriage even when I've been in the field more than at home. My heart is always with you. For my children, thank you for refraining from driving me to complete insanity, for keeping me young(er) at heart, and for your support and interest in my experiments.

Dedicated to the memory of my father, Italo Benito Bongioanni (1952 – 1999).

TABLE OF CONTENTS

LIST OF FIGURES

LIST OF TABLES

CHAPTER 1 - INTRODUCTION

A roadway's surface texture is the primary influencing factor over several critical tire/pavement interactions. Chief among these are the important safety concerns of friction (Wambold et al. 1995) and splash and spray (Weir et al. 1978). Several studies (Roe et al. 1998; Parry and Viner 2005) have shown a correlation between texture and vehicle crashes in wet weather. Secondary to safety concerns are user and environmental concerns such as rolling resistance (Sandberg et al. 2011) and road noise (Descornet et al. 2000). Unlike other areas in the world, the United States has no requirement for macrotexture of newly constructed or resurfaced roads, despite the evidence that macrotexture is related to these safety, environmental, and social factors.

The World Road Association defines macrotexture as “surface irregularities of a road pavement with horizontal dimensions ranging between 0.5 mm and 50 mm and vertical dimensions between 0.2 and 10 mm” (PIARC 2016). Surface texture smaller than this is typically referred to as "microtexture," and larger texture as "megatexture" or, if larger still, as the "roughness" of a road. As water film thickness increases, the pavement’s macrotexture provides drainage paths for water beneath the tire to escape, reducing hydroplaning potential and allowing for greater tire/pavement adhesion (a function of the pavement’s microtexture). Also, macrotexture provides friction through hysteresis (lost energy from the tire’s rubber sticking larger asperities of the pavement aggregate surface in an asymmetric fashion. The hysteresis effect increases exponentially with increasing vehicle speed, accounting for 95 percent of available friction at speeds above 65 mph (Hall et al. 2009).

Macrotexture measurements of a roadway are split into two general categories: stationary and dynamic. Stationary measurements are typically made with hand-placed devices or manual tests and gather a relatively small quantity of data when compared to the overall surface area of the pavement (i.e., several linear or square inches vs. many linear miles of the road surface). Dynamic tests, on the other hand, gather continuous (or near-continuous) data, providing larger representative samples of the surface. Many modern profilers used to determine the International Roughness Index (IRI) on roads can be used to gather macrotexture measurements, meaning this valuable information can be collected for minimal additional cost. As most efforts to gather macrotexture data are concerned with network-level detection, dynamic methods are more

common at present. However, static means still play an important role in spot-checks (i.e., at a job site with a newly surfaced road) or to verify dynamically-measuring equipment.

Static Measurements

These measurement methods require the data collection team to hand-place a device or manually perform the test on the surface of interest. Several data points are required on homogeneous pavement surfaces to find the representative characteristics of the surface. Operator judgment is needed to determine how many samples to collect, where to collect, and what constitutes a "homogeneous pavement section." These measurement methods always require traffic control and pose a significant risk to those collecting the data from oncoming traffic. These methods, however, are generally regarded as "ground truth". They can measure the surface texture with a high degree of accuracy because they can record several samples at different orientations in one placement, use a physical medium to discretely measure texture, or they sample a near-continuous 3-D profile of the pavement. Stationary methods generally fall into three categories: volumetric, 2-D profiles, and 3-D profiles.

Volumetric devices use a known volume of a physical medium such as sand, glass spheres, or grease to fill the pavement texture. The resulting measure is that of a Mean Texture Depth (MTD). This is the average distance (typically measured in mm or thousandths of an inch from the peaks of the large aggregate to the bottoms of the valleys between. A variation of the volumetric device is the outflow meter which uses a known volume of water in a graduated cylinder. Outflow devices have the benefit of quantifying sub surface interconnected voids from surfaces such as porous or pervious pavements which have been challenging for contactless texture meters.

Two-dimensional profiles have become the de-facto standard used in gathering macrotexture data, given the most prevalent technologies used to gather texture data are 2-D. This has given rise to the prevalence of Mean Profile Depth (MPD) as the parameter of choice in the United States for describing a pavement's macrotexture. Three-dimensional surface maps can also be sampled and recorded of a pavement's texture. A distinct advantage over 2-D stationary profiles is a larger quantity of data gathered over a larger surface area. This additional data can shed further light on a pavement surface by addressing directionality, spacing, and the orientation of asperities. It also enables more direct conversion to physical parameters such as

Mean Texture Depth. 3-D profiles, on the other hand, take longer to capture (due to slower sampling rates, this can be problematic if mounted to a moving vehicle), can require more post-processing of the data to interpret the results of the scan, and are less widely used at present.

Dynamic Measurements

Walking Speed

These devices often use the same types of sensors as stationary machines; an operator pushes the device at walking speed. An advantage over stationary devices is that walking speed systems gather a larger sample of the pavement texture, and both 2-D and 3-D information can be collected. These devices are typically used to gather project-level macrotexture measurements, collect data on a section of interest (i.e., in response to an accident), for calibration of other data collection devices, or anywhere small-scale data collection is needed such as research.

Highway Speed

These devices gather continuous (or near continuous) data over large portions of the road network in a single run at high speed. No traffic control is required, given the vehicles travel at the speed of traffic and use contactless sensors. To date, no such devices have been considered to have the necessary resolution and sampling rate combination to gather continuous 3-D macrotexture data in the longitudinal (traffic) direction, so continuous longitudinal 2-D profiles are typically collected.

The most common devices are high-speed laser equipped (HSLE) systems that use the single-spot laser (SSL) triangulation method. Under this approach, a single laser beam (generally smaller than 1mm in diameter at its standoff distance in the center of its measurement range) is emitted from the device. The light is reflected from a discrete point of the pavement to the device's light sensor (typically a charged couple device or CMOS sensor like the one in a digital camera). Triangulation is then used to determine the distance between the instrument and the pavement surface at the point measured. Distance triangulation can be performed on any right triangle if at least one angle (based on the angle of the sensor relative to the laser) and one distance (the orthogonal distance from the laser beam to the position on the sensor) is known. Line lasers operate on a similar principle; however, the laser is spread into a beam through optics

before striking its target and a 2D sensor is used to record many individual center-weighted light points. Triangulation is then carried out for these many distances and angles.

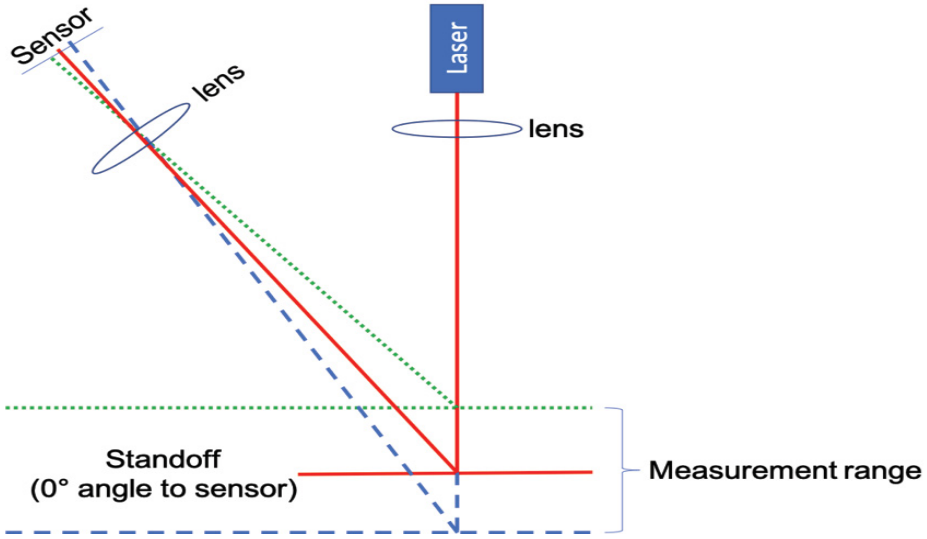

Figure 1-1 - Diagram of Single Spot Laser triangulation device.

Profiles from lasers can be defined as "continuous" if the sampling rate of the sensor is high enough to provide continuous coverage of the surface at the speed driven. Some manufacturers have reported sampling rates as high as 100,000 samples per second (100kHz). However, faster sampling rates often result in higher signal noise (Schleppi et al. 2016), especially when used on challenging surfaces such as dark and/or reflective pavements. If the sampling rate is too slow (i.e., the device is not "fast" enough), information about the shape of pavement asperities can be lost, as demonstrated by Liu et al. (2016).

The measurement method on the horizon for macrotexture is three-dimensional. A laser light is emitted from a diode (just as with the SSL process), however, the beam is diffused into a line by optics. Instead of a single point reflected to the sensor, the line covers many points on the grid of pixels of the sensor; each is taken as an individual data point. The number of data points taken per profile is dependent on the sensor used (how many pixels per row) and the laser line's width (field of view) is determined by the optical diffuser used and the mounting height of the device.

Water evacuation potential, which is the predominant factor in wet weather handling and in the splash and spray context, can be estimated from 2-D profiles. However, the ability of a parameter such as MPD to exhaustively describe road-tire interaction has been called into

question (Leandri and Losa 2015). In a 3-D environment, the prospects for meaningfully estimating a traveled surface's ability to move water is enhanced. Surfaces with anisotropic features (e.g., tined or grooved concrete) are more complicated and may be better characterized by 3-D technologies, especially if important features are oriented in the longitudinal direction.

Problem Statement

Current capabilities and technology to measure and analyze pavement macrotexture are not in use within the state agencies at the network level. These data are sometimes collected during annual road survey for information such as roughness, rutting, and pavement distress; however, they are infrequently made of any use. Practitioners indicated a lack of guidance and experience with using macrotexture data as the culprits. Furthermore, current standards provide only general guidance for issues such as outlier removal, data filtering, and the equipment to be used when gathering data. In addition, current macrotexture characterization parameters may not be the most appropriate for network-level macrotexture characterization.

Objectives

The goal of this work will be to provide practice-ready research in support of state agencies and data collection entities. The following are the main objectives of this work:

1. Produce the needed research for the industry to move forward with network-level macrotexture measurement standards in support of state and private entities. Both 2-D and 3-D approaches were evaluated.
2. Conduct an equipment comparison experiment to establish the repeatability and reproducibility of available macrotexture measurement equipment.
3. Develop a method to remove outliers in 3-D data to provide more accurate representations of the measured surface for further analysis.
4. Evaluate the effectiveness of current macrotexture characterization parameters and seek to develop parameters that are better related to other pavement surface properties.

Secondary objectives of this work:

1. Test the developed 3-D outlier removal routine on various pavement types for comparison against industry-accepted devices such as the Circular Track Meter

2. Provide a model to predict the change in macrotexture given repeated vehicular traffic. This will enhance an engineer's ability to effectively plan paving projects.
3. Test novel parameters on a variety of road surfaces to analyze their effectiveness at improving correlation to other pavement surface properties.

Research Approach

In order to further the work and achieve the stated objectives, the following tasks were conducted:

1. Comparison of network-level macrotexture equipment
    a. Data collection and processing
    b. Data analysis
        i. Repeatability and reproducibility (static, slow-speed and high-speed) – profile and macrotexture parameters
        ii. Impact of operational factors
        iii. Accuracy with respect to reference surfaces
        iv. Relationship with other pavement surface characteristics
2. Assessment of the change of macrotexture with traffic
    a. Data collection and processing
    b. Data analysis
3. 3-D macrotexture characterization
    a. Data collection and processing
    b. Outliers removal from 3-D macrotexture data

These research tasks are summarized in the flowchart in Figure 1-2. Manuscripts are designated in green.

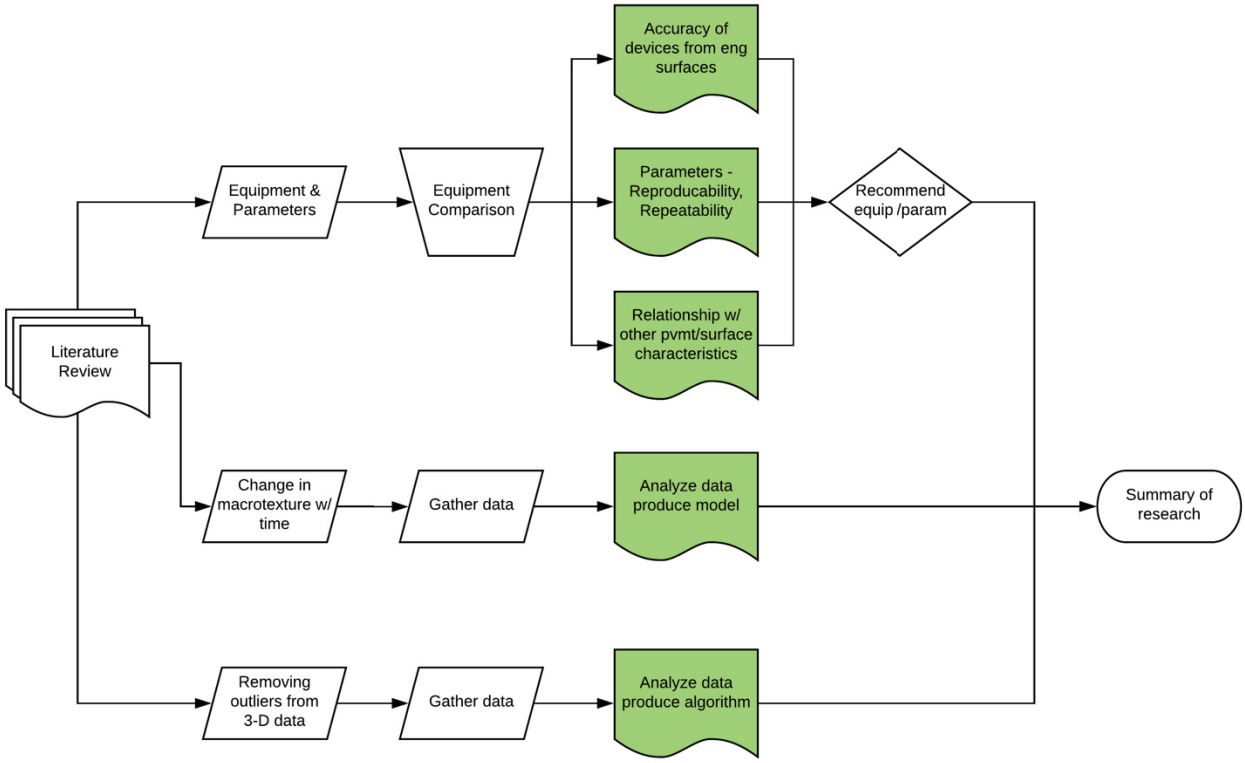

Figure 1-2 – Flowchart of research tasks

The first manuscript presents a methodology to follow to compare various macrotexture measurement equipment. An agency may wish to compare a candidate device to a reference device but will need to know how close the candidate device's measurements will be to the reference or current device used. A methodology for repeatability testing is prosed to gauge the candidate device's ability to produce measurements similar to itself. A limits of agreement analysis is then used to compare candidate device (or devices) against one another. This information can then be used by agencies to gauge the need for updating existing databases or future measurements based on the new equipment.

The second manuscript addresses methods by which an agency can analyze the accuracy of candidate devices evaluated using the methods detailed in the first manuscript to confirm the accuracy of in-service devices. Reference surfaces were engineered to represent various typical pavement surfaces. These surfaces were measured in the laboratory using a custom line-laser device and in the field using commercial off-the-shelf equipment under various vehicle speed and sensor exposure conditions. A methodology is then proposed to compare these

measurements and thresholds is suggested for agencies to predict how these devices will perform in the field.

The third manuscript addresses the emergence of 3-D macrotexture measurement equipment in the field and the data preparation necessary to ensure accurate representation of pavement surface properties. Specifically, outliers are identified by control of the false discovery rate. This is a powerful statistical tool that guarantees data points fit to a custom distribution that are identified as outliers will be false discoveries no more than a user-defined level (i.e., 10% was used in this work). The identified outliers are then replaced by fitting those points with those of a 2-D moving average filter of the original scanned surface. This results in a final 3-D profile that is free of outliers and ready for further analysis.

The fourth manuscript addresses the change of pavement macrotexture with time. This is important to help shape network level pavement monitoring plans based on real-time vehicle traffic information. Specifically, a rich mix of asphalt pavement is monitored for changes in pavement macrotexture while tracking equivalent single axle load information for the investigation sites. Given the richness of the pavement mix, the distress of bleeding (secretion of asphalt binder above the surface) is observed. A model is fit to this empirical data to aid agencies in predicting the macrotexture of a given rich-mix pavement at some future time as determined by vehicle traffic.

The fifth manuscript addresses what to do with pavement macrotexture data once it has been appropriately captured by a calibrated device and pre-processed to remove outlier data. Devices were used to measure the pavement surface properties of friction and noise. A large library of current and novel macrotexture parameters was then correlated to these pavement surface properties through simple least squares linear regression and multiple regression. Models improved through the use of multiple regression and as longer evaluation lengths were used.

Significance

There is no standardized method for collecting network-level macrotexture data in the US today. Standards do exist for the determination of macrotexture parameters such as Mean Texture Depth (MTD) produced by sand patch tests or for single Mean Profile Depth (MPD) calculations taken by non-contacting means. However, the sand patch test is clearly not appropriate for network-level investigations and the collection methods and requirements of

macrotexture data at the network level need further development to become viable. The presence of outliers in 3-D data will affect the accuracy of analysis and potentially rule out this data collection stream before it has a chance to prove its worth in this field. Furthermore, state agencies need a wider range of methods and guidance to compare and calibrate candidate equipment, collect macrotexture to utilize this important data in network analysis. Agencies will be able to better predict both future macrotexture levels and associated pavement phenomena such as wet friction and noise.

Attributions

This work includes five independent papers developed at the Center for Sustainable Transportation Infrastructure at the Virginia Tech Transportation Institute. This attribution section clarifies all co-authors contributions in these manuscripts.

Chapter 3: Repeatability and Agreement of Various High-Speed Macrotexture Measurement Devices. Vincent Bongioanni conceived the experiment details, performed all coding, prepared and processed all data and drafted the manuscript. Kyle Maeger provided inputs for the manuscript, performed the statistical analysis, calculated repeatability coefficients and limits of agreement. Vincent Bongioanni and Kyle Maeger collected the data, parsed the data for further analysis, and interpreted the results. Edgar de Leon Izeppi provided guidance for implementation of a repeatability and agreement analysis. Gerardo Flintsch reviewed the manuscript and provided suggestions for improvement of the work throughout its development.

Chapter 4: Evaluating non-contacting Macrotexture Laser Displacement Device Accuracy at Highway Speeds. Vincent Bongioanni collected, parsed, pre-processed, and analyzed the data for the high-speed devices; drafted the manuscript. Emmanuel Fernando and Sheng Hu of the Texas Transportation Institute provided the reference measurements of the engineered surfaces. Gerardo Flintsch reviewed and edited the manuscript.

Chapter 5: Removing Outliers from 3-D Macrotexture Data by Controlling the False Discovery Rate. Vincent Bongioanni planned and conducted field testing, conducted the literature review, wrote most of the code, and prepared the paper. Samer Katicha developed part of the computer code, was key in the development of the algorithm, and provided significant revisions to the paper to include comparison of the proposed method to other available methods.

Gerardo Flintsch and Edgar de León Izeppi reviewed the paper and provided suggestions for revisions.

Chapter 6: Change in Macrotexture Due to Traffic and Bleeding in an Accelerated Pavement Testing Machine. Vincent Bongioanni conceived the idea for the experiment, wrote the code to analyze all data, and provided inputs for the manuscript. Kyle Maeger performed the statistical analysis and drafted the manuscript. Vincent Bongioanni and Kyle Maeger collected the data in the HVS and interpreted the results. Gerardo Flintsch reviewed the manuscript and provided suggestions in analysis to include resulting RMS calculations being better predictors of degradation than MPD.

Chapter 7: Standard and Novel Pavement Macrotexture Characterization Parameters and their Relationship to Other Pavement Surface Properties. Vincent Bongioanni conceived the experiment, collected, parsed, pre-processed, and analyzed the data for the high-speed macrotexture data; drafted the manuscript. Lucas Spies collected, parsed, pre-processed, and analyzed the data for the OBSI and provided inputs for the manuscript. Gerardo Flintsch, Edgar de Leon Izeppi, and Samer Katicha reviewed the manuscript and provided inputs for the data analysis.

References

Descornet, G., Faure, B., Hamet, J., Kestemont, X., Luminari, M., Quaresma, L., and Sandulli, D. (2000). "Traffic noise and road surfaces: state of the art." *Belgian Road Research Centre, Brussels*.

Hall, J. W., Smith, K. L., Titus-Glover, L., Wambold, J. C., Yager, T. J., and Rado, Z. (2009). "Guide for Pavement Friction." 257p.

Leandri, P., and Losa, M. (2015). "Peak Friction Prediction Model Based on Surface Texture Characteristics." *Transportation Research Record: Journal of the Transportation Research Board*(2525), pp 91–99.

Liu, Q., Kavanagh, L., Shalaby, A., and Izevbekhai, B. I. (2016). "Comparison of Pavement Texture Measurements from a Three-Dimensional Profiler and a Circular Track Meter at MnROAD Test Facilities." *Transportation Research Record: Journal of the Transportation Research Board*(2591), pp 121–129.

Parry, A., and Viner, H. (2005). "Accidents And The Skidding Resistance Standard For Strategic Roads In England." *TRL report*, TRL Limited, Wokingham, Berkshire, UK.

PIARC (2016). "Road Dictionary." <http://www.piarc.org/en/Terminology-Dictionaries-Road-Transport-Roads/>. (16 December 2016).

Roe, P. G., Parry, A. R., and Viner, H. E. (1998). "High and low speed skidding resistance: the influence of texture depth." TRL Limited, Crowthorne, Berkshire, U.K., 22p.

Sandberg, U., Bergiers, A., Ejsmont, J. A., Goubert, L., Karlsson, R., and Zöller, M. (2011). "Road surface influence on tyre/road rolling resistance." *Models for Rolling Resistance in Road Infrastructure Asset Management Systems (MIRIAM),(http://miriam-co2. net/Publications/MIRIAM_SP1_Road-Surf-Infl_Report*, 20111231.

Schleppi, B. L., Maikhail, M. Y., and Chang, G. K. (2016). "International Experience and Perspective of Pavement Texture Measurements and Evaluation." *Transportation Research Circular*, E-C216.

Wambold, J., Antle, C., Henry, J., Rado, Z., Descornet, G., Sandberg, U., Gothié, M., and Huschek, S. (1995). "International PIARC Experiment to Compare and Harmonize Skid Resistance and Texture Measurements (Paris: PIARC) Publication n 01.04." PIARC, Paris, France.

Weir, D., Strange, J., and Heffley, R. (1978). "Reduction Of Adverse Aerodynamic Effects Of Large Trucks Volume I: Technical Report."

CHAPTER 2 - BACKGROUND

This section provides a summary of the relevant current literature on the subject of pavement macrotexture. As previously stated, there is no requirement in the US to collect macrotexture data. In Europe, project ROSANNE was initiated to study more closely pavement surface-related phenomena. This project is principally concerned with phenomena such as rolling resistance, skid resistance, and noise emission. However, macrotexture is also an item of interest as it is a major contributor in each of the phenomena evaluated. The project also assessed the implementation of 3-D texture measurement equipment on European roads (Goubert 2016). 3-D measurements were not adopted as a standard due to the issues previously mentioned including sampling rate, cost, product availability, and huge raw datasets.

The United Kingdom has long recognized the importance of texture measurements on their road networks. They perform Traffic Speed Condition Surveys (Ferne 2015) on an annual basis, a survey that uses multi-purpose vehicles that are equipped with single spot lasers. The vehicles gather Sensor Measured Profile Depths (SMPD). SMPD values can easily be transformed into an estimated texture depth for comparison to legacy volumetric-based data. Texture measurements complement friction data collected network-wide using their Sideways-force Coefficient Routine Investigation Machines (SCRIMs) and high-speed friction measurements such as locked-wheel skid testers. The SCRIM reading is generally regarded as a microtexture reading due to the relative speed under which the test is carried out. Correlations have been made between high and low-speed friction data and macrotexture measurements. The work is moving forward in the hope that eventually a contactless measurement method can be used to determine friction levels of roadways.

In terms of standards organizations, the American Society of Tests and Measures (ASTM) is constantly reviewing and updating their standards (e.g., ASTM E965 (2015); ASTM E1845 (2015); ASTM E2380 (2015)) as needed. Meanwhile, the International Organization for Standardization (ISO) has initiated an overhaul of their ISO 13473-1 (1997) for the measurement of macrotexture. ISO noted a need for a major revision given the wide variability and poor repeatability between various measurement devices used in the field today. Some devices even give seemingly unreasonable values due to a range of issues such as sampling rate, vehicle speed, and processing techniques.

Several friction harmonization efforts such as HERMES (Descornet 2004), TYROSAFE (Scharnigg et al. 2011), NASA friction workshops (Wambold et al. 2002), Virginia Tech Transportation Institute (VTTI) Pavement Surface Properties Consortium Rodeos (Flintsch et al. 2012) have taken place. Each has identified pavement texture as a major contributor to pavement friction. Harmonization seeks to compare devices against a reference device to produce a model for the pairing of interest. In this way, the results of the device tested can be normalized to the reference device for comparison against other devices. This requires each device be tested under the same conditions as the reference device. Furthermore, devices of the same make and model should not be assumed to have the same correlation as the original device tested. The World Road Association (PIARC) took an early interest in macrotexture as it relates to friction in their development of their well-known International Friction Index (IFI). IFI uses the macrotexture parameter of Mean Profile Depth (MPD) to calculate their speed constant which is critical to the analysis.

Parameters to Describe Macrotexture

Several parameters have been developed and implemented over the years to convey macrotexture data in a single, useful term for further analysis of pavement surface-related phenomena. Table 2-1 is a summary of the most common macrotexture parameters and their constituents in use today.

For 2-D measurements, the MPD and the root mean square (RMS) are typically used with laser devices such as the CT Meter or vehicle-mounted devices to characterize macrotexture. ASTM Standard E-1845 (the procedure in ISO 13473-1 (1997) is nearly identical) provides the methodology for calculating MPD from a pavement profile. MPD was derived from the physical medium sand patch but in 2-D. MPD is the average height of the two highest peaks in an equally divided 100mm-long segment above the mean height of the segment. Slopes are suppressed by subtracting a linear regression from the base length.

Table 2-1 - Currently Used Macrotexture Parameters

Available Parameters				
	Parameter	Reference	Strengths	Limitations
1.	MTD - Mean Texture Depth	ASTM E965 (2015)	Time-tested	Operator error
2.	MPD – Mean Profile Depth	ISO 13473-1 (1997); ASTM E1845 (2015)	Time-tested, widely used	Typically, limited sampling of roadway
3.	ETD - Estimated Texture Depth	ISO 13473-1 (1997); ASTM E1845 (2015)	Relation to MTD Collected by MPD equipment	Correlation-based parameter
4.	SMTD - Sensor Measured Texture Depth	Roe et al. (1998)	Uses statistical measure (vs. MPD's 2 peaks)	Typically limited sampling of roadway
5.	PD – Profile Depth	ASTM E1845 (2015)	Basic measure, information can be further processed	Uses single peak height as reference
6.	TD - Texture Depth	ISO 13473-1 (1997)	Basic measure, information can be further processed	Uses average of three highest peaks in 3-D profile
7.	RMS - Root Mean Square	Wennink and Gerritsen (2000)	Stronger statistical basis, describes variation	Not widely used in the US
8.	Texture Spectra PSD – Power Spectral Density Texture Power Spectra TL – Texture Level	Anfosso-Lédée and Do (2002), Goubert (2007), Leandri and Losa (2015)	Relation to road noise, some operations computationally simpler	Not widely used in the US, can require additional analysis

The RMS is essentially the standard deviation of texture profile measurements for a zero-mean segment. RMS has traditionally been more popular outside of the United States. Proponents of RMS argue that it is a more reliable amplitude-based macrotexture measurement than MTD (Liu et al. 2016). Large variations mean large deviations from the mean texture level.

Many other parameters have been suggested in the literature but have not been widely adopted across the United States. Table 2-2 provides the more commonly referenced emerging parameters.

Table 2-2 - Emerging Macrotexture Parameters

Emerging Parameters				
	Parameter	Reference	Strength	Limitation
1.	MTD3 - Digitally Simulated 3-D Mean Texture Depth	Liu et al. (2016)	High Resolution; correlation to established parameters	Typically gathered by stationary device
2.	RMSD3 – 3D Root Mean Square Deviation	Liu et al. (2016)	High Resolution; correlation to established parameters	Typically gathered by stationary device
3.	MPDi - Mean Profile Depth from 3-D image measurements	El Gendy and Shalaby (2007)	High Resolution; correlation to established parameters	Typically gathered by stationary device
4.	Enveloping Profiles (Goubert 2007) Empirical Physical Spectral Effective Area of Water Evacuation	Clapp (1983), Von Meier et al. (1992), Klein et al. (2004), Mogrovejo et al. (2016)	Accounts for a more realistic area for water evacuation. Improved correlations to friction and noise	Not implemented in existing software or measurement schemes
5.	Wavelet Transformations	Zelelew et al. (2013), Leandri and Losa (2015),	Greater granularity on measured profile waveform	Processing intensive
6.	HHT - Huang–Hilbert transform	Rado and Kane (2014)	Good correlation to friction	Limited testing; intense post-processing
7.	Summit Analysis	Le Gal et al. (2008)	In depth analysis of macrotexture asperities	Intense post-processing; limited testing
8.	3D Void Volume	Sanders et al. (2014)	High-resolution 3D data	Very sensitive to outliers
9.	Geometric Statistical Methods Mean Profile Depth (avg roughness, R_a) Mean Square Roughness (R_q) Skewness (R_{sk}) Kurtosis (R_{ku})	ISO 4288 (1996), ISO 4287 (1997), ASME B46.1 (2009)	Common set of tools available to multiple disciplines	Not widely used in common pavement surface vernacular
10.	Tortuosity	Praticò et al. (2017)	Use in pervious and porous pavements	Difficult to characterize on network level
11.	Rugosity	Du Preez (2015)	Relates micro/macrotexture	Difficult to characterize network

Some measures that could enhance the characterization of the pavement surface include MTD3 and RMSD3, which are 3-D versions of their 2-D counterparts suggested by Liu et al. (2016). Skewness and Kurtosis are measures of texture distribution and peak characteristics and can be gathered via both 2-D and 3-D sensors.

Positive and Negative Textures

The plot in Figure 2-1a shows an unfiltered profile taken from the Smart Road at the Virginia Tech Transportation Institute. The negative value for skewness indicates a negative texture; meaning there is more area in the valley below the average than in the peaks above. Figure 2-1b is the same profile flipped at zero on the horizontal axis. The value for skewness now becomes positive, indicating positive texture, which is expected for a profile with opposite peak and valley characteristics. The RMS value for the two surfaces is the same (the variations from the means are equivalent). The MPD for the negatively textured pavement in Figure 2-1a, however, is less than that of the positively textured pavement.

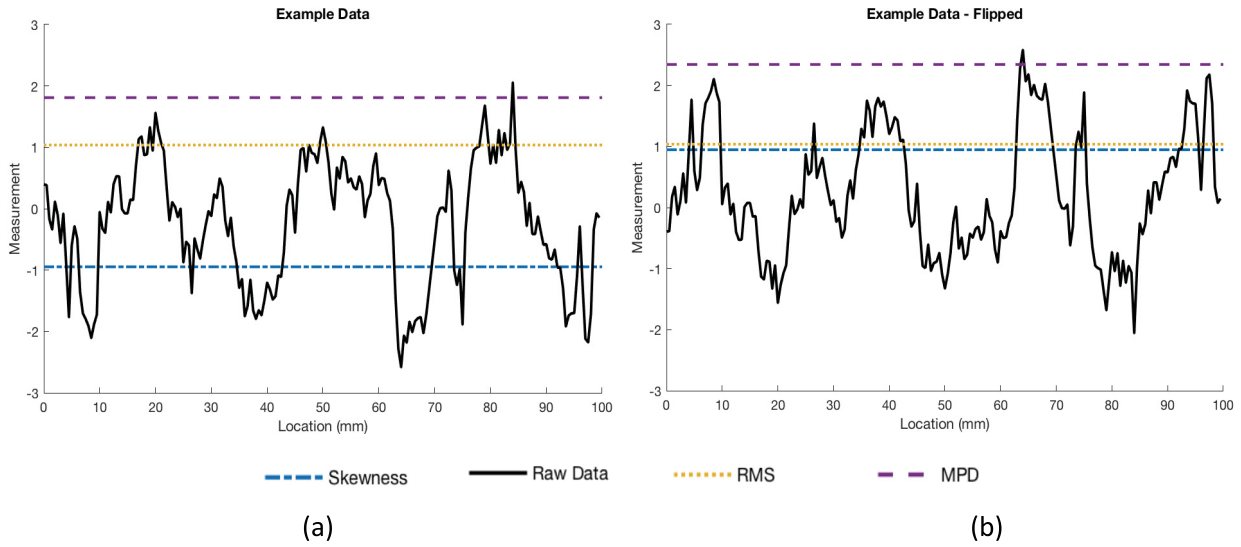

Figure 2-1 - Examples of (a) positive and (b) negative texture (negative skewness indicates negative textures).

Water evacuation

Another important issue is that is often overlooked is the free space between the actual tire and the pavement. Most engineers recognize its importance, as well as the difference that exists between asphalt surfaces and tining/grooving of concrete pavements. One very promising parameter that addresses this free space between the tire and the pavement is the Effective Area

of Water Evacuation (EAWE) proposed by Mogrovejo et al. (2016). This is a single parameter that places the enveloping profile (Klein et al. 2004) of a tire over the measured pavement surface to identify the free space between the two. An enveloping profile of a tire is one that accounts for deformations in the tire surface due to its placement on the rough pavement's surface. Mogrovejo found that the use of this parameter as a descriptor of macrotexture better characterized the pavement's ability to evacuate water beneath the tire than MPD alone. Correlation to friction and noise were also improved using this parameter.

Uses of Macrotexture Measurements

Once a high-quality profile has been collected on a road surface, the data must be processed into accurate and usable data. The processing involved depends largely on the application. The main uses for macrotexture include the following:

Friction

Macrotexture's relationship with friction (especially wet weather friction) is perhaps the most critical. A vehicle's ability to maintain good traction on the road and avoid hydroplaning is critical to driver safety. The World Road Association (PIARC) took an early interest in macrotexture as it relates to friction in the development of the International Friction Index (IFI). IFI uses the MPD to calculate the critical speed constant (S_p) that is used to determine the friction sensitivity to sliding speed using the formula found in Wambold et al. (1995). However, there is difficulty in harmonizing friction tester results as demonstrated in the HERMES (Descornet 2004) project. The follow-on TYROSAFE (Scharnigg et al. 2011) project, therefore, recommended categorizing friction testing vehicles according to operating principles and test conditions.

Rolling resistance

The surface characteristics of a road affect the amount of resistance a vehicle experiences to forward movement. To ensure environmentally sustainable roads, we can quantify the amount of resistance a vehicle will encounter. One approach is through the equation developed through the MIRIAM (Models for rolling resistance In Road Infrastructure Asset Management systems) study (Sandberg et al. 2011).

Rolling resistance is a complex issue and there are still several factors to be determined in the development of a complete model. The MIRIAM model was developed using light vehicle (passenger cars) data and is recommended for use only in the speed range of 50-110 km/h. Although complex, this is an important issue as the study found an increase in rolling resistance (from 21 to 55 percent) as macrotexture increased (from 0.08 to 2.77mm) as measured via MPD. This increase in rolling resistance leads to additional fuel consumption of between 7 and 18 percent (Sandberg et al. 2011). Harvey et al. (2016) also demonstrated excess fuel consumption due to the mechanical response of the pavement structure to a lesser extent, approximately one-half a percent in hot climates. The same study found fuel consumption to decrease as IRI is reduced.

Splash and Spray

This is a complex phenomenon that poses a safety risk to motorists but is more widely viewed as a nuisance issue. The issue was divided into four distinct contributors by Weir et al. (1978): Capillary Adhesion (CA), Bow Wave (BW), Side Wave (SW), and Tread Pickup (TP). (Flintsch and Viner 2016) sums mass flow for each of the four possible sources for splash and spray into an overall spray density. Each source has its own model that results in the mass flow for the component. As this is a cumbersome task for road agencies to calculate, a tool was developed (Flintsch et al. 2014; Flintsch and Viner 2016) that takes the input parameters of the cross slope, drainage path length, and rainfall intensity to calculate the overall spray density. This spray density can then be converted into a nuisance index.

Tire and pavement noise

Higher macrotexture levels combined with high porosity can be favorable (Sandberg and Descornet 1980) for reduction of noise caused by tire interactions with the pavement. This is because air can be expressed through the channels below the tire contact area of the surface in much the same way as water to reduce the risk of a slide in wet weather. However, certain amplitudes/frequencies of pavement texture (some within the macrotexture range) can create noise through what is known as “knocking” where the rubber of the tire strikes the protuberances from the smooth surface.

Road noise analysis is almost always carried out in the frequency domain. This is a natural relationship as our auditory perception is most commonly described in terms of decibels and frequencies. The concept in pavements, while not typically immediately apparent, is relatively straight forward. A road's surface is composed of many repeating patterns. For instance, we see a repeating pattern in our rumble strips. For macrotexture, however, the visualization begins to break down due to the relatively random texture found on most roads, especially asphalt. The repeating patterns are, however, present in macrotexture. We typically see texture measurements to be used in noise and other analysis in terms of frequency "buckets" (bandwidths) on a horizontal axis and texture levels (height measurements converted to decibels) on a vertical axis.

Determination of construction uniformity

Since macrotexture analysis measures the variation of the pavement's surface from a flat plane, it is a natural analysis tool for pavement defects that deal with material uniformity. AC defects such as segregation have been successfully detected using macrotexture (McGhee et al. 2003). Segregation of asphalt mixtures can lead to early and localized raveling (Tsai and Wang 2015), longitudinal cracking, fatigue cracking, and rutting (Khedaywi and White 1996). PCC defects such as non-conformity to the texturing requirements, pop-outs, faulting, and delamination should also be evident.

Macrotexture Collection Practices of State Agencies

Pavement surface characterization experts at state departments of transportation were asked about their current practices regarding macrotexture data collection. In general, the questions addressed whether macrotexture measurements were made, and if so, with what equipment was used and what parameters were collected. Of the states who provided responses, those shown in green in Figure 2-2 reported presently collecting macrotexture data on the network-level.

Of the states that do not collect macrotexture measurements at the network level, four reported it was because they did not believe the technology was mature enough, seven said it was due to the cost of data collection, and 10 reported a lack of available workforce to collect the data.

When asked "when are macrotexture measurements performed," the majority of states indicated "while profiling the pavement;" showing an additional sensor is added to the profiling vehicle to gather macrotexture data. Several states reported "while collecting friction data," indicating an additional sensor is attached to the friction tester and macrotexture data is collected at the same frequency as friction data (usually annually or less than annually for the entire network).

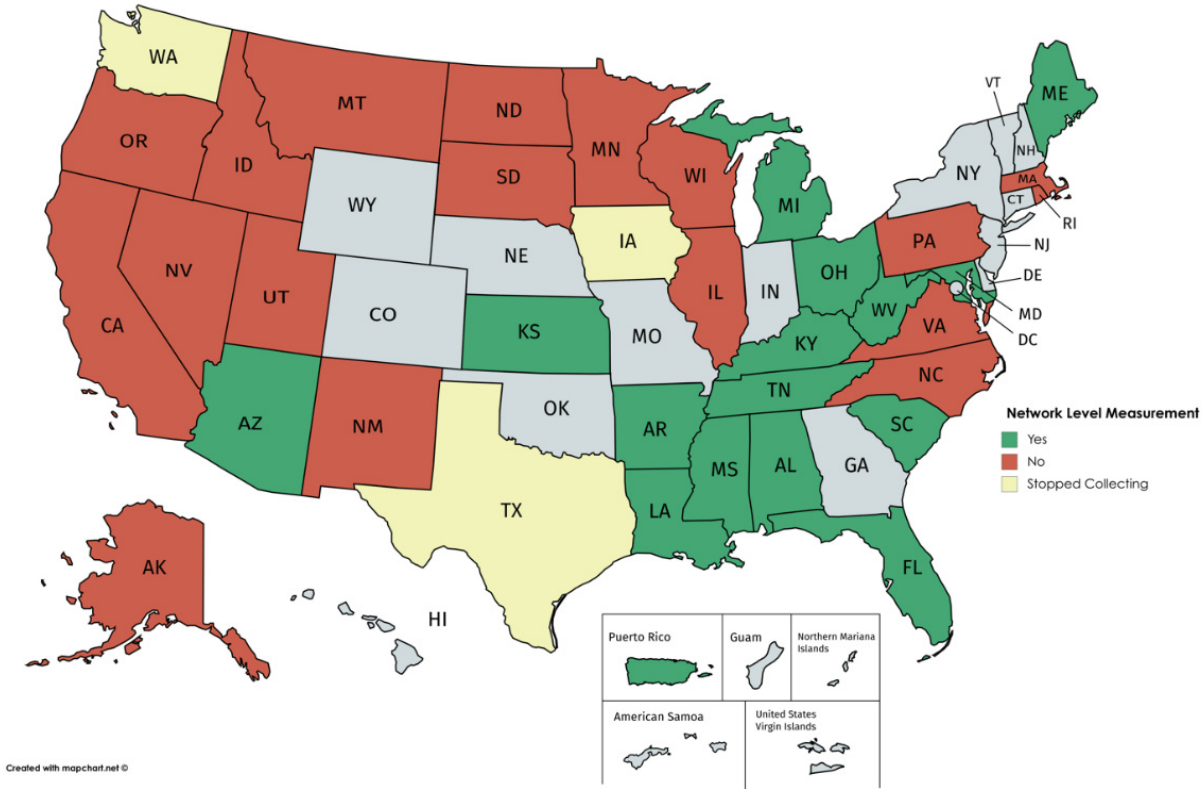

Figure 2-2 - Macrotexture data collection status on the network level.

Project level macrotexture data

Other states indicated collecting macrotexture data at the project level for specific newly installed surfaces such as high friction courses or micro milling. Of the states providing responses, those shaded green in Figure 2-3 reported that they collect project-level macrotexture measurements.

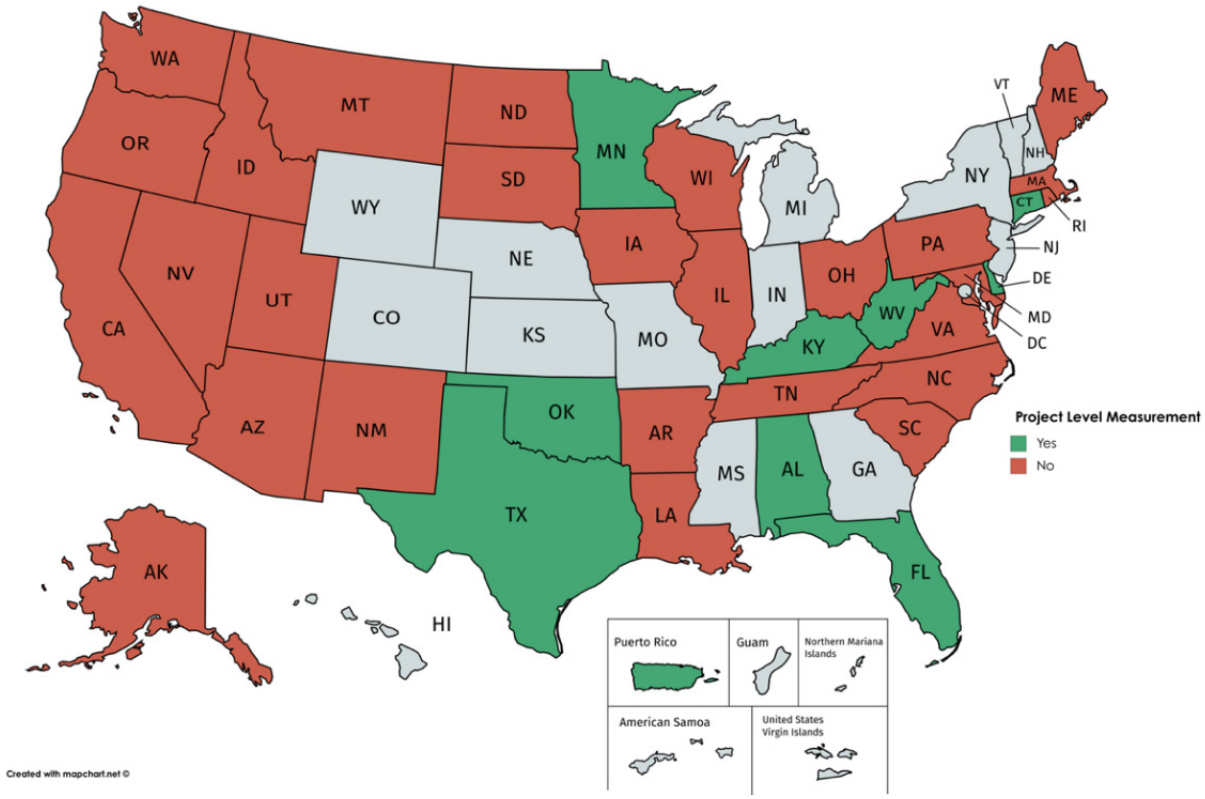

Figure 2-3 - Macrotexture data collection status on the project level.

As with network-level collection, five states indicated that they felt the technology was not yet sufficiently mature, 11 cited cost as being a deterrent, and 12 noted a lack of available human resources as reasons for not collecting macrotexture data at the project level. Additional reasons specific to project-level measurements included:

- No trigger levels (i.e., watch, action, etc.) established for macrotexture
- Different sensor set up from network level sensor with different results created a lack of faith in the measurements
- Macrotexture data only collected for projects (e.g., High Friction Surface Treatment, HFST) where macrotexture is used for acceptance

Equipment used to gather macrotexture data

States were asked what equipment they use to collect macrotexture data if it is recorded at all. Below is a summary of their responses. The most common methods are the CT Meter for

project-level data and a single spot laser for network level. A small number of states indicated that they are beginning to use line laser systems.

Table 2-3 - Summary of Equipment and Parameters Used to Characterize Macrotexture

Equipment	Network	Project
Volumetric		
Sand patch	1	6
HydroTimer	0	2
Stationary Laser Systems		
C.T. Meter	1	7
Laser Texture Scanner	0	3
Walking Speed Laser System		
TM2 Texture Meter	1	2
High-Speed Laser Equipment (HSLE)		
HSLE (Single spot laser)	10	4
HSLE (Line laser)	1	1
3-D Laser/ camera	7	1
Other		
Florida texture meter	0	1
ARAN Pave 2D LRMS (64 kHz)	0	1
In house 3-D system	0	1
Contour/ tire depth gauge for tined/ grooved surfaces	0	1
Parameter		
Mean Texture Depth (MTD)	7	7
Mean Profile Depth (MPD)	7	6
Root Mean Square (RMS)	2	3
Estimated Texture Depth (ETD)	0	3
Other		
Skewness, Kurtosis, PSD	1	0
Digital Sand Patch (LCMS)	1	0

Parameters used to describe macrotexture

When asked which parameters were used to report macrotexture data, the majority of states that collect data reported MTD and MPD. Several states are also using RMS. summarizes states' responses to the question.

Uses of macrotexture data

When asked "How does your agency currently use macrotexture measurements," states responded fairly equally that they currently use the measurements as a compliment to friction

measurements (i.e., as a screening tool for problem areas where macrotexture is low and friction demand is high), for safety reasons (i.e., at specific locations in response to incidents), for adding the information to their Pavement Management System (PMS), and for project acceptance (i.e., for projects with specific macrotexture requirements such as HFST and PCC texturing). The information is currently used to a lesser extent to characterize mixes and surface treatments.

Other general observations from the survey

When asked where on the pavement macrotexture data is gathered, the majority of states that responded (seventeen) indicated it was in the rightmost travel lane. States are much more likely to collect the information on other lanes at the project level (six) rather than at the network level (one).

When asked if the agencies envisioned additional changes in data collection activities over the next several years, more agencies responded that they did (thirteen) than did not (ten). Numerous agencies indicated that they planned on adding a macrotexture sensor to future equipment purchases (i.e., inertial profiler, friction measuring equipment). At least one state plans to use 3-D data collected from LCMS measurements along with friction measurements to identify high-risk curves and with accident data to identify areas that require treatment. One state plans to set minimum values, especially for PCC where a macrotexture threshold can be used in lieu of tine-depth specifications. Another state plans to replace cumbersome sand patch tests with a 3-D laser texture scanner.

Several states indicated they would look at ways to express macrotexture data in more useful ways such as on a Geographic Information System for easier visualization of texture data over time. Several states indicated 3-D macrotexture measurements as being the next level of data granularity they are seeking to obtain. In final comments, many states are desirous for standardized macrotexture procedures. They seek consensus on parameters/ indices to use for macrotexture, and improvement of their QA/QC processes.

Summary

Several different methods exist for measuring macrotexture. Selecting a method is typically based on the application. For example, localized or small-scale projects typically employ static or walking-speed measurements. The most common approach for measuring macrotexture today

is via 2-D profile representation through a contactless sensor. These profiles are typically measured in the longitudinal direction (since that is the direction of the measuring vehicle) however, lateral or other measurements can also be made. Three dimensional (3-D) measurements are emerging with several state agencies already reporting 3-D data collection of some form.

Once a high-fidelity profile has been collected for a pavement surface, it must then be processed and communicated via a relevant index. The most common indices for reporting macrotexture are the MPD (used primarily in the U.S.) and the RMS. These parameters are typically computed using data collected with a single-spot laser that provides a 2-D description of the pavement's profile. This profile is of a spot less than 1 mm wide and as long as the distance measured by the device. Several emerging parameters were provided in Table 2-2. For example, vertical resolution and sampling rate of line lasers are improving and the applicability and usefulness of the 3-D versions of MPD and RMS or other 3-D-based parameters are under investigation. Particularly within the context of wet-pavement safety, macrotexture parameters should also take into account the enveloping effect of tires to include the contribution of tire stiffness on effective void space beneath the tire and traveled surface.

A survey of state transportation agencies revealed that only 38% of the states that provided responses collect macrotexture at the network level. Reasons for not collecting such data generally revolved around a lack of clear actions to take with collected data. A lack of workforce or resources to collect the data was also cited several times. Of the states that do collect macrotexture data, the most common methods are the CT meter at the project level (6 of 10 states) and single-spot HSLE at the network level (8 of 16 states). The use of 3-D measurements is also gaining popularity for network level use. Most states (14 of 16) that do collect macrotexture data do so at the same time as profiling for roughness measurements, indicating an extra sensor is simply added to the profiling vehicle to collect the data. Most agencies see macrotexture data as being useful in conjunction with other data, especially friction data, to identify areas that require some form of treatment. Many states also recognize macrotexture data as valuable for work acceptance at the project level. In final comments, many states are desirous for standardized macrotexture procedures, consensus on parameters/ indices, and improvement of their QA/QC processes.

References

Anfosso-Lédée, F., and Do, M.-T. (2002). "Geometric descriptors of road surface texture in relation to tire-road noise." *Transportation Research Record: Journal of the Transportation Research Board*(1806), 160-167.

ASME B46.1 (2009). "Surface Texture (Surface Roughness, Waviness, and Lay)." The American Society of Mechanical Engineers.

ASTM E965 (2015). "Standard Test Method for Measuring Pavement Macrotexture Depth Using a Volumetric Technique." ASTM International.

ASTM E1845 (2015). "Standard Practice for Calculating Pavement Macrotexture Mean Profile Depth." ASTM International.

ASTM E2380 (2015). "Standard Test Method for Measuring Pavement Texture Drainage Using an Outflow Meter." ASTM International.

Clapp, T. G. (1983). *Spectral correlation of the surface profile in the development of a tire and pavement interaction force model*.

Descornet, G. "The HERMES project." *Proc., Symposium on Pavement Surface Characteristics [of Roads and Airports], 5th, 2004, Toronto, Ontario, Canada*.

Du Preez, C. (2015). "A new arc–chord ratio (ACR) rugosity index for quantifying three-dimensional landscape structural complexity." *Landscape Ecology*, 30(1), 181-192.

El Gendy, A., and Shalaby, A. (2007). "Mean Profile Depth of Pavement Surface Macrotexture Using Photometric Stereo Techniques." *Journal of Transportation Engineering*, 133(7), pp 433-440.

Ferne, B. (2015). "UK experiences on pavement texture measurement and interpretation." *Transportation Research Circular*, International Experience and Perspective of Pavement Texture Measurements and Evaluation(E-C216), 26-41.

Flintsch, G. W., McGhee, K., de León Izeppi, E., and Najafi, S. (2012). "The little book of tire pavement friction." *Pavement Surface Properties Consortium*.

Flintsch, G. W., Tang, L., Katicha, S., de León Izeppi, E., Viner, H., Dunford, A., Nesnas, K., Coyle, F., Sanders, P., and Gibbons, R. B. (2014). "Splash and Spray Assessment Tool Development Program." Virginia Tech. Virginia Tech Transportation Institute.

Flintsch, G. W., and Viner, H. "Highway Splash and Spray Assessment Tool." *Proc., Transportation Research Board 95th Annual Meeting*, 17p.

Goubert, L. "Road Surface Texture and Traffic Noise." *Proc., NPRA workshop Texture and Road traffic noise*.

Goubert, L. (2016). "Rolling Resistance, Skid Resistance, and Noise Emission Measurement Standards for Road Surfaces." *Transportation Research Circular*, International Experience and Perspective of Pavement Texture Measurements and Evaluation(E-C216), 83-97.

Harvey, J., Lea, J. D., and Kim, C. "Simulation of Annual Excess Fuel Consumption from Pavement Structural Response for California Test Sections." 20p.

ISO 4287 (1997). "Geometrical Product Specifications (GPS) -- Surface texture: Profile method -- Terms, definitions and surface texture parameters."

ISO 4288 (1996). "Geometrical Product Specifications (GPS) -- Surface texture: Profile method -- Rules and procedures for the assessment of surface texture." International Organization for Standardization, 8.

ISO 13473-1 (1997). "Characterization of pavement texture by use of surface profiles - Part 1: Determination of Mean Profile Depth." *Part 1: Determination of Mean Profile Depth*, International Organization for Standardization.

Khedaywi, T., and White, T. (1996). "Effect of segregation on fatigue performance of asphalt paving mixtures." *Transportation Research Record: Journal of the Transportation Research Board*(1543), 63-70.

Klein, P., Hamet, J., and Anfosso-Ledee, F. "An envelopment procedure for tire-road contact." 10p.

Le Gal, A., Guy, L., Orange, G., Bomal, Y., and Klüppel, M. (2008). "Modelling of sliding friction for carbon black and silica filled elastomers on road tracks." *Wear*, 264(7), 606-615.

Leandri, P., and Losa, M. (2015). "Peak Friction Prediction Model Based on Surface Texture Characteristics." *Transportation Research Record: Journal of the Transportation Research Board*(2525), pp 91–99.

Liu, Q., Gonzalez, M., Tighe, S. L., and Shalaby, A. (2016). "Three-dimensional surface texture of Portland cement concrete pavements containing nanosilica." *International Journal of Pavement Engineering*, 1-8.

Liu, Q., Kavanagh, L., Shalaby, A., and Izevbekhai, B. I. (2016). "Comparison of Pavement Texture Measurements from a Three-Dimensional Profiler and a Circular Track Meter at MnROAD Test Facilities." *Transportation Research Record: Journal of the Transportation Research Board*(2591), pp 121–129.

McGhee, K. K., Flintsch, G. W., and de Leon Izeppi, E. (2003). "Using high-speed texture measurements to improve the uniformity of hot-mix asphalt." Virginia Center for Transportation Innovation and Research.

Mogrovejo, D. E., Flintsch, G. W., Katicha, S. W., de León Izeppi, E. D., and McGhee, K. K. (2016). "Enhancing Pavement Surface Macrotexture Characterization by Using the Effective Area for Water Evacuation." *Transportation Research Record: Journal of the Transportation Research Board*(2591), pp 80–93.

Praticò, F. G., Fedele, R., and Vizzari, D. (2017). "Significance and reliability of absorption spectra of quiet pavements." *Construction and Building Materials*, 140, 274-281.

Rado, Z., and Kane, M. (2014). "An initial attempt to develop an empirical relation between texture and pavement friction using the HHT approach." *Wear*, 309(1), 233-246.

Roe, P. G., Parry, A. R., and Viner, H. E. (1998). "High and low speed skidding resistance: the influence of texture depth." TRL Limited, Crowthorne, Berkshire, U.K., 22p.

Sandberg, U., Bergiers, A., Ejsmont, J. A., Goubert, L., Karlsson, R., and Zöller, M. (2011). "Road surface influence on tyre/road rolling resistance." *Models for Rolling Resistance in Road Infrastructure Asset Management Systems (MIRIAM),(http://miriam-co2. net/Publications/MIRIAM_SP1_Road-Surf-Infl_Report*, 20111231.

Sandberg, U., and Descornet, G. "ROAD SURFACE INFLUENCE ON TIRE/ROAD NOISE--1." *Proc., Proceedings of the International Conference Noise Control Engineering, Noise Control for the 80's, Inter-Noise 80, Vol. 1, Miami, Florida, December 8-10, 1980.*

Sanders, P. D., Morosiuk, K., and Peeling, J. R. (2014). "Road surface properties and high speed friction." 41p.

Scharnigg, K., Schwalbe, G., and Haider, M. "TYROSAFE: tyre and road surface optimisation for skid resistance and further effects." 14p.

Tsai, Y., and Wang, Z. (2015). "Development of an Asphalt Pavement Raveling Detection Algorithm Using Emerging 3D Laser Technology and Macrotexture Analysis." Transportation Research Board, 50p.

Von Meier, A., Van Blokland, G., and Descornet, G. "The influence of texture and sound absorption on the noise of porous road surfaces." *Proc., Second International Symposium on Road Surface Characteristics, Berlin*.

Wambold, J., Antle, C., Henry, J., Rado, Z., Descornet, G., Sandberg, U., Gothié, M., and Huschek, S. (1995). "International PIARC Experiment to Compare and Harmonize Skid Resistance and Texture Measurements (Paris: PIARC) Publication n 01.04." PIARC, Paris, France.

Wambold, J. C., Henry, J. J., Transport, C., and Incorporated, C. (2002). "NASA WALLOPS TIRE/RUNWAY FRICTION WORKSHOPS: 1993-2002." 155 p.

Weir, D., Strange, J., and Heffley, R. (1978). "Reduction Of Adverse Aerodynamic Effects Of Large Trucks Volume I: Technical Report."

Wennink, M., and Gerritsen, W. "Detection of changes of pavement texture material recognition." *Proc., International symposium on pavement surface characteristics of roads and airfields*, 153-162.

Zelelew, H., Papagiannakis, A., and de León Izeppi, E. (2013). "Pavement macro-texture analysis using wavelets." *International Journal of Pavement Engineering*, 14(8), 725-735.

CHAPTER 3 - REPEATABILITY AND AGREEMENT OF VARIOUS HIGH-SPEED MACROTEXTURE MEASUREMENT DEVICES[1]

Abstract

Five high-speed macrotexture measurement devices were tested on a variety of asphalt and Portland Cement Concrete pavement surfaces to evaluate their repeatability and their pairwise agreement. Experiments were run under three speed conditions: highway speed, varying constant speeds, and various acceleration and deceleration profiles. Data were processed and reduced per current industry standards. A novel approach for outlier removal from line laser devices was developed. The pairwise device agreement was evaluated using a Limits of Agreement analysis. The results demonstrate good repeatability for each of the devices tested. The agreement analysis showed that not all high-speed distance triangulation devices can be used interchangeably for all pavement surfaces. Data acquisition speed was found to be a factor in macrotexture parameter calculation for two of the five devices. The effect of speed was found to be worse on randomly textured surfaces than on transversely textured surfaces. Finally, acceleration was shown to have an effect on the parameters produced by one of the devices, giving further credence to the fact that care should be taken to gather high-quality datasets for the critical pavement characteristic of macrotexture.

Keywords: Macrotexture, Limits of Agreement, Repeatability, MPD, Surface

---

[1] This manuscript (TRB Paper #19-01177R2) was accepted for presentation and publication at the 98th Annual Meeting of the Transportation Research Board. The final published version can be found in the Transportation Research Record at: https://doi.org/10.1177/0361198119830309. Preliminary findings were presented at the 30th Annual Road Profile User's Group meeting held at Rapid City, SD in September 2018. Coauthors for this paper are Kyle Maeger, Dr. Samer W. Katicha, Dr. Edgar de Leon Izeppi, Dr. Gerardo Flintsch.

Introduction

Background

Various US and international standards exist to calculate parameters that describe a road surface's macrotexture.
However, the US currently has no standard for gathering network-level macrotexture measurements. Several high-speed devices were tested on the Virginia Smart Road to assess their ability to characterize the macrotexture of various road surfaces.

Typical means of data comparison, such as regression analysis with associated correlation coefficients, can be misleading in comparing datasets from two or more devices. Correlation only shows how strongly the data are related (Altman and Bland 1983), and depends on both the measurement errors and the true variability of macrotexture. For data to be well-correlated, it just needs to fall along a straight line or follow any selected function. Therefore, correlation is not appropriate to determine the repeatability (i.e., its ability to produce the same results under the same conditions) of a given device.

In the past, the typical approach was to perform harmonization studies to allow the results of pavement surface interaction characteristics from different devices (PIARC 1987; Descornet 2004; Sandberg et al. 2011; Haider et al. 2016) to be compared. However, the true value of the parameter measured is unknown for the entire surface. One could try to use a mechanical stylus or perform sand patch tests on an entire wheel path, but manual tests have been known to be susceptible to operator error (Mokarem 2006).

Another issue with harmonization studies is that results are often difficult to replicate (Vos and Groenendijk ; Flintsch et al. 2009; Fuentes and Gunaratne 2010). Given the shortcomings of harmonization between macrotexture measurement devices, another method is needed. Izeppi et al. (2012) showed that valid comparisons between various friction measuring devices can be made in the absence of a true value via agreement methods first used in the biopharmaceutical field (Martin Bland and Altman 1986; Bland and Altman 1999; Barnhart et al. 2007; Bland 2007; Carstensen et al. 2008). These methods assess the agreement or closeness between readings of the devices evaluated (Barnhart et al. 2007). Katicha et al. (2014) used this method to compare Falling Weight Deflectometer (FWD) and Traffic Speed Deflectometer

(TSD) measurements. However, no such analysis has been carried out to compare an array of macrotexture measurement devices.

Problem Statement

No guidance exists for network-level macrotexture data collection in the US. Comparison of devices to measure macrotexture can be difficult as the true macrotexture is unknown for the entire roadway. Furthermore, correlation comparisons can be misleading for the purposes of device comparisons (Carstensen et al. 2008).

Objective

The objective of this study is to evaluate the ability of various macrotexture measurement devices to measure typical pavement surfaces to determine if they can be used interchangeably within an acceptable range. As network-level measurements are envisioned to be made on a reoccurring basis, the ability of a device to produce consistent results on given surfaces (its repeatability) is also studied. Finally, since data collection does not occur in an ideal world, the effects of operational factors such as speed, acceleration, and deceleration on the measurements are also evaluated.

Methodology

Experiment Setup

Vehicles with high-speed macrotexture scanning equipment were used to make measurements on the Virginia Smart Road. The Smart Road is a 2.2-mile test track dedicated to research located in Blacksburg, Virginia. It offers a variety of surfaces, including Dense Graded Hot Mix Asphalt (DGHMA), an Open-Graded Friction Course (OGFC), proprietary High-Friction Surface Treatments (HFST), as well as grooved, tined, or ground Portland Cement Concrete (PCC) sections as shown in Figure 3-1. More information is given in Appendix A.

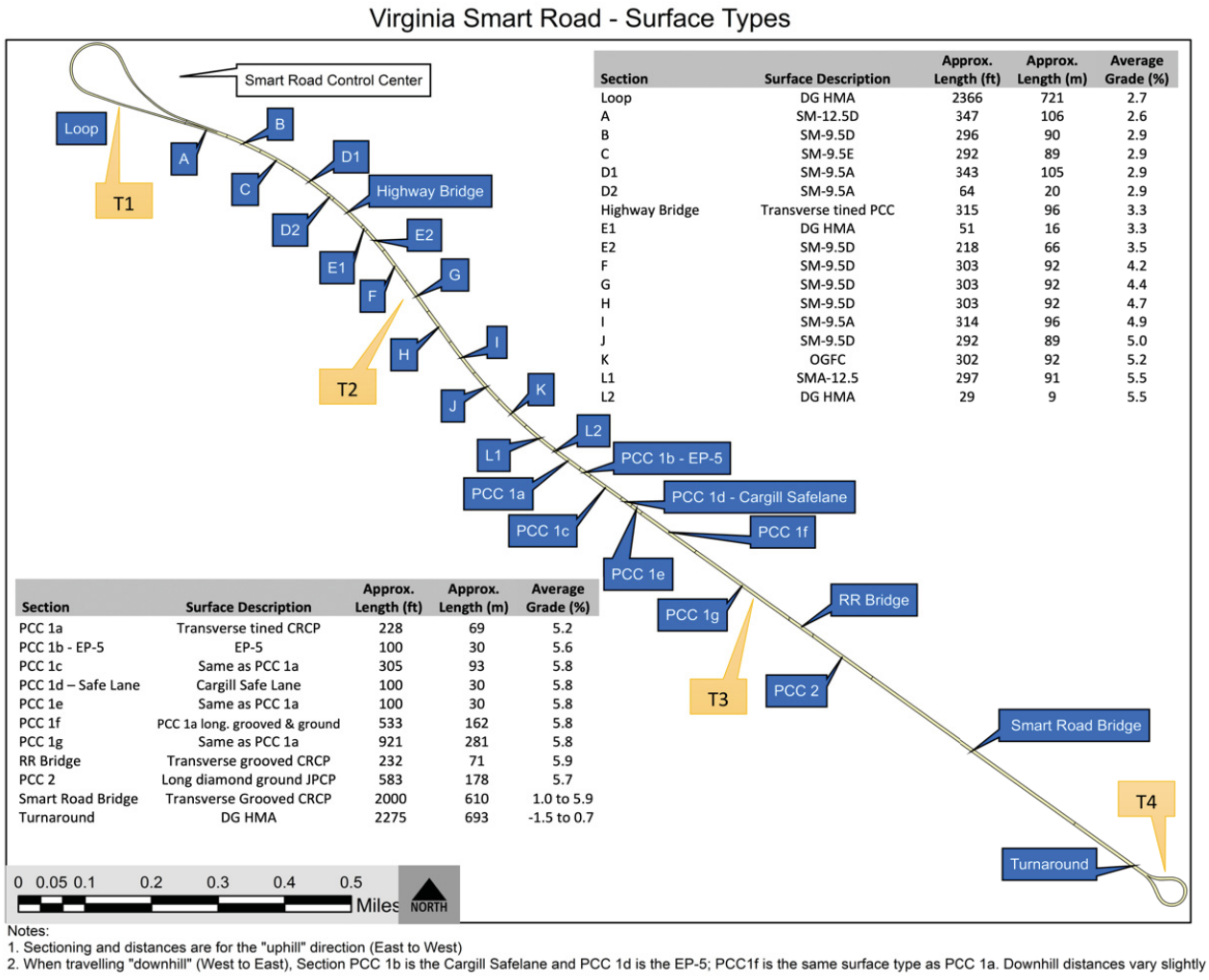

Section	Surface Description	Approx. Length (ft)	Approx. Length (m)	Average Grade (%)
Loop	DG HMA	2366	721	2.7
A	SM-12.5D	347	106	2.6
B	SM-9.5D	296	90	2.9
C	SM-9.5E	292	89	2.9
D1	SM-9.5A	343	105	2.9
D2	SM-9.5A	64	20	2.9
Highway Bridge	Transverse tined PCC	315	96	3.3
E1	DG HMA	51	16	3.3
E2	SM-9.5D	218	66	3.5
F	SM-9.5D	303	92	4.2
G	SM-9.5D	303	92	4.4
H	SM-9.5D	303	92	4.7
I	SM-9.5A	314	96	4.9
J	SM-9.5D	292	89	5.0
K	OGFC	302	92	5.2
L1	SMA-12.5	297	91	5.5
L2	DG HMA	29	9	5.5

Section	Surface Description	Approx. Length (ft)	Approx. Length (m)	Average Grade (%)
PCC 1a	Transverse tined CRCP	228	69	5.2
PCC 1b - EP-5	EP-5	100	30	5.6
PCC 1c	Same as PCC 1a	305	93	5.8
PCC 1d – Safe Lane	Cargill Safe Lane	100	30	5.8
PCC 1e	Same as PCC 1a	100	30	5.8
PCC 1f	PCC 1a long. grooved & ground	533	162	5.8
PCC 1g	Same as PCC 1a	921	281	5.8
RR Bridge	Transverse grooved CRCP	232	71	5.9
PCC 2	Long diamond ground JPCP	583	178	5.7
Smart Road Bridge	Transverse Grooved CRCP	2000	610	1.0 to 5.9
Turnaround	DG HMA	2275	693	-1.5 to 0.7

Notes:
1. Sectioning and distances are for the "uphill" direction (East to West)
2. When travelling "downhill" (West to East), Section PCC 1b is the Cargill Safelane and PCC 1d is the EP-5; PCC1f is the same surface type as PCC 1a. Downhill distances vary slightly

Figure 3-1 - Virginia Smart Road sections and surface types

Data Collection

Data were collected using five vehicles, each fitted with laser triangulation sensors capable of collecting pavement macrotexture information at the rates shown in Table 3-1. All data were gathered in the left wheelpath of the ‘uphill” lane (the lane runs from east to west). Data were received in the raw spatial form from the operators. Height measurements were given with the fixed sampling interval shown in Table 3-1. In the case of Device 3, the authors interpolated time-domain data into spatial-domain data according to the maximum interval observed for the speeds used. The operators performed no filtering or outlier correction. Raw data were requested to enable an objective comparison of all data by applying the same analysis methods to remove variables such as filtering, outlier correction, and method of parameter

calculation. Note that device 15 was mounted directly behind Device 1 on the same vehicle to test the effects of vehicle motion and driver wander.

Table 3-1 - Data collection equipment information

Device ID	Laser Type	Make	Sampling Frequency (kHz)	Raw Data Spatial Interval (mm)	Vertical Resolution (± mm)
1	Single Spot	Acuity (custom)	100	0.25	0.020
2	Single Spot	Limab SR TexRough	32	1	0.010
3	Single Spot	LMI Gocator 1300 series	32	0.9	0.049
4	Single Spot	Acuity (custom)	100	0.5	0.020
5	Line Laser	LMI Gocator	5	0.3 (transverse) 25 (longitudinal)	0.015 to 0.040
15	Single Spot	LMI Opticator	62.4	0.25	0.045

The Virginia Smart Road was prepared by placing rubber strips at or near the pavement section transitions of the surfaces tested. These were used to accurately identify the boundaries between the different surfaces. Traffic cones with a strip of reflective tape along the entire height were also placed on the road's shoulder to trigger photocells to mark where each transition occurred. Operators calibrated their distance measurement equipment at 105 km/h using survey points placed on the road for that purpose.

Three sets of tests were completed at high speed and are summarized in Table 3-2. The first test, High Speed, was aimed at studying the overall repeatability and agreement of the various devices. The high-speed test commenced with the test vehicle on the Virginia Smart Road turnaround (labeled "T4" in Figure 3-1). The vehicle subsequently accelerated to the test speed and remained at this speed (typically through the use of cruise control) across all the surfaces tested. To study the possible effect of speed on a device, the second test, Constant Speed, started at T3 and ended at T2. This test involved a PCC section and an AC section. The vehicle commenced at T3, accelerated to the test speed before crossing into the test sections and remained at that speed for the duration of the test. The speeds listed in Table 3-2 were used in the constant speed test. The third test, Variable Speed, evaluated the effect of acceleration on measurements. It commenced at Section H and ran through Section F. As shown in Figure 3-1, the surface type is the same for these sections, so they can be considered as one section. Four

speed profiles were used, and drivers were instructed to achieve the initial speed from T3 and then perform the test action (acceleration or deceleration) by the mid-point of the test section, which was marked by a cone. The vehicles then proceeded through the remainder of the test section at that speed or accelerated to the next required speed by the end of the test section.

Table 3-2 - Summary of tests performed

Test Name	Speed	# runs	Section Tested
High Speed (HS)	55 mph (89 km/h)	5	Smart Road Bridge through Section C
Constant Speed (CS)	15 mph to 65 mph (24 km/h to 105 km/h) in 10 mph (16 km/h) increments	4	PCC 1a, Section L
Variable Speed (VS)	25 mph (40 km/h) speed up to 50 mph (80 km/h) 50 mph (80 km/h), slow to 25 mph (40 km/h) 50 mph (80 km/h), full stop, 50 mph (80 km/h) 50 mph (80 km/h), slow to 25 mph (40 km/h), speed up to 50 mph (80 km/h)	4	Section H through F

Data Preparation

For the high-speed runs, data were collected without interruption along the length of the road. To break these datasets into individual sections (i.e., various surface types), reflective cones were placed to trigger event markers using the various devices' photocell triggers, and bump strips of known dimensions were placed across the width of the lane. The reflective cones did not always trigger an event marker for all devices, so the bump strips were used to locate the beginning and end of each section definitively. These bumps were meticulously located in the data for each of five runs of the 18 sections of interest for all six devices. This ensured that each section's set of data had a common starting point across devices and runs to minimize the effect of vehicle wander on profile lengths compared to simply using the overall test start and stop points. The start/stop bumps were similarly located for the constant speed and variable speed tests data.

Once sections were parceled out, 3 meters were cut off the beginning and end of all data. This was done to ensure that the bump strip would not affect the data analysis. The length of 3 meters was selected also to minimize the effect of inconsistencies in the road surface. For example, steel bridge expansion joints, areas of PCC near the start of a section that could not receive grinding/grooving to match subsequent pavement, and abrupt transitions between PCC/AC or surface treatments were all removed in this manner. This provides a more consistent surface profile from which to calculate macrotexture parameters.

The mean profile depth (MPD) was selected as the parameter to represent the macrotexture as it is widely used in both the US and abroad. An initial analysis of variance (ANOVA) of repeated runs of the same devices showed that aggregating MPD to a 1-meter or greater reporting length resulted in failure to reject the null hypothesis, indicating that means are equal for each run. For this reason, MPDs aggregated to 1 meter are used for the entirety of the analysis in this work. Aggregation reduces the negative impacts of slight vehicle wander, operator experience, and misalignment of individual runs.

Outlier Removal

As noted in various standards for calculating MPD (ISO 13473-1 1997; ASTM E1845 2015), outliers in the data must first be removed. This is especially important for MPD calculations as they are sensitive to large data variations. All data from single-spot laser devices were treated with the same adaptive outlier removal routine as described by Katicha et al. (Katicha et al. 2015). Figure 3-2 provides an example of profiles before and after outlier removal.

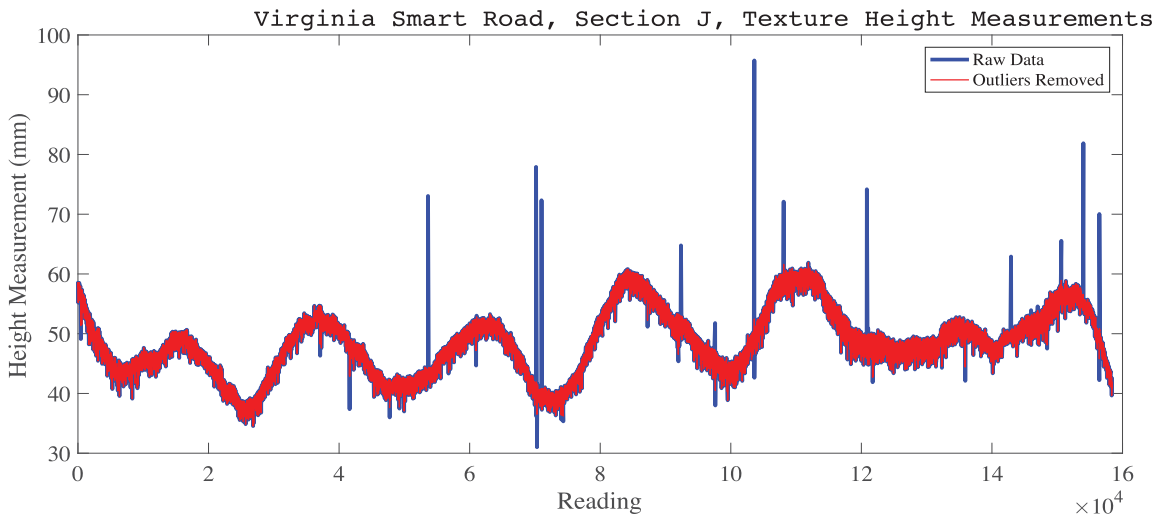

Figure 3-2 - Example outlier removal of single-spot lasers

The data from the line laser (Device 5) presented a challenge that inspired a novel approach to dropout and outlier removal from wide-footprint data sets. Relatively large quantities of dropouts (data points not recorded by the device at the specified sampling time) were found in the raw data from the line laser. These dropouts occurred most typically along the edges of the laser footprint or, at times, across the entire width of the laser for one or more samples. To overcome these missing data and proceed to subsequent outlier removal, transverse rows of data were completely removed if more than 10% (as ASTM E1845 (2015) suggests), of the data points were dropouts. Next, columns of data outside of the central 100-mm footprint (the base length for our MPD calculation) were removed, which eliminated the majority of remaining dropouts along the edges. Then, for the remaining rows, the mean value of valid measurements was calculated, and the few remaining dropouts were then replaced with this value. The dataset was now ready for outlier removal. The authors wanted to use a consistent approach to outlier removal for all datasets. The false discovery rate method we employed is a statistics-based approach that adapts to the given dataset to select an appropriate threshold that guarantees that no more than a certain percentage (10% in our case) of outliers are incorrectly identified. Due to its statistical nature, large datasets should be used, so consecutive rows of line laser data were concatenated according to equation 1 to create a dataset similar in size to those of the single-spot lasers for their outlier elimination.

$$\begin{bmatrix} h_{1,1} & h_{1,2} & \dots & h_{1,n} \\ \dots & & & \\ h_{m,1} & h_{m,2} & \dots & h_{m,n} \end{bmatrix} \xrightarrow{yields} [h_{1,1} \quad \dots \quad h_{m,n}] \qquad \textit{(Equation 3-1)}$$

where:
h = texture height
m = row
n = column

To minimize edge effects in the concatenation, the profile was detrended via a simple linear regression subtracted from the row of interest which suppressed the slope and set the mean of the row to zero. After outlier removal, the dataset is reconstructed to the original matrix dimensions. The result (Figure 3-3) is a 3-D profile with outliers removed whose profile was untouched in areas not containing outliers.

(a

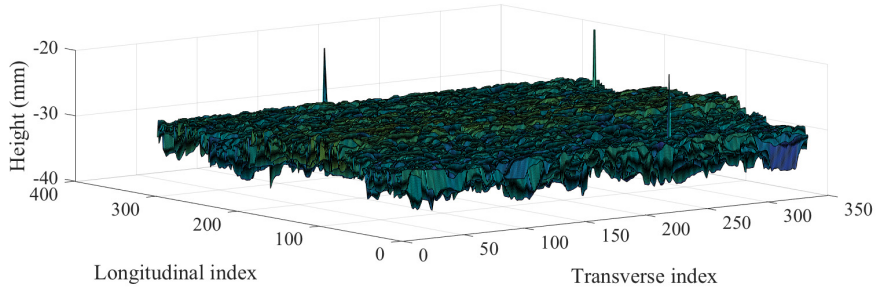

(b

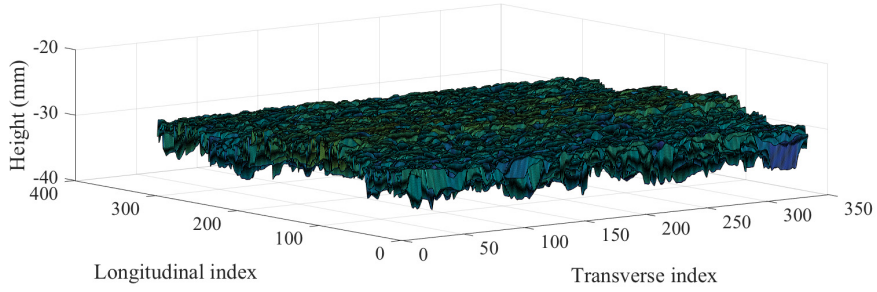

Figure 3-3 - Example raw (a) line laser profile and (b) profile with outliers removed

After outlier removal, all data were filtered to ensure only the wavelengths of interest for macrotexture are evaluated. A low-pass, lowest-order Butterworth Infinite Impulse Response filter was designed for each device based on the sampling interval used according to the guidance in ASTM E1845 (ASTM E1845 2015). All long wavelength trends (i.e., grade of the road, slope due to position of the vehicle-mounted sensor relative to the surface) of the 100mm MPD base lengths were removed. This was accomplished by subtracting a first-order regression line from the profile of each base length, resulting in a zero-mean, zero-slope (detrended) base

length. Finally, MPDs were calculated for every 100 mm of longitudinal travel in the left wheelpath according to ASTM E1845. For Device 5, a line laser, MPD values were calculated in the transverse direction and then arithmetic means were calculated to harmonize the reporting length of the line laser with the results of the single spot lasers. For example, MPDs were calculated for each transverse line laser scan and all MPD values within the 100mm of interest. This means the data from typically four measurements (given the 25mm longitudinal sampling interval) are averaged for every MPD reported by the devices with single spot lasers.

Device Comparison

To overcome the shortcomings in other forms of device comparison (i.e., ANOVA, correlation, and harmonization), the repeatability of each device against itself and the agreement in measurement between the devices (which also sheds light on an instrument's bias) were evaluated. Conducting an ANOVA can show if means are equal for multiple runs of a device, where a high *p*-value corresponds to a failure to reject the null hypothesis, meaning that the means of repeated measurements taken are equal. However, this approach is limited when comparing devices one with another because a device with high variance in collected data tolerates a more substantial difference in means before rejecting the null hypothesis of equal means than a device with lower variance. Correlation analysis for the purpose comparing devices can also be misleading as it shows only the strength of the relationship between devices, but does not quantify the differences (or, conversely, agreement) between devices. Harmonization studies have been used in the past to compare a device against a "ground truth" in order to force measurements to be more similar to another device. This is difficult for a pavement's macrotexture as the true value of macrotexture us unknown for the surfaces measured; in other words, there is no "ground truth." Furthermore, these studies have been difficult to replicate under differing experimental conditions (Vos and Groenendijk ; Flintsch et al. 2009; Fuentes and Gunaratne 2010). The methods employed to quantify repeatability and agreement are described below.

Repeatability

Repeatability determines the extent to which a device can reproduce its previous results. In this study, this is accomplished by quantitatively by calculating a device's repeatability

coefficient. A repeatability coefficient is superior to a coefficient of correlation as the former provides a specific quantity (i.e., difference in MPD measured in millimeters), whereas the latter only provides a proportion of the relationship (1.0 being a perfect relationship) between the repeat runs of the device. With the specific quantity provided by the repeatability coefficient, engineering judgement can be used to determine if the device has sufficient repeatability for the planned purpose. For example, a device with a repeatability coefficient of 0.09mm may be deemed sufficient for measuring macrotexture as this is within the resolution required to delineate between investigatory and intervention levels which is often given in tenths of a millimeter. The repeatability coefficient is derived from the device's mean square error (MSE) for several runs over the same pavement section, where MSE is essentially the variance of the device. The repeatability coefficient is derived from the within-device standard deviation as proposed by Bartlett and Frost (2008):

$$c_r = 1.96 * \sqrt{2} * SD \qquad \textit{(Equation 3-2)}$$

As multiple runs were made with each device, SD (the within-device standard deviation) in equation 2 is calculated by taking the square root of the MSE after performing an ANOVA. Appendices B through F contain ANOVA results for the devices tested. The interpretation of the test is that two measurements made on a subject by a device should differ by no more than the repeatability coefficient 95% of the time, assuming a normal distribution of differences between measurements (Bartlett and Frost 2008). For each device, the ANOVA was conducted for the High-Speed data with pavement section as the input and MPD as the model effect. For all the analyses, 1-meter aggregated data collected over the pavement sections were averaged to a single average MPD for each pavement section for each of the five runs. Additional data on device repeatability is available in Appendix G.

Device Agreement

Limits of agreement (LOA) is presented by Bland and Altman (Martin Bland and Altman 1986) as a superior device comparison method for correlation coefficients because a strong correlation between devices does not necessarily guarantee strong agreement between them. This method explores the differences between measurements made by any two devices and quantifies these differences against the mean of the measurements made. Five runs of High-Speed data

were collected over the 18 pavement sections as shown in Table 3-2. A data table for the calculation of LOA can be found in Appendix H. The LOA method used assumes that the true value measured does not change and that measurements are made in quick succession to minimize effects caused by changes in experimental conditions. To ensure that the true value of the pavement macrotexture does not change, the standard deviation of runs for each section should be constant and not related to the magnitude of the measurements. This is checked by plotting the standard deviation against the mean for each device (Bland 2007).

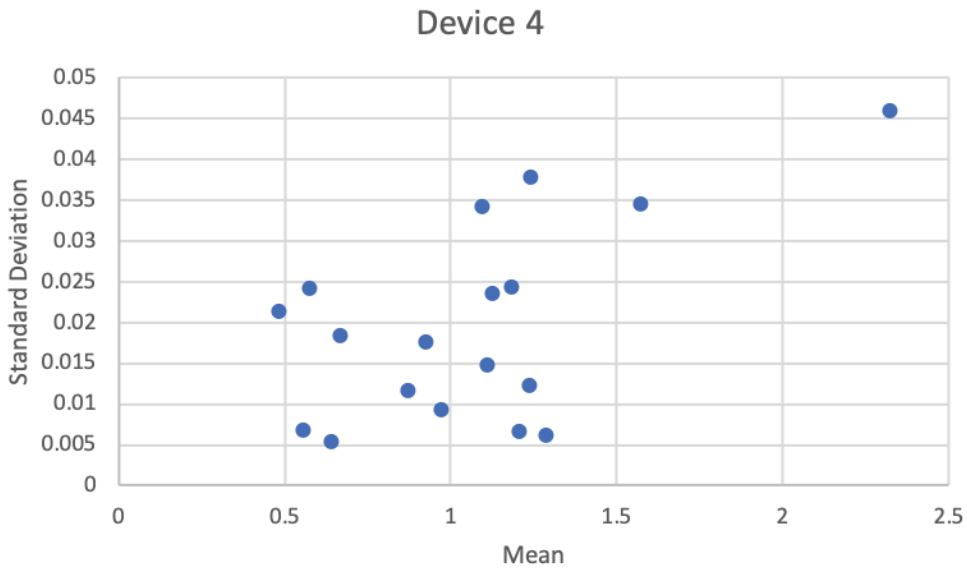

Figure 3-4 - Determination of constant means for Device 4

Figure 3-4 is an example of this check for Device 4 and appears to show no clear relation between standard deviation and magnitude of mean values, which suggests the constant standard deviation assumption can be used. The 95% confidence LOA are calculated as prescribed by Bland and Altman (Bland 2007):

$$LOA = 1.96 * S_c \qquad \textit{(Equation 3-3)}$$

where:

S_c is the corrected standard deviation of differences = $\sqrt{S_D{}^2 + f_1 \cdot S_1{}^2 + f_2 \cdot S_2{}^2}$;

S_D = standard deviation of the difference between the mean of the runs for each road section by two devices compared;

f_1 and $f_2 = 1 - \frac{1}{m}$ (m is the number of runs for each section). Each section had 5 runs; therefore, $f_1 = f_2 = 0.8$.

S_1^2 and $S_2^2$are the variances of the devices (MSE determined from an ANOVA of the device with the pavement section as the model input and average MPD as the response).

The boundaries for LOA are the mean of the differences for the devices over the sections ± the LOA. The LOA are plotted with the mean of the two devices' measurements on the *x*-axis and the difference between the devices on the *y*-axis.

Operational Factors Test

For the Constant-Speed tests, an ANOVA was conducted for both pavement sections with speed as a continuous variable model input and MPD as the response. Using a significance level of 0.05, a failure to reject the null hypothesis demonstrates no effect of speed, and rejection of the null hypothesis demonstrates an effect of speed.

For the Variable-Speed tests, an ANOVA was conducted with the four various acceleration conditions as the model input and MPD as the response. Using a significance level of 0.05, a failure to reject the null hypothesis demonstrates no effect of variable speeds, and rejection of the null hypothesis demonstrates an effect of the variable speeds.

Results

To begin the analysis, a two-way factorial ANOVA was performed on the entire data set of 55 mph runs of all devices. In this analysis, the device, pavement section, and interaction term of device*section are all used as model effects with average MPD for the section as the response. The resulting *p*-values (all < 0.0001) indicated that all model effects were significant to the analysis. The effects test of the device was used to determine if any of the devices differ. From the two-way ANOVA, a Tukey's Honest Significant Difference (HSD) test with connecting letters report from JMP software was used to make a preliminary evaluation of device agreement. It should be noted that Tukey's HSD is a very sensitive test and small differences may show as disagreement of an entire device. Only devices 2 and 4 were shown to provide the same overall readings. Further light is shed in subsequent pairwise LOA comparisons in this work.

Repeatability

All datasets received the same outlier removal, detrending, and filtering treatments before the data was analyzed. The calculated coefficients of repeatability are found in Table 3-3 for the data analyzed according to the procedures described above. C_r for all devices tested was in a similar range (from 0.063 to 0.088 mm), meaning that measurements on pavement types similar to those tested by the devices used will differ by no more than the repeatability coefficient (i.e., 0.063 mm) on 95% of occasions. This is thought to be sufficient since the repeatability of sand patch tests has been found to vary by approximately 24% of the mean value of each test location in another study (Doty 1975), indicating that these high-speed, non-contact means are an improvement to manual means.

Table 3-3 - Summary of device repeatability

	Device 1	**Device 2**	**Device 3**	**Device 4**	**Device 5**	**Device 15**
MSE	7.3 E-4	6.7 E-4	10.07 E-4	5.27 E-4	5.2 E-4	9.38 E-4
$\mathbf{c_r}$	0.075	0.072	0.088	0.064	0.063	0.085

Device Agreement

The mean of all 1-meter MPDs for each run of a particular pavement section was calculated. The results are plotted in Figure 3-5 for each of the devices tested. From the figure, it is easy to discern that the results were similar for most of the surfaces tested. For example, PCC1e had relatively low MPDs, and asphalt section K (an open-graded friction course) had relatively high MPDs reported by all devices. It is also apparent in PCC1f (a longitudinally ground and grooved PCC section) that one device yielded much higher results than the other four devices tested for each of its runs. PCC2 shows a similar but less extreme trend. The next task is to quantify the agreement (or lack thereof) between devices.

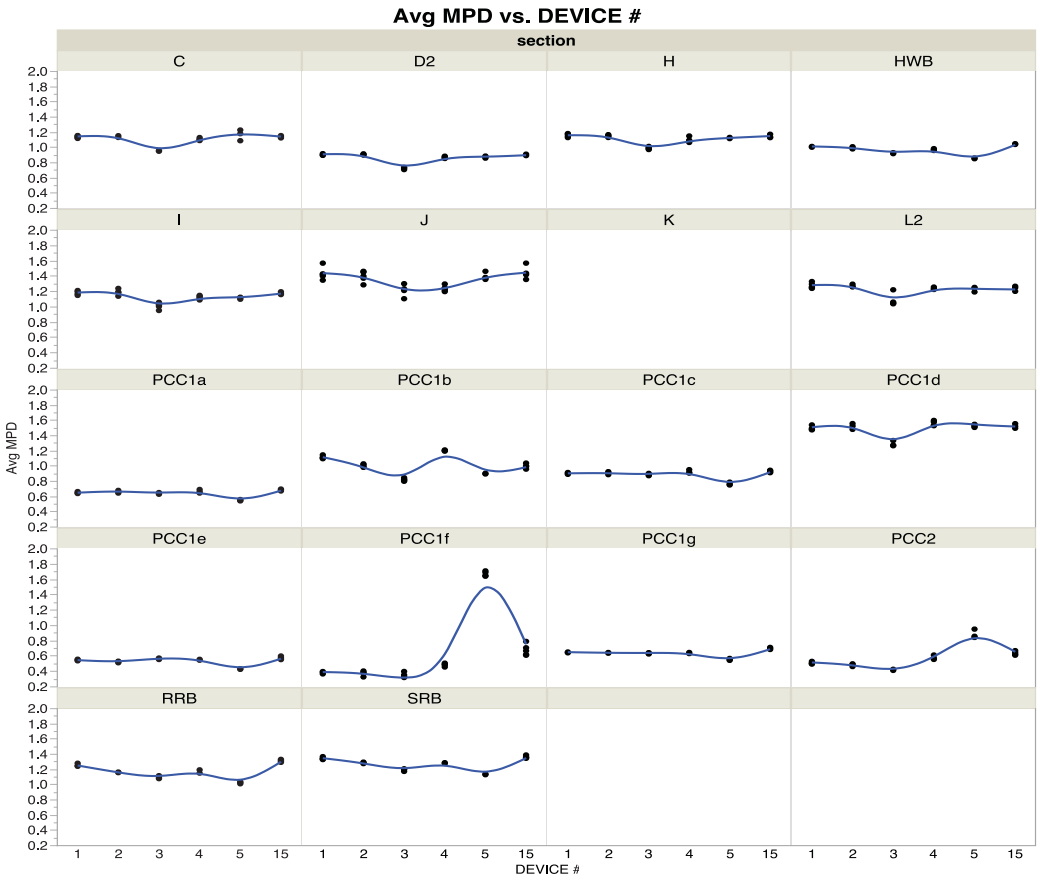

Figure 3-5 - Mean MPD results for each section tested

The LOAs were initially calculated for pairs of all devices and all sections of pavement. However, the agreement of all devices against the transversely mounted line laser (Device 5) is poor compared to the pairwise comparisons of the other devices. The difference in MPD for Device 5 is seen in Figure 3-5; note all five runs are plotted for each device but are typically too close to distinguish at this scale as quantified by their repeatability coefficients in the previous sections. The plots in Figure 3-5 show that there is a difference for the longitudinally texture surfaces, and the plots in Figure 3-6 show how much the single-spot lasers disagree with the line laser system. Note the narrow band of agreement of two single-spot laser devices (Figure 3-6a) and a wider range for the single-spot laser compared to the line laser (Figure 3-6b). This does not mean that the readings made by either of the devices are necessarily poor, it demonstrates that the devices are not interchangeable for certain pavement types. Additional data and plots for all devices tested are available in Appendices I though N.

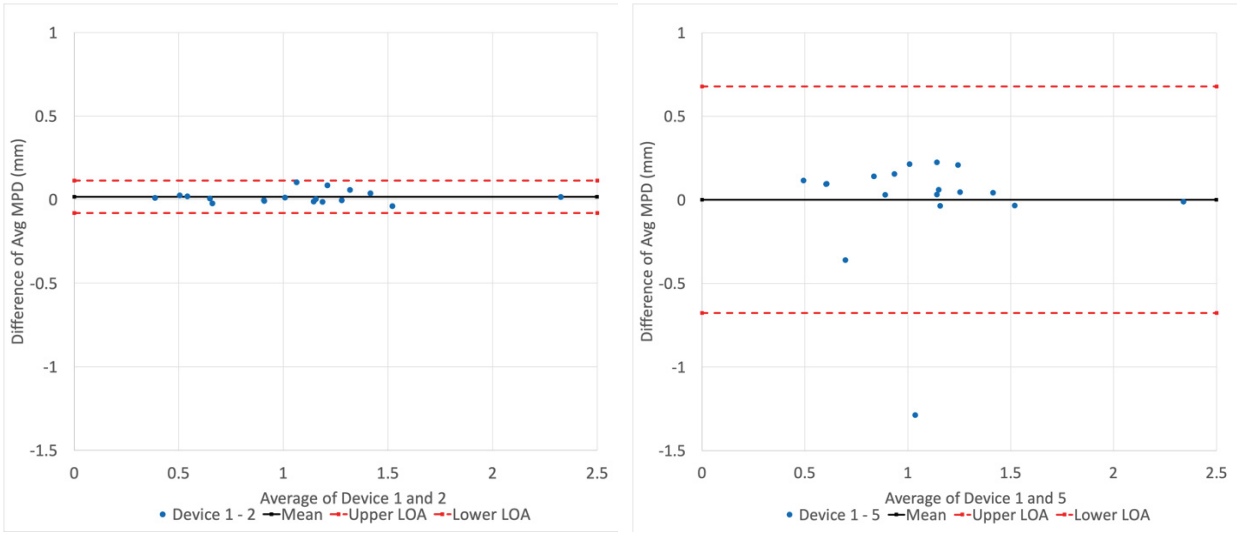

(a) (b)

Figure 3-6 - Bland-Altman plots for all sections tested device pair s(a) 1-2 and (b) 1-5

This prompted the evaluation of the pavement sections with no directional texturing (i.e., asphalt, and PCC1b and PCC1d, which are similar to asphalt), hence the pavement surface groupings shown in Table 3-4. The "Random" texture (asphalt-like sections) columns show better agreement for the line laser (Device 5) with all other devices when compared to the LOA for all pavement surface types. In fact, the LOA drops (improves) by an average of 74%. Since it was apparent that the engineered directional textures (i.e., grooves and tine marks) created poor agreement between the single-spot and line laser devices, LOA analysis was then carried out on the PCC sections, first those with longitudinal texture (PCC2 and PCC1f, "longitudinal only" in Table 3-4), next those with transverse grooves or tine marks (the remaining PCC-surfaced sections, "transverse only" in Table 3-4).

Table 3-4 - Summary of LOAs

	Texture Type							
	All		Random		Longitudinal Only		Transverse only	
Device Pair	Mean of Difference	LOA	Mean of Difference	LOA	Mean of Difference	LOA	Mean of Difference	LOA
1,2	0.02	0.10	0.01	0.12	0.02	0.05	0.02	0.08
1,3	0.13	0.19	0.20	0.12	0.07	0.08	0.06	0.14
1,4	0.01	0.15	0.03	0.18	-0.07	0.07	0.02	0.08
1,5	0.00	0.68	0.04	0.17	-0.82	1.29	0.15	0.10
1,15	-0.03	0.18	0.02	0.12	-0.21	0.25	-0.04	0.04
2,3	0.11	0.18	0.19	0.10	0.05	0.08	0.04	0.09
2,4	0.00	0.16	0.02	0.20	-0.09	0.06	0.00	0.05
2,5	-0.03	0.67	0.03	0.12	-0.84	1.27	0.13	0.06
2,15	-0.04	0.18	0.01	0.10	-0.23	0.24	-0.06	0.09
3,4	-0.12	0.21	-0.17	0.23	-0.14	0.06	-0.04	0.08
3,5	-0.14	0.66	-0.16	0.14	-0.89	1.22	0.09	0.06
3,15	-0.15	0.17	-0.18	0.11	-0.27	0.20	-0.09	0.15
4,5	-0.03	0.63	0.01	0.25	-0.75	1.24	0.13	0.06
4,15	-0.04	0.19	-0.01	0.23	-0.13	0.21	-0.06	0.09
5,15	-0.01	0.55	-0.02	0.13	0.62	1.06	-0.18	0.11

Note the line laser again showed poor agreement with all devices (as expected) for the "Longitudinal Only" sections (the line laser can capture this texture and the other devices cannot). However, it is interesting to note that the best agreement between all devices was for the PCC sections with transverse texturing with LOA ranging from 0.05 mm to 0.14 mm. A transverse-mounted line laser theoretically should fall either into a peak or a valley for each reading. The close agreement, however, indicates that the line laser does not always run parallel to the transverse groove or tine and, therefore, captures peak and valley information similar to the single-spot laser systems. Device comparisons and Normal-Quantile plots are available in Appendix O. Table 3-4 shows that the two technologies (single-spot and line lasers) cannot be used interchangeably for all pavement types.

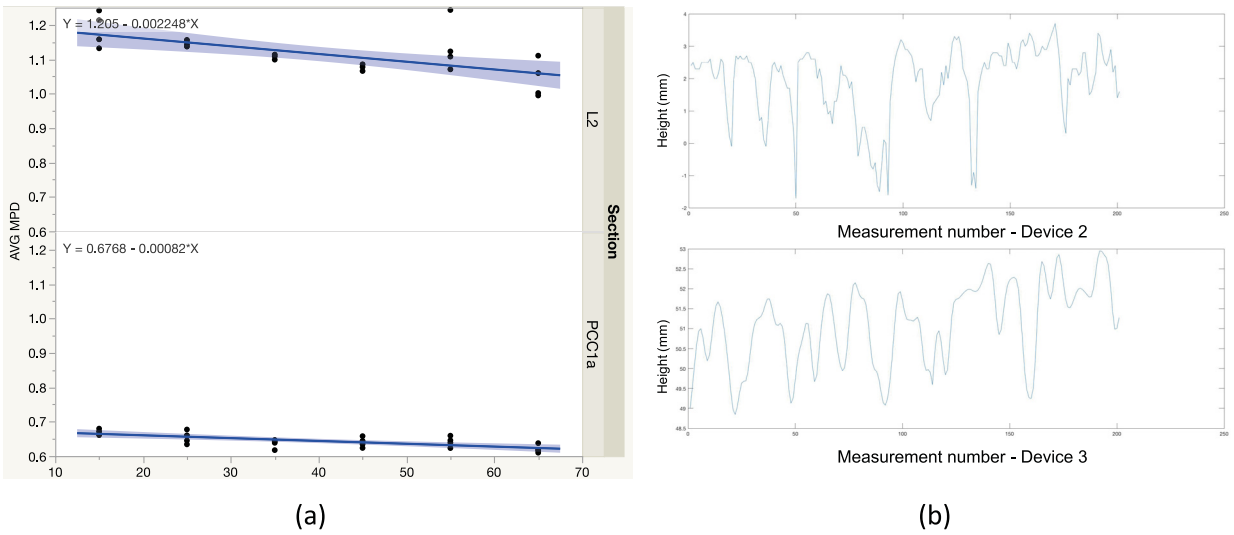

Figure 3-7 - MPDs (a) for all runs of Device 3 in the constant speed experiment and raw data profiles (b) of two single-spot laser devices from the experiment

It is also noted that Device 3 has a consistent bias of approximately 0.1mm (see the "Mean of Difference" column in Table 3-4) when compared to all other devices. Table 3-5shows the difference in means between any two devices to show where the greatest agreements and disagreements were for each pavement section. In reviewing the data for Devices 2 and 3 (both equipped with 32kHz sensors), the raw profiles captured for Device 3 were smoother with less aggressive peaks than those of device 2. See Figure 3-7(b). This was before the data was manipulated with any software filtering by the authors. This smoother signal is thought to account for the difference in MPD between these devices.

Table 3-5 - Summary pf difference of mean MPD values between device pairs

Sec	1-15	2-15	3-15	4-15	5-15	1-2	1-3	1-4	1-5	2-3	2-4	2-5	3-4	3-5	4-5
SRB	-0.02	-0.07	-0.17	-0.08	-0.23	0.06	0.15	0.06	0.21	0.09	0.00	0.15	-0.09	0.06	0.15
PCC2	-0.12	-0.15	-0.21	-0.07	0.24	0.03	0.09	-0.06	-0.36	0.06	-0.08	-0.39	-0.15	-0.45	-0.30
RRB	-0.06	-0.15	-0.22	-0.14	-0.29	0.09	0.16	0.07	0.23	0.07	-0.01	0.14	-0.08	0.07	0.15
PCC1g	-0.05	-0.05	-0.06	-0.06	-0.14	0.01	0.01	0.01	0.10	0.01	0.00	0.09	0.00	0.08	0.08
PCC1f	-0.29	-0.30	-0.33	-0.20	1.00	0.01	0.04	-0.09	-1.29	0.03	-0.10	-1.30	-0.13	-1.33	-1.20
PCC1e	-0.03	-0.05	-0.01	-0.02	-0.14	0.02	-0.02	-0.01	0.12	-0.04	-0.03	0.10	0.01	0.13	0.12
PCC1d	-0.02	0.02	-0.22	0.05	0.01	-0.04	0.20	-0.07	-0.03	0.24	-0.03	0.00	-0.27	-0.24	0.04
PCC1c	-0.03	-0.02	-0.05	-0.01	-0.17	-0.01	0.02	-0.02	0.14	0.02	-0.01	0.15	-0.04	0.12	0.16
PCC1b	0.11	0.01	-0.18	0.21	-0.10	0.10	0.29	-0.09	0.21	0.19	-0.20	0.11	-0.38	-0.08	0.31
PCC1a	-0.04	-0.02	-0.04	-0.02	-0.13	-0.02	0.01	-0.02	0.10	0.03	0.01	0.12	-0.02	0.09	0.11
L2	0.05	0.05	-0.14	0.01	0.00	0.00	0.19	0.04	0.05	0.19	0.04	0.05	-0.15	-0.14	0.01
K	0.06	0.04	-0.14	0.05	0.07	0.02	0.21	0.01	-0.01	0.19	-0.01	-0.03	-0.20	-0.22	-0.02
J	-0.01	-0.05	-0.22	-0.20	-0.05	0.04	0.21	0.19	0.04	0.18	0.16	0.01	-0.02	-0.17	-0.15
I	0.01	0.02	-0.16	-0.05	-0.06	-0.01	0.17	0.06	0.06	0.18	0.07	0.07	-0.11	-0.10	0.00
H	0.00	0.00	-0.16	-0.06	-0.03	0.00	0.16	0.06	0.03	0.16	0.06	0.03	-0.10	-0.13	-0.03
HWB	-0.03	-0.05	-0.12	-0.08	-0.19	0.01	0.08	0.04	0.16	0.07	0.03	0.14	-0.04	0.07	0.11
D2	0.00	0.01	-0.17	-0.03	-0.03	0.00	0.17	0.03	0.03	0.18	0.04	0.03	-0.14	-0.14	0.00
C	0.00	0.01	-0.18	-0.03	0.03	-0.01	0.18	0.03	-0.04	0.19	0.04	-0.03	-0.15	-0.22	-0.06

One concern with performing network-level macrotexture data collection is that uncontrolled factors such as vehicle wander and a driver's ability to reproduce a vehicle's path will distort the data. Recall that Device 15 was mounted to the same vehicle and directly in-line with Device 1. Note the LOA for Devices 1 and 15 are extremely similar to those of all other single-spot laser devices with the exception of the longitudinally-textured sections where single-spot lasers have been shown to be ineffective. This means that MPD measurements are not significantly affected by vehicle wander and macrotexture measurement path.

Operational Factors Tests

Constant Speed

To analyze the effect of speed (24 km/h to 105 km/h in 16-km/h increments) on the devices tested, an ANOVA was performed for each device on the two sections tested. A significance level of 0.05 was selected, above which we fail to reject the null hypothesis that speed does not affect the mean 1-meter MPD calculated. The results are presented in Figure 3-6. Recall that section L2 is a dense-graded hot mix asphalt and PCC1a is a transversely tined PCC section.

Table 3-6 - Summary of ANOVA results for the constant-speed experiment

Device	Section	*p*-value
1	L2	0.3854
2	L2	0.5966
3	L2	**0.0009**
4	L2	0.3977
5	L2	**0.0001**
1	PCC1a	0.0607
2	PCC1a	0.2206
3	PCC1a	**0.0001**
4	PCC1a	0.4951
5	PCC1a	**<0.0001**

As seen in Table 3-6, Devices 3 and 5 reject the null hypothesis that speed has no effect on MPD calculated. Recall that Device 3 and 5 have lower sampling frequencies: 32 kHz and 5 kHz, respectively. Device 5 is a line laser and captures over 300 points transversely 5,000 times per second. Figure 3-7(a) shows the average of 1-meter MPDs calculated for Device 3 for each of the test speeds. Here, a clear linear trend is seen with MPD negatively correlated to speed. The range of the data, however, is entirely different for the two pavement types tested. For Section L2 (DGHMA) the range of MPDs through the speeds was from 1.24 down to 0.99 mm for a spread of 0.25 mm. For the transverse-tined section PCC1a, the data ranged from 0.68 down to 0.61 (a spread of 0.07 mm), which is within the range of good repeatability for the device. Because we reject the null hypothesis that means are equal for devices 3 and 5, there is statistical evidence that speed does affect the reading of average MPD for these devices. However, as the range of data for the PCC section was within the range of repeatability coefficients for both devices, speed may not have an effect on these devices on PCC. As the range of data for the asphalt sections was outside of the range of repeatability coefficients for both devices, speed does have an effect on these devices (both with lower sampling frequencies) on asphalt pavements.

Device 5 had the same negative correlation as Device 3. It also shared similar range characteristics with a spread of only 0.054 mm (MPDs from 0.60 down to 0.54 mm) for the PCC1a section. For the asphalt section L2, MPDs ranged from 1.32 down to 1.20 mm. This is a

spread of 0.129 mm which is larger than the repeatability of the device. When the raw profiles were investigated, it was noted that the profiles were smoother and more closely resembled a flat line as speed increased. This could be due to an averaging effect on the signal with increased vehicle speed and constant exposure time on the device's sensor. Users can adjust the 'exposure time' or, more accurately, the amount of time photons are collected on the device's charged-couple device (CCD) before the CCD is cleared for the next reading. Devices are also capable of adjusting this exposure time to compensate for the surface being measured. Lighter surfaces reflect more light and require less exposure time. Darker surfaces reflect less light and, therefore, more exposure time allows more of these scare photons to be collected. With longer exposure time, more features of the surface scanned are collected on one single line of data, averaging peaks and valleys and forming flatter surfaces as can be observed in Figure 3-8. This indicates that not only does speed have an influence, but that surface type tends to either magnify or reduce this effect.

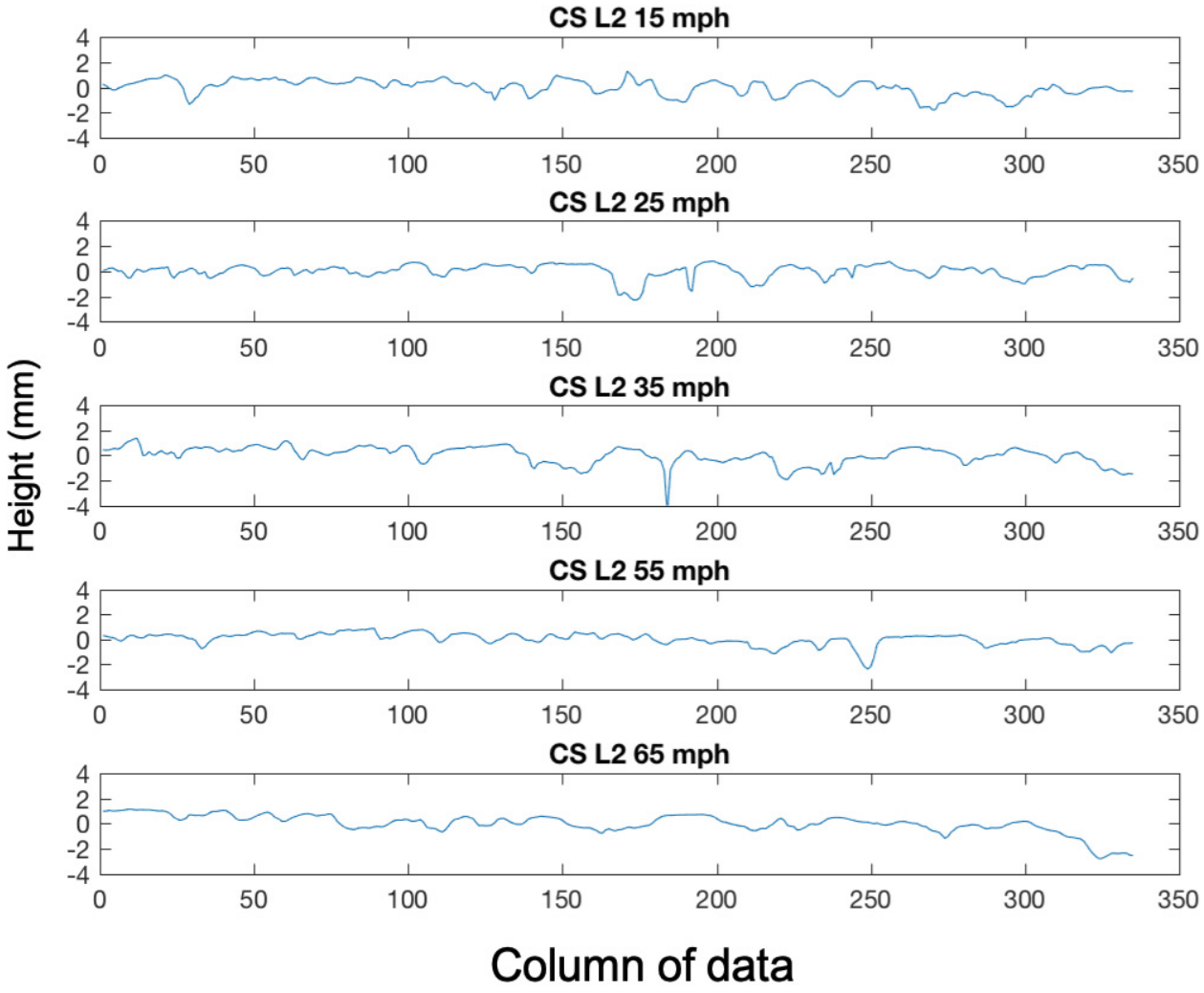

Figure 3-8 - Smoothing of line laser readings as speed increases

Variable Speed

The effect of acceleration (both speeding up and braking) was evaluated similarly to the constant speed experiment. An ANOVA analysis with the four various acceleration conditions as the model input and MPD as the response was completed. Results are summarized in **Table *3-7***.

Table 3-7 - Summary of ANOVA analysis for variable speed experiment

Device	*p*-Value
1	0.4653
2	0.6184
3	0.4306
4	0.8423
5	**0.0051**

Only the device with a line laser rejected the null hypothesis that acceleration does not affect the MPD calculated. Box plots of the processed data collected by this device are shown in Figure 3-9. Processing included outlier removal, low-pass filtering, profile detrending, and calculation of MPD. Although the null hypothesis was rejected, it should be noted that the data ranged from 1.23 down to 1.17 mm (a spread of only 0.06 mm), which is within the range of good repeatability for the device. Because we fail to reject the null hypothesis for the other devices, there is statistical evidence that the variable speeds tested do not affect the reading of average MPD for single-spot devices. However, the good repeatability shown for the line laser indicates that the ANOVA may be penalizing the line laser data due to its low variance. In other words, with low variability, a small deviation from the mean causes a rejection of the null hypothesis that all means are equal. Acceleration of the test device was found to be statistically significant for the line laser. However, since the range of 1-meter MPDs (0.06 mm) for the variable speed test is within the device's coefficient of repeatability, the effect is found to be negligible.

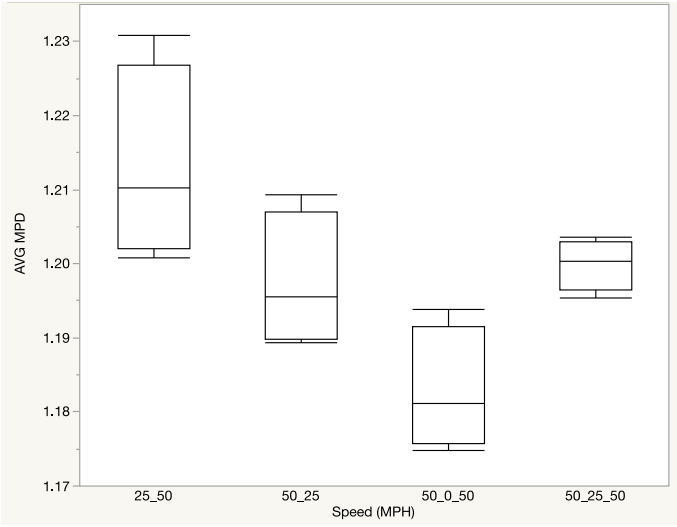

Figure 3-9 – Processed data collected by Device 5 during the variable speed experiment.

Summary and Conclusions

- A novel approach to removing dropouts and outliers from near-continuous line laser data was presented. The approach is adaptable to the given dataset and guarantees that the rate of falsely discovered outliers is limited to a pre-determined threshold.
- All devices tested showed good repeatability for all surfaces tested with coefficients of repeatability ranging from 0.063 to 0.088 mm.
- Low agreement was found for the line laser when compared to all other single-spot laser devices on all sections in a LOA analysis.
    - This does not necessarily mean that the measurements taken by this type of technology are bad. The wide band of agreement is likely because the line laser measures the peaks and valleys of longitudinal texturing whereas single spot lasers cannot. All pairwise comparisons of the line laser and the other devices yielded similar results when only transverse grooved sections were considered.
    - Agreement improved significantly (lack of agreement fell by more than half) when considering only surfaces similar to asphalt (i.e., SMA, OGFC, and HFST) in the LOA analysis.
- Device 3, a 32 kHz single-spot laser with a smoother raw data signal than the other single spot lasers tested appears to have a bias in calculated MPD of approximately 0.1mm when compared to all other devices.
- Speed is a significant factor in determining a pavement's macrotexture for some devices with sampling frequencies ≤ 32 kHz.
    - Smoothing of the signal before data manipulation appears to determine if speed will affect the results.
    - None of the devices appear to be affected on the PCC surface tested, however, two devices (each with sampling rates ≤ 32 kHz) showed a negative correlation to increasing speed on the asphalt section tested. This demonstrates the difficulty of capturing darker surfaces that require longer exposure time of sensors resulting in a smoothing effect on the profile.
- Acceleration is not a significant factor for devices equipped with single-spot lasers. ANOVA revealed that, statistically, acceleration is a significant factor for the line-laser-equipped

device. However, since the range of 1-meter MPDs (0.06 mm) for the variable speed test is within the device's coefficient of repeatability, the effect is found to be negligible.

- The best agreement between all devices comes when considering only PCC surfaces with transverse texturing. This is likely due to the fact that the line laser does not always run parallel to the transverse groove or tine and, therefore, captures peak and valley information similar to the single-spot laser systems.
- Readings from single-spot and transversely mounted line lasers should not be used interchangeably on longitudinally textured surfaces such as tined, grooved, or ground PCC surfaces.

Future Research

Only one device was fitted with a line laser and this device could only measure the surface with the laser line perpendicular to the direction of travel. It is recommended that additional line lasers with lines at differing orientations be studied to determine if there is an effect on repeatability, agreement, and operational factors. Exposure time should be tested to determine if speed is a factor for darker-colored pavements such as asphalt.

Acknowledgement

The authors would like to extend our sincere appreciation to those who performed the macrotexture measurements at the Virginia Smart Road.

References

Altman, D. G., and Bland, J. M. (1983). "Measurement in medicine: the analysis of method comparison studies." *The statistician*, 307-317.

ASTM E1845 (2015). "Standard Practice for Calculating Pavement Macrotexture Mean Profile Depth." ASTM International.

Barnhart, H. X., Haber, M. J., and Lin, L. I. (2007). "An overview on assessing agreement with continuous measurements." *Journal of biopharmaceutical statistics*, 17(4), 529-569.

Bartlett, J., and Frost, C. (2008). "Reliability, repeatability and reproducibility: analysis of measurement errors in continuous variables." *Ultrasound in Obstetrics and Gynecology: The Official Journal of the International Society of Ultrasound in Obstetrics and Gynecology*, 31(4), 466-475.

Bland, J. M., and Altman, D. G. (1999). "Measuring agreement in method comparison studies." *Statistical methods in medical research*, 8(2), 135-160.

Bland, J. M. A., Douglas G (2007). "Agreement between methods of measurement with multiple observations per individual." *Journal of biopharmaceutical statistics*, 17(4), 571-582.

Carstensen, B., Simpson, J., and Gurrin, L. C. (2008). "Statistical models for assessing agreement in method comparison studies with replicate measurements." *The international journal of biostatistics*, 4(1).

Descornet, G. "The HERMES project." *Proc., Symposium on Pavement Surface Characteristics [of Roads and Airports], 5th, 2004, Toronto, Ontario, Canada*.

Doty, R. N. (1975). "Study of the sand patch and outflow meter methods of pavement surface texture measurement." *Surface Texture Versus Skidding: Measurements, Frictional Aspects, and Safety Features of Tire-Pavement Interactions*, ASTM International.

Flintsch, G., de León Izeppi, E., McGhee, K., and Roa, J. (2009). "Evaluation of international friction index coefficients for various devices." *Transportation Research Record: Journal of the Transportation Research Board*(2094), 136-143.

Fuentes, L., and Gunaratne, M. (2010). "Evaluation of the Speed Constant and Its Effect on the Calibration of Friction-Measuring Devices." *Transportation Research Record: Journal of the Transportation Research Board*, 2155, 134-144.

Haider, M., Conter, M., Green, M., Schmidt, B., and Sandberg, U. (2016). "Status of the EU-project ROSANNE." *Transportation Research Procedia*, 14, 2946-2955.

ISO 13473-1 (1997). "Characterization of pavement texture by use of surface profiles - Part 1: Determination of Mean Profile Depth." *Part 1: Determination of Mean Profile Depth*, International Organization for Standardization.

Izeppi, E. d. L., Flintsch, G., and McGhee, K. (2012). "Limits of Agreement Method for Comparison of Pavement Friction Measurement." *Transportation Research Record: Journal of the Transportation Research Board*, 2306, 188-195.

Katicha, S. W., Flintsch, G. W., Ferne, B., and Bryce, J. (2014). "Limits of agreement (LOA) method for comparing TSD and FWD measurements." *Journal of Pavement Engineering*, 15, 6.

Katicha, S. W., Mogrovejo, D. E., Flintsch, G. W., and Izeppi, E. D. d. L. (2015). "Adaptive Spike Removal Method for High-Speed Pavement Macrotexture Measurements by Controlling the False Discovery Rate." *Transportation Research Record: Journal of the Transportation Research Board*(2525), pp 100–110.

Martin Bland, J., and Altman, D. (1986). "Statistical Methods for Assessing Agreement Between Two Methods of Clinical Measurement." *The Lancet*, 327(8476), 307-310.

Mokarem, D. W. (2006). "Use of the Digital Surface Roughness Meter in Virginia." Virginia Transportation Research Council.

PIARC (1987). "Technical Committee Report On Surface Characteristics --Piarc XVIII World Road Congress, Brussels, Belgium, September 13-19, 1987." World Road Association, Permanent International Assoc of Road Congresses (PIARC), 108 p.

Sandberg, U., Bergiers, A., Ejsmont, J. A., Goubert, L., Karlsson, R., and Zöller, M. (2011). "Road surface influence on tyre/road rolling resistance." *Models for Rolling Resistance in Road Infrastructure Asset Management Systems (MIRIAM),(http://miriam-co2. net/Publications/MIRIAM_SP1_Road-Surf-Infl_Report*, 20111231.

Vos, E., and Groenendijk, J. "Report on Analysis of Previous Skid Resistance Harmonization Research Projects. FEHRL, Brussels, Belgium, 2009."

CHAPTER 4 - EVALUATING NON-CONTACTING MACROTEXTURE LASER DISPLACEMENT DEVICE ACCURACY AT HIGHWAY SPEEDS

Abstract

Testing the accuracy of highway-speed macrotexture measurement devices under field conditions is problematic. As the true value of macrotexture of a roadway is unknown, measurements of the pavement surface cannot be used. For this purpose, machined reference surfaces were developed and machined out of billet aluminum to test device accuracy at highway speeds. These surfaces were measured in the lab with calipers and non-contacting laser displacement technology and in the field using non-contacting laser triangulation devices mounted to test vehicles. Various speed and exposures settings were evaluated for every plate and test device. Clear effects of vehicle speed and extreme sensor exposure time are demonstrated. A methodology was developed to compare lab and field measurements and a threshold level between the two is suggested.

Keywords: macrotexture, pavement, reference, calibration, accuracy, line laser

Introduction

The World Road Association defines macrotexture as "surface irregularities of a road pavement with horizontal dimensions ranging between 0.5 mm and 50 mm and vertical dimensions between 0.2 and 10 mm" (PIARC 2016). A pavement's macrotexture is crucial in providing a safer driving environment for motorists. Hydroplaning risk is reduced by providing a drainage path for water to provide "dry" pavement for tire contact to maintain vehicle control. In addition, the hysteresis component of friction is provided by macrotexture. The effect of these asymmetric deformations of the vehicle tire as it strikes the large asperities of the surface in the macrotexture range increases exponentially with increasing vehicle speed, accounting for 95 percent of available friction at speeds above 65 mph (Hall et al. 2009).

Commercial test vehicles exist to measure macrotexture using non-contacting laser displacement devices. However, accuracy checks for these vehicles are typically carried out in a static setting using gauge blocks. These conditions do not adequately reproduce the conditions of the field. There are no vehicle dynamics to perturb the distance measurement equipment and ambient light and surface metrology do not simulate the pavement's surface. Furthermore, any measurement of a pavement surface is not valuable in an analysis of accuracy as the true value of macrotexture is unknown (Izeppi et al. 2012) and since measurement paths cannot be aligned to guarantee the same pavement profile is measured.

The ISO (ISO 13473-1 1997) suggests using a rotating disc with shapes cut into it to test device accuracy. This approach was also investigated by the Australian Road Research Board (Wix and Leschinski 2010). However, this requires a test vehicle be able to simulate a data collection run at a given speed and not all vehicles are equipped to do so. Also, a rotating disc is not appropriate for measuring the newer class of line lasers employed by some vendors. ISO 13473-1 (2019) suggests a similar rotating disc approach or use of a single machined plate. However, various plate shapes are not suggested, and the effects of vehicle speed and exposure settings are not addressed.

This work used machined reference plates developed by Huang et al. (2013) at the Texas Department of Transportation. Their study tested a lab-built line laser system mounted to a high-speed vehicle. However, the effects of filtering and the use of single-spot lasers at various testing speeds and exposure settings were not addressed. Single spot lasers (SSL) project a circular laser point on the pavement surface and triangulation is used to determine the distance of the surface

from the laser. Samples are collected typically in excess of 32kHz, forming a series of texture heights one data point wide for the length of the test surface. Line lasers (LL) first diffuse the laser light through optics into a line that is projected onto the pavement surface. A line of texture heights is then triangulated on a sensor with many (typically several hundred) measurement rows. In the current work, vehicles fitted with commercial off the shelf single SSL and LL are tested at various travel speeds and exposure settings. Both raw and filtered data are analyzed.

Problem Statement

The true value of a pavement's macrotexture is unknown. Therefore, there is no standard against which to compare macrotexture readings from high-speed devices. Furthermore, the effect of vehicle speed, exposure settings of test equipment and signal filtering should be evaluated to enable recommending reference surface characteristics.

Objective

The main objective of this work is to analyze the ability of various devices to reproduce surface profiles at high speed. Secondary objectives include:

1. Determine if speed is a significant factor in the determination of derived parameters.
2. Determine if exposure is a significant factor for devices tested.
3. Compare reference measurements to field measurements.
4. Guide development of specifications for reference surfaces.

Methodology

Reference surfaces of known geometry (see Figure 4-3) were designed to represent shapes similar to those encountered on roadways. All plates were cut on a computer numeric control machining device from a single billet of aluminum 6061 alloy. The reflective machine marks that could cause unpredictable reflection of laser light were masked using a surface coating of matte red primer paint. Media blasting was considered and tested on other reference surfaces; however, this type of finish is prone to scratching (which would remove the matte finish) and the heat generated in the blasting process can warp the material blasted resulting in an inconsistent shape. After surface preparation, the plates were measured to determine their final dimensions. Digital calipers were used by two separate technicians to measure groove depths and

peak/valley widths. However, these measurements were inconsistent between the two operators (see Table 4-2). To obtain final reference measurements, a non-contacting laser distance measurement device was developed and used as described later.

Once reference measurements were made, the plates were measured in the laboratory with a reference measurement system and in the field by high-speed devices fitted with laser profilers. Equipment characteristics are given in Table 4-1. The LLL and LLT are the same sensor. However, for the LLL the laser line was oriented parallel to the direction of travel, see Figure 4-1(b), and the LLT was oriented perpendicular to the direction of travel. Additional detail of line laser orientation is given in Appendix P. As only one sensor could be fit to the center vehicle position, measurements were first taken in the LLL configuration and then the device was reoriented in the LLT direction.

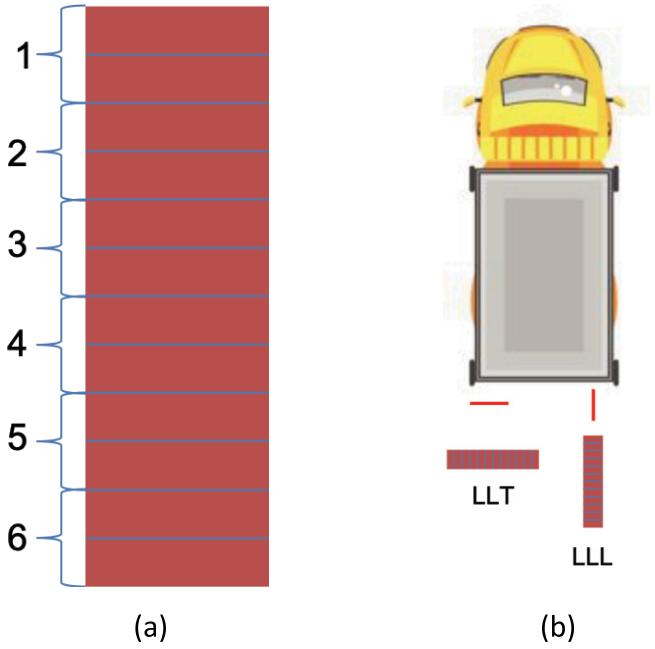

Figure 4-1 – Reference plates (a) segmentation and (b) orientation of the line lasers used

To analyze the data, an n-way analysis of variance (ANOVA) was performed on all measurements made under each of the given experimental conditions. The goal of the ANOVA is to determine if speed and exposure time have an effect on the final measurements. For this study, Mean Profile Depth (MPD) was used as the macrotexture metric as this is the most prevalent descriptor of macrotexture in use today. Both raw and filtered datasets were calculated. Finally, field measurements are compared to laboratory measurements via a forest plot analysis

to determine if the differences between measurements are statistically the same for all experimental conditions.

Equipment Used

The equipment used for the experiment is summarized in Table 4-1. The LLL and LLT are the high-speed line lasers mounted in the configurations shown in Figure 4-1. The SSL is likewise a commercial off-the-shelf device that uses a single spot to gather a single-point stream of texture heights. The LAPS is a purpose-built reference measurement device that was used to measure the reference surfaces in the laboratory as described below.

Table 4-1 – High-speed equipment used to gather data

Device ID	Laser Orientation	Make	Sampling Frequency (kHz)	Raw Data Spatial Interval (mm)	Vertical Resolution (± mm)
SSL	Single Spot	Acuity (custom) AR550-200	100	0.25	0.020
LLL	Line Laser Longitudinal	LMI Gocator 2342	5	25 (transverse) 0.5 (longitudinal)	0.015 to 0.040
LLT	Line Laser Transverse	LMI Gocator 2342	5	0.5 (transverse) 25 (longitudinal)	0.015 to 0.040
LAPS	Reference Line Laser	Keyence LJ-V7200	0.5 (tested)	0.02 (transverse) 0.112 (longitudinal)	0.001

Reference measurements with the Laser Analyzer for Pavement Surfaces (LAPS)

To overcome the shortcomings of caliper measurements, the LAPS device was developed and used to measure all reference surfaces in the controlled conditions of the laboratory. LAPS has a commercially-available line laser and camera sensor and is mounted to an aluminum rail equipped with a stepper motor to automatically control movement along the rail for a measurement length of 1.2 meters. Plates were first scanned with the laser line parallel to the grooves in the plates; however, this proved challenging for the device on some plates as the abrupt changes from peak to slope and vice-versa caused specular reflections which resulted in outlier data that over-estimated plate depths estimated by the caliper measurements. Final reference measurements were made by sliding the laser line along the length of the plate with the

line perpendicular to the grooves. This method is more similar to the measurement style of the SSL and LLL.

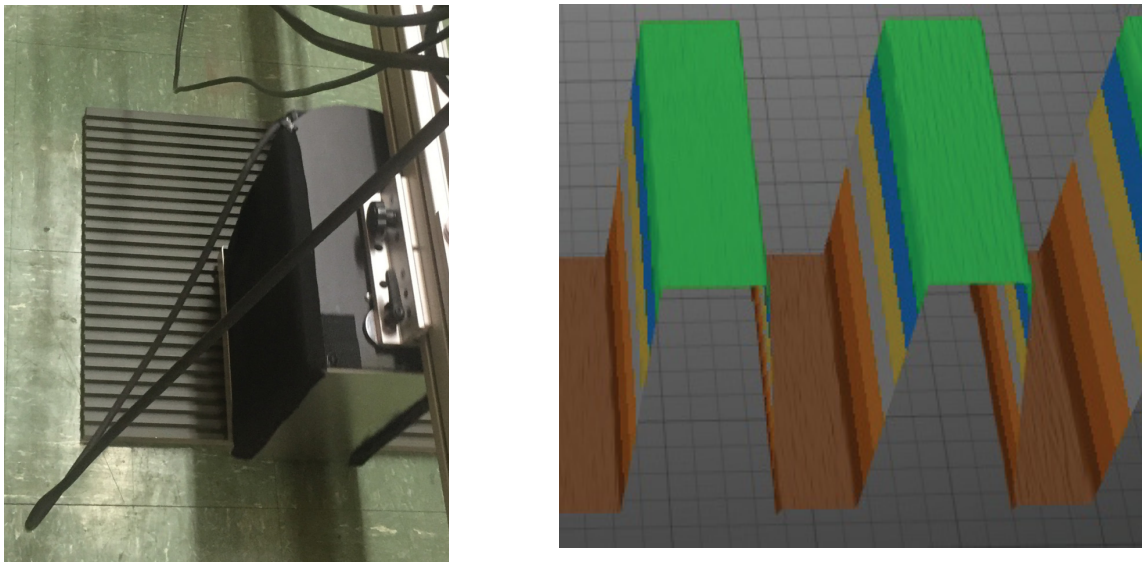

(a) (b)

Figure 4-2 - LAPS reference measurement device showing (a) lab setup and (b) resulting 3D surface profile

Engineered surfaces studied

The reference surfaces engineered to test macrotexture devices are described in Table 4-2 and shown in Figure 4-3 below. The smallest shape (plate 1) is a triangular "sawtooth" pattern. This is representative of fine mixes such as surface dressings and high-friction surface treatments. The mid-sized shape (plate 5) has a hexagonal half-shape and represents typical dense-graded asphalt mixes. The largest shape (plate 6) is similar to plate 5 but has deeper channels, more similar to larger aggregate or tined or grooved concrete.

Table 4-2 - Engineered reference surface characteristics

Attribute	Plate 1	Plate 5	Plate 6
Design MPD (mm)	1.25	3.75	5.15
Tech cal depth #1 (mm)	2.6	7.95	10.3
Tech cal depth #2 (mm)	2.0	7.5	10.5
Avg LAPS MPD (mm)	1.054	3.872	5.161
SD of Avg LAPS MPD (mm)	0.007	0.037	0.093

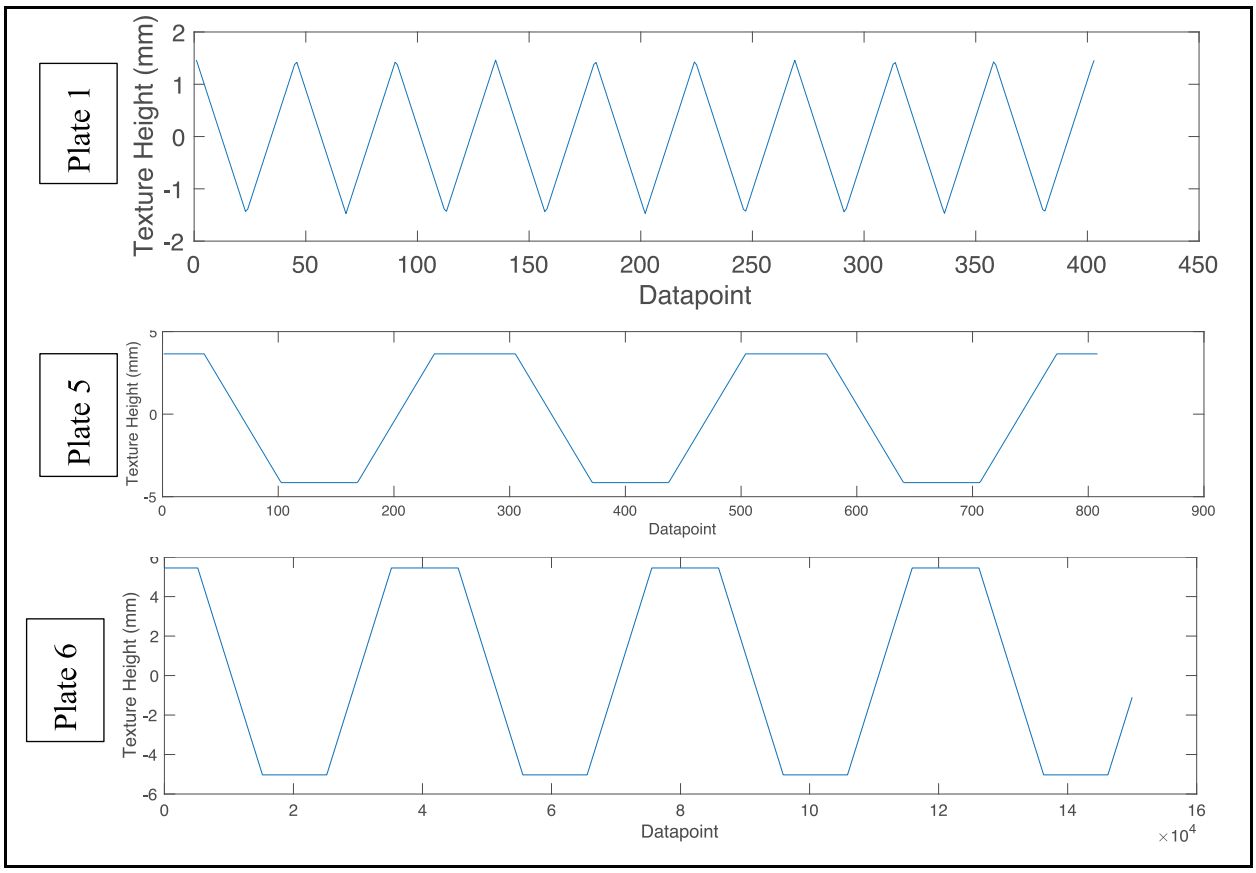

Figure 4-3 - Cross sections of reference surfaces

Segmentation of plates

Each plate is approximately 150mm wide and 600mm long. Plates are segmented as shown in Figure 4-1 into base lengths approximately 100mm in length. These base lengths are used to calculate MPD as specified in ASTM E1845 (2015). However, strict 100mm base lengths could not be used as starting and end points do not align with repeatable waveform locations. This resulted in incorrect mean line and regression determination which affects the MPD calculated. As seen in Figure 4-4, a 100mm base length resulted in an MPD of 5.18mm whereas a base length of 119mm (which included a multiple of whole waveforms) resulted in a MPD of 5.47mm. This difference in MPD could differentiate between investigatory and intervention levels on a road surface and are, therefore, unacceptable. For this experiment, base lengths as close to 100mm as possible were selected by taking points at the center of shape peaks to result in vertical and horizontal symmetry and stable, accurate MPD results.

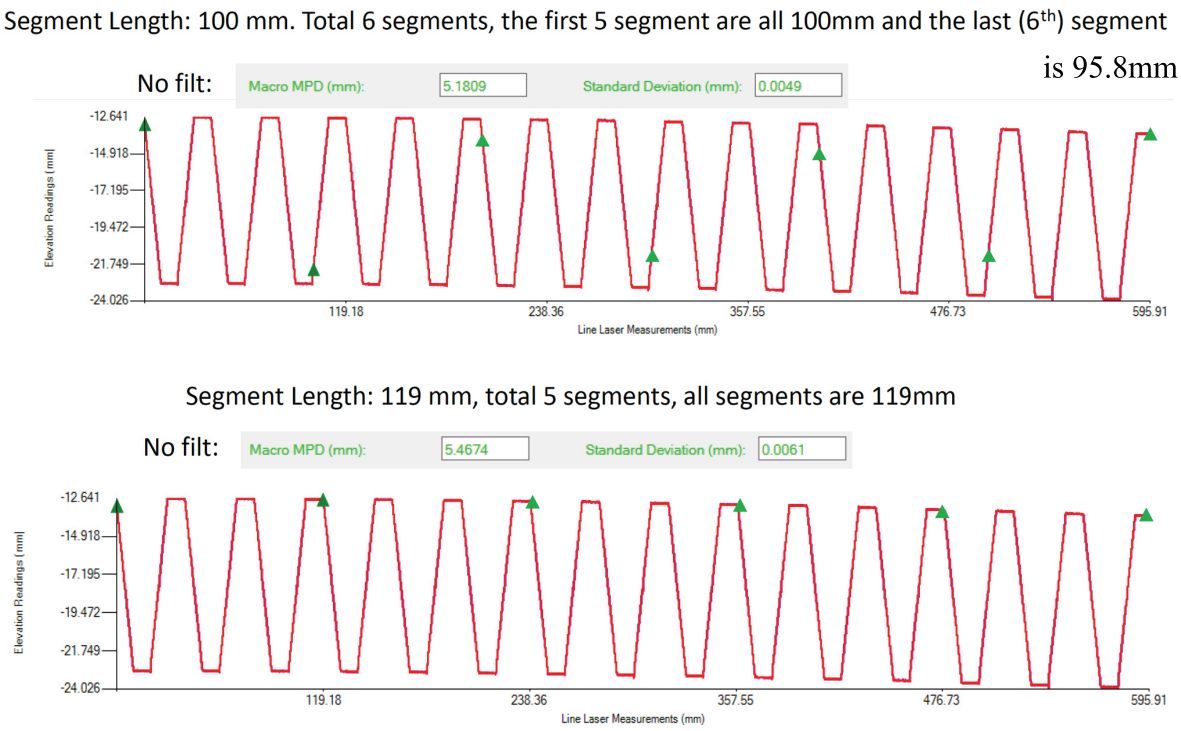

Figure 4-4 - examples of various segment lengths tried for the experiment

The center of each peak at the beginning of a given segment was found in the raw data profile and then a subsequent center of peak was found approximately 100mm from the first point. This was the base length used, repeated for all segments for all segments of each plate, for every test condition used for the LAPS and high-speed data collection effort. To test the effect of filtering on their result, the same start and stop points were used on profiles that were first filtered using a low-pass infinite impulse response filter conforming to ASTM E1845 (2015). The filter was applied to the entire profile (with several meters of lead-in and lead-out data included) for the SSL measurements. For all line laser measurements, profiles were first unfolded by mirroring at least 2.5mm (the cutoff wavelength of the filter used) on both sides of the profile and then filtered.

High-speed Data Collected

To meet the stated objectives, the vehicle speeds and sensor exposure settings listed in Table 4-3 were used. Speeds for all vehicles were the same and were held constant by using in-vehicle cruise control. Sensor exposure time describes the length of time photons are collected

by the triangulation sensor by the electronic shutter. Exposure can be adjusted in the device software to the lengths listed in Table 4-3. Note the line lasers have an "auto exposure" setting that adjusts the exposure time to best expose the height data collected per the manufacturer's algorithm. The SSL device does not have an auto exposure setting; instead, ranges of exposure times were selected. The normal operating condition for the particular SSL tested is 5 – 12 μs. The line laser uses a diffuse laser projection, therefore there are fewer photons available per unit area as the return light is collected. For this reason, the line laser exposure times are higher than the SSL, allowing more photons to reflect off the surface to read the height. As the exposure times for the two technologies (SSL and line lasers) differ, levels of "Short, Medium, and Long" were established. For each plate, six MPD measurements were taken of approximately 100mm base length, as described above and shown in Figure 4-1.

Table 4-3 - Experimental travel speeds and exposure settings

Attribute	SSL	LLL	LLT
Speed	25 mph (40 km/hr), 40 mph (64 km/hr), 55 mph (89km/hr)		
"Short" exposure	5 – 12 μs	40 μs	40 μs
"Medium" exposure	10 - 20 μs	80 μs	80 μs
"Long" exposure	30 - 40 μs	160 μs	160 μs
"Auto" exposure	n/a	varies	varies

Results and Discussion

MPDs were calculated using the test data from all devices collected on all plates for each speed and exposure time combination of the test matrix. Results are summarized as plate mean MPD values in Table 4-4 through Table 4-5. In general, MPD results tend to be negatively correlated to vehicle speed and exposure time. This, however, was not always the case and is explored further in the ANOVA and forest plot analysis.

Table 4-4 - Summary of MPD values measured by high-speed devices for plate 1

		Plate 1 mean MPD (mm) - raw			Plate 1 mean MPD (mm) - E1845 filt		
Exp	**Speed (mph)**	**SSL**	**LLL**	**LLT**	**SSL**	**LLL**	**LLT**
Auto	**Mean**	**-**	**1.12**	**1.18**	**-**	**0.93**	**0.96**
	25	-	1.16	1.17	-	0.94	0.98
	40	-	1.11	1.18	-	0.93	0.95
	55	-	1.10	1.19	-	0.93	0.96
Long	**Mean**	**0.88**	**0.72**	**1.34**	**0.74**	**0.60**	**1.03**
	25	0.92	0.99	1.32	0.79	0.84	1.03
	40	0.90	0.73	1.36	0.75	0.61	1.03
	55	0.81	0.45	1.33	0.69	0.34	1.04
Medium	**Mean**	**1.04**	**1.05**	**1.23**	**0.89**	**0.90**	**0.98**
	25	1.04	1.15	1.23	0.89	0.95	0.98
	40	1.05	1.05	1.24	0.89	0.90	0.98
	55	1.04	0.95	1.21	0.89	0.84	0.99
Short	**Mean**	**1.03**	**1.15**	**1.21**	**0.88**	**0.94**	**0.96**
	25	1.03	1.16	1.21	0.87	0.95	0.95
	40	1.05	1.15	1.18	0.89	0.94	0.95
	55	1.03	1.13	1.23	0.87	0.94	0.96

Table 4-4 shows the MPD results for each of the devices tested at each of the travel speed and exposure settings laid out on Table 4-3. Results are given for both raw (unfiltered) profiles and for profiles that were first filtered according to the parameters given in ASTM E1845 (2015). For the SSL profiles, filtering was completed on the entire measured profile (which includes several meters of lead-in and lead-out data before and after each plate). For the Line laser profiles, each 100mm (approx.) base length was first unfolded by 2.5mm (the wavelength of the lowpass filter used) by mirroring the start and end. This was done in order to avoid distortion of the beginning and end of the profile. Mirrored portions were removed after filtering was complete. It can be seen that, for the longest exposure time, MPD decreases with speed. This is observed to a lesser extent (or not at all) as exposure time is made shorter. Filtering lowers the MPD of all devices at all speeds and exposures by 16 (for short exposures) to 22 percent (for longer exposures). These trends can be seen in Figure 4-5 and Figure 4-6. Additional plots for all devices and plates tested are available in Appendix Q.

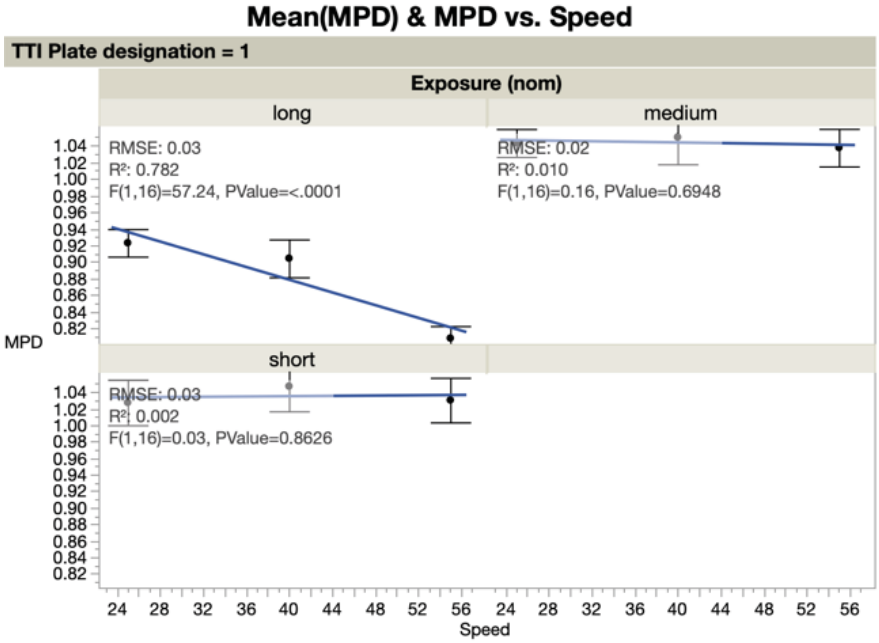

Figure 4-5 - Example MPD results - SSL

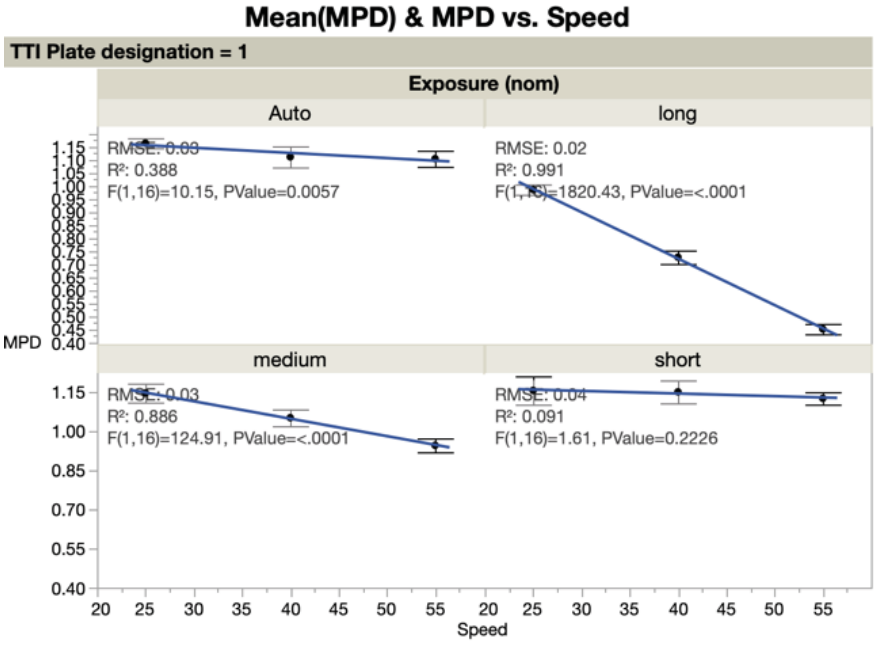

Figure 4-6 - Example MPD results - LLL

Table 4-5 - Summary of MPD values measured by high-speed devices for plates 5 and 6

		Plate 5 mean MPD (mm) - raw			Plate 5 mean MPD (mm) - E1845 filt			Plate 6 mean MPD (mm) - raw			Plate 6 mean MPD (mm) - E1845 filt		
Exp	**Speed (mph)**	**SSL**	**LLL**	**LLT**	**SSL**	**LLL**	**LLT**	**SSL**	**LLL**	**LLT**	**SSL**	**LLL**	**LLT**
Auto	**Mean**	**-**	**3.92**	**3.92**	**-**	**3.94**	**3.94**	**-**	**5.06**	**5.20**	**-**	**5.07**	**5.21**
	25	-	3.95	3.90	-	3.96	3.92	-	4.83	5.20	-	4.83	5.20
	40	-	3.91	3.96	-	3.93	3.98	-	5.17	5.12	-	5.18	5.14
	55	-	3.90	3.90	-	3.92	3.92	-	5.18	5.27	-	5.18	5.29
Long	**Mean**	**3.93**	**3.93**	**3.93**	**3.88**	**3.94**	**3.96**	**5.19**	**5.17**	**5.16**	**5.16**	**5.18**	**5.19**
	25	3.89	3.95	3.99	3.87	3.96	4.01	5.14	5.16	5.11	5.13	5.16	5.13
	40	3.92	3.93	3.91	3.87	3.94	3.94	5.22	5.16	5.12	5.18	5.16	5.15
	55	3.98	3.92	3.90	3.90	3.92	3.92	5.21	5.20	5.26	5.16	5.20	5.27
Medium	**Mean**	**3.88**	**3.92**	**3.93**	**3.89**	**3.93**	**3.95**	**5.18**	**5.20**	**5.20**	**5.18**	**5.20**	**5.22**
	25	3.88	3.93	3.90	3.89	3.95	3.92	5.17	5.23	5.13	5.18	5.24	5.15
	40	3.89	3.91	3.89	3.89	3.93	3.92	5.14	5.17	5.20	5.15	5.18	5.22
	55	3.87	3.91	4.00	3.88	3.93	4.02	5.22	5.19	5.25	5.21	5.19	5.27
Short	**Mean**	**3.88**	**3.96**	**3.89**	**3.89**	**3.97**	**3.90**	**5.20**	**5.23**	**5.17**	**5.20**	**5.24**	**5.18**
	25	3.87	3.97	3.90	3.89	3.98	3.92	5.16	5.22	5.11	5.17	5.21	5.12
	40	3.88	3.97	3.90	3.89	3.98	3.91	5.18	5.21	5.13	5.18	5.22	5.14
	55	3.90	3.94	3.86	3.89	3.95	3.88	5.26	5.28	5.28	5.26	5.28	5.30

Raw data profiles of the first 100mm of the high-speed measurements of the SSL are shown in Figure 4-7 through Figure 4-9. As evidenced in Figure 4-7, the plate with the small waveform (plate 1) shape proved difficult to profile. This difficulty was exacerbated by increased speed and exposure time. Inaccuracy of profile reproduction increased as vehicle speed and sensor exposure time increased. For the fastest test speed (55mph or 88.5 km/hr) and longest exposure time (30-40 μs), the profile is quite degraded. The signal is smoothed by an averaging effect of the long exposure time (both slope and peak data is captured in a single sample), resulting in lowered MPD value.

The profiles shown in Figure 4-8 and Figure 4-9 demonstrate more stable measurement of the plate profiles. However, small “lobes” can be seen in the raw data profile near the edges of the peak and valley plateaus. This ca be attributed to either light dispersion or hardware filtering at these sharp corners and represents a shortcoming of this measurement approach for sharp features. The effect of these edges is averaged into the surrounding profile by low-pass filtering shown in the respective figures.

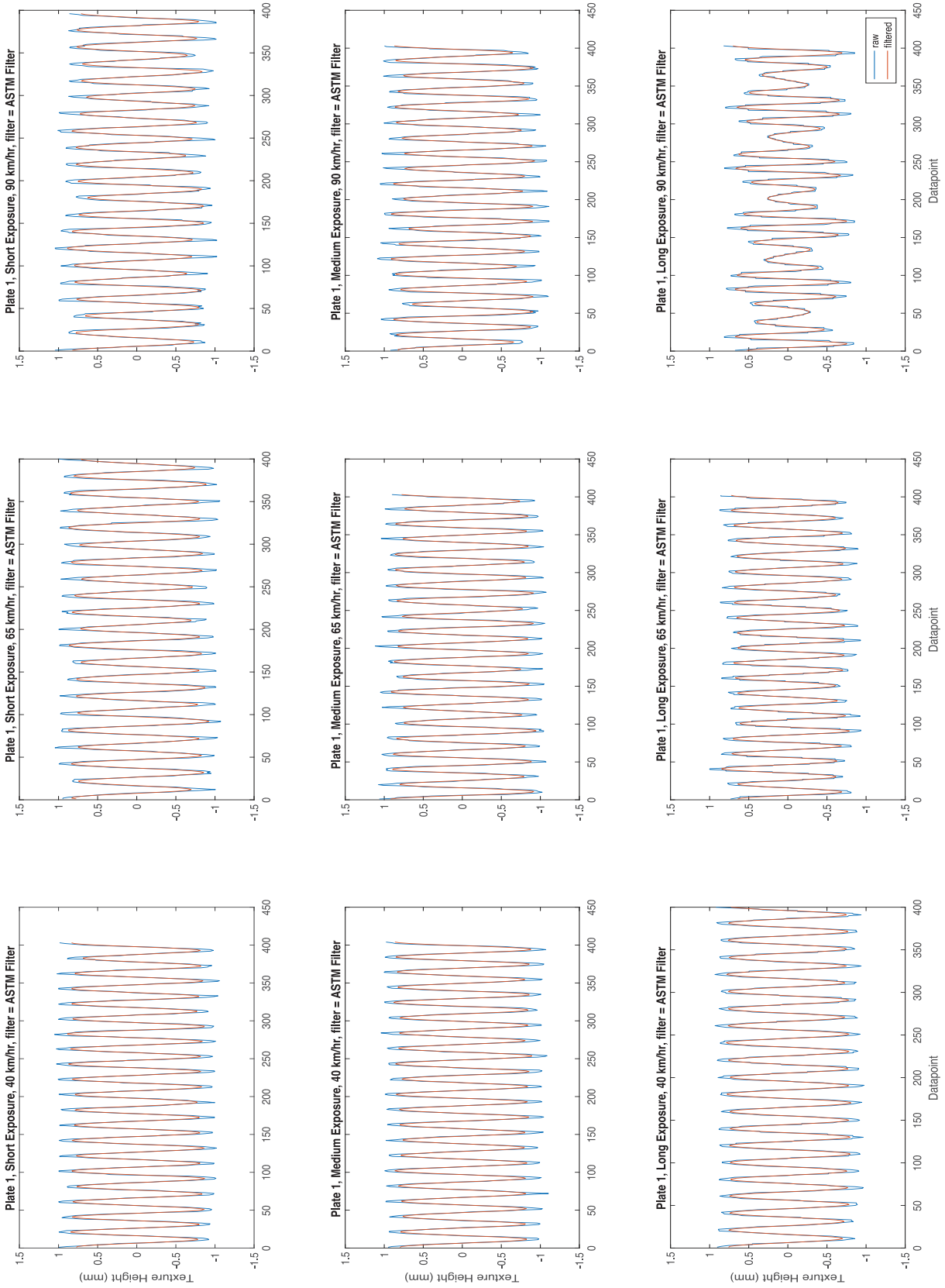

Figure 4-7 - SSL Plate 1 first 100mm all exposures and speeds

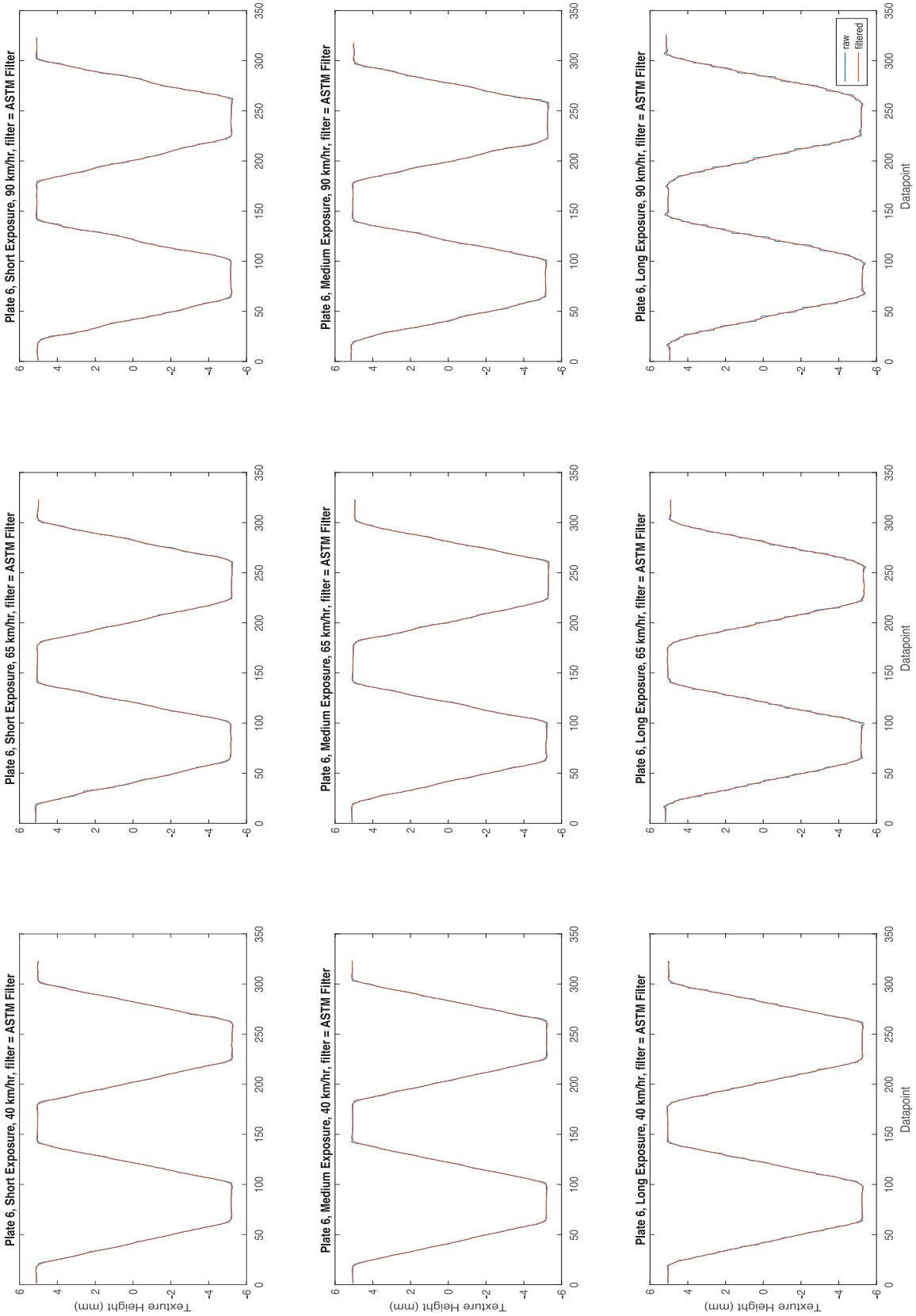

Figure 4-8 - SSL Plate 5 first 100mm all exposures and speeds

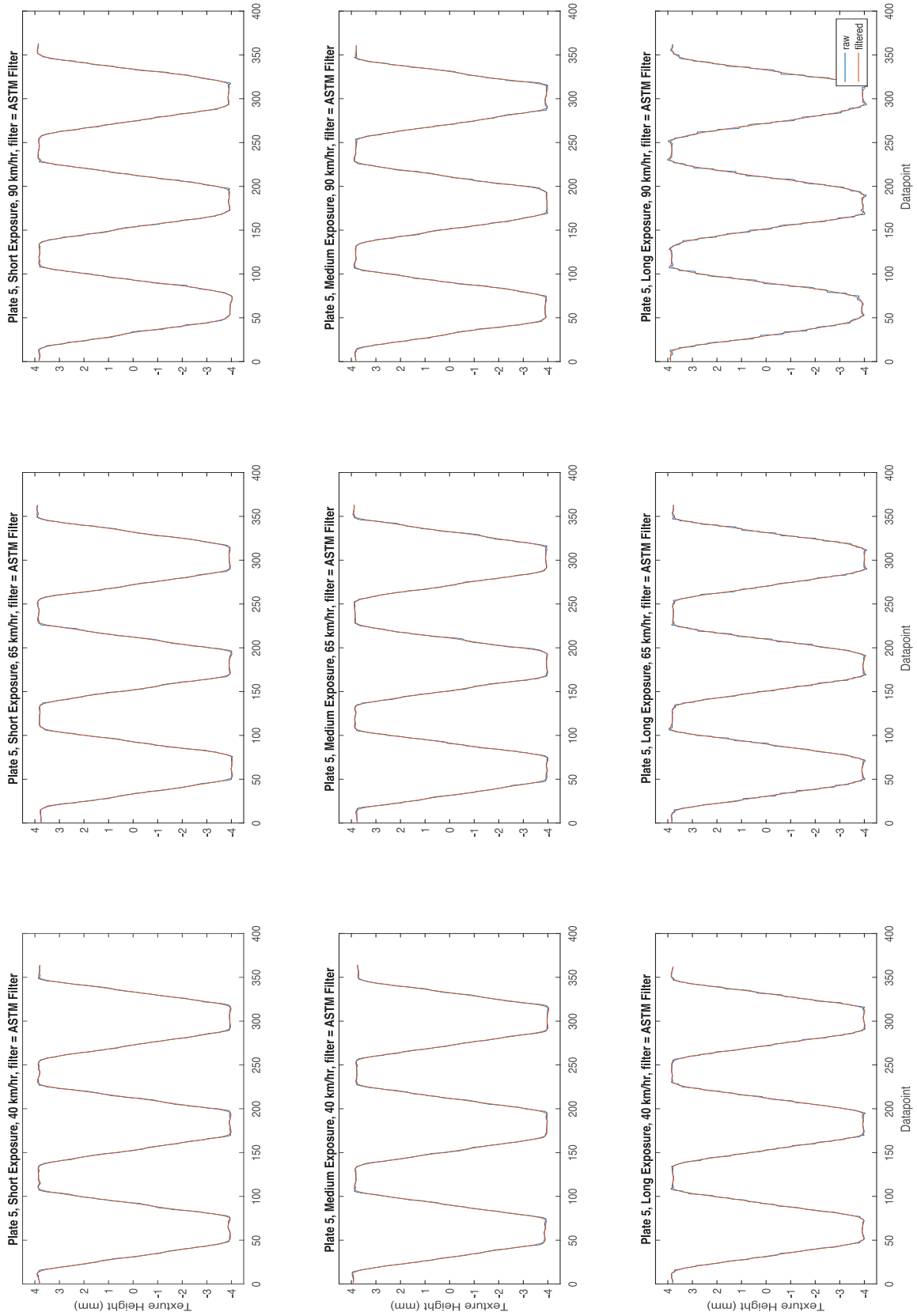

Figure 4-9 - SSL Plate 6 first 100mm all exposures and speed

Analysis of Variance

To make an initial analysis of the effect of vehicle speed and exposure settings on final MPD calculation, a n-way ANOVA was completed using MPD as the response variable and speed, exposure time and the interaction between speed and exposure time as model effects. A full factorial analysis was completed to include these effects. The resulting p-values (shown in Table 4-6) reveal that speed and exposure time are significant factors (effects tests are given in Appendix R) in obtaining MPDs from measured road profiles. Specifically, the null hypothesis that the mean MPDs measured are the same for each device and plate was rejected in eight of nine cases and seven of nine cases when using filtered data. However, there are shortcomings with this approach. Given nine tests were completed for each case and with a 95% confidence level, we can expect a difference in one of twenty cases. This means the average MPDs for plate 5 where the p-values are above the significance level of 0.05 may not be the same. The ANOVA also fails to show us what effects (speed and exposure time) cause mean MPDs to differ from each other for the same reference plate and the extents of these differences.

Table 4-6 - P-values from n-way ANOVA

	P-Value unfiltered			**P-Value - E1845 filt**		
	SSL	**LLL**	**LLT**	**SSL**	**LLL**	**LLT**
Plate 1	<.0001*	<.0001*	<.0001*	<.0001*	<.0001*	<.0001*
Exp	<.0001*	<.0001*	0.8558	<.0001*	<.0001*	0.2805
Speed	<.0001*	<.0001*	<.0001*	<.0001*	<.0001*	<.0001*
Speed*Exp	<.0001*	<.0001*	0.368	<.0001*	<.0001*	0.2627
Plate 5	<.0001*	0.7961	<.0001*	0.066	0.79	<.0001*
Exp	0.0001*	0.3163	0.5831	0.4216	0.2687	0.8399
Speed	<.0001*	0.2952	0.0002*	0.524	0.3132	<.0001*
Speed*Exp	0.0003*	0.9917	<.0001*	0.0195*	0.9943	<.0001*
Plate 6	0.0402*	0.0030*	<.0001*	0.0490*	0.0024*	<.0001*
Exp	0.0076*	0.0708	<.0001*	0.0503	0.0674	<.0001*
Speed	0.503	0.0099*	0.0671	0.0934	0.0104*	0.0819
Speed*Exp	0.2348	0.0299*	0.0025*	0.2259	0.0222*	0.0028*

** Indicates p-value is below the significance level of 0.05*

Detailed Analysis

To obtain more granularity on which plate and speed/exposure combinations cause unequal means, forest plots are used. Forest plots are graphical depictions of given center values and a range. In our case, we are interested in the difference between two devices, the reference (LAPS) device and the field device. Therefore, center values used for the forest plot are the difference in means between the two devices for a given plate, speed, exposure combination. Since the reference device was used in a laboratory setting without varying the speed or exposure time, one set of six mean segment depths (MSDs), one from each segment shown in Figure 4-1, are used to represent each plate for the LAPS. Six MSDs were likewise used for each high-speed device and speed/exposure combinations. These six measurements from the high-speed devices were averaged together via arithmetic mean to compare against the average MSD (the MPD) from the LAPS.

The range used on the forest plots in Figure 4-8 and Figure 4-9 are representative of the 95% confidence interval for the measurements made. To obtain this interval, standard errors for each of the plate and speed/exposure combinations were calculated for each device using a pooled estimate obtained from the 12 MSDs from both the reference measurement and the high-speed device. The 95% confidence interval was then calculated by adding (for the upper interval) or subtracting (for the lower interval) the product of the standard error and 1.96 (given the desired confidence level was 95%). This means we are 95% confident that the mean MPD difference at a given speed/exposure combination for a given plate will fall somewhere on the line plotted in Figure 4-8. In this way, we can visualize the variance of a given device.

As seen in Figure 4-8, ranges that contain zero are colored black. This can be interpreted as no difference between the reference and field measurements as we are 95% confident the field measurement will fall somewhere on this line. Since field measurements can be lower or higher than the zero-line drawn, it can be said that, statistically, the difference between the two devices is zero. The central green zone on each plot represents a difference in means of 0.1mm. Some agencies have established normal, investigation, and intervention levels of macrotexture and these levels are separated by 0.1mm MPD. As such, it is useful to see if the difference between reference and field measurements is within this threshold to assess its practical significance. Center values (difference in means) that fall within this green zone indicate the mean field measurements were within this tolerance of the mean reference measurements.

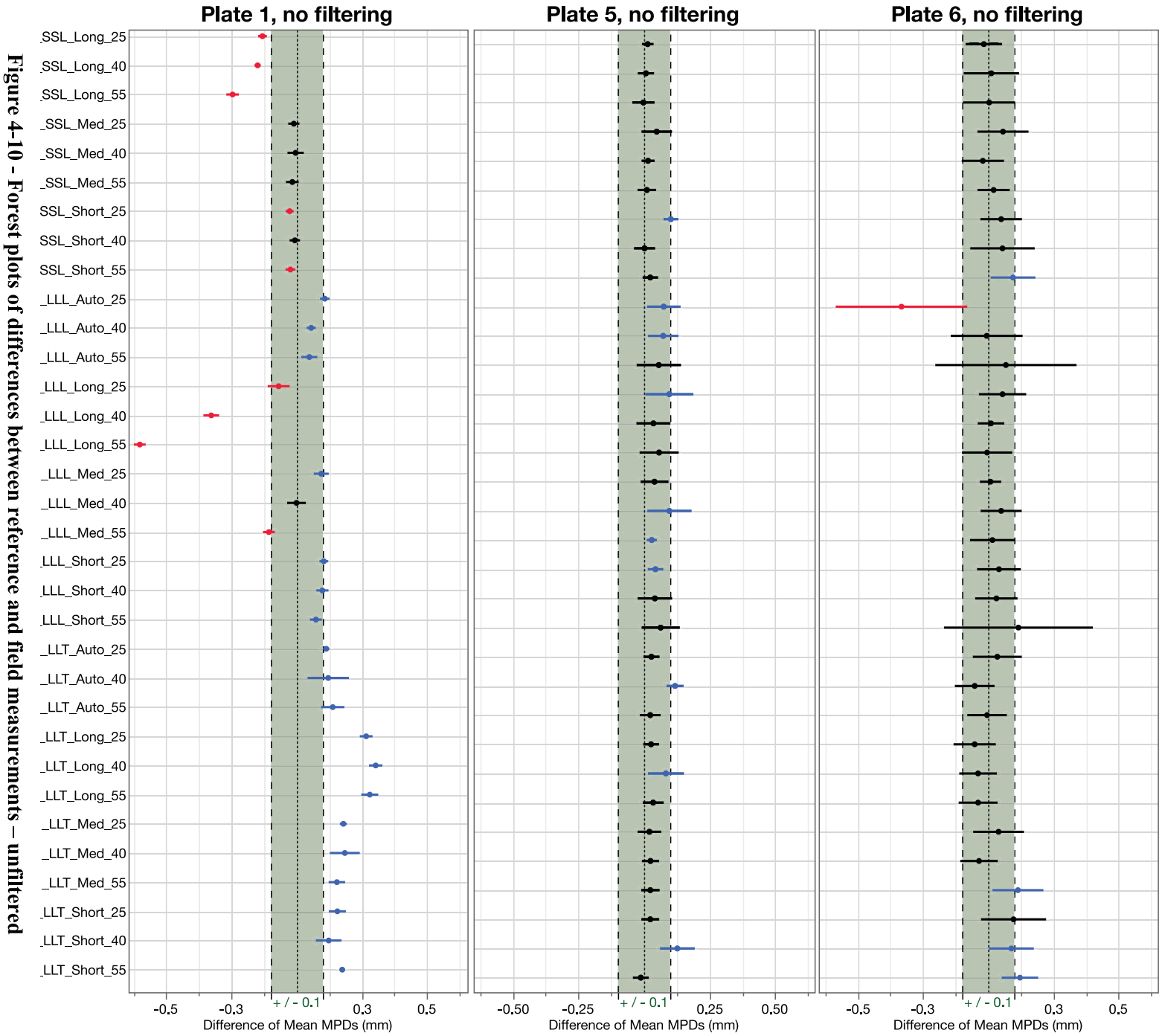

Figure 4-10 - Forest plots of differences between reference and field measurements – unfiltered

Plate 1

As seen above, the transverse line laser did not reliably reproduce the plate with the smallest waveform (plate 1). The single spot laser and the longitudinally-oriented line lasers were both effective at reproducing the waveform at short, medium and auto (for the LLL) exposure settings at the fastest speeds tested (with the exception of LLL, medium exposure time). Many of the SSL measurements for plate 1 contained zero within their confidence interval, meaning the difference between the reference measurements and the highspeed device were effectively zero. The LLT, on the other hand, did not reproduce the waveform of plate 1 at any speed or exposure setting. It should be noted that line lasers inherently have a longer exposure time than single-spot lasers. In fact, the line laser's shortest exposure is similar to the single spot's longest exposure. This causes an averaging of peaks and slope readings which results in a lower MPD reading. This is also seen generally as speed increases (the same exposure time covers more distance on the ground), resulting in lower MPDs. However, the opposite can be true if laser light is reflected off the narrow valleys of plate 1 and bounce between the subsequent peaks, causing an erroneous reflection back to the sensor. This is why high-speed measurements may be higher than the laboratory reference measurements. For the SSL and LLL, speed had little effect on the result, with the exception of longest exposure times.

Plate 5

This plate has deeper groove depths than plate 1 and valleys that match the designed peak, the LLT high speed measurements were higher than the LAPS. The worst cases were observed on the long exposure settings. In fact, speed was observed to have little effect on the difference of means between the reference measurements and the LLT. The LLT, however, had the greatest observed variances (as shown by the confidence interval bands in Figure 4-8) of the devices tested. Most of the measurements made by all devices on plate 5 contained zero within the 95% pooled confidence interval, indicating the lab reference measurements were the same statistically as the field measurements. Likewise, difference of means between the lab and most field measurements were observed to be within our tolerance of 0.1mm as indicated by the central dots within the green boundary area. A large majority of high-speed field measurements were higher than lab reference measurements, indicating erroneous reflections back to the laser.

The LLT was the only device to have two difference of mean measurements outside of the 0.1mm tolerance limit established.

Plate 6

This plate contained readings with the greatest variation as demonstrated by the large confidence interval bands in Figure 4-8. Note the scales on all plots in Figure 4-8 are identical to allow for the most straight-forward comparisons. Note that plate 6 has the deepest groove depth. The greatest variations were seen using the auto exposure setting. This setting dynamically changes the exposure setting to anywhere within the exposure bands tested in this work to obtain an "optimal exposure" according to the device's algorithm. However, larger variations may be seen due to the sudden change in surface color and reflectivity, initiating a change in exposure, causing readings in a spread of values that is larger than those of the fixed-exposure setting. A majority of device 95% confidence intervals contained zero, meaning the difference between the reference and field measurements were statistically zero. All devices tested were able to accurately reproduce the waveform at the various speed/exposures combinations. This is true for most of the LLT readings; however, several of the difference of means fall very nearly outside of the 0.1mm tolerance and confidence intervals are very close to not containing zero. This means that the LLT had the greatest difficulty of the devices tested in accurately reproducing the waveform. In cases where the LLT was close to the thresholds defined, the high-speed measurements were higher than the lab reference measurements. This is thought to be due to the lobes created on the signal (see Figure 4-6 and Figure 4-7) at higher speeds and exposure settings.

Effect of Filtering

Figure 4-9 shows the effect of ASTM E1845-compliant low-pass filtering on the MPD results. The effect of this filtering is visualized in Figure 4-5 through Figure 4-7. In general, waveforms are smoother and appear to better represent the total peak height of the reference plate. For plate 1, however, the raw waveform is reduced significantly as the half-period of the wave (2.5mm) is the same wavelength as the cutoff frequency of the filter designed for the purpose of smoothing the signal. This results in a waveform that appears to be over-damped. However, if the waveforms taken by the reference equipment are treated with the same filtering, the two signals can be quite comparable as demonstrated by Figure 4-9. Filtering, due to its averaging effect, tends to lower the variance of the results slightly, as seen in all plots of Figure

4-9 when compared to Figure 4-8. The difference in means is also shifted slightly to the left for all plates and devices. This means the field measurements are made lower than the LAPS measurements, since there is a sort of double-penalty applied to the field measurements, first with the synthetic filter, next with the filtering that occurs as the greater ground covered for a given exposure tends to smooth the signal out. Filtering does, however, have the distinct advantage of removing the lobes created on the raw profiles (see Figure 4-6 and Figure 4-7) from specular reflection at the peak corner points.

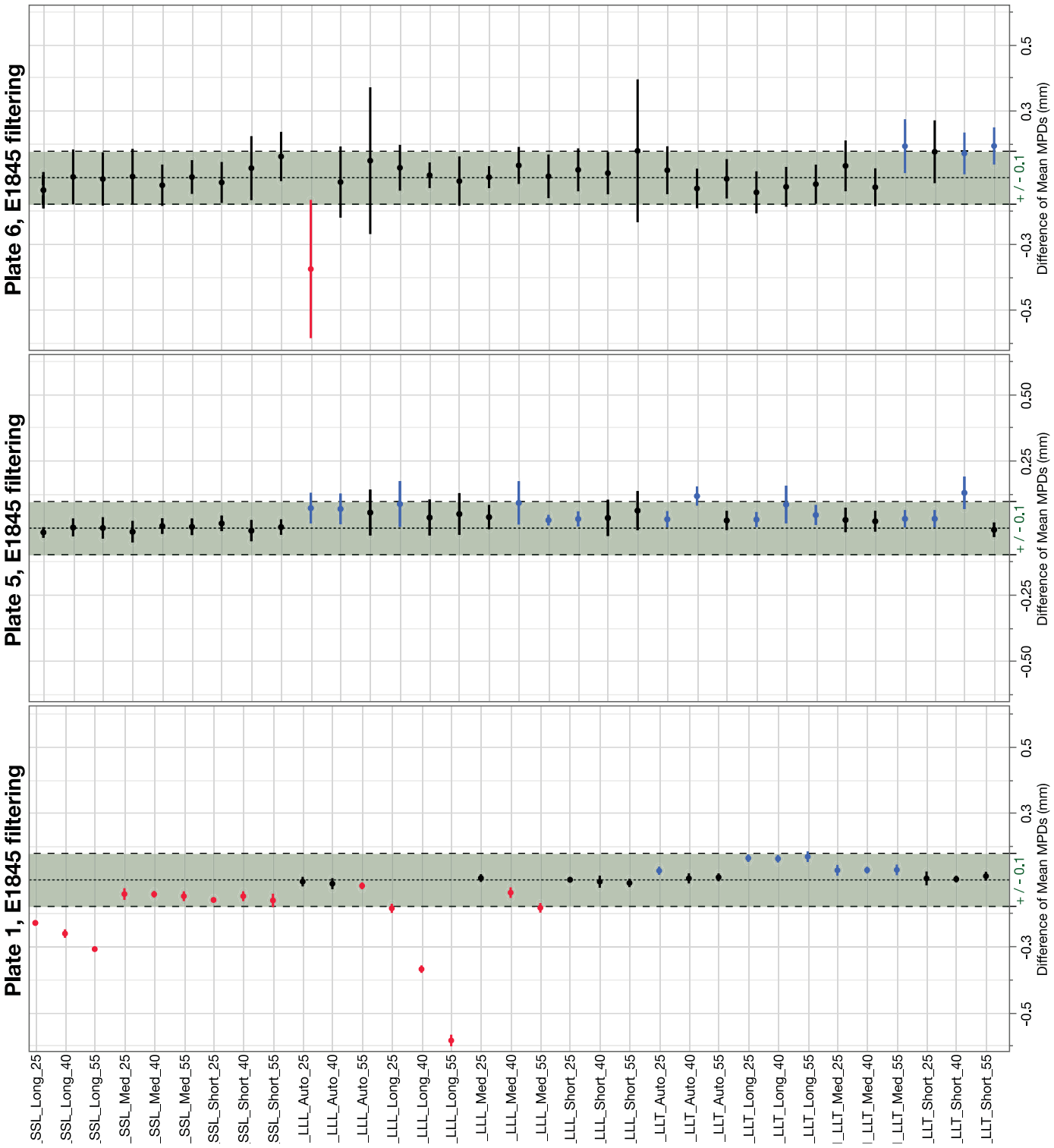

Figure 4-11 - Forest plots of mean differences: reference field measurements – E1845 filtering

Findings

The base lengths selected for MPD analysis in this work were meticulously selected from the raw signal data, resulting in waveforms that were symmetric about a vertical axis so regression lines and calculated mean profile lines were unaffected. Plate shapes in the future should be designed in such a way that the wavelength is a multiple of the selected base length (peak to peak) selected for evaluation. This would greatly aid in automating the MPD calculation. Plate base material should always be surface treated to reduce the specular reflections of the plate, especially at peak corner points. The plates in this experiment were coated in matte primer. This treatment worked well, powered coating could also be a viable alternative or potential improvement if the coating is more durable and results in improved proper reflection.

Tolerances should be established to compare lab (reference) measurements and high-speed field measurements to assess the practical significance of their differences in additions to their statistical significance. In this work, the tolerance selected was $\pm$ 0.1mm, the resolution used by some agencies to identify pavement as needing further investigation or even rehabilitation. As was shown in this work, an effective way of visualizing both adherence to this tolerance and the variation inherent to any given system is the use of forest plots to show the difference in means and the 95% confidence interval. This means a given device is within the tolerance selected if the difference in means is contained within the green bands of the forest plot. Bias can be shown and variability assessed by the 95% confidence intervals calculated using the pooled measurement data from the reference device and the field device. A confidence interval that contains zero (no difference in means) can be said to statistically measure the same as the reference device.

Slower speeds can lead to more accurate readings, but speed is dictated by traffic conditions on road networks. Exposure settings, on the other hand, can be controlled by the operator. In general, shorter exposure settings are desired. As exposure settings were lengthened, resulting MPDs were shown to decrease. This is a function of the averaging of peak data with slope data of the waveforms measured, resulting in lower MPDs. Filtering was found to lower the variance of measurements and bring difference of means (between reference and field measurements) closer to zero. Filtering was also observed to reduce the magnitude of the lobes caused by machine marks, hardware filtering, or sharp transitions between slopes and

peaks/valleys. If filtering is used on resulting data, lab reference measurements must also first be filtered to create more similar waveforms for comparison, especially in the case of the smallest waveforms.

Conclusions and Recommendations

Reference surfaces, such as those used in this experiment are effective at testing the accuracy of laser triangulation devices at high speed. This is because the reference surfaces can be manufactured to known dimensions for comparison to device-measured values. Waveform periods should be selected as multiples of the base length to be evaluated to ensure proper detrending can be performed for accurate results. Vehicle speed and sensor exposure time were found to be significant factors. A deeper analysis of individual sensor and speed/exposure pairings through visualizing data on forest plots showed that speed and exposure are more critical for smaller waveforms, especially at higher speeds and longer exposure times. Speed and exposure were not found to bring high-speed values out of the 0.1mm tolerance established for this experiment. For the Deepest plate (Plate 6), however, larger variations were observed. This is due to the deepness and steepness of the machined channels and possibly by the sharp corners. For these reasons, it is recommended that a shape similar to Plate 5 be used with a tolerance of ±0.1mm from a reference measurement. Filtering did not have any beneficial effect on the larger waveforms (Plates 5 and 6) and caused MPD values for Plate 1 to drop significantly, therefore, filtering is not recommended for measurement of the reference surfaces. Care should be taken, however, to ensure excessive outlier values are not contained in the profiles through careful control of the plate manufacturing process.

Future Research

The triangular pattern used for the smallest waveform (plate 1) presented difficulty in measuring with non-contacting laser displacement equipment. This is likely due to the interactions caused in the valleys of the shape. As there is still value in determining if a device can accurately measure such small shapes (the are within the range of macrotexture characteristics), the valleys should be widened to more closely resemble plates 5 and 6 while still keeping the peaks triangular in shape.

Acknowledgements

The author wishes to extend his heartfelt appreciation to the Texas Transportation institute for the use of their test track at the RELLIS Campus of Texas A & M University and for furnishing the LAPS data and plates used in this experiment

References

ASTM E1845 (2015). "Standard Practice for Calculating Pavement Macrotexture Mean Profile Depth." ASTM International.

Hall, J. W., Smith, K. L., Titus-Glover, L., Wambold, J. C., Yager, T. J., and Rado, Z. (2009). "Guide for Pavement Friction." 257p.

Huang, Y., Copenhaver, T., Hempel, P., and Mikhail, M. (2013). "Development of Texture Measurement System Based on Continuous Profiles from Three-Dimensional Scanning System." *Transportation Research Record: Journal of the Transportation Research Board*(2367), pp 13–22.

ISO 13473-1 (1997). "Characterization of pavement texture by use of surface profiles - Part 1: Determination of Mean Profile Depth." *Part 1: Determination of Mean Profile Depth*, International Organization for Standardization.

ISO 13473-1 (2019). "Characterization of pavement texture by use of surface profiles - Part 1: Determination of Mean Profile Depth."

Izeppi, E. d. L., Flintsch, G., and McGhee, K. (2012). "Limits of Agreement Method for Comparison of Pavement Friction Measurement." *Transportation Research Record: Journal of the Transportation Research Board*, 2306, 188-195.

PIARC (2016). "Road Dictionary." <http://www.piarc.org/en/Terminology-Dictionaries-Road-Transport-Roads/>. (16 December 2016).

Wix, R., and Leschinski, R. "How Coarse was my Texture?" *Proc., 24th ARRB Conference*, ARRB.

CHAPTER 5 - REMOVING OUTLIERS FROM 3-D MACROTEXTURE DATA BY CONTROLLING THE FALSE DISCOVERY RATE[2]

Abstract

Measurement of pavement macrotexture by non-contacting means is often contaminated by erroneous readings made by the instrument. These errors can be caused by extreme diffusion or refraction of the light source by aggregate or bitumen and are manifest in the data as outliers in both the positive and negative directions. In three dimensions, these errors can manifest themselves along the width and length of the measured profile as singularities or packets of continuous data. The problem is confounded by the constantly changing nature of pavement surfaces and large quantity of data gathered in 3-D applications. The identification and treatment of outliers proposed in this work is a new method that effectively treats outliers while continuously adapting to the surface measured. This is done by controlling the rate of false discoveries (measurements incorrectly identified as outliers) without affecting adjacent, correct, measurements.

Keywords: macrotexture, outliers, spikes, dropouts

---

[2] This manuscript was published by the American Society of Civil Engineers (ASCE) in the Journal of Transportation Engineering, Part B: Pavements. The final revised version is included in this work. This material may be downloaded for personal use only. Any other use requires prior permission of the American Society of Civil Engineers. This material may be found at https://ascelibrary.org/doi/abs/10.1061/JPEODX.0000119. Preliminary results were presented at the 8th Symposium on Pavement Surface Characteristics (SURF) 2018 in Brisbane, Australia. Coauthors on the work were Dr. Samer Katicha and Dr. Gerardo Flintsch.

Introduction

Pavement macrotexture is a critical indicator of several key pavement-vehicle interactions. These include wet and dry weather friction (Parry and Viner 2005; Loprencipe and Cantisani 2013; de Leon et al. 2016), rolling resistance (Haider et al. 2016), in-vehicle noise (Loprencipe and Cantisani 2013), tire-pavement interface noise (Rasmussen 2009)), tire wear (Lowne 1970; Gunaratne et al. 2000), and the quantity of water that will be splashed or sprayed (Flintsch and Viner 2016) when the pavement is wet or damp. Accurate measurements of macrotexture are needed to reliably quantify these interactions and allow planners to appropriately manage their pavement systems. Measurement errors will affect how the pavement surface is characterized which can have devastating effects, especially for safety-related vehicle pavement interactions. One source of error in measurement manifests itself in the form of outlier data. Identification and elimination of outlier data from pavement macrotexture data sets is, therefore, of extreme importance.

Background

The World Road Association (Permanent International Association of Road Congress [PIARC]) defines macrotexture as "surface irregularities of a road pavement with horizontal dimensions ranging between 0.5 mm and 50 mm and vertical dimensions between 0.2 and 10 mm" (PIARC 2016). A pavement's macrotexture can generally be thought of as the deviations from a horizontal plane that can be seen from a standing position with the naked eye. Examples include the large aggregate in asphalt cement (AC) pavements or brush, tine, grooving, or grinding marks on portland cement concrete (PCC). Surface profiles can be gathered in a myriad of different ways, however, one of the most common ways to gather macrotexture data is via contactless means such as laser distance triangulation. A profile can be gathered using a single laser point moving along the road's surface. In recent years, development of scanning and line lasers has resulted in 3-D profiles of road surfaces which typically contain several orders of magnitude more information than do single point profiles. These 3-D profiles, while extremely valuable, are not without their challenges in obtaining accurate surface profiles.

Challenges in measurement

Pavement represents a challenging surface to measure for several key reasons:

Large volume of data collected

Road networks are comprised of thousands of miles of pavement, often several lanes wide with traffic flowing in both directions. In the United States alone, there are an estimated 2.5 million centerline miles (ASCE 2017). Since the Macrotexture band of wavelengths is on the millimeter scale, vast amounts of data need to be collected to appropriately characterize the surface for even relatively small surface samples. As the quantity of data collected increases, so does the potential for erroneous measurements. Furthermore, identifying the erroneous data becomes much harder akin to finding the needles in a haystack. Erroneous data can be eliminated by setting a threshold beyond which measurements will be considered incorrect. However, eliminating out too much data tends to negate the benefit of increased data collection, especially since some proportion of the data may be accurate.

Constantly varying surface

Any traveled surface can change in a multitude of ways. Relatively isotropic surfaces such as finished PCC can change to anisotropic asphalt cement surfaces in all their varieties and then back again to PCC on the surfaces measured. Seemingly minor changes in slope and elevation, if not appropriately treated, can have great impacts on the parameters used to characterize the macrotexture of a surface. Furthermore, aggregates and cements can be sources of error for profiles measured by noncontact equipment.

Sources of error from equipment

Shiny surfaces can cause laser light to reflect in unpredictable ways. In pavements this occurs on newly laid asphalt, highly polished aggregates, and aggregates containing highly reflective minerals. Newly laid asphalt has the additional drawback of being a dark surface which absorbs larger amounts of measurement light creating errors in sensing the true position (Schleppi et al. 2016) of the measured surface. ASTM International defines “an outlying observation, or ‘outlier,’ is an extreme one in either direction that appears to deviate markedly from other members of the sample in which it occurs” (ASTM E178 2016). In measured profiles, these can be seen as outliers which extend far above or far below the surrounding profile. These outliers can occur both globally such as a spike that extends far above the entire measured profile and locally as outliers that deviate from the immediate surrounding profile but within the global profile. In 3-D measurements, this outlier data can be found along both the length and width of the measured profile.

Outlier Detections

Spikes in macrotexture laser measurements are unwanted anomalies. Detection of anomalies is a challenging problem affecting many application areas. Chandola et al. (2009) list 6 techniques used for anomaly detection. These are "classification based, clustering based, nearest neighbor based, statistical, information-theoretic, and spectral." All techniques to some extent rely on defining or finding a normal region that encompasses normal behavior. Statistical techniques rely on the assumption that a stochastic model can generate normal data and that anomalies have a low probability of occurrence under that model (Chandola et al. 2009). In the parametric approach, the stochastic model is assumed to be a parametric distribution. Because a parametric distribution can well approximate macrotexture measurements (Katicha et al. 2015), and the spikes in the data are extreme values, the parametric statistical approach is well suited to detect these spikes.

The most studied parametric distribution is the Gaussian distribution. In this case, the z-value has been used to define possible outliers (Chandola et al. 2009; Aggarwal 2015). A z-value of 3 (or -3) has been the traditional threshold to label an observation an outlier. This is because within the standard Gaussian distribution, 99.7% of the observations are between 3 and -3 standard deviations and observations outside of this range are highly unlikely. This approach is similar in concept to the box plot rule which labels deviations that are larger than 1.5x the IQR from the upper and lower quartiles as outliers. The drawback of using a fixed threshold is that for large datasets, a number of observations that are perfectly normal would be flagged as outliers. For example, with 10,000 measurements, a z-value threshold of 3 flags about 30 normal observations as outliers. Methods that adjust for the number of observations such as the Bonferroni correction and the Grubbs method (they are equivalent for large datasets from a normal distribution) adjust the threshold depending on the number of observations. However, they are known to have low power (Benjamini and Hochberg 1995; Storey and Tibshirani 2003). To increase power, Benjamini and Hochberg (1995) recommended controlling the false discovery rate (FDR). The FDR procedure adapts to the data both concerning the number of observations as well as the presence of outliers to produce a threshold with increased power without the drawbacks of a fixed threshold. Figure 5-1 illustrates the drawbacks of a fixed threshold and Bonferroni correction while showing how the FDR approach can adapt to the data and provide an adequate threshold whether outliers are present in the data or not. This clearly

shows that any method that suggests a fixed threshold or a threshold that only depends on the number of observations without taking into account the actual data suffers from instances where it fails in the detection of outliers. The FDR approach has the advantage of implicitly accounting for the presence and number of outliers.

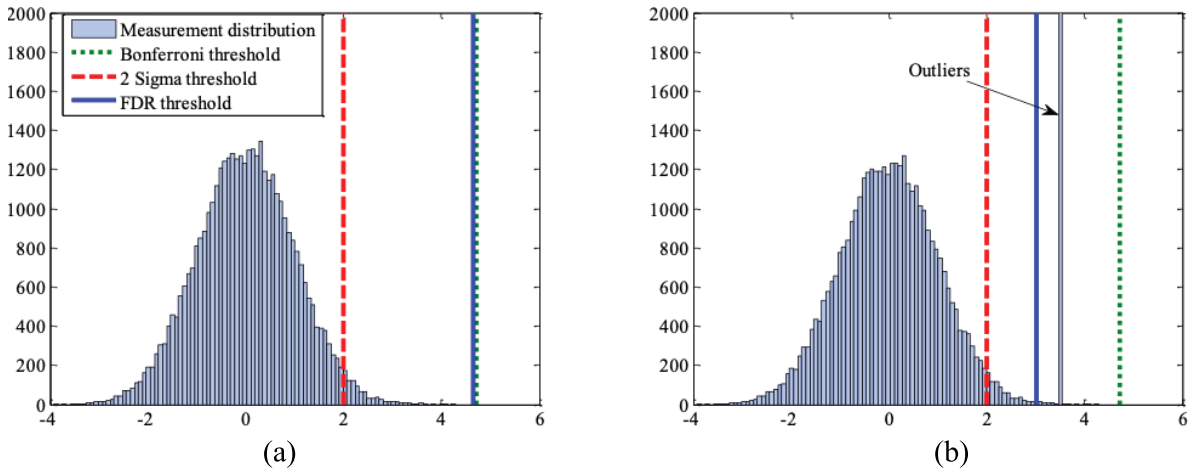

Figure 5-1 - Threshold selection based on 2 sigma, Bonferroni correction, and FDR for Gaussian distributions: (a) without outliers and (b) with outliers. The 2 sigma and Bonferroni thresholds are constant while the FDR threshold adapts to the measurements

The FDR approach is not restricted to the Gaussian distribution and can be applied to any probability distribution. Katicha et al. (2015) showed that texture measurements significantly deviate from a Gaussian distribution and found that a generalized Gaussian distribution (GGD) is appropriate to represent macrotexture measurements. Therefore, the use of the GGD with FDR control is an effective approach to deal with spikes in macrotexture measurements.

Problem Statement

3-D representations of pavement texture are often contaminated by outliers (large local and global deviations from the data set) which seriously affect the analysis of the data. To obtain accurate representations of the pavement texture, these outliers need to be removed. The method used to identify these outliers should be robust so that it correctly identifies outliers and adapts the identification threshold to different types of surfaces with a high probability.

Objective

The objective is to develop an approach that can detect and remove the outliers from 3-D pavement macrotexture measurements without reliance on a set threshold for outlier identification.

Methodology

The algorithm developed to meet the objective of this study is outlined in Figure 5-2 and explained in further detail in subsequent text.

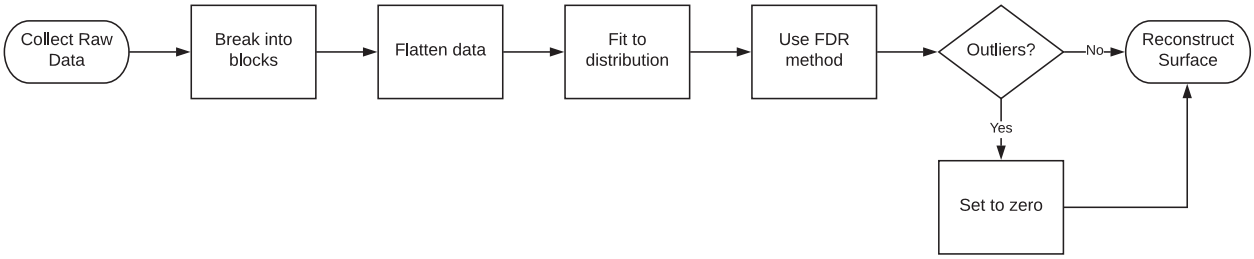

Figure 5-2 - Overview of outlier elimination algorithm

Break dataset into blocks of data

To address the large surface area of data that can be gathered in 3-D, profiles should be broken into smaller subsets as seen in Figure 5-3. Since we are dealing with three dimensions, the data is broken into blocks of a given length (m) and width (n). One challenge in three-dimensional data is that outliers can exist as singularities, or as many connected points along the length and/or width of the profile. This issue is addressed by analyzing blocks of measurements surrounding the point in question.

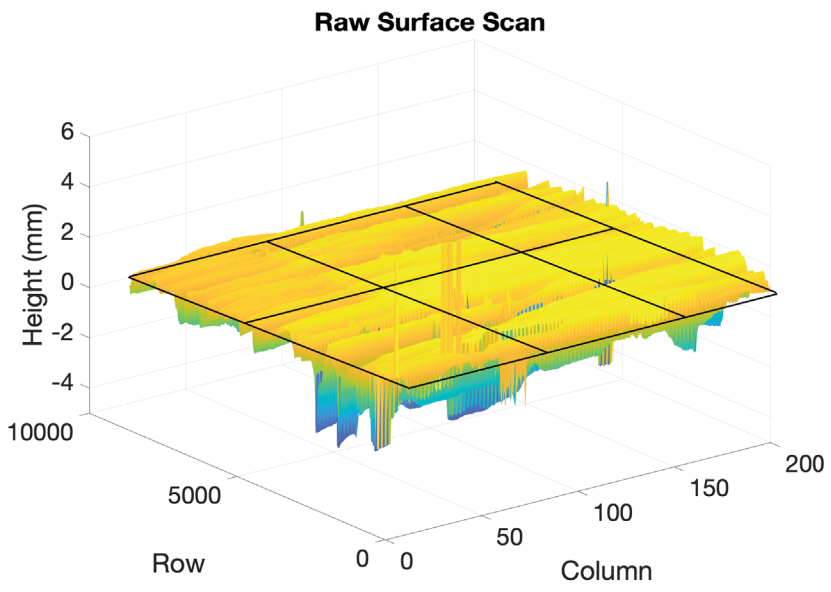

Figure 5-3 - Raw data is broken into sections

Low Pass Filtering

Measurements are processed with a low pass filter to remove wavelengths outside the range of macrotexture. The low pass filter used is based on a 2-D weighted moving average. The smoothed signal, "y", in equation 1 is obtained by taking a response matrix and convolving it against the signal of interest. This low pass filtering approach results in the measurements having a zero-mean distribution. Therefore, outliers and other large deviations are more easily identified as the measurements that significantly deviate from the distribution of the remaining measurements.

$$y[m,n] = \sum_{j=-\infty}^{\infty} \sum_{i=-\infty}^{\infty} x[i,j] \cdot h[m-i, n-j] \qquad \textit{(Equation 5-1)}$$

Fit data to distribution

To be able to identify the outliers, we first have to define the distribution of correct texture measurements. Having done so, the outliers are identified as measurements that have a very low probability of belonging to that distribution. Due to the variable nature of pavement, the distribution of texture depths is frequently not normally distributed and can vary for different pavements. Therefore, the family of GGDs is selected to fit our model. GGDs are a parameterized family of symmetric distributions that are particularly useful in our case as the thickness of the tails adjusts to better fit the different pavement surfaces based on the collected

data. Since the distribution of values of a block can be different for positive and negative values (i.e., peaks and valleys with respect to a mean of zero), separate models are fit to these data classes.

$$\frac{\beta}{2\alpha\Gamma\left(1/\beta\right)}\, e^{-\left(\frac{|x-\mu|}{\alpha}\right)^{\beta}} \qquad \textit{(Equation 5-2)}$$

Where:
α is a scale parameter (defines the spread of the distribution)
β is a shape parameter (thicker tails as β increases)
Γ represents the gamma function equal to $(n-1)!$
n is the number of points evaluated

False Discovery Rate

With the data fit to a GGD, a threshold can now be selected beyond which, values will be identified as outliers. Again, given the large quantity of data collected and the wide range of surface textures, pavement types, and local geometry of the pavement surface, this is not a straightforward task. A fixed threshold such as identifying data more than two or three standard deviations from the mean as outliers does not automatically adapt to the variable proportion of outliers and may always underestimate or overestimate the number of outliers. On the other hand, a method such as the Bonferroni correction which considers the number of samples in a dataset will always push the thresholds toward the extreme ends of the tails as the number of samples increase, which may underestimate the number of true outliers. A threshold selection method is needed which adapts to the data supplied even if the number of samples is large. For example, a small portion of the roadway, say a 10 cm^2 3-D profile sampled at 0.5mm longitudinally and laterally contains over 40,000 points! Benjamini and Hochberg (1995) demonstrated a method of meeting these two demands. The method seeks to control the expected proportion (rate) of falsely rejected discoveries (FDR). In the FDR approach, we first determine and sort all P-Values for all hypothesis (samples) in ascending order. Next, we identify the largest value of the point evaluated (i) for which:

$$P_i \leq \frac{i}{m}\, q^* \qquad \textit{(Equation 5-3)}$$

Where:
P_i is the P-value for the ith hypothesis (observation)
m is the total number of observations
q^* is the selected false discovery rate

All observations at or below this value are identified as discoveries. In our case, discoveries are values deemed to be outliers. Benjamini and Hochberg (1995) showed that the false discovery proportion (i.e., samples wrongfully identified as outliers) will never be in excess of the value of q* selected. For example, given a dataset of 1,000 samples, if 10 samples are identified as outliers, a maximum of one of these samples may not actually be an outlier value. Katicha et al. (2015) showed that controlling the FDR is an effective way to remove outliers from 2-D macrotexture data.

Address Outliers

Once values are identified as outliers, there are several approaches one can take to correct the dataset. For example, the data may be bridged by interpolating between valid (non-outlier) points. In our case, we temporarily set outlier values equal to zero since this is the mean value of the flattened dataset. The 2-D moving average of the surface is then added back to flattened dataset. This returns all valid measurements (non-outliers) to their original (raw) values and all points identified as outliers to the values of the surface created by the moving average filter. In this way, non-outlier data is unchanged and outlier data takes on the characteristics of the neighborhood of points surrounding them. Figure 5-4 shows an example of data processed with the FDR approach of outlier removal.

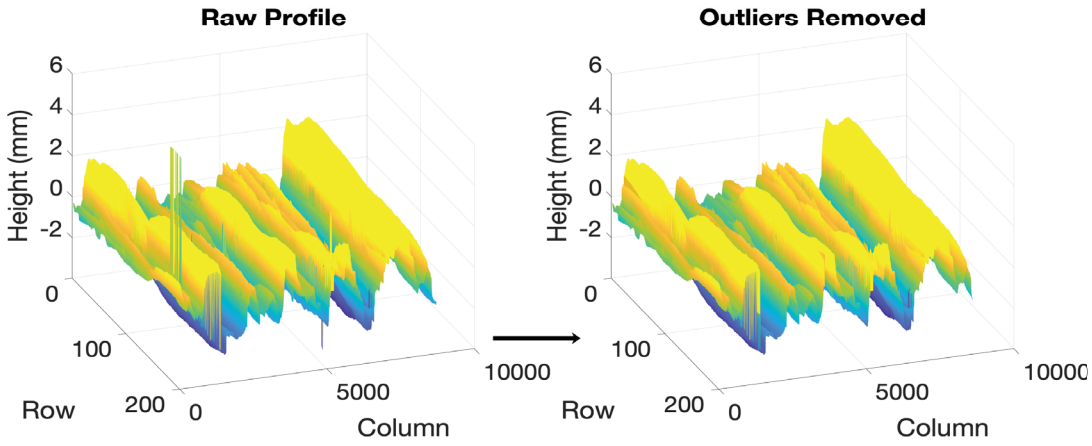

Figure 5-4 - Raw profile and profile after application of the algorithm

Equipment Used

Two devices were used to gather data to demonstrate the proposed method. The first was a device capable of gathering 3-D pavement profiles, the Ames Engineering Laser Texture Scanner (LTS) model 9300. The second device was the Nippo Sangyo Circular Track Meter (CT Meter). The CT Meter is a 2-D profile laser triangulation scanner. It was used to check the results of the 3-D scanner using the proposed algorithm. Measurement characteristics of the two devices are given in Table 5-1.

Table 5-1 - Device Characteristics

Characteristic	**LTS MPD**	**CT Meter**
Vertical Resolution	0.015 mm	0.03 mm
Laser spot size @ typical standoff distance	~0.050 mm	0.07 mm
Minimum spacing between measurements	Lateral: 0.024694mm Longitudinal: 0.0121648mm	0.87 mm
Profile Scanned	108 x 72 mm max (8848 x 2,916 samples)	142 mm circular (1,024 samples)

The surfaces scanned by the two devices were not precisely the same (which is characteristic of repeated sampling in an operational environment), due to the nature of the measurement schemes employed by the two devices. The 3-D LTS uses a single spot laser to scan one line (2-D profile) over its maximum longitudinal scan length. Scans are repeated at

desired lateral spacing along the device's scan width until the desired number of scans are achieved. This results in a (typically dense) point cloud of texture heights which can be analyzed as a 3-D surface. The CT Meter also uses a single spot laser to perform distance triangulation, however, the scan path is in eight continuous arcs about the devices center point. This results in a circular 2-D profile. In this way, repeated measurements for statistical analysis are possible in one placement of the CT Meter, and data can be analyzed for various phenomena such as directionality by using the separate measurement arcs. The CT Meter was placed in the immediate vicinity of the surfaces tested by the LTS.

Surfaces Studied

To test the outlier removal algorithm, several surfaces were measured at the Virginia Smart Road. This is a closed-track set of pavement surfaces in Southwest Virginia owned, operated, and managed by VTTI and Virginia DoT. It is a full-scale controlled test bed 3.5 km in length with differing surface types as shown in Figure 5-5. For this study, the surfaces shown in Table 5-2 were scanned with both devices.

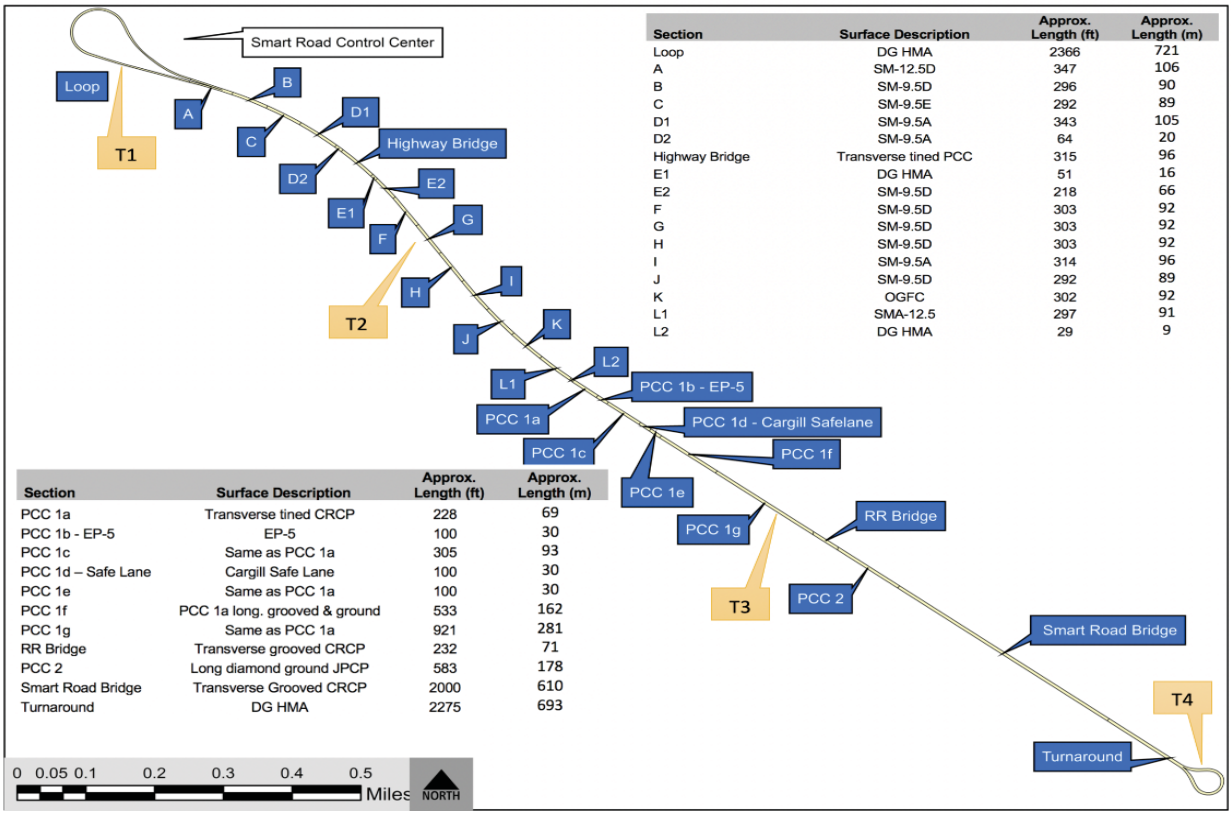

Section	Surface Description	Approx. Length (ft)	Approx. Length (m)
Loop	DG HMA	2366	721
A	SM-12.5D	347	106
B	SM-9.5D	296	90
C	SM-9.5E	292	89
D1	SM-9.5A	343	105
D2	SM-9.5A	64	20
Highway Bridge	Transverse tined PCC	315	96
E1	DG HMA	51	16
E2	SM-9.5D	218	66
F	SM-9.5D	303	92
G	SM-9.5D	303	92
H	SM-9.5D	303	92
I	SM-9.5A	314	96
J	SM-9.5D	292	89
K	OGFC	302	92
L1	SMA-12.5	297	91
L2	DG HMA	29	9

Section	Surface Description	Approx. Length (ft)	Approx. Length (m)
PCC 1a	Transverse tined CRCP	228	69
PCC 1b - EP-5	EP-5	100	30
PCC 1c	Same as PCC 1a	305	93
PCC 1d – Safe Lane	Cargill Safe Lane	100	30
PCC 1e	Same as PCC 1a	100	30
PCC 1f	PCC 1a long. grooved & ground	533	162
PCC 1g	Same as PCC 1a	921	281
RR Bridge	Transverse grooved CRCP	232	71
PCC 2	Long diamond ground JPCP	583	178
Smart Road Bridge	Transverse Grooved CRCP	2000	610
Turnaround	DG HMA	2275	693

Figure 5-5 - The Virginia Smart Road

Table 5-2 - Surfaces Studied

Section	Surface Type	Nominal Max Aggregate Size (mm)	Texture description
B	AC	12.5	Dense Graded Hot Mix Asphalt (HMA)
J	AC	9.5	Dense Graded HMA
L1	AC	12.5	Dense Graded HMA
PCC 1f	PCC	-	PCC – longitudinally ground and grooved CRCP
PCC 2	PCC	-	PCC – longitudinally ground JPCP

Results

The LTS was used to record 3-D profiles of the surfaces tested with longitudinal spacing of 0.01216 mm (approximately 8,700 rows) and lateral spacing of 0.02469 mm (200 columns) for a total of approximately 1.75 million samples per scan location. One 3-D profile was recorded for every surface tested. The CT Meter was used to collect data to cross-check the results of the outlier removal from the 3-D data. The CT Meter collects 1,024 samples along its circular scan path. The CT Meter was selected as it has wide acceptance by researchers and state departments of transportation to measure macrotexture. Due to the differences in scan areas (large circular track vs more concentrated rectangular area), several repeat scans of the CT Meter were made in the vicinity of the LTS measurements. Nine separate CT Meter scans were recorded in a grid pattern surrounding the surface scanned by the LTS. Each of the eight CT Meter sectors were treated separately, resulting in 72 profiles of approximately 100mm in length to compare against the 200 profiles of approximately 100 mm in length of the LTS. The 3-D data from the LTS was treated with the proposed outlier removal algorithm. 3-D surface plots of the surfaces scanned are shown in Figure 5-6 for both the raw datasets and for datasets for which outliers have been removed.

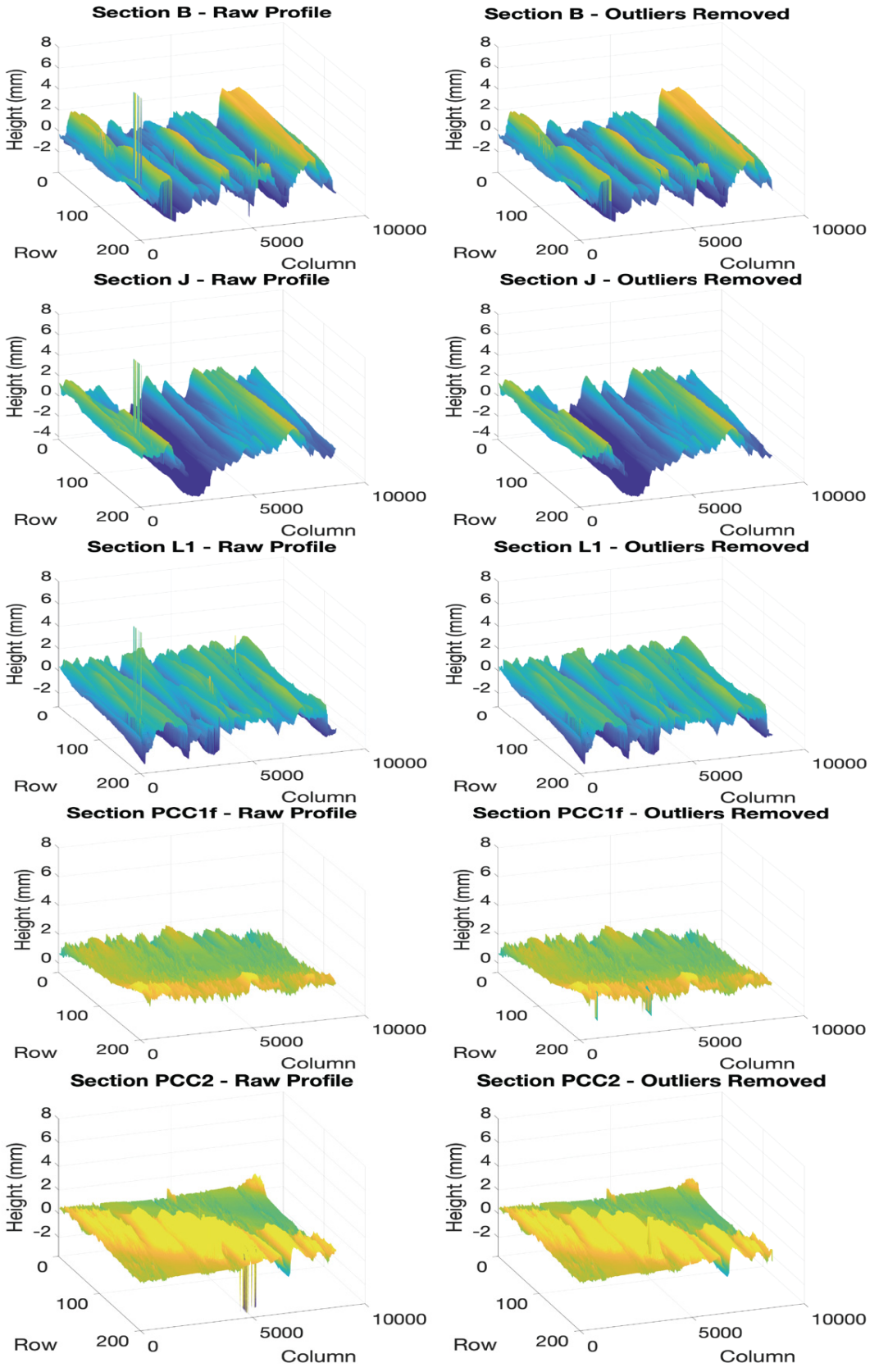

Figure 5-6 - 3-D surface plots of raw data and data with outliers removed

Mean Profile Depths (MPDs) were then calculated according to ASTM E1845 (2015). This was accomplished for each of the 200 columns of data contained in the 3-D scan for both the raw data and the data with outliers removed. In this way, the readings of the CT meter could be compared to results. One obvious deviation from the MPD calculation was for the raw LTS data as outliers were not removed beforehand as required by the standard. MPDs were calculated by the manufacturer software for each of the 72 profiles taken by the CT Meter for each test section. Results of the outlier removal algorithm proposed in this work are presented in Table 5-3, all MPD results are millimeters.

Table 5-3 - Results of outlier removal on surfaces tested

	LTS				CT Meter	
Section	Mean MPD (raw)	Standard Deviation	Mean MPD (no outliers)	Standard Deviation	Mean MPD	Standard Deviation
B	2.29	1.3	1.99	0.09	1.82	0.3
J	2.21	1.29	1.91	0.1	1.58	0.36
L1	1.38	1.08	1.13	0.13	1.12	0.23
PCC 1f	0.46	0.23	0.46	0.23	1.82	0.34
PCC 2	0.81	0.36	0.79	0.3	1.03	0.23

Discussion

In Table 5-3, we see that the mean MPD from sections B, J, and L1 all move toward the mean of MPD readings recorded by the CT Meter when outliers are removed from the raw 3-D data by use of this method. The algorithm works on both positive and negative outliers, however, in each of these sections the MPD is reduced. This is due largely to the fact that MPD is a measurement of peaks, therefore, any reduction in height (i.e. treatment of upward outlier values) results in a corresponding reduction in MPD. Similarly, when negative outliers are identified and removed, the mean value of the base length is correspondingly reduced (i.e., the mean is closer to the peaks), which also results in a reduction of MPD. For the PCC sections, the mean MPD values for the raw 3-D data and the 3-D data with outliers removed remain much more stable. This indicates there were not as many outliers to remove as there were in the asphalt sections, as can be seen subjectively in Figure 5-6. The greater incidence of outliers in the asphalt surfaces may occur due to the difficultly in measuring the surface via optical methods such as laser light.

The dark color of the binder can absorb more of the source light than will lighter surfaces and the shiny surface of the bitumen can cause more scattering of the light source (ISO 13473-1 1997).

The mean MPD values for the PCC sections as measured by the CT Meter are very different than the raw and despiked data taken by the LTS. This highlights the difficulty in quantifying these types of surface texture by methods such as MPD. Both sections have isotropic finishes of longitudinal grinding for PCC 2 and longitudinal grinding and grooving for section PCC 1f. Profiles collected by a single laser point run parallel to grinding and grooving will fall in and out of the valleys created by these texturing methods at a different rate than profiles collected perpendicular to these finishing marks.

Qualitatively, the results of the proposed method are shown in Figure 5-7. The blue lines show a single column of the original (raw) profile as gathered by the LTS. The profile treated by this approach is overlain over the raw data in red. This illustrates that the algorithm is effective in automatically removing outlier data from a local area of the profile as well as data that is globally more extreme than the entire profile. Because 2-D neighborhoods are considered for the 3-D profile as part of the procedure, the approach is also effective in determining if several continuous or non-continuous extreme data points are outliers in the same neighborhood. This is evidenced in the top plot of Figure 5-7 as several outlier points have been identified and eliminated. Figure 5-7 also demonstrates that the original (non-outlier) profile is preserved when outliers are not present by using the proposed approach.

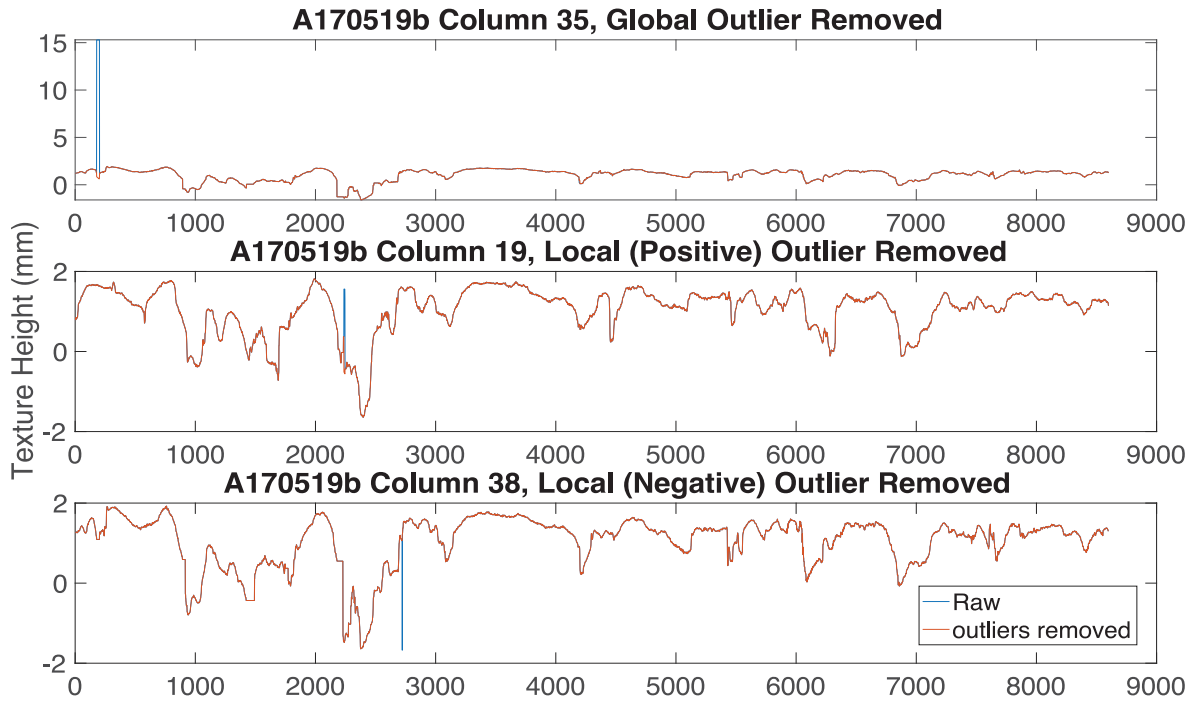

Figure 5-7 - Typical results of algorithm for a single column of LTS data showing global and local (positive and negative) removal of outlier data

Conclusions

3-D data is contaminated by outliers in both directions of data collection (transverse and longitudinal). We have seen that controlling the FDR is an innovative and effective way to remove outliers from 3-D macrotexture data. Outliers are identified by fitting data to specialized distributions and are removed when above a threshold that constantly adapts to the dataset analyzed. The method preserves the raw data profile while removing both global and local outliers from the large datasets created in 3-D surface profiling. The newly-proposed method removes outliers from 3-D scans of pavement surface where outlier data can seriously affect parameter calculation (i.e. MPD) of macrotexture data. These effects would lead to incorrect characterization of the pavement surface's ability to do critical things such as drain water away from the contact area of a tire, prevent splash and spray in rain events, or provide sound attenuation.

References

Aggarwal, C. C. "Outlier analysis." *Proc., Data mining*, Springer, 237-263.

ASCE (2017). "2017 Report Card for America's Infrastucture - Roads Report." <http://www.infrastructurereportcard.org>. (March 2017).

ASTM E178 (2016). "Standard Practice for Dealing With Outlying Observations."
ASTM E1845 (2015). "Standard Practice for Calculating Pavement Macrotexture Mean Profile Depth." ASTM International.
Benjamini, Y., and Hochberg, Y. (1995). "Controlling the false discovery rate: a practical and powerful approach to multiple testing." *Journal of the royal statistical society. Series B (Methodological)*, 289-300.
Chandola, V., Banerjee, A., and Kumar, V. (2009). "Anomaly Detection: A Survey, ACM Computing Surveys, Vol. 41 (3), Article 15."
Flintsch, G. W., and Viner, H. "Highway Splash and Spray Assessment Tool." *Proc., Transportation Research Board 95th Annual Meeting*, 17p.
Gunaratne, M., Bandara, N., Medzorian, J., Chawla, M., and Ulrich, P. (2000). "Correlation of tire wear and friction to texture of concrete pavements." *Journal of materials in civil engineering*, 12(1), 46-54.
Haider, M., Conter, M., Green, M., Schmidt, B., and Sandberg, U. (2016). "Status of the EU-project ROSANNE." *Transportation Research Procedia*, 14, 2946-2955.
ISO 13473-1 (1997). "Characterization of pavement texture by use of surface profiles - Part 1: Determination of Mean Profile Depth." *Part 1: Determination of Mean Profile Depth*, International Organization for Standardization.
Katicha, S. W., Mogrovejo, D. E., Flintsch, G. W., and Izeppi, E. D. d. L. (2015). "Adaptive Spike Removal Method for High-Speed Pavement Macrotexture Measurements by Controlling the False Discovery Rate." *Transportation Research Record: Journal of the Transportation Research Board*(2525), pp 100–110.
Loprencipe, G., and Cantisani, G. (2013). "Unified analysis of road pavement profiles for evaluation of surface characteristics." *Modern Applied Science*, 7(8), 1.
Lowne, R. W. (1970). "The effect of road surface texture on tyre wear." *Wear*, 15(1), 57-70.
PIARC (2016). "Road Dictionary." <http://www.piarc.org/en/Terminology-Dictionaries-Road-Transport-Roads/>. (16 December 2016).
Rasmussen, R. "Relating Texture to Tire-Pavement Noise." *Proc., 21st Annual Road Profile User's Group*.
Schleppi, B. L., Maikhail, M. Y., and Chang, G. K. (2016). "International Experience and Perspective of Pavement Texture Measurements and Evaluation." *Transportation Research Circular*, E-C216.
Storey, J. D., and Tibshirani, R. (2003). "Statistical significance for genomewide studies." *Proceedings of the National Academy of Sciences*, 100(16), 9440-9445.

CHAPTER 6 - CHANGE IN MACROTEXTURE DUE TO TRAFFIC AND BLEEDING IN AN ACCELERATED PAVEMENT TESTING MACHINE

Abstract

This study sought to model the behavior of a binder-rich stone matrix asphalt overlay of jointed plain concrete pavement when subjected to traffic loading using a heavy vehicle simulator to report the effect on pavement macrotexture. The change in macrotexture due to traffic loading was measured periodically with a circular track meter. Overall, as the cumulative load increased, the macrotexture decreased due to bleeding on the pavement's surface. A regression model was produced for the center of the wheel path which determined that, on average, the macrotexture's root mean square (RMS) decreased 0.14 mm per million equivalent single axle loads applied, with a coefficient of determination of $R^2 = 0.507$. The relatively low R^2 was a result of high variability within the collected data. A comparison of RMS and mean profile depth (MPD) outputs indicated that RMS was a more appropriate measure of macrotexture when bleeding was present. No clear model was determined for measurements outside the center of the wheel path. In one case, the buildup of material from bleeding caused measures of MPD to increase while RMS decreased when calculated from the same profiles. In another case, both RMS and MPD measurements showed macrotexture increasing with bleeding due to buildup of material on the surface. This study showed traffic-induced bleeding can have a tendency to both decrease macrotexture by filling in voids between aggregates and increase macrotexture by creating a ridges of binder material on the surface.

Keywords: Accelerated Pavement Testing, Macrotexture, Surface Properties

Background

A roadway's texture is the primary influencing factor over several critical tire-pavement interactions. Chief among these are the important safety concerns of friction (Wambold et al. 1995) and splash and spray (Weir et al. 1978). Several studies (Roe et al. 1998; Parry and Viner 2005) have shown a correlation between texture and vehicle crashes in wet weather. Secondary to safety concerns, in terms of pavement macrotexture, are user and environmental concerns, such as rolling resistance (Sandberg et al. 2011) and road noise (Descornet et al. 2000).

The World Road Association defines macrotexture as “surface irregularities of a road pavement with horizontal dimensions ranging between 0.5 mm and 50 mm and vertical dimensions between 0.2 and 10 mm” (PIARC 2016). Surface texture smaller than this is typically referred to as "microtexture," and larger texture as "megatexture" or, if larger still, as the "roughness" of a road. As water film thickness increases, the pavement’s macrotexture provides drainage paths for water beneath the tire to escape, reducing hydroplaning potential and allowing for greater tire-pavement adhesion (a function of the pavement’s microtexture). Macrotexture also provides friction through hysteresis (energy loss due to asymmetrical deformation of the tire). The hysteresis effect increases exponentially with increasing vehicle speed, accounting for 95% of available friction at speeds above 65 mph (Hall et al. 2009).

There are a variety of devices, both dynamic and static, that are used to measure macrotexture. Dynamic devices collect data while moving and vary in operation from manually pushed walking speed devices to vehicle-mounted highway speed devices. Static measurement methods require the data collection team to hand-place a device and manually perform the test on the surface of interest. Several data points are required on homogeneous pavement surfaces to find a surface’s representative characteristics. Operator judgment is needed to determine how many samples to collect, where to collect them, and what constitutes a “homogeneous pavement section.” These methods are generally regarded as “ground truth,” and can provide a high degree of measurement accuracy because they can record several samples at different orientations in one placement.

Two common measures of macrotexture are RMS and MPD. MPD is taken by averaging together the peak heights of two half-segments of a standard 100mm base length above the segment mean (typically zero after slope suppression), as illustrated below (Figure 6-1). Because MPD is peak-based, it is sensitive to outliers and spikes within the collected data. Various

filtering and outlier removal techniques address these concerns. Many macrotexture measurement devices and software have automated data processing routines that perform the required data filtering.

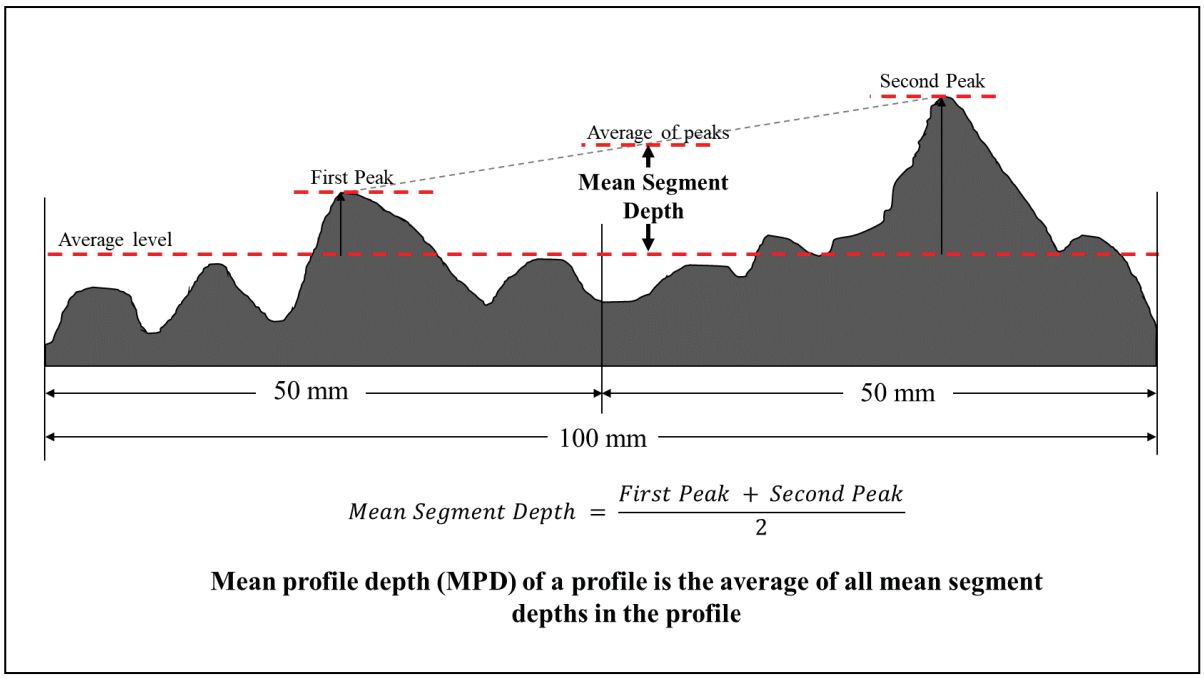

Figure 6-1 - Mean profile depth – adapted from ASTM E1845 2015 (ASTM E1859 2015)

RMS is akin to a standard deviation of the profile data for a segment and is in theory more robust against outliers than MPD because it is not based on single peaks within a given profile. It is calculated by the following equation from ISO 13473-2 (2002):

$$RMS = \sqrt{\frac{1}{l}\int_0^l Z^2(x)dx} \qquad \textit{(Equation 6-1)}$$

Where:
Z(x) are ordinate values of texture height measurements
l is the evaluation length

Previous research on macrotexture has shown that the change in macrotexture of a pavement's surface can vary depending on the surface type as well as the distresses observed. Macrotexture is a common measure of chip seal performance, and models for the decrease in chip seal

macrotexture with traffic are best fit with logarithmic functions (Aktaş et al. 2013). It has been shown that the sand patch-measured MTD of seal coats decrease with time and traffic, with this decrease attributed to wear of aggregates and embedment (Roque et al. 1991). Another study also showed a logarithmic relationship between the macrotexture of various pavement preservation techniques and the independent variable of time to model deterioration for use in pavement management systems (Riemer and Pittenger 2012). Lin and Wang showed that macrotexture decreased with load initially but reached a stable level at around 30,000 loading cycles of the Model Mobile Load Simulator (Lin and Tongjing 2018). Alternatively, it has been shown that traffic loading can lead to an increase in macrotexture due to raveling of aggregate (Powell and Buchanan 2012). For stone mastic asphalt, a study showed a logarithmic relationship between macrotexture and the number of gyrations in a gyratory compactor used to compact test samples. However, when simulated traffic was applied using a road test machine, the samples with lower initial macrotexture showed little change as a result of traffic, while samples with "greatest values of initial macrotexture showed an increase in texture in the later stages of simulated trafficking," which was attributed to raveling (Woodward et al. 2016).

Objective

This study sought to model the behavior of binder rich stone matrix asphalt (SMA) overlay of jointed plain concrete pavement (JPCP) when subjected to traffic loading using a heavy vehicle simulator to isolate the effect of traffic from other environmental effects and report the effect on pavement macrotexture. For this study, a decrease in pavement macrotexture was expected; however, as indicated, the distresses induced under loading can vary the effect on macrotexture. In binder-rich mixes, bleeding or flushing are commonly observed distresses. Therefore, the focus of this study was to model the effects of traffic-induced bleeding on macrotexture through analysis of variance (ANOVA) and linear regression.

Methodology

Pavement Structure

The structure of the pavement tested in this study is shown below (Figure 6-2). The surface was comprised of two binder-rich (6.7%, by mass, binder content) lifts of SMA, each of

75mm thickness and identical mix design with a nominal maximum aggregate size (NMAS) of 12.5 mm. A binder content report of the surface mix is given in Appendix T. A JPCP underlaid the SMA founded upon an intermediate layer of dense-graded asphalt with a NMAS of 19 mm that ranged from 25 to 38 mm in thickness to create a level bedding course for the JPCP. The base course was a Virginia Department of Transportation aggregate blend "21-B," which was specified to be a non-plastic select material comprised of crushed materials with a minimum California Bearing Ratio (CBR) of 30 (Virginia Department of Transportation 2014). The subbase is a select material with a minimum CBR of 7.5. The construction began with excavations to a depth 1.50 m across the entire test lane with two layers of geogrid material placed above the natural foundation and 150 mm of 21-B material placed above and below each geogrid.

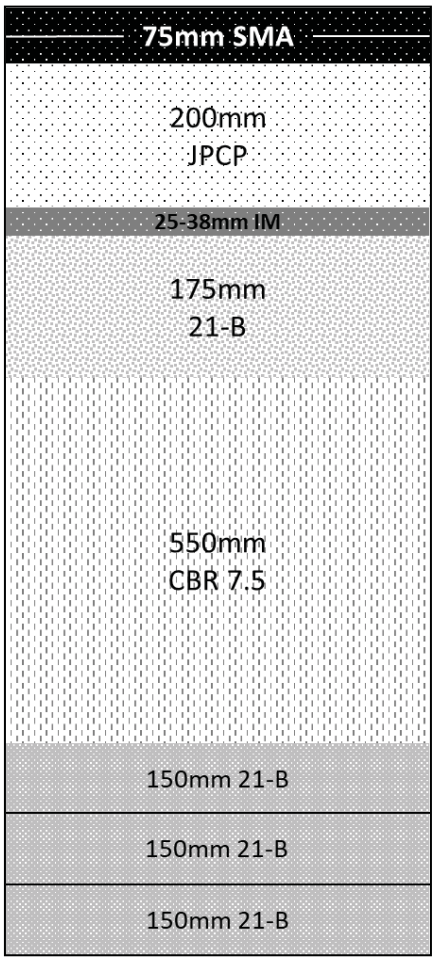

Figure 6-2 - Pavement cross-section.

Equipment

This study utilized accelerated pavement testing to simulate traffic loading on the pavement using the Dynatest Mk VI Heavy Vehicle Simulator (HVS). Additionally, the HVS environmental chamber was used to keep the pavement surface temperature at approximately 50°F and protect the pavement from weather effects.

This experiment expressed the traffic applied by the HVS in cumulative equivalent single axle load (ESAL). ESAL is a preferred parameter to measure traffic as it is the primary measure of traffic loading used in mechanistic-empirical pavement design methods. Theoretically, an ESAL is the summation of the equivalent axel load factor (EALF) for axle load groups multiplied by the number of passes of that axle load group for all axle load groups applied to pavement. The EALF is the ratio of pavement damage induced from a pass of the axle load group to the damage from a standard 18-kip single axle.

$$EALF = \frac{Damage\ from\ pass\ of\ axle\ in\ load\ group}{damage\ from\ a\ 18{-}kip\ single\ axle} \qquad \textit{(Equation 6-2)}$$

$$ESAL = \sum F_i N_i \qquad \textit{(Equation 6-3)}$$

Where:
F_i *is* the EALF
N_i is the number of passes for the i^{th} axle load group (Huang 2004)

The ESALs applied by each pass of the HVS dual wheel are estimated by (D. Jones 2006):

$$ESALs = Number\ of\ Passes \cdot \left(\frac{HVS\ Load\ Applied}{9\ Kips}\right)^{4.2} \qquad \textit{(Equation 6-4)}$$

The equipment used to measure the macrotexture was the Nippo Sangyo Co. Circular Track Meter (CT Meter), shown in Figure 6-3. The CT Meter is a stand-alone device that uses a single laser on a circular track with a radius of 142 mm to collect a two-dimensional profile. It collects 1,024 data points in eight arc segments (111.5 mm) with 128 points each (Nippo Sangyo Co. 2018). The macrotexture is reported in MPD and RMS.

Figure 6-3 - CT Meter

Experiment Setup

This experiment consisted of a single test lane trafficked using the HVS with the traffic loading applied at a normal distribution to simulate the effect of wander from the wheel path. The wander effect was applied by adjusting the transverse position of the HVS wheel apparatus after the prescribed number of passes. The distribution of passes in the HVS used the default wander from the Mechanistic-Empirical Pavement Design Guide and is depicted below (Figure 6-4).

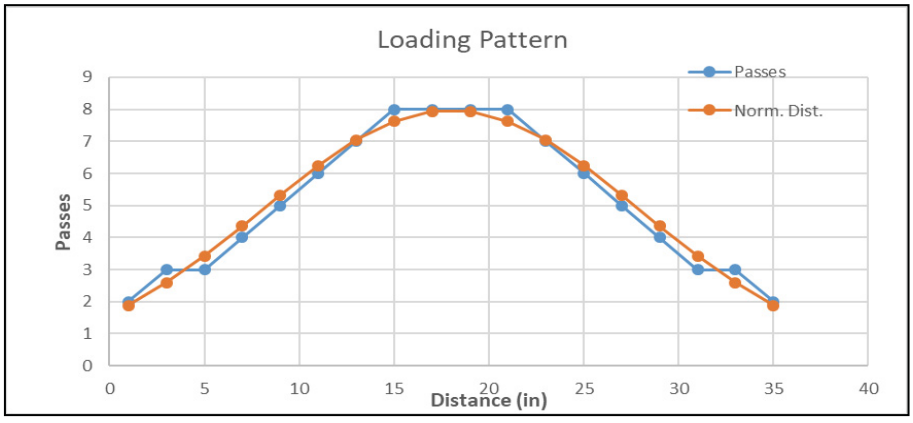

Figure 6-4 - HVS load distribution.

Initial macrotexture measurements were taken on the surface before traffic load was applied and were continued periodically, roughly once per week, as the cumulative traffic load increased on the pavement. Initially, daily measurements were taken; however, due to the low initial HVS load, there was little change over the initial 3 weeks of the experiment. These measurements have therefore been omitted from the analysis.

For each interval of loading at which macrotexture was measured a total of 20 measurements were taken on the traffic surface. The measurements were taken at five transverse positions along the width of the trafficked surface at each of four stations along the longitudinal length. One additional measurement was taken on a non-trafficked portion (Figure 6-5).

The red circles represent the path of the CT Meter laser. An alternate approach for determining the distribution of load of the tire group is the equivalent circle method shown in Appendix S. The centerline measurements identified by C in Figure 6-5 are of primary interest as they represent the center of the wheelpath, and therefore have the most impact to pavement-tire interactions. Additionally, network level macrotexture collection typically occurs in the wheelpath. The remainder of the measurements—L, LC, R, RC which correspond to left, left-center, right and right-center as relative positions transversely with respect to the direction of travel—were used to determine if an overall pavement macrotexture effect occurred as a result of traffic along the entire width of wander around the wheel path. Additonally, the measurements outside of the wheelpath enabled analysis of distresses observed in those areas of the pavement. Herein, measurement locations are referred to by the station (1 through 4) and position (R, RC, C, LC, L, EDGE)—i.e., the center of station 4 would be “4C”.

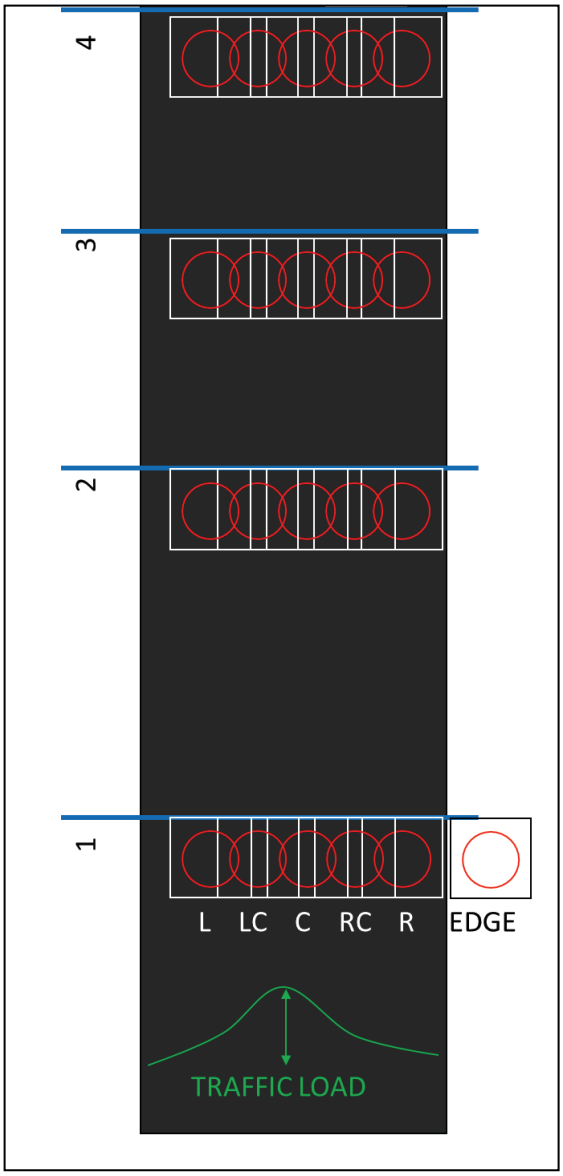

Figure 6-5 - Experiment measurement locations.

The methods of data analysis included statistical testing through ANOVA to determine if the application of traffic load effect on macrotexture was significant and the development of a regression model of observed behavior. JMP statistical software was used for all statistical analysis. Additionally, photographs taken at measurement locations over time as traffic load was applied were used to identify changes and distresses that developed in the pavement surface that indicated the causes of observed changes in macrotexture.

Results

Because the CT Meter produces both MPD and RMS macrotexture parameters, an initial analysis of the data to determine the most appropriate dependent variable response was conducted. The summary statistics of the data collected on the un-trafficked 1EDGE measurement show that MPD gave more consistent results with a smaller range and lower standard deviation (Table 6-1). However, comparing regression models for the data, RMS yielded a better coefficient of determination, R^2 (Figure 6-6 and Figure 6-7).

Table 6-1 - Comparison of MPD and RMS on Un-Trafficked Surface

Date	Avg MPD	Avg RMS
1/17/2018	0.81	0.96
1/24/2018	0.76	0.97
1/31/2018	0.79	0.96
2/8/2018	0.79	0.95
2/14/2018	0.87	1.38
2/21/2018	0.8	1.02
2/28/2018	0.8	1.02
3/7/2018	0.77	1.03
3/15/2018	0.78	1.01
3/21/2018	0.77	0.96
3/28/2018	0.82	1.15
4/3/2018	0.86	1.17
4/13/2018	0.85	0.97
4/18/2018	0.79	0.9
4/25/2018	0.8	1.03
5/10/2018	0.76	0.83
5/17/2018	0.75	0.89
Mean	0.80	1.01
Max	0.87	1.38
Min	0.75	0.83
Range	0.12	0.55
Std Dev	0.04	0.13

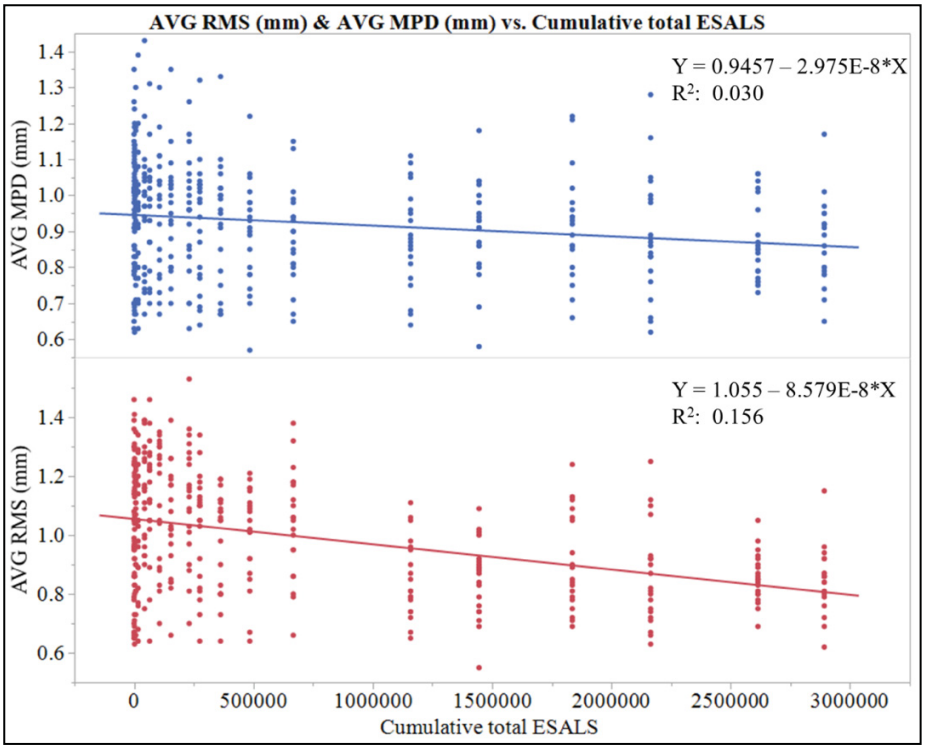

Figure 6-6 - Comparison of RMS and MPD for full data set.

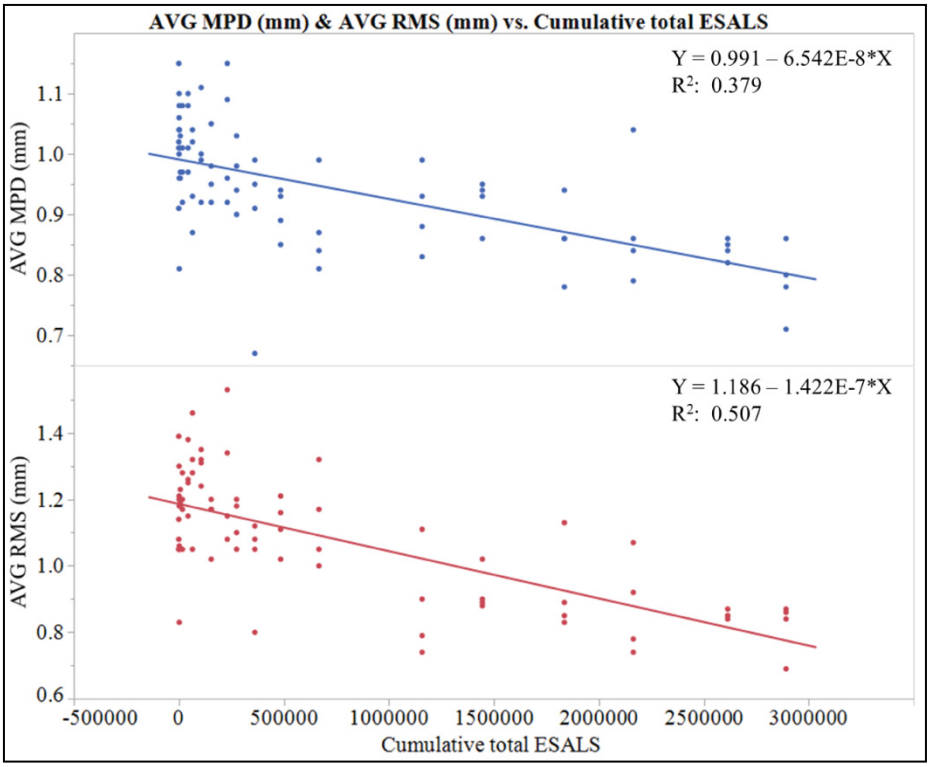

Figure 6-7 - Comparison of RMS and MPD for center of wheelpath only.

Because RMS yielded a better coefficient of determination for both the full data set and center of wheel path measurements, it was used as the primary macrotexture measurement for the remainder of the analysis.

Figure 6-6 also indicates a high degree of variability within the data collected, which was primarily due to the way in which the traffic load was applied. The measurement locations at the edges did not receive the same amount of simulated traffic as the center. It was therefore expected that the distresses would develop more quickly and have more severity closer to the center, and less so towards the edges. An analysis was conducted in which the fraction of the traffic load that was applied at the transverse positions was used as the independent variable instead of the total load; however, this analysis produced no significant improvement to the overall model and was therefore excluded from this study.

Given the high variability of the dataset and the difference in how the measurement positions received the traffic load, it is helpful to visualize the data for each measurement location separately (Figure 6-8). While generally all the measurement locations showed a decrease in macrotexture from traffic load, the slopes vary, and in one case (4R) show an increase in macrotexture, which is discussed further in the following section.

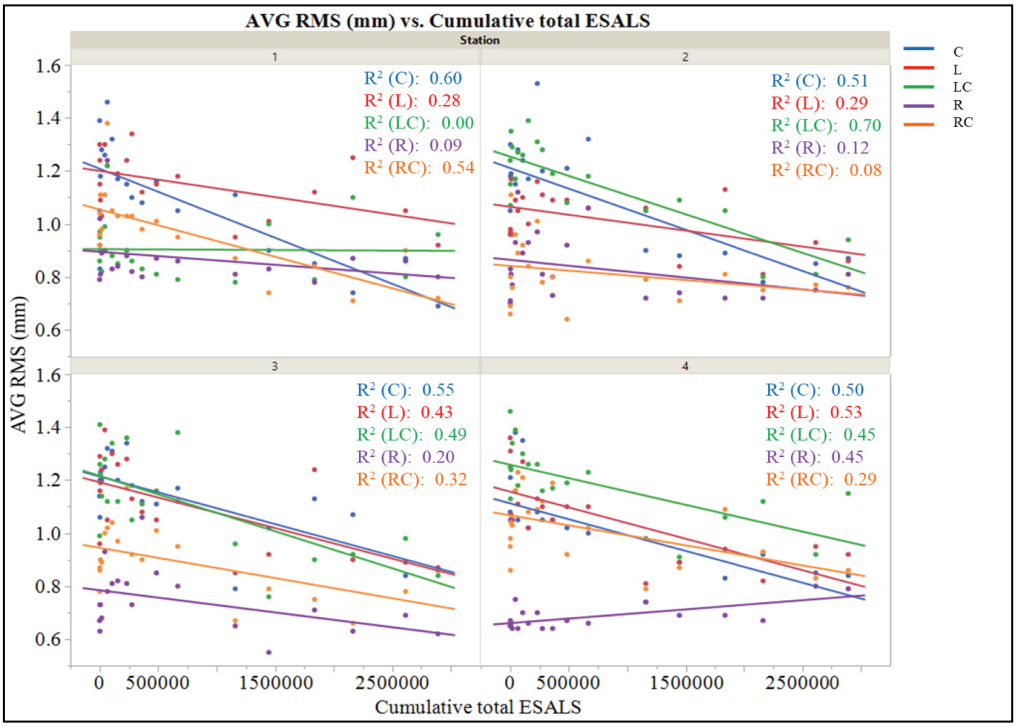

Figure 6-8 - Individual measurement location ESAL vs RMS.

Figure 6-9 shows the deterioration of the pavement over time in the center of the wheel path measurement locations. For each measurement location 1C through 4C, the picture on the left shows the pavement before traffic was applied and the picture on the right shows pavement after the final load of 2,891,714 ESALs. The middle picture shows pavement at an intermediate loading. The photographs demonstrate that as the cumulative traffic load increased, bleeding on the surface caused the gaps between the aggregates to be filled with binder, reducing the macrotexture.

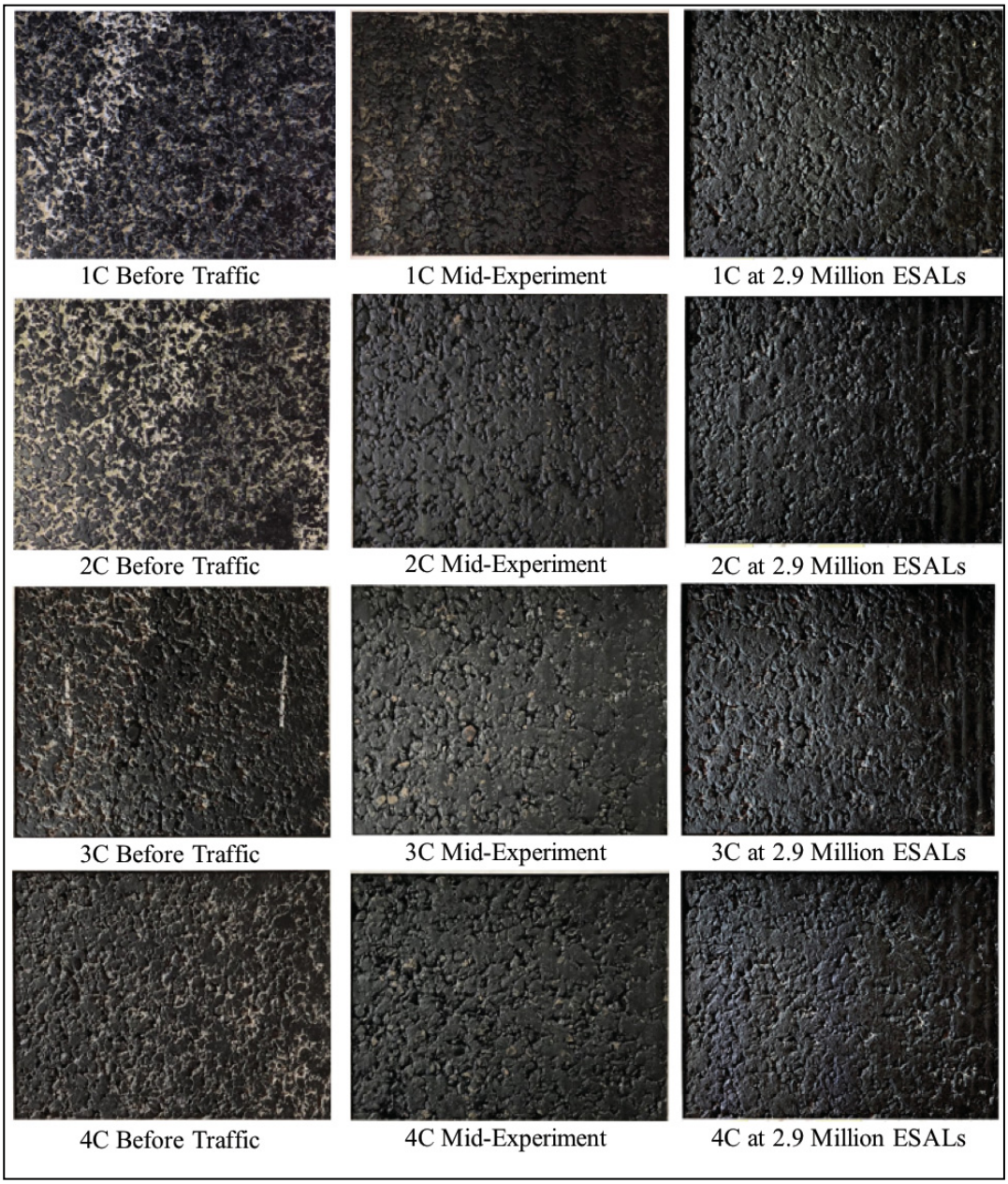

Figure 6-9 - Photographs of center measurements over time.

ANOVA Results

Table 6-2 shows the results of a 2nd degree factorial ANOVA of the full data set. The station and position of the measurements were used as blocking factors, the load in ESALs is the primary model effect, and RMS the response variable. The ANOVA showed a significant effect of traffic load on RMS with a P-value less than 0.0001. However, the effect test of the blocking factors showed the transverse position to be significant as well with a P-value less than 0.0001, and as Figure 6-8 above indicated, the different measurements are not completely co-directional. Additionally, the interaction terms that include the transverse position are significant, indicating that an overall effect is masked by either the variability, an unmeasured model effect, or both. For this reason, the full data set was not ideal for the development of a regression model.

Table 6-2 - Full Data Set 2nd Degree Factorial ANOVA

Analysis of Variance					
Source	**DF**	**Sum of Squares**	**Mean Square**	**F Ratio**	**Prob > F**
Model	27	11.1775	0.4140	30.7718	<.0001*
Error	371	4.9912	0.0134		
Cumulative Total	398	16.1687			
Effect Tests					
Source	**Nparm**	**DF**	**Sum of Squares**	**F Ratio**	**Prob > F**
Cumulative total ESALS	1	1	2.5326	188.2550	<.0001*
Station	3	3	0.0127	0.31570	0.814
Position	4	4	6.0141	111.7610	<.0001*
Cumulative total ESALS*Station	3	3	0.0336	0.8331	0.4763
Cumulative total ESALS*Position	4	4	0.4888	9.0834	<.0001*
Station*Position	12	12	2.1186	13.1236	<.0001*

Table 6-3 shows a one-way ANOVA and linear regression model of the load in ESALS and the effect on RMS with only the data collected from the center measurement locations. It shows that the effect of traffic is significant, with a P-value less than 0.0001. The regression model indicates that the macrotexture in RMS will decrease by -1.42E-07 mm per ESAL applied, or 0.142 mm per million ESALs. The coefficient of determination, $R^2 = 0.507$, indicates that a little more than half of the variability in the data is explained by the effect of traffic loading. The

low R^2 is likely due to high variability in the data as well as some unique observed phenomena on the pavement surface during the study, which are discussed following.

Table 6-3 - Center of Wheelpath Data ANOVA

Summary of Fit				
RSquare	0.5072			
RSquare Adj	0.5010			
Root Mean Square Error	0.1313			
Mean of Response	1.083			
Observations (or Sum wgts)	80			
Analysis of Variance				
Source	**DF**	**Sum of Squares**	**Mean Square**	**F Ratio**
Model	1	1.3838	1.3838	80.3040
Error	78	1.3441	0.0172	Prob > F
C. Total	79	2.7279		<.0001*
Parameter Estimates				
Term	Estimate	Std Error	t Ratio	Prob > |t|
Intercept	1.1864	0.0187	63.58	<.0001*
Cumulative total ESALS	-1.42E-07	1.59E-08	-8.96	<.0001*

Discussion of Results and Observed Phenomena

As previously indicated, change in macrotexture due to load can vary greatly based on the distresses that development in the pavement surface. This experiment showed that when bleeding is the primary distress that develops, the macrotexture will decrease with traffic. This is expected, as bleeding fills in the voids on the surface between aggregates. However, there were some anomalies in this study that did not follow that trend. One unique observation was that a buildup of material on the surface from bleeding caused an increase in macrotexture at 4R.

Figure 6-10 shows photographs taken over the course of this study, where the top picture is before the application of traffic and the bottom represents the maximum load applied. These photographs clearly show the development of ridges on the pavement surface from buildup of the binder material bleeding up from the pavement matrix. As Figure 6-11 indicates, the result was that the macrotexture as measured by RMS increased with the cumulative traffic.

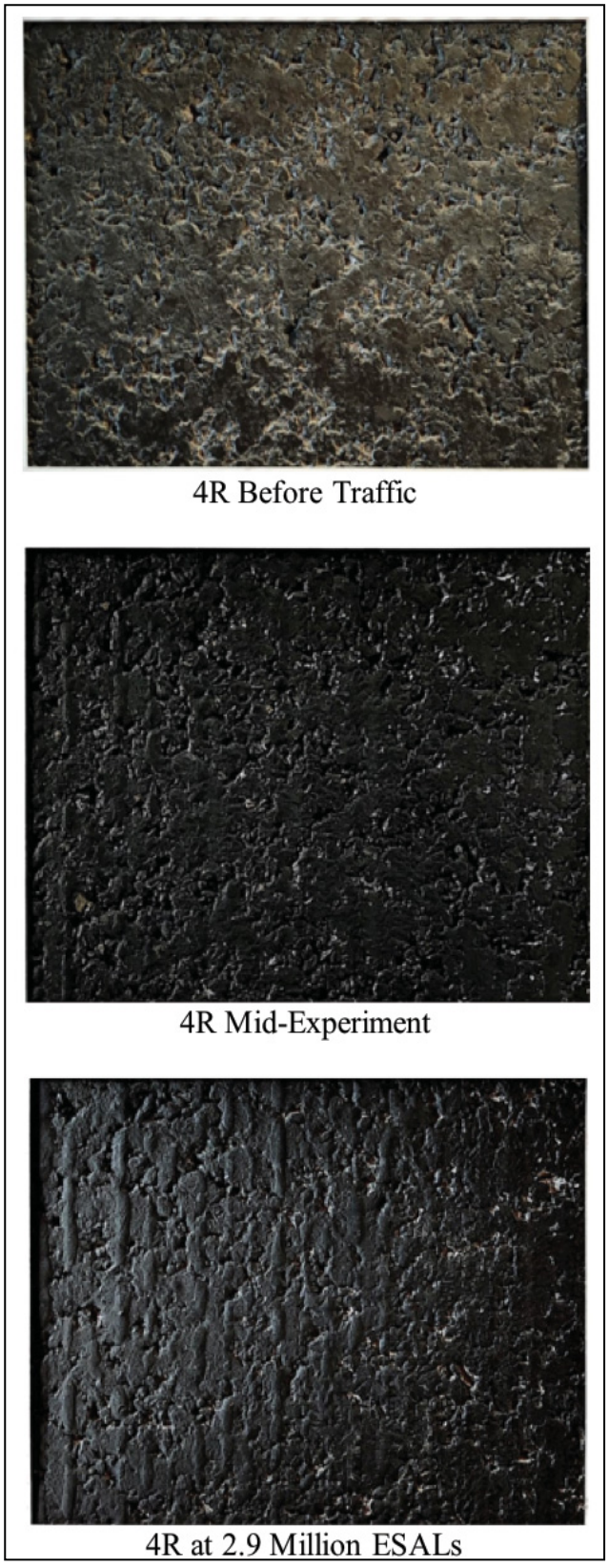

Figure 6-10 - Photographs from Position 4R.

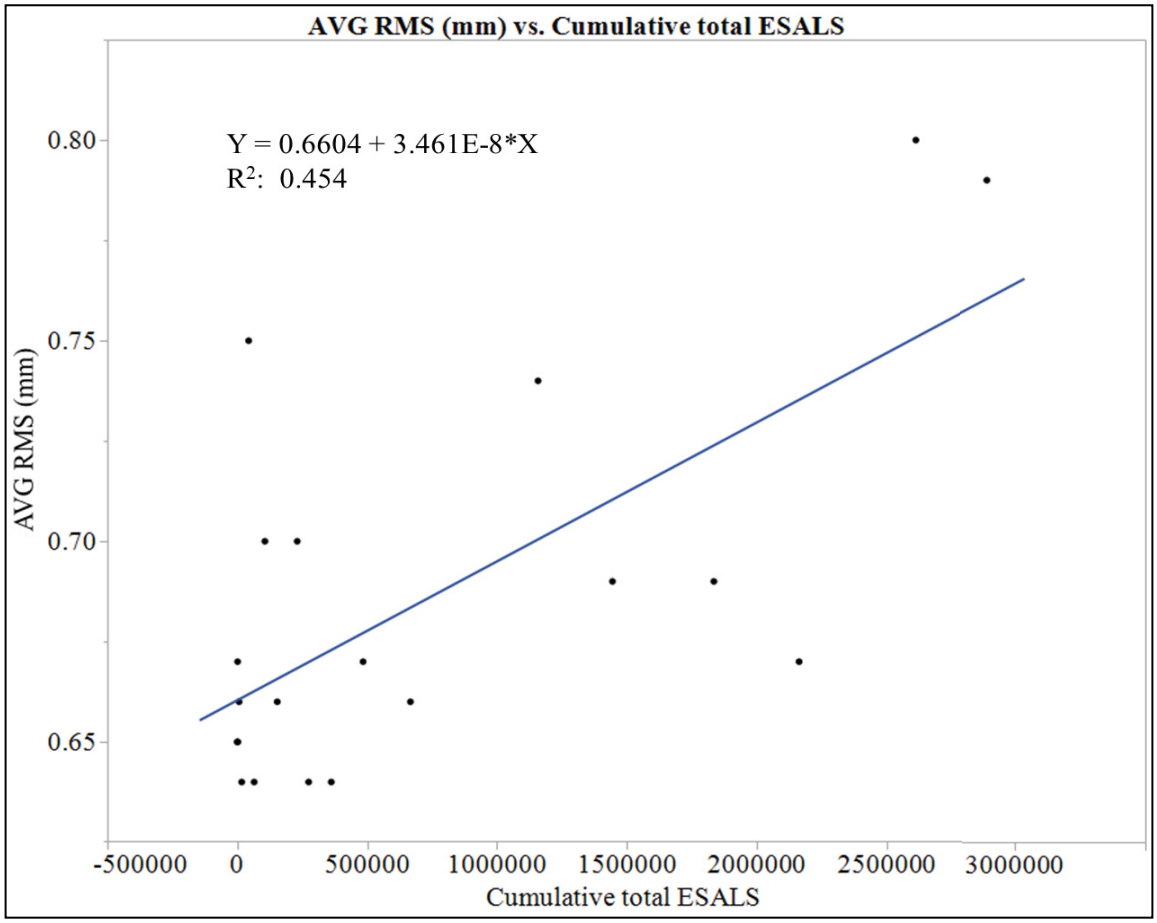

Figure 6-11 - ESALs vs RMS for Position 4R.

Another interesting observation was that in some areas, RMS and MPD showed opposite trends as bleeding occurred. Position 2R was the most pronounced example of this. The photographs in Figure 6-12 below show the development of bleeding and accumulation of material on the surface forming ridges similar to position 4R. However, these ridges appear to be somewhat wider. Interestingly, the macrotexture measured in MPD shows an increase with traffic loading while the trend of RMS was a decrease of similar magnitude (Figure 6-13). It appears that as the buildup of material occurred due to bleeding, the ridges of buildup created peaks in the CT Meter profile that affected the device's calculation of MPD, which is based on peaks, as previously described. Because bleeding would be expected to lead to a decrease in friction, and friction is correlated with macrotexture, these results indicate that RMS is a more appropriate macrotexture measure when bleeding results in surface binder accumulation, which would likely decrease friction.

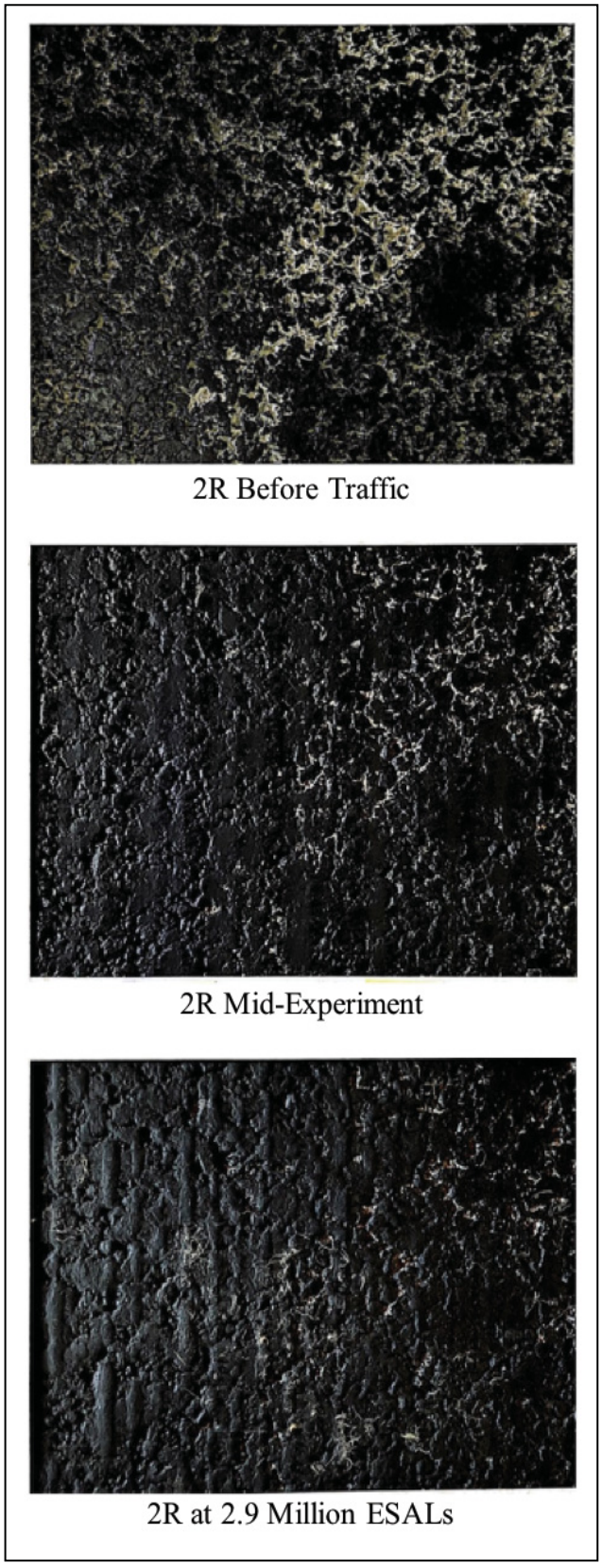

Figure 6-12 - Photographs from position 2R

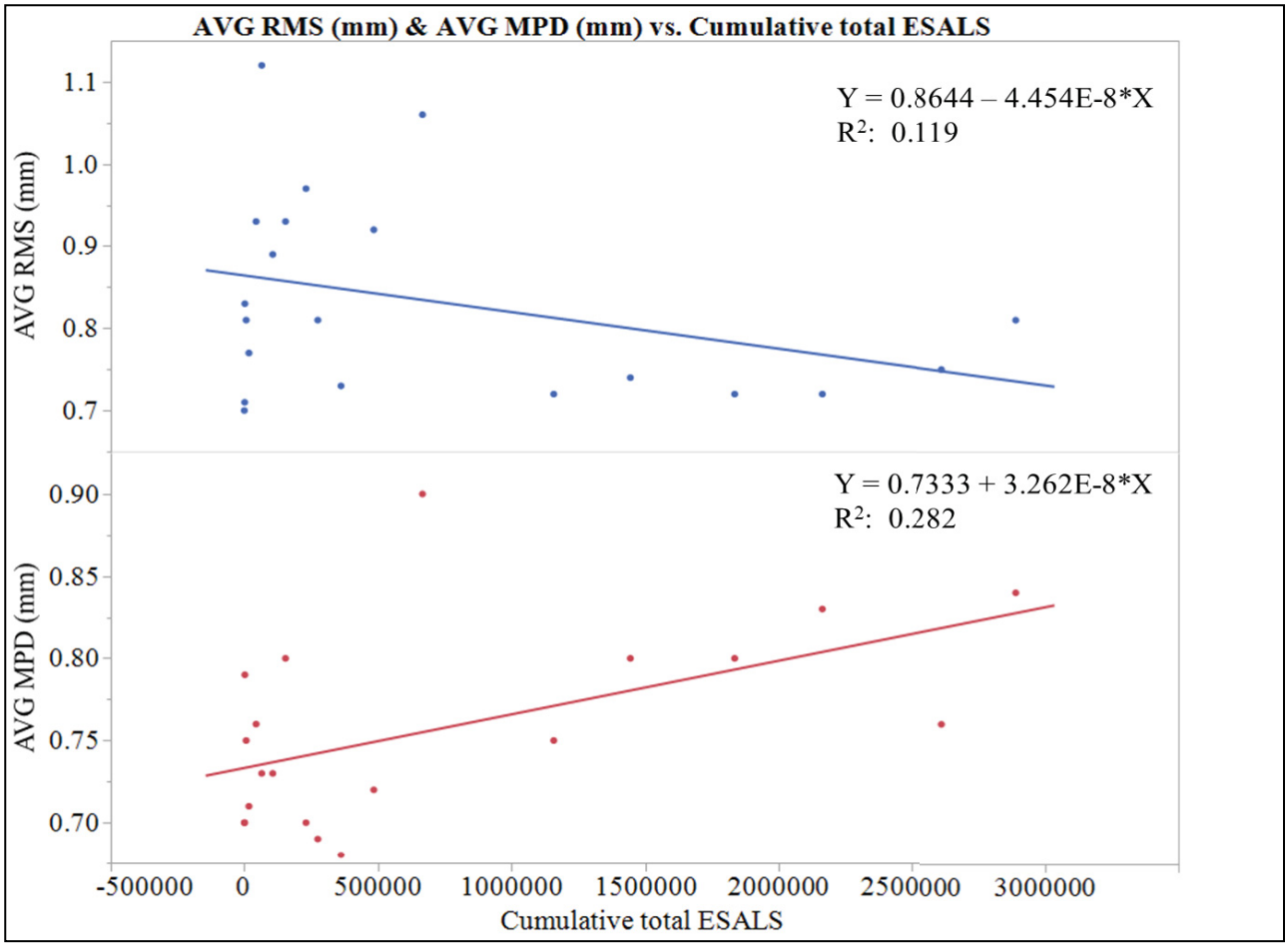

Figure 6-13 - Comparison of RMS and MPD for position 2R

A final observation is that the way in which material built up on the surface of the pavement due to bleeding is likely a source of the considerable variability in the data collected. In one instance near the midpoint of the study, wearing of the surface, which exposed aggregates, began to occur while binder simultaneously began to accumulate nearby (Figure 6-14). There are also indications that the high load used in the HVS caused rubber for the tires to accumulate on the pavement surface as shown by the wearing on the outside edge of the tires (Figure 6-15).

This type of varied response to the traffic load made modeling the overall change in macrotexture difficult, which is reflected in the spread of the data points and the lower coefficient of determination for the centerline position regression model.

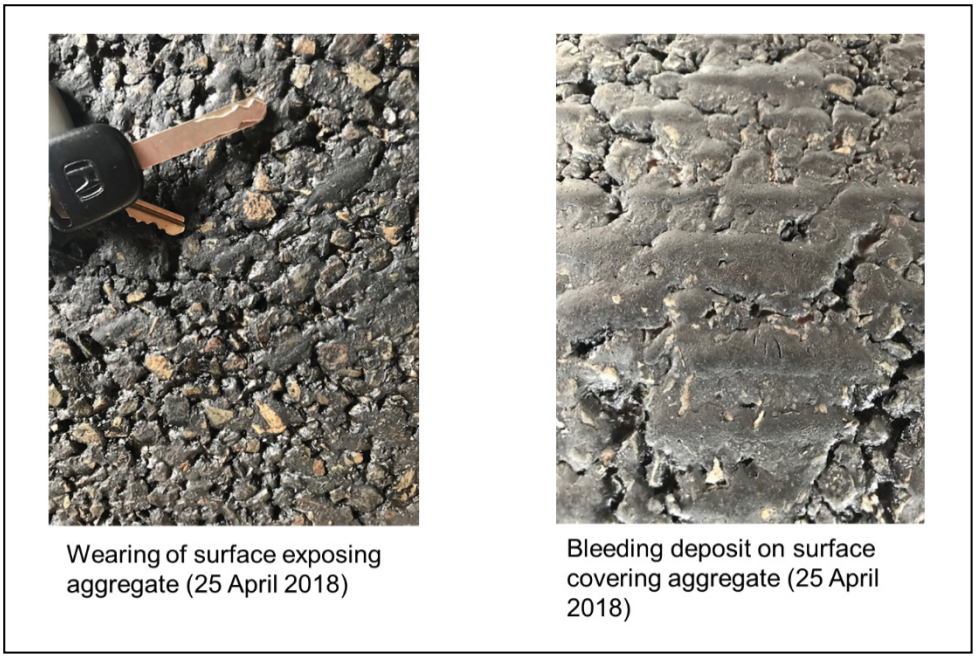

Figure 6-14 - Simultaneous wear and buildup of binder

Figure 6-15 - Wear of HVS Tires

Summary and Conclusions

This study sought to observe and model the development of bleeding and its effect on macrotexture under simulated traffic loading from an HVS. More research is needed to determine the relationship between traffic-induced bleeding and macrotexture, preferably by testing various binder contents and severities of bleeding and correlating resulting surfaces with friction. While overall this study showed that macrotexture decreases with bleeding due to traffic load, there are instances where it can increase due to the buildup of material from bleeding. The results also indicate that RMS is a more effective measurement for macrotexture when buildup from bleeding occurs. This is because the peaks created by the buildup may artificially inflate the readings when using MPD and would, therefore, be less likely to correlate with friction.

The possibility that the observed phenomena are unique to the experimental conditions created by the HVS and not representative of real-world observations must be considered. These experimental conditions include the temperature control, high loads and channelized nature of the HVS passes.

While data collected outside of the wheel path was useful for modeling the bleeding observed along the edge of the pavement, the variability in the data was higher for readings taken outside of the center of the wheel path. The center of the wheel path is the measurement location typical for network level macrotexture collection and this study indicates that the measurements within the wheel path are more predictable as load is applied and are subject to less variability in measurements than other areas on the pavement surface.

Acknowledgement

The authors would like to express our gratitude to Brian Diefenderfer for his oversight of accelerated pavement testing at Virginia Tech Transportation Institute.

References

Aktaş, B., Karaşahin, M., and Tiğdemir, M. (2013). "Developing a macrotexture prediction model for chip seals." *Construction and Building Materials*, 41, 784-789.

ASTM E1859 (2015). "Standard Test Method for Friction Coefficient Measurements Between Tire and Pavement Using a Variable Slip Technique." ASTM International.

D. Jones, R. J. H. (2006). "Reflective Cracking Study: First-LEvel Report on HVS Testing on Section 586RF -- 45 mm MB15-G Overlay." University of California Pavement Research Center UC Davis, UC Berkeley.

Descornet, G., Faure, B., Hamet, J., Kestemont, X., Luminari, M., Quaresma, L., and Sandulli, D. (2000). "Traffic noise and road surfaces: state of the art." *Belgian Road Research Centre, Brussels*.

Hall, J. W., Smith, K. L., Titus-Glover, L., Wambold, J. C., Yager, T. J., and Rado, Z. (2009). "Guide for Pavement Friction." 257p.

Huang, Y. H. (2004). *Pavement Analysis and Design, 2nd Ed.*, Pearson Prentice Hall.

ISO 13473-2 (2002). "Characterization of pavement texture by use of surface profiles - Part 2: Terminology and basic requirements related to pavement texture profile analysis." *Part 2: Terminology and basic requirements related to pavement texture profile analysis*, International Organization for Standardization.

Lin, C., and Tongjing, W. (2018). "Effect of fine aggregate angularity on skid-resistance of asphalt pavement using accelerated pavement testing." *Construction and Building Materials*, 168, 41-46.

Nippo Sangyo Co. (2018). "Circular Track Meter Product Guide." <http://www.nippou.com/en/products/ct.html>. (1 June 2018, 2018).

Parry, A., and Viner, H. (2005). "Accidents And The Skidding Resistance Standard For Strategic Roads In England." *TRL report*, TRL Limited, Wokingham, Berkshire, UK.

PIARC (2016). "Road Dictionary." <http://www.piarc.org/en/Terminology-Dictionaries-Road-Transport-Roads/>. (16 December 2016).

Powell, R. B., and Buchanan, S. (2012). "Long Term Performance of a Thin Asphalt Overlay on the NCAT Pavement Test Track." *TRB*.

Riemer, C., and Pittenger, D. (2012). "Modeling Pavemnt Texture Deterioration as a Pavement Preservation Management System Tool." *TRB*.

Roe, P. G., Parry, A. R., and Viner, H. E. (1998). "High and low speed skidding resistance: the influence of texture depth." TRL Limited, Crowthorne, Berkshire, U.K., 22p.

Roque, R., Anderson, D., and Thompson, M. (1991). "Effect of Material, Design, and Construction Variables on Seal-Coat Performance." *Transportation Research Record No. 1300, Asphalt Pavement and Surface Treatments: Construction and Performance 1991*.

Sandberg, U., Bergiers, A., Ejsmont, J. A., Goubert, L., Karlsson, R., and Zöller, M. (2011). "Road surface influence on tyre/road rolling resistance." *Models for Rolling Resistance in Road Infrastructure Asset Management Systems (MIRIAM),(http://miriam-co2. net/Publications/MIRIAM_SP1_Road-Surf-Infl_Report*, 20111231.

Virginia Department of Transportation (2014). "Pavement Design Guide for Subdivision and Secondary Roads In Virginia."

Wambold, J., Antle, C., Henry, J., Rado, Z., Descornet, G., Sandberg, U., Gothié, M., and Huschek, S. (1995). "International PIARC Experiment to Compare and Harmonize Skid Resistance and Texture Measurements (Paris: PIARC) Publication n 01.04." PIARC, Paris, France.

Weir, D., Strange, J., and Heffley, R. (1978). "Reduction Of Adverse Aerodynamic Effects Of Large Trucks Volume I: Technical Report."

Woodward, D., Millar, P., Lantieri, C., Sangiorgi, C., and Vignali, V. (2016). "The wear of Stone Mastic Asphalt due to slow speed high stress simulated laboratory trafficking." *Construction and Building Materials*, 110, 270-277.

CHAPTER 7 – STANDARD AND NOVEL PAVEMENT MACROTEXTURE PARAMETERS AND THEIR RELATIONSHIP TO OTHER PAVEMENT SURFACE PROPERTIES

Abstract

Pavement macrotexture characteristics are key indicators of several critical tire/pavement interactions. Chief among these are the wet weather friction and vehicle splash and spray, due to safety risks posed. Also important are interactions that affect society such as road noise. Road profiles necessary for macrotexture analysis are relatively simple to collect if sensors with the required vertical resolution and sampling rate are used during mandatory annual road roughness (IRI) surveys. This paper seeks to improve prediction of pavement friction and noise characteristics by testing and combining several existing macrotexture measures with new or lesser-used measures. Single-variable and multi-variable linear regression are used for this analysis. Several parameters are found that outperform the de facto standards of MPD and RMS in both single and multiple variable models. Models that included parameters that account for the tire's enveloped profile, the prominence of peaks within a base length, and road geometry were found to significantly improve predictions.

Keywords: macrotexture parameters, friction, noise, OBSI, CMFE

Introduction

Over 1.2 million vehicle crashes are caused annually in the US by weather-related events. Of these, over 70% are due to wet pavement resulting in nearly 325,000 injuries and 4,000 fatalities (Federal Highway Administration 2018). Pavement macrotexture is related with several pavement surface properties. Most important are those associated with safety concerns such as pavement to tire friction (Wambold et al. 1995) and the splashing and spraying of water from the roadway to vehicle windshields or within the driver's field of view (Weir et al. 1978). Studies (Roe et al. 1998; Parry and Viner 2005) have shown a correlation between pavement texture and vehicle crashes in wet weather. Aside from safety matters, user and environmental concerns such as rolling resistance (Sandberg et al. 2011) and road noise (Descornet et al. 2000) are associated with a pavement's macrotexture.

The World Road Association defines macrotexture as "surface irregularities of a road pavement with horizontal dimensions ranging between 0.5 mm and 50 mm and vertical dimensions between 0.2 and 10 mm" (PIARC 2016). Pavement macrotexture provides a drainage path for water and air beneath the tire to be expelled, reducing hydroplaning potential and allowing for greater tire/pavement adhesion. In addition to adhesion, the hysteresis effect provides traction for vehicles to stay on the roadway. With increasing speed, the hysteresis effect increases exponentially. At speeds above 65mph, Hall et al. (2009) found hysteresis to account for 95 percent of available friction.

Background

The results of several studies [e.g., HERMES (Descornet 2004), TYROSAFE (Scharnigg et al. 2011; Haider et al. 2014), NASA friction workshops(Wambold et al. 2002; Yager 2005), Virginia Tech Transportation Institute (VTTI) Pavement Surface Properties Consortium Rodeos (Flintsch et al. 2012), etc.] have identified pavement texture as a major contributor to pavement friction. In the United Kingdom, yearly road surveys are made to record pavement profiles and derive macrotexture parameters (along with road roughness information as part of their pavement management plan (Ferne 2015). The International Friction Index (IFI) used by The World Road Association (PIARC) uses the macrotexture measure of MPD to determine the friction sensitivity to sliding by calculating the critical speed constant (S_p) as suggested by Wambold et al. (1995).

Higher macrotexture levels combined with high porosity were found by Sandberg and Descornet (1980) to reduce pavement noise. Despite the evidence of the benefits of measuring macrotexture, the United States currently has no requirement for state or federal agencies to measure macrotexture. However, the ability of a parameter such as MPD to exhaustively describe road-tire interaction has been called into question (Leandri and Losa 2015).

Informal interviews with state pavement engineers reviled that a majority of states do not collect pavement macrotexture data at the network level on a recurring basis. This partly because such surveys are not required of state agencies (as they are for road's roughness). Many of the engineers reported they lacked clear direction of what to do with macrotexture information. However, most of the states that do collect macrotexture information do so via high-speed single-spot laser triangulation devices. The primary parameter used to characterize macrotexture is either MPD or Root mean Square data. Engineers indicated a desire for better macrotexture characterization parameters.

Problem Statement

Wet pavement is associated with over 4,000 fatalities in the US per year. A portion of these crashes could be prevented via simple macrotexture surveys collected by the same vehicles collecting mandated IRI data by attaching additional sensors (or using the roughness sensors to collect macrotexture data). Compelling evidence of improved measures must be provided so practitioners will have more confidence in gathering macrotexture data to inform their pavement management decisions.

Objective

Identify the best macrotexture parameters from a suite of existing and newly-developed parameters (aimed at improving correlation with pavement surface properties) to predict a roadway's frictional and noise characteristics without the use of additional specialized equipment for the collection of friction and noise data.

Methodology

The left wheelpath of the "uphill" travel lane of Virginia Smart Road (see Figure 7-1) was measured with a single-spot laser device to capture the pavement surface macrotexture at 55

mph. The same path was measured with two continuous friction measurement devices and a test vehicle capable of measuring road noise. The friction and sound data were then distilled into the parameters we will attempt to predict (predicted variables) from either a single macrotexture parameter (predictor variable) via for single-variable linear regression or several predictor variables via multiple linear regression.

Equipment Used

Table 7-1 - Equipment used to gather data

Measurement	Manufacturer	Model	Specification
Macrotexture	Ames Engineering	Accutexture 100	100 kHz single-spot laser triangulation profiler
Friction	WDM Ltd.	Sideway-force Coefficient Routine Investigation Machine (SCRIM)	Continuous Friction Measurement Device, standard tire
Friction	Findlay Irvine	Grip Tester Mark III (GT)	Continuous Friction Measurement Device, smooth tire
Noise	AVEC, Inc.	Custom	On Board Sound Intensity (OBSI) with optical sensor for tire noise separation

The devices listed in Table 7-1 gather continuous data of the road network in a single run at high speed. The vehicles travel at the speed of traffic and use contactless sensors, so no traffic control is necessary. For macrotexture measurements, a single spot laser beam is emitted from the device. The light is reflected from a discrete point of the pavement surface to the device's light sensor (typically a charged couple device or CMOS sensor like the one in your digital camera). Triangulation is then used to determine the distance between the instrument and the pavement surface at the point measured.

The SCRIM was operated according to normal operating procedures (The Highways Agency 1999) at 50 km/hr. The GT was likewise operated at 50 km/hr according to the manufacturer's standard operating procedure (RoadBase operator's manual). The OBSI was operated at 50km/hr. From the raw data, Overall A-weighted Sound Pressure Levels were calculated. One advantage of the device used in this testing is the addition of an optical sensor. This was done to register the one per revolution signal. The tire revolution signal was used to remove [per Feng (2017)] the tire tread pattern noise component from the total tire noise.

Surfaces Studied

The pavement measured in this experiment each come from the Virginia Smart Road. This offers a wide variety of pavement surfaces typically encountered in the US. The surfaces selected were the continuous surfaces from the Smart Road bridge to pavement section C. See Figure 7-1. The turn-arounds and sections A and B were excluded from the study as similar pavements are already present on the test track and so vehicles can maintain the target test speed of 50 km/hr.

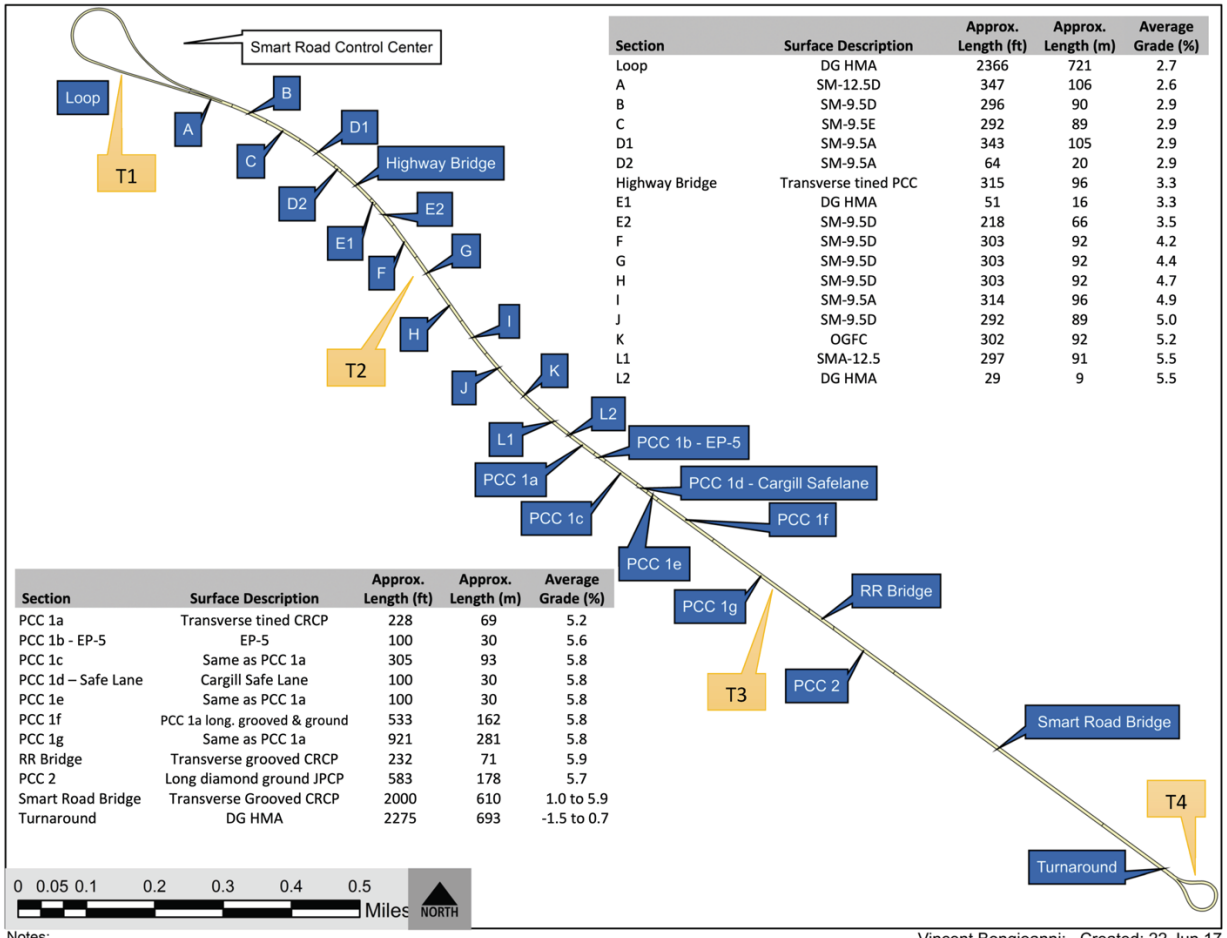

Section	Surface Description	Approx. Length (ft)	Approx. Length (m)	Average Grade (%)
Loop	DG HMA	2366	721	2.7
A	SM-12.5D	347	106	2.6
B	SM-9.5D	296	90	2.9
C	SM-9.5E	292	89	2.9
D1	SM-9.5A	343	105	2.9
D2	SM-9.5A	64	20	2.9
Highway Bridge	Transverse tined PCC	315	96	3.3
E1	DG HMA	51	16	3.3
E2	SM-9.5D	218	66	3.5
F	SM-9.5D	303	92	4.2
G	SM-9.5D	303	92	4.4
H	SM-9.5D	303	92	4.7
I	SM-9.5A	314	96	4.9
J	SM-9.5D	292	89	5.0
K	OGFC	302	92	5.2
L1	SMA-12.5	297	91	5.5
L2	DG HMA	29	9	5.5

Section	Surface Description	Approx. Length (ft)	Approx. Length (m)	Average Grade (%)
PCC 1a	Transverse tined CRCP	228	69	5.2
PCC 1b - EP-5	EP-5	100	30	5.6
PCC 1c	Same as PCC 1a	305	93	5.8
PCC 1d – Safe Lane	Cargill Safe Lane	100	30	5.8
PCC 1e	Same as PCC 1a	100	30	5.8
PCC 1f	PCC 1a long. grooved & ground	533	162	5.8
PCC 1g	Same as PCC 1a	921	281	5.8
RR Bridge	Transverse grooved CRCP	232	71	5.9
PCC 2	Long diamond ground JPCP	583	178	5.7
Smart Road Bridge	Transverse Grooved CRCP	2000	610	1.0 to 5.9
Turnaround	DG HMA	2275	693	-1.5 to 0.7

Notes:
1. Sectioning and distances are for the "uphill" direction (East to West)
2. When travelling "downhill" (West to East), Section PCC 1b is the Cargill Safelane and PCC 1d is the EP-5; PCC1f is the same surface type as PCC 1a. Downhill distances vary slightly

Vincent Bongioanni; Created: 22 Jun 17

Figure 7-1 - The Virginia Smart Road Pavement Surface Characteristics

Surface photos of each of the surfaces studied are provided in Figure 7-2. All photos were taken from approximately a 3-ft focal length. Each photo has been scaled to show relative textures. As transitions between different surface types may have adverse effects on any given

device's various measurements, the first and last 1 meter of each section was removed from the pavement dataset.

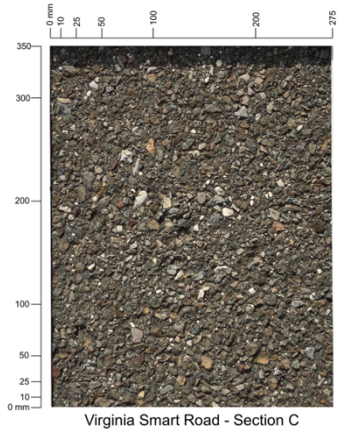

Virginia Smart Road - Section C

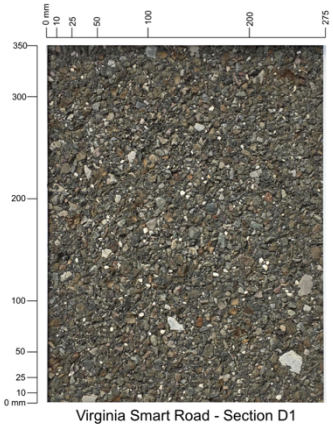

Virginia Smart Road - Section D1

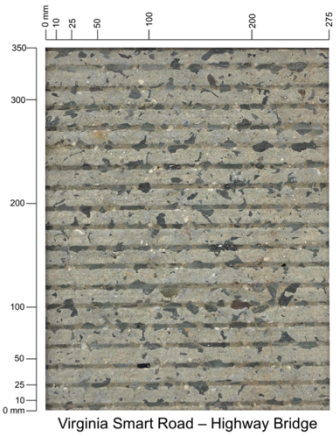

Virginia Smart Road – Highway Bridge

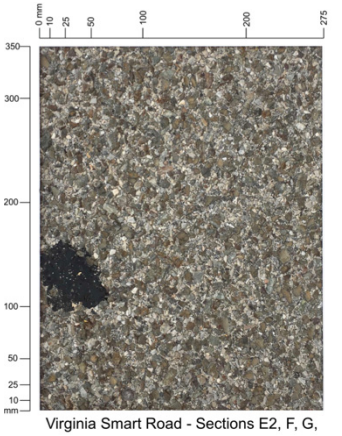

Virginia Smart Road - Sections E2, F, G,

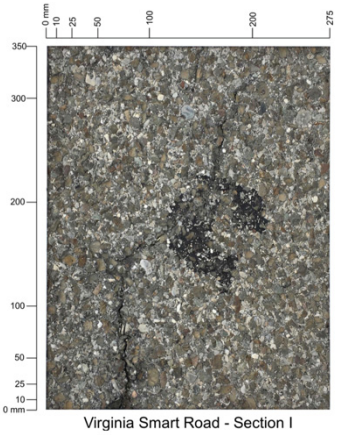

Virginia Smart Road - Section I

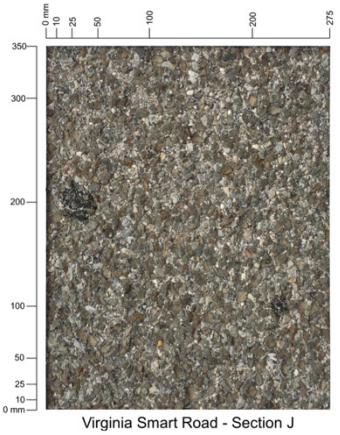

Virginia Smart Road - Section J

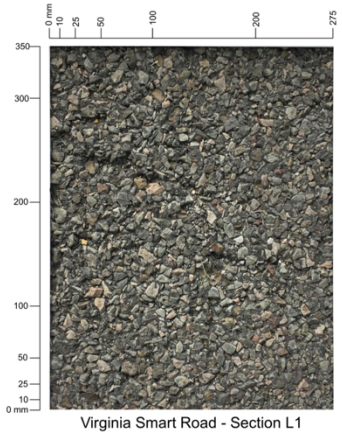

Virginia Smart Road - Section L1

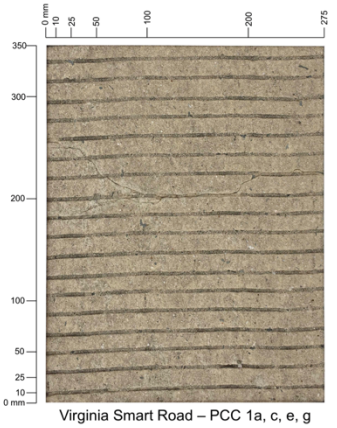

Virginia Smart Road – PCC 1a, c, e, g

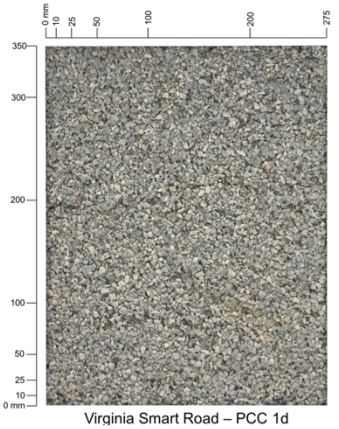

Virginia Smart Road – PCC 1d

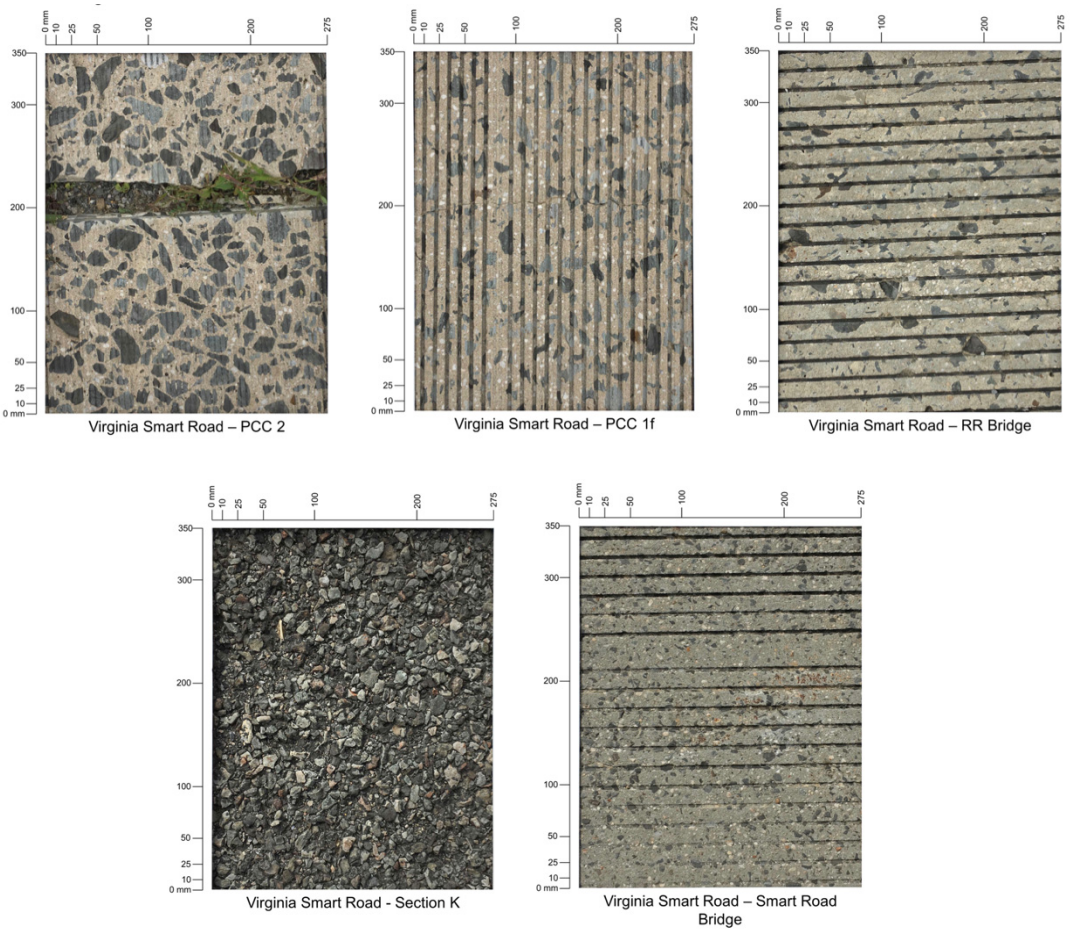

Figure 7-2 - Virginia Smart Road Pavement Surfaces

Predicted Variables

The focus of this experiment is to predict friction (as measured by the SCRIM and GT) and noise (as measured by the OBSI) from pavement surface profiles in the macrotexture range. As such, the data collected by the devices to be predicted was treated using the manufacture's software to derive the predicted variables. The SCRIM was run at 50 km/hr and SCRIM readings (SR) were output from the system software. Data is typically evaluated at 50km/hr. To allow for small variations in vehicle travel speed, data is corrected [per The Highways Agency (1999)] to a constant equivalent SCRIM reading at 50 km/hr (SR_{50}), using the following equation:

$$SR_{50} = SR(100) * \frac{(-0.0152s^2 + 4.77s + 799)}{1000} \qquad \textit{(Equation 7-1)}$$

where:
s = instantaneous speed (km/hr) of the individual measurement

GT data was collected at 50 km/hr along the left wheelpath of the uphill lane of the Virginia Smart Road. The GT device software outputs Grip Numbers (GN) which range from 0.0 to 1.0 and are dimensionless. These GNs are the pavement coefficient of friction as measured by the GT via the relationship:

$$GN = \frac{f_d}{f_n} \qquad \textit{(Equation 7-2)}$$

where:
f_d = drag force (N)
f_n = normal force (N)

Noise data was collected in the right wheelpath of the uphill lane of the Virginia Smart Road. The parameter distilled from the raw noise data is the Overall A-Weighted Sound Pressure Level (OASPL). This is essentially the total sound pressure as measured by the OBSI. The A weighting is applied to take into account the relative loudness perceived by the human ears. Tire tread pattern noise was removed using the optical sensor data applying the tire noise separation procedure.

Predictor Variables

The single-spot laser device was used to record a raw texture height profile of all road surfaces. Measurements were taken in the left wheelpath at 90 km/hr. All raw time-domain data was converted to spatial data via linear interpolation based on texture height data and distances pulses gathered by a wheel encoder mounted to the driver-side rear tire. The minimum spatial sampling distance of one-quarter mm was used for all profiles as determined by the following calculation:

$$\frac{88.5\ km}{hr}\ x\ \frac{1{,}000{,}000\ mm}{km}\ x\ \frac{hr}{3{,}600\ s}\ x\ \frac{1\ s}{100{,}000\ samples} = \frac{0.25mm}{sample} \qquad \textit{(Equation 7-3)}$$

Once a raw spatial-domain profile was obtained, the profile was distilled into a suite of macrotexture parameters including the most popular parameters used in the US, MPD and RMS as well as less widespread parameters from literature (i.e., Skewness, Kurtosis, and Mean Depth of Elevation). The authors also devised many additional parameters with the intent

of obtaining better correlations with the predicted variables. These parameters are described below.

Outliers were removed from the raw pavement profile following the methods described in Katicha et al. (2015). Filtering per ASTM E1845 (2015) was performed on each pavement surface profile before parameter calculation unless denoted to the contrary. The majority of parameters used a base length of 100mm for each calculation and slope suppression via simple linear regression was performed on each base length for all parameters with the exception of those derived by wavelet transformation as described below. A base length that has had the slope removed is referred to as a detrended base length in this paper.

Table 7-2 - Summary of Predictor Parameters

Var #	Parameter	Reference
1	Mean Profile Depth (MPD)	ISO 13473-1 (1997); ASTM E1845 (2015)
2	Root Mean Square (RMS)	Wennink and Gerritsen (2000), ISO 13473-2 (2002),
3	Mean Difference of Elevation (MDE)	Chou et al. (2017)
4 – 7 22-25	Enveloping Profiles Empirical Physical Effective Area of Water Evacuation (EAWE)	Clapp (1983), Von Meier et al. (1992), Klein et al. (2004),Goubert (2007), Mogrovejo et al. (2016)
8 – 9	Geometric Statistical Methods Skewness (R_{sk}) Kurtosis (R_{ku})	ISO 4288 (1996), ISO 4287 (1997), ASME B46.1 (2009)
10	Maximum Height (Max H)	New
11 – 13	Percentile MPD (MPD_{95}, MPD_{97}, MPD_{99})	New
14 - 21	Tire Contact Length (TCL)	New
26 – 55	Wavelet Transformations ($w_{d\,x}$) Various statistical measures of Haar details	New, more information in Zelelew et al. (2013), Leandri and Losa (2015)
56 – 60	Enveloped Profile MPD (MPD_e)	New, more information given in Goubert and Sandberg (2018)
61	Profile Length Ratio (PLR)	New
62 – 79	Peak Data Parameters Mean Peak height above Zero (MPGZ) Mean peak above zero Separation (MSEPGZ) Mean Prominence Separation Ratio (MPMSR) Mean Prominence above zero (MPROMGZ) Mean width of peaks above zero (MWGZ) Mean Prominence to Width Ratio (MPWR) Mean peak Width Mean peak Separation Ratio (MWMSR) Number of Peaks above zero (NPGZ)	New

Traditional Measures

MPD and RMS are well-documented macrotexture parameters, information on their calculation can be obtained in the references given in Table 7-2. MDE takes the average difference of profile points above a

$$MDE = \frac{\sum_{i=1}^{n-1} DE_i}{n-1} \qquad \textit{(Equation 7-4)}$$

where:
DE = difference in elevation between point of interest on a detrended base length and the successive point
n = number of points in the base length

Enveloping Profiles

Enveloping profiles account for the free space between tire and pavement. This enveloped profile can be used in a host of ways, we include for evaluation the Effective Area of Water Evacuation (EAWE) proposed by Mogrovejo et al. (2016). This is a single parameter that places the enveloping profile (Klein et al. 2004) of a tire over the measured pavement surface and calculates the area between the two. This method requires the use of a tire stiffness coefficients (d*) to determine the extent of tire rubber penetration into the pavement surface. In our analysis, the following coefficients were used:

Table 7-3 - Tire stiffness coefficients used in tire envelopment procedure

Tire Stiffness	d*
Soft tire	1E-2
Medium-soft tire	1E-3
Medium-stiff tire	1E-4
Stiff tire	1E-5

Traditional Statistical Moments

Skewness (R_{sk}) and Kurtosis (R_{ku}) are the third and fourth statistical moments. Skewness can be used to capture positive or negative texture behavior. Negative skewness values indicate a negative texture (more troughs than peaks). Kurtosis can generally be used to describe the peakedness (i.e., how severe peaks and troughs are) of a roughness profile. In image processing, kurtosis can be used to describe the uniformity of the grayscale distribution.

$$R_{sk} = \frac{\sum_{i=1}^{n} y_i^3}{n(R_q^3)} \qquad \textit{(Equation 7-5)}$$

$$R_{ku} = \frac{\sum_{i=1}^{n} y_i^4}{n(R_q^4)} \qquad \textit{(Equation 7-6)}$$

Maximum Height

Maximum height is a simple measure of the distance between the maximum peak height in a detrended base length and the minimum valley distance in the same detrended base length. Percentile MPDs are calculated by finding not by the maximum height in a half-base length but a value near the maximum height. This is helpful if many outliers are suspected in a profile. Pavement texture heights in a detrended half base length are sorted and the n^{th} percentile value is taken and averaged with the n^{th} percentile value of the second half base length. For our analysis, the 95^{th}, 97^{th}, and 99^{th} percentiles were used.

Tire Contact Length

Tire Contact Length (TCL) is a measure of the percentage of pavement in contact with the tire. This is important for two reasons. First, it describes the percentage of the pavement that is taking advantage of the adhesive properties (a function of microtexture) of the pavement. Secondly, it helps to describe the percentage of pavement that is being used to evacuate water beneath the tire contact area. TCL is calculated by first deriving an enveloped profile using the Klein et al. (2004) method with tire stiffness coefficients given in Table 7-3. Next, the pavement profile points that coincide with the enveloped profile (to within a specified tolerance) are counted and the ratio of coincident points to base length is taken as the TCL.

Measures of Wavelet Transformations

Wavelets are methods to approximate the characteristics of a measured waveform. Wavelets are localized in both time and frequency whereas the Fourier transformation is only localized in frequency. A short-period mother wavelet is selected and then scaled and shifted along the signal to decompose the signal into the wavelet transformation. In our case, we used the Haar mother wavelet which is a square-wavelet comprised of two complimentary components, the difference in magnitude between two points (the details) and the average value (the amplitude data) of the two points. The wavelet decomposition is performed numerous times (levels) to the signal to gain insights of different scales of data decomposition that may shed light on wavelengths of interest for pavement surface properties. Each successive level is a wavelet decomposition of the previous level. The decomposition is complimentary because the details and amplitude information of two successive levels can be used to reconstruct the previous level. The various levels of the details of the wavelet decomposition are independent (orthogonal) to

one another are, therefore, not colinear. In our case, we decomposed the raw data profile into 10 levels. As each of data points is spaced the minimum spatial distance obtainable by the measurement device (0.25mm), the 10-level decomposition provides information up to the 0.25 * 2^{10} = 256mm scale. The details of each wavelet decomposition level were then processed to gather the following predictor parameters (as described elsewhere in this work): RMS, $R_{sk,}$ R_{ku}. This resulted in 30 predictor parameters derived from each of the 10 levels of the wavelet decompositions.

Enveloped Profile MPD

Enveloped Profile MPD (MPD_e) were proposed by Goubert and Sandberg (2018). This is the MPD taken of an enveloped profile. For our analysis, the enveloped profile was calculated using the Klein et al. (2004) method with tire stiffness coefficients given in Table 7-3. Next, a mean profile depth is calculated for the enveloped profile according to the procedures in ASTM E1845 (2015), however, no filter is performed on the relatively smooth enveloped profile.

Pavement Length Ratio

Another measure of the measured profile to a theoretical length is that of the Pavement Length Ratio (PLR). This is taken as the ratio between the length of the measured profile, calculated via the sum of Euclidian distances between two data points in the base length and the base length. A perfectly flat and smooth surface would have a PLR of 1.0 and PLR increases with increasing texture height.

$$PLR = \frac{\sum_{i=1}^{n-1} \sqrt{(h_{i+1} - h_i)^2 + (\Delta x)^2}}{base\ length} \qquad \textit{(Equation 7-7)}$$

Peak Parameter Measures

A variety of peak data parameters were developed for this work by using various peak height characteristics. Peaks were found using various capabilities of the 'findpeaks' function in MATLAB (Mathworks 2016). Within the function, the minimum peak prominence can be specified. This is a measure of the prominence of the peak due to its intrinsic height and location characteristics relative to other peaks. This helps to identify peaks that stand out by themselves. A low and isolated peak can have a greater prominence than a peak near another peak at a similar height. This is done by finding all peaks (any point with a height greater than the points immediately preceding and following the point) and then extending a horizontal line in the

forward and reverse directions of the signal from each peak until the line crosses the signal (or reaches the end of the signal). The minima (i.e., see labels A and B in Figure 7-3) are then found within these two intervals of the horizontal line. The higher minimum value is used as a reference level and the peak height above this reference level is calculated. This is the peak prominence. Any peak with a prominence greater than the user-specified value is then identified. For our analysis, peak prominence of 0.1 and 0.25mm respectively were used.

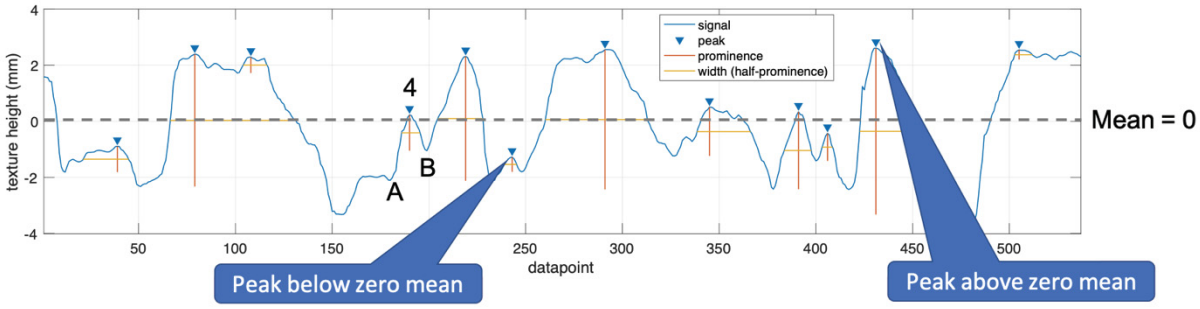

Figure 7-3 – Peaks with minimum prominence of 0.25mm

The base length used for all peak parameters is 100mm and each base length is detrended (slope removed and mean of base length set to zero) by subtracting its linear regression from itself. From this detrended profile, the following parameters are calculated for the minimum prominence levels specified:

MPGZ = mean peak height for peaks above the zero-mean line

MSEPGZ = separation (in mm) between peaks in a base length

MPMSR = $\frac{MPGZ}{MSEPGZ}$

MPROMGZ = mean of prominence for all peaks greater than zero

MWGZ = mean of peak width (equal to half the peak prominence) for all peaks > zero

MPWR = $\frac{MPROMGZ}{MWGZ}$

MWMSR = $\frac{MPGMWGZ}{MSEPGZ}$

NPGZ = count of peaks above zero mean line in a base length

Results and Discussion

After all parameters (three predicted and 79 predictor parameters) were calculated for each section of the road, data measures spaced less than one meter were averaged to a length of

one meter via arithmetic means. Next, distances were aligned via linear interpolation. Minor differences in measured distance occur due to experimental error such as distance measurement sensor calibration issues or interruptions to distance measurement such as if the measurement device bounced and lost contact with the surface momentarily. The distances of the predicted variables were brought to match those of the predictor parameters (which were all the same as the same non-contacting displacement device measured the original pavement surface profile from which the variables were derived). Linear interpolation was accomplished via the method in the following equation. The values of x_a and x_b were taken as the linear space between zero and one for the number of samples of the parameter to be interpolated. The values of x were taken as the linear space between zero and one for the number of samples in the parameter for which we wish to match its length (i.e., the predictor parameters). In this way, the values are still valid one-meter samples (or, the interpolated value between two valid one-meter samples) but have been scaled to match the one-meter values recorded by the pavement profiler.

$$y = y_a + (y_a - y_b)\frac{(x - x_a)}{(x_b - x_a)} \qquad \textit{(Equation 7-8)}$$

Where:
x_a and y_a are coordinates for the data point before the desired interpolation point
x_b and y_b are coordinates for the data point after the desired interpolation point
y is the interpolated vertical value between x_a and x_b
x is the interpolated horizontal value of y

After bringing all parameters to the same scale so equal numbers of samples could be evaluated, pairwise multivariate linear regression was performed on all datasets. In pairwise multivariate linear regression, each possible combination of variables is correlated via least-squares regression and Pearson Correlation Coefficients (ρ) are calculated for each pair. More than 2,600 rows of one-meter data for each of the 82 variables (3 predicted variable and 79 predictor variables) were correlated resulting in a 6,724-cell matrix of correlations coefficients. Strengths of relationships could be visualized with this matrix and its corresponding scatterplot matrix. More importantly, the predicted variables' correlation coefficients could be examined to find the best predictor parameters to predict the variables of interest.

To simplify the results, the absolute values of the correlation coefficients were sorted, and the 10 largest values were taken as the best single-variable parameters to predict the parameter of interest. The results are summarized in Table 7-4 and Table 7-5 for the random textured and transverse textured surfaces, respectively. The pavement of the Virginia Smart Road has been broken into two general categories based on their surface texture characteristics. Random textures are surfaces such as HMA, OGFC, SMA, or the EP-5 or Cargill Safe Lane surface treatments. Transverse textures include PCC surfaces which have been tined or grooved perpendicularly to the direction of travel. This single-variable analysis is beneficial to agencies desiring to minimize the amount of calculations needed to predict friction or noise data from a pavement surface profile. Correlations between the predicted variable column and MPD and RMS as well as the other predicted variables are also given at the bottom of each table for reference.

Table 7-4 - Single Variable Pearson Correlation Coefficients - Random Texture

SCRIM		GT		OBSI	
EAWE (filt, d*=1E-2)	-0.64	PLR (no filt)	-0.69	$W_{d,,\,RMS}$ (lvl 7, no filt)	0.34
PLR (no filt)	-0.61	EAWE (filt, d*=1E-2)	-0.69	$W_{d,,\,RMS}$ (lvl 9, no filt)	0.34
TCL (filt, tol = 0.1, d*=1E-2)	0.61	$W_{d,,\,RMS}$ (lvl 1, no filt)	-0.68	$W_{d,,\,RMS}$ (lvl 10, no filt)	0.34
EAWE (no filt, d*=1E-2)	-0.61	$W_{d,,\,RMS}$ (lvl 2, no filt)	-0.68	NPGZ (filt, P = 0.1)	-0.34
$W_{d,,\,RMS}$ (lvl 1, no filt)	-0.60	TCL (filt, tol = 0.1, d*=1E-2)	0.68	$W_{d,,\,RMS}$ (lvl 8, no filt)	0.34
$W_{d,,\,RMS}$ (lvl 2, no filt)	-0.59	EAWE (no filt, d*=1E-2)	-0.68	$W_{d,,\,RMS}$ (lvl 6, no filt)	0.33
$W_{d,,\,RMS}$ (lvl 3, no filt)	-0.59	$W_{d,,\,RMS}$ (lvl 3, no filt)	-0.68	RMS	0.33
$W_{d,,\,RMS}$ (lvl 4, no filt)	-0.58	$W_{d,,\,RMS}$ (lvl 4, no filt)	-0.67	MPD_{95}	0.32
MDE	-0.57	MDE	-0.67	MPD_{97}	0.32
MPMSR (filt, P = 0.25)	-0.56	MPMSR (filt, P = 0.25)	-0.66	Max H	0.32
MPD	-0.42	MPD	-0.57	MPD	0.31
RMS	-0.49	RMS	-0.61	RMS	0.33
SCRIM	1	SCRIM	0.80	SCRIM	0.07
GT	0.80	GT	1	GT	0.02
OBSI	0.07	OBSI	0.02	OBSI	1

Table 7-5 - Single Variable Pearson Correlation Coefficients - Transverse Texture

SCRIM		GT		OBSI	
MWMSR (filt, P = 0.1)	-0.22	TCL (no filt, tol= 0.1, d*=1E-4)	0.51	EAWE (filt, d*=1E-2)	0.26
MPMSR (filt, P = 0.1)	-0.20	MPD_e (no filt, d*=1E-4)	-0.50	NPGZ (filt, P = 0.1)	0.24
MPMSR (filt, P = 0.25)	-0.20	TCL (no filt, tol= 0.1, d*=1E-5)	0.48	MWGZ (filt, P = 0.1)	-0.24
MWGZ (filt, P = 0.1)	0.20	MPMSR (filt, P = 0.25)	-0.47	EAWE (filt, d*=1E-2)	0.23
$W_{d,,\ RKU}$ (lvl 4, no filt)	0.19	MPD_e (no filt, d*=1E-3)	-0.46	MWGZ (filt, P = 0.25)	-0.23
MSEPGZ (filt, P = 0.1)	0.18	TCL (no filt, tol= 0.1, d*=1E-3)	0.43	NPGZ (filt, P = 0.25)	0.23
$W_{d,,\ RKU}$ (lvl 5, no filt)	0.18	MPD_e (no filt, d*=1E-5)	-0.43	PLR (no filt)	0.21
MWGZ (filt, P = 0.25)	0.17	MWMSR (filt, P = 0.1)	-0.43	MSEPGZ (filt, P = 0.1)	-0.21
$W_{d,,\ RKU}$ (lvl 6, no filt)	0.17	EAWE (filt, d*=1E-5)	-0.41	MPMSR (filt, P = 0.1)	0.21
NPGZ (filt, P = 0.1)	-0.17	MWMSR (filt, P = 0.25)	-0.41	TCL (filt, tol= 0.1, d*=1E-2)	-0.21
MPD	-0.13	MPD	-0.38	MPD	0.16
RMS	-0.12	RMS	-0.31	RMS	0.17
SCRIM	1	SCRIM	0.14	SCRIM	-0.09
GT	0.14	GT	1	GT	-0.22
OBSI	-0.09	OBSI	-0.22	OBSI	1

The best parameters to predict friction from the SCRIM or the GT from a pavement surface profile are the same for randomly-textured surfaces. Small differences in order based on correlation coefficients exist due to minor variations in the data. In general, the best performers for the single-variable correlation are those that account for the tire's enveloped profile (i.e., EAWE and TCL) and the PLR which is a measure of how much texture is provided by the pavement in comparison to a perfectly smooth surface. RMS of several levels of the details of the Haar wavelet decompositions also perform well, especially when compared to the RMS values given near the bottom of the table on a filtered, detrended profile. MDE (a differencing algorithm similar to the details of the Haar wavelet decomposition on the raw pavement profile) and MPMSR (a ratio parameter between the mean peak height of peaks with a prominence of at least 0.25mm and their spacing) round off the list with correlation coefficients greater than 0.5. Note the sign of correlation coefficient is positive in some cases and negative in others. For example, EAWE has a negative sign and TCL is positive. This is likely due to the fact that there is an inverse relationship between the two parameters. If TCL is high, the tire will be in contact with more of the surface, leaving less space for an effective area of water evacuation.

Correlation between the randomly-textured pavement surface profile and noise (as characterized by the overall sound pressure level measured by OBSI) is best with variations of the statistical measure of RMS or peak information such as MPD, Max Height of peaks above

the lowest valley, or number of peaks above the mean profile (NPGZ) line of a 100mm base length also outperform the rest of the variables for noise prediction. The correlation coefficients, however, are low for all measures evaluated with no more than 34% strength of relation.

Also note that each of the top-ten predictor parameters in Table 7-4 outperform the most commonly-used pavement macrotexture characterization parameters of MPD and RMS, however, correlation coefficients can still be relatively small. The reader should also be note that the Pearson Correlation Coefficient between the SCRIM and GT (two devices that both characterize pavement friction via a rubber tire in contact with the road and lubricated by a thin fil of water) is 0.8. Despite differences in operating principles (i.e., slip speed, normal loads used, water flow rates, etc.), we can expect any given predictor parameter to have a maximum correlation in a similar range given the two devices should, in theory, measure wet weather friction.

The correlations for all predictor variables for SCRIM and OBSI are all low for the transverse textured pavements, however, Table 7-5 still proves useful as it shows each of the top 10 predictor variables outperform MPD and RMS, the most commonly-used parameters used to describe a pavement's macrotexture. This shows that improvements can be made to these common predictors to enable better pavement management in the future. Stronger relationships were found for GT data by several proposed macrotexture parameters. The best being those that account for the deformed shape of the vehicle's tire into the pavement texture: TCL, MPD_e as well as peak analysis-based parameters that account for the separation of peaks above a certain prominence or the widths associated with these peaks.

Multiple Regression

Each of the aforementioned predictor parameters bring their own strengths to the single-variable linear regression. For example, some characterize the peaks of the base length evaluated, others give various measures of the enveloped tire profile on the surface, still others evaluate the statistical measures of the base length at various wavelet-decomposed scales. The next objective of this work is to determine if the power of the model developed to predict friction or noise from surface profile measurements can be increased. This can done by taking into consideration several variables to relate pavement surface properties to the desired objective predicted variable. Multiple linear regression results in additional coefficients for the linear model. A similar

approach was taken by Sohaney and Rasmussen (2013) on their analysis of 3-D macrotexture data measured by a walking-speed semi-autonomous vehicle. This type of data stream is not yet available for high-speed network-level analysis, hence the use in this work of single-spot laser triangulation data which is commonly available. In our analysis, the additional parameters of pavement geometry (grade, crossfall, curvature) were also added to the predictor parameters outlined in Table 7-2 for the multiple linear regression. These measurements can be collected by the same vehicle gathering the pavement surface profile by the addition of another laser for lane crossfall and inertial measurement unit for curvature information.

One approach to arrive at a multiple regression model would be to include all predictor variables in the model. This approach would, however, have several significant problems in our analysis. Chiefly, the complexity of the final model and need for calculation of additional predictor parameters would greatly increase, possibly without any benefit to the final model. Too many parameters will most often result in a model that is overfit. The predictor variables may also bring multicollinearity issues to the model, thereby falsely inflating our confidence in the final model.

To select the best parameters for our final model and avoid overfitting, a least absolute shrinkage and selection operator (LASSO) model was developed using JMP software. LASSO is a minimization problem similar to basis pursuit denoising used in signals processing. The approach (in the least-squares case, as was used in the following analysis) forces regression coefficients to be less than a fixed value (t) as shown in the equation below (Tibshirani 1996). In so doing, some coefficients are forced down to zero, which removes them from the final model. This approach is also similar to ridge regression; however, ridge regression only reduces the magnitude of the regression coefficients it does not set some to zero (remove them) based on predetermined criteria.

$$\min_{\beta_o,\beta} \left\{ \frac{1}{N} \sum_{i=1}^{N} (y_i - \beta_o - x_i^T \beta)^2 \right\} \quad such\ that \ \sum_{j=1}^{p} |\beta_j| \leq t \qquad \textit{(Equation 7-9)}$$

where:
N is number of cases (observations)
p is number of predictor variables
y is outcome (predicted variable)
x is the covariate vector of predictor variables for the ith case
1_N is a vector of ones

Variance Inflation

If the predictor variables are not independent (i.e., collinear), several regression parameters will be found to be solutions to the minimization problem described above. For this work, to avoid collinearity, Variance Inflation Factors (VIF) were considered. VIF were calculated in a pairwise fashion for all parameters selected be the LASSO analysis. VIF are calculated as inverse correlations of the ith pair of variables.

$$VIF_i = \frac{1}{1 - R_i^2} \qquad \textit{(Equation 7-10)}$$

where:
R_i^2 is the coefficient of variation of the ith pair of variables

In general, VIF is sought to be brought below 4 (Hair et al. 2011). VIFs between 5 and 10 indicate high correlation between predictor variables and values above 10 will likely produce poor estimates due to stronger multicollinearity. VIF values for variables selected by the LASSO analysis were sorted and the variable with the highest VIF removed. VIFs were then again calculated for the model and the process was repeated until all remaining variables had VIFs lower than 4. Summaries of the selected variables, their coefficients for the model equation, and descriptors of their goodness of fit (ρ and RMSE) are given below. LASSO minimization plots and resulting models are given in Appendix U.

After valid parameters were selected for the model, the dataset was divided for cross validation. This was accomplished by designating 8 of 10 data points to a training dataset, the remainder being reserved for validation. Models were formed using the training dataset and cross validated using the validation dataset. The results are summarized in Table 7-6 and Table 7-7, respectively.

Table 7-6 - Summary of Model Coefficients, ρ, and RMSE values - Random Texture

SCRIM		GT		OBSI	
Intercept	145.06	Intercept	1.48	Intercept	103.30
Wd, RKU (lvl 3, no filt)	-2.26	Rsk	-0.05	TCL (filt, tol= 0.1, d*=1E-2)	0.08
NPGZ (filt, P = 0.25)	-1.49	TCL (filt, tol= 0.1, d*=1E-5)	-0.08	MWMSR (filt, P = 0.1)	-4.27
MPMSR (filt, P = 0.1)	-177.16	Wd, RKU (lvl 3, no filt)	-0.02	Grade	0.40
MWMSR (filt, P = 0.1)	-59.33	Wd, SKU (lvl 3, no filt)	0.05		
Grade	2.19	Wd, SKU (lvl 7, no filt)	0.04		
		MPMSR (filt, P = 0.25)	-1.94		
		NPGZ (filt, P = 0.25)	-0.01		
		MWMSR (filt, P = 0.1)	-0.73		
		Grade	0.01		
Model ρ (training)	0.75		0.77		0.41
Model ρ (validation)	0.75		0.76		0.38
SCRIM Mean	79.09		0.74		102.67
SCRIM St Dev	6.76		0.07		0.96
Model RMSE (training)	4.52		0.05		0.88
Model RMSE (validation)	4.48		0.05		0.89

The use of multiple regression increased Pearson Correlation Coefficients by 10 – 20% for random-textured pavements when compared to single-variable regression analysis. The friction-related predicted values (SCRIM and GT) both included the peak-related predictors of NPGZ, MPMSR, and the kurtosis of the details of a Haar wavelet transform as common predictors. The GT data benefited from taking into account the tire's interaction with the surface in the for of TCL. The noise-related parameter of OASPL as measured by OBSI included the peak-related parameter dealing with the ratio of Mean Peak with and Mean peak Spacing (MWMSR) and the influence of the deformed tire into the pavement surface (TCL). Each of the predicted parameters benefitted from including the road geometry measure of grade. The ρ and RMSEs of the training and validation sets were very close to one another, indicating good cross-validation of the model.

Table 7-7 - Summary of Model Coefficients, ρ, and RMSE values - Transverse Texture

SCRIM		GT		OBSI	
Intercept	71.54	Intercept	1.06	Intercept	101.22
Wd, R_{KU} (lvl 4, no filt)	0.68	TCL (filt, tol= 0.1, d*=1E-5)	0.09	TCL (filt, tol= 0.1, d*=1E-3)	-0.81
Wd, R_{KU} (lvl 10, no filt)	1.84	EAWE (filt, d*=1E-2)	0.0002	Wd, R_{SK} (lvl 4, no filt)	-1.01
Wd, R_{SK} (lvl 1, no filt)	-1.50	MWMSR (filt, P = 0.25)	0.001	MWMSR (filt, P = 0.25)	3.44
MWGZ (filt, P = 0.1)	0.41	MWGZ (filt, P = 0.25)	-0.47	Grade	0.08
Grade	-0.30	Crossfall	0.01	Crossfall	-0.19
Curvature	545.10	Curvature	-10.72		
Model ρ (training)	0.31		0.69		0.53
Model ρ (validation)	0.31		0.65		0.59
SCRIM Mean	81.02		0.74		104.13
SCRIM St Dev	2.75		0.04		1.11
Model RMSE (training)	2.64		0.03		0.94
Model RMSE (validation)	2.64		0.03		0.97

Prediction of SCRIM and noise (OASPL) data measured by the OBSI proved again to be difficult on transversely-texture pavements. Pearson Correlation Coefficients increased dramatically compared to single-variable regression coefficients, however, ρ still remains at or below 0.5 for these two parameters. Prediction of GT from a pavement surface profile (as measured by ρ) rose by 35% when compared to single-variable regression. Taking tire envelopment (TCL and EAWE) into account and aggregate width and separation information resulted in higher ρfor transversely textured pavements. Road geometry information such as grade, cross fall, and curvature were also found to be significant in the model. RMSEs and correlation coefficients of the training and validation sets were very close to one another, indicating good cross-validation of the model.

Aggregation of predictor variables

Inclusion of multiple parameters to describe a pavement's macrotexture resulted in an appreciable increase in the ability to predict all three predictor variables (SCRIM, GT and OBSI). These models were built and validated on one-meter data taken from the Virginia Smart Road. 100mm pavement macrotexture parameters were aggregated to one-meter data via arithmetic mean to match the minimum reporting length of the devices to be predicted. However, most state transportation officials do not store or analyze data based on one-meter data. Linear referencing and required storage space for the data begin to become problematic for tens of thousands of kilometers of road data. Furthermore, roads are not managed on a meter-by meter

basis. It would be rare for a project to be initiated based on a single one-meter variable and road projects are always carried out on a much larger scale, not through the replacement of a single meter of pavement.

Therefore, it is of particular interest to aggregate the data (predicted and predictor variables) in this experiment to test the models developed. Predicted and predictor variables were aggregated by taking arithmetic means of the data to arrive at data at 1, 3, 10, and 20m intervals. The proposed multivariable linear models were then applied to the aggregated datasets of predictor variables and correlations coefficients were calculated on the predicted variables for the SCRIM, GT, and OBSI. Results of this aggregation are given in Table 7-8 and Table 7-9.

Table 7-8 - Summary model performance, various distance aggregations - random texture

		1m	3m	10m	20m
SCRIM	*Model ρ*	0.75	0.79	0.84	0.86
	Model RMSE	4.52	4.10	3.65	3.45
	SCRIM Mean	79.09	79.11	79.06	79.17
GT	*Model ρ*	0.76	0.79	0.88	0.94
	Model RMSE	0.05	0.04	0.03	0.03
	GT Mean	0.74	0.74	0.74	0.74
OBSI	*Model ρ*	0.41	0.47	0.55	0.58
	Model RMSE	0.88	0.76	0.64	0.60
	OASPL Mean	102.67	102.68	102.68	102.68

Table 7-9 - Summary model performance, various distance aggregations - transverse texture

		1m	3m	10m	20m
SCRIM	*Model ρ*	0.29	0.39	0.45	0.54
	Model RMSE	2.63	2.01	1.74	1.54
	SCRIM Mean	81.02	81.02	81.01	81.07
GT	*Model ρ*	0.66	0.73	0.80	0.88
	Model RMSE	0.03	0.03	0.02	0.02
	GT Mean	0.74	0.74	0.74	0.74
OBSI	*Model ρ*	0.54	0.60	0.70	0.76
	Model RMSE	0.94	0.81	0.65	0.58
	OASPL Mean	104.12	104.12	104.12	104.11

The data presented in Table 7-8 and Table 7-9 represent the correlation coefficients and RMSE to SCRIM, GT and OASPL measured by OBSI that agencies can expect if the models proposed in Table 7-6 and Table 7-7 are employed at the reporting interval maintained by the

agency for their road profile data. Note, these values (as is the case for all presented in this work) apply for road networks comprised of pavement surfaces similar to those represented in this experiment. In general, all correlation coefficients improve with greater aggregated distance data. This is because local changes in macrotexture on smaller scales are attenuated by surrounding values in the aggregation process. The Root Mean Square Error values decrease with larger aggregations for SCRIM and OBSI, values remain essentially constant for the GT. This disparity may be explained by the relatively large scale of SCRIM and OBSI values which are two orders of magnitude larger than GT values.

Findings

- The top-10 single-variable predictor parameters for random, transverse, and longitudinally-textured pavements all outperformed the most commonly used predictor parameters of MPD and RMS.
- For randomly-textured pavement (i.e., asphalt), the best single-variable predictors of friction (as measured by the SCRIM and GT) the are those that account for the tire's enveloped profile (i.e., EAWE and TCL) and the PLR which is a measure of how much texture is provided by the pavement in comparison to a perfectly smooth surface.
    - The maximum Pearson Correlation Coefficient for randomly-textured pavements for the SCRIM and GT were 0.64 and 0.69, respectively.
    - It should be noted that the correlation coefficient between the SCRIM and GT (two devices that measure friction in a similar way) is 0.8. It is reasonable to assume any single predictor variable taken from a road profile should have a correlation coefficient lower than this.
- For transversely-textured pavements, SCRIM and OBSI correlations were low but outperformed the common measures of MPD and RMS. Two parameters had correlation coefficients greater than 0.5 for the GT, these parameters were derived in part by first producing an enveloped tire profile over the particular pavement evaluated and then characterizing the free space below this enveloped profile in the case of EAWE or the proportion of pavement in contact with the tire in the case of TCL.
- For randomly-textured surfaces, the use of multiple regression increased Pearson Correlation Coefficients by 10 – 20% when compared to single-variable regression analysis.

    - GT and SCRIM data were better predicted when including both peak (including NPGZ and MPMSR) and kurtosis of the details of a Haar wavelet transform as common predictors. The GT data benefited from taking into account the tire's interaction with the surface in the for of TCL.
    - The noise-related parameter of OASPL as measured by OBSI included the peak-related parameter dealing with the ratio of Mean Peak with and Mean peak Spacing (MWMSR) and the influence of the deformed tire into the pavement surface (TCL).
    - Each of the predicted parameters benefitted from including the road geometry measure of grade.
    - Correlation coefficients and RMSEs of the training and validation sets were very close to one another, indicating good cross-validation of the model.
- Improvement were made in the prediction of SCRIM and noise (OASPL) data measured by the OBSI via multiple linear regression, however, correlation coefficients still remain at or below 0.5 for these two parameters. Prediction of GT from a pavement surface profile (as measured by correlation coefficients) rose by 35% when compared to single-variable regression. Taking tire envelopment (TCL and EAWE) into account and aggregate width and separation information resulted in higher correlation coefficients for transversely textured pavements when compared to any single-variable model. Road geometry information such as grade, cross fall, and curvature were also found to be significant in the multiple linear regression models. correlation coefficients and RMSEs of the training and validation sets were very close to one another, indicating good cross-validation of the model.
- Aggregation of pavement macrotexture data into longer reporting lengths is favorable for both the confidence in model coefficients and effective management of road networks.

Conclusions

The de facto standards for macrotexture measurement of MPD and RMS can be improved upon for better predictions of wet weather friction and pavement noise. A variety of existing and newly-developed macrotexture parameters were shown to outperform these two standards in single-variable linear regression models for randomly-texture and transverse-textured pavements. Little improvement was found over MPD or RMS for noise levels measured in OASPL by OBSI. Correlation coefficients improved by using multiple linear regression (care

was taken to avoid multicollinearity by controlling the VIF). All models were formed using one-meter datasets, correlations improved on all fronts when data was aggregated to larger reporting distances. Agencies should consider further investigation of these new parameters and the use of larger reporting distances for their pavement management systems.

Future Research

The conclusions made above apply to the road surfaces tested in this experiment. The Virginia Smart Road has relatively high friction and low traffic. Subsequent testing can be accomplished on diverse road surfaces in other locations using the analysis method and parameters outlined in this work.

Acknowledgements

The authors wish to extend our heartfelt appreciation to the Virginia Tech Department of Mechanical Engineering for their data analysis of OBSI with tire tread cancelling optical sensor. Also, many thanks go out to Austin Cole and Danni Lu of the Virginia Tech Statistical Applications and Innovations Group for their guidance in using the statistical approaches used in this work.

References

ASME B46.1 (2009). "Surface Texture (Surface Roughness, Waviness, and Lay)." The American Society of Mechanical Engineers.

ASTM E1845 (2015). "Standard Practice for Calculating Pavement Macrotexture Mean Profile Depth." ASTM International.

Chou, C.-P., Lee, C.-C., Chen, A.-C., and Wu, C.-Y. (2017). "Using a constructive pavement texture index for skid resistance screening." *International Journal of Pavement Research and Technology*, 10(4), 360-368.

Clapp, T. G. (1983). *Spectral correlation of the surface profile in the development of a tire and pavement interaction force model*.

Descornet, G. "The HERMES project." *Proc., Symposium on Pavement Surface Characteristics [of Roads and Airports], 5th, 2004, Toronto, Ontario, Canada*.

Descornet, G., Faure, B., Hamet, J., Kestemont, X., Luminari, M., Quaresma, L., and Sandulli, D. (2000). "Traffic noise and road surfaces: state of the art." *Belgian Road Research Centre, Brussels*.

Federal Highway Administration, R. W. M. P. (2018). "How Do Weather Events Impact Roads?"Washington, DC.

Feng, J. (2017). "Separation of tread-pattern noise in tire-pavement interaction noise." Virginia Tech.

Ferne, B. (2015). "UK experiences on pavement texture measurement and interpretation." *Transportation Research Circular*, International Experience and Perspective of Pavement Texture Measurements and Evaluation(E-C216), 26-41.
Flintsch, G. W., McGhee, K., de León Izeppi, E., and Najafi, S. (2012). "The little book of tire pavement friction." *Pavement Surface Properties Consortium*.
Goubert, L. "Road Surface Texture and Traffic Noise." *Proc., NPRA workshop Texture and Road traffic noise*.
Goubert, L., and Sandberg, U. "Enveloping texture profiles for better modelling of the rolling resistance and acoustic qualities of road pavements." 12p.
Haider, M., Conter, M., Wehr, R., Sandberg, U., and Anfosso, F. "Project ROSANNE: Rolling resistance, Skid resistance, and Noise Emission measurement standards for road surfaces." *Proc., Proc. Internoise*.
Hair, J. F., Ringle, C. M., and Sarstedt, M. (2011). "PLS-SEM: Indeed a silver bullet." *Journal of Marketing theory and Practice*, 19(2), 139-152.
Hall, J. W., Smith, K. L., Titus-Glover, L., Wambold, J. C., Yager, T. J., and Rado, Z. (2009). "Guide for Pavement Friction." 257p.
ISO 4287 (1997). "Geometrical Product Specifications (GPS) -- Surface texture: Profile method -- Terms, definitions and surface texture parameters."
ISO 4288 (1996). "Geometrical Product Specifications (GPS) -- Surface texture: Profile method -- Rules and procedures for the assessment of surface texture." International Organization for Standardization, 8.
ISO 13473-1 (1997). "Characterization of pavement texture by use of surface profiles - Part 1: Determination of Mean Profile Depth." *Part 1: Determination of Mean Profile Depth*, International Organization for Standardization.
ISO 13473-2 (2002). "Characterization of pavement texture by use of surface profiles - Part 2: Terminology and basic requirements related to pavement texture profile analysis." *Part 2: Terminology and basic requirements related to pavement texture profile analysis*, International Organization for Standardization.
Katicha, S. W., Mogrovejo, D. E., Flintsch, G. W., and Izeppi, E. D. d. L. (2015). "Adaptive Spike Removal Method for High-Speed Pavement Macrotexture Measurements by Controlling the False Discovery Rate." *Transportation Research Record: Journal of the Transportation Research Board*(2525), pp 100–110.
Klein, P., Hamet, J., and Anfosso-Ledee, F. "An envelopment procedure for tire-road contact." 10p.
Leandri, P., and Losa, M. (2015). "Peak Friction Prediction Model Based on Surface Texture Characteristics." *Transportation Research Record: Journal of the Transportation Research Board*(2525), pp 91–99.
Mathworks, T. 2016. Find Peaks, version Copyright 2007-2016 The MathWorks, Inc.
Mogrovejo, D. E., Flintsch, G. W., Katicha, S. W., de León Izeppi, E. D., and McGhee, K. K. (2016). "Enhancing Pavement Surface Macrotexture Characterization by Using the Effective Area for Water Evacuation." *Transportation Research Record: Journal of the Transportation Research Board*(2591), pp 80–93.
Parry, A., and Viner, H. (2005). "Accidents And The Skidding Resistance Standard For Strategic Roads In England." *TRL report*, TRL Limited, Wokingham, Berkshire, UK.
PIARC (2016). "Road Dictionary." <http://www.piarc.org/en/Terminology-Dictionaries-Road-Transport-Roads/>. (16 December 2016).

Roe, P. G., Parry, A. R., and Viner, H. E. (1998). "High and low speed skidding resistance: the influence of texture depth." TRL Limited, Crowthorne, Berkshire, U.K., 22p.
Sandberg, U., Bergiers, A., Ejsmont, J. A., Goubert, L., Karlsson, R., and Zöller, M. (2011). "Road surface influence on tyre/road rolling resistance." *Models for Rolling Resistance in Road Infrastructure Asset Management Systems (MIRIAM),(http://miriam-co2. net/Publications/MIRIAM_SP1_Road-Surf-Infl_Report*, 20111231.
Sandberg, U., and Descornet, G. "ROAD SURFACE INFLUENCE ON TIRE/ROAD NOISE--1." *Proc., Proceedings of the International Conference Noise Control Engineering, Noise Control for the 80's, Inter-Noise 80, Vol. 1, Miami, Florida, December 8-10, 1980.*
Scharnigg, K., Schwalbe, G., and Haider, M. "TYROSAFE: tyre and road surface optimisation for skid resistance and further effects." 14p.
Sohaney, R. C., and Rasmussen, R. O. (2013). "Pavement Texture Evaluation and Relationships to Rolling Resistance at MnROAD." Department of Transportation, Research Services Section.
The Highways Agency (1999). "Design Manual For Roads and Bridges." *Volume 7 - Pavement Design and Maintenance*, The Highways Agency, 623.
Tibshirani, R. (1996). "Regression shrinkage and selection via the lasso." *Journal of the Royal Statistical Society. Series B (Methodological)*, 267-288.
Von Meier, A., Van Blokland, G., and Descornet, G. "The influence of texture and sound absorption on the noise of porous road surfaces." *Proc., Second International Symposium on Road Surface Characteristics, Berlin*.
Wambold, J., Antle, C., Henry, J., Rado, Z., Descornet, G., Sandberg, U., Gothié, M., and Huschek, S. (1995). "International PIARC Experiment to Compare and Harmonize Skid Resistance and Texture Measurements (Paris: PIARC) Publication n 01.04." PIARC, Paris, France.
Wambold, J. C., Henry, J. J., Transport, C., and Incorporated, C. (2002). "NASA WALLOPS TIRE/RUNWAY FRICTION WORKSHOPS: 1993-2002." 155 p.
Weir, D., Strange, J., and Heffley, R. (1978). "Reduction Of Adverse Aerodynamic Effects Of Large Trucks Volume I: Technical Report."
Wennink, M., and Gerritsen, W. "Detection of changes of pavement texture material recognition." *Proc., International symposium on pavement surface characteristics of roads and airfields*, 153-162.
Yager, T. J. (2005). "An Overview of the Annual NASA Tire/Runway Friction Workshop and Lessons Learned."
Zelelew, H., Papagiannakis, A., and de León Izeppi, E. (2013). "Pavement macro-texture analysis using wavelets." *International Journal of Pavement Engineering*, 14(8), 725-735.

CHAPTER 8 - SUMMARY, FINDINGS, CONCLUSIONS, AND RECOMMENDATIONS

This work sought to enable widespread collection, preparation, processing, and use of network-level macrotexture data. This data can then, in turn be used by agencies for project-level decision making and overall pavement network management. This was done through several experiments that collected data in both laboratory and field environments. The results of these experiments and the procedures used to obtain the data used are detailed in the manuscripts within this work.

To do so, a cradle-to-grave approach was used that can be followed by an agency to effectively manage their road network. To start, proper equipment must be obtained to gather the raw data necessary for further analysis. A framework was laid out to compare candidate device (either initial purchases or to compare against legacy equipment) repeatability and a limits of agreement approach to compare against any other device. Both single-spot and line lasers (that gather profile data along the length and width of the road) were evaluated. Next, agencies are presented with recommendations for creation of reference surfaces and a methodology to test the accuracy of their new or in-service equipment. Data processing begins with removing outliers to ensure the device does not poison the well and erroneously affect pavement management decisions throughout the lifecycle. These errors could be either overly-conservative, increasing expenditures on unneeded maintenance and rehabilitation projects or true surface problems could be overlooked, risking lives. A new statistical method of outlier removal is presented for 3-D datasets, an emerging technology that shows great promise in the field. Once proper data streams are secured from the field, a model is presented for pavement managers to use to predict pavement macrotexture throughout the lifecycle of the pavement. This was accomplished using an accelerated pavement testing device on an asphalt-rich pavement surface. Finally, a suite of existing and novel macrotexture characterization parameters is used with friction and noise data to develop models for the prediction of these important pavement surface characteristics. Many parameters were found that improve upon the results obtained by the current de facto standards of MPD and RMS. These macrotexture parameters can be used by engineers and traffic safety professionals to effectively manage their pavement network.

Findings

The salient findings from the various work described above are summarized below:

- High-speed macrotexture measurement devices tested were shown to have repeatability coefficients ranging from 0.063 to 0.088mm. Measurements made on the same pavements by the same device will differ by no more than this coefficient. This holds true on 95% of occasions.
- High-speed devices tested at the Virginia Smart Road agreed well with one another except for comparisons between single-spot and line lasers.
    - Agreement improved when pavements were grouped based on their predominant texture direction (random, transverse, or longitudinal).
    - Poor agreement between SSL and LL is not necessarily a negative result, given the different measurement approaches.
- Speed and acceleration were shown to be insignificant in MPD results for single spot lasers when devices are operated in their normal range. Testing need not be re-accomplished due to the occurrence of these phenomena during network testing.
    - Speed was found to be a significant effect on calculation of MPD for two devices tested.
    - Raw data profiles showed a "smoothing" of signals with increased speed.
    - Longer sensor exposure times were found to be the cause.
- Acceleration was found to be a significant factor for the line laser device tested via ANOVA. However, the range of data for this device was within the device's calculated coefficient of repeatability. It is, therefore possible acceleration is not a significant factor as the device has a low variance. This is studied further in chapter 5 of this work.
- Analysis of variance of the engineered reference surfaces indicated the mean macrotexture measurements for the majority of vehicle test speed and sensor exposure combinations were not the same.
    - The quantity of tests performed, however, result in an increased likelihood that one or more combinations will fall outside of the 0.05 significance level.
    - ANOVA indicated there is a difference in measurements but did not quantify the differences for interpretation and application of engineering judgement.

    - A comparison of differences of means between the reference device and each device tested via forest plots revealed the effect of testing conditions on the final measured values.
- Use of standard base lengths for calculation of macrotexture parameters from a reference surface can lead to erroneous results if the base length is not a multiple of the plate waveform. Base lengths of profiles should be symmetrical about a vertical axis
- Mean MPD values from a 3-D data cloud show better agreement with the reference device when the algorithm described in this work is applied.
    - The algorithm is effective with both large upward and downward outlier data points. The overall resulting MPD was always found to be lower as this is a measure of peak height and removal of erroneous deep valleys only result in a lowering of the mean signal line in proportion to the number of downward outliers removed.
    - The algorithm presented is effective in removing outliers that are either global (i.e., unique to the entire dataset analyzed) or local (i.e., an outlier within the range of normal values of the surrounding data).
- Fewer outliers were found on lighter surfaces with less aggressive texture (i.e., PCC) as the material has better reflective qualities when compared to darker surfaces such as AC or surface treatments.
- The model describing the change in macrotexture over time is applicable to rich-mix asphalt pavements prone to bleeding. Generally speaking, the pavement macrotexture decreased with increased passes. However, the macrotexture was also shown to increase in areas where severe bleeding had occurred, and binder material was built up by the tire contact area.
- The following model can be applied to predict future macrotexture levels for pavements demonstrating bleeding as a primary distress:
    - $RMS = 1.186 - 1.422\text{E-}07 \times \#\ ESALs$
    - This represents a decrease of 0.1mm for every million ESALs, which may trigger agency intervention after the application of the next million EASLs.

    - RMS was shown to be less sensitive to pavement macrotexture changes due to loading that causes severe bleeding. This is due to the artificial peaks that were created by the tire on the surface.
- Several macrotexture characterization parameters developed by the author were shown to outperform the de facto standards of MPD and RMS.
    - Correlation coefficients were improved by as much as 57% in single-variable linear regression at the 1m level.
    - No fewer than six previously published or novel parameters for each of the three predicted variables (friction as measured by SCRIM, friction as measured by GT, and the noise measurement of OASPL as measured by OBSI) outperformed MPD and RMS for both randomly-textured and transversely-textured surfaces.
- Several correlations that account for the enveloped shape of the tire performed very well. The sign of the correlation coefficient is reversed when considering the space below a tire's enveloped profile and the proportion of the pavement surface in contact with the tire. Both were found to have higher correlations than RMS and MPD.
- The correlation coefficient between SCRIM and GT was found to be 0.8
    - Correlations between two non-identical properties, macrotexture and friction, shouldn't be expected to outperform two devices that measure the same property in a similar fashion.
    - Novel correlations between macrotexture and GT were found to be within as much as 86% of the correlation between SCRIM and GT.
- Correlations to friction and noise were improved via multiple regression. Cross validation through training and validation sets had very similar results, demonstrating the robustness of the model. Models were optimized via a LASSO analysis. Further simplifications and protections against multi-collinearity were made by screening variables according to VIF.
- Via correlations to SCRIM and GT-measured friction, it was demonstrated that the space below a tire and the proportion of tire in contact with the pavement surface have nearly equal importance.
- Correlations to friction and noise improved by 53 to 87% when data was aggregated from 1m to as much as 20m. Most road agencies don't analyze or plan on a 1m scale.

Conclusions

Below are the major conclusions of this work:

1. Single spot and line laser MPD results should not be used interchangeably when longitudinal pavement texturing is present. SSLs are not capable of adequately capturing longitudinal pavement texture when compared to line lasers.
2. Most commercial off-the-shelf macrotexture equipment are repeatable and agree well with one another if similar sensing technologies are used (i.e., single spot lasers). However, tolerances should be established based on agency needs for acceptance of a particular macrotexture measurement device.
3. Outlier data must be removed from datasets before further analysis is made. For example, including erroneous data in a model that relies on macrotexture data to predict important safety measures such as wet pavement friction will overestimate the pavement's ability to provide adequate friction. As macrotexture datasets are large (especially those in 3-D), statistical measures are more robust and efficient than other techniques. The method proposed was effective in identifying and removing outliers as confirmed by comparing results with the industry standard reference device of the CT meter.
4. Macrotexture parameters that account for the enveloped shape of the tire on the pavement's surface or that considered alternate peak information correlated better to friction and noise than MPD and RMS for random and transverse textures
    - Noise measured as OASPL by an OBSI was better predicted when using enveloped profiles as well.
    - OASPL was better predicted by pavement profile peak information data such as the RMS several levels of a Haar wavelet decomposition and the number of peaks in a base length.

Significance

A comprehensive review of the state of the art and practice of network-level macrotexture is provided. Methods are provided to evaluate candidate equipment precision, repeatability, and comparison against other or legacy equipment. These methods can be employed with or without specialized equipment. A method for removing outliers from 3-D data sets while constantly automatically updating the removal threshold based on sample size and

outlier intensity was provided. This is a critical step in ensuring equipment is providing reasonable values. Three Dimensional macrotexture equipment is the technology on the horizon of macrotexture measurement and efficient but robust means are needed to pre-process the data. Using the methods developed, agencies will be able to predict future macrotexture performance of asphalt-rich pavement surfaces. This is very useful for organizations that do not perform recurring assessments or for surfaces that are difficult to reach. Finally, several parameters are proposed that correlate better to the critical attributes of wet weather friction and pavement noise than the current standards.

Recommendations

For network-level macrotexture measurement, the following recommendations are made:

- Agencies use the proposed outlier detection method to their 3-D datasets to ensure proper profiles are used in subsequent analysis.
- The proposed device repeatability determination method should be used by agencies wishing to perform network-level macrotexture measurements.
- The proposed device comparison technique be used for organizations considering new equipment or comparing contracted results with previous results stored in pavement management systems.
- Engineered surfaces with properly prepared surfaces be used to test both single spot and line-laser equipped devices as this is a more universal test method than that of a spinning object for single spot lasers and static shapes for line lasers. The base lengths of selected plate shape for high-speed device accuracy testing should be a multiple of the waveform used to facilitate result calculation and interpretation. Use 0.1mm as the tolerance level for MPD the difference between measurements of reference and high-speed equipment. This will show if a device is capable of providing the needed information for proper investigation and intervention decision making. Filtering, if applied, should be applied to both reference and filed test results in an equivalent manner.
- High-speed devices should use the shortest exposure time practical for a given pavement surface.
- Agencies should strongly consider macrotexture parameters that account for a tire's enveloped profile (EAWE and TCL) and several novel measures of pavement peak data

that factor in peak prominence and widths as they have been shown to correlate better to wet weather friction and noise on the surfaces tested in this work than the current most prominent measures.

For future research, the following recommendations are made:

- Apply the proposed methods for outlier removal and new macrotexture parameters to an expanded set of pavement surfaces with frictional and texture surfaces not available at the Virginia Smart Road.
- Apply the model developed in this work to other surfaces mixes in an HVS or real-world traffic locations where bleeding is a major distress.
    - determine if the channelization of traffic induced by the HVS test tire caused the increase in MPD noted or if this is a phenomenon that is universal to the distress.
    - apply these findings to other channelization-based experiments as autonomous vehicles will likely decrease wheel wander widths and increase the damage due to channelization of traffic.
    - The degradation model can be improved by performing friction testing on trafficked surfaces within the HVS for correlation of the macrotexture to this critical pavement surface property.
- Expand the equipment comparison experiment to multiple vehicles equipped with line lasers as this technology becomes more prevalent.
- Redesign the smallest waveform tested on the accuracy plate to include a broad valley area between peaks to avoid erroneous measurements due to this challenging geometry. Perhaps 3-D printed references surfaces can be designed and included with standards for testing high-speed macrotexture equipment. The reproducibility and precision of the 3-D printed media should be tested before implementation.

Table of Appendices

Appendix A Virginia Smart Road Information

The Virginia Smart Road is a unique, state-of-the-art, full-scale, closed test-bed research facility managed by VTTI and owned and maintained by the Virginia Department of Transportation (VDOT). The Smart Road continues to play an important role in the overall success of the institute and its research endeavors. Transportation scientists and product developers have spent more than 20,000 hours conducting research on this high-tech highway since its opening. The Virginia Smart Road is even a FAA approved testing facility for flight!

SMART ROAD FEATURES

- A 2.2-mile, controlled-access test track built to FHWA standards
- Two paved lanes
- Three bridges, including the Smart Road Bridge (tallest state-maintained bridge in VA)
- Full-time staff that coordinate all road activities
- 24/7 access control and oversight
- Lighting and weather system controls
- Safety assurance and surveillance
- Seven roadside equipment units that facilitate connected-vehicle communications
- Two mobile roadside equipment sites
- A connected-vehicle-compatible intersection controller model
- Fourteen pavement sections, including an open-grade friction course
- In-pavement sensors (that detect such factors as moisture, temperature, strain, vibration, and weigh-in-motion)
- A zero-crown pavement section designed for flooded pavement testing
- An American Association of State Highway and Transportation Officials (AASHTO)-designated surface friction testing facility
- Seventy-five weather-making towers
- Artificial snow production of ~4 inches per hour (based on suitable weather conditions)
- Production of differing intensities of rain with varying droplet sizes
- Fog production
- Two weather stations with official NOAA weather available within one mile
- Variable pole spacing designed to replicate 95 percent of national highway systems
- Multiple luminaire heads, including light-emitting diode (LED) modules
- An optical fiber communication system
- Ethernet fiber transceivers and Ethernet switches
- A differential GPS base station for precise vehicle locating
- A signalized intersection w/ signal phase and timing (SPaT) using remote controls
- Wide shoulders for safe maneuvering during experimental testing

Virginia Smart Road - Surface Types

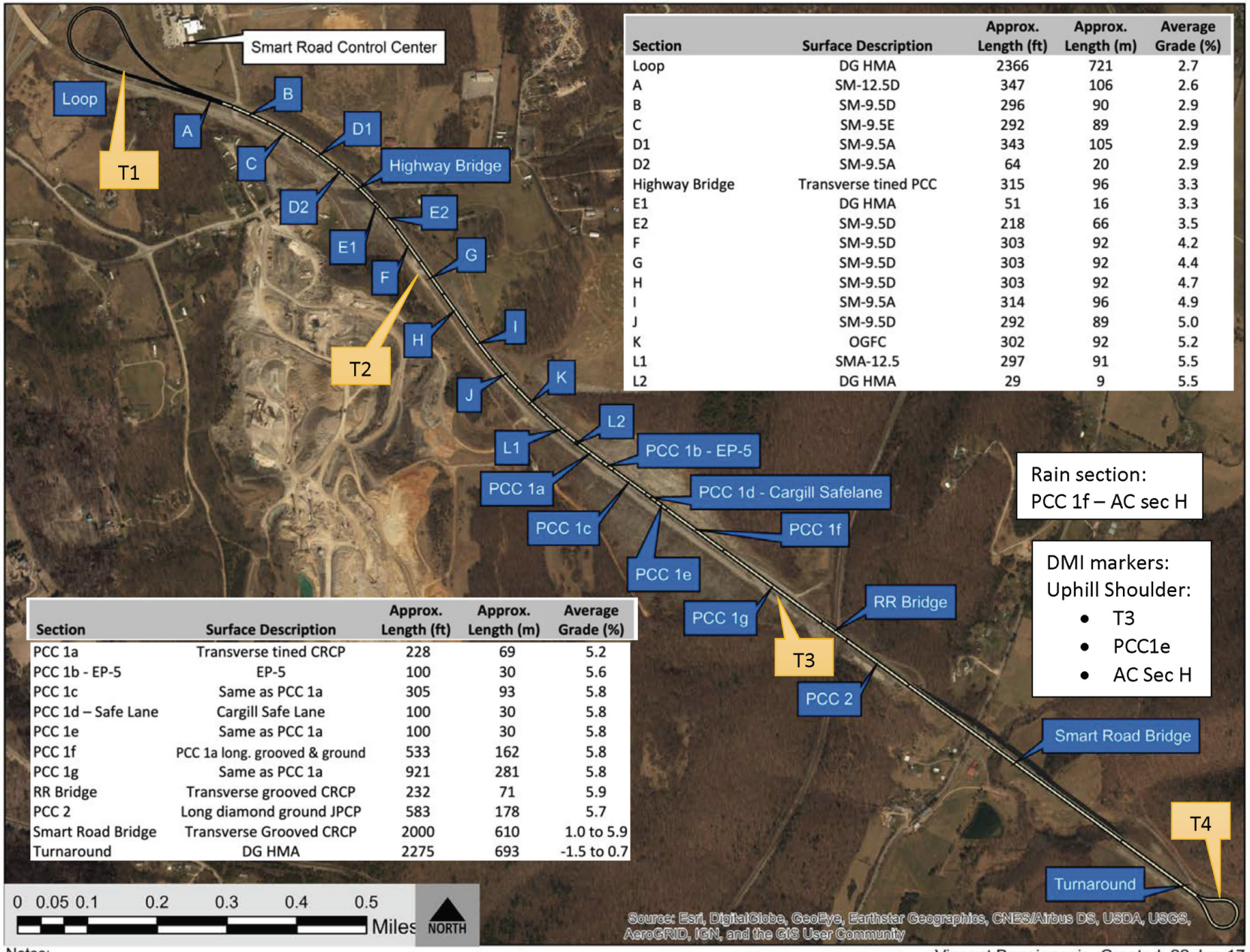

Section	Surface Description	Approx. Length (ft)	Approx. Length (m)	Average Grade (%)
Loop	DG HMA	2366	721	2.7
A	SM-12.5D	347	106	2.6
B	SM-9.5D	296	90	2.9
C	SM-9.5E	292	89	2.9
D1	SM-9.5A	343	105	2.9
D2	SM-9.5A	64	20	2.9
Highway Bridge	Transverse tined PCC	315	96	3.3
E1	DG HMA	51	16	3.3
E2	SM-9.5D	218	66	3.5
F	SM-9.5D	303	92	4.2
G	SM-9.5D	303	92	4.4
H	SM-9.5D	303	92	4.7
I	SM-9.5A	314	96	4.9
J	SM-9.5D	292	89	5.0
K	OGFC	302	92	5.2
L1	SMA-12.5	297	91	5.5
L2	DG HMA	29	9	5.5

Section	Surface Description	Approx. Length (ft)	Approx. Length (m)	Average Grade (%)
PCC 1a	Transverse tined CRCP	228	69	5.2
PCC 1b - EP-5	EP-5	100	30	5.6
PCC 1c	Same as PCC 1a	305	93	5.8
PCC 1d – Safe Lane	Cargill Safe Lane	100	30	5.8
PCC 1e	Same as PCC 1a	100	30	5.8
PCC 1f	PCC 1a long. grooved & ground	533	162	5.8
PCC 1g	Same as PCC 1a	921	281	5.8
RR Bridge	Transverse grooved CRCP	232	71	5.9
PCC 2	Long diamond ground JPCP	583	178	5.7
Smart Road Bridge	Transverse Grooved CRCP	2000	610	1.0 to 5.9
Turnaround	DG HMA	2275	693	-1.5 to 0.7

Notes:
1. Sectioning and distances are for the "uphill" direction (East to West)
2. When travelling "downhill" (West to East), Section PCC 1b is the Cargill Safelane and PCC 1d is the EP-5; PCC1f is the same surface type as PCC 1a. Downhill distances vary slightly

Vincent Bongioanni; Created: 22 Jun 17

Virginia Smart Road - Surface Types

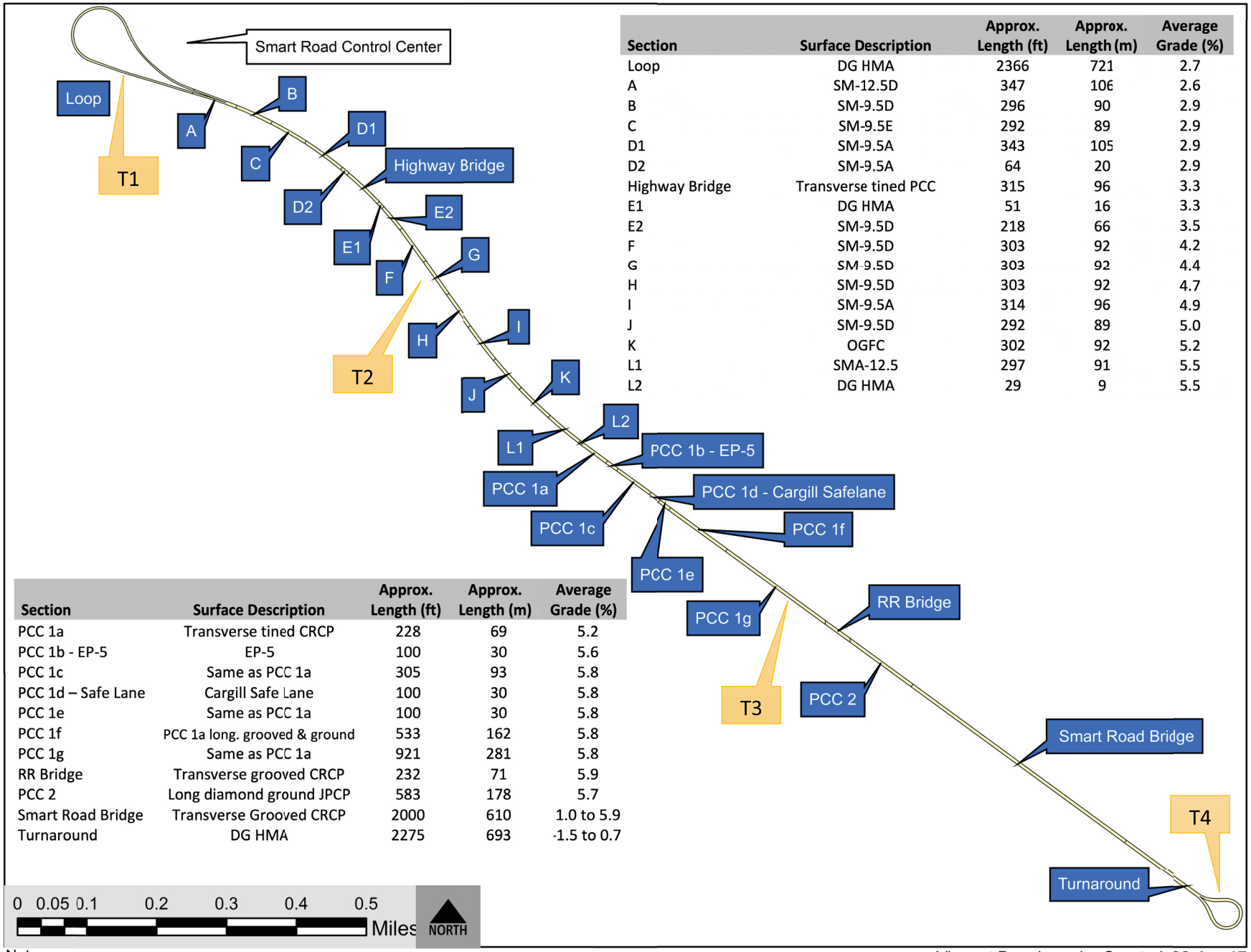

Section	Surface Description	Approx. Length (ft)	Approx. Length (m)	Average Grade (%)
Loop	DG HMA	2366	721	2.7
A	SM-12.5D	347	106	2.6
B	SM-9.5D	296	90	2.9
C	SM-9.5E	292	89	2.9
D1	SM-9.5A	343	105	2.9
D2	SM-9.5A	64	20	2.9
Highway Bridge	Transverse tined PCC	315	96	3.3
E1	DG HMA	51	16	3.3
E2	SM-9.5D	218	66	3.5
F	SM-9.5D	303	92	4.2
G	SM-9.5D	303	92	4.4
H	SM-9.5D	303	92	4.7
I	SM-9.5A	314	96	4.9
J	SM-9.5D	292	89	5.0
K	OGFC	302	92	5.2
L1	SMA-12.5	297	91	5.5
L2	DG HMA	29	9	5.5

Section	Surface Description	Approx. Length (ft)	Approx. Length (m)	Average Grade (%)
PCC 1a	Transverse tined CRCP	228	69	5.2
PCC 1b - EP-5	EP-5	100	30	5.6
PCC 1c	Same as PCC 1a	305	93	5.8
PCC 1d – Safe Lane	Cargill Safe Lane	100	30	5.8
PCC 1e	Same as PCC 1a	100	30	5.8
PCC 1f	PCC 1a long. grooved & ground	533	162	5.8
PCC 1g	Same as PCC 1a	921	281	5.8
RR Bridge	Transverse grooved CRCP	232	71	5.9
PCC 2	Long diamond ground JPCP	583	178	5.7
Smart Road Bridge	Transverse Grooved CRCP	2000	610	1.0 to 5.9
Turnaround	DG HMA	2275	693	-1.5 to 0.7

Notes:
1. Sectioning and distances are for the "uphill" direction (East to West)
2. When travelling "downhill" (West to East), Section PCC 1b is the Cargill Safelane and PCC 1d is the EP-5; PCC1f is the same surface type as PCC 1a. Downhill distances vary slightly

Vincent Bongioanni; Created: 22 Jun 17

Provided by VTTI controllers, use the following nomenclature for radio calls

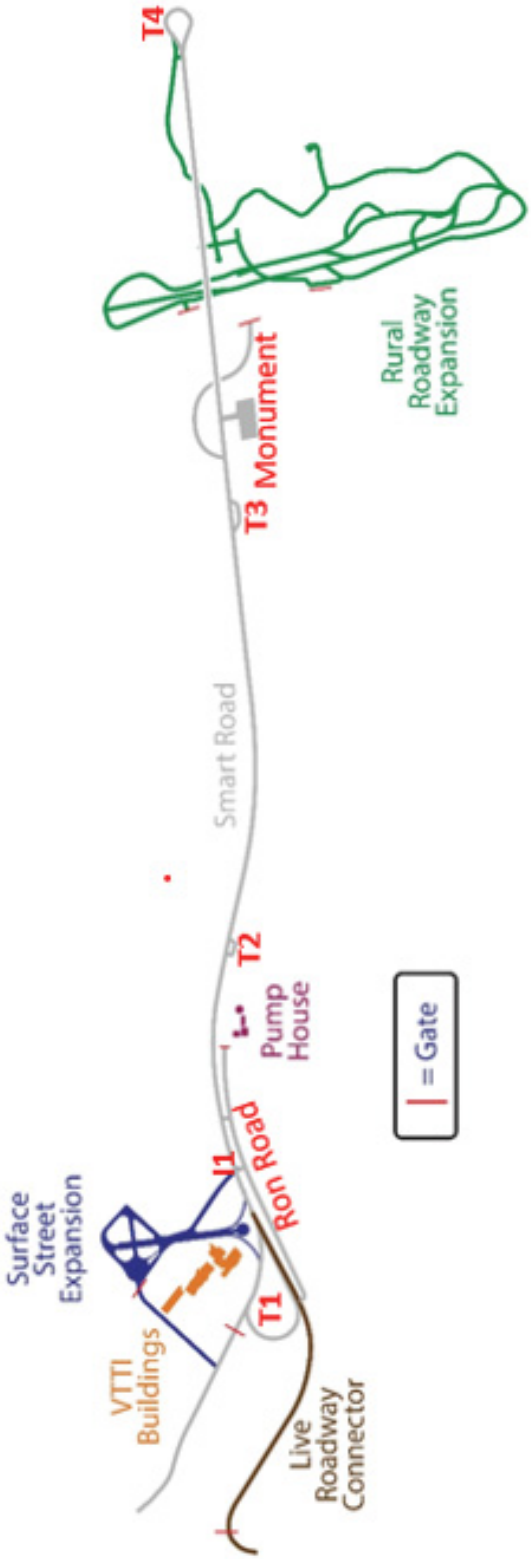

Notes:
Turnaround 1 (T1) is referred to as the “Loop” elsewhere in this document
T2 is between AC sections F and G
T3 is on PCC 1G
T4 is referred to as the “Turnaround” elsewhere in this document

Smart Road Flexible Pavement Sections

Weather Section

Rigid Pavement

A	B	C	D	E	F	G	H	I	J	K	L	CRCP
SM-12.5D (38mm)	SM-9.5D (38mm)	SM-9.5E (38mm)	SM-9.5A (38mm)	SM-9.5D (38mm)	SM-9.5D (38mm)	SM-9.5D (38mm)	SM-9.5D (38mm)	SM-9.5A* (38mm)	SM-9.5D (38mm)	OGFC (19mm) / SM-9.5D (19mm)	SMA-12.5 (38mm)	Concrete (250mm)
BM-25.0 (150mm)	BM-25.0 (150mm)	BM-25.0 (150mm)	BM-25.0 (150mm)	BM-25.0 (225mm)	BM-25.0 (150mm)	BM-25.0 (100mm) / SM-9.5A (50mm)	BM-25.0 (100mm) / SM-9.5A (50mm)	BM-25.0 (100mm) / SM-9.5A (50mm)	BM-25.0 (225mm)	BM-25.0 (225mm)	BM-25.0 (150mm)	
OGDL (75mm)	OGDL (75mm)	OGDL (75mm)	OGDL (75mm)	21A Cement Stabilized (150mm)	21A Cement Stabilized (150mm)	21A Cement Stabilized (150mm)	OGDL (75mm)	OGDL (75mm)	OGDL (75mm)	Cement OGDL (75mm)	Cement OGDL (75mm)	OGDL (75mm) / Cement OGDL (75mm)
21A Cement Stabilized (150mm)	21A Cement Stabilized (150mm)	21A Cement Stabilized (150mm)	21A Cement Stabilized (150mm)	21B (75mm)	21B (150mm)	21B (150mm)	21A Cement Stabilized (150mm)	21A Cement Stabilized (150mm)	21B (150mm)	21B (150mm)	21A Cement Stabilized (150mm)	21A Cement Stabilized (150mm)
21B (175mm)	21B (175mm)	21B (175mm)	21B (175mm)				21B (75mm)	21B (75mm)			21B (75mm)	21B (75mm)

SM-9.5A in Section I was designed with high lab compaction.
Sec. B, C, D, E, and G have woven geotextile separation barrier.
Sec. I and L have a reinforcing steel mesh.
Sec. J has a moisture barrier geocomposite membrane.
Sec. K has a stress relief geocomposite membrane.

Section	Surface Description	Approx. Length (ft)	Approx. Length (m)	Average Grade (%)
Loop	DG HMA	2366	721	2.7
A	SM-12.5D	347	106	2.6
B	SM-9.5D	296	90	2.9
C	SM-9.5E	292	89	2.9
D1	SM-9.5A	343	105	2.9
D2	SM-9.5A	64	20	2.9
Highway Bridge	Transverse tined PCC	315	96	3.3
E1	DG HMA	51	16	3.3
E2	SM-9.5D	218	66	3.5
F	SM-9.5D	303	92	4.2
G	SM-9.5D	303	92	4.4
H	SM-9.5D	303	92	4.7
I	SM-9.5A	314	96	4.9
J	SM-9.5D	292	89	5.0
K	OGFC	302	92	5.2
L1	SMA-12.5	297	91	5.5
L2	DG HMA	29	9	5.5
PCC 1a	Transverse tined CRCP	228	69	5.2
PCC 1b - EP-5	EP-5	100	30	5.6
PCC 1c	Same as PCC 1a	305	93	5.8
PCC 1d – Safe Lane	Cargill Safe Lane	100	30	5.8
PCC 1e	Same as PCC 1a	100	30	5.8
PCC 1f	PCC 1a long. grooved & ground	533	162	5.8
PCC 1g	Same as PCC 1a	921	281	5.8
RR Bridge	Transverse grooved CRCP	232	71	5.9
PCC 2	Long diamond ground JPCP	583	178	5.7
Smart Road Bridge	Transverse Grooved CRCP	2000	610	1.0 to 5.9
Turnaround	DG HMA	2275	693	-1.5 to 0.7

Section Scale for overlaying on data plots, uphill (East to West)

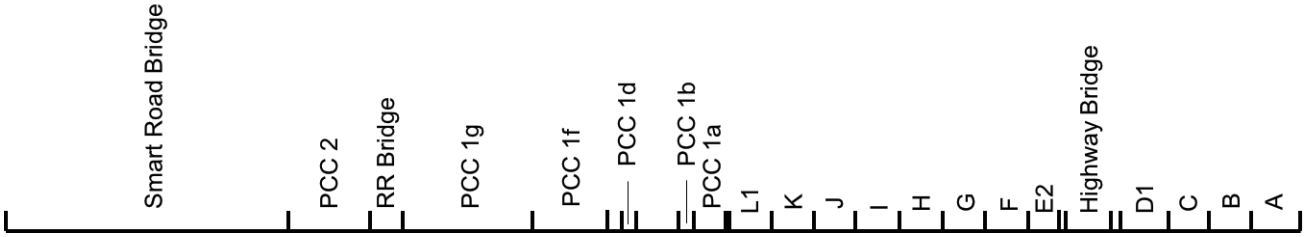

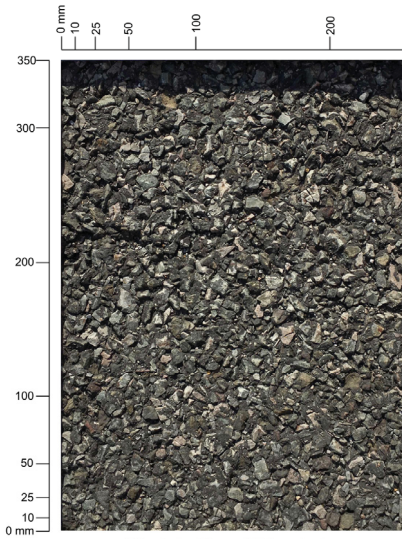

Virginia Smart Road - Loop

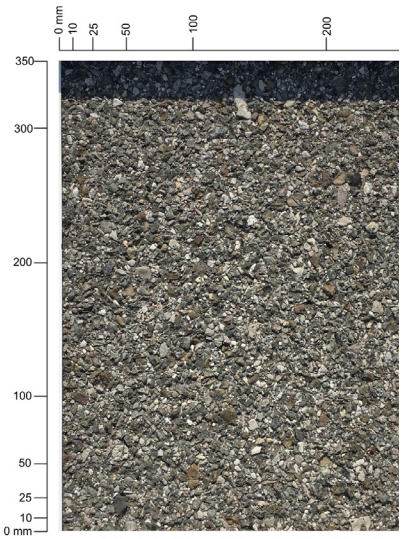

Virginia Smart Road – Section A

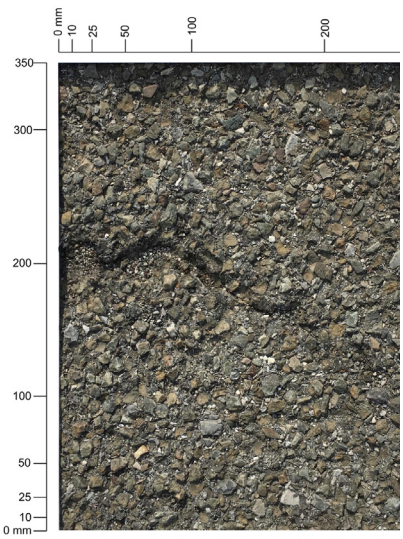

Virginia Smart Road – Section B

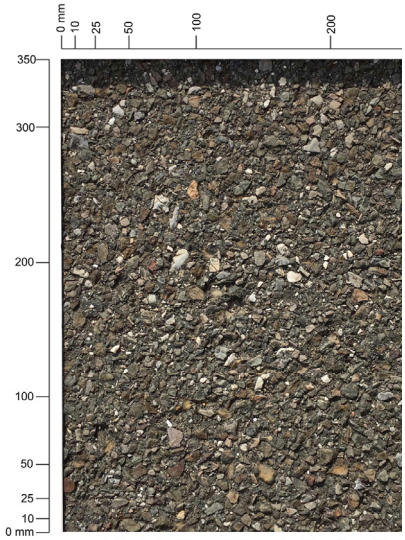

Virginia Smart Road - Section C

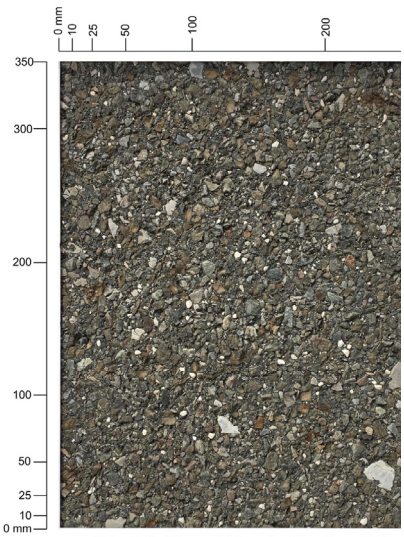

Virginia Smart Road - Section D1

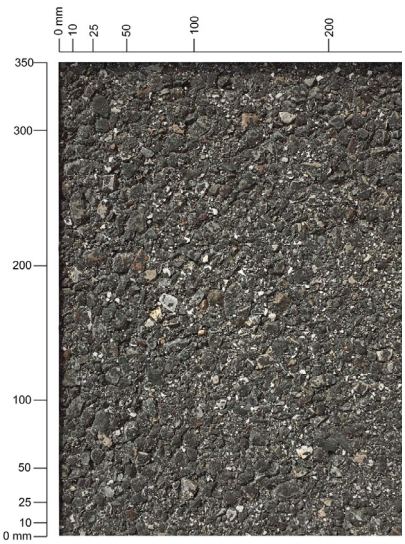

Virginia Smart Road - Section D2

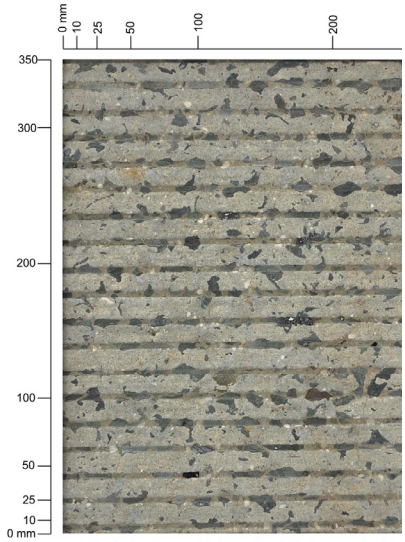

Virginia Smart Road – Highway Bridg

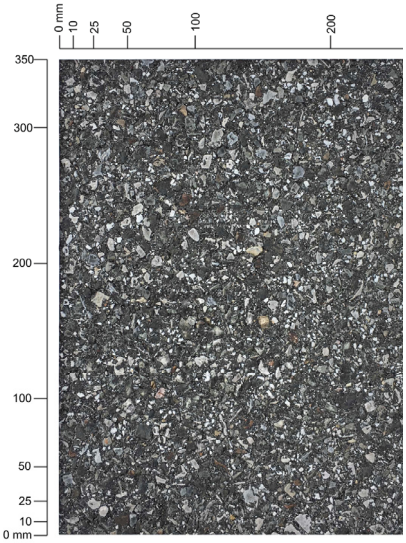

Virginia Smart Road - Section E1

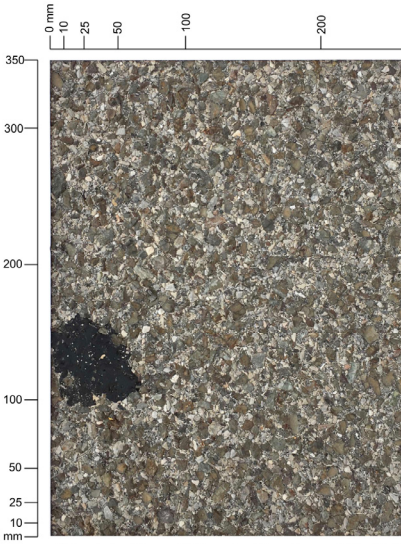

Virginia Smart Road - Sections E2, F, G and H

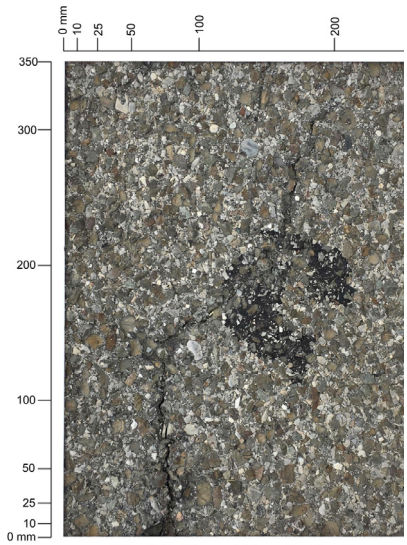

Virginia Smart Road - Section I

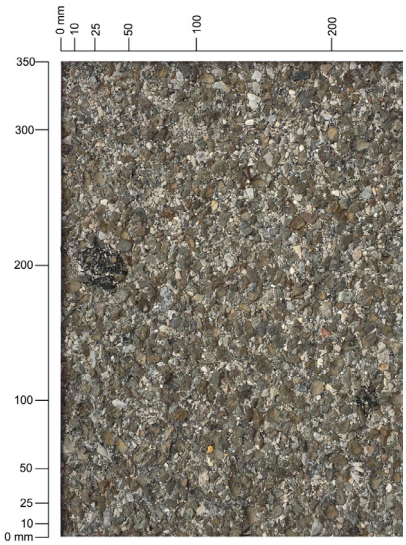

Virginia Smart Road - Section J

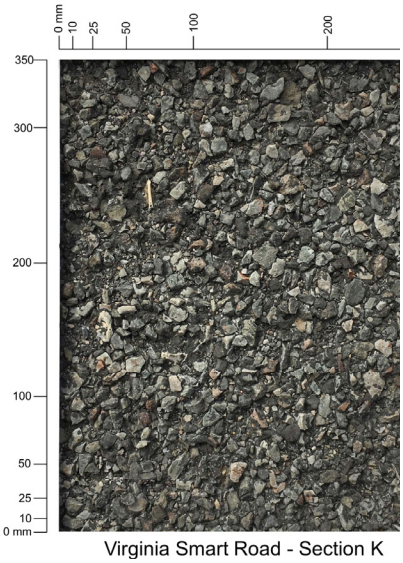

Virginia Smart Road - Section K

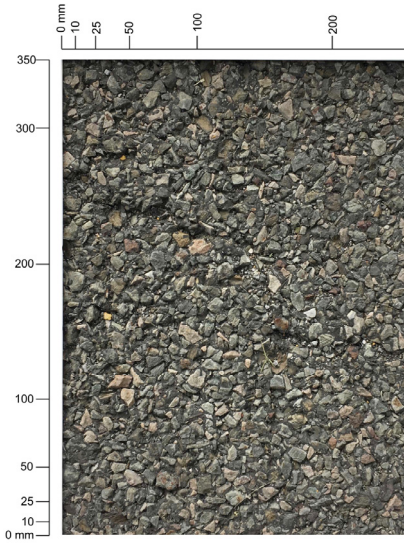

Virginia Smart Road - Section L1

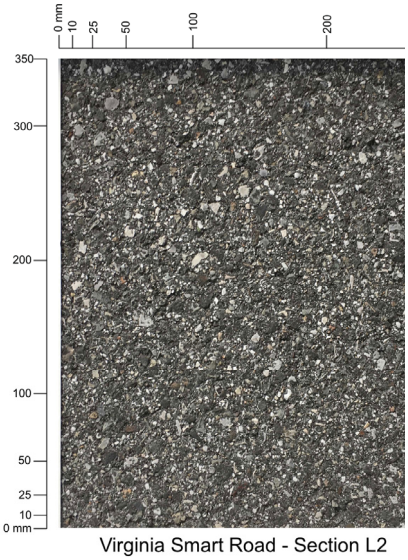

Virginia Smart Road - Section L2

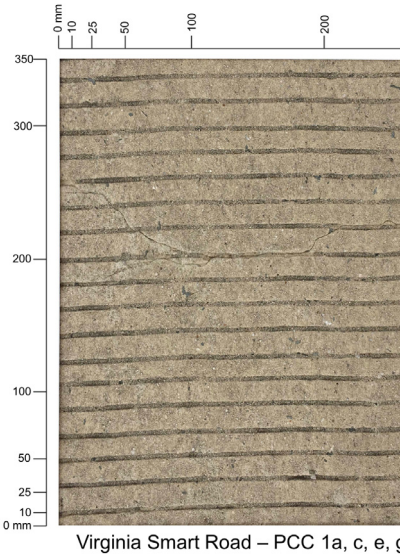

Virginia Smart Road – PCC 1a, c, e, g

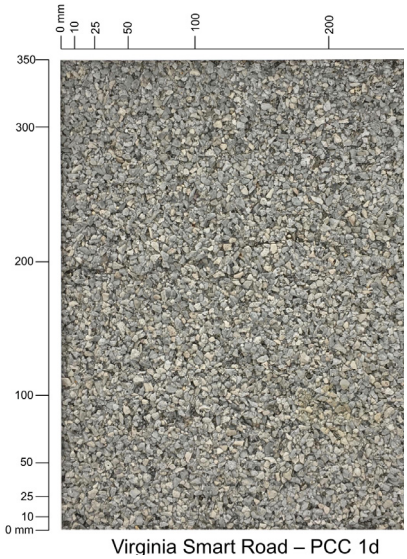

Virginia Smart Road – PCC 1d

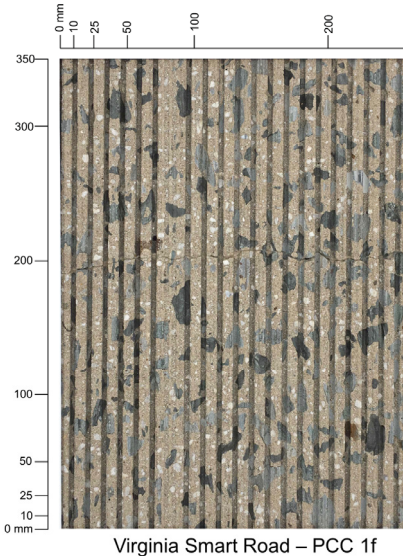

Virginia Smart Road – PCC 1f

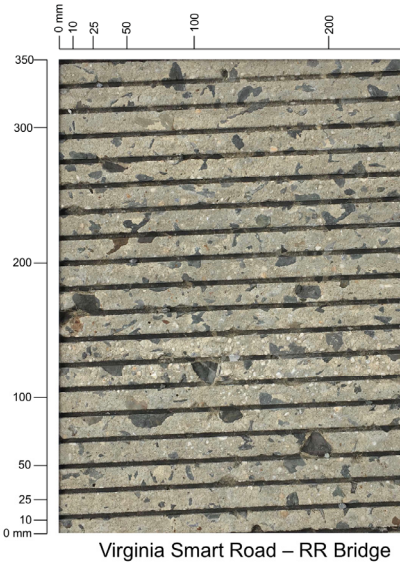

Virginia Smart Road – RR Bridge

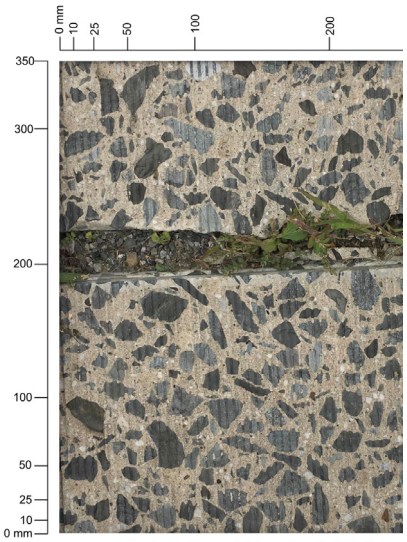

Virginia Smart Road – PCC 2

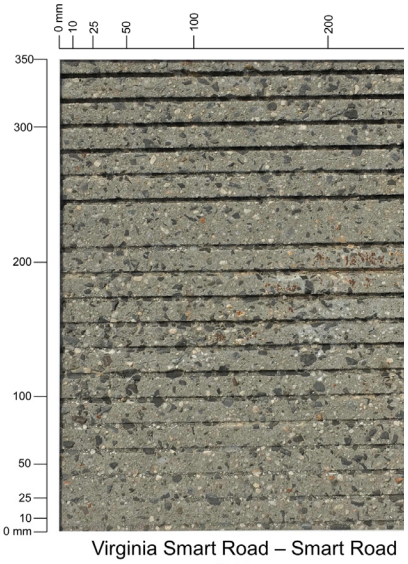

Virginia Smart Road – Smart Road Bridge

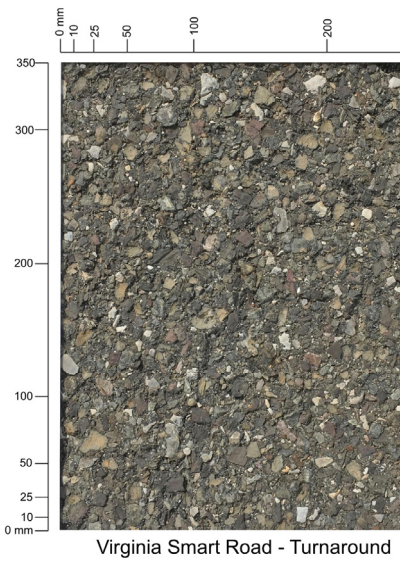

Virginia Smart Road - Turnaround

Appendix B Chapter 3 Device 1 ANOVA Data

DEVICE 1 ANOVA Tables and Figures (Produced in JMP software):
MSE from these ANOVA tables was used to produce repeatability Coefficients and device variability used in Limits of Agreement. Only 55 MPH 1m aggregated data was used in the manuscript.

HIGH SPEED REPEATABILITY

DEVICE_1_HS_55MPH_Raw_Trimmed_dsp_**MPD_1m** (Repeatability JMP Table)					
Analysis of Variance					
Source	DF	Sum of Squares	Mean Square	F Ratio	Prob > F
Model	17	17.70447	1.04144	1430.987	<.0001
Error	72	0.0524	0.00073		
C. Total	89	17.75687			
DEVICE_1_HS_55MPH_Raw_Trimmed_dsp_**MPD_0_1m** (Repeatability JMP Table)					
Analysis of Variance					
Source	DF	Sum of Squares	Mean Square	F Ratio	Prob > F
Model	17	17.70879	1.04169	1420.357	<.0001
Error	72	0.052805	0.00073		
C. Total	89	17.7616			

Comparison of .1m aggregated data vs 1m aggregated data revealed no significant difference in MSE. 1m aggregated data is used through out the rest of the analysis.

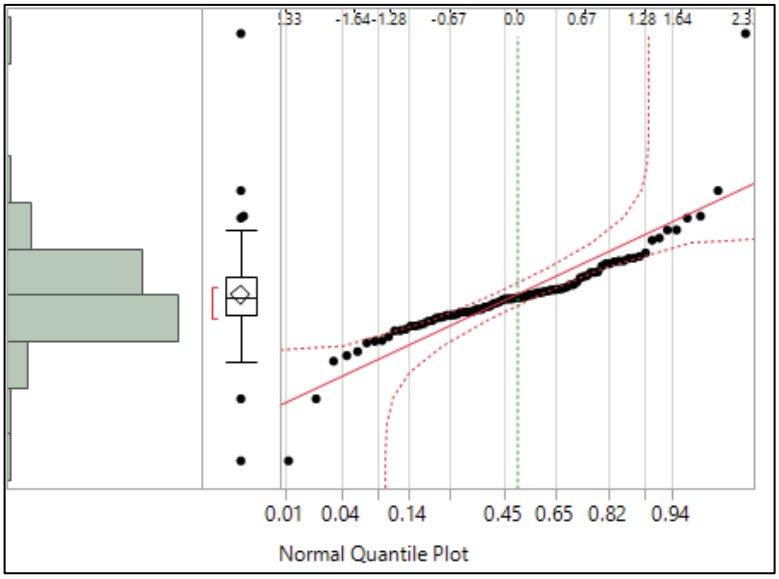

Based on Normal Quantile Plot assumptions for ANOVA are acceptably met

CONSTANT SPEED ANOVA (SECTIONS SEPARATE)
DEVICE_1_OF_CS_Raw_Trimmed_dsp_MPD_1m (ANOVA JMP Table)
Note: Speed was defined as a continuous variable in the ANOVA

L2					
Analysis of Variance					
Source	DF	Sum of Squares	Mean Square	F Ratio	Prob > F
Model	1	0.002716	0.002716	0.7844	0.3854
Error	22	0.076177	0.003463		
C. Total	23	0.078893			
Parameter Estimates					
Term	Estimate	Std Error	t Ratio	Prob>|t|	
Intercept	1.251253	0.03059	40.9	<.0001	
Speed (MPH)	0.000623	0.000703	0.89	0.3854	
Effect Tests					
Source	Nparm	DF	Sum of Squares	F Ratio	Prob > F
Speed (MPH)	1	1	0.002716	0.7844	0.3854

P-value of 0.3854 fails to reject the null hypothesis, therefore the speed had no effect on the device for asphalt section L2.

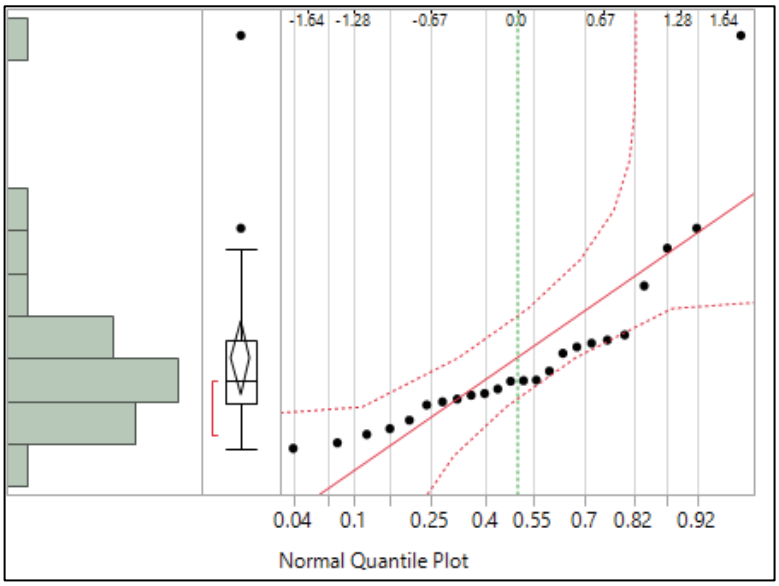

Based on Normal Quantile Plot assumptions for ANOVA are acceptably met

PCC1a					
Analysis of Variance					
Source	DF	Sum of Squares	Mean Square	F Ratio	Prob > F
Model	1	0.001355	0.001355	3.9095	0.0607
Error	22	0.007627	0.000347		
C. Total	23	0.008982			
Parameter Estimates					
Term	Estimate	Std Error	t Ratio	Prob>|t|	
Intercept	0.687302	0.009679	71.01	<.0001	
Speed (MPH)	-0.00044	0.000223	-1.98	0.0607	
Effect Tests					
Source	Nparm	DF	Sum of Squares	F Ratio	Prob > F
Speed (MPH)	1	1	0.001355	3.9095	0.0607

P-value of 0.0607 fails to reject the null hypothesis, therefore the speed had no effect on the device for section PCC1a.

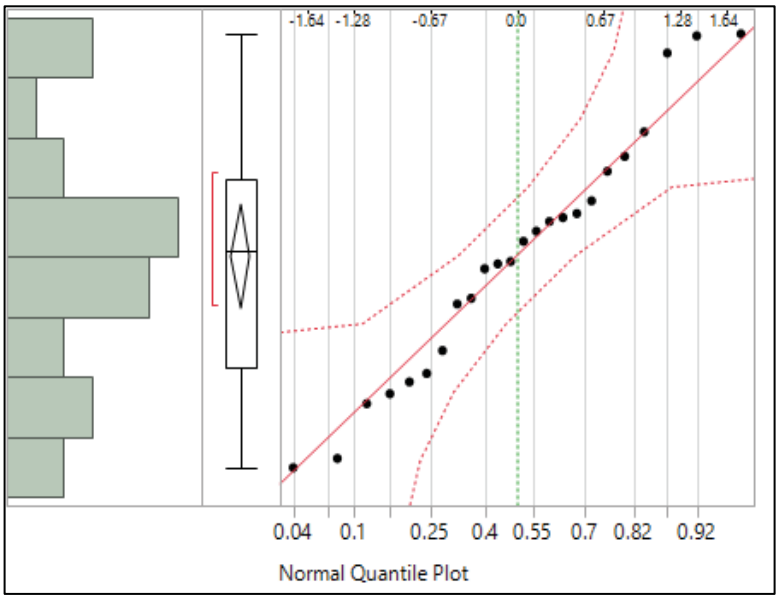

Based on Normal Quantile Plot assumptions for ANOVA are acceptably met

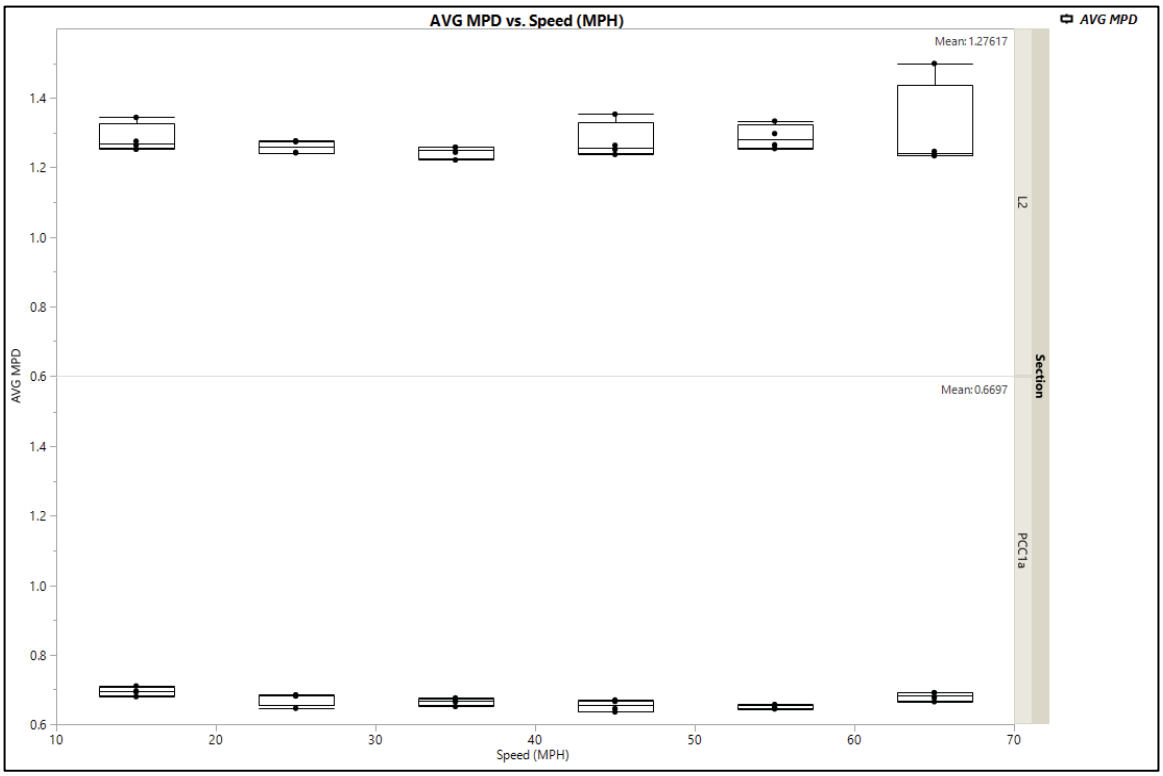

Box plots of constant speed demonstrate no effect of speed on MPD

Range of data points:

PCC1a	
max	0.710262005
min	0.635562394
diff	0.07469961
L2	
max	1.499444398
min	1.221672805
diff	0.277771594

VARIABLE SPEED ANOVA

AME_OF_VS_Raw_Trimmed_dsp_MPD_1m (ANOVA JMP Table)

Analysis of Variance					
Source	DF	Sum of Squares	Mean Square	F Ratio	Prob > F
Model	3	0.001601	0.000534	0.9095	0.4653
Error	12	0.007039	0.000587		
C. Total	15	0.00864			
Parameter Estimates					
Term	Estimate	Std Error	t Ratio	Prob>|t|	
Intercept	1.162006	0.006055	191.91	<.0001	
Speed (MPH)[25_50]	-0.00292	0.010487	-0.28	0.7858	
Speed (MPH)[50_0_50]	0.010777	0.010487	1.03	0.3244	
Speed (MPH)[50_25]	-0.01499	0.010487	-1.43	0.1784	
Effect Tests					
Source	Nparm	DF	Sum of Squares	F Ratio	Prob > F
Speed (MPH)	3	3	0.001601	0.9095	0.4653

P-value of 0.4653 fails to reject the null hypothesis, therefore the speed had no effect on the device.

Based on Normal Quantile Plot assumptions for ANOVA are acceptably met

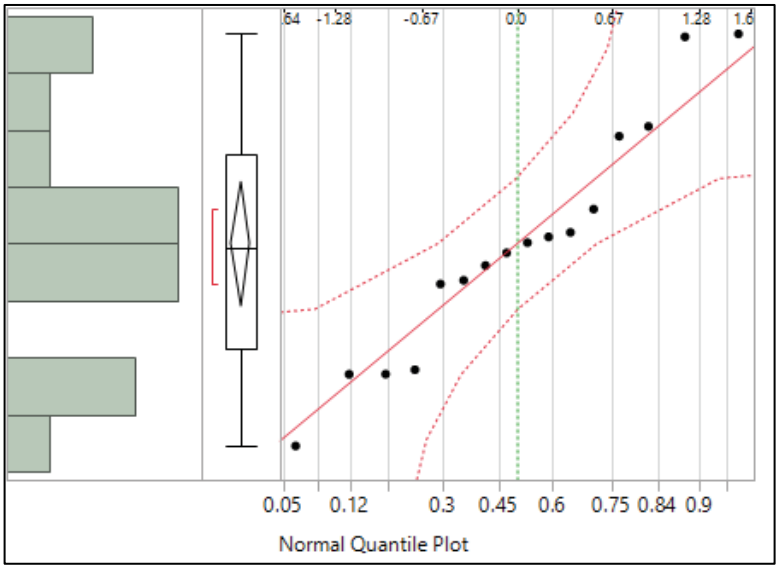

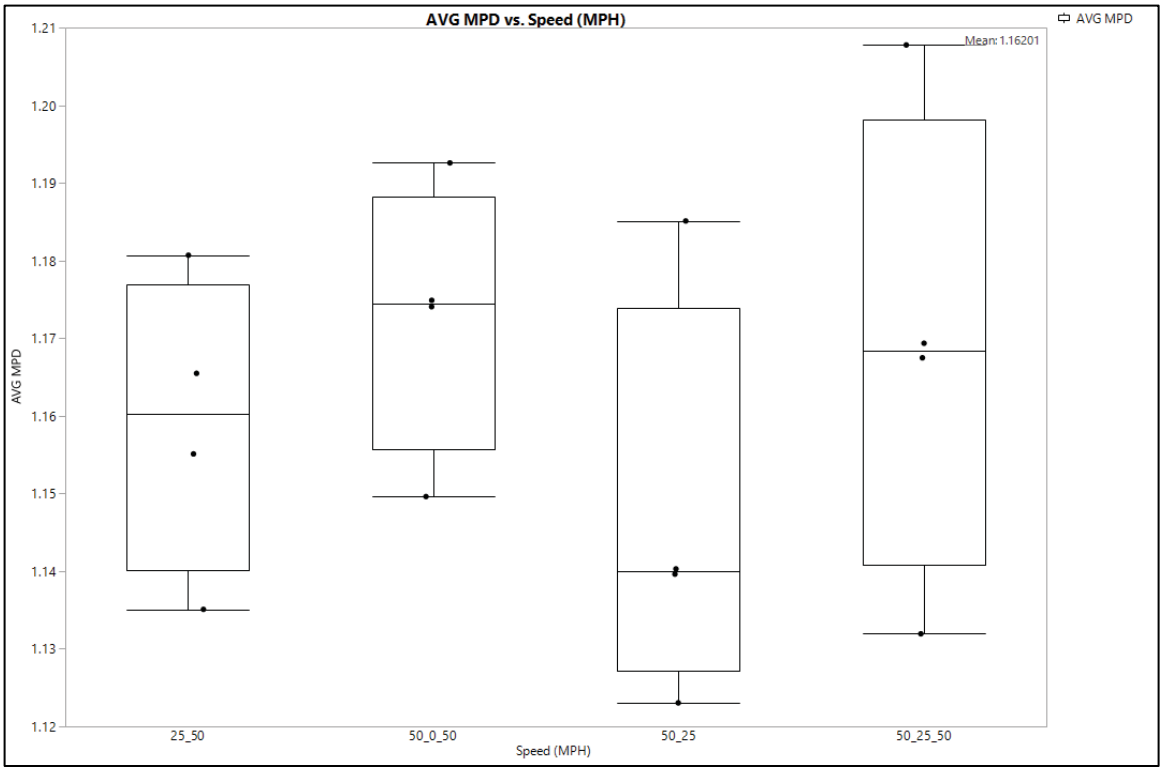

Box plots of variable speed demonstrate no effect of speed on MPD

Range of data points:

max	1.207767191
min	1.123038961
diff	0.08472823

Appendix C Chapter 3 Device 2 ANOVA Data

DEVICE 2 ANOVA Tables and Figures (Produced in JMP software):
MSE from these ANOVA tables was used to produce repeatability Coefficients and device variability used in Limits of Agreement. Only 55 MPH 1m aggregated data was used in the manuscript.

HIGH SPEED REPEATABILITY

AAR_HS_55mph_Raw_Trimmed_dsp_MPD_1m (Repeatability JMP Table)					
Analysis of Variance					
Source	DF	Sum of Squares	Mean Square	F Ratio	Prob > F
Model	17	17.55437	1.03261	1537.453	<.0001
Error	72	0.048358	0.00067		
C. Total	89	17.60273			

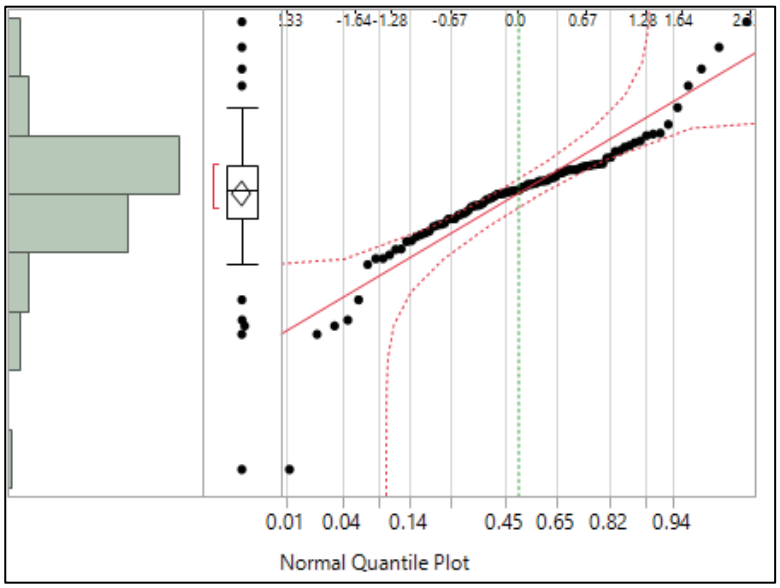

Based on Normal Quantile Plot assumptions for ANOVA are acceptably met

CONSTANT SPEED ANOVA (SECTIONS SEPARATE)
DEVICE_2_OF_CS_Raw_Trimmed_dsp_MPD_1m (ANOVA JMP Table)
Note: Speed was defined as a continuous variable in the ANOVA

L2					
Analysis of Variance					
Source	DF	Sum of Squares	Mean Square	F Ratio	Prob > F
Model	1	0.000345	0.000345	0.2884	0.5966
Error	22	0.026341	0.001197		
C. Total	23	0.026686			
Parameter Estimates					
Term	Estimate	Std Error	t Ratio	Prob>|t|	
Intercept	1.285919	0.017988	71.49	<.0001	
Speed (MPH)	-0.00022	0.000414	-0.54	0.5966	
Effect Tests					
Source	Nparm	DF	Sum of Squares	F Ratio	Prob > F
Speed (MPH)	1	1	0.000345	0.2884	0.5966

P-value of 0.5966 fails to reject the null hypothesis, therefore the speed had no effect on the device for asphalt section L2.

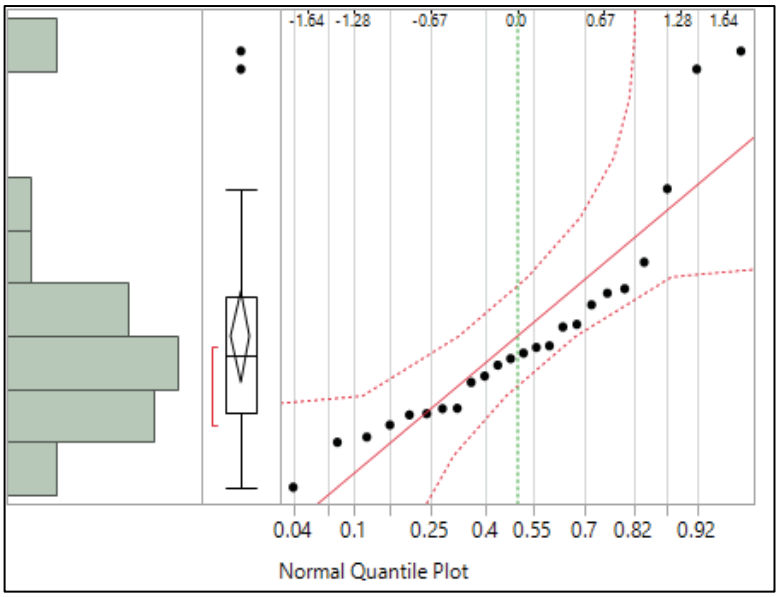

Based on Normal Quantile Plot assumptions for ANOVA are acceptably met

PCC1a					
Analysis of Variance					
Source	DF	Sum of Squares	Mean Square	F Ratio	Prob > F
Model	1	0.000439	0.000439	1.5892	0.2206
Error	22	0.006079	0.000276		
C. Total	23	0.006518			
Parameter Estimates					
Term	Estimate	Std Error	t Ratio	Prob>|t|	
Intercept	0.679175	0.008641	78.59	<.0001	
Speed (MPH)	-0.00025	0.000199	-1.26	0.2206	
Effect Tests					
Source	Nparm	DF	Sum of Squares	F Ratio	Prob > F
Speed (MPH)	1	1	0.000439	1.5892	0.2206

P-value of 0.2206 fails to reject the null hypothesis, therefore the speed had no effect on the device for section PCC1a.

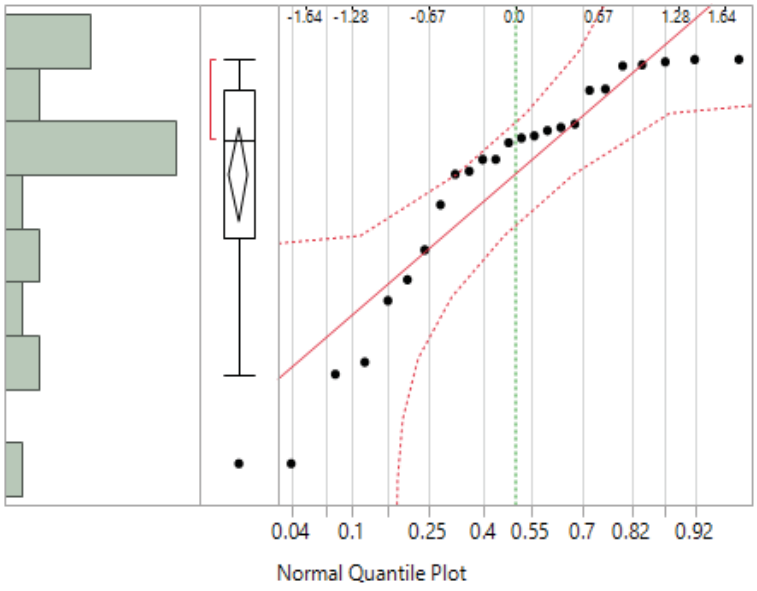

Based on Normal Quantile Plot assumptions for ANOVA are acceptably met

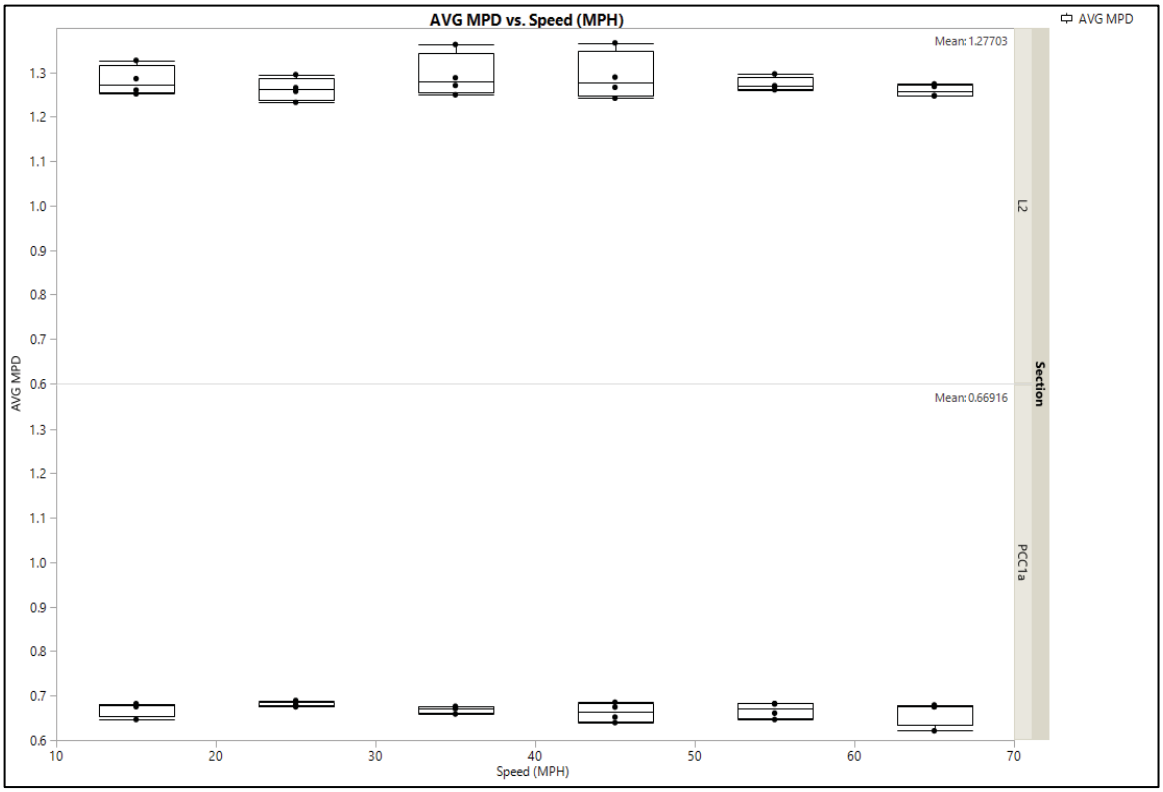

Box plots of constant speed demonstrate no effect of speed on MPD

Range of data points:

PCC1a	
max	0.68927
min	0.621116
diff	0.068154
L2	
max	1.366642
min	1.232927
diff	0.133715

VARIABLE SPEED ANOVA

DEVICE_2_OF_VS_Raw_Trimmed_dsp_MPD_1m (ANOVA JMP Table)

Analysis of Variance					
Source	DF	Sum of Squares	Mean Square	F Ratio	Prob > F
Model	3	0.000288	0.000096	0.6149	0.6184
Error	12	0.00187	0.000156		
C. Total	15	0.002158			
Parameter Estimates					

Term	Estimate	Std Error	t Ratio	Prob>|t|	
Intercept	1.180519	0.003121	378.23	<.0001	
Speed (MPH)[25_50]	-0.00316	0.005406	-0.58	0.5697	
Speed (MPH)[50_0_50]	-0.00511	0.005406	-0.94	0.3635	
Speed (MPH)[50_25]	0.003222	0.005406	0.6	0.5622	
Effect Tests					
Source	Nparm	DF	Sum of Squares	F Ratio	Prob > F
Speed (MPH)	3	3	0.000288	0.6149	0.6184

P-value of 0.6184 fails to reject the null hypothesis, therefore the speed had no effect on the device.

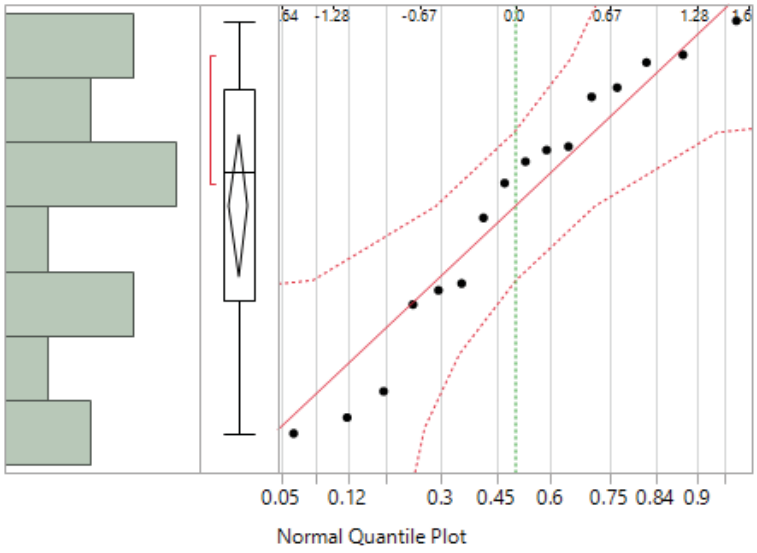

Based on Normal Quantile Plot assumptions for ANOVA are acceptably met

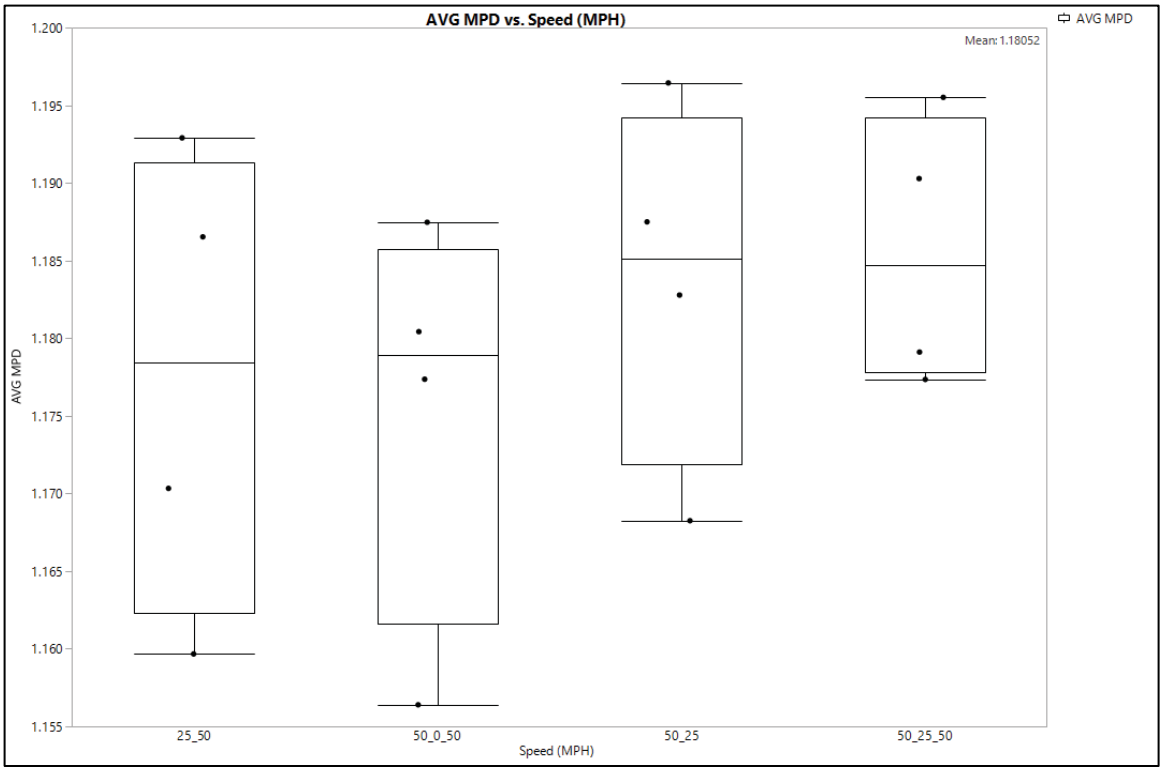

Box plots of variable speed demonstrate no effect of speed on MPD

Range of data points:

max	1.19644
min	1.156396
diff	0.040044

Appendix D Chapter 3 Device 3 ANOVA Data

DEVICE_3 ANOVA Tables and Figures (Produced in JMP software):
MSE from these ANOVA tables was used to produce repeatability Coefficients and device variability used in Limits of Agreement. Only 55 MPH 1m aggregated data was used in the manuscript.

HIGH SPEED REPEATABILITY

DEVICE_3_HS_55mph_Raw_Trimmed_dsp_MPD_1m (Repeatability JMP Table)					
Analysis of Variance					
Source	DF	Sum of Squares	Mean Square	F Ratio	Prob > F
Model	17	13.64222	0.802483	796.8858	<.0001
Error	72	0.072506	0.001007		
C. Total	89	13.71472			

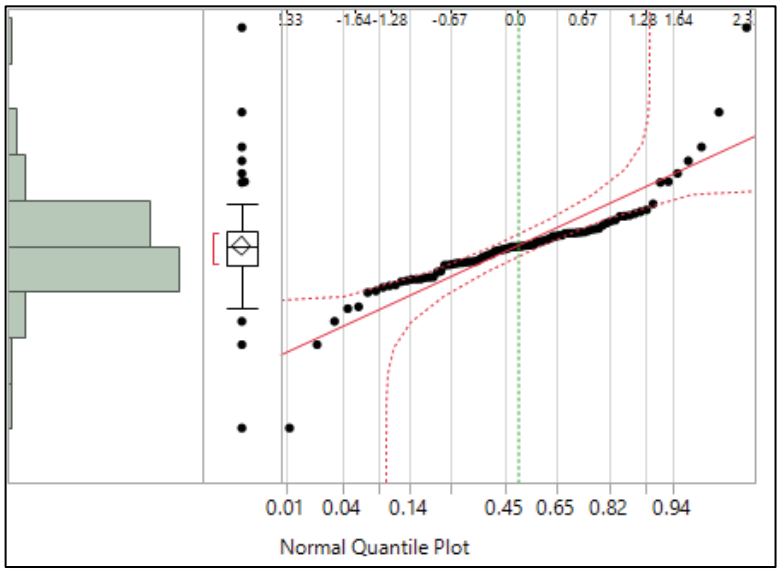

Based on Normal Quantile Plot assumptions for ANOVA are acceptably met

CONSTANT SPEED ANOVA (SECTIONS SEPARATE)
DEVICE_3_OF_CS_Raw_Trimmed_dsp_MPD_1m (ANOVA JMP Table)
Note: Speed was defined as a continuous variable in the ANOVA

L2					
Analysis of Variance					
Source	DF	Sum of Squares	Mean Square	F Ratio	Prob > F
Model	1	0.035371	0.035371	14.7538	0.0009
Error	22	0.052744	0.002397		
C. Total	23	0.088115			
Parameter Estimates					
Term	Estimate	Std Error	t Ratio	Prob>|t|	
Intercept	1.205052	0.025453	47.34	<.0001	
Speed (MPH)	-0.00225	0.000585	-3.84	0.0009	
Effect Tests					
Source	Nparm	DF	Sum of Squares	F Ratio	Prob > F
Speed (MPH)	1	1	0.035371	14.7538	0.0009

P-value of 0.0009 rejects the null hypothesis, therefore the speed had an effect on the device for asphalt section L2.

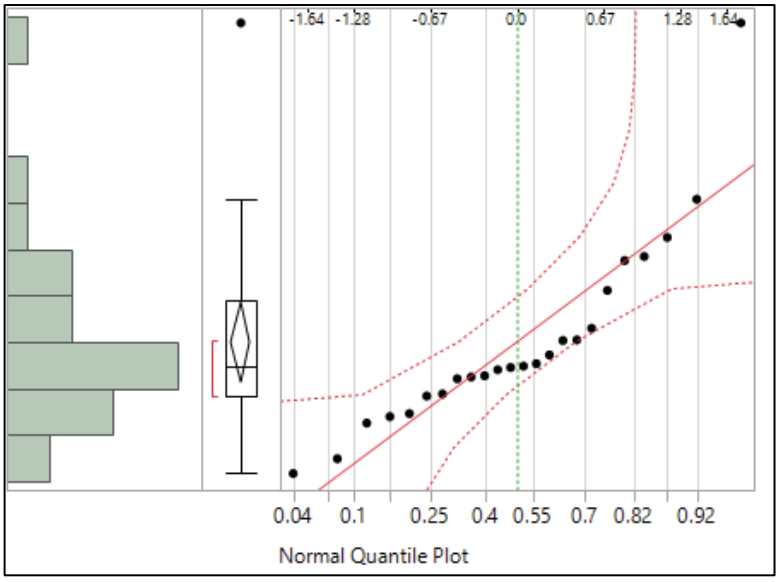

Based on Normal Quantile Plot assumptions for ANOVA are acceptably met

PCC1a					
Analysis of Variance					
Source	DF	Sum of Squares	Mean Square	F Ratio	Prob > F
Model	1	0.004704	0.004704	22.0646	0.0001
Error	22	0.00469	0.000213		
C. Total	23	0.009394			
Parameter Estimates					
Term	Estimate	Std Error	t Ratio	Prob>|t|	
Intercept	0.676822	0.00759	89.17	<.0001	
Speed (MPH)	-0.00082	0.000175	-4.7	0.0001	
Effect Tests					
Source	Nparm	DF	Sum of Squares	F Ratio	Prob > F
Speed (MPH)	1	1	0.004704	22.0646	0.0001

P-value of 0.0001 rejects the null hypothesis, therefore the variable speed had an effect on the device for section PCC1a.

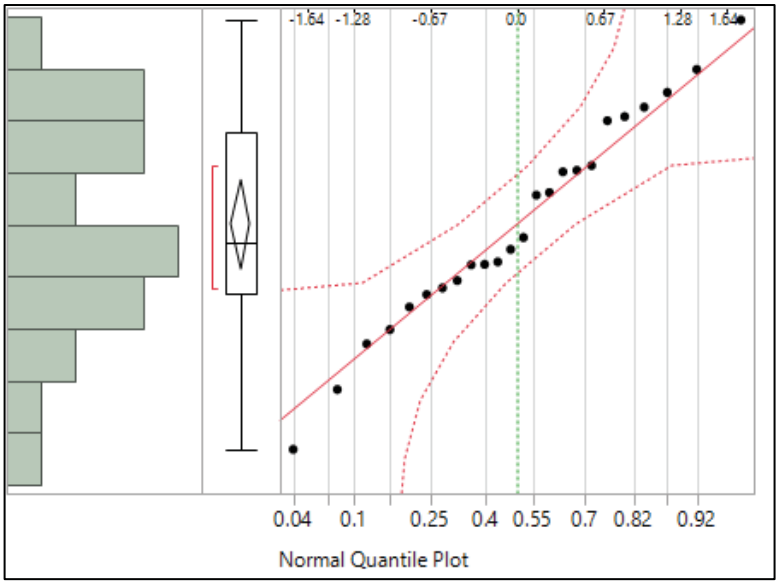

Based on Normal Quantile Plot assumptions for ANOVA are acceptably met

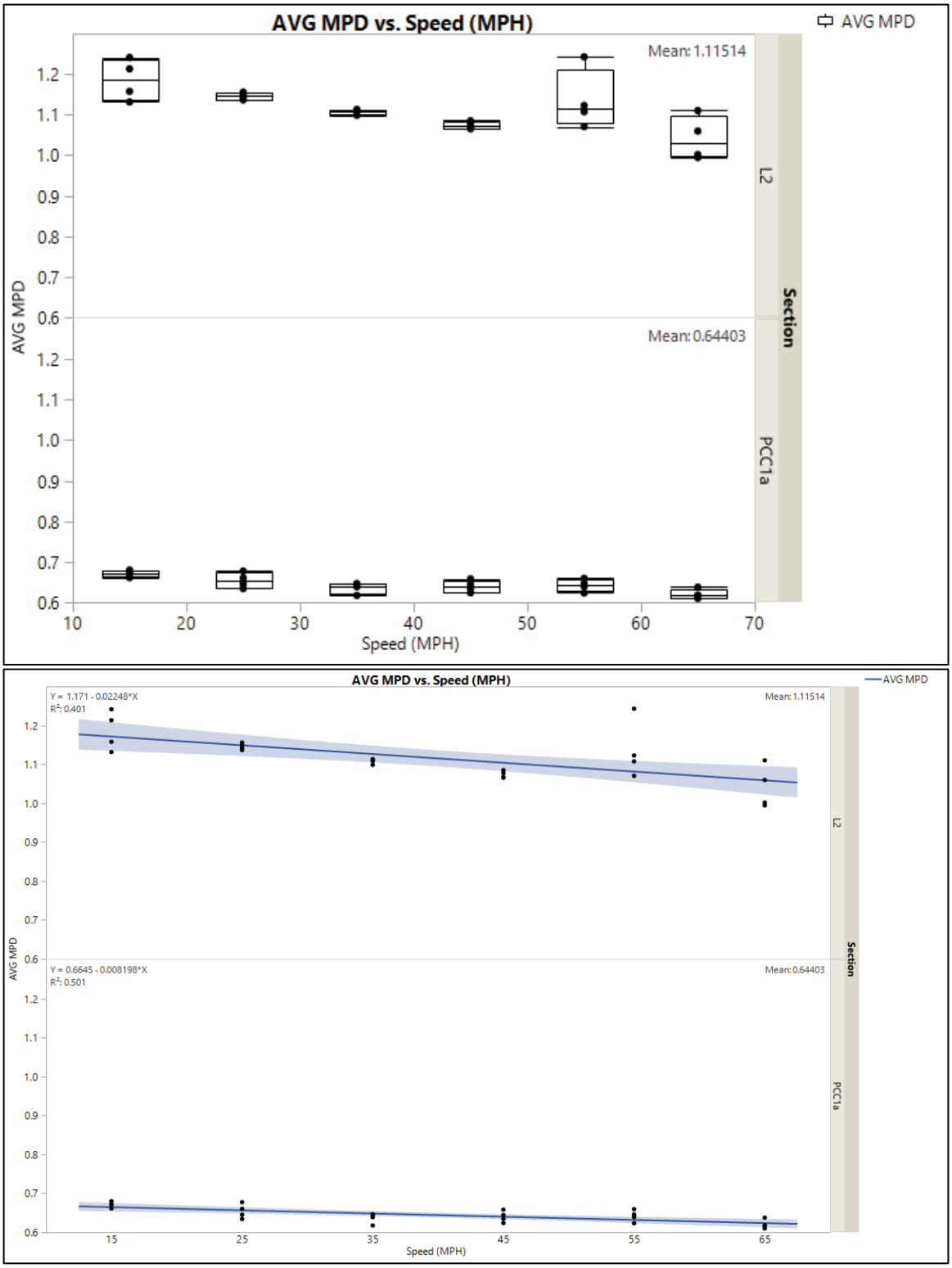

Box plots and linear regression of constant speed demonstrate the effect of speed on MPD

PCC1a	
max	**0.679869**
min	**0.609823**
diff	**0.070046**
L2	
max	**1.242914**
min	**0.994503**
diff	**0.248411**

Analysis of the range of data points shows that given the effect of speed on MPD, PCC1a measurements are still within a good range of repeatability, however measurements on section L2 are not.

VARIABLE SPEED ANOVA

DEVICE_3_OF_VS_Raw_Trimmed_dsp_MPD_1m (ANOVA JMP Table)

Analysis of Variance					
Source	DF	Sum of Squares	Mean Square	F Ratio	Prob > F
Model	3	0.003271	0.00109	0.9895	0.4306
Error	12	0.013221	0.001102		
C. Total	15	0.016492			
Parameter Estimates					
Term	Estimate	Std Error	t Ratio	Prob>|t|	
Intercept	1.024426	0.008298	123.45	<.0001	
Speed (MPH)[25_50]	-0.01264	0.014373	-0.88	0.3965	
Speed (MPH)[50_0_50]	-0.01585	0.014373	-1.1	0.2918	
Speed (MPH)[50_25]	0.014962	0.014373	1.04	0.3184	
Effect Tests					
Source	Nparm	DF	Sum of Squares	F Ratio	Prob > F
Speed (MPH)	3	3	0.003271	0.9895	0.4306

P-value of 0.4306 fails to reject the null hypothesis, therefore the speed had no effect on the device.

Based on Normal Quantile Plot assumptions for ANOVA are acceptably met

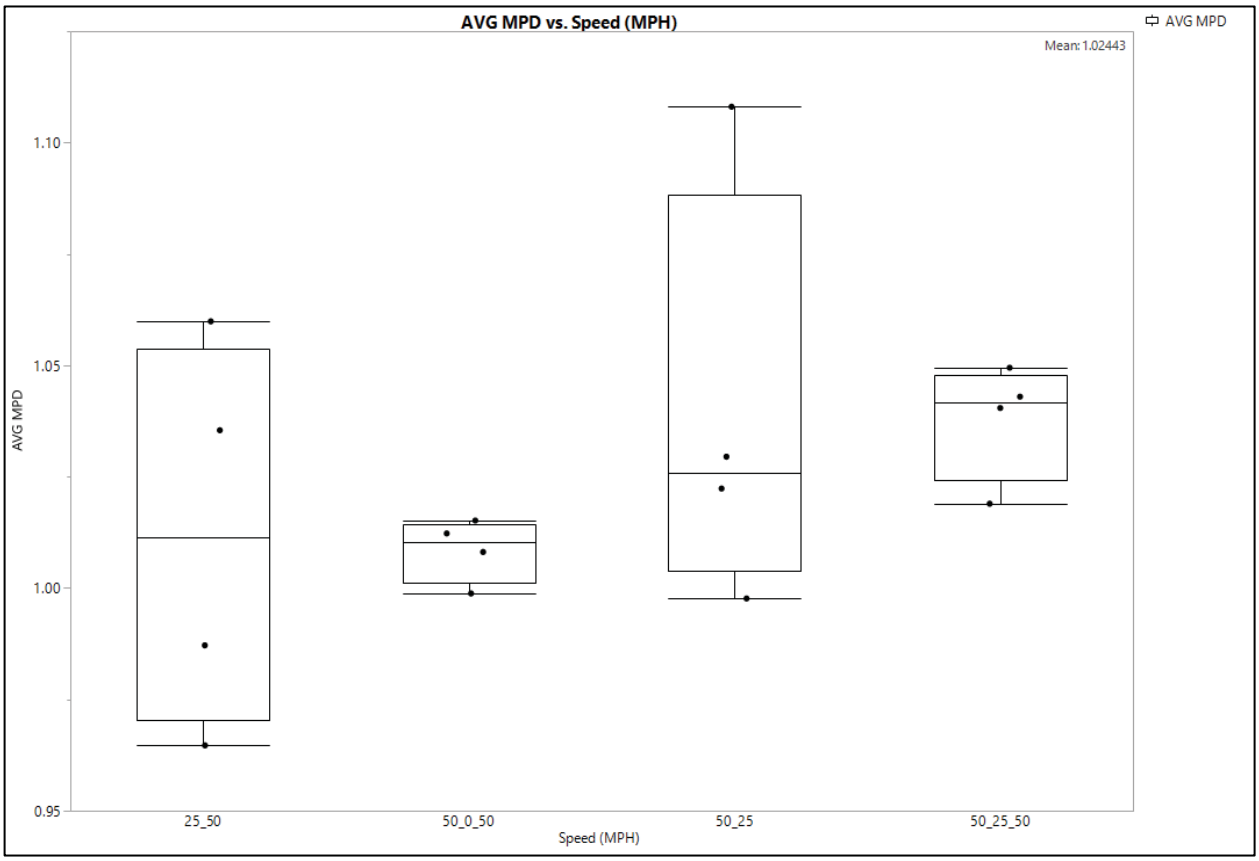

Box plots of variable speed demonstrate no effect of speed on MPD

Range of data points:

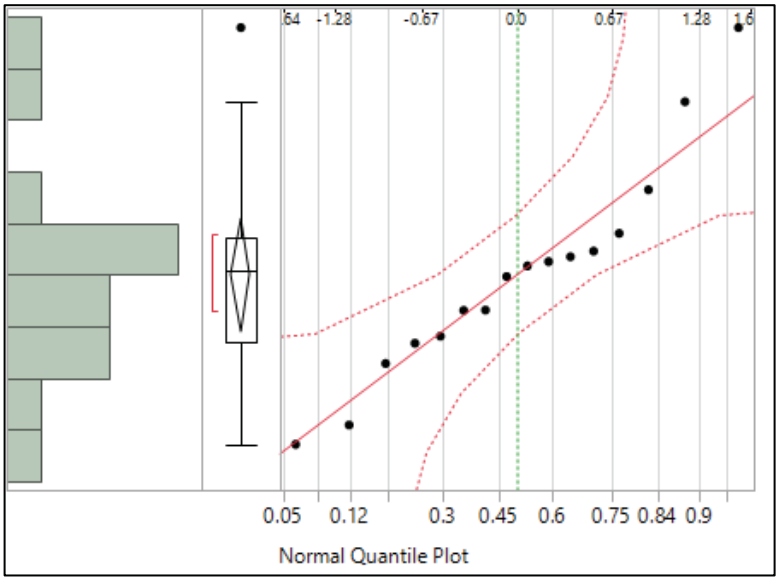

max	1.108059
min	0.964687
difff	0.143372

Appendix E Chapter 3 Device 4 ANOVA Data

DEV_4 ANOVA Tables and Figures (Produced in JMP software):
MSE from these ANOVA tables was used to produce repeatability Coefficients and device variability used in Limits of Agreement. Only 55 MPH 1m aggregated data was used in the manuscript.

HIGH SPEED REPEATABILITY

DEVICE_4_HS_55mph_Raw_Trimmed_dsp_MPD_1m (Repeatability JMP Table)					
Analysis of Variance					
Source	DF	Sum of Squares	Mean Square	F Ratio	Prob > F
Model	17	16.18045	0.951791	1805.474	<.0001
Error	72	0.037956	0.000527		
C. Total	89	16.21841			

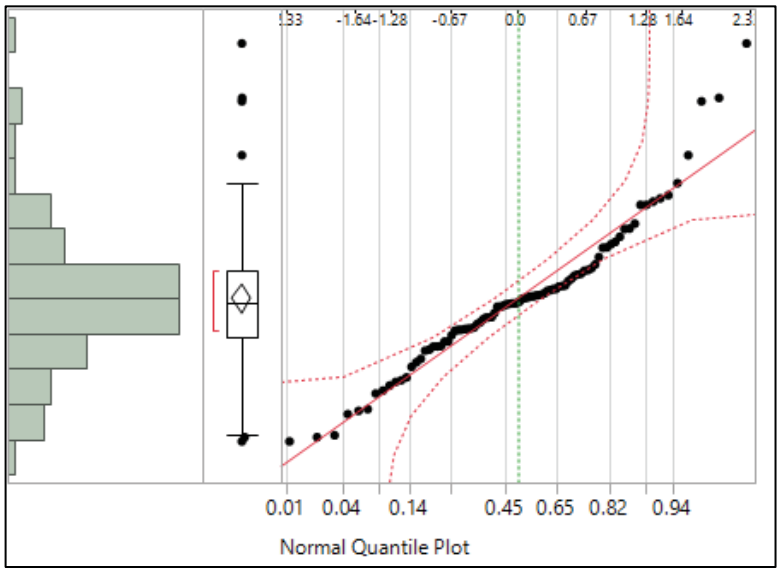

Based on Normal Quantile Plot assumptions for ANOVA are acceptably met

CONSTANT SPEED ANOVA (SECTIONS SEPARATE)
DEVICE_4_OF_CS_raw_trimmed_dsp_MPD_1m (ANOVA JMP Table)
Note: Speed was defined as a continuous variable in the ANOVA

L2					
Analysis of Variance					
Source	DF	Sum of Squares	Mean Square	F Ratio	Prob > F
Model	1	0.002314	0.002314	0.7439	0.3977
Error	22	0.068444	0.003111		
C. Total	23	0.070758			
Parameter Estimates					
Term	Estimate	Std Error	t Ratio	Prob>|t|	
Intercept	1.290611	0.028995	44.51	<.0001	
Speed (MPH)	-0.00058	0.000667	-0.86	0.3977	
Effect Tests					
Source	Nparm	DF	Sum of Squares	F Ratio	Prob > F
Speed (MPH)	1	1	0.002314	0.7439	0.3977

P-value of 0.3977 fails to reject the null hypothesis, therefore the speed had no effect on the device for asphalt section L2.

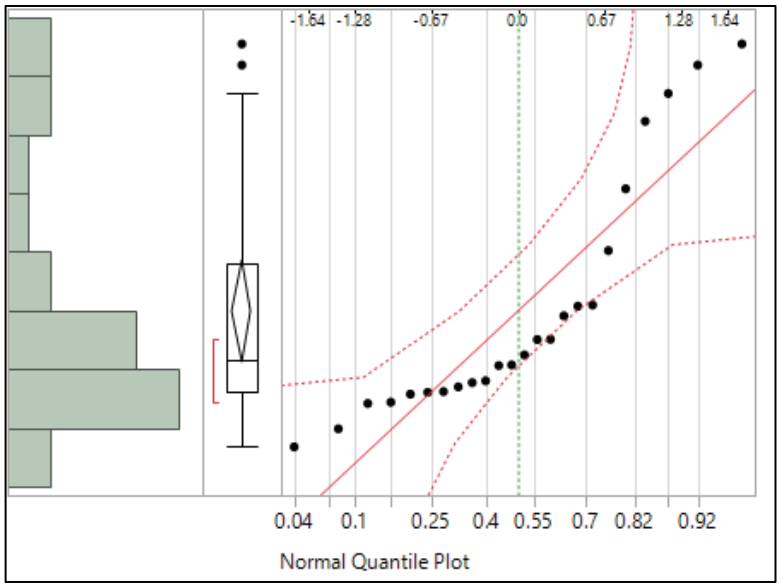

Based on Normal Quantile Plot assumptions for ANOVA are acceptably met

PCC1a					
Analysis of Variance					
Source	DF	Sum of Squares	Mean Square	F Ratio	Prob > F
Model	1	5.45E-05	0.000055	0.4812	0.4951
Error	22	0.002492	0.000113		
C. Total	23	0.002546			
Parameter Estimates					
Term	Estimate	Std Error	t Ratio	Prob>|t|	
Intercept	0.685096	0.005532	123.83	<.0001	
Speed (MPH)	-8.82E-05	0.000127	-0.69	0.4951	
Effect Tests					
Source	Nparm	DF	Sum of Squares	F Ratio	Prob > F
Speed (MPH)	1	1	5.45E-05	0.4812	0.4951

P-value of 0.4951 fails to reject the null hypothesis, therefore the speed had no effect on the device for section PCC1a.

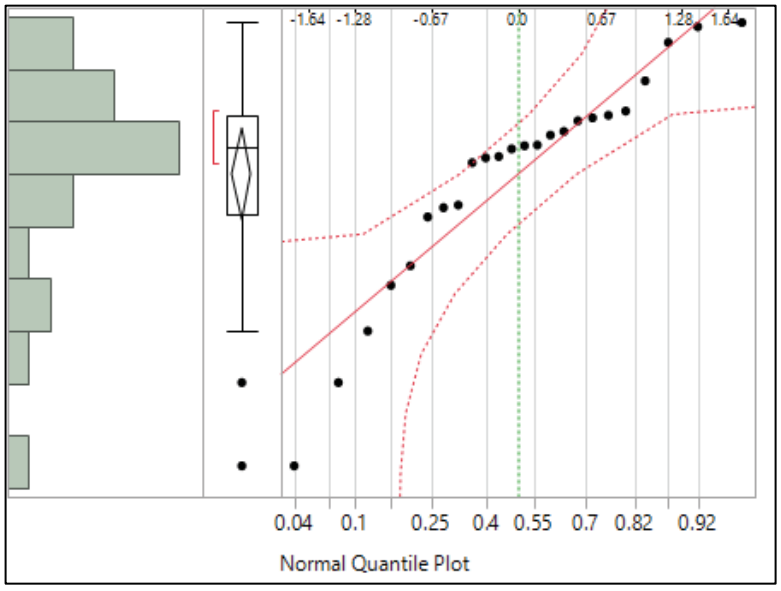

Based on Normal Quantile Plot assumptions for ANOVA are acceptably met

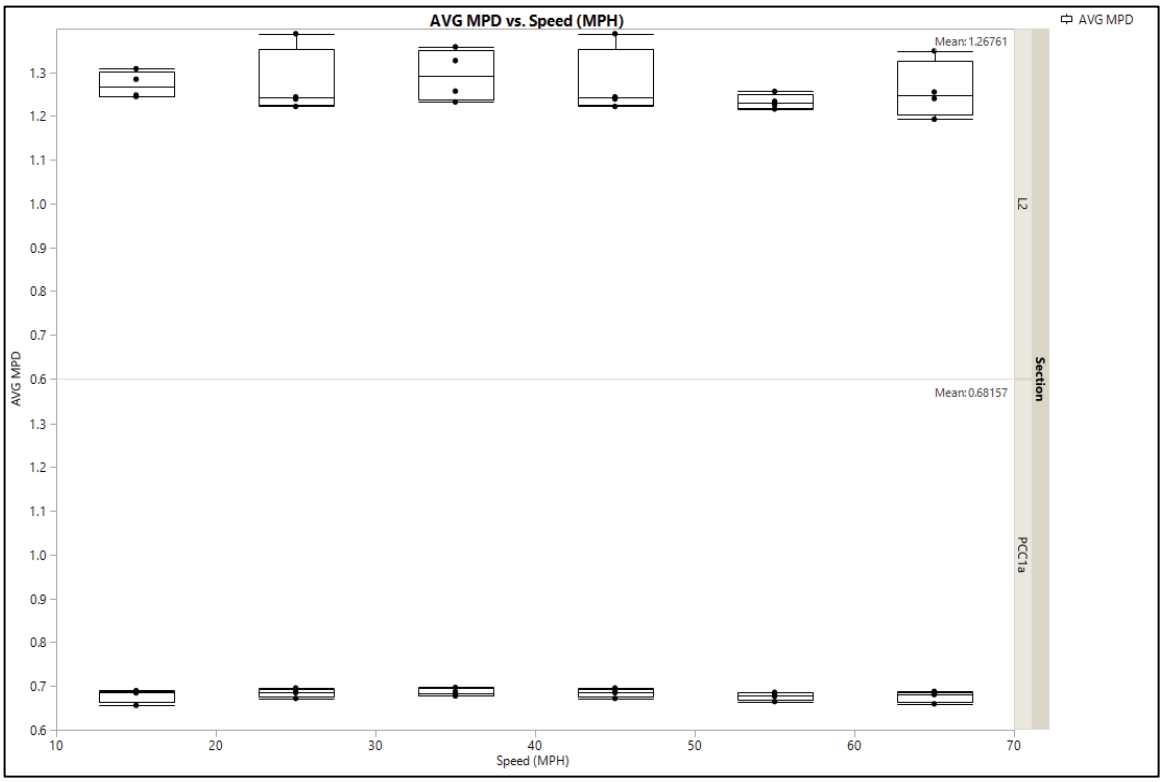

Box plots of constant speed demonstrate no effect of speed on MPD

Range of data points:

pcc1a	
max	0.696991
min	0.656145
diff	0.040846
L2	
max	1.388574
min	1.192978
diff	0.195596

VARIABLE SPEED ANOVA

DEVICE_4_OF_VS_Raw_Trimmed_dsp_MPD_1m (ANOVA JMP Table)

Analysis of Variance					
Source	DF	Sum of Squares	Mean Square	F Ratio	Prob > F
Model	3	0.00036	0.00012	0.2751	0.8423
Error	12	0.00524	0.000437		
C. Total	15	0.005601			
Parameter Estimates					
Term	Estimate	Std Error	t Ratio	Prob>|t|	
Intercept	1.120877	0.005224	214.55	<.0001	
Speed (MPH)[25_50]	0.002629	0.009049	0.29	0.7764	
Speed (MPH)[50_0_50]	0.004116	0.009049	0.45	0.6573	
Speed (MPH)[50_25]	-0.00804	0.009049	-0.89	0.392	
Effect Tests					
Source	Nparm	DF	Sum of Squares	F Ratio	Prob > F
Speed (MPH)	3	3	0.00036	0.2751	0.8423

P-value of 0.8423 fails to reject the null hypothesis, therefore the speed had no effect on the device.

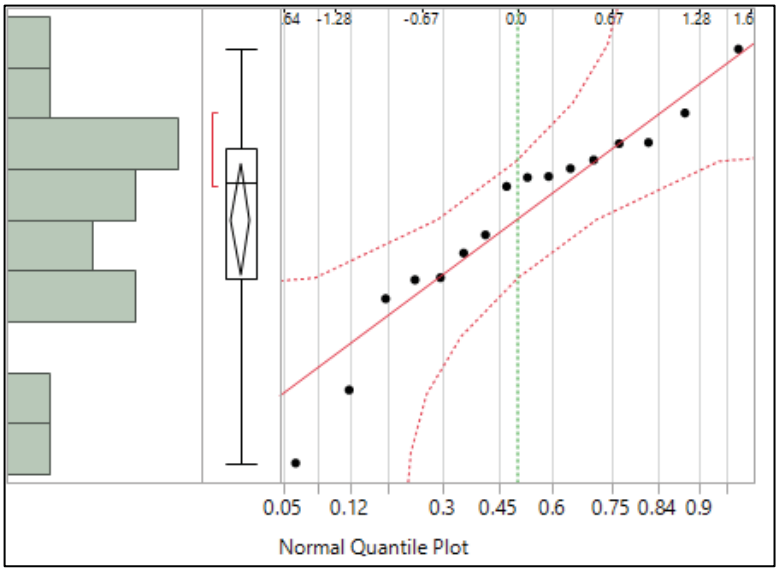

Based on Normal Quantile Plot assumptions for ANOVA are acceptably met

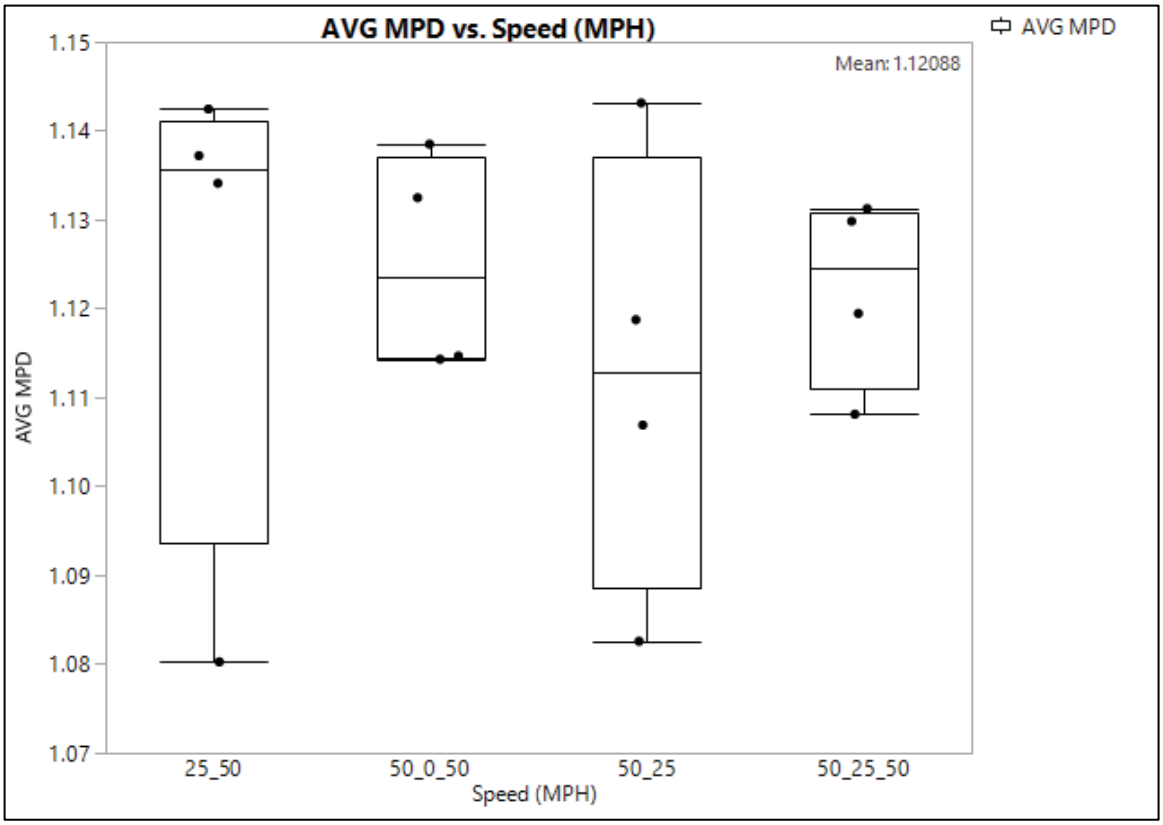

Box plots of variable speed demonstrate no effect of speed on MPD

Range of data points:

max	1.143145
min	1.080253
difff	0.062892

Appendix F Chapter 3 Device 5 ANOVA Data

DEVICE_5 ANOVA Tables and Figures (Produced in JMP software):
MSE from these ANOVA tables was used to produce repeatability Coefficients and device variability used in Limits of Agreement. Only 55 MPH 1m aggregated data was used in the manuscript.

HIGH SPEED REPEATABILITY

DEVICE_5_HS_55mph_Raw_Trimmed_dsp_MPD_1m CORRECTED FILTER (Repeatability JMP Table)					
Analysis of Variance					
Source	DF	Sum of Squares	Mean Square	F Ratio	Prob > F
Model	17	17.66562	1.03915	1989.966	<.0001
Error	72	0.037598	0.00052		
C. Total	89	17.70321			

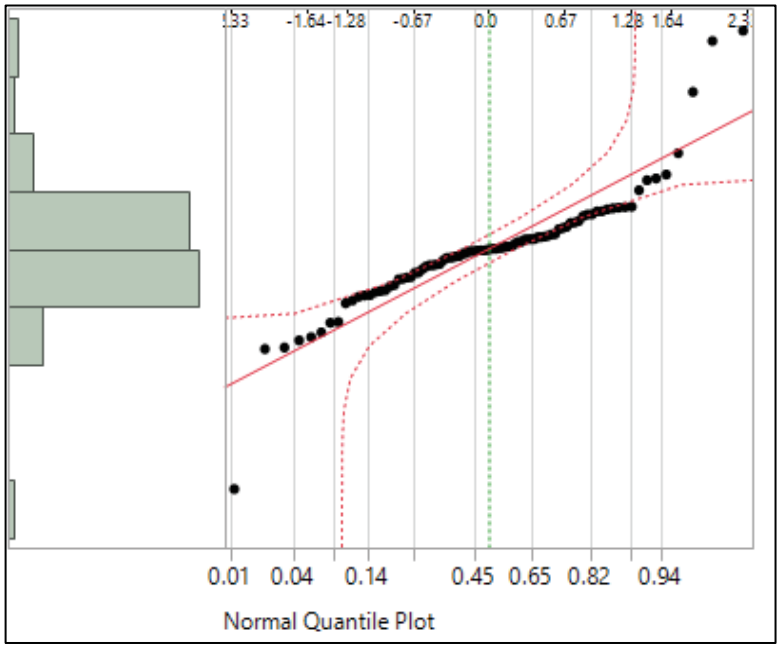

Based on Normal Quantile Plot assumptions for ANOVA are acceptably met

CONSTANT SPEED ANOVA (SECTIONS SEPARATE)

DEVICE_5_OF_CS_Raw_Trimmed_dsp_MPD_1m (ANOVA JMP Table)

Note: Speed was defined as a continuous variable in the ANOVA

L2					
Analysis of Variance					
Source	DF	Sum of Squares	Mean Square	F Ratio	Prob > F
Model	1	0.017455	0.017455	21.663	0.0001
Error	22	0.017727	0.000806		
C. Total	23	0.035182			
Parameter Estimates					
Term	Estimate	Std Error	t Ratio	Prob>|t|	
Intercept	1.326271	0.014756	89.88	<.0001	
Speed (MPH)	-0.00158	0.000339	-4.65	0.0001	
Effect Tests					
Source	Nparm	DF	Sum of Squares	F Ratio	Prob > F
Speed (MPH)	1	1	0.017455	21.663	0.0001

P-value of 0.0001 rejects the null hypothesis, therefore the speed has an effect on the device for asphalt section L2.

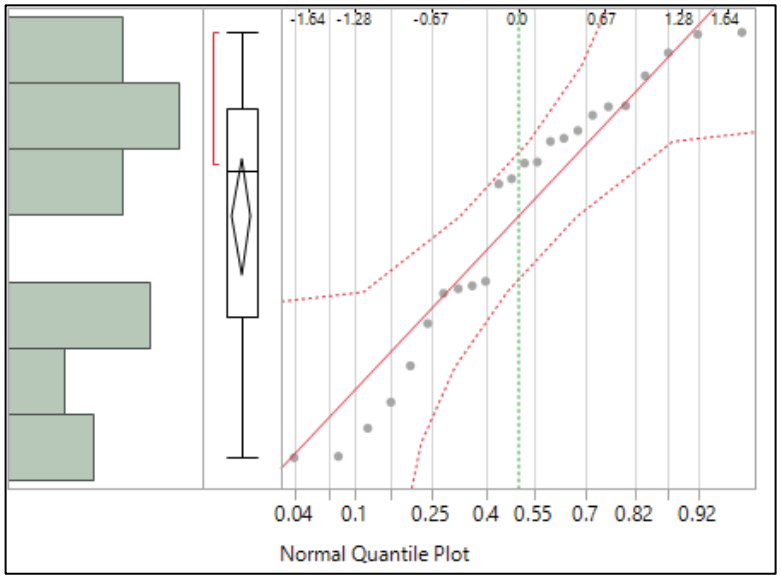

Based on Normal Quantile Plot assumptions for ANOVA are acceptably met

PCC1a					
Analysis of Variance					
Source	DF	Sum of Squares	Mean Square	F Ratio	Prob > F
Model	1	0.003053	0.003053	28.8525	<.0001
Error	22	0.002328	0.000106		
C. Total	23	0.005381			
Parameter Estimates					
Term	Estimate	Std Error	t Ratio	Prob>|t|	
Intercept	0.5987	0.005347	111.96	<.0001	
Speed (MPH)	-0.00066	0.000123	-5.37	<.0001	
Effect Tests					
Source	Nparm	DF	Sum of Squares	F Ratio	Prob > F
Speed (MPH)	1	1	0.003053	28.8525	<.0001

P-value of less than .0001 rejects the null hypothesis, therefore the speed has an effect on the device for section PCC1a.

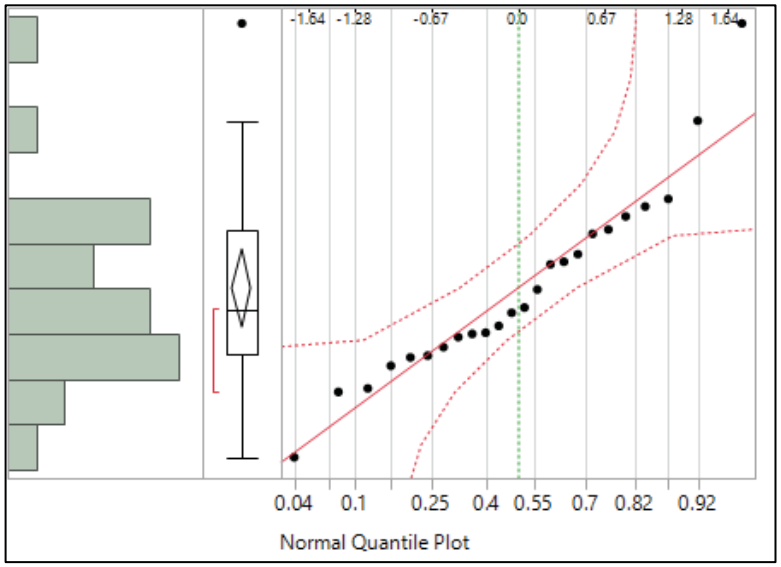

Based on Normal Quantile Plot assumptions for ANOVA are acceptably met

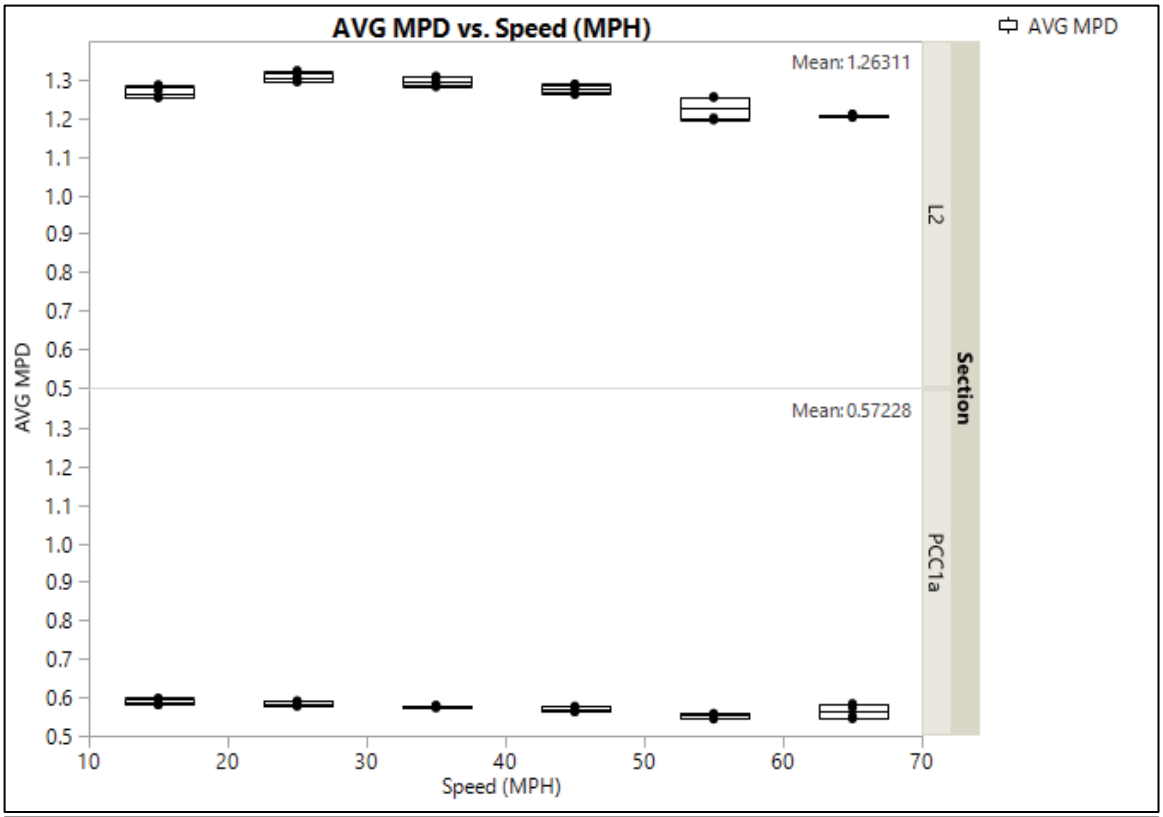
AVG MPD vs. Speed (MPH)
AVG MPD
Mean: 1.26311
Mean: 0.57228
L2
PCC1a
Section
AVG MPD
Speed (MPH)

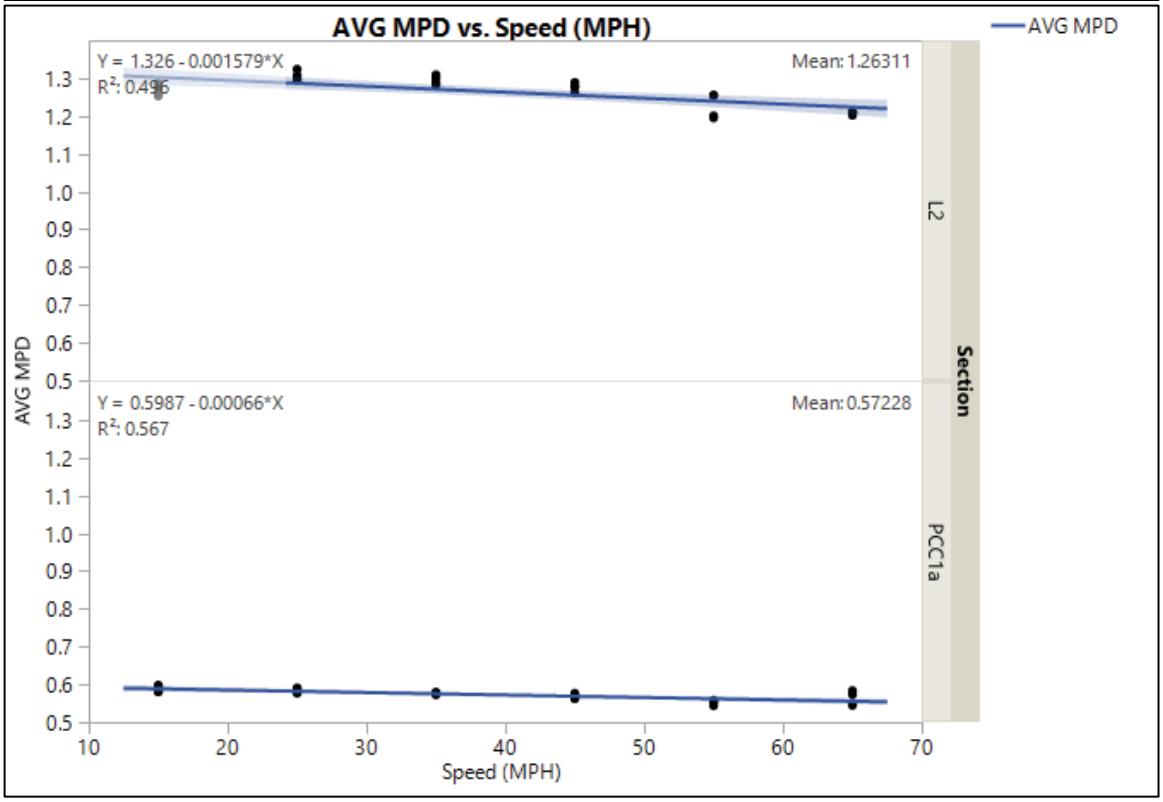
AVG MPD vs. Speed (MPH)
AVG MPD
Y = 1.326 - 0.001579*X
R²: 0.496
Mean: 1.26311
Y = 0.5987 - 0.00066*X
R²: 0.567
Mean: 0.57228
L2
PCC1a
Section
AVG MPD
Speed (MPH)

Box plots and linear regression of constant speed demonstrate effect of speed on MPD
Range of data points:

PCC1a	
max	0.598234
min	0.543973
diff	0.054261
L2	
max	1.324007
min	1.195473
diff	0.128534

Although rejection of the null hypothesis shows an effect of speed on the device, the range of the data points for section PCC1a is still wthin good repeatability, however the range of the data for section L2 is not.

VARIABLE SPEED ANOVA

DEV_3_OF_VS_Raw_Trimmed_dsp_MPD_1m (ANOVA JMP Table)

Analysis of Variance					
Source	DF	Sum of Squares	Mean Square	F Ratio	Prob > F
Model	3	0.001841	0.000614	7.1925	0.0051
Error	12	0.001024	0.000085		
C. Total	15	0.002864			
Parameter Estimates					
Term	Estimate	Std Error	t Ratio	Prob>|t|	
Intercept	1.198276	0.002309	518.95	<.0001	
Speed (MPH)[25_50]	0.01473	0.003999	3.68	0.0031	
Speed (MPH)[50_0_50]	-0.01549	0.003999	-3.87	0.0022	
Speed (MPH)[50_25]	-0.00085	0.003999	-0.21	0.8346	
Effect Tests					
Source	Nparm	DF	Sum of Squares	F Ratio	Prob > F
Speed (MPH)	3	3	0.001841	7.1925	0.0051

P-value of 0.0051 rejects the null hypothesis, therefore the variable speed has an effect on the device.

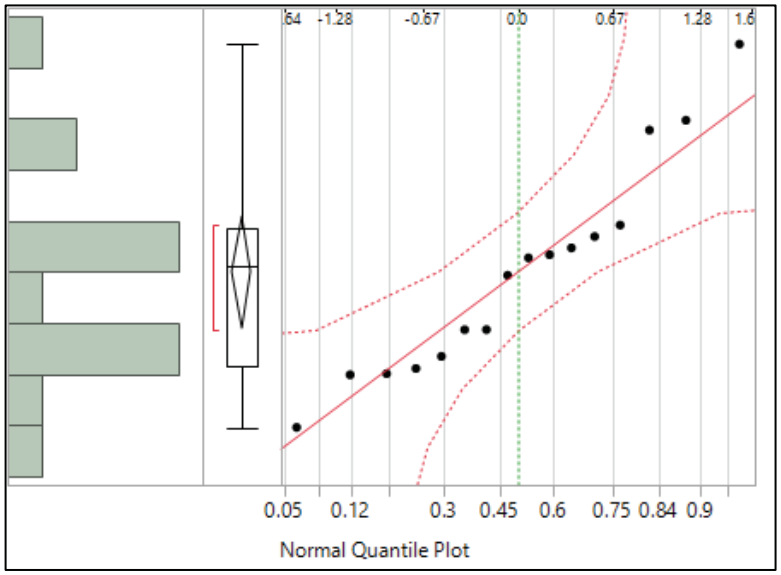

Based on Normal Quantile Plot assumptions for ANOVA are acceptably met

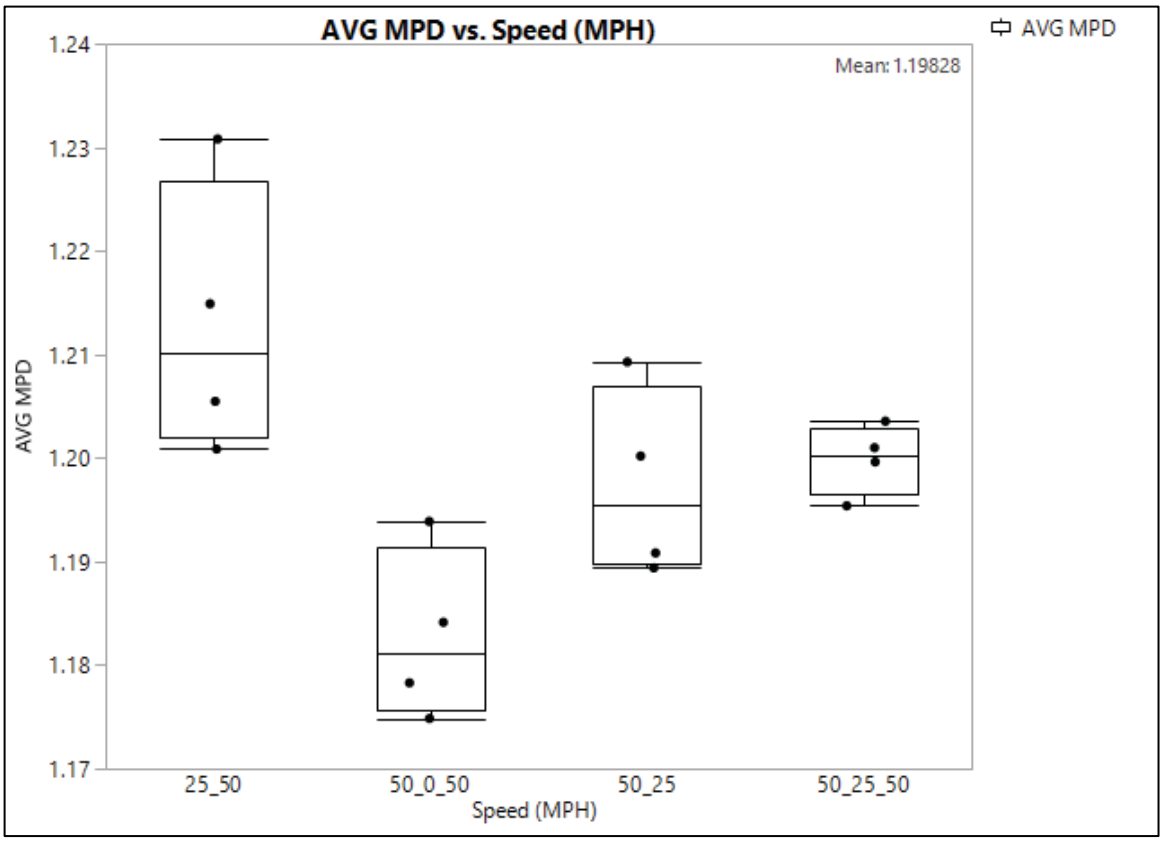

Box plots of variable speed demonstrate the effect of speed on MPD

Range of data points:

max	1.230804
min	1.17485
diff	0.055954

Although speed has an effect on the device the range of the data is within good repeatability

Appendix G Chapter 3 Device Repeatability

Repeatability coefficient is calculated as $\sqrt{MSE} \times 1.96 \times \sqrt{2}$
Repeatability and ANOVA P-Value Interpretations for all pavement sections, α = .05

		AMES		ARRB		ICC		VTTI		SSI	
		DEVICE 1		DEVICE 2		DEVICE 3		DEVICE 4		DEVICE 5	
High Speed		ANOVA MSE	Repeatability Coefficient	ANOVA MSE	Repeatability Coefficient	ANOVA MSE	Repeatability Coefficient	ANOVA MSE	Repeatability Coefficient	ANOVA MSE	Repeatability Coefficient
	HS_55MPH	0.00073	0.074891495	0.00067	0.07174778	0.001007	0.087960118	0.000527	0.063632118	0.00052	0.063208101
	HS_65MPH	0.001314	0.100477484	0.00046	0.059449743	0.000691	0.072863511	0.000892	0.082785351	0.00034	0.051110547

		AMES		ARRB		ICC		VTTI		SSI	
		DEVICE 1		DEVICE 2		DEVICE 3		DEVICE 4		DEVICE 5	
Constant Speed 15,25,35,45,55,65 MPH		ANOVA P-Value	Interpretation	ANOVA P-Value	Interpretation	ANOVA P-Value	Interpretation	ANOVA P-Value	Interpretation	ANOVA P-Value	Interpretation
	L2	0.3854	No effect of speed	0.5966	No effect of speed	0.0009	Speed has effect on device	0.3977	No effect of speed	0.0001	Speed has effect on device
		ANOVA MSE	Repeatability Coefficient	ANOVA MSE	Repeatability Coefficient	ANOVA MSE	Repeatability Coefficient	ANOVA MSE	Repeatability Coefficient	ANOVA MSE	Repeatability Coefficient
		0.003463	0.163116282	0.001197	0.095899898	0.002397	0.135707886	0.003111	0.154604124	0.000806	0.078693451
		ANOVA P-Value	Interpretation	ANOVA P-Value	Interpretation	ANOVA P-Value	Interpretation	ANOVA P-Value	Interpretation	ANOVA P-Value	Interpretation
	PCC1a	0.0607	No effect of speed	0.2206	No effect of speed	0.0001	Speed has effect on device	0.4951	No effect of speed	<.0001	Speed has effect on device
		ANOVA MSE	Repeatability Factor	ANOVA MSE	Repeatability Factor	ANOVA MSE	Repeatability Coefficient	ANOVA MSE	Repeatability Coefficient	ANOVA MSE	Repeatability Coefficient
		0.000347	0.051634004	0.000276	0.046049573	0.000213	0.040453944	0.000113	0.029465261	0.000106	0.028538031

		AMES		ARRB		ICC		VTTI		SSI	
		DEVICE 1		DEVICE 2		DEVICE 3		DEVICE 4		DEVICE 5	
Variable Speed		ANOVA P-Value	Interpretation	ANOVA P-Value	Interpretation	ANOVA P-Value	Interpretation	ANOVA P-Value	Interpretation	ANOVA P-Value	Interpretation
		0.4653	No effect of variable speed	0.6184	No effect of variable speed	0.4306	No effect of variable speed	0.8423	No effect of variable speed	0.0051	Speed has effect on device
	Repeatability	ANOVA MSE	Repeatability Coefficient	ANOVA MSE	Repeatability Coefficient	ANOVA MSE	Repeatability Coefficient	ANOVA MSE	Repeatability Coefficient	ANOVA MSE	Repeatability Coefficient
		0.000587	0.067156819	0.000156	0.034620503	0.001102	0.092015686	0.000437	0.057944442	0.000085	0.025555273

Repeatability for random texture (asphalt like) sections only

	AMES		ARRB		ICC		VTTI		SSI	
	DEVICE 1		DEVICE 2		DEVICE 3		DEVICE 4		DEVICE 5	
	ANOVA MSE	Repeatability Coefficient	ANOVA MSE	Repeatability Coefficient	ANOVA MSE	Repeatability Coefficient	ANOVA MSE	Repeatability Coefficient	ANOVA MSE	Repeatability Coefficient
HS_55MPH	0.001319	0.10066847	0.001115	0.092556837	0.001792	0.117338376	0.00078	0.077413797	0.000682	0.072387446

Repeatability for longitudinally grooved sections only

	AMES		ARRB		ICC		VTTI		SSI	
	DEVICE 1		DEVICE 2		DEVICE 3		DEVICE 4		DEVICE 5	
	ANOVA MSE	Repeatability Coefficient	ANOVA MSE	Repeatability Coefficient	ANOVA MSE	Repeatability Coefficient	ANOVA MSE	Repeatability Coefficient	ANOVA MSE	Repeatability Coefficient
HS_55MPH	0.000112	0.029334594	0.000135	0.032206086	0.000127	0.03123726	0.000206	0.039783655	0.000071	0.023356096

Appendix H Chapter 3 Data used for LOA

Run	section	Avg MPD	DEVICE	DEVICE #	avg of runs	Std Dev of runs
1	SRB	1.3513	DEV_1	1	1.347874599	0.014404
2	SRB	1.3695	DEV_1	1		
3	SRB	1.34821	DEV_1	1		
4	SRB	1.33895	DEV_1	1		
5	SRB	1.33142	DEV_1	1		
1	PCC2	0.50484	DEV_1	1	0.516419294	0.016276
2	PCC2	0.53384	DEV_1	1		
3	PCC2	0.49753	DEV_1	1		
4	PCC2	0.51347	DEV_1	1		
5	PCC2	0.53242	DEV_1	1		
1	RRB	1.28287	DEV_1	1	1.253528075	0.01675
2	RRB	1.24579	DEV_1	1		
3	RRB	1.24284	DEV_1	1		
4	RRB	1.24433	DEV_1	1		
5	RRB	1.25181	DEV_1	1		
1	PCC1g	0.65944	DEV_1	1	0.653092814	0.005749
2	PCC1g	0.65091	DEV_1	1		
3	PCC1g	0.64437	DEV_1	1		
4	PCC1g	0.6548	DEV_1	1		
5	PCC1g	0.65595	DEV_1	1		
1	PCC1f	0.40235	DEV_1	1	0.391018779	0.013267
2	PCC1f	0.36904	DEV_1	1		
3	PCC1f	0.39499	DEV_1	1		
4	PCC1f	0.38914	DEV_1	1		
5	PCC1f	0.39957	DEV_1	1		
1	PCC1e	0.54932	DEV_1	1	0.55072603	0.007412
2	PCC1e	0.5532	DEV_1	1		
3	PCC1e	0.53989	DEV_1	1		
4	PCC1e	0.55078	DEV_1	1		
5	PCC1e	0.56044	DEV_1	1		
1	PCC1d	1.49885	DEV_1	1	1.501181435	0.024972
2	PCC1d	1.47721	DEV_1	1		
3	PCC1d	1.50256	DEV_1	1		
4	PCC1d	1.48535	DEV_1	1		
5	PCC1d	1.54194	DEV_1	1		
1	PCC1c	0.91002	DEV_1	1	0.904966385	0.009253
2	PCC1c	0.89299	DEV_1	1		
3	PCC1c	0.91674	DEV_1	1		
4	PCC1c	0.90593	DEV_1	1		
5	PCC1c	0.89915	DEV_1	1		
1	PCC1b	1.14823	DEV_1	1	1.114724255	0.02028

2	PCC1b	1.09963	DEV_1	1		
3	PCC1b	1.11714	DEV_1	1		
4	PCC1b	1.11029	DEV_1	1		
5	PCC1b	1.09833	DEV_1	1		
1	PCC1a	0.64365	DEV_1	1	0.650074524	0.009835
2	PCC1a	0.64866	DEV_1	1		
3	PCC1a	0.64089	DEV_1	1		
4	PCC1a	0.65103	DEV_1	1		
5	PCC1a	0.66615	DEV_1	1		
1	L2	1.26325	DEV_1	1	1.277114508	0.036523
2	L2	1.29688	DEV_1	1		
3	L2	1.25192	DEV_1	1		
4	L2	1.3311	DEV_1	1		
5	L2	1.24242	DEV_1	1		
1	K	2.32138	DEV_1	1	2.333629406	0.03558
2	K	2.34292	DEV_1	1		
3	K	2.27938	DEV_1	1		
4	K	2.37337	DEV_1	1		
5	K	2.35109	DEV_1	1		
1	J	1.42168	DEV_1	1	1.435228453	0.082324
2	J	1.40347	DEV_1	1		
3	J	1.43135	DEV_1	1		
4	J	1.57094	DEV_1	1		
5	J	1.34871	DEV_1	1		
1	I	1.17026	DEV_1	1	1.180456531	0.0251
2	I	1.16968	DEV_1	1		
3	I	1.15079	DEV_1	1		
4	I	1.19748	DEV_1	1		
5	I	1.21407	DEV_1	1		
1	H	1.13169	DEV_1	1	1.156019496	0.022885
2	H	1.13796	DEV_1	1		
3	H	1.17495	DEV_1	1		
4	H	1.18423	DEV_1	1		
5	H	1.15128	DEV_1	1		
1	HWB	1.01562	DEV_1	1	1.012769687	0.005035
2	HWB	1.00514	DEV_1	1		
3	HWB	1.01045	DEV_1	1		
4	HWB	1.01481	DEV_1	1		
5	HWB	1.01783	DEV_1	1		
1	D2	0.92019	DEV_1	1	0.905469661	0.008887
2	D2	0.90549	DEV_1	1		
3	D2	0.89784	DEV_1	1		
4	D2	0.89912	DEV_1	1		

5	D2	0.9047	DEV_1	1		
1	C	1.15082	DEV_1	1	1.139378884	0.01519
2	C	1.12064	DEV_1	1		
3	C	1.15813	DEV_1	1		
4	C	1.1371	DEV_1	1		
5	C	1.1302	DEV_1	1		
1	SRB	1.27994	DEV_2	2	1.288432914	0.009198
2	SRB	1.2972	DEV_2	2		
3	SRB	1.28881	DEV_2	2		
4	SRB	1.27838	DEV_2	2		
5	SRB	1.29783	DEV_2	2		
1	PCC2	0.50001	DEV_2	2	0.49066238	0.015355
2	PCC2	0.49192	DEV_2	2		
3	PCC2	0.46506	DEV_2	2		
4	PCC2	0.50472	DEV_2	2		
5	PCC2	0.49159	DEV_2	2		
1	RRB	1.16693	DEV_2	2	1.167064948	0.004744
2	RRB	1.16683	DEV_2	2		
3	RRB	1.15945	DEV_2	2		
4	RRB	1.17095	DEV_2	2		
5	RRB	1.17117	DEV_2	2		
1	PCC1g	0.63963	DEV_2	2	0.644288617	0.004588
2	PCC1g	0.64935	DEV_2	2		
3	PCC1g	0.64794	DEV_2	2		
4	PCC1g	0.64503	DEV_2	2		
5	PCC1g	0.6395	DEV_2	2		
1	PCC1f	0.37935	DEV_2	2	0.379345684	0.029574
2	PCC1f	0.40665	DEV_2	2		
3	PCC1f	0.39368	DEV_2	2		
4	PCC1f	0.38751	DEV_2	2		
5	PCC1f	0.32954	DEV_2	2		
1	PCC1e	0.53077	DEV_2	2	0.529468812	0.00964
2	PCC1e	0.53473	DEV_2	2		
3	PCC1e	0.51466	DEV_2	2		
4	PCC1e	0.52693	DEV_2	2		
5	PCC1e	0.54026	DEV_2	2		
1	PCC1d	1.55989	DEV_2	2	1.539058402	0.034442
2	PCC1d	1.56291	DEV_2	2		
3	PCC1d	1.56195	DEV_2	2		
4	PCC1d	1.5269	DEV_2	2		
5	PCC1d	1.48365	DEV_2	2		
1	PCC1c	0.9276	DEV_2	2	0.910926056	0.01863
2	PCC1c	0.91347	DEV_2	2		

3	PCC1c	0.92987	DEV_2	2		
4	PCC1c	0.89473	DEV_2	2		
5	PCC1c	0.88896	DEV_2	2		
1	PCC1b	1.01843	DEV_2	2	1.0102524	0.018697
2	PCC1b	0.99723	DEV_2	2		
3	PCC1b	1.03035	DEV_2	2		
4	PCC1b	0.98471	DEV_2	2		
5	PCC1b	1.02053	DEV_2	2		
1	PCC1a	0.68158	DEV_2	2	0.670703241	0.016302
2	PCC1a	0.64658	DEV_2	2		
3	PCC1a	0.68256	DEV_2	2		
4	PCC1a	0.66088	DEV_2	2		
5	PCC1a	0.68191	DEV_2	2		
1	L2	1.26834	DEV_2	2	1.279984114	0.01887
2	L2	1.26114	DEV_2	2		
3	L2	1.29685	DEV_2	2		
4	L2	1.27012	DEV_2	2		
5	L2	1.30347	DEV_2	2		
1	K	2.27427	DEV_2	2	2.316092071	0.037199
2	K	2.28816	DEV_2	2		
3	K	2.30937	DEV_2	2		
4	K	2.35006	DEV_2	2		
5	K	2.3586	DEV_2	2		
1	J	1.40158	DEV_2	2	1.396605228	0.07111
2	J	1.45431	DEV_2	2		
3	J	1.37483	DEV_2	2		
4	J	1.46436	DEV_2	2		
5	J	1.28794	DEV_2	2		
1	I	1.18403	DEV_2	2	1.192092096	0.036263
2	I	1.24124	DEV_2	2		
3	I	1.19697	DEV_2	2		
4	I	1.19826	DEV_2	2		
5	I	1.13996	DEV_2	2		
1	H	1.1327	DEV_2	2	1.151242653	0.013618
2	H	1.14682	DEV_2	2		
3	H	1.14961	DEV_2	2		
4	H	1.1575	DEV_2	2		
5	H	1.16958	DEV_2	2		
1	HWB	1.00331	DEV_2	2	0.99960517	0.010509
2	HWB	1.0111	DEV_2	2		
3	HWB	0.99861	DEV_2	2		
4	HWB	1.00236	DEV_2	2		
5	HWB	0.98265	DEV_2	2		

1	D2	0.90404	DEV_2	2	0.907801313	0.005966
2	D2	0.91745	DEV_2	2		
3	D2	0.90931	DEV_2	2		
4	D2	0.90575	DEV_2	2		
5	D2	0.90245	DEV_2	2		
1	C	1.15571	DEV_2	2	1.148895706	0.012904
2	C	1.16056	DEV_2	2		
3	C	1.13648	DEV_2	2		
4	C	1.15834	DEV_2	2		
5	C	1.1334	DEV_2	2		
1	SRB	1.20948	DEV_3	3	1.195408994	0.016659
2	SRB	1.21063	DEV_3	3		
3	SRB	1.20171	DEV_3	3		
4	SRB	1.17569	DEV_3	3		
5	SRB	1.17954	DEV_3	3		
1	PCC2	0.43351	DEV_3	3	0.425884009	0.008902
2	PCC2	0.42911	DEV_3	3		
3	PCC2	0.43398	DEV_3	3		
4	PCC2	0.41512	DEV_3	3		
5	PCC2	0.4177	DEV_3	3		
1	RRB	1.09725	DEV_3	3	1.096984327	0.013983
2	RRB	1.09467	DEV_3	3		
3	RRB	1.11917	DEV_3	3		
4	RRB	1.0933	DEV_3	3		
5	RRB	1.08053	DEV_3	3		
1	PCC1g	0.63839	DEV_3	3	0.639016818	0.006377
2	PCC1g	0.64359	DEV_3	3		
3	PCC1g	0.62908	DEV_3	3		
4	PCC1g	0.64553	DEV_3	3		
5	PCC1g	0.6385	DEV_3	3		
1	PCC1f	0.33592	DEV_3	3	0.348051347	0.032214
2	PCC1f	0.40067	DEV_3	3		
3	PCC1f	0.35589	DEV_3	3		
4	PCC1f	0.32564	DEV_3	3		
5	PCC1f	0.32213	DEV_3	3		
1	PCC1e	0.56812	DEV_3	3	0.567863684	0.008654
2	PCC1e	0.57554	DEV_3	3		
3	PCC1e	0.55715	DEV_3	3		
4	PCC1e	0.56144	DEV_3	3		
5	PCC1e	0.57706	DEV_3	3		
1	PCC1d	1.33738	DEV_3	3	1.297670608	0.03615
2	PCC1d	1.33693	DEV_3	3		
3	PCC1d	1.27586	DEV_3	3		

4	PCC1d	1.26958	DEV_3	3		
5	PCC1d	1.2686	DEV_3	3		
1	PCC1c	0.90503	DEV_3	3	0.886290083	0.011494
2	PCC1c	0.88621	DEV_3	3		
3	PCC1c	0.886	DEV_3	3		
4	PCC1c	0.87914	DEV_3	3		
5	PCC1c	0.87507	DEV_3	3		
1	PCC1b	0.81084	DEV_3	3	0.822887792	0.01815
2	PCC1b	0.83068	DEV_3	3		
3	PCC1b	0.82208	DEV_3	3		
4	PCC1b	0.80198	DEV_3	3		
5	PCC1b	0.84885	DEV_3	3		
1	PCC1a	0.65571	DEV_3	3	0.643009639	0.011224
2	PCC1a	0.6423	DEV_3	3		
3	PCC1a	0.63136	DEV_3	3		
4	PCC1a	0.63268	DEV_3	3		
5	PCC1a	0.65299	DEV_3	3		
1	L2	1.2234	DEV_3	3	1.088091022	0.076245
2	L2	1.0637	DEV_3	3		
3	L2	1.04115	DEV_3	3		
4	L2	1.04901	DEV_3	3		
5	L2	1.06319	DEV_3	3		
1	K	2.14535	DEV_3	3	2.127029813	0.03995
2	K	2.0891	DEV_3	3		
3	K	2.10617	DEV_3	3		
4	K	2.1063	DEV_3	3		
5	K	2.18823	DEV_3	3		
1	J	1.21494	DEV_3	3	1.22030933	0.071301
2	J	1.10717	DEV_3	3		
3	J	1.30313	DEV_3	3		
4	J	1.23612	DEV_3	3		
5	J	1.24019	DEV_3	3		
1	I	1.03334	DEV_3	3	1.015186299	0.039612
2	I	1.02343	DEV_3	3		
3	I	1.06002	DEV_3	3		
4	I	1.00536	DEV_3	3		
5	I	0.95377	DEV_3	3		
1	H	1.01522	DEV_3	3	0.99419308	0.016149
2	H	0.98411	DEV_3	3		
3	H	0.99213	DEV_3	3		
4	H	0.97466	DEV_3	3		
5	H	1.00484	DEV_3	3		
1	HWB	0.93372	DEV_3	3	0.929944273	0.006239

2	HWB	0.93272	DEV_3	3		
3	HWB	0.92701	DEV_3	3		
4	HWB	0.92044	DEV_3	3		
5	HWB	0.93583	DEV_3	3		
1	D2	0.73928	DEV_3	3	0.730880666	0.012035
2	D2	0.71104	DEV_3	3		
3	D2	0.72944	DEV_3	3		
4	D2	0.73345	DEV_3	3		
5	D2	0.7412	DEV_3	3		
1	C	0.95815	DEV_3	3	0.957882676	0.004433
2	C	0.95228	DEV_3	3		
3	C	0.9551	DEV_3	3		
4	C	0.96373	DEV_3	3		
5	C	0.96015	DEV_3	3		
1	SRB	1.27972	DEV_4	4	1.287211749	0.006115
2	SRB	1.28994	DEV_4	4		
3	SRB	1.29602	DEV_4	4		
4	SRB	1.28556	DEV_4	4		
5	SRB	1.28481	DEV_4	4		
1	PCC2	0.57334	DEV_4	4	0.573446815	0.024134
2	PCC2	0.55954	DEV_4	4		
3	PCC2	0.56088	DEV_4	4		
4	PCC2	0.55822	DEV_4	4		
5	PCC2	0.61524	DEV_4	4		
1	RRB	1.15333	DEV_4	4	1.181077239	0.024362
2	RRB	1.20146	DEV_4	4		
3	RRB	1.19586	DEV_4	4		
4	RRB	1.19907	DEV_4	4		
5	RRB	1.15566	DEV_4	4		
1	PCC1g	0.64081	DEV_4	4	0.64022361	0.005455
2	PCC1g	0.64849	DEV_4	4		
3	PCC1g	0.64121	DEV_4	4		
4	PCC1g	0.63464	DEV_4	4		
5	PCC1g	0.63597	DEV_4	4		
1	PCC1f	0.49394	DEV_4	4	0.481878451	0.021412
2	PCC1f	0.45884	DEV_4	4		
3	PCC1f	0.50918	DEV_4	4		
4	PCC1f	0.46191	DEV_4	4		
5	PCC1f	0.48552	DEV_4	4		
1	PCC1e	0.56386	DEV_4	4	0.55687032	0.006816
2	PCC1e	0.55136	DEV_4	4		
3	PCC1e	0.5619	DEV_4	4		
4	PCC1e	0.5591	DEV_4	4		

5	PCC1e	0.54813	DEV_4	4		
1	PCC1d	1.60098	DEV_4	4	1.571798753	0.034467
2	PCC1d	1.53187	DEV_4	4		
3	PCC1d	1.60544	DEV_4	4		
4	PCC1d	1.539	DEV_4	4		
5	PCC1d	1.58171	DEV_4	4		
1	PCC1c	0.92319	DEV_4	4	0.924113839	0.017602
2	PCC1c	0.90918	DEV_4	4		
3	PCC1c	0.95424	DEV_4	4		
4	PCC1c	0.91866	DEV_4	4		
5	PCC1c	0.91529	DEV_4	4		
1	PCC1b	1.19787	DEV_4	4	1.207250894	0.006712
2	PCC1b	1.213	DEV_4	4		
3	PCC1b	1.20505	DEV_4	4		
4	PCC1b	1.20585	DEV_4	4		
5	PCC1b	1.21448	DEV_4	4		
1	PCC1a	0.64681	DEV_4	4	0.66545677	0.018419
2	PCC1a	0.69372	DEV_4	4		
3	PCC1a	0.65145	DEV_4	4		
4	PCC1a	0.66607	DEV_4	4		
5	PCC1a	0.66923	DEV_4	4		
1	L2	1.23958	DEV_4	4	1.238712766	0.012339
2	L2	1.25898	DEV_4	4		
3	L2	1.23725	DEV_4	4		
4	L2	1.22797	DEV_4	4		
5	L2	1.22978	DEV_4	4		
1	K	2.32676	DEV_4	4	2.323260993	0.045923
2	K	2.32084	DEV_4	4		
3	K	2.39767	DEV_4	4		
4	K	2.2895	DEV_4	4		
5	K	2.28154	DEV_4	4		
1	J	1.24875	DEV_4	4	1.240633388	0.037832
2	J	1.21627	DEV_4	4		
3	J	1.20015	DEV_4	4		
4	J	1.23885	DEV_4	4		
5	J	1.29914	DEV_4	4		
1	I	1.13991	DEV_4	4	1.123415882	0.023559
2	I	1.11083	DEV_4	4		
3	I	1.09111	DEV_4	4		
4	I	1.15071	DEV_4	4		
5	I	1.12452	DEV_4	4		
1	H	1.07076	DEV_4	4	1.094626675	0.034251
2	H	1.06774	DEV_4	4		

3	H	1.08544	DEV_4	4		
4	H	1.15216	DEV_4	4		
5	H	1.09703	DEV_4	4		
1	HWB	0.97135	DEV_4	4	0.971077375	0.009249
2	HWB	0.96195	DEV_4	4		
3	HWB	0.96496	DEV_4	4		
4	HWB	0.97119	DEV_4	4		
5	HWB	0.98595	DEV_4	4		
1	D2	0.87762	DEV_4	4	0.870987279	0.011639
2	D2	0.86957	DEV_4	4		
3	D2	0.88679	DEV_4	4		
4	D2	0.85694	DEV_4	4		
5	D2	0.86402	DEV_4	4		
1	C	1.10165	DEV_4	4	1.110134657	0.014739
2	C	1.11165	DEV_4	4		
3	C	1.11291	DEV_4	4		
4	C	1.13196	DEV_4	4		
5	C	1.09251	DEV_4	4		
1	SRB	1.13245	DEV_5	5	1.137906121	0.004022
2	SRB	1.13629	DEV_5	5		
3	SRB	1.14229	DEV_5	5		
4	SRB	1.13707	DEV_5	5		
5	SRB	1.14143	DEV_5	5		
1	PCC2	0.84487	DEV_5	5	0.875965345	0.043646
2	PCC2	0.95307	DEV_5	5		
3	PCC2	0.86077	DEV_5	5		
4	PCC2	0.86141	DEV_5	5		
5	PCC2	0.85971	DEV_5	5		
1	RRB	1.03959	DEV_5	5	1.027968828	0.009577
2	RRB	1.03145	DEV_5	5		
3	RRB	1.02812	DEV_5	5		
4	RRB	1.01315	DEV_5	5		
5	RRB	1.02753	DEV_5	5		
1	PCC1g	0.55637	DEV_5	5	0.555903098	0.009346
2	PCC1g	0.57068	DEV_5	5		
3	PCC1g	0.54601	DEV_5	5		
4	PCC1g	0.55629	DEV_5	5		
5	PCC1g	0.55017	DEV_5	5		
1	PCC1f	1.64319	DEV_5	5	1.678486599	0.02936
2	PCC1f	1.71239	DEV_5	5		
3	PCC1f	1.69186	DEV_5	5		
4	PCC1f	1.65247	DEV_5	5		
5	PCC1f	1.69252	DEV_5	5		

1	PCC1e	0.43412	DEV_5	5	0.434128905	0.003268
2	PCC1e	0.43746	DEV_5	5		
3	PCC1e	0.43598	DEV_5	5		
4	PCC1e	0.42882	DEV_5	5		
5	PCC1e	0.43426	DEV_5	5		
1	PCC1d	1.522	DEV_5	5	1.535190488	0.019328
2	PCC1d	1.55597	DEV_5	5		
3	PCC1d	1.54982	DEV_5	5		
4	PCC1d	1.50945	DEV_5	5		
5	PCC1d	1.53871	DEV_5	5		
1	PCC1c	0.7553	DEV_5	5	0.763583109	0.015203
2	PCC1c	0.75293	DEV_5	5		
3	PCC1c	0.75648	DEV_5	5		
4	PCC1c	0.7633	DEV_5	5		
5	PCC1c	0.78989	DEV_5	5		
1	PCC1b	0.90586	DEV_5	5	0.900551533	0.003327
2	PCC1b	0.89978	DEV_5	5		
3	PCC1b	0.90142	DEV_5	5		
4	PCC1b	0.89765	DEV_5	5		
5	PCC1b	0.89805	DEV_5	5		
1	PCC1a	0.55148	DEV_5	5	0.554051589	0.006747
2	PCC1a	0.54397	DEV_5	5		
3	PCC1a	0.55505	DEV_5	5		
4	PCC1a	0.55829	DEV_5	5		
5	PCC1a	0.56147	DEV_5	5		
1	L2	1.25457	DEV_5	5	1.230257387	0.029635
2	L2	1.20083	DEV_5	5		
3	L2	1.25521	DEV_5	5		
4	L2	1.19547	DEV_5	5		
5	L2	1.24521	DEV_5	5		
1	K	2.34803	DEV_5	5	2.343352833	0.012731
2	K	2.35563	DEV_5	5		
3	K	2.35325	DEV_5	5		
4	K	2.32698	DEV_5	5		
5	K	2.33288	DEV_5	5		
1	J	1.37318	DEV_5	5	1.39136086	0.042112
2	J	1.46485	DEV_5	5		
3	J	1.35912	DEV_5	5		
4	J	1.37451	DEV_5	5		
5	J	1.38515	DEV_5	5		
1	I	1.11877	DEV_5	5	1.119545842	0.012188
2	I	1.13285	DEV_5	5		
3	I	1.10042	DEV_5	5		

4	I	1.11905	DEV_5	5		
5	I	1.12664	DEV_5	5		
1	H	1.12004	DEV_5	5	1.124056998	0.00587
2	H	1.11832	DEV_5	5		
3	H	1.12489	DEV_5	5		
4	H	1.12359	DEV_5	5		
5	H	1.13343	DEV_5	5		
1	HWB	0.85369	DEV_5	5	0.856855861	0.003686
2	HWB	0.8554	DEV_5	5		
3	HWB	0.86201	DEV_5	5		
4	HWB	0.8538	DEV_5	5		
5	HWB	0.85938	DEV_5	5		
1	D2	0.87657	DEV_5	5	0.874058806	0.010754
2	D2	0.86136	DEV_5	5		
3	D2	0.87826	DEV_5	5		
4	D2	0.88844	DEV_5	5		
5	D2	0.86565	DEV_5	5		
1	C	1.23061	DEV_5	5	1.175121347	0.051375
2	C	1.09037	DEV_5	5		
3	C	1.18297	DEV_5	5		
4	C	1.18732	DEV_5	5		
5	C	1.18434	DEV_5	5		

Appendix I Chapter 3 LOA – All Sections

From the LOA Data Table, the mean is plotted against the standard deviation to check that the standard deviation of runs for each section should is constant and not related to the magnitude of the measurements. The ANOVA tables from which the MSE used as the device's are in the ANOVA appendices for each of the devices.

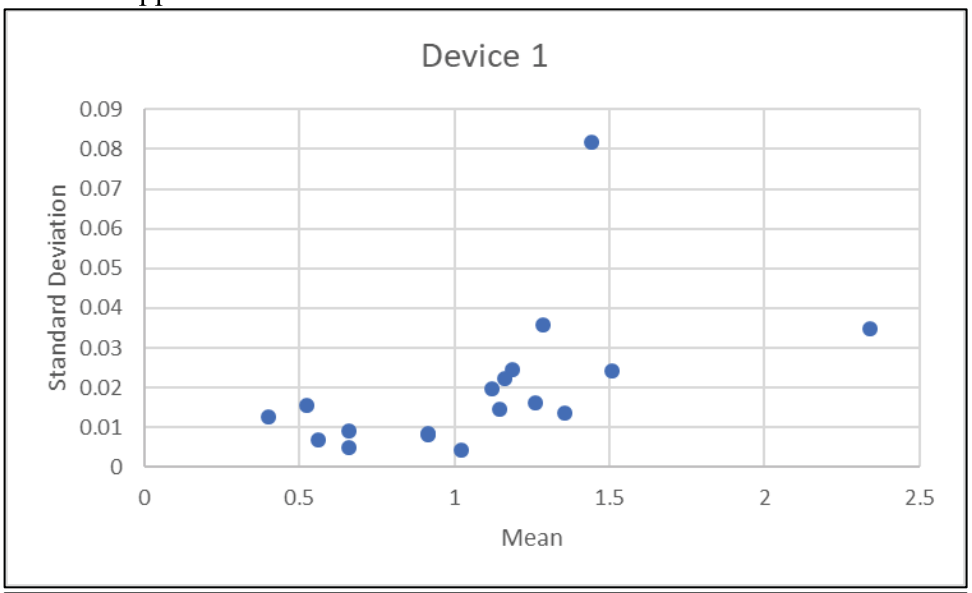

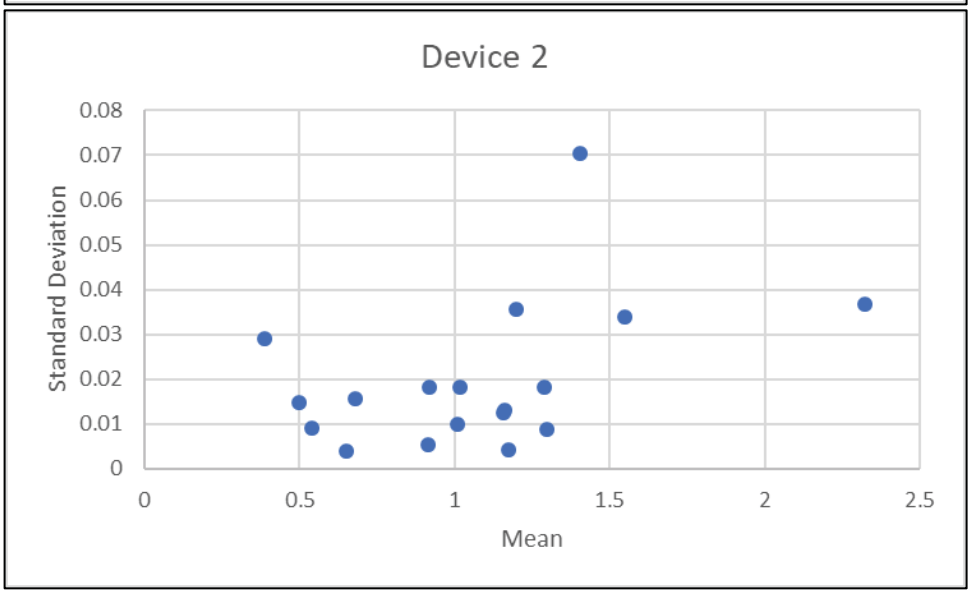

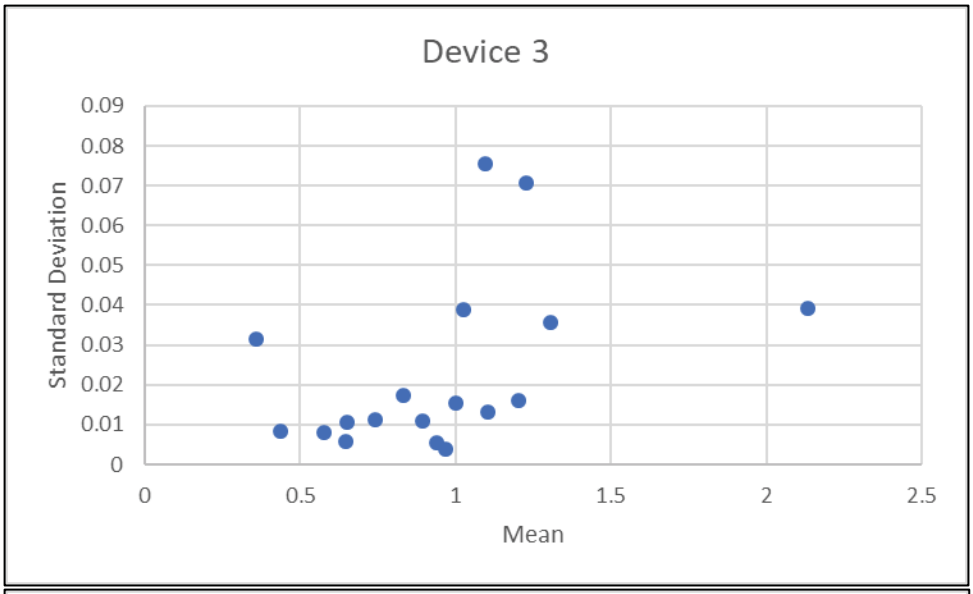
Device 3
Standard Deviation
0.09
0.08
0.07
0.06
0.05
0.04
0.03
0.02
0.01
0
0
0.5
1
1.5
2
2.5
Mean

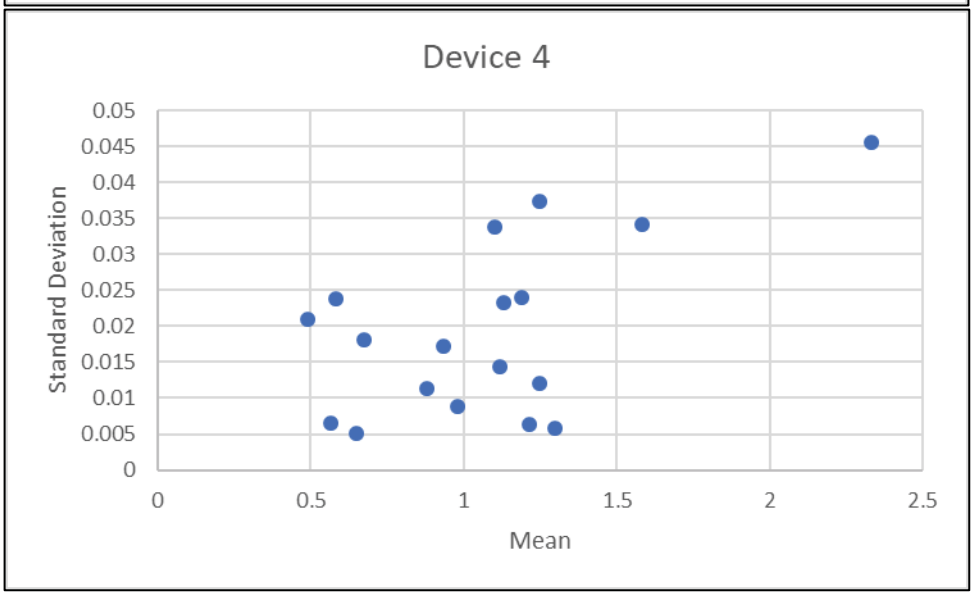
Device 4
Standard Deviation
0.05
0.045
0.04
0.035
0.03
0.025
0.02
0.015
0.01
0.005
0
0
0.5
1
1.5
2
2.5
Mean

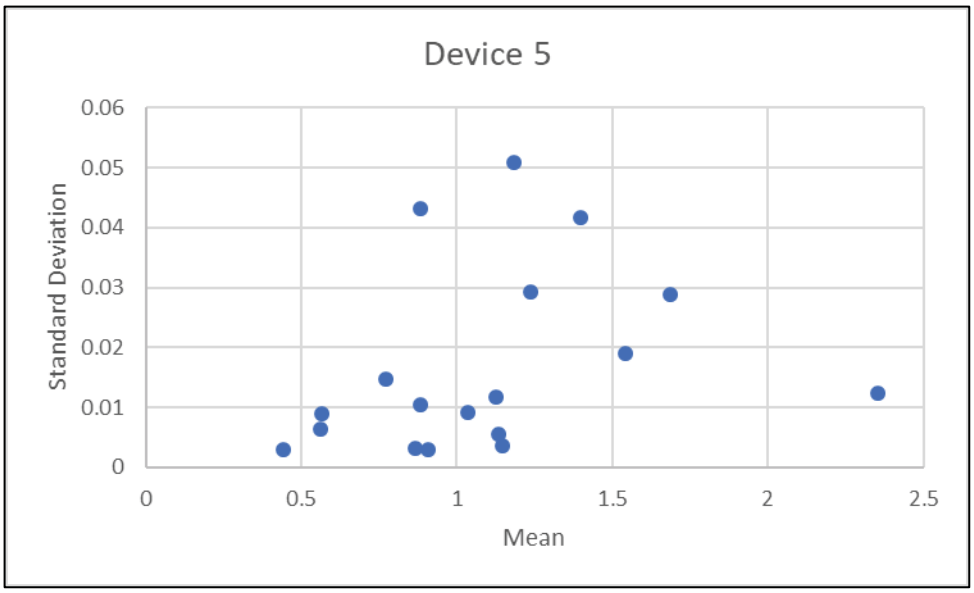
Device 5
Standard Deviation
0.06
0.05
0.04
0.03
0.02
0.01
0
0
0.5
1
1.5
2
2.5
Mean

LOA calculations and Plots:

1 - 2			
		Diff 1 - 2	avg (1&2)
	SRB	0.059442	1.318153756
	PCC2	0.025757	0.503540837
	RRB	0.086463	1.210296512
	PCC1g	0.008804	0.648690715
	PCC1f	0.011673	0.385182231
	PCC1e	0.021257	0.540097421
	PCC1d	-0.03788	1.520119919
	PCC1c	-0.00596	0.90794622
	PCC1b	0.104472	1.062488327
	PCC1a	-0.02063	0.660388882
	L2	-0.00287	1.278549311
	K	0.017537	2.324860738
	J	0.038623	1.41591684
	I	-0.01164	1.186274314
	H	0.004777	1.153631074
	HWB	0.013165	1.006187429
	D2	-0.00233	0.906635487
	C	-0.00952	1.144137295
mean diff		0.016731	
std dev diff	0.036255		
variance diff	0.001314		
		Variance for Factor 1:	0.00073
		Variance for Factor 2:	0.00067
		variance of difference 1&2	0.00131
		Corrected variance of differences between means s_c^2	0.00243
		Corrected std dev of differences between means s_c	0.04934
		LOA=1.96*s_c=	0.09671
		Range	0.19341
		Lower limit	-0.07998
		Upper Limit	0.11344

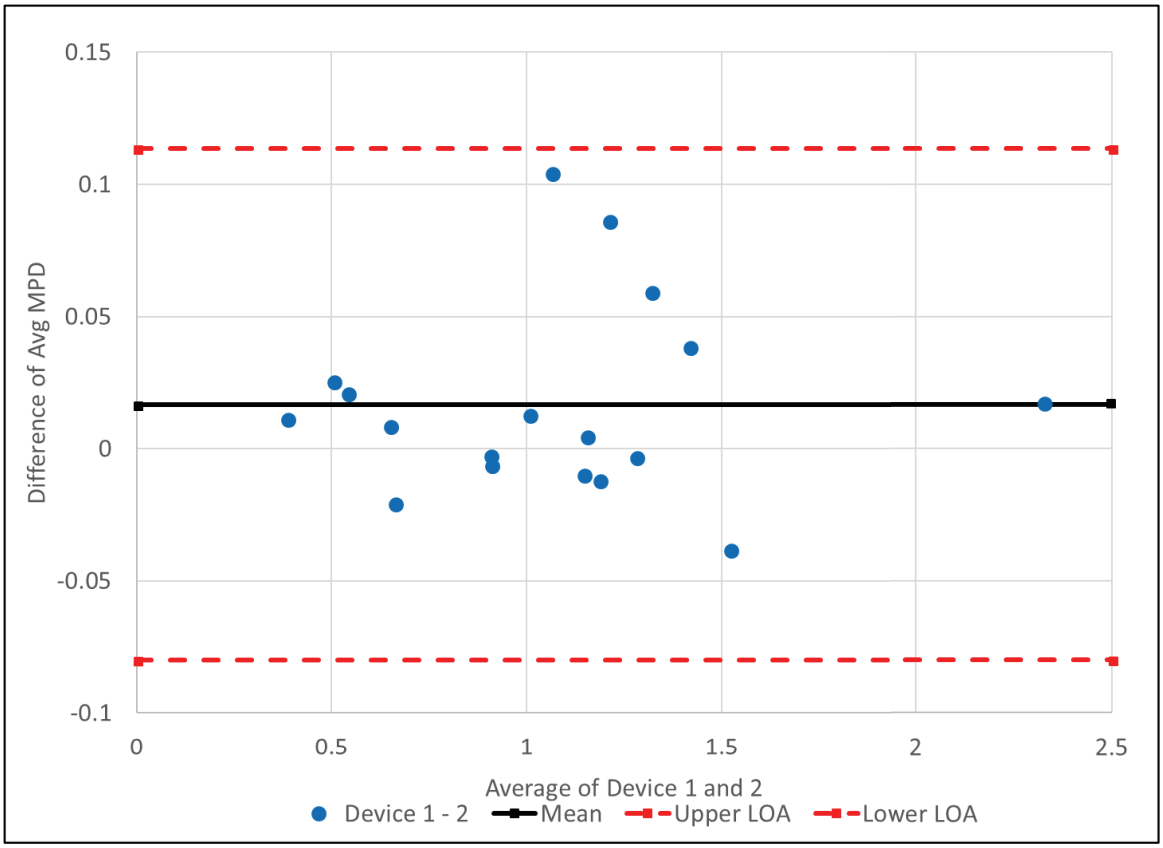
0.15
0.1
0.05
0
-0.05
-0.1
Difference of Avg MPD
0
0.5
1
1.5
2
2.5
Average of Device 1 and 2
Device 1 - 2
Mean
Upper LOA
Lower LOA

1 - 3			
		Diff 1 - 3	avg (1&3)
	SRB	0.152466	1.271641796
	PCC2	0.090535	0.471151652
	RRB	0.156544	1.175256201
	PCC1g	0.014076	0.646054816
	PCC1f	0.042967	0.369535063
	PCC1e	-0.01714	0.559294857
	PCC1d	0.203511	1.399426021
	PCC1c	0.018676	0.895628234
	PCC1b	0.291836	0.968806023
	PCC1a	0.007065	0.646542082
	L2	0.189023	1.182602765
	K	0.2066	2.230329609
	J	0.214919	1.327768891
	I	0.16527	1.097821415
	H	0.161826	1.075106288
	HWB	0.082825	0.97135698
	D2	0.174589	0.818175164
	C	0.181496	1.04863078
mean		0.129838	
std dev	0.08752		
variance	0.00766		
		Variance for Factor 1:	0.00073
		Variance for Factor 3:	0.00101
		variance of difference between means 1&3	0.00766
		Corrected variance of differences between means s_c^2	0.00905
		Corrected std dev of differences between means s_c	0.09513
		LOA=1.96*s_c=	0.18645
		Range	0.37290
		Lower limit	-0.05661
		Upper Limit	0.31629

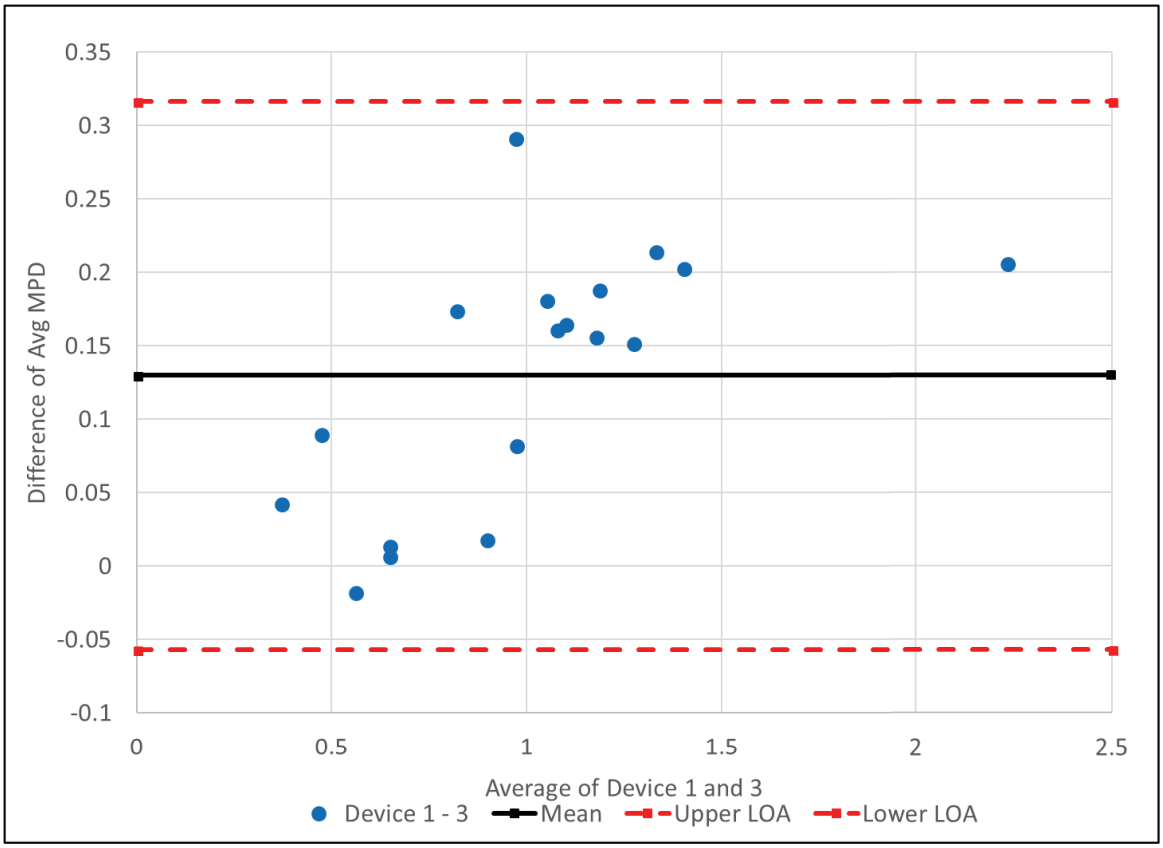
0.35
0.3
0.25
0.2
0.15
0.1
0.05
0
-0.05
-0.1
Difference of Avg MPD
0
0.5
1
1.5
2
2.5
Average of Device 1 and 3
Device 1 - 3
Mean
Upper LOA
Lower LOA

1 - 4			
		Diff 1 - 4	avg (1&4)
	SRB	0.060663	1.317543174
	PCC2	-0.05703	0.544933055
	RRB	0.072451	1.217302657
	PCC1g	0.012869	0.646658212
	PCC1f	-0.09086	0.436448615
	PCC1e	-0.00614	0.553798175
	PCC1d	-0.07062	1.536490094
	PCC1c	-0.01915	0.914540112
	PCC1b	-0.09253	1.160987575
	PCC1a	-0.01538	0.657765647
	L2	0.038402	1.257913637
	K	0.010368	2.3284452
	J	0.194595	1.33793092
	I	0.057041	1.151936206
	H	0.061393	1.125323085
	HWB	0.041692	0.991923531
	D2	0.034482	0.88822847
	C	0.029244	1.124756771
mean		0.014528	
std dev	0.069132		
variance	0.004779		
		Variance for Factor 1:	0.00073
		Variance for Factor 4:	0.00053
		variance of difference between means 1&4	0.00478
		Corrected variance of differences between means s_c^2	0.00578
		Corrected std dev of differences between means s_c	0.07606
		LOA=1.96*s_c=	0.14907
		Range	0.29815
		Lower limit	-0.13455
		Upper Limit	0.16360

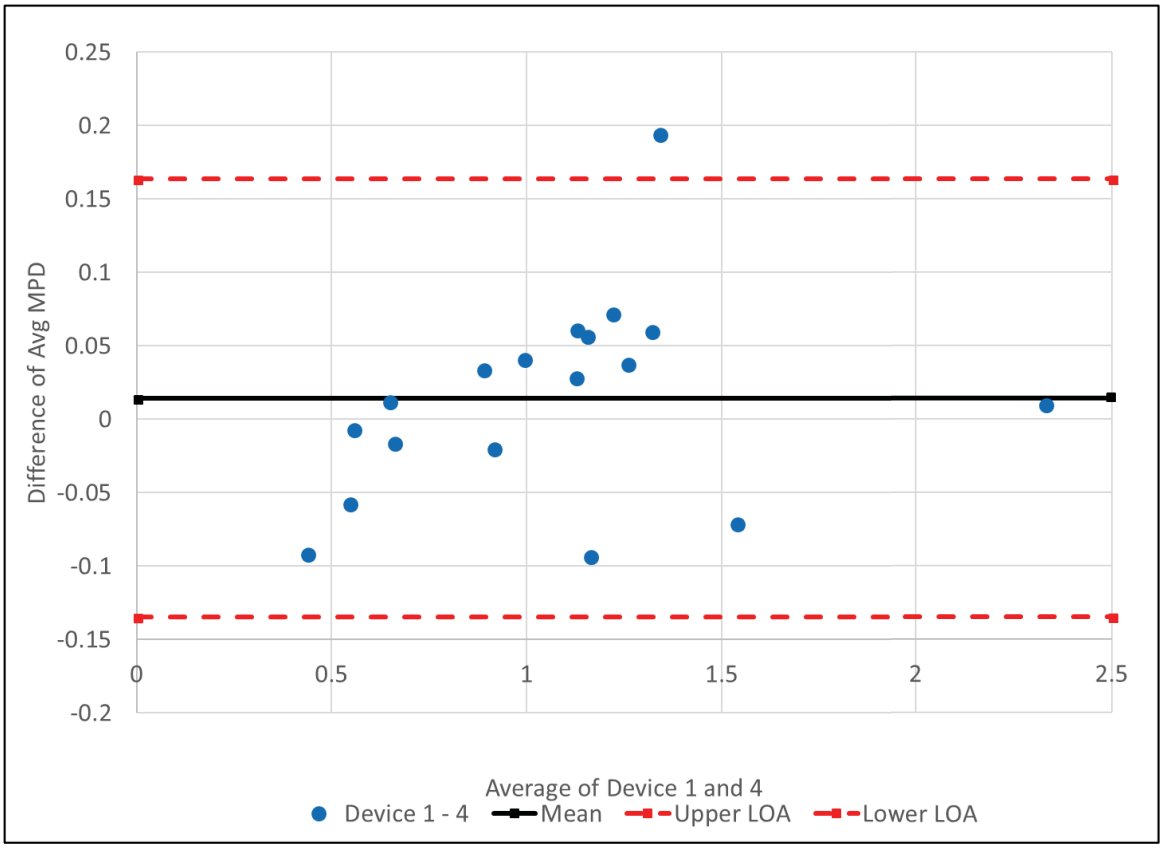
0.25
0.2
0.15
0.1
0.05
0
-0.05
-0.1
-0.15
-0.2
Difference of Avg MPD
0
0.5
1
1.5
2
2.5
Average of Device 1 and 4
Device 1 - 4
Mean
Upper LOA
Lower LOA

1 - 5			
		Diff 1 - 5	avg (1&5)
	SRB	0.209968	1.24289036
	PCC2	-0.35955	0.69619232
	RRB	0.225559	1.140748452
	PCC1g	0.09719	0.604497956
	PCC1f	-1.28747	1.034752689
	PCC1e	0.116597	0.492427467
	PCC1d	-0.03401	1.518185961
	PCC1c	0.141383	0.834274747
	PCC1b	0.214173	1.007637894
	PCC1a	0.096023	0.602063056
	L2	0.046857	1.253685948
	K	-0.00972	2.33849112
	J	0.043868	1.413294656
	I	0.060911	1.150001187
	H	0.031962	1.140038247
	HWB	0.155914	0.934812774
	D2	0.031411	0.889764234
	C	-0.03574	1.157250116
mean		0	
std dev	0.34411		
variance	0.118412		
		Variance for Factor 1:	0.00073
		Variance for Factor 5:	0.00052
		variance of difference between means 1&5	0.11841
		Corrected variance of differences between means s_c^2	0.11941
		Corrected std dev of differences between means s_c	0.34556
		LOA=1.96*s_c=	0.67730
		Range	1.35460
		Lower limit	-0.67730
		Upper Limit	0.67730

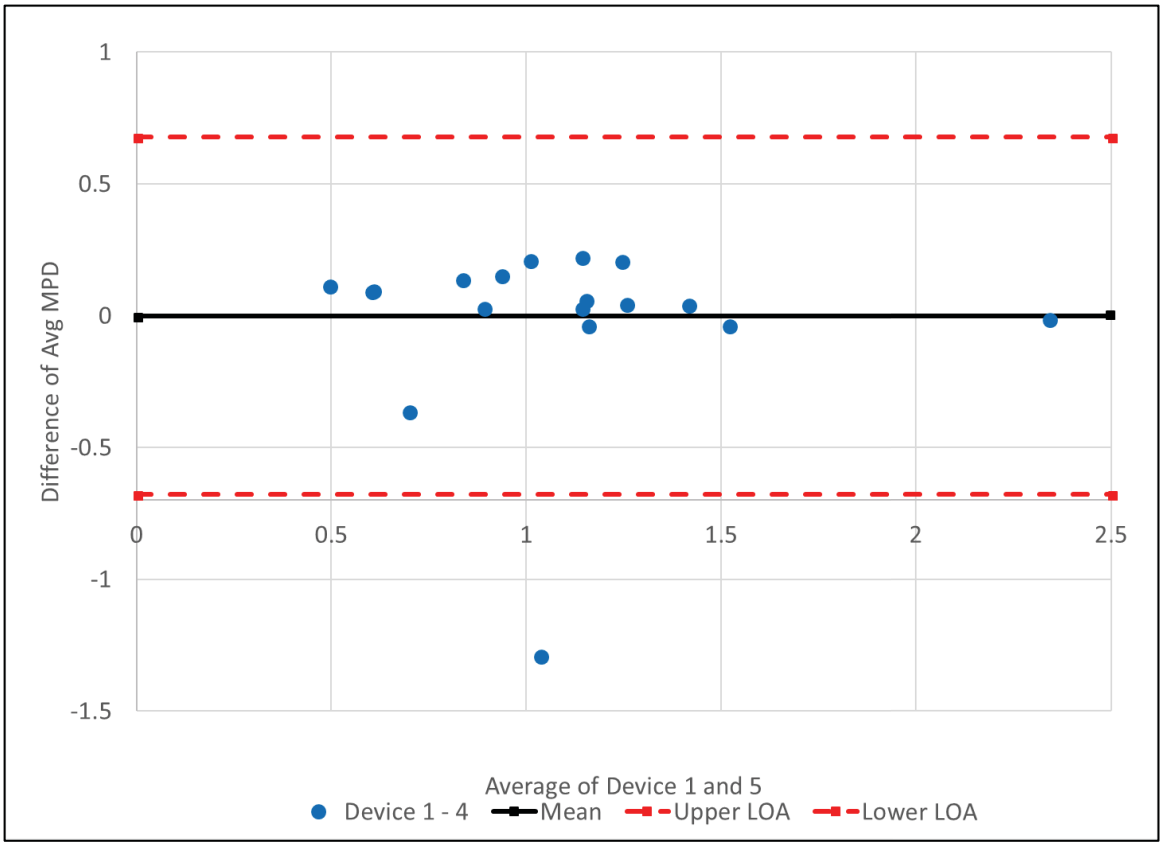
1
0.5
0
-0.5
-1
-1.5
0
0.5
1
1.5
2
2.5
Difference of Avg MPD
Average of Device 1 and 5
Device 1 - 4
Mean
Upper LOA
Lower LOA

2-3			
		Diff 2-3	avg (2&3)
	SRB	0.093024	1.241920954
	PCC2	0.064778	0.458273195
	RRB	0.070081	1.132024638
	PCC1g	0.005272	0.641652718
	PCC1f	0.031294	0.363698516
	PCC1e	-0.03839	0.548666248
	PCC1d	0.241388	1.418364505
	PCC1c	0.024636	0.89860807
	PCC1b	0.187365	0.916570096
	PCC1a	0.027694	0.65685644
	L2	0.191893	1.184037568
	K	0.189062	2.221560942
	J	0.176296	1.308457279
	I	0.176906	1.103639198
	H	0.15705	1.072717866
	HWB	0.069661	0.964774722
	D2	0.176921	0.81934099
	C	0.191013	1.053389191
mean		0.113108	
std dev	0.082945		
variance	0.00688		
		Variance for Factor 2:	0.00067
		Variance for Factor 3:	0.00101
		variance of difference between means 2&3	0.00688
		Corrected variance of differences between means s_c^2	0.00822
		Corrected std dev of differences between means s_c	0.09067
		LOA=1.96*s_c=	0.17772
		Range	0.35543
		Lower limit	-0.06461
		Upper Limit	0.29082

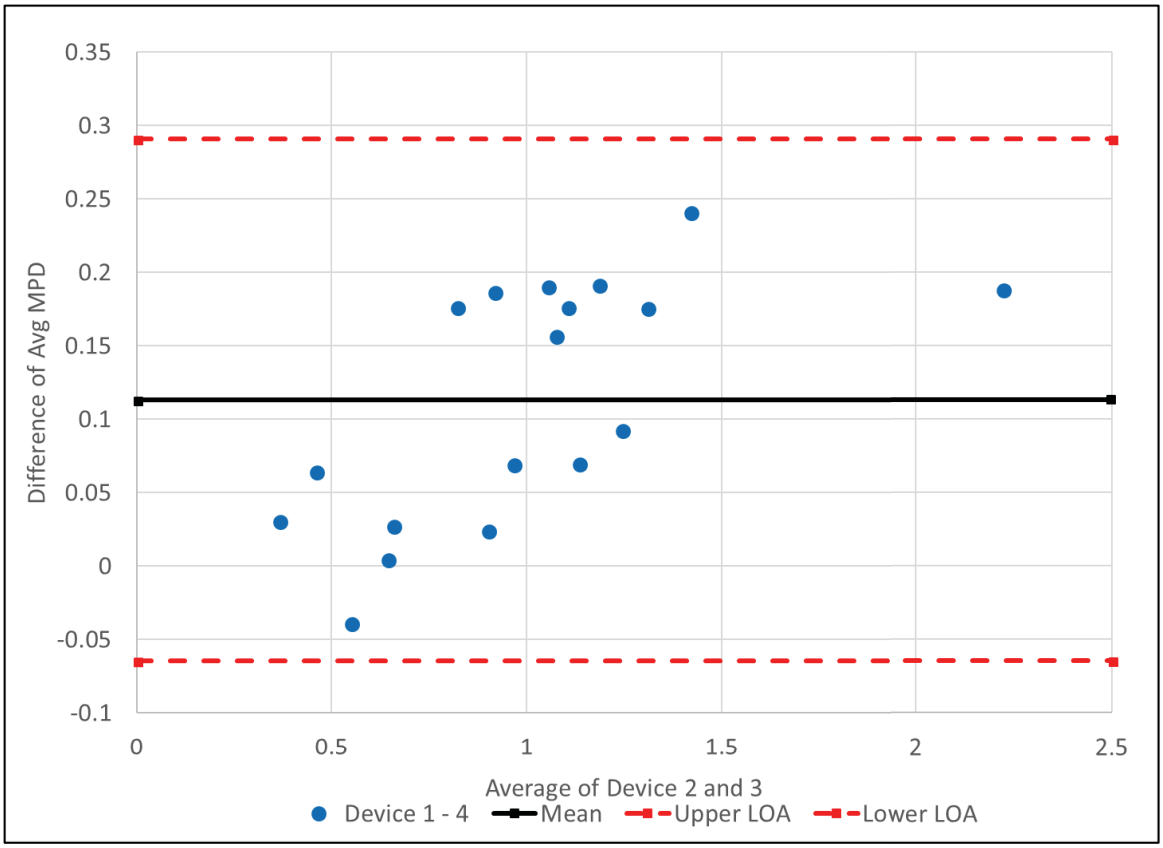
0.35
0.3
0.25
0.2
0.15
0.1
0.05
0
-0.05
-0.1
Difference of Avg MPD
0
0.5
1
1.5
2
2.5
Average of Device 2 and 3
Device 1 - 4
Mean
Upper LOA
Lower LOA

2-4			
		Diff 2-4	avg (2&4)
	SRB	0.001221	1.287822331
	PCC2	-0.08278	0.532054597
	RRB	-0.01401	1.174071094
	PCC1g	0.004065	0.642256114
	PCC1f	-0.10253	0.430612067
	PCC1e	-0.0274	0.543169566
	PCC1d	-0.03274	1.555428578
	PCC1c	-0.01319	0.917519948
	PCC1b	-0.197	1.108751647
	PCC1a	0.005246	0.668080006
	L2	0.041271	1.25934844
	K	-0.00717	2.319676532
	J	0.155972	1.318619308
	I	0.068676	1.157753989
	H	0.056616	1.122934664
	HWB	0.028528	0.985341273
	D2	0.036814	0.889394296
	C	0.038761	1.129515181
mean		-0.0022	
std dev	0.075147		
variance	0.005647		
		Variance for Factor 2:	0.00067
		Variance for Factor 4:	0.00053
		variance of difference between means 2&4	0.00565
		Corrected variance of differences between means s_c^2	0.00660
		Corrected std dev of differences between means s_c	0.08127
		LOA=1.96*s_c=	0.15929
		Range	0.31858
		Lower limit	-0.16149
		Upper Limit	0.15709

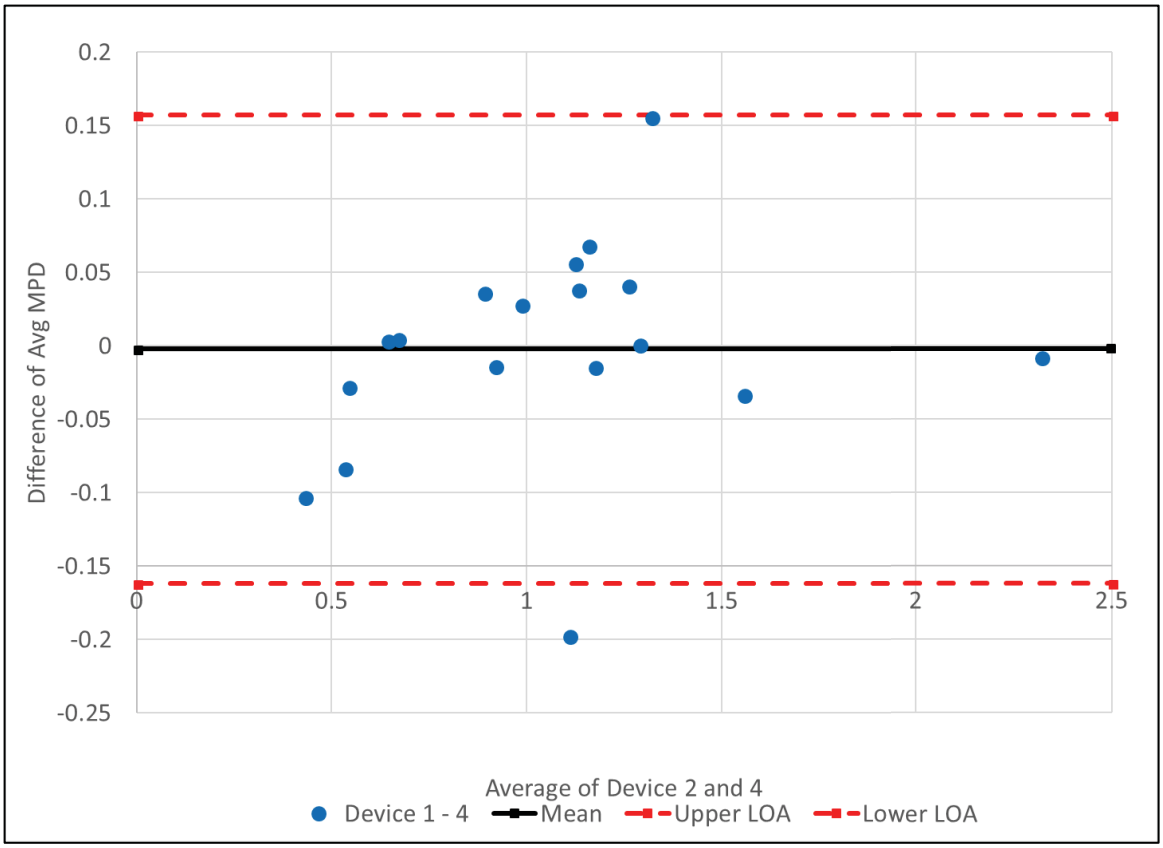
0.2
0.15
0.1
0.05
0
-0.05
-0.1
-0.15
-0.2
-0.25
Difference of Avg MPD
0
0.5
1
1.5
2
2.5
Average of Device 2 and 4
Device 1 - 4
Mean
Upper LOA
Lower LOA

2-5			
		Diff 2-5	avg (2&5)
	SRB	0.150527	1.213169517
	PCC2	-0.3853	0.683313863
	RRB	0.139096	1.097516888
	PCC1g	0.088386	0.600095858
	PCC1f	-1.29914	1.028916142
	PCC1e	0.09534	0.481798858
	PCC1d	0.003868	1.537124445
	PCC1c	0.147343	0.837254582
	PCC1b	0.109701	0.955401966
	PCC1a	0.116652	0.612377415
	L2	0.049727	1.25512075
	K	-0.02726	2.329722452
	J	0.005244	1.393983044
	I	0.072546	1.155818969
	H	0.027186	1.137649825
	HWB	0.142749	0.928230516
	D2	0.033743	0.89093006
	C	-0.02623	1.162008526
mean		-0.03088	
std dev	0.339271		
variance	0.115105		
		Variance for Factor 2:	0.00067
		Variance for Factor 5:	0.00052
		variance of difference between means 2&5	0.11511
		Corrected variance of differences between means s_c^2	0.11606
		Corrected std dev of differences between means s_c	0.34067
		LOA=1.96*s_c=	0.66772
		Range	1.33543
		Lower limit	-0.69860
		Upper Limit	0.63684

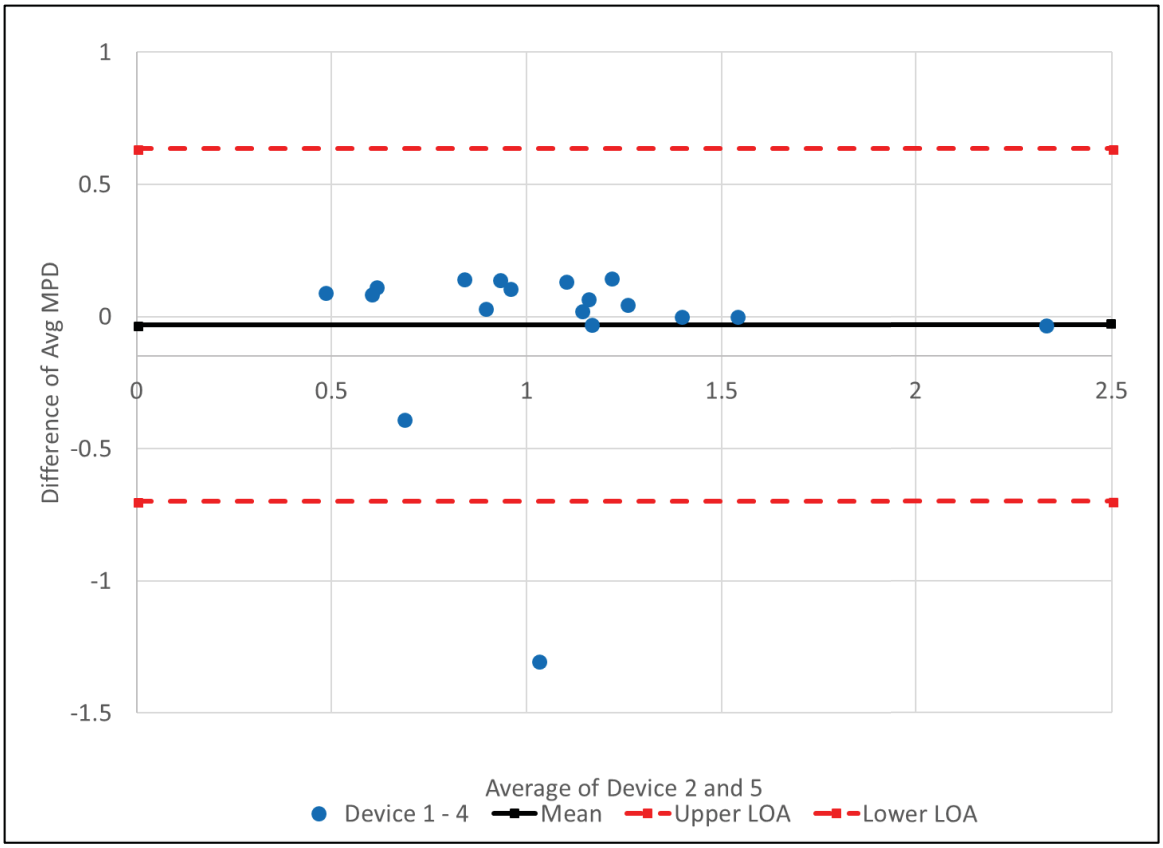
1
0.5
0
-0.5
-1
-1.5
Difference of Avg MPD
0
0.5
1
1.5
2
2.5
Average of Device 2 and 5
Device 1 - 4
Mean
Upper LOA
Lower LOA

3-4			
		Diff 3-4	avg (3&4)
	SRB	-0.0918	1.241310371
	PCC2	-0.14756	0.499665412
	RRB	-0.08409	1.139030783
	PCC1g	-0.00121	0.639620214
	PCC1f	-0.13383	0.414964899
	PCC1e	0.010993	0.562367002
	PCC1d	-0.27413	1.434734681
	PCC1c	-0.03782	0.905201961
	PCC1b	-0.38436	1.015069343
	PCC1a	-0.02245	0.654233205
	L2	-0.15062	1.163401894
	K	-0.19623	2.225145403
	J	-0.02032	1.230471359
	I	-0.10823	1.06930109
	H	-0.10043	1.044409877
	HWB	-0.04113	0.950510824
	D2	-0.14011	0.800933973
	C	-0.15225	1.034008666
mean		-0.11531	
std dev	0.099615		
variance	0.009923		
		Variance for Factor 3:	0.00101
		Variance for Factor 4:	0.00053
		variance of difference between means 3&4	0.00992
		Corrected variance of differences between means s_c^2	0.01115
		Corrected std dev of differences between means s_c	0.10560
		LOA=1.96*s_c=	0.20697
		Range	0.41393
		Lower limit	-0.32228
		Upper Limit	0.09166

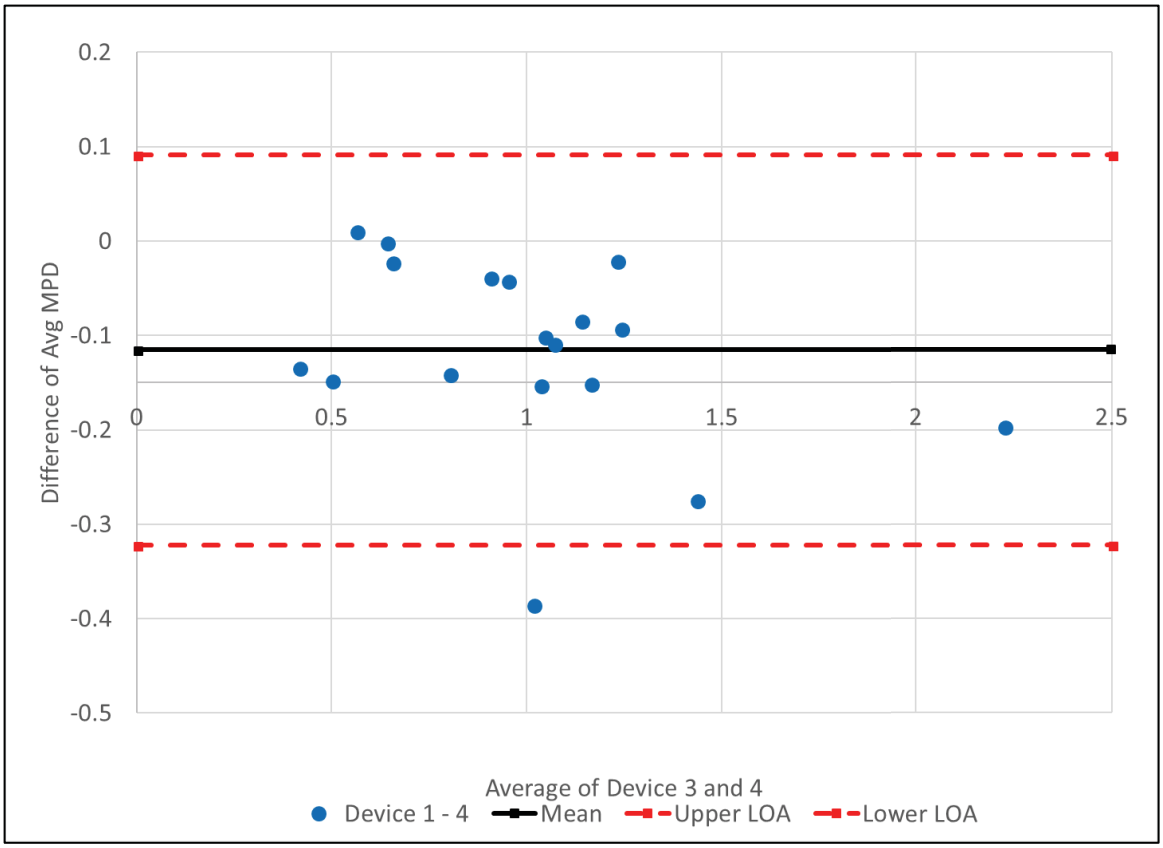
0.2
0.1
0
-0.1
-0.2
-0.3
-0.4
-0.5
Difference of Avg MPD
0
0.5
1
1.5
2
2.5
Average of Device 3 and 4
Device 1 - 4
Mean
Upper LOA
Lower LOA

3-5			
		Diff 3-5	avg (3&5)
	SRB	0.057503	1.166657557
	PCC2	-0.45008	0.650924677
	RRB	0.069015	1.062476578
	PCC1g	0.083114	0.597459958
	PCC1f	-1.33044	1.013268973
	PCC1e	0.133735	0.500996294
	PCC1d	-0.23752	1.416430548
	PCC1c	0.122707	0.824936596
	PCC1b	-0.07766	0.861719662
	PCC1a	0.088958	0.598530614
	L2	-0.14217	1.159174204
	K	-0.21632	2.235191323
	J	-0.17105	1.305835095
	I	-0.10436	1.067366071
	H	-0.12986	1.059125039
	HWB	0.073088	0.893400067
	D2	-0.14318	0.802469736
	C	-0.21724	1.066502012
mean		-0.14399	
std dev	0.335611		
variance	0.112635		
		Variance for Factor 3:	0.00101
		Variance for Factor 5:	0.00052
		variance of difference between means 3&5	0.11263
		Corrected variance of differences between means s_c^2	0.11386
		Corrected std dev of differences between means s_c	0.33743
		LOA=1.96*s_c=	0.66135
		Range	1.32271
		Lower limit	-0.80534
		Upper Limit	0.51737

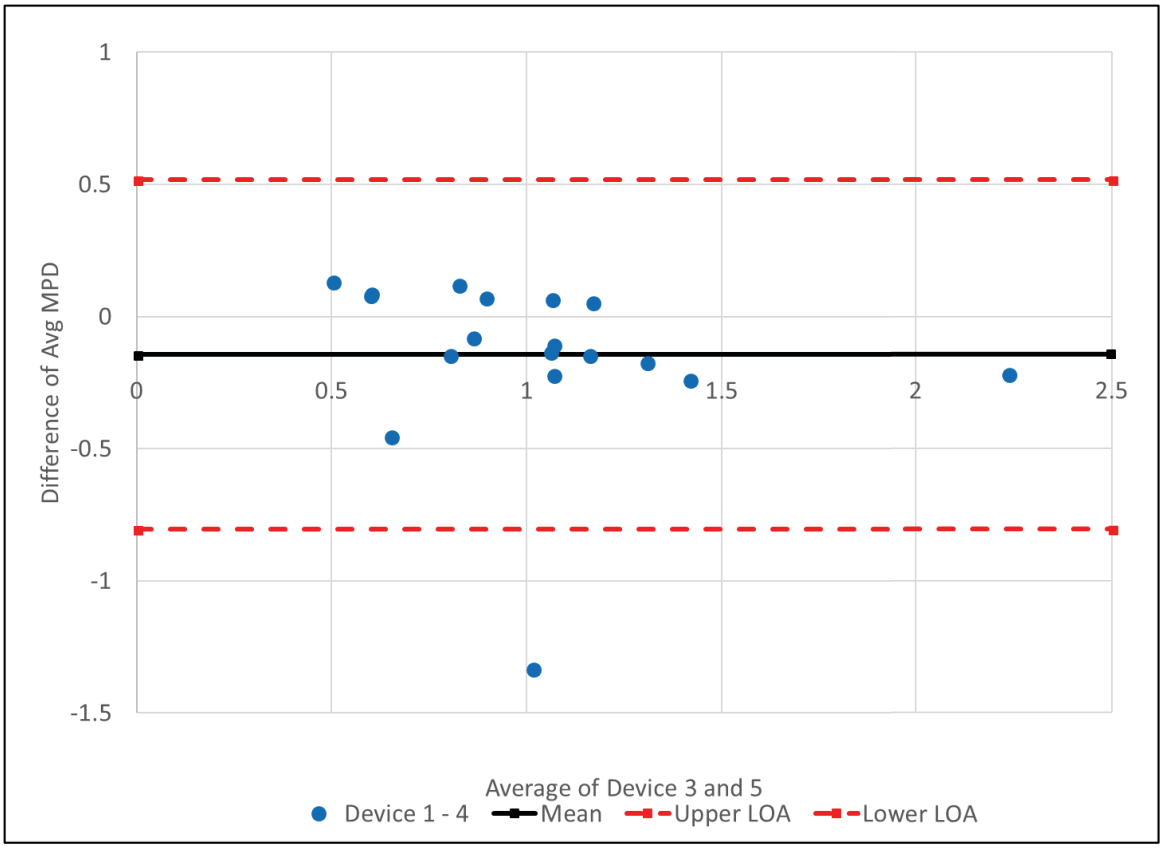
1
0.5
0
-0.5
-1
-1.5
Difference of Avg MPD
0
0.5
1
1.5
2
2.5
Average of Device 3 and 5
Device 1 - 4
Mean
Upper LOA
Lower LOA

4-5			
		Diff 4-5	avg (4&5)
	SRB	0.149306	1.212558935
	PCC2	-0.30252	0.72470608
	RRB	0.153108	1.104523034
	PCC1g	0.084321	0.598063354
	PCC1f	-1.19661	1.080182525
	PCC1e	0.122741	0.495499612
	PCC1d	0.036608	1.553494621
	PCC1c	0.160531	0.843848474
	PCC1b	0.306699	1.053901214
	PCC1a	0.111405	0.60975418
	L2	0.008455	1.234485076
	K	-0.02009	2.333306913
	J	-0.15073	1.315997124
	I	0.00387	1.121480862
	H	-0.02943	1.109341836
	HWB	0.114222	0.913966618
	D2	-0.00307	0.872523043
	C	-0.06499	1.142628002
mean		-0.02868	
std dev	0.320976		
variance	0.103026		
		Variance for Factor 4:	0.00053
		Variance for Factor 5:	0.00052
		variance of difference between means 4&5	0.10303
		Corrected variance of differences between means s_c^2	0.10386
		Corrected std dev of differences between means s_c	0.32228
		LOA=1.96*s_c=	0.63167
		Range	1.26333
		Lower limit	-0.66034
		Upper Limit	0.60299

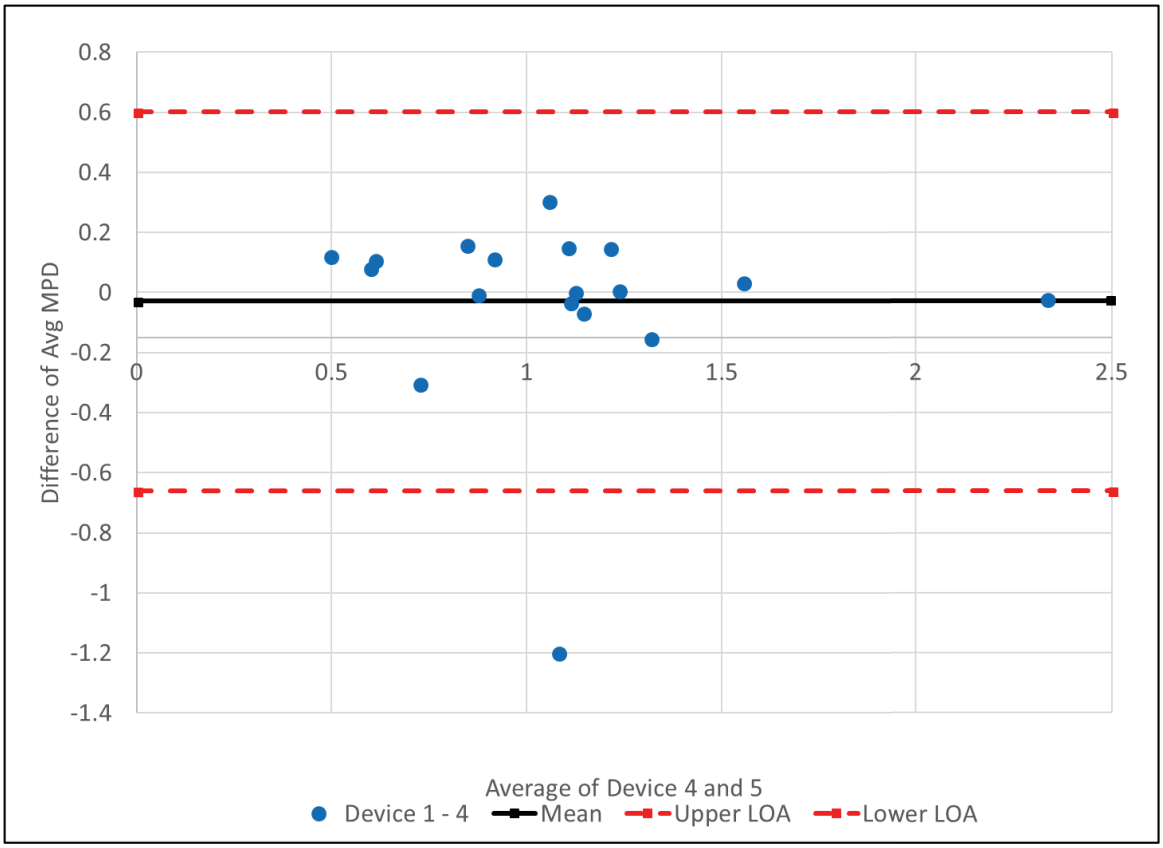
0.8
0.6
0.4
0.2
0
-0.2
-0.4
-0.6
-0.8
-1
-1.2
-1.4
Difference of Avg MPD
0
0.5
1
1.5
2
2.5
Average of Device 4 and 5
Device 1 - 4
Mean
Upper LOA
Lower LOA

Appendix J Chapter 3 LOA – Smart Road (Longitudinal Sections Removed)

ANOVA tables for MSE to use as device variance

DEVICE#1					
Analysis of Variance					
Source	DF	Sum of Squares	Mean Square	F Ratio	Prob > F
Model	15	13.343188	0.889546	1124.311	<.0001
Error	64	0.050636	0.000791		
C. Total	79	13.393824			

DEVICE#2					
Analysis of Variance					
Source	DF	Sum of Squares	Mean Square	F Ratio	Prob > F
Model	15	13.173707	0.878247	1279.883	<.0001
Error	64	0.043916	0.000686		
C. Total	79	13.217623			

DEVICE#3					
Analysis of Variance					
Source	DF	Sum of Squares	Mean Square	F Ratio	Prob > F
Model	15	10.140137	0.676009	635.8894	<.0001
Error	64	0.068038	0.001063		
C. Total	79	10.208174			

DEVICE#4					
Analysis of Variance					
Source	DF	Sum of Squares	Mean Square	F Ratio	Prob > F
Model	15	12.983276	0.865552	1639.278	<.0001
Error	64	0.033793	0.000528		
C. Total	79	13.017068			

DEVICE#5					
Analysis of Variance					
Source	DF	Sum of Squares	Mean Square	F Ratio	Prob > F
Model	15	15.651354	1.04342	2517.071	<.0001
Error	64	0.02653	0.00041		
C. Total	79	15.677884			

1 - 2			
		Diff 1 - 2	avg (1&2)
	SRB	0.059442	1.318153756
	RRB	0.086463	1.210296512
	PCC1g	0.008804	0.648690715
	PCC1e	0.021257	0.540097421
	PCC1d	-0.03788	1.520119919
	PCC1c	-0.00596	0.90794622
	PCC1b	0.104472	1.062488327
	PCC1a	-0.02063	0.660388882
	L2	-0.00287	1.278549311
	K	0.017537	2.324860738
	J	0.038623	1.41591684
	I	-0.01164	1.186274314
	H	0.004777	1.153631074
	HWB	0.013165	1.006187429
	D2	-0.00233	0.906635487
	C	-0.00952	1.144137295
mean diff		0.016483	
std dev diff	0.038503		
variance diff	0.001482		
		Variance for Factor 1:	0.00079
		Variance for Factor 2:	0.00069
		variance of difference 1&2	0.00148
		Corrected variance of differences between means s_c^2	0.00266
		Corrected std dev of differences between means s_c	0.05161
		LOA=1.96*s_c=	0.10116
		Range	0.20233
		Lower limit	-0.08468
		Upper Limit	0.11765

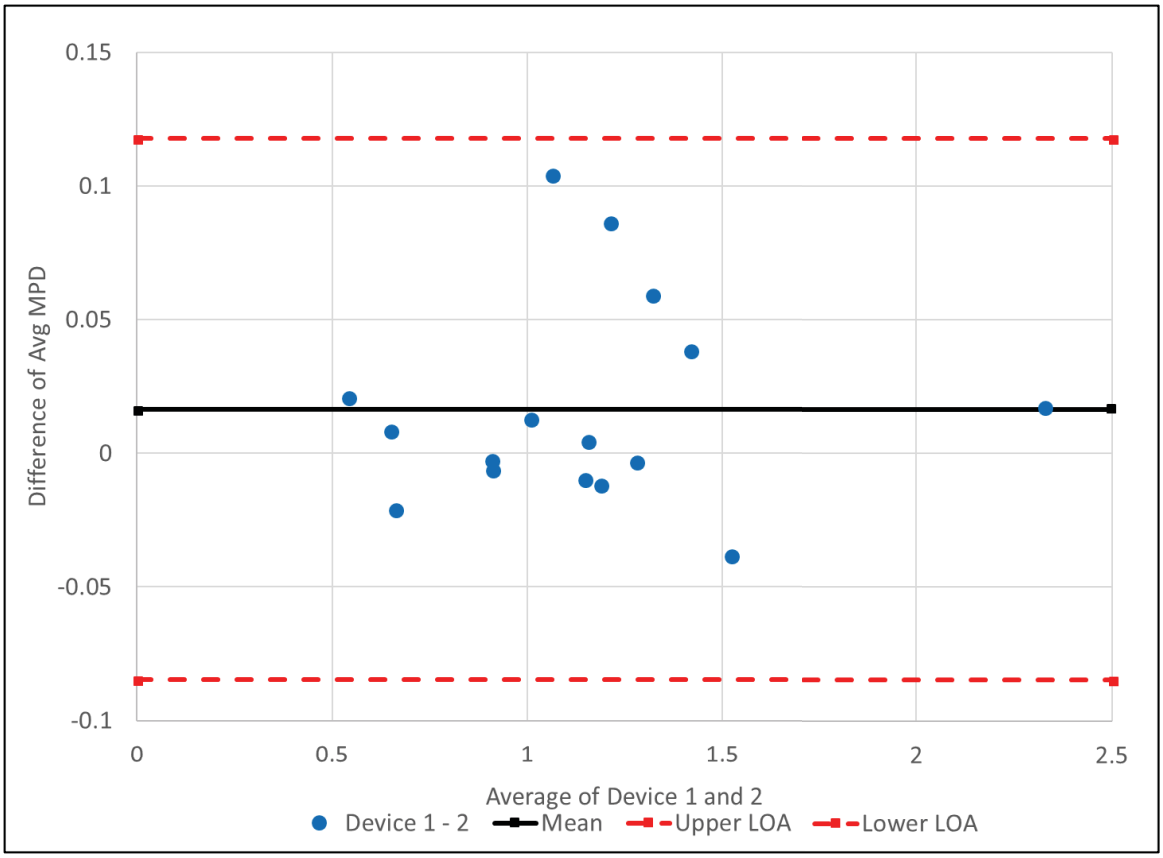
0.15
0.1
0.05
0
-0.05
-0.1
Difference of Avg MPD
0
0.5
1
1.5
2
2.5
Average of Device 1 and 2
Device 1 - 2
Mean
Upper LOA
Lower LOA

1 - 3			
		Diff 1 - 3	avg (1&3)
	SRB	0.152466	1.271641796
	RRB	0.156544	1.175256201
	PCC1g	0.014076	0.646054816
	PCC1e	-0.01714	0.559294857
	PCC1d	0.203511	1.399426021
	PCC1c	0.018676	0.895628234
	PCC1b	0.291836	0.968806023
	PCC1a	0.007065	0.646542082
	L2	0.189023	1.182602765
	K	0.2066	2.230329609
	J	0.214919	1.327768891
	I	0.16527	1.097821415
	H	0.161826	1.075106288
	HWB	0.082825	0.97135698
	D2	0.174589	0.818175164
	C	0.181496	1.04863078
mean		0.137724	
std dev	0.089491		
variance	0.008009		
		Variance for Factor 1:	0.00079
		Variance for Factor 3:	0.00106
		variance of difference between means 1&3	0.00801
		Corrected variance of differences between means s_c^2	0.00949
		Corrected std dev of differences between means s_c	0.09743
		LOA=1.96*s_c=	0.19095
		Range	0.38191
		Lower limit	-0.05323
		Upper Limit	0.32868

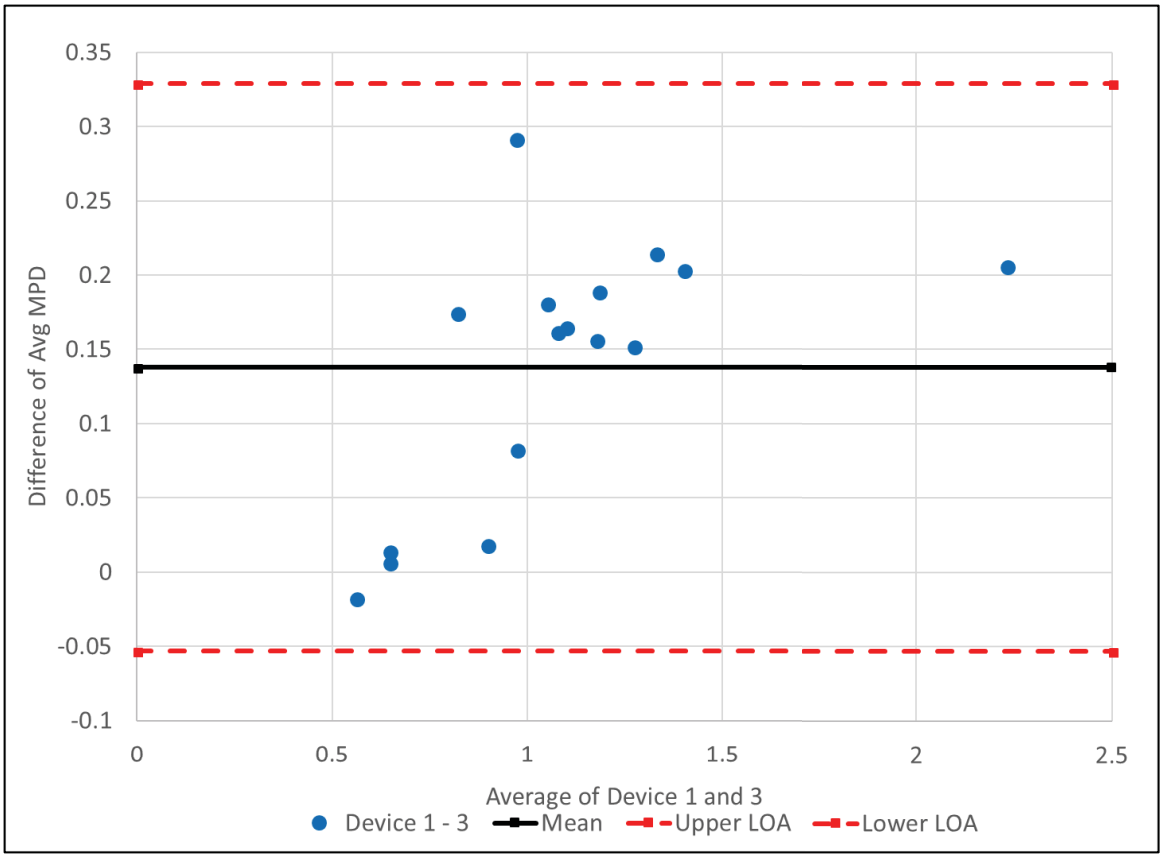
0.35
0.3
0.25
0.2
0.15
0.1
0.05
0
-0.05
-0.1
Difference of Avg MPD
0
0.5
1
1.5
2
2.5
Average of Device 1 and 3
Device 1 - 3
Mean
Upper LOA
Lower LOA

1 - 4			
		Diff 1 - 4	avg (1&4)
	SRB	0.060663	1.317543174
	RRB	0.072451	1.217302657
	PCC1g	0.012869	0.646658212
	PCC1e	-0.00614	0.553798175
	PCC1d	-0.07062	1.536490094
	PCC1c	-0.01915	0.914540112
	PCC1b	-0.09253	1.160987575
	PCC1a	-0.01538	0.657765647
	L2	0.038402	1.257913637
	K	0.010368	2.3284452
	J	0.194595	1.33793092
	I	0.057041	1.151936206
	H	0.061393	1.125323085
	HWB	0.041692	0.991923531
	D2	0.034482	0.88822847
	C	0.029244	1.124756771
mean		0.025586	
std dev	0.06484		
variance	0.004204		
		Variance for Factor 1:	0.00079
		Variance for Factor 4:	0.00053
		variance of difference between means 1&4	0.00420
		Corrected variance of differences between means s_c^2	0.00526
		Corrected std dev of differences between means s_c	0.07252
		LOA=1.96*s_c=	0.14214
		Range	0.28429
		Lower limit	-0.11656
		Upper Limit	0.16773

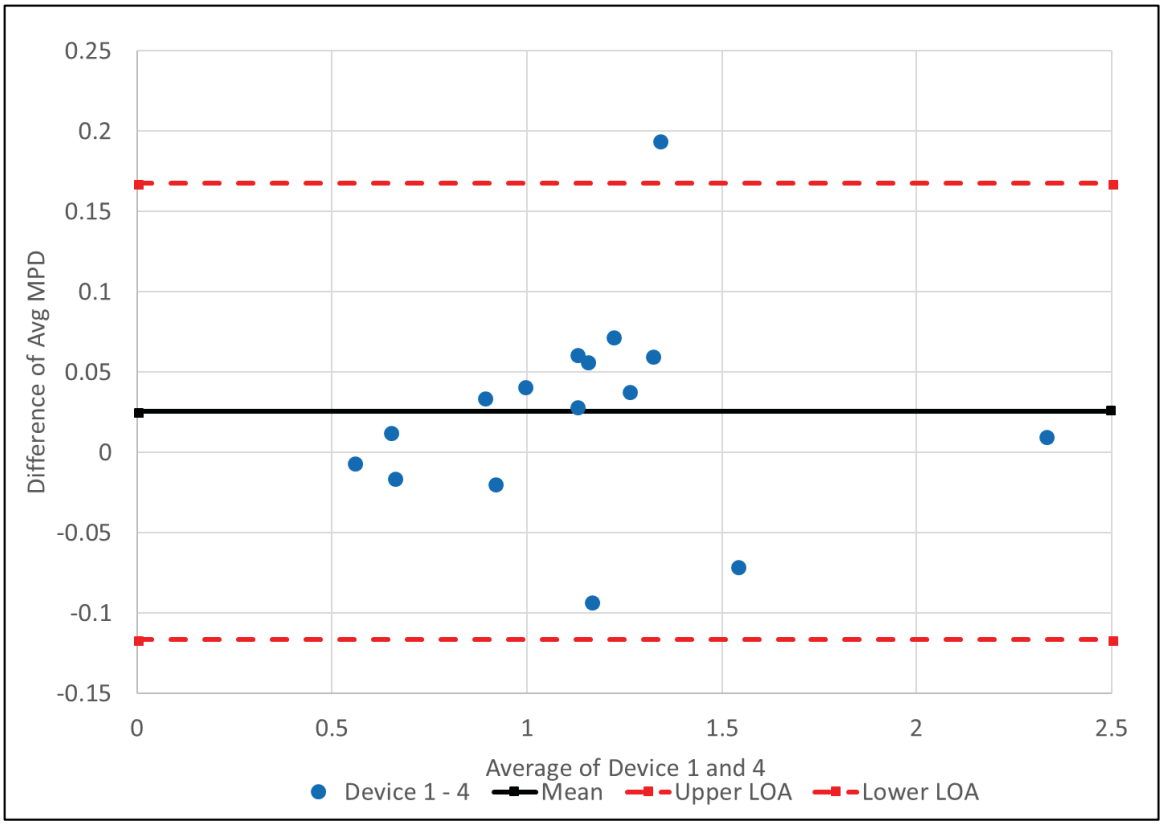
0.25
0.2
0.15
0.1
0.05
0
-0.05
-0.1
-0.15
Difference of Avg MPD
0
0.5
1
1.5
2
2.5
Average of Device 1 and 4
Device 1 - 4
Mean
Upper LOA
Lower LOA

1 - 5			
		Diff 1 - 5	avg (1&5)
	SRB	0.209968	1.24289036
	RRB	0.225559	1.140748452
	PCC1g	0.09719	0.604497956
	PCC1e	0.116597	0.492427467
	PCC1d	-0.03401	1.518185961
	PCC1c	0.141383	0.834274747
	PCC1b	0.214173	1.007637894
	PCC1a	0.096023	0.602063056
	L2	0.046857	1.253685948
	K	-0.00972	2.33849112
	J	0.043868	1.413294656
	I	0.060911	1.150001187
	H	0.031962	1.140038247
	HWB	0.155914	0.934812774
	D2	0.031411	0.889764234
	C	-0.03574	1.157250116
mean		0.087021	
std dev	0.085087		
variance	0.00724		
		Variance for Factor 1:	0.00079
		Variance for Factor 5:	0.00041
		variance of difference between means 1&5	0.00724
		Corrected variance of differences between means s_c^2	0.00820
		Corrected std dev of differences between means s_c	0.09056
		LOA=1.96*s_c=	0.17749
		Range	0.35498
		Lower limit	-0.09047
		Upper Limit	0.26451

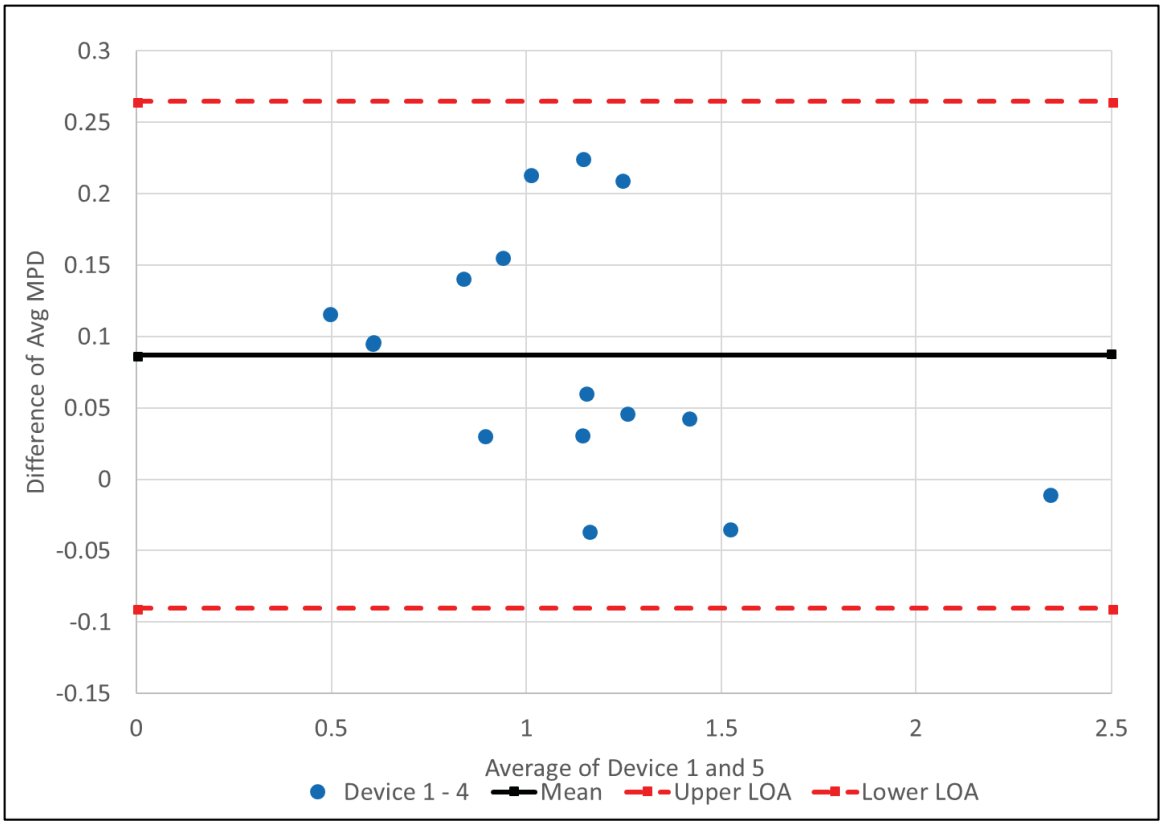
0.3
0.25
0.2
0.15
0.1
0.05
0
-0.05
-0.1
-0.15
Difference of Avg MPD
0
0.5
1
1.5
2
2.5
Average of Device 1 and 5
Device 1 - 4
Mean
Upper LOA
Lower LOA

2-3			
		Diff 2-3	avg (2&3)
	SRB	0.093024	1.241920954
	RRB	0.070081	1.132024638
	PCC1g	0.005272	0.641652718
	PCC1e	-0.03839	0.548666248
	PCC1d	0.241388	1.418364505
	PCC1c	0.024636	0.89860807
	PCC1b	0.187365	0.916570096
	PCC1a	0.027694	0.65685644
	L2	0.191893	1.184037568
	K	0.189062	2.221560942
	J	0.176296	1.308457279
	I	0.176906	1.103639198
	H	0.15705	1.072717866
	HWB	0.069661	0.964774722
	D2	0.176921	0.81934099
	C	0.191013	1.053389191
mean		0.121242	
std dev	0.084408		
variance	0.007125		
		Variance for Factor 2:	0.00069
		Variance for Factor 3:	0.00106
		variance of difference between means 2&3	0.00712
		Corrected variance of differences between means s_c^2	0.00852
		Corrected std dev of differences between means s_c	0.09232
		LOA=1.96*s_c=	0.18096
		Range	0.36191
		Lower limit	-0.05971
		Upper Limit	0.30220

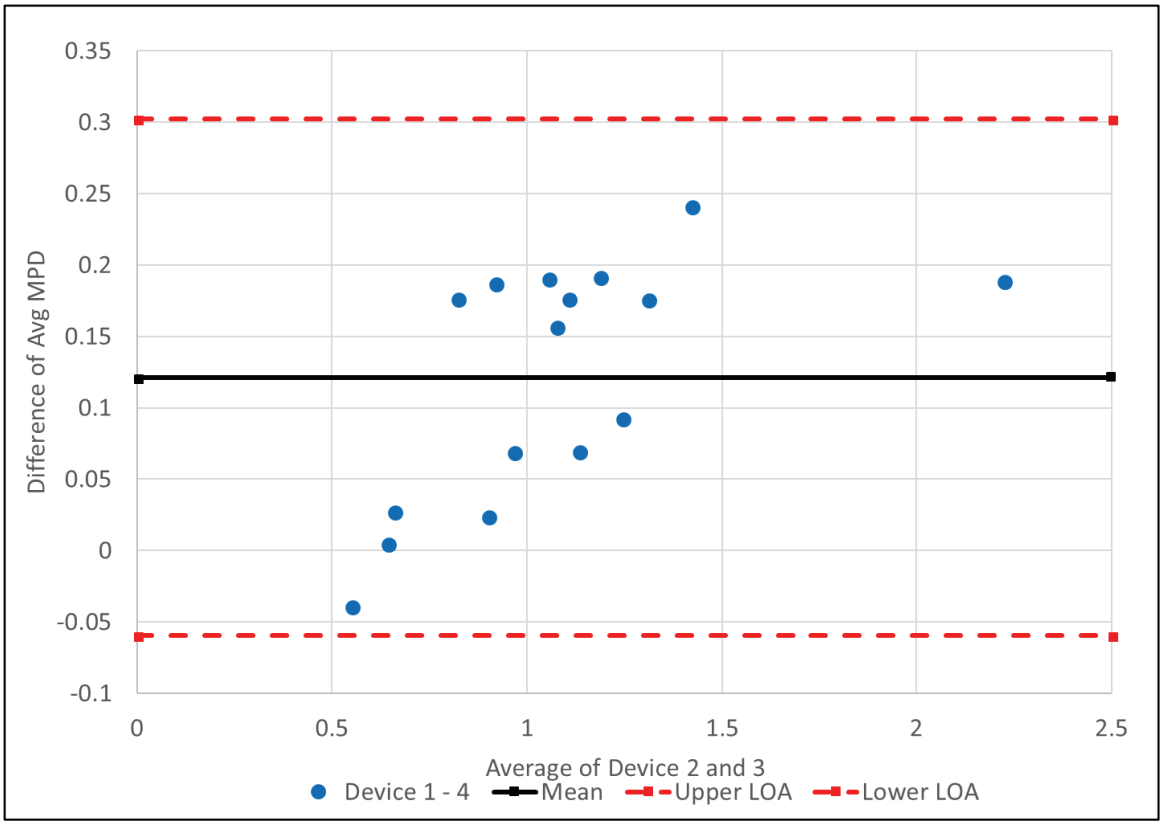
0.35
0.3
0.25
0.2
0.15
0.1
0.05
0
-0.05
-0.1
Difference of Avg MPD
0
0.5
1
1.5
2
2.5
Average of Device 2 and 3
Device 1 - 4
Mean
Upper LOA
Lower LOA

2-4			
		Diff 2-4	avg (2&4)
	SRB	0.001221	1.287822331
	RRB	-0.01401	1.174071094
	PCC1g	0.004065	0.642256114
	PCC1e	-0.0274	0.543169566
	PCC1d	-0.03274	1.555428578
	PCC1c	-0.01319	0.917519948
	PCC1b	-0.197	1.108751647
	PCC1a	0.005246	0.668080006
	L2	0.041271	1.25934844
	K	-0.00717	2.319676532
	J	0.155972	1.318619308
	I	0.068676	1.157753989
	H	0.056616	1.122934664
	HWB	0.028528	0.985341273
	D2	0.036814	0.889394296
	C	0.038761	1.129515181
mean		0.009104	
std dev	0.071831		
variance	0.00516		
		Variance for Factor 2:	0.00069
		Variance for Factor 4:	0.00053
		variance of difference between means 2&4	0.00516
		Corrected variance of differences between means s_c^2	0.00613
		Corrected std dev of differences between means s_c	0.07830
		LOA=1.96*s_c=	0.15347
		Range	0.30694
		Lower limit	-0.14436
		Upper Limit	0.16257

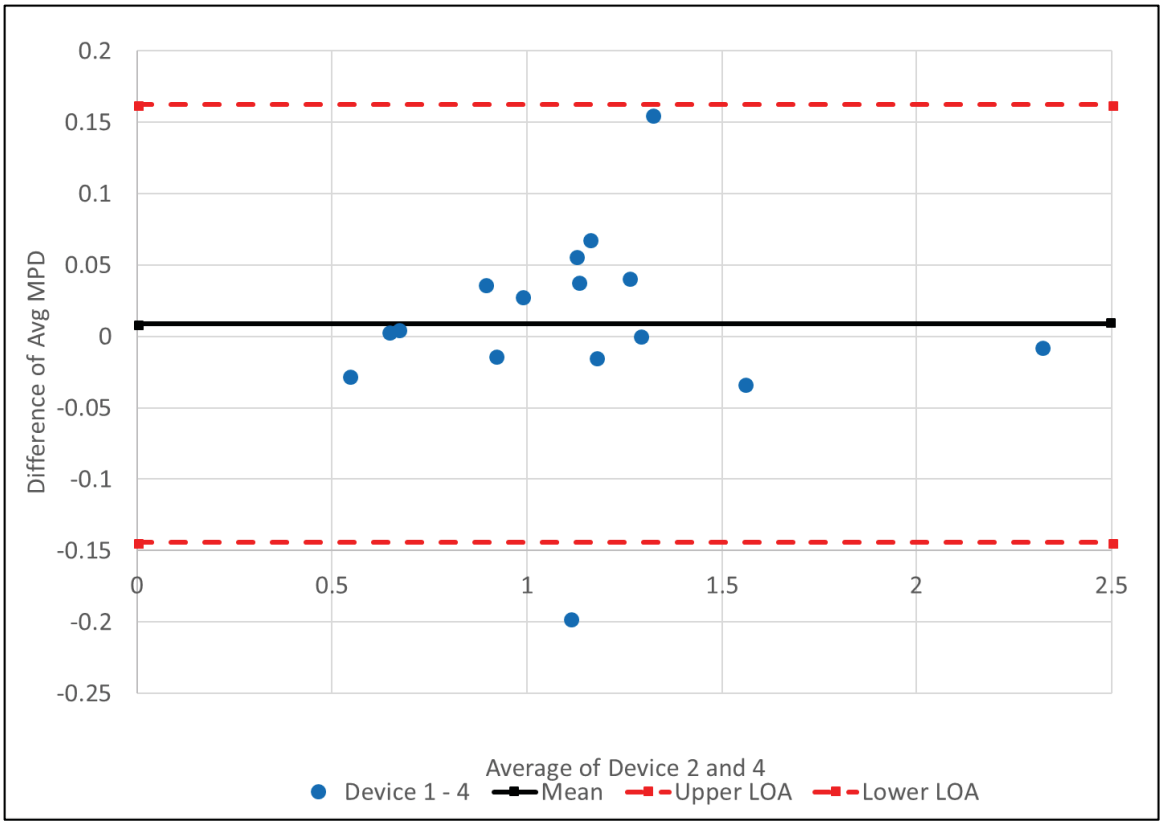
0.2
0.15
0.1
0.05
0
-0.05
-0.1
-0.15
-0.2
-0.25
Difference of Avg MPD
0
0.5
1
1.5
2
2.5
Average of Device 2 and 4
Device 1 - 4
Mean
Upper LOA
Lower LOA

2-5			
		Diff 2-5	avg (2&5)
	SRB	0.150527	1.213169517
	RRB	0.139096	1.097516888
	PCC1g	0.088386	0.600095858
	PCC1e	0.09534	0.481798858
	PCC1d	0.003868	1.537124445
	PCC1c	0.147343	0.837254582
	PCC1b	0.109701	0.955401966
	PCC1a	0.116652	0.612377415
	L2	0.049727	1.25512075
	K	-0.02726	2.329722452
	J	0.005244	1.393983044
	I	0.072546	1.155818969
	H	0.027186	1.137649825
	HWB	0.142749	0.928230516
	D2	0.033743	0.89093006
	C	-0.02623	1.162008526
mean		0.070539	
std dev	0.062243		
variance	0.003874		
		Variance for Factor 2:	0.00069
		Variance for Factor 5:	0.00041
		variance of difference between means 2&5	0.00387
		Corrected variance of differences between means s_c^2	0.00475
		Corrected std dev of differences between means s_c	0.06893
		LOA=1.96*s_c=	0.13510
		Range	0.27019
		Lower limit	-0.06456
		Upper Limit	0.20564

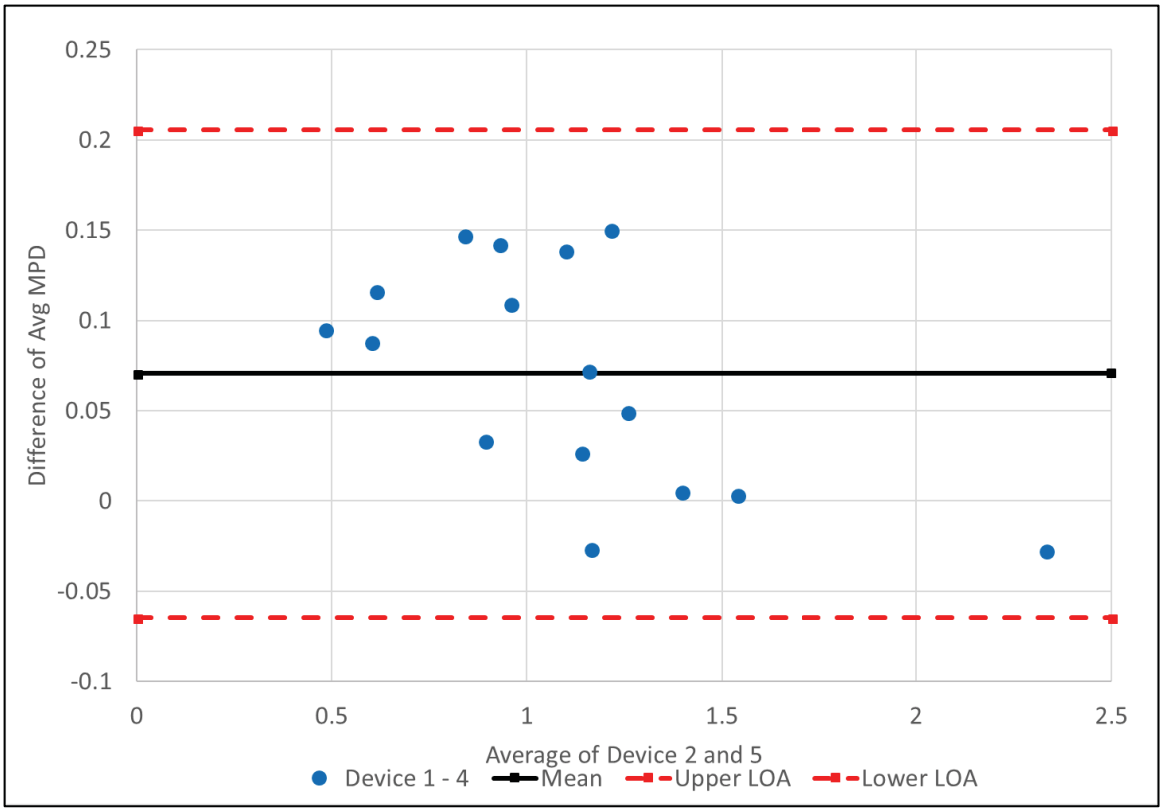
0.25
0.2
0.15
0.1
0.05
0
-0.05
-0.1
Difference of Avg MPD
0
0.5
1
1.5
2
2.5
Average of Device 2 and 5
Device 1 - 4
Mean
Upper LOA
Lower LOA

3-4			
		Diff 3-4	avg (3&4)
	SRB	-0.0918	1.241310371
	RRB	-0.08409	1.139030783
	PCC1g	-0.00121	0.639620214
	PCC1e	0.010993	0.562367002
	PCC1d	-0.27413	1.434734681
	PCC1c	-0.03782	0.905201961
	PCC1b	-0.38436	1.015069343
	PCC1a	-0.02245	0.654233205
	L2	-0.15062	1.163401894
	K	-0.19623	2.225145403
	J	-0.02032	1.230471359
	I	-0.10823	1.06930109
	H	-0.10043	1.044409877
	HWB	-0.04113	0.950510824
	D2	-0.14011	0.800933973
	C	-0.15225	1.034008666
mean		-0.11214	
std dev	0.105562		
variance	0.011143		
		Variance for Factor 3:	0.00106
		Variance for Factor 4:	0.00053
		variance of difference between means 3&4	0.01114
		Corrected variance of differences between means s_c^2	0.01242
		Corrected std dev of differences between means s_c	0.11143
		LOA=1.96*s_c=	0.21840
		Range	0.43680
		Lower limit	-0.33054
		Upper Limit	0.10626

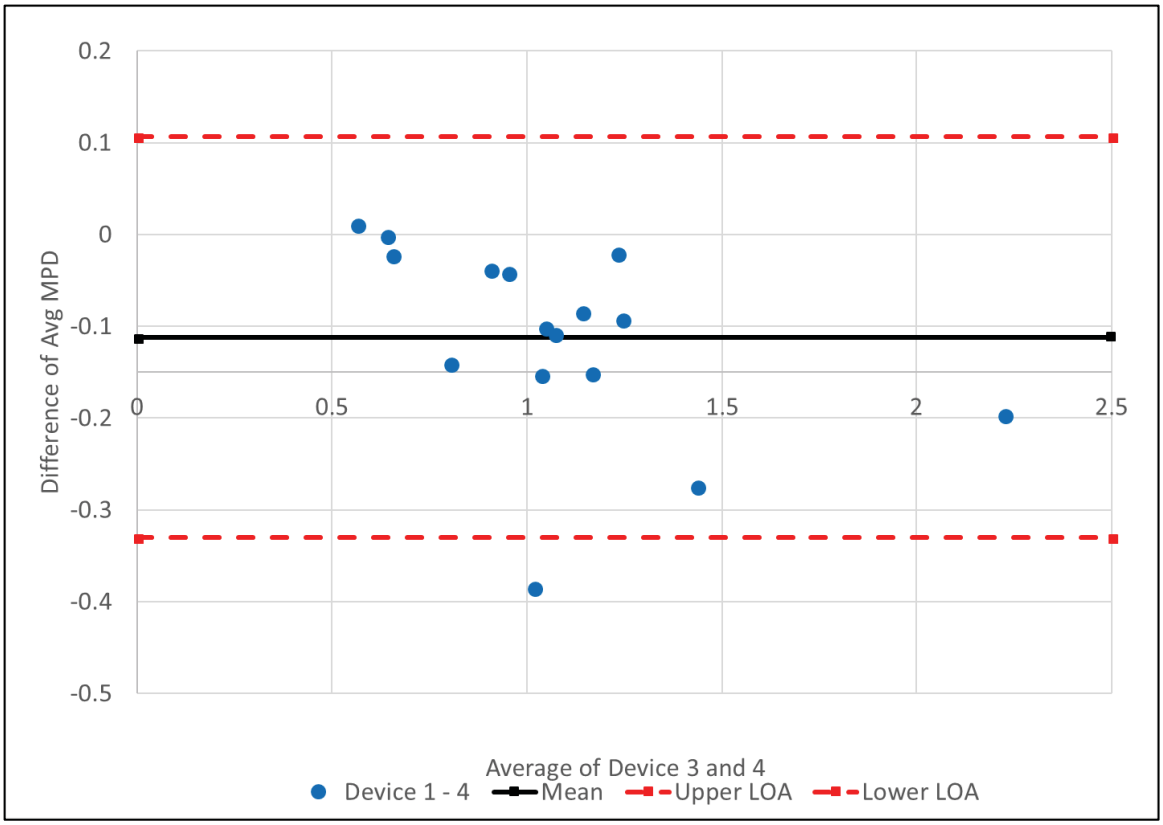
0.2
0.1
0
-0.1
-0.2
-0.3
-0.4
-0.5
Difference of Avg MPD
0
0.5
1
1.5
2
2.5
Average of Device 3 and 4
Device 1 - 4
Mean
Upper LOA
Lower LOA

3-5			
		Diff 3-5	avg (3&5)
	SRB	0.057503	1.166657557
	RRB	0.069015	1.062476578
	PCC1g	0.083114	0.597459958
	PCC1e	0.133735	0.500996294
	PCC1d	-0.23752	1.416430548
	PCC1c	0.122707	0.824936596
	PCC1b	-0.07766	0.861719662
	PCC1a	0.088958	0.598530614
	L2	-0.14217	1.159174204
	K	-0.21632	2.235191323
	J	-0.17105	1.305835095
	I	-0.10436	1.067366071
	H	-0.12986	1.059125039
	HWB	0.073088	0.893400067
	D2	-0.14318	0.802469736
	C	-0.21724	1.066502012
mean		-0.0507	
std dev	0.135204		
variance	0.01828		
		Variance for Factor 3:	0.00106
		Variance for Factor 5:	0.00041
		variance of difference between means 3&5	0.01828
		Corrected variance of differences between means s_c^2	0.01946
		Corrected std dev of differences between means s_c	0.13949
		LOA=1.96*s_c=	0.27341
		Range	0.54682
		Lower limit	-0.32411
		Upper Limit	0.22271

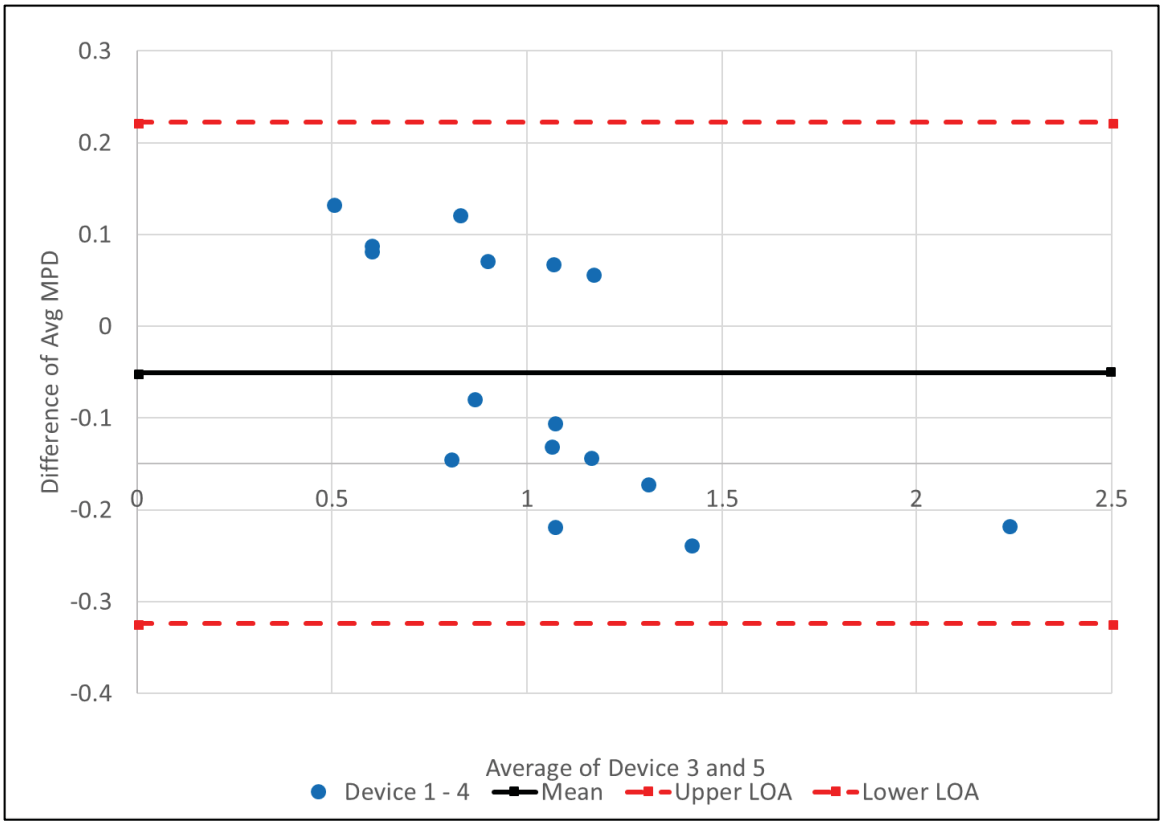
0.3
0.2
0.1
0
-0.1
-0.2
-0.3
-0.4
Difference of Avg MPD
0
0.5
1
1.5
2
2.5
Average of Device 3 and 5
Device 1 - 4
Mean
Upper LOA
Lower LOA

4-5			
		Diff 4-5	avg (4&5)
	SRB	0.149306	1.212558935
	RRB	0.153108	1.104523034
	PCC1g	0.084321	0.598063354
	PCC1e	0.122741	0.495499612
	PCC1d	0.036608	1.553494621
	PCC1c	0.160531	0.843848474
	PCC1b	0.306699	1.053901214
	PCC1a	0.111405	0.60975418
	L2	0.008455	1.234485076
	K	-0.02009	2.333306913
	J	-0.15073	1.315997124
	I	0.00387	1.121480862
	H	-0.02943	1.109341836
	HWB	0.114222	0.913966618
	D2	-0.00307	0.872523043
	C	-0.06499	1.142628002
mean		0.061435	
std dev	0.110291		
variance	0.012164		
		Variance for Factor 4:	0.00053
		Variance for Factor 5:	0.00041
		variance of difference between means 4&5	0.01216
		Corrected variance of differences between means s_c^2	0.01291
		Corrected std dev of differences between means s_c	0.11364
		LOA=1.96*s_c=	0.22274
		Range	0.44548
		Lower limit	-0.16130
		Upper Limit	0.28417

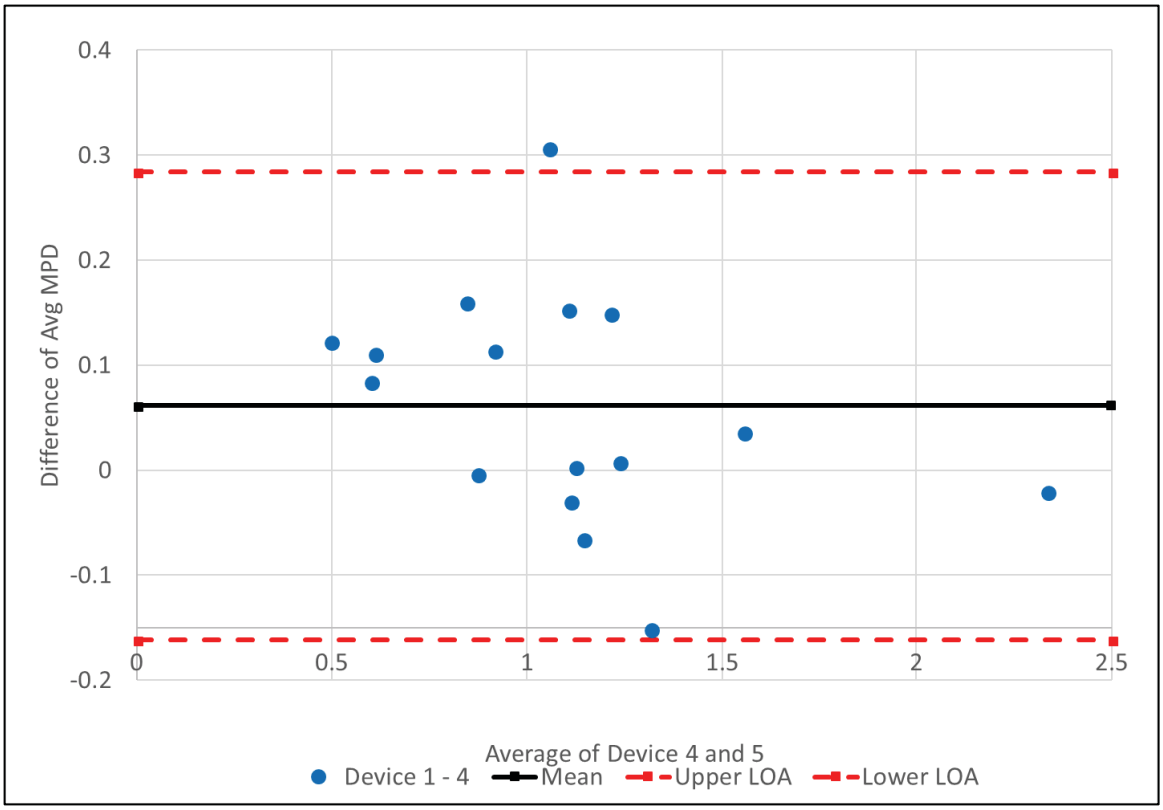
0.4
0.3
0.2
0.1
0
-0.1
-0.2
Difference of Avg MPD
0
0.5
1
1.5
2
2.5
Average of Device 4 and 5
Device 1 - 4
Mean
Upper LOA
Lower LOA

Appendix K Chapter 3 LOA – Asphalt Sections

ANOVA tables to determine MSE used as device variance

DEVICE#1					
Analysis of Variance					
Source	DF	Sum of Squares	Mean Square	F Ratio	Prob > F
Model	8	6.8269405	0.853368	646.7431	<.0001
Error	36	0.0475014	0.001319		
C. Total	44	6.8744419			

DEVICE#2					
Analysis of Variance					
Source	DF	Sum of Squares	Mean Square	F Ratio	Prob > F
Model	8	6.9359784	0.866997	777.5948	<.0001
Error	36	0.040139	0.001115		
C. Total	44	6.9761174			

DEVICE#3					
Analysis of Variance					
Source	DF	Sum of Squares	Mean Square	F Ratio	Prob > F
Model	8	6.730859	0.841357	469.6289	<.0001
Error	36	0.0644953	0.001792		
C. Total	44	6.7953543			

DEVICE#4					
Analysis of Variance					
Source	DF	Sum of Squares	Mean Square	F Ratio	Prob > F
Model	8	7.1477783	0.893472	1147.701	<.0001
Error	36	0.0280256	0.000778		
C. Total	44	7.1758039			

DEVICE#5					
Analysis of Variance					
Source	DF	Sum of Squares	Mean Square	F Ratio	Prob > F
Model	8	7.8860257	0.985753	1445.753	<.0001
Error	36	0.0245458	0.000682		
C. Total	44	7.9105715			

1 - 2			
		Diff 1 - 2	avg (1&2)
	PCC1d	-0.03788	1.520119919
	PCC1b	0.104472	1.062488327
	L2	-0.00287	1.278549311
	K	0.017537	2.324860738
	J	0.038623	1.41591684
	I	-0.01164	1.186274314
	H	0.004777	1.153631074
	D2	-0.00233	0.906635487
	C	-0.00952	1.144137295
mean diff		0.011242	
std dev diff	0.040733		
variance diff	0.001659		
		Variance for Factor 1:	0.00132
		Variance for Factor 2:	0.00112
		variance of difference 1&2	0.00166
		Corrected variance of differences between means s_c^2	0.00361
		Corrected std dev of differences between means s_c	0.06005
		LOA=1.96*s_c=	0.11770
		Range	0.23541
		Lower limit	-0.10646
		Upper Limit	0.12895

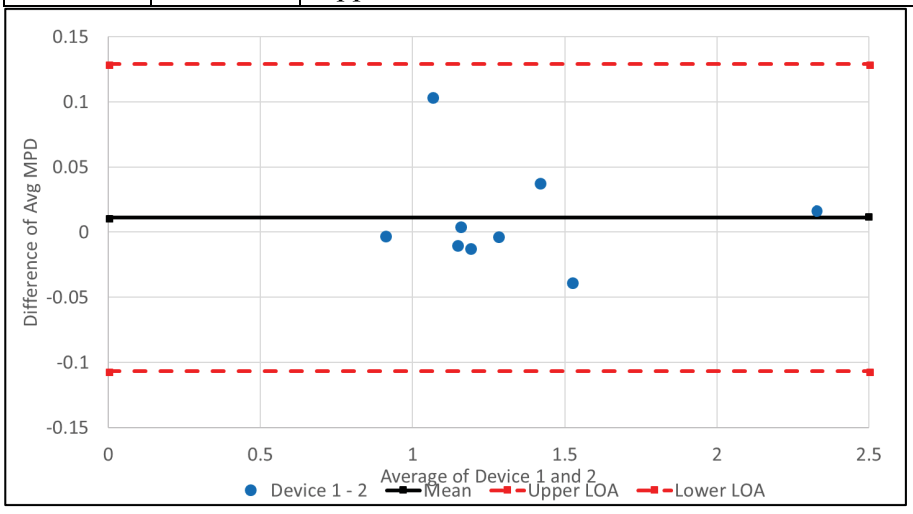

1 - 3			
		Diff 1 - 3	avg (1&3)
	PCC1d	0.203511	1.399426021
	PCC1b	0.291836	0.968806023
	L2	0.189023	1.182602765
	K	0.2066	2.230329609
	J	0.214919	1.327768891
	I	0.16527	1.097821415
	H	0.161826	1.075106288
	D2	0.174589	0.818175164
	C	0.181496	1.04863078
mean		0.198786	
std dev	0.039483		
variance	0.001559		
		Variance for Factor 1:	0.00132
		Variance for Factor 3:	0.00179
		variance of difference between means 1&3	0.00156
		Corrected variance of differences between means s_c^2	0.00405
		Corrected std dev of differences between means s_c	0.06362
		LOA=1.96*s_c=	0.12470
		Range	0.24940
		Lower limit	0.07409
		Upper Limit	0.32348

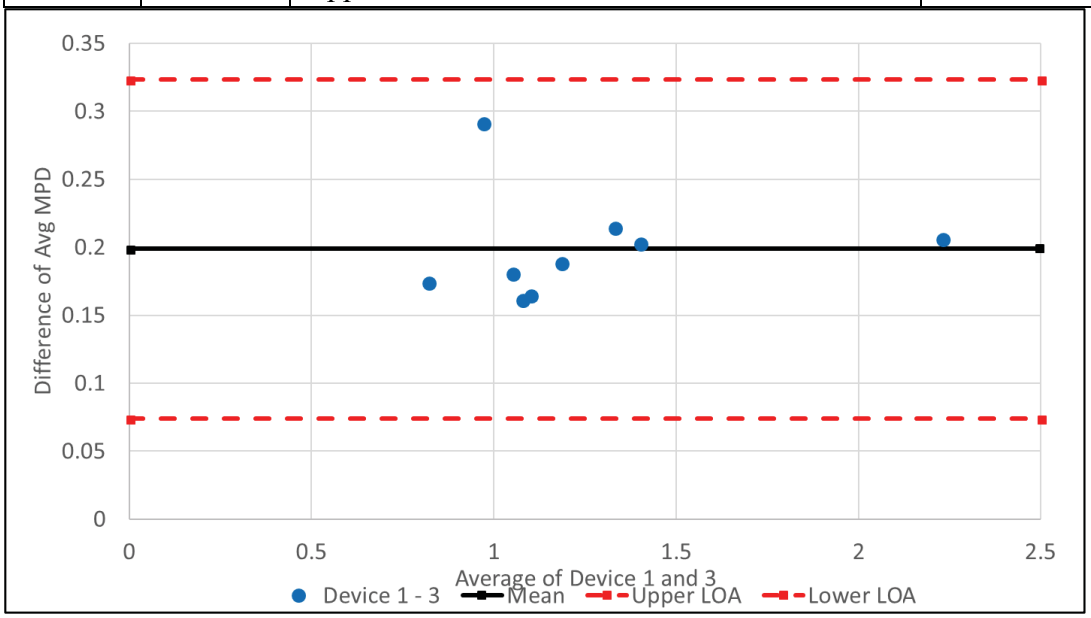

1 - 4			
		Diff 1 - 4	avg (1&4)
	PCC1d	-0.07062	1.536490094
	PCC1b	-0.09253	1.160987575
	L2	0.038402	1.257913637
	K	0.010368	2.3284452
	J	0.194595	1.33793092
	I	0.057041	1.151936206
	H	0.061393	1.125323085
	D2	0.034482	0.88822847
	C	0.029244	1.124756771
mean		0.029153	
std dev	0.082474		
variance	0.006802		
		Variance for Factor 1:	0.00132
		Variance for Factor 4:	0.00078
		variance of difference between means 1&4	0.00680
		Corrected variance of differences between means s_c^2	0.00848
		Corrected std dev of differences between means s_c	0.09208
		LOA=1.96*s_c=	0.18048
		Range	0.36097
		Lower limit	-0.15133
		Upper Limit	0.20964

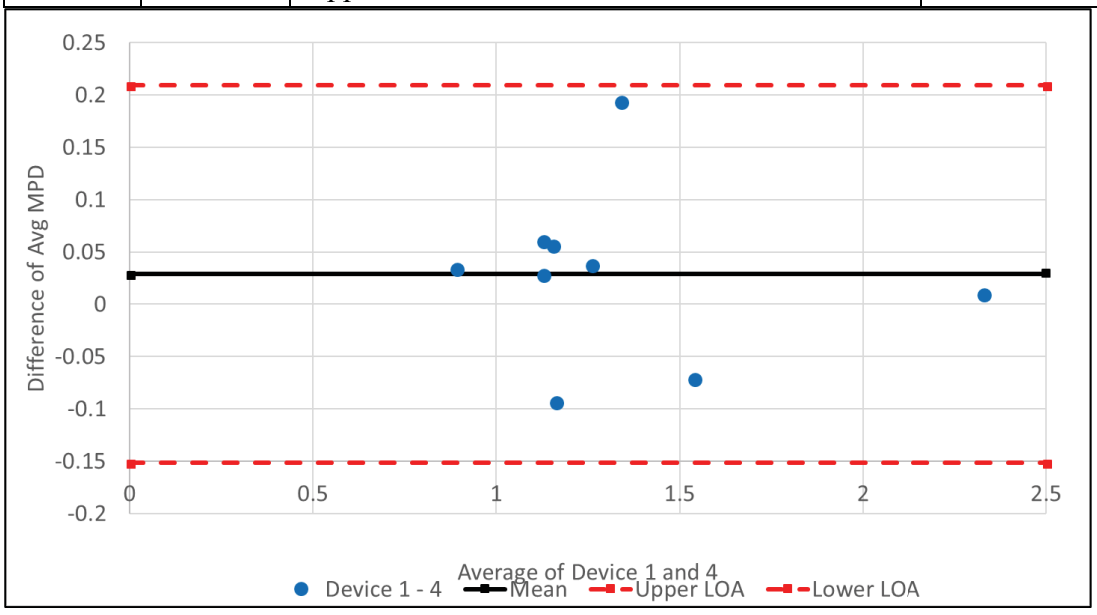

1 - 5			
		Diff 1 - 5	avg (1&5)
	PCC1d	-0.03401	1.518185961
	PCC1b	0.214173	1.007637894
	L2	0.046857	1.253685948
	K	-0.00972	2.33849112
	J	0.043868	1.413294656
	I	0.060911	1.150001187
	H	0.031962	1.140038247
	D2	0.031411	0.889764234
	C	-0.03574	1.157250116
mean		0.038856	
std dev	0.074707		
variance	0.005581		
		Variance for Factor 1:	0.00132
		Variance for Factor 5:	0.00068
		variance of difference between means 1&5	0.00558
		Corrected variance of differences between means s_c^2	0.00718
		Corrected std dev of differences between means s_c	0.08475
		LOA=1.96*s_c=	0.16610
		Range	0.33220
		Lower limit	-0.12725
		Upper Limit	0.20496

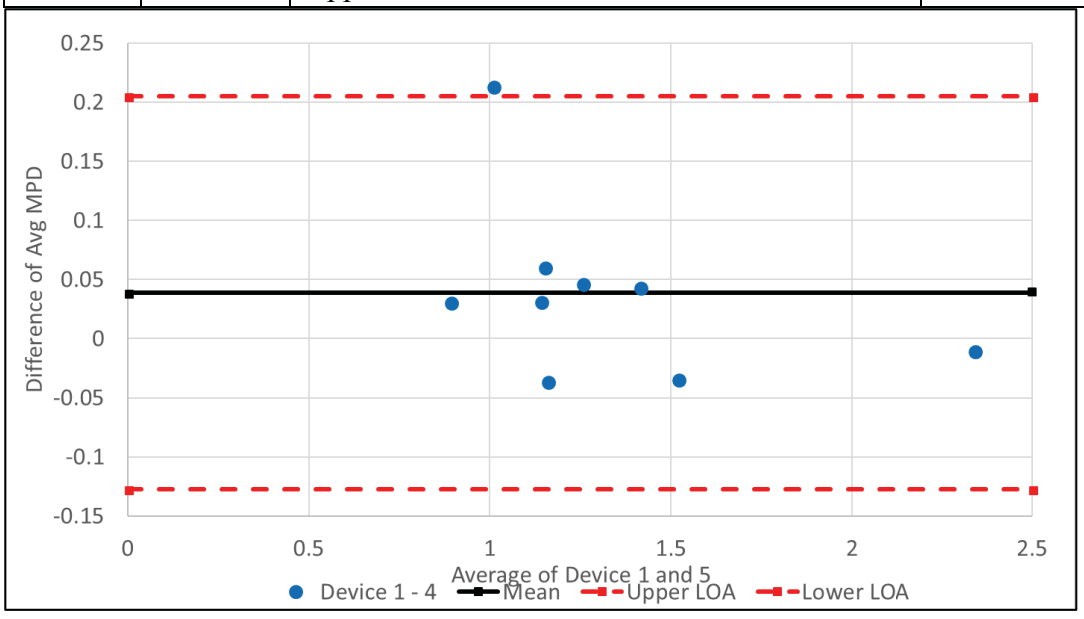

2-3			
		Diff 2-3	avg (2&3)
	PCC1d	0.241388	1.418364505
	PCC1b	0.187365	0.916570096
	L2	0.191893	1.184037568
	K	0.189062	2.221560942
	J	0.176296	1.308457279
	I	0.176906	1.103639198
	H	0.15705	1.072717866
	D2	0.176921	0.81934099
	C	0.191013	1.053389191
mean		0.187544	
std dev	0.022953		
variance	0.000527		
		Variance for Factor 2:	0.00112
		Variance for Factor 3:	0.00179
		variance of difference between means 2&3	0.00053
		Corrected variance of differences between means s_c^2	0.00285
		Corrected std dev of differences between means s_c	0.05341
		LOA=1.96*s_c=	0.10468
		Range	0.20936
		Lower limit	0.08286
		Upper Limit	0.29222

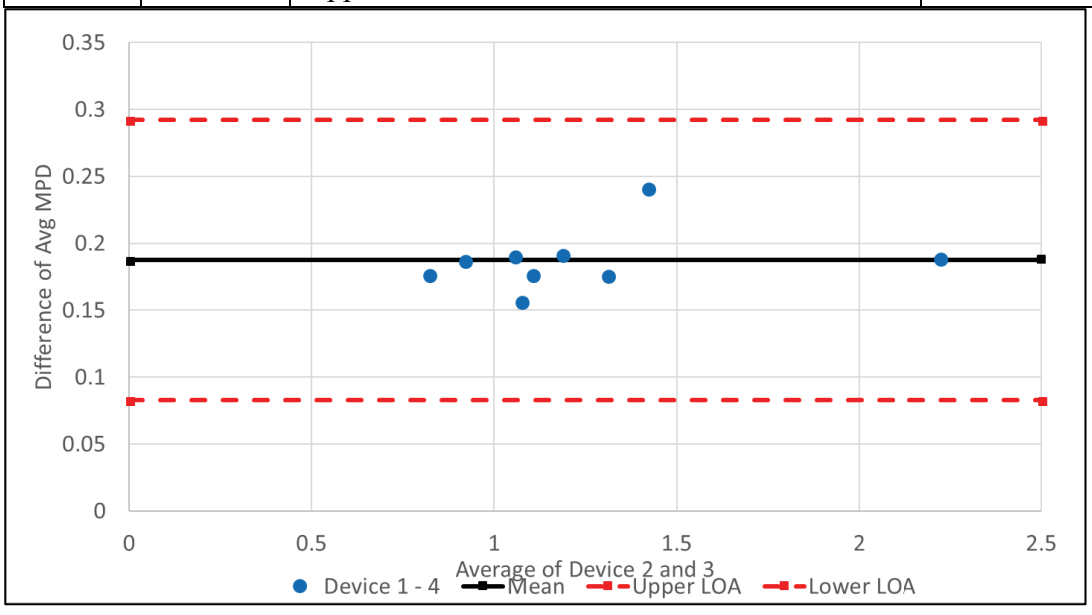

2-4			
		Diff 2-4	avg (2&4)
	PCC1d	-0.03274	1.555428578
	PCC1b	-0.197	1.108751647
	L2	0.041271	1.25934844
	K	-0.00717	2.319676532
	J	0.155972	1.318619308
	I	0.068676	1.157753989
	H	0.056616	1.122934664
	D2	0.036814	0.889394296
	C	0.038761	1.129515181
mean		0.017911	
std dev	0.096082		
variance	0.009232		
		Variance for Factor 2:	0.00112
		Variance for Factor 4:	0.00078
		variance of difference between means 2&4	0.00923
		Corrected variance of differences between means s_c^2	0.01075
		Corrected std dev of differences between means s_c	0.10366
		LOA=1.96*s_c=	0.20318
		Range	0.40636
		Lower limit	-0.18527
		Upper Limit	0.22109

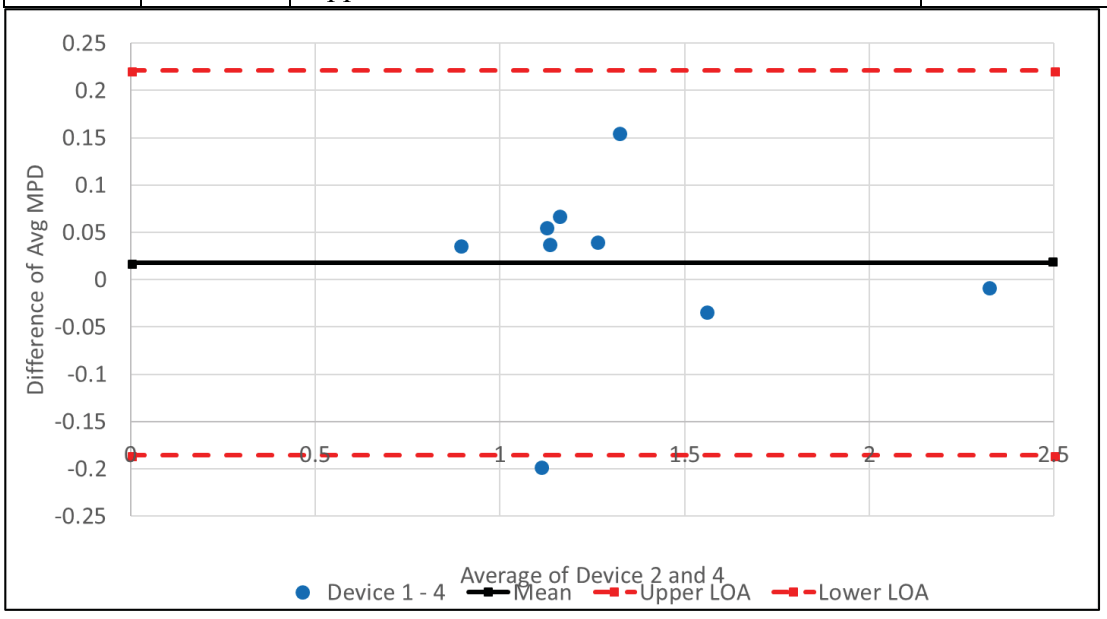

2-5			
		Diff 2-5	avg (2&5)
	PCC1d	0.003868	1.537124445
	PCC1b	0.109701	0.955401966
	L2	0.049727	1.25512075
	K	-0.02726	2.329722452
	J	0.005244	1.393983044
	I	0.072546	1.155818969
	H	0.027186	1.137649825
	D2	0.033743	0.89093006
	C	-0.02623	1.162008526
mean		0.027614	
std dev	0.045081		
variance	0.002032		
		Variance for Factor 2:	0.00112
		Variance for Factor 5:	0.00068
		variance of difference between means 2&5	0.00203
		Corrected variance of differences between means s_c^2	0.00347
		Corrected std dev of differences between means s_c	0.05891
		LOA=1.96*s_c=	0.11545
		Range	0.23091
		Lower limit	-0.08784
		Upper Limit	0.14307

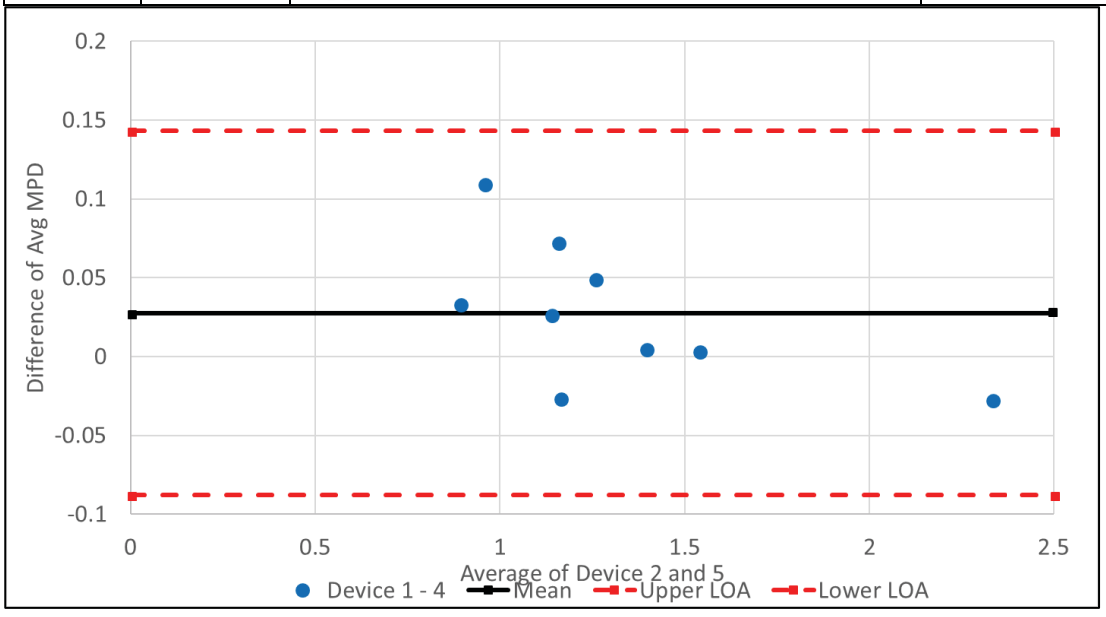

3-4			
		Diff 3-4	avg (3&4)
	PCC1d	-0.27413	1.434734681
	PCC1b	-0.38436	1.015069343
	L2	-0.15062	1.163401894
	K	-0.19623	2.225145403
	J	-0.02032	1.230471359
	I	-0.10823	1.06930109
	H	-0.10043	1.044409877
	D2	-0.14011	0.800933973
	C	-0.15225	1.034008666
mean		-0.16963	
std dev	0.106139		
variance	0.011265		
		Variance for Factor 3:	0.00179
		Variance for Factor 4:	0.00078
		variance of difference between means 3&4	0.01127
		Corrected variance of differences between means s_c^2	0.01332
		Corrected std dev of differences between means s_c	0.11542
		LOA=1.96*s_c=	0.22622
		Range	0.45244
		Lower limit	-0.39585
		Upper Limit	0.05659

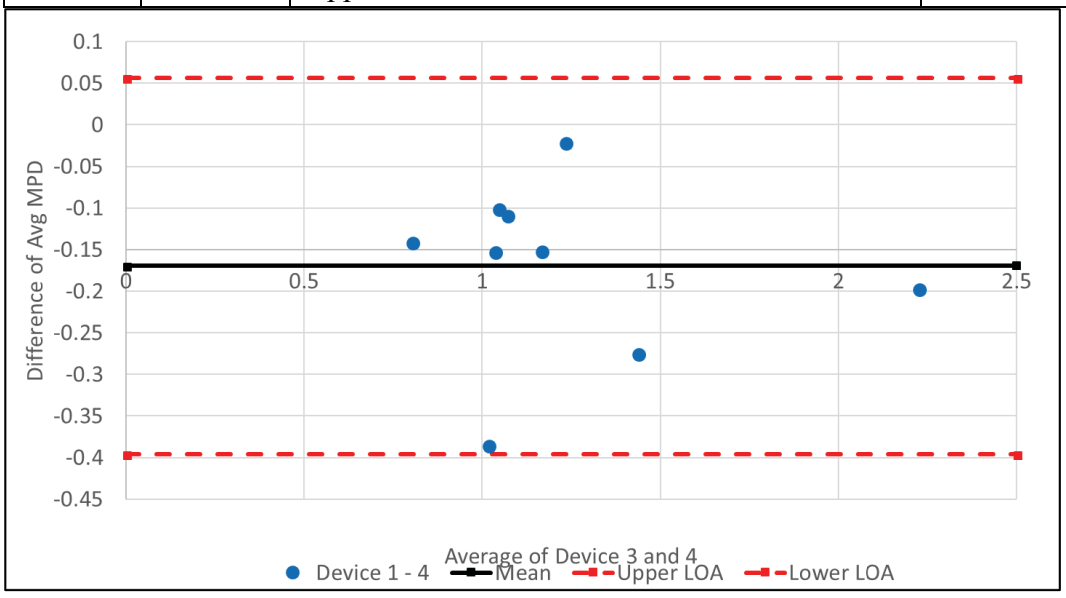

3-5			
		Diff 3-5	avg (3&5)
	PCC1d	-0.23752	1.416430548
	PCC1b	-0.07766	0.861719662
	L2	-0.14217	1.159174204
	K	-0.21632	2.235191323
	J	-0.17105	1.305835095
	I	-0.10436	1.067366071
	H	-0.12986	1.059125039
	D2	-0.14318	0.802469736
	C	-0.21724	1.066502012
mean		-0.15993	
std dev	0.054731		
variance	0.002996		
		Variance for Factor 3:	0.00179
		Variance for Factor 5:	0.00068
		variance of difference between means 3&5	0.00300
		Corrected variance of differences between means s_c^2	0.00497
		Corrected std dev of differences between means s_c	0.07053
		LOA=1.96*s_c=	0.13824
		Range	0.27648
		Lower limit	-0.29817
		Upper Limit	-0.02169

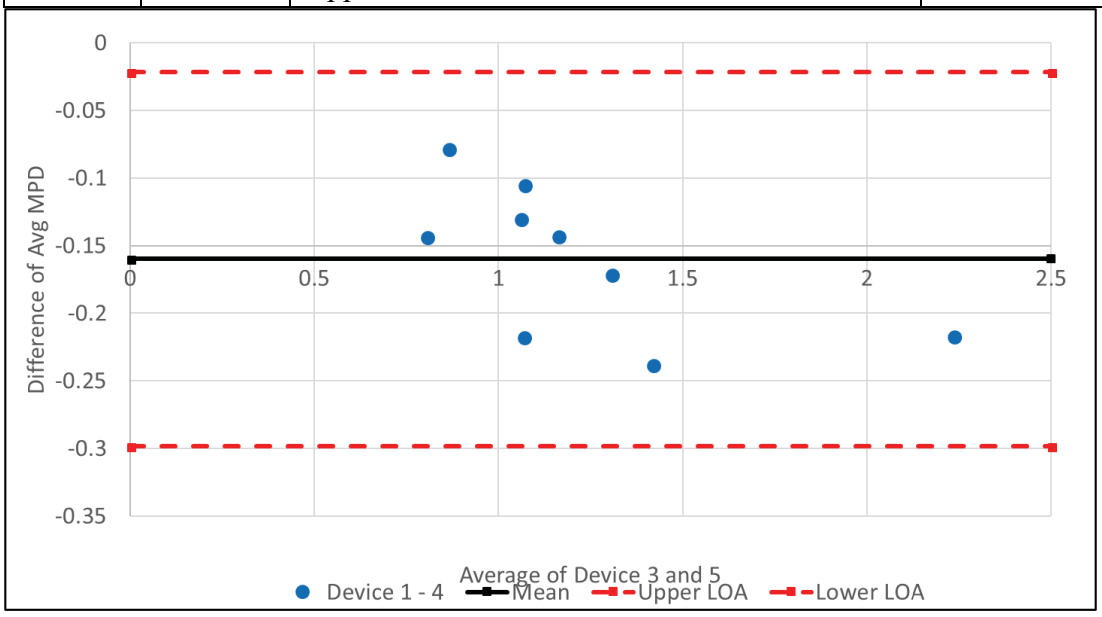

4-5			
		Diff 4-5	avg (4&5)
	PCC1d	0.036608	1.553494621
	PCC1b	0.306699	1.053901214
	L2	0.008455	1.234485076
	K	-0.02009	2.333306913
	J	-0.15073	1.315997124
	I	0.00387	1.121480862
	H	-0.02943	1.109341836
	D2	-0.00307	0.872523043
	C	-0.06499	1.142628002
mean		0.009703	
std dev	0.123928		
variance	0.015358		
		Variance for Factor 4:	0.00078
		Variance for Factor 5:	0.00068
		variance of difference between means 4&5	0.01536
		Corrected variance of differences between means s_c^2	0.01653
		Corrected std dev of differences between means s_c	0.12855
		LOA=1.96*s_c=	0.25197
		Range	0.50393
		Lower limit	-0.24226
		Upper Limit	0.26167

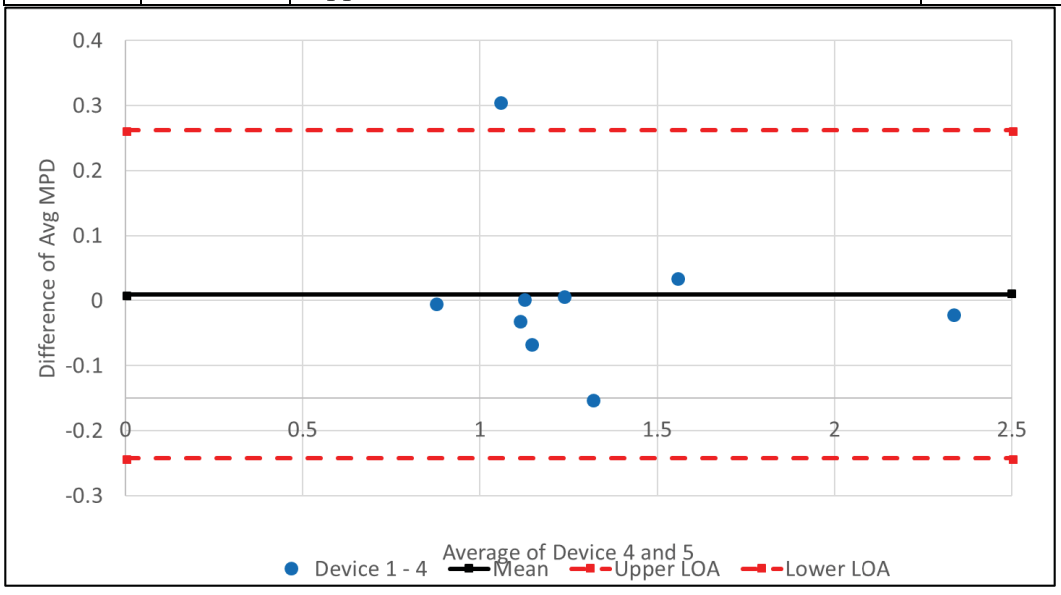

Appendix L Chapter 3 LOA – longitudinal only sections

ANOVA Tables for MSE to use as device variance:

DEVICE#1					
Analysis of Variance					
Source	DF	Sum of Squares	Mean Square	F Ratio	Prob > F
Model	1	0.03931322	0.039313	178.3268	<.0001
Error	8	0.00176365	0.00022		
C. Total	9	0.04107687			

DEVICE#2					
Analysis of Variance					
Source	DF	Sum of Squares	Mean Square	F Ratio	Prob > F
Model	1	0.03097852	0.030979	55.7984	<.0001
Error	8	0.00444149	0.000555		
C. Total	9	0.03542001			

DEVICE#3					
Analysis of Variance					
Source	DF	Sum of Squares	Mean Square	F Ratio	Prob > F
Model	1	0.01514481	0.015145	27.1178	0.0008
Error	8	0.00446785	0.000558		
C. Total	9	0.01961266			

DEVICE#4					
Analysis of Variance					
Source	DF	Sum of Squares	Mean Square	F Ratio	Prob > F
Model	1	0.02096191	0.020962	40.2755	0.0002
Error	8	0.0041637	0.00052		
C. Total	9	0.02512562			

DEVICE#5					
Analysis of Variance					
Source	DF	Sum of Squares	Mean Square	F Ratio	Prob > F
Model	1	1.6101009	1.6101	1163.821	<.0001
Error	8	0.0110677	0.00138		
C. Total	9	1.6211686			

1 - 2			
		Diff 1 - 2	avg (1&2)
	SRB	0.025757	0.503540837
	PCC2	0.011673	0.385182231
mean diff		0.018715	
std dev diff	0.009959		
variance diff	9.92E-05		
		Variance for Factor 1:	0.00022
		Variance for Factor 2:	0.00056
		variance of difference 1&2	0.00010
		Corrected variance of differences between means s_c^2	0.00072
		Corrected std dev of differences between means s_c	0.02682
		LOA=1.96*s_c=	0.05256
		Range	0.10512
		Lower limit	-0.03385
		Upper Limit	0.07128

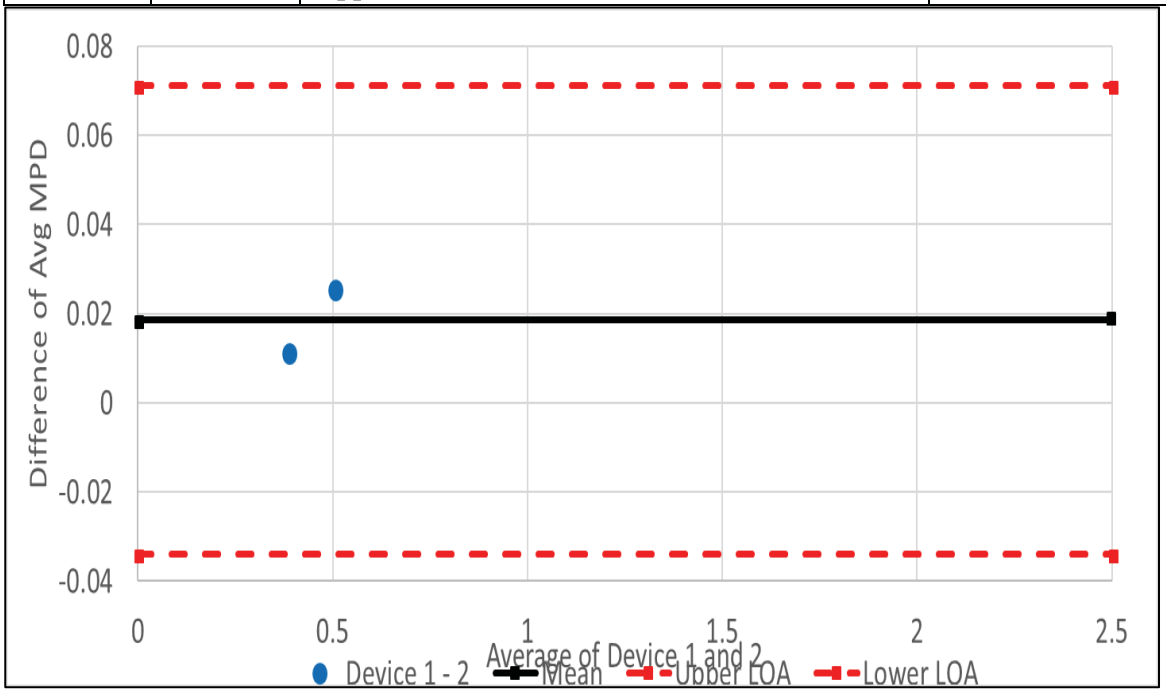

1 - 3			
		Diff 1 - 3	avg (1&3)
	SRB	0.090535	0.471151652
	PCC2	0.042967	0.369535063
mean		0.066751	
std dev	0.033636		
variance	0.001131		
		Variance for Factor 1:	0.00022
		Variance for Factor 3:	0.00056
		variance of difference between means 1&3	0.00113
		Corrected variance of differences between means s_c^2	0.00175
		Corrected std dev of differences between means s_c	0.04188
		LOA=1.96*s_c=	0.08208
		Range	0.16416
		Lower limit	-0.01533
		Upper Limit	0.14883

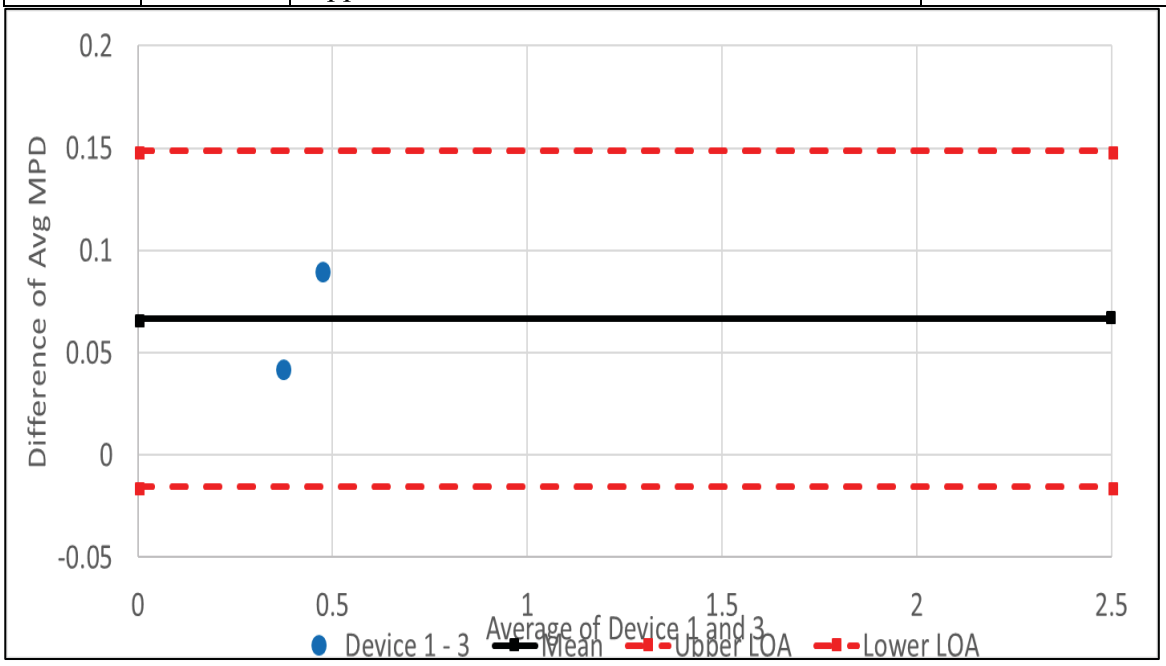

1 - 4			
		Diff 1 - 4	avg (1&4)
	SRB	-0.05703	0.544933055
	PCC2	-0.09086	0.436448615
mean		-0.07394	
std dev	0.023923		
variance	0.000572		
		Variance for Factor 1:	0.00022
		Variance for Factor 4:	0.00052
		variance of difference between means 1&4	0.00057
		Corrected variance of differences between means s_c^2	0.00116
		Corrected std dev of differences between means s_c	0.03412
		LOA=1.96*s_c=	0.06688
		Range	0.13376
		Lower limit	-0.14082
		Upper Limit	-0.00706

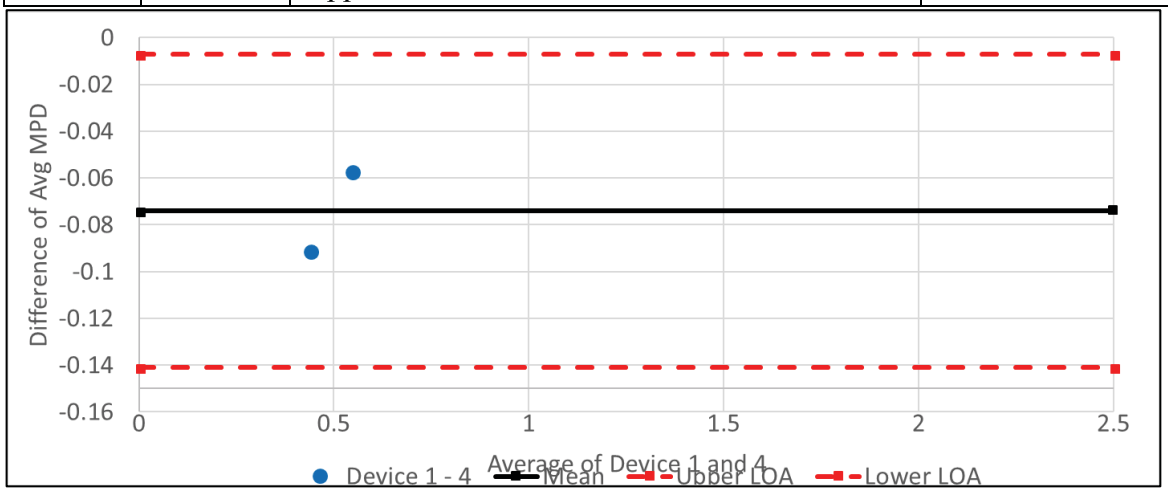

1 - 5			
		Diff 1 - 5	avg (1&5)
	SRB	-0.35955	0.69619232
	PCC2	-1.28747	1.034752689
mean		-0.82351	
std dev	0.65614		
variance	0.430519		
		Variance for Factor 1:	0.00022
		Variance for Factor 5:	0.00138
		variance of difference between means 1&5	0.43052
		Corrected variance of differences between means s_c^2	0.43180
		Corrected std dev of differences between means s_c	0.65711
		LOA=1.96*s_c=	1.28794
		Range	2.57589
		Lower limit	-2.11145
		Upper Limit	0.46444

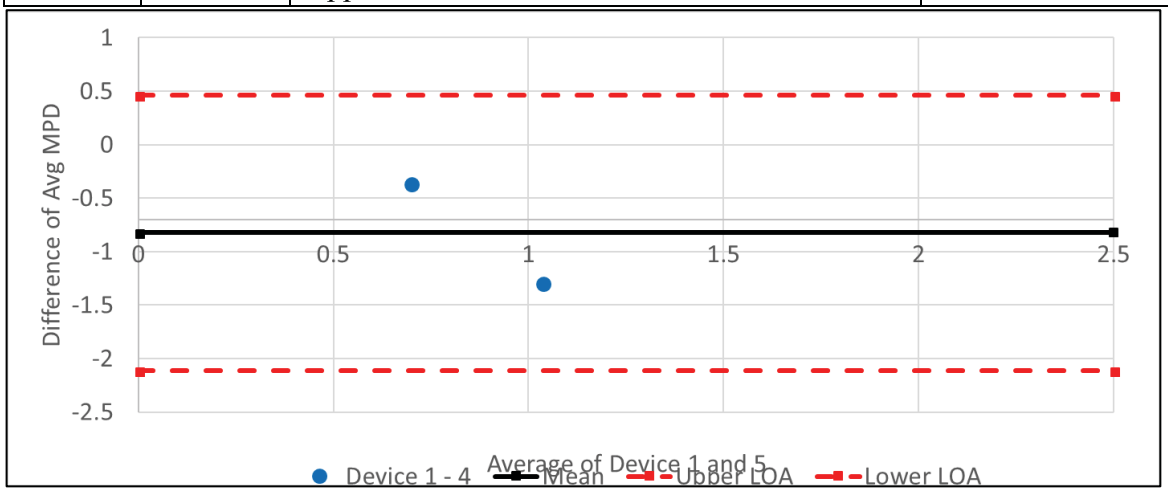

2-3			
		Diff 2-3	avg (2&3)
	SRB	0.064778	0.458273195
	PCC2	0.031294	0.363698516
mean		0.048036	
std dev	0.023677		
variance	0.000561		
		Variance for Factor 2:	0.00056
		Variance for Factor 3:	0.00056
		variance of difference between means 2&3	0.00056
		Corrected variance of differences between means s_c^2	0.00145
		Corrected std dev of differences between means s_c	0.03809
		LOA=1.96*s_c=	0.07466
		Range	0.14932
		Lower limit	-0.02662
		Upper Limit	0.12270

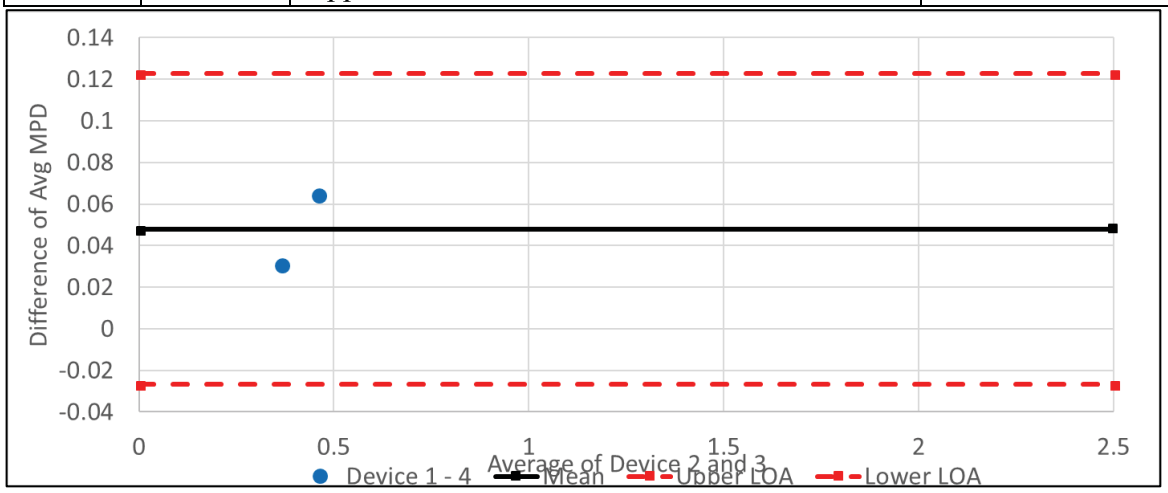

2-4			
		Diff 2-4	avg (2&4)
	SRB	-0.08278	0.532054597
	PCC2	-0.10253	0.430612067
mean		-0.09266	
std dev	0.013964		
variance	0.000195		
		Variance for Factor 2:	0.00056
		Variance for Factor 4:	0.00052
		variance of difference between means 2&4	0.00019
		Corrected variance of differences between means s_c^2	0.00105
		Corrected std dev of differences between means s_c	0.03248
		LOA=1.96*s_c=	0.06366
		Range	0.12732
		Lower limit	-0.15632
		Upper Limit	-0.02900

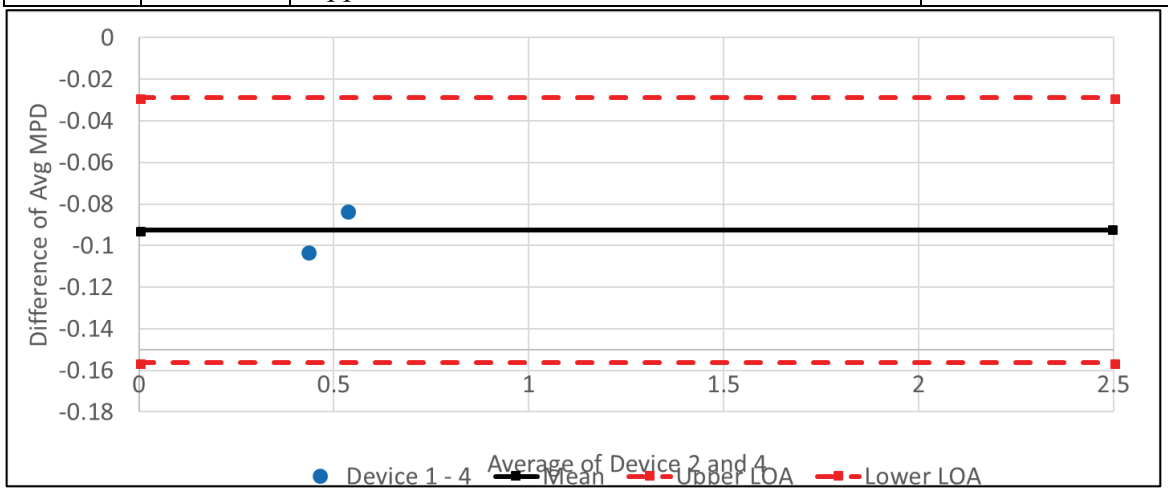

2-5			
		Diff 2-5	avg (2&5)
	SRB	-0.3853	0.683313863
	PCC2	-1.29914	1.028916142
mean		-0.84222	
std dev	0.646181		
variance	0.41755		
		Variance for Factor 2:	0.00056
		Variance for Factor 5:	0.00138
		variance of difference between means 2&5	0.41755
		Corrected variance of differences between means s_c^2	0.41910
		Corrected std dev of differences between means s_c	0.64738
		LOA=1.96*s_c=	1.26886
		Range	2.53772
		Lower limit	-2.11108
		Upper Limit	0.42664

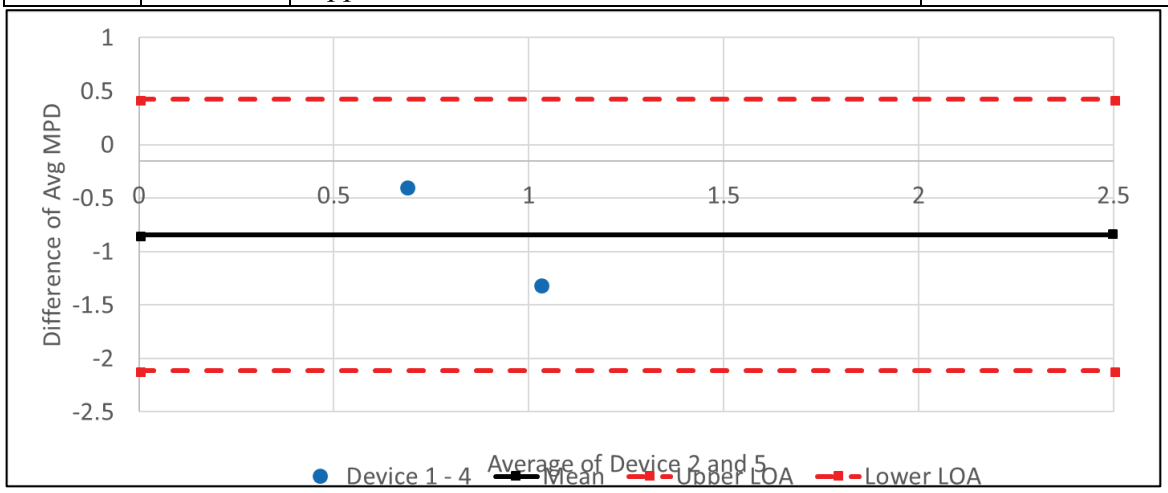

3-4			
		Diff 3-4	avg (3&4)
	SRB	-0.14756	0.499665412
	PCC2	-0.13383	0.414964899
mean		-0.14069	
std dev	0.009713		
variance	9.43E-05		
		Variance for Factor 3:	0.00056
		Variance for Factor 4:	0.00052
		variance of difference between means 3&4	0.00009
		Corrected variance of differences between means s_c^2	0.00096
		Corrected std dev of differences between means s_c	0.03093
		LOA=1.96*s_c=	0.06063
		Range	0.12125
		Lower limit	-0.20132
		Upper Limit	-0.08007

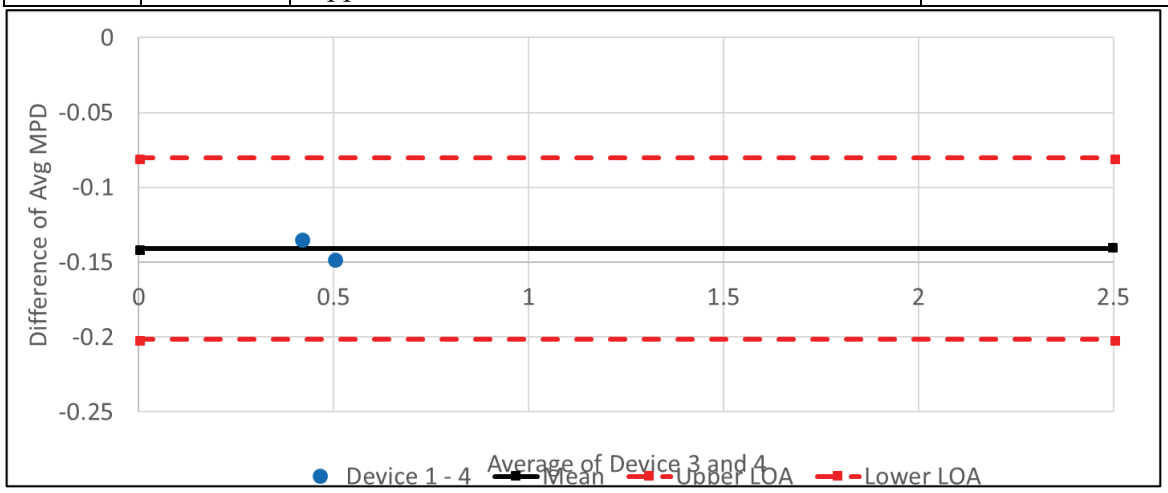

3-5			
		Diff 3-5	avg (3&5)
	SRB	-0.45008	0.650924677
	PCC2	-1.33044	1.013268973
mean		-0.89026	
std dev	0.622504		
variance	0.387512		
		Variance for Factor 3:	0.00056
		Variance for Factor 5:	0.00138
		variance of difference between means 3&5	0.38751
		Corrected variance of differences between means s_c^2	0.38906
		Corrected std dev of differences between means s_c	0.62375
		LOA=1.96*s_c=	1.22255
		Range	2.44509
		Lower limit	-2.11280
		Upper Limit	0.33229

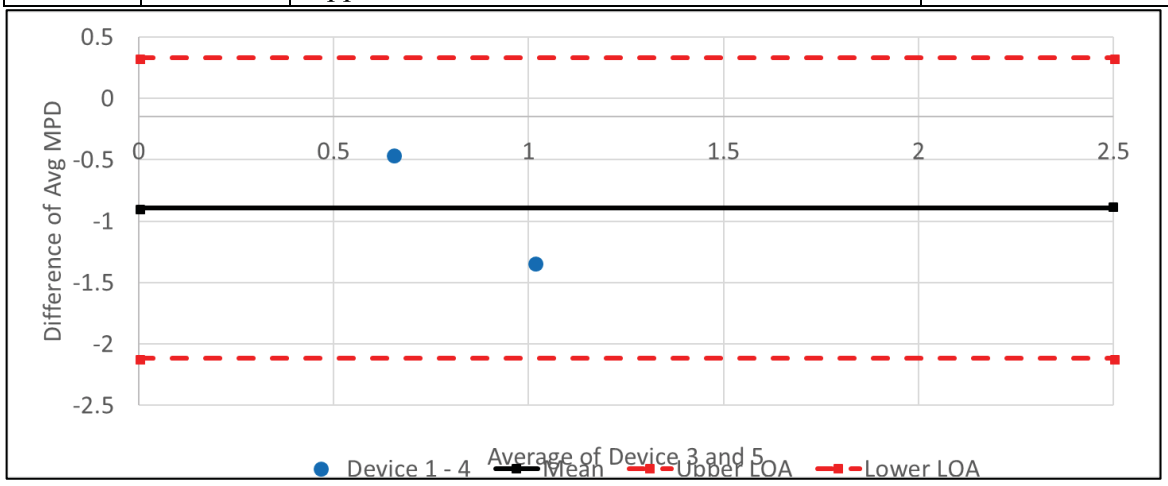

4-5			
		Diff 4-5	avg (4&5)
	SRB	-0.30252	0.72470608
	PCC2	-1.19661	1.080182525
mean		-0.74956	
std dev	0.632217		
variance	0.399698		
		Variance for Factor 4:	0.00052
		Variance for Factor 5:	0.00138
		variance of difference between means 4&5	0.39970
		Corrected variance of differences between means s_c^2	0.40122
		Corrected std dev of differences between means s_c	0.63342
		LOA=1.96*s_c=	1.24150
		Range	2.48300
		Lower limit	-1.99106
		Upper Limit	0.49194

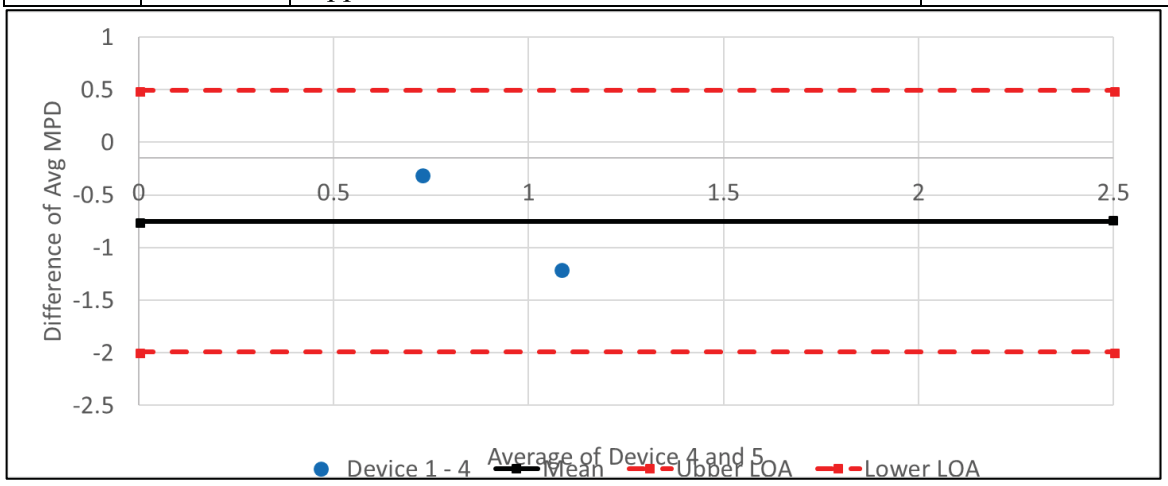

Appendix M Chapter 3 LOA – Transverse only Sections

ANOAV tables for MSE to use as device variance

DEVICE#1					
Analysis of Variance					
Source	DF	Sum of Squares	Mean Square	F Ratio	Prob > F
Model	6	2.9148584	0.48581	4339.167	<.0001
Error	28	0.0031349	0.000112		
C. Total	34	2.9179932			

DEVICE#2					
Analysis of Variance					
Source	DF	Sum of Squares	Mean Square	F Ratio	Prob > F
Model	6	2.4317924	0.405299	3004.336	<.0001
Error	28	0.0037773	0.000135		
C. Total	34	2.4355697			

DEVICE#3					
Analysis of Variance					
Source	DF	Sum of Squares	Mean Square	F Ratio	Prob > F
Model	6	1.7748307	0.295805	2337.997	<.0001
Error	28	0.0035426	0.000127		
C. Total	34	1.7783733			

DEVICE#4					
Analysis of Variance					
Source	DF	Sum of Squares	Mean Square	F Ratio	Prob > F
Model	6	2.3701073	0.395018	1917.926	<.0001
Error	28	0.0057669	0.000206		
C. Total	34	2.3758742			

DEVICE#5					
Analysis of Variance					
Source	DF	Sum of Squares	Mean Square	F Ratio	Prob > F
Model	6	2.0713052	0.345218	4870.262	<.0001
Error	28	0.0019847	0.000071		
C. Total	34	2.0732899			

1 - 2			
		Diff 1 - 2	avg (1&2)
	SRB	0.059442	1.318153756
	RRB	0.086463	1.210296512
	PCC1g	0.008804	0.648690715
	PCC1e	0.021257	0.540097421
	PCC1c	-0.00596	0.90794622
	PCC1a	-0.02063	0.660388882
	HWB	0.013165	1.006187429
mean diff		0.02322	
std dev	0.037414		
variance	0.0014		
		Variance for Factor 1:	0.00011
		Variance for Factor 2:	0.00014
		variance of difference 1&2	0.00140
		Corrected variance of differences between means s_c^2	0.00160
		Corrected std dev of differences between means s_c	0.03997
		LOA=1.96*s_c=	0.07834
		Range	0.15667
		Lower limit	-0.05512
		Upper Limit	0.10156

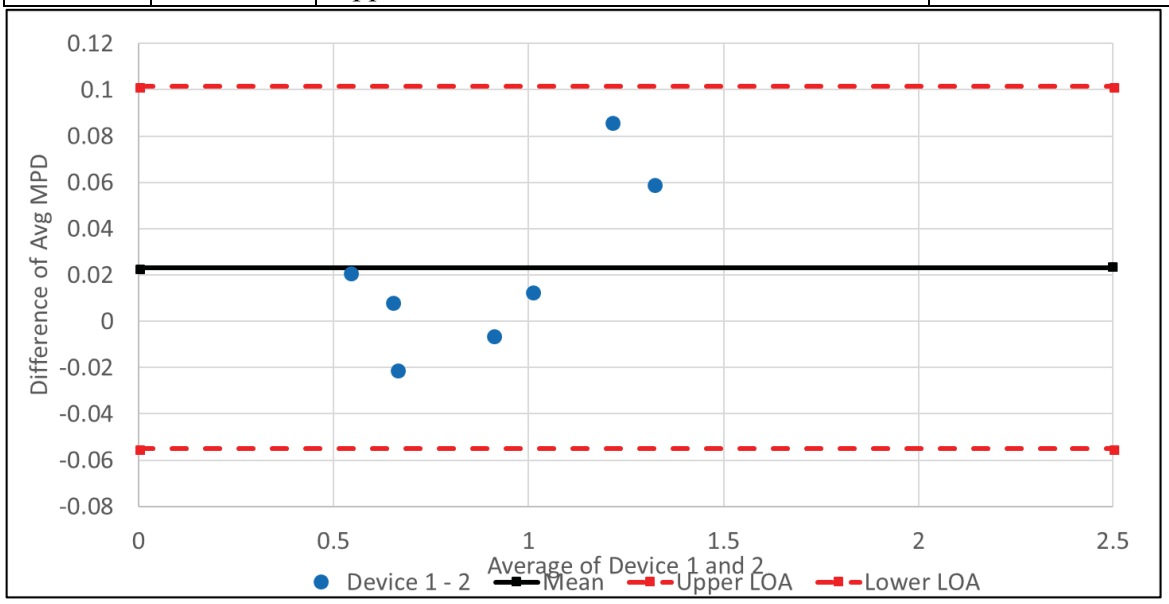

1 - 3			
		Diff 1 - 3	avg (1&3)
	SRB	0.152466	1.271641796
	RRB	0.156544	1.175256201
	PCC1g	0.014076	0.646054816
	PCC1e	-0.01714	0.559294857
	PCC1c	0.018676	0.895628234
	PCC1a	0.007065	0.646542082
	HWB	0.082825	0.97135698
mean		0.059216	
std dev	0.071829		
variance	0.005159		
		Variance for Factor 1:	0.00011
		Variance for Factor 3:	0.00013
		variance of difference between means 1&3	0.00516
		Corrected variance of differences between means s_c^2	0.00535
		Corrected std dev of differences between means s_c	0.07315
		LOA=1.96*s_c=	0.14337
		Range	0.28674
		Lower limit	-0.08415
		Upper Limit	0.20259

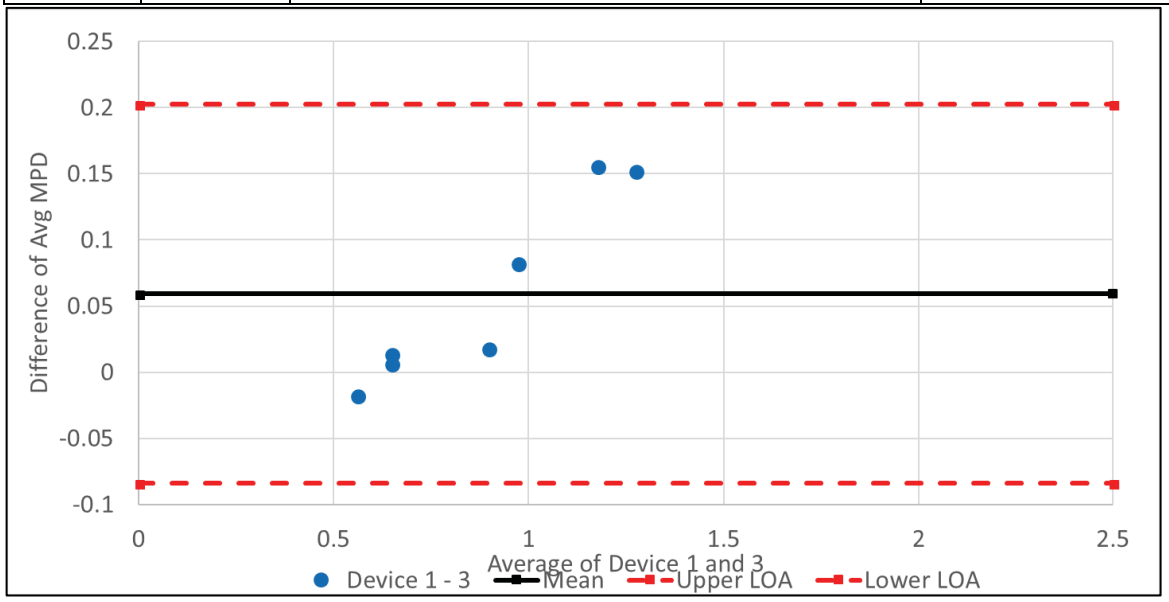

1 - 4			
		Diff 1 - 4	avg (1&4)
	SRB	0.060663	1.317543174
	RRB	0.072451	1.217302657
	PCC1g	0.012869	0.646658212
	PCC1e	-0.00614	0.553798175
	PCC1c	-0.01915	0.914540112
	PCC1a	-0.01538	0.657765647
	HWB	0.041692	0.991923531
mean		0.021	
std dev	0.037387		
variance	0.001398		
		Variance for Factor 1:	0.00011
		Variance for Factor 4:	0.00021
		variance of difference between means 1&4	0.00140
		Corrected variance of differences between means s_c^2	0.00165
		Corrected std dev of differences between means s_c	0.04065
		LOA=1.96*s_c=	0.07967
		Range	0.15934
		Lower limit	-0.05867
		Upper Limit	0.10067

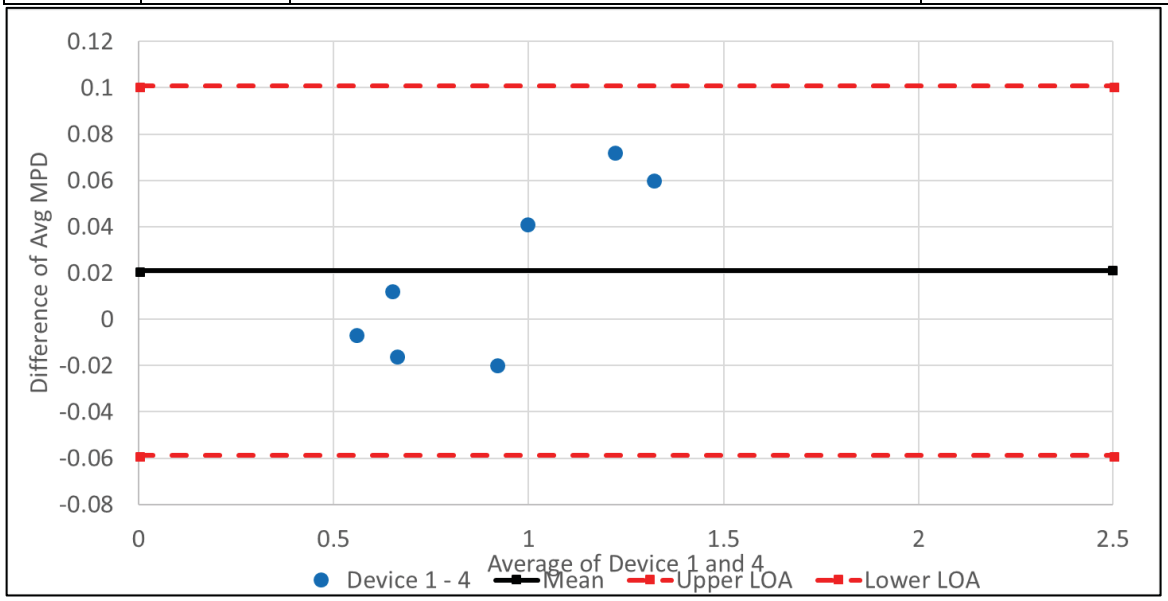

1 - 5			
		Diff 1 - 5	avg (1&5)
	SRB	0.209968	1.24289036
	RRB	0.225559	1.140748452
	PCC1g	0.09719	0.604497956
	PCC1e	0.116597	0.492427467
	PCC1c	0.141383	0.834274747
	PCC1a	0.096023	0.602063056
	HWB	0.155914	0.934812774
mean		0.148948	
std dev	0.052002		
variance	0.002704		
		Variance for Factor 1:	0.00011
		Variance for Factor 5:	0.00007
		variance of difference between means 1&5	0.00270
		Corrected variance of differences between means s_c^2	0.00285
		Corrected std dev of differences between means s_c	0.05339
		LOA=1.96*s_c=	0.10465
		Range	0.20929
		Lower limit	0.04430
		Upper Limit	0.25359

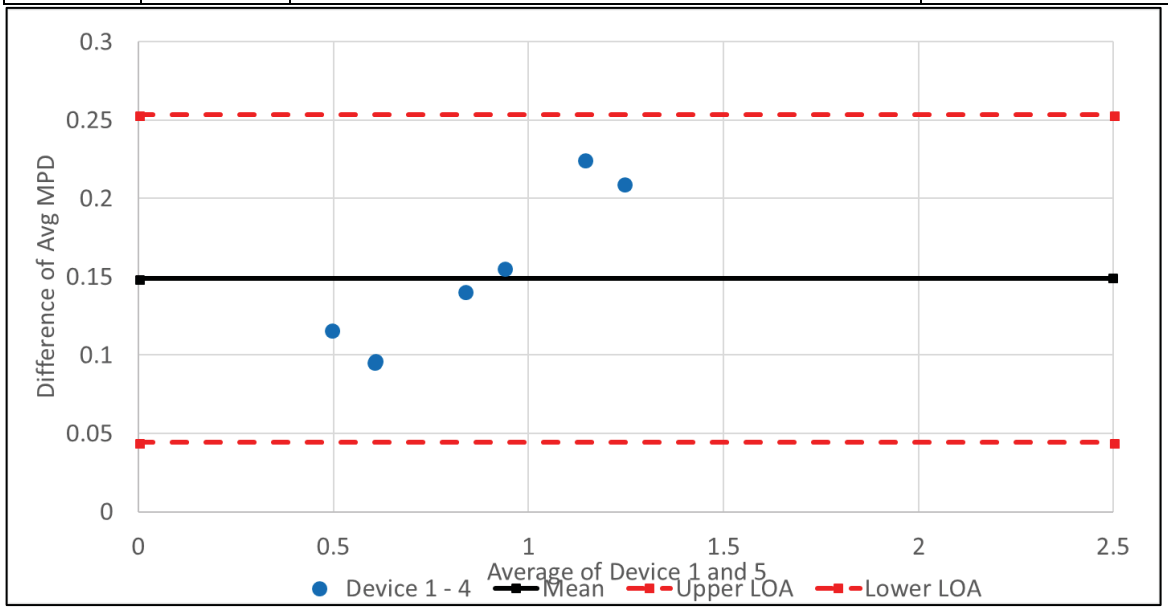

2-3			
		Diff 2-3	avg (2&3)
	SRB	0.093024	1.241920954
	RRB	0.070081	1.132024638
	PCC1g	0.005272	0.641652718
	PCC1e	-0.03839	0.548666248
	PCC1c	0.024636	0.89860807
	PCC1a	0.027694	0.65685644
	HWB	0.069661	0.964774722
mean		0.035996	
std dev	0.045135		
variance	0.002037		
		Variance for Factor 2:	0.00014
		Variance for Factor 3:	0.00013
		variance of difference between means 2&3	0.00204
		Corrected variance of differences between means s_c^2	0.00225
		Corrected std dev of differences between means s_c	0.04740
		LOA=1.96*s_c=	0.09290
		Range	0.18581
		Lower limit	-0.05691
		Upper Limit	0.12890

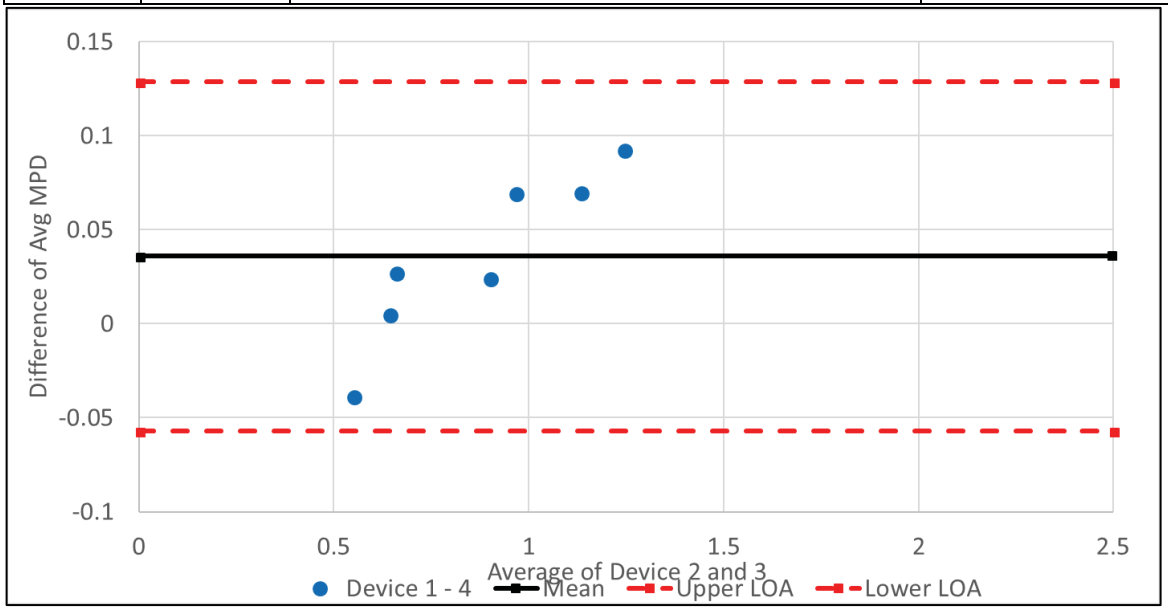

2-4			
		Diff 2-4	avg (2&4)
	SRB	0.001221	1.287822331
	RRB	-0.01401	1.174071094
	PCC1g	0.004065	0.642256114
	PCC1e	-0.0274	0.543169566
	PCC1c	-0.01319	0.917519948
	PCC1a	0.005246	0.668080006
	HWB	0.028528	0.985341273
mean		-0.00222	
std dev	0.018009		
variance	0.000324		
		Variance for Factor 2:	0.00014
		Variance for Factor 4:	0.00021
		variance of difference between means 2&4	0.00032
		Corrected variance of differences between means s_c^2	0.00060
		Corrected std dev of differences between means s_c	0.02444
		LOA=1.96*s_c=	0.04790
		Range	0.09579
		Lower limit	-0.05012
		Upper Limit	0.04567

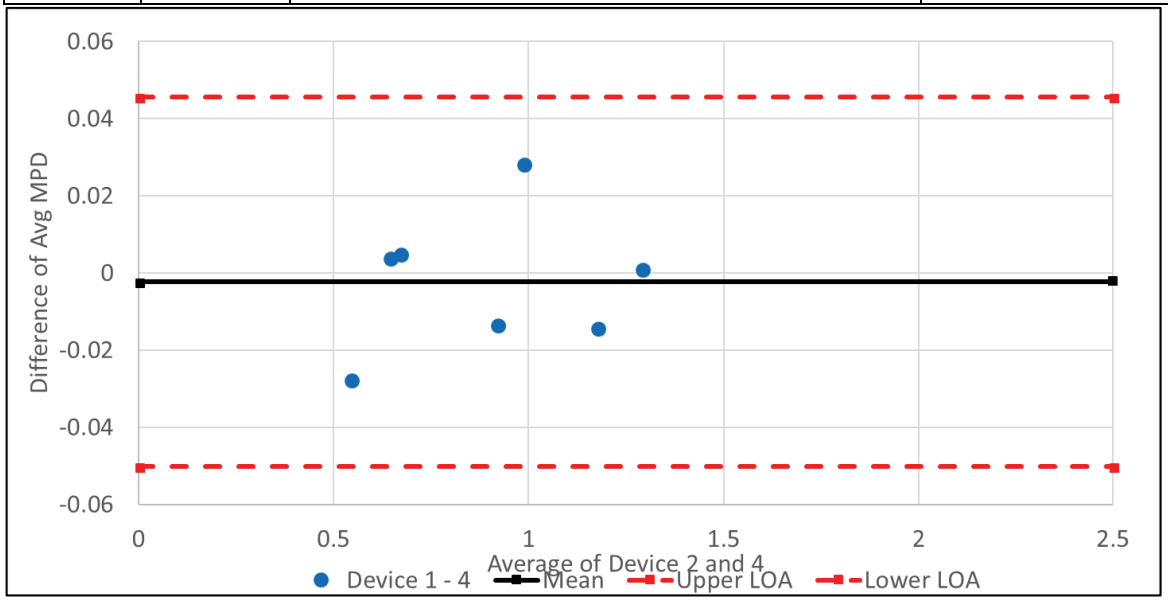

2-5			
		Diff 2-5	avg (2&5)
	SRB	0.150527	1.213169517
	RRB	0.139096	1.097516888
	PCC1g	0.088386	0.600095858
	PCC1e	0.09534	0.481798858
	PCC1c	0.147343	0.837254582
	PCC1a	0.116652	0.612377415
	HWB	0.142749	0.928230516
mean		0.125727	
std dev	0.025661		
variance	0.000658		
		Variance for Factor 2:	0.00014
		Variance for Factor 5:	0.00007
		variance of difference between means 2&5	0.00066
		Corrected variance of differences between means s_c^2	0.00082
		Corrected std dev of differences between means s_c	0.02869
		LOA=1.96*s_c=	0.05624
		Range	0.11248
		Lower limit	0.06949
		Upper Limit	0.18197

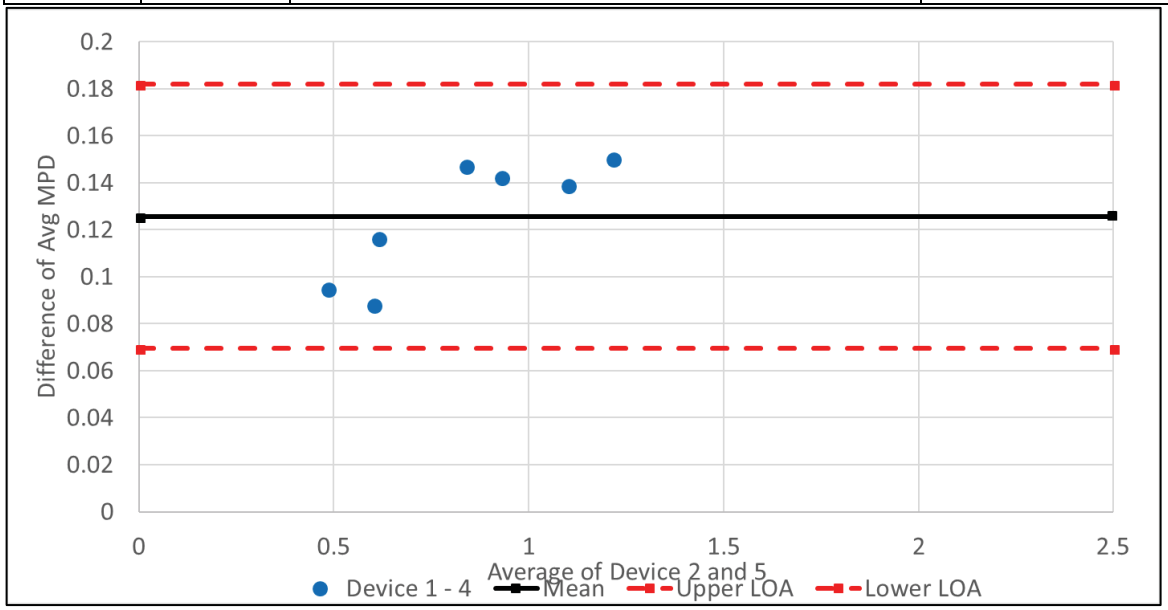

3-4			
		Diff 3-4	avg (3&4)
	SRB	-0.0918	1.241310371
	RRB	-0.08409	1.139030783
	PCC1g	-0.00121	0.639620214
	PCC1e	0.010993	0.562367002
	PCC1c	-0.03782	0.905201961
	PCC1a	-0.02245	0.654233205
	HWB	-0.04113	0.950510824
mean		-0.03822	
std dev	0.038783		
variance	0.001504		
		Variance for Factor 3:	0.00013
		Variance for Factor 4:	0.00021
		variance of difference between means 3&4	0.00150
		Corrected variance of differences between means s_c^2	0.00177
		Corrected std dev of differences between means s_c	0.04208
		LOA=1.96*s_c=	0.08247
		Range	0.16494
		Lower limit	-0.12069
		Upper Limit	0.04426

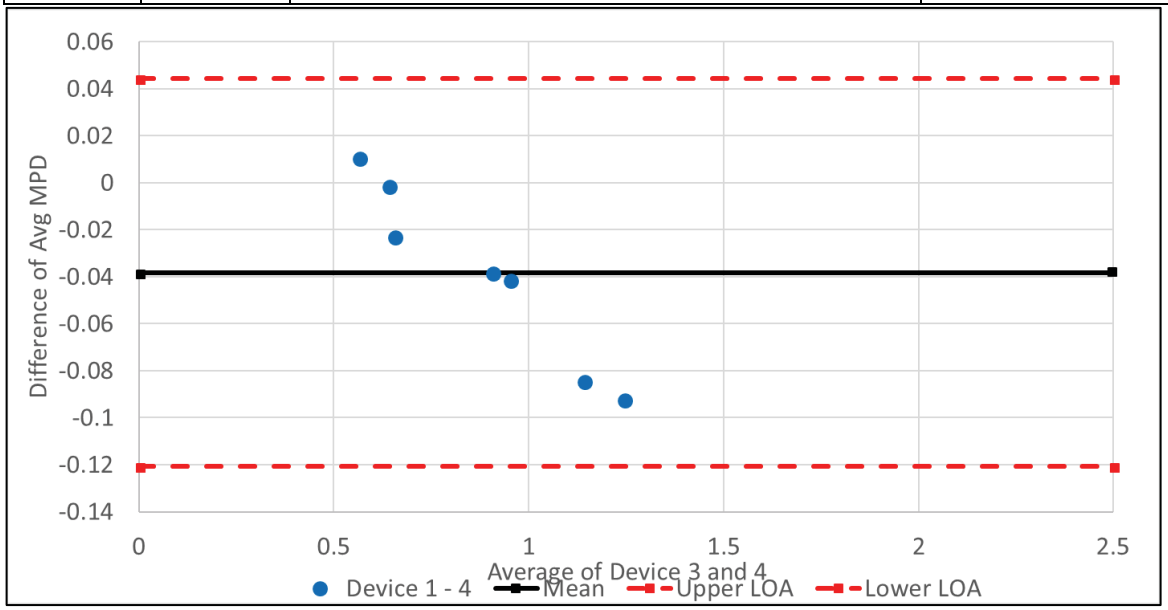

3-5			
		Diff 3-5	avg (3&5)
	SRB	0.057503	1.166657557
	RRB	0.069015	1.062476578
	PCC1g	0.083114	0.597459958
	PCC1e	0.133735	0.500996294
	PCC1c	0.122707	0.824936596
	PCC1a	0.088958	0.598530614
	HWB	0.073088	0.893400067
mean		0.089731	
std dev	0.028322		
variance	0.000802		
		Variance for Factor 3:	0.00013
		Variance for Factor 5:	0.00007
		variance of difference between means 3&5	0.00080
		Corrected variance of differences between means s_c^2	0.00096
		Corrected std dev of differences between means s_c	0.03099
		LOA=1.96*s_c=	0.06075
		Range	0.12149
		Lower limit	0.02899
		Upper Limit	0.15048

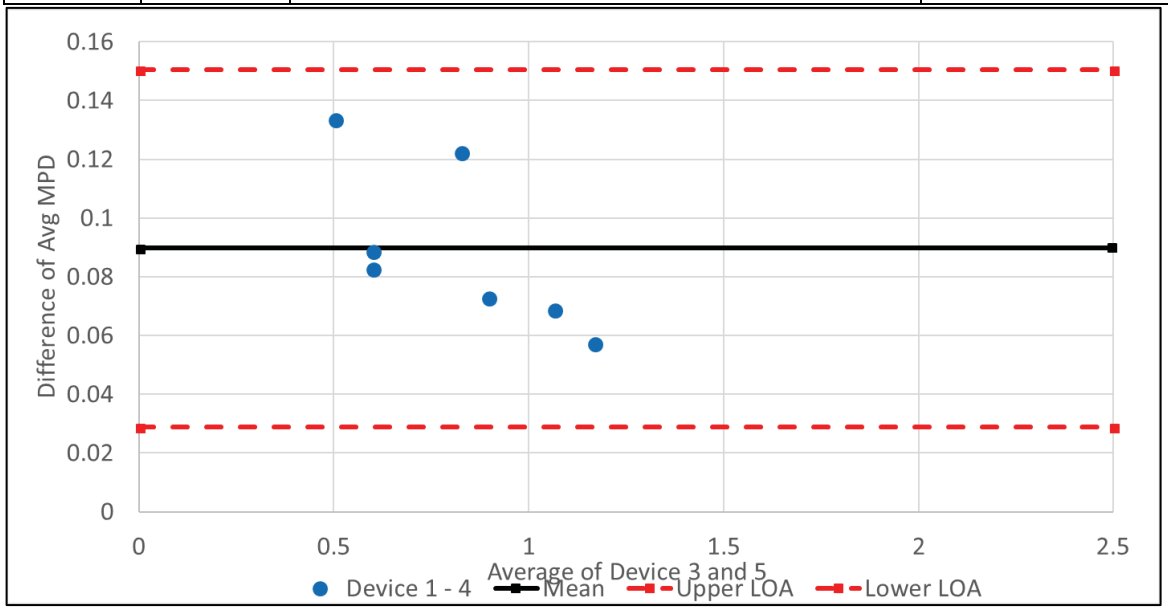

4-5			
		Diff 4-5	avg (4&5)
	SRB	0.149306	1.212558935
	RRB	0.153108	1.104523034
	PCC1g	0.084321	0.598063354
	PCC1e	0.122741	0.495499612
	PCC1c	0.160531	0.843848474
	PCC1a	0.111405	0.60975418
	HWB	0.114222	0.913966618
mean		0.127948	
std dev	0.027518		
variance	0.000757		
		Variance for Factor 4:	0.00021
		Variance for Factor 5:	0.00007
		variance of difference between means 4&5	0.00076
		Corrected variance of differences between means s_c^2	0.00098
		Corrected std dev of differences between means s_c	0.03129
		LOA=1.96*s_c=	0.06132
		Range	0.12264
		Lower limit	0.06663
		Upper Limit	0.18927

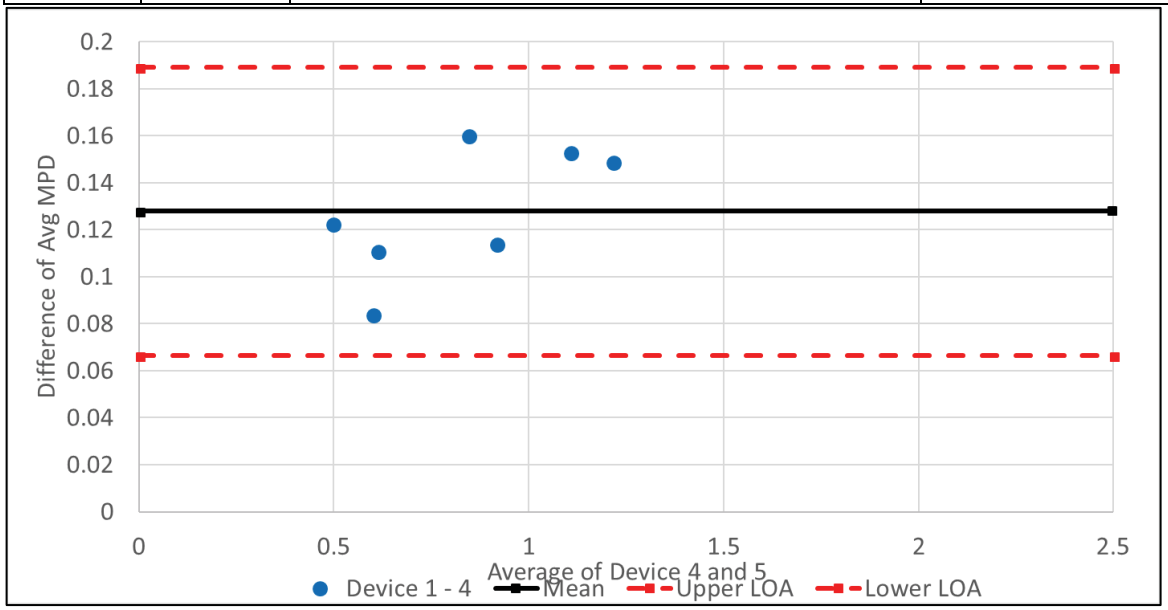

Appendix N Chapter 3 Orthogonal regression of Devices

Bivariate Fit of 2 By 1

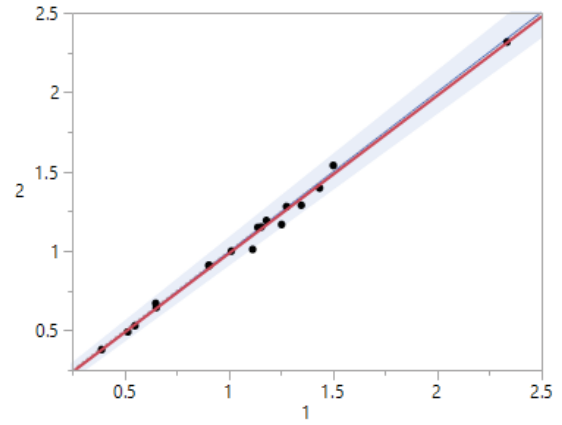

Equality
Passing-Bablok
Orthogonal Fit Ratio=0.992

Passing-Bablok Regression

Parameter	Estimate	LowerCL	UpperCL
Intercept	-0.0144	-0.051	0.0356
Slope	1.00801	0.95723	1.05158
Tau	0.96078	.	.

Orthogonal Fit Ratio=0.992

Variable	Mean	Std Dev	Variance Ratio	Correlation
1	1.073537	0.456386	0.991522	0.9968
2	1.056807	0.454447		

Intercept	Slope	LowerCL	UpperCL	Alpha
-0.01217	0.995752	0.954553	1.03873	0.05000

Bivariate Fit of 3 By 1

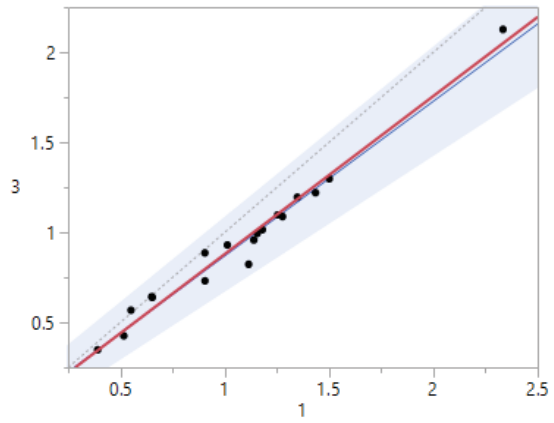

Equality
Passing-Bablok
Orthogonal Fit Ratio=0.771

Passing-Bablok Regression

Parameter	Estimate	LowerCL	UpperCL
Intercept	0.01009	-0.0836	0.1421
Slope	0.85907	0.75425	0.94535
Tau	0.93464	.	.

Orthogonal Fit Ratio=0.771

Variable	Mean	Std Dev	Variance Ratio	Correlation
1	1.073537	0.456386	0.770552	0.9876
3	0.943699	0.40062		

Intercept	Slope	LowerCL	UpperCL	Alpha
0.001336	0.877811	0.806607	0.955301	0.05000

Bivariate Fit of 4 By 1

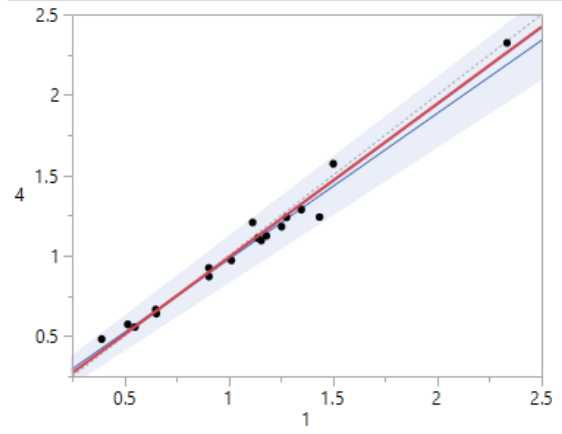

Equality
Passing-Bablok
Orthogonal Fit Ratio=0.914

Passing-Bablok Regression

Parameter	Estimate	LowerCL	UpperCL
Intercept	0.0688	-0.0128	0.13351
Slope	0.90847	0.84264	0.99074
Tau	0.88235	.	.

Orthogonal Fit Ratio=0.914

Variable	Mean	Std Dev	Variance Ratio	Correlation
1	1.073537	0.456386	0.913919	0.9890
4	1.05901	0.436301		

Intercept	Slope	LowerCL	UpperCL	Alpha
0.032718	0.955991	0.883034	1.034977	0.05000

Bivariate Fit of 1 By 5

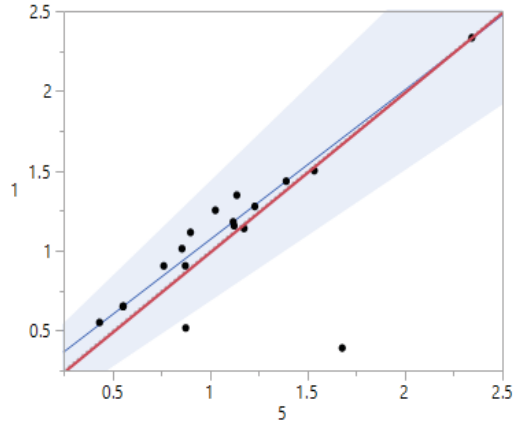

Equality
Passing-Bablok
Orthogonal Fit Ratio=1.002

Passing-Bablok Regression

Parameter	Estimate	LowerCL	UpperCL
Intercept	0.13059	-0.1367	0.25088
Slope	0.93771	0.82113	1.18349
Tau	0.59477	.	.

Orthogonal Fit Ratio=1.002

Variable	Mean	Std Dev	Variance Ratio	Correlation
5	1.087686	0.455885	1.002199	0.7154
1	1.073537	0.456386		

Intercept	Slope	LowerCL	UpperCL	Alpha
-0.01534	1.001099	0.56445	1.775533	0.05000

Bivariate Fit of 3 By 2

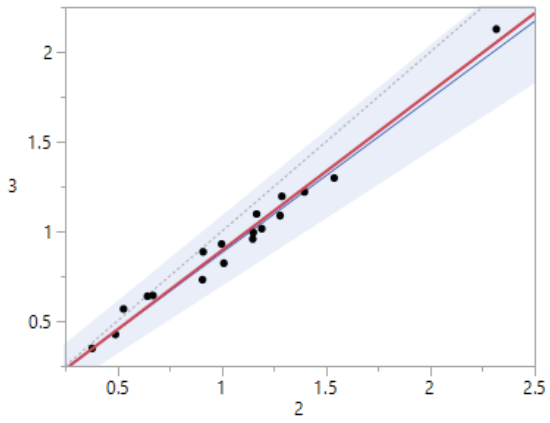

Passing-Bablok Regression

Parameter	Estimate	LowerCL	UpperCL
Intercept	0.02024	-0.0578	0.13736
Slope	0.86032	0.75391	0.95076
Tau	0.94771	.	.

Orthogonal Fit Ratio=0.777

Variable	Mean	Std Dev	Variance Ratio	Correlation
2	1.056807	0.454447	0.777141	0.9891
3	0.943699	0.40062		

Intercept	Slope	LowerCL	UpperCL	Alpha
0.012065	0.881556	0.814431	0.954214	0.05000

Bivariate Fit of 4 By 2

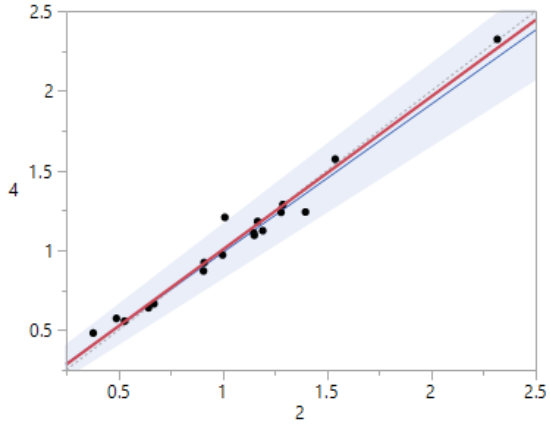

Passing-Bablok Regression

Parameter	Estimate	LowerCL	UpperCL
Intercept	0.05647	-0.0089	0.16116
Slope	0.92991	0.83027	1.00652
Tau	0.89542	.	.

Orthogonal Fit Ratio=0.922

Variable	Mean	Std Dev	Variance Ratio	Correlation
2	1.056807	0.454447	0.921733	0.9866
4	1.05901	0.436301		

Intercept	Slope	LowerCL	UpperCL	Alpha
0.044402	0.960069	0.879278	1.048284	0.05000

Bivariate Fit of 2 By 5

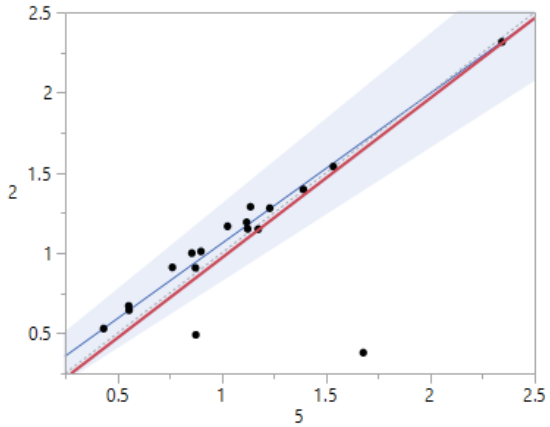

Passing-Bablok Regression

Parameter	Estimate	LowerCL	UpperCL
Intercept	0.12365	-0.0085	0.24608
Slope	0.93579	0.83324	1.06185
Tau	0.5817	.	.

Orthogonal Fit Ratio=0.994

Variable	Mean	Std Dev	Variance Ratio	Correlation
5	1.087686	0.455885	0.993703	0.7222
2	1.056807	0.454447		

Intercept	Slope	LowerCL	UpperCL	Alpha
-0.02745	0.996846	0.56972	1.744193	0.05000

Bivariate Fit of 4 By 3

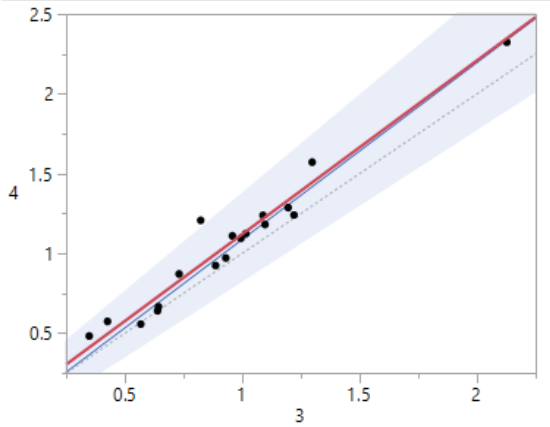

Passing-Bablok Regression

Parameter	Estimate	LowerCL	UpperCL
Intercept	-0.0216	-0.1272	0.15109
Slope	1.10887	0.95041	1.23049
Tau	0.86928	.	.

Orthogonal Fit Ratio=1.186

Variable	Mean	Std Dev	Variance Ratio	Correlation
3	0.943699	0.40062	1.186057	0.9753
4	1.05901	0.436301		

Intercept	Slope	LowerCL	UpperCL	Alpha
0.031263	1.089062	0.965214	1.228802	0.05000

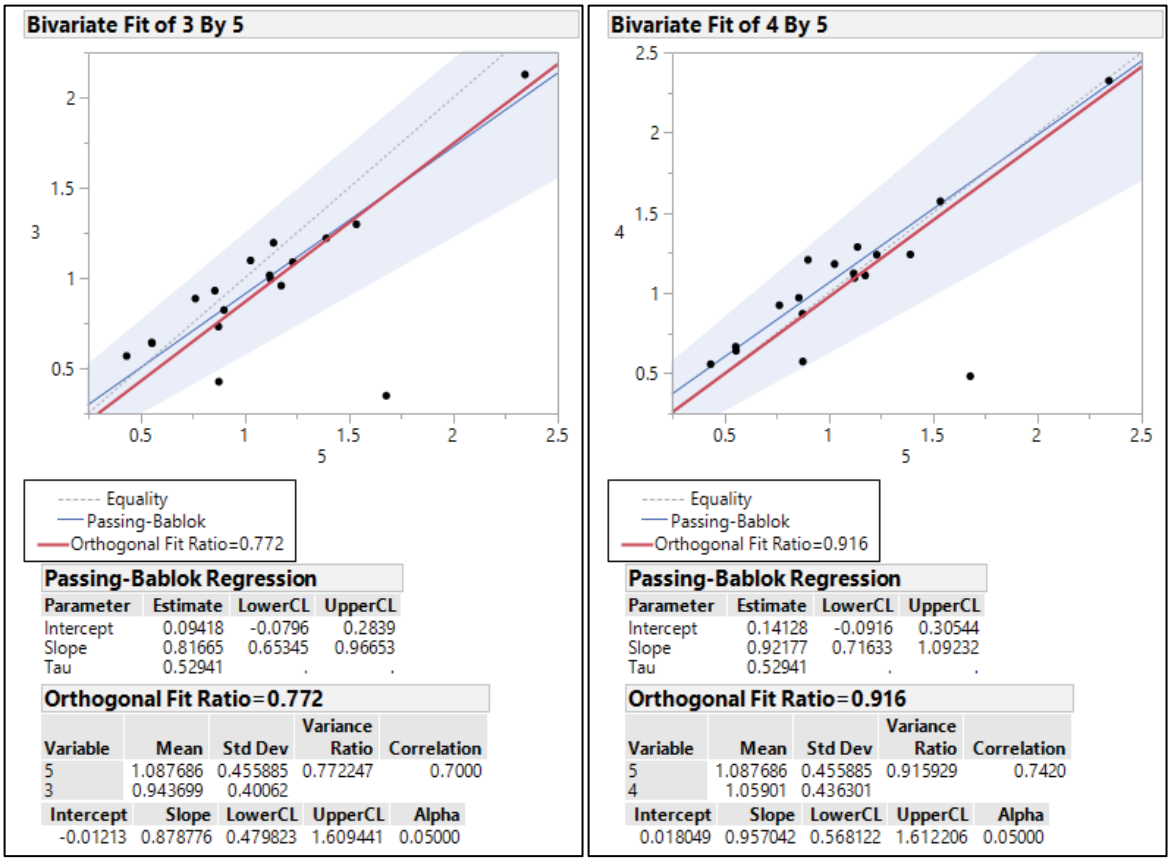

Plots and tables produced in JMP software with the 55 MPH HS data for all sections

Appendix O Chapter 3 Device Comparison

ANOVA of 55 MPH high speed runs, all devices, all sections

Summary of Fit					
RSquare	0.997044				
RSquare Adj	0.996314				
Root Mean Square Error	0.02629				
Mean of Response	1.044148				
Observations (or Sum Wgts)	450				
Analysis of Variance					
Source	DF	Sum of Squares	Mean Square	F Ratio	Prob > F
Model	89	83.93785	0.943122	1364.548	<.0001
Error	360	0.248818	0.000691		
C. Total	449	84.18667			
Effect Tests					
Source	Nparm	DF	Sum of Squares	F Ratio	Prob > F
DEVICE #	4	4	1.190734	430.7006	<.0001
section	17	17	74.49565	6340.198	<.0001
section*DEVICE #	68	68	8.251473	175.5672	<.0001

Normal Quantile Plot demonstrates assumptions for ANOVA are acceptably met.

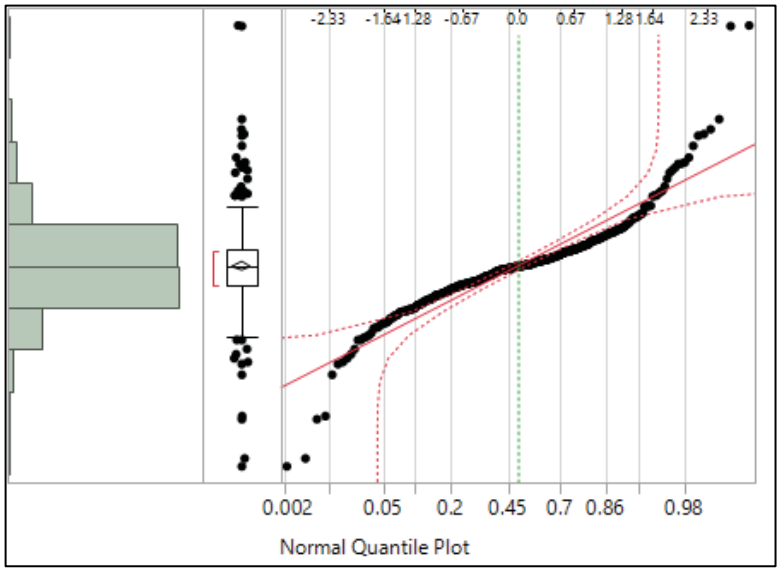

LSMeans Differences Tukey HSD

Alpha= 0.050 Q= 2.74167

LSMean[j]

LSMean[i] / Mean[i]-Mean[j] / Std Err Dif / Lower CL Dif / Upper CL Dif	1	2	3	4	5
1	0	0.01673	0.12984	0.01453	-0.0141
	0	0.00392	0.00392	0.00392	0.00392
	0	0.00599	0.11909	0.00378	-0.0249
	0	0.02748	0.14058	0.02527	-0.0034
2	-0.0167	0	0.11311	-0.0022	-0.0309
	0.00392	0	0.00392	0.00392	0.00392
	-0.0275	0	0.10236	-0.0129	-0.0416
	-0.006	0	0.12385	0.00854	-0.0201
3	-0.1298	-0.1131	0	-0.1153	-0.144
	0.00392	0.00392	0	0.00392	0.00392
	-0.1406	-0.1239	0	-0.1261	-0.1547
	-0.1191	-0.1024	0	-0.1046	-0.1332
4	-0.0145	0.0022	0.11531	0	-0.0287
	0.00392	0.00392	0.00392	0	0.00392
	-0.0253	-0.0085	0.10457	0	-0.0394
	-0.0038	0.01295	0.12606	0	-0.0179
5	0.01415	0.03088	0.14399	0.02868	0
	0.00392	0.00392	0.00392	0.00392	0
	0.0034	0.02013	0.13324	0.01793	0
	0.02489	0.04162	0.15473	0.03942	0

Level					Least Sq Mean
5	A				1.0876859
1		B			1.0735374
4			C		1.0590099
2			C		1.0568068
3				D	0.9436991

Levels not connected by same letter are significantly different.

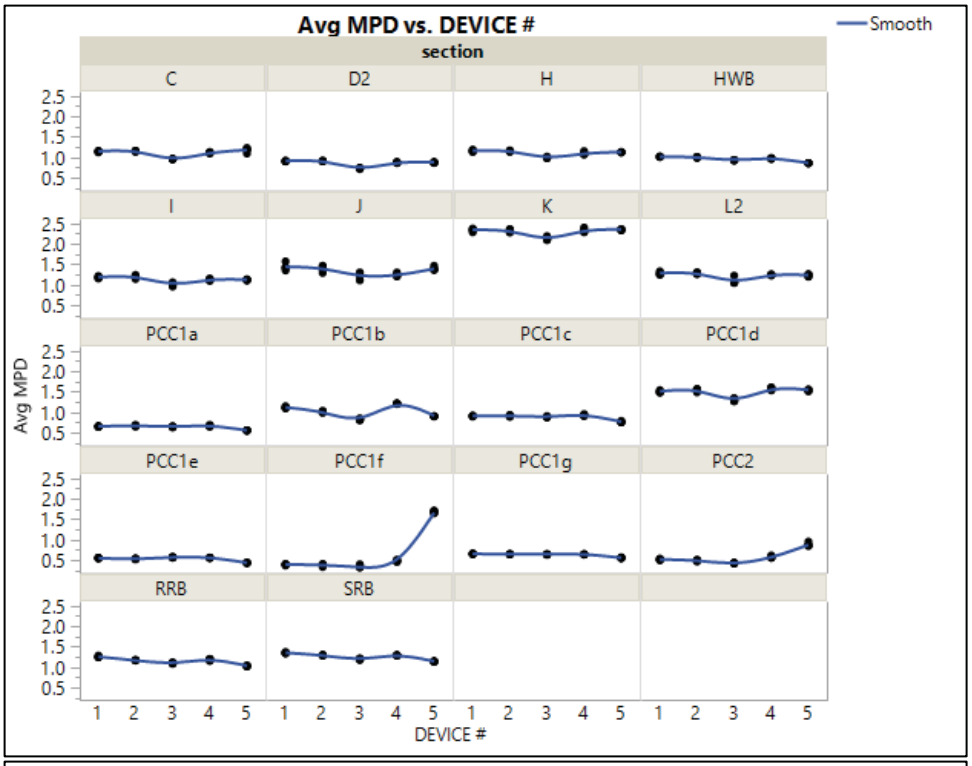
Avg MPD vs. DEVICE #
Smooth
section
C
D2
H
HWB
I
J
K
L2
PCC1a
PCC1b
PCC1c
PCC1d
PCC1e
PCC1f
PCC1g
PCC2
RRB
SRB
Avg MPD
DEVICE #

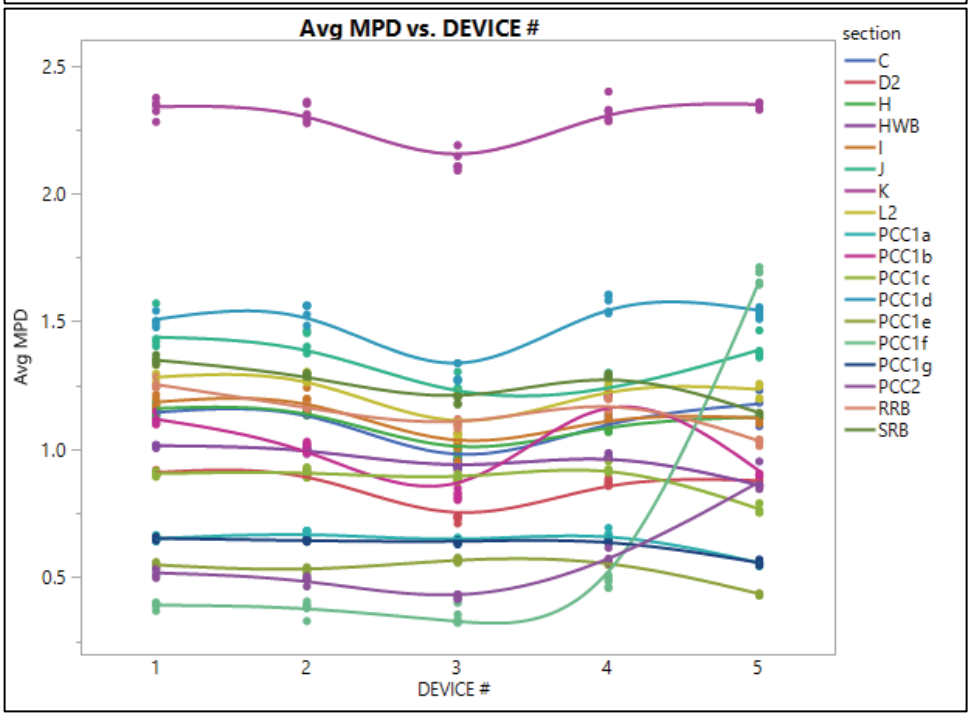
Avg MPD vs. DEVICE #
section
C
D2
H
HWB
I
J
K
L2
PCC1a
PCC1b
PCC1c
PCC1d
PCC1e
PCC1f
PCC1g
PCC2
RRB
SRB
Avg MPD
DEVICE #

ANOVA of 55 MPH high speed runs, all devices, longitudinally grooved sections only

Summary of Fit					
RSquare	0.996455				
RSquare Adj	0.995658				
Root Mean Square Error	0.025448				
Mean of Response	0.616116				
Observations (or Sum Wgts)	50				
Analysis of Variance					
Source	DF	Sum of Squares	Mean Square	F Ratio	Prob > F
Model	9	7.282236	0.809137	1249.422	<.0001
Error	40	0.025904	0.000648		
C. Total	49	7.30814			
Effect Tests					
Source	Nparm	DF	Sum of Squares	F Ratio	Prob > F
DEVICE #	4	4	5.565737	2148.569	<.0001
section	1	1	0.078568	121.3195	<.0001
section*DEVICE #	4	4	1.637932	632.2991	<.0001

Normal Quantile Plot demonstrates assumptions for ANOVA are acceptably met.

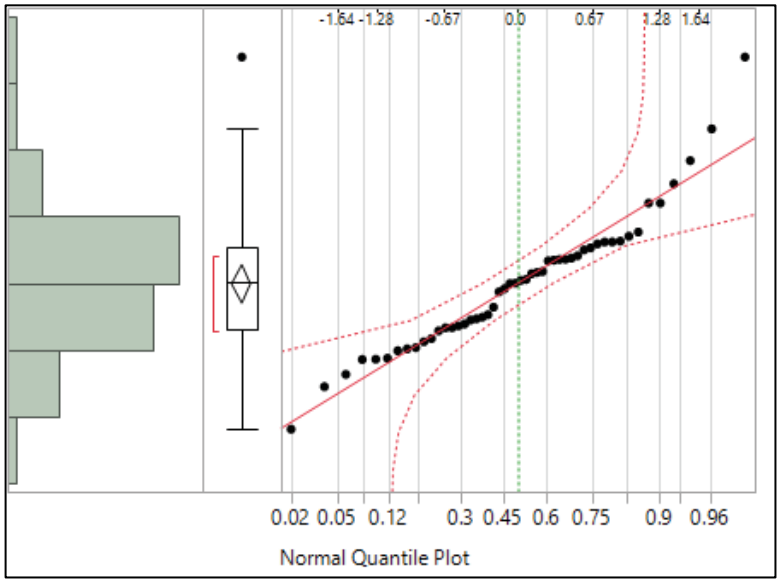

LSMeans Differences Tukey HSD

Alpha= 0.050 Q= 2.85609

LSMean[i]	Mean[i]-Mean[j] Std Err Dif Lower CL Dif Upper CL Dif	LSMean[j] 1	2	3	4	5
1		0	0.01872	0.06675	-0.0739	-0.8235
		0	0.01138	0.01138	0.01138	0.01138
		0	-0.0138	0.03425	-0.1064	-0.856
		0	0.05122	0.09926	-0.0414	-0.791
2		-0.0187	0	0.04804	-0.0927	-0.8422
		0.01138	0	0.01138	0.01138	0.01138
		-0.0512	0	0.01553	-0.1252	-0.8747
		0.01379	0	0.08054	-0.0602	-0.8097
3		-0.0668	-0.048	0	-0.1407	-0.8903
		0.01138	0.01138	0	0.01138	0.01138
		-0.0993	-0.0805	0	-0.1732	-0.9228
		-0.0342	-0.0155	0	-0.1082	-0.8578
4		0.07394	0.09266	0.14069	0	-0.7496
		0.01138	0.01138	0.01138	0	0.01138
		0.04144	0.06015	0.10819	0	-0.7821
		0.10645	0.12516	0.1732	0	-0.7171
5		0.82351	0.84222	0.89026	0.74956	0
		0.01138	0.01138	0.01138	0.01138	0
		0.791	0.80972	0.85775	0.71706	0
		0.85601	0.87473	0.92276	0.78207	0

Level					Least Sq Mean
5	A				1.2772260
4		B			0.5276626
1			C		0.4537190
2			C		0.4350040
3				D	0.3869677

Levels not connected by same letter are significantly different.

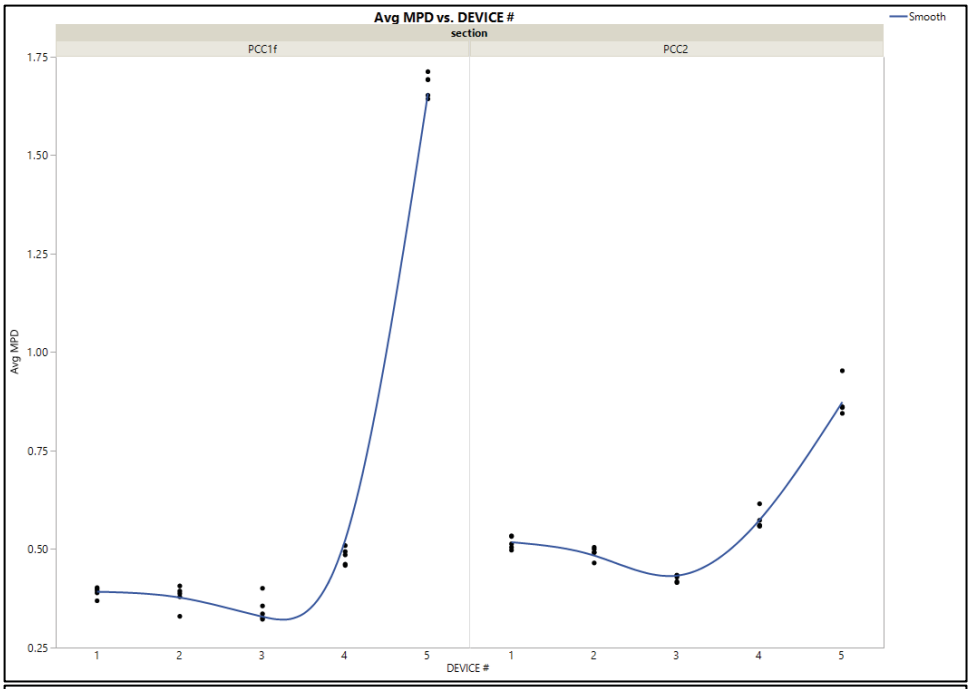
Avg MPD vs. DEVICE #
section
PCC1f
PCC2
Smooth
Avg MPD
DEVICE #
1.75
1.50
1.25
1.00
0.75
0.50
0.25
1
2
3
4
5

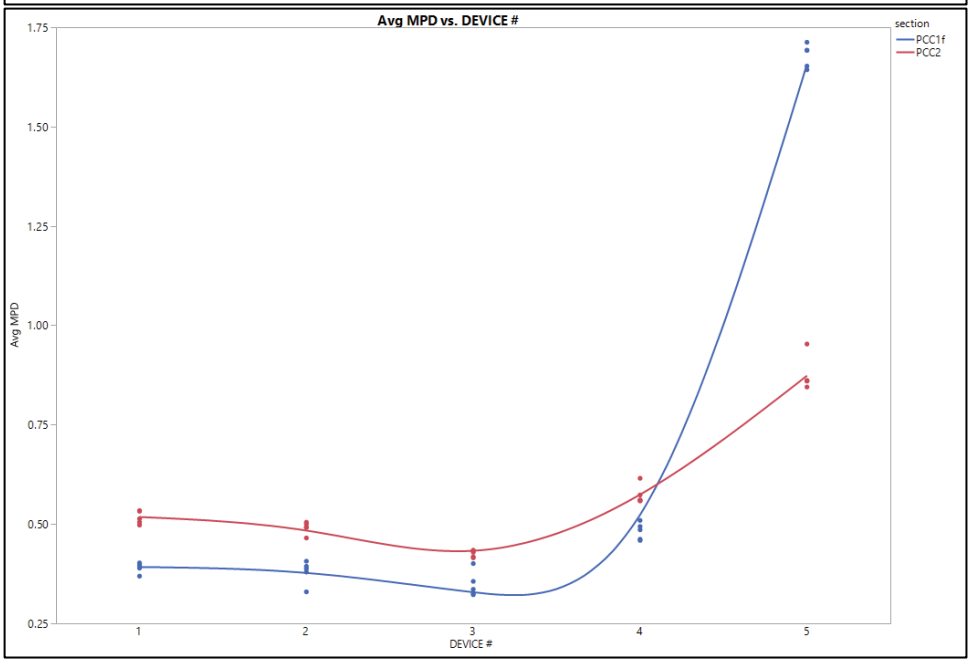
Avg MPD vs. DEVICE #
section
PCC1f
PCC2
Avg MPD
DEVICE #
1.75
1.50
1.25
1.00
0.75
0.50
0.25
1
2
3
4
5

ANOVA of 55 MPH high speed runs, all devices, all sections excluding longitudinally grooved sections

Summary of Fit					
RSquare	0.996652				
RSquare Adj	0.995825				
Root Mean Square Error	0.026393				
Mean of Response	1.097652				
Observations (or Sum Wgts)	400				
Analysis of Variance					
Source	DF	Sum of Squares	Mean Square	F Ratio	Prob > F
Model	79	66.34998	0.839873	1205.667	<.0001
Error	320	0.222914	0.000697		
C. Total	399	66.57289			
Effect Tests					
Source	Nparm	DF	Sum of Squares	F Ratio	Prob > F
DEVICE #	4	4	1.058319	379.8134	<.0001
section	15	15	64.11144	6135.611	<.0001
section*DEVICE #	60	60	1.180219	28.2374	<.0001

Normal Quantile Plot demonstrates assumptions for ANOVA are acceptably met.

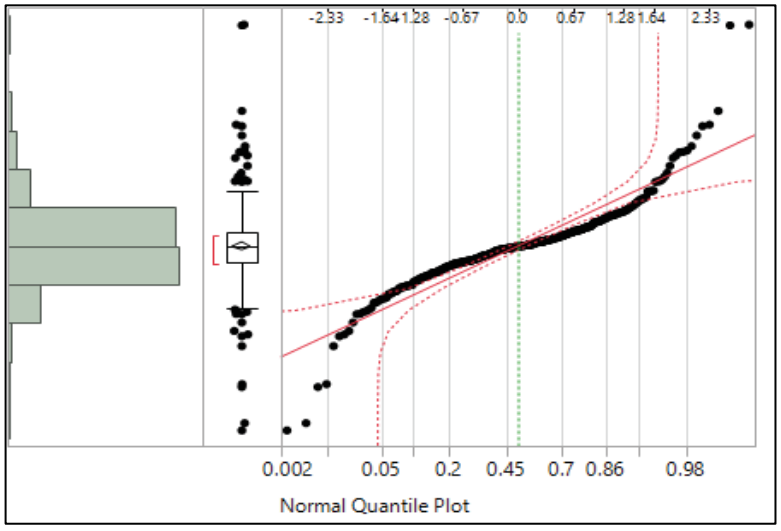

LSMeans Differences Tukey HSD

Alpha= 0.050 Q= 2.74341

LSMean[j]

LSMean[i]	Mean[i]-Mean[j] Std Err Dif Lower CL Dif Upper CL Dif	1	2	3	4	5
	1	0 0 0 0	0.01648 0.00417 0.00503 0.02793	0.13772 0.00417 0.12628 0.14917	0.02559 0.00417 0.01414 0.03704	0.08702 0.00417 0.07557 0.09847
	2	-0.0165 0.00417 -0.0279 -0.005	0 0 0 0	0.12124 0.00417 0.10979 0.13269	0.0091 0.00417 -0.0023 0.02055	0.07054 0.00417 0.05909 0.08199
	3	-0.1377 0.00417 -0.1492 -0.1263	-0.1212 0.00417 -0.1327 -0.1098	0 0 0 0	-0.1121 0.00417 -0.1236 -0.1007	-0.0507 0.00417 -0.0622 -0.0393
	4	-0.0256 0.00417 -0.037 -0.0141	-0.0091 0.00417 -0.0206 0.00234	0.11214 0.00417 0.10069 0.12359	0 0 0 0	0.06143 0.00417 0.04999 0.07288
	5	-0.087 0.00417 -0.0985 -0.0756	-0.0705 0.00417 -0.082 -0.0591	0.0507 0.00417 0.03925 0.06215	-0.0614 0.00417 -0.0729 -0.05	0 0 0 0

Level						Least Sq Mean
1	A					1.1510147
2		B				1.1345321
4		B				1.1254283
5			C			1.0639934
3				D		1.0132906

Levels not connected by same letter are significantly different.

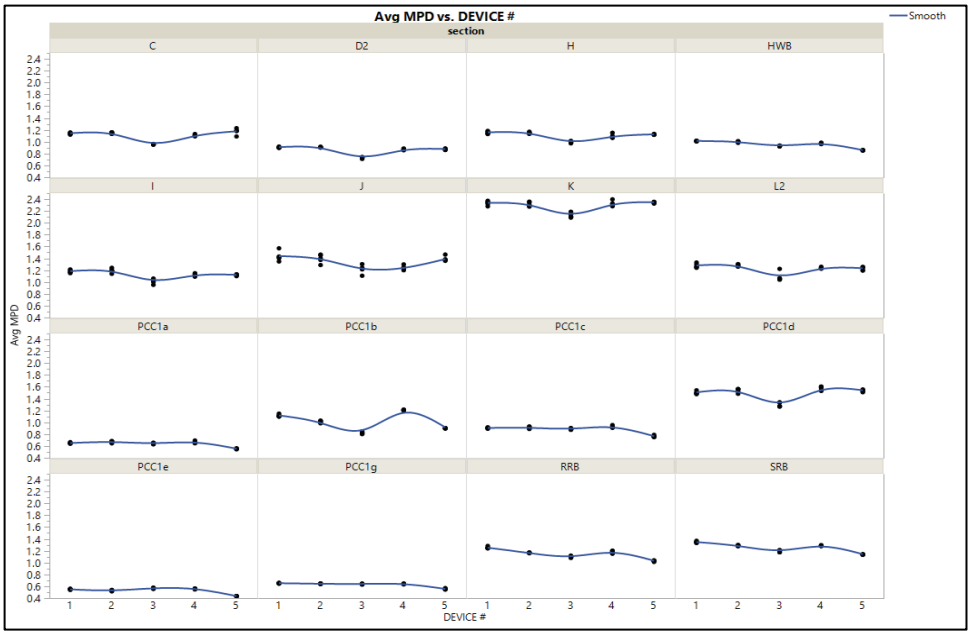
Avg MPD vs. DEVICE #
section
Smooth
C
D2
H
HWB
I
J
K
L2
PCC1a
PCC1b
PCC1c
PCC1d
PCC1e
PCC1g
RRB
SRB
Avg MPD
DEVICE #

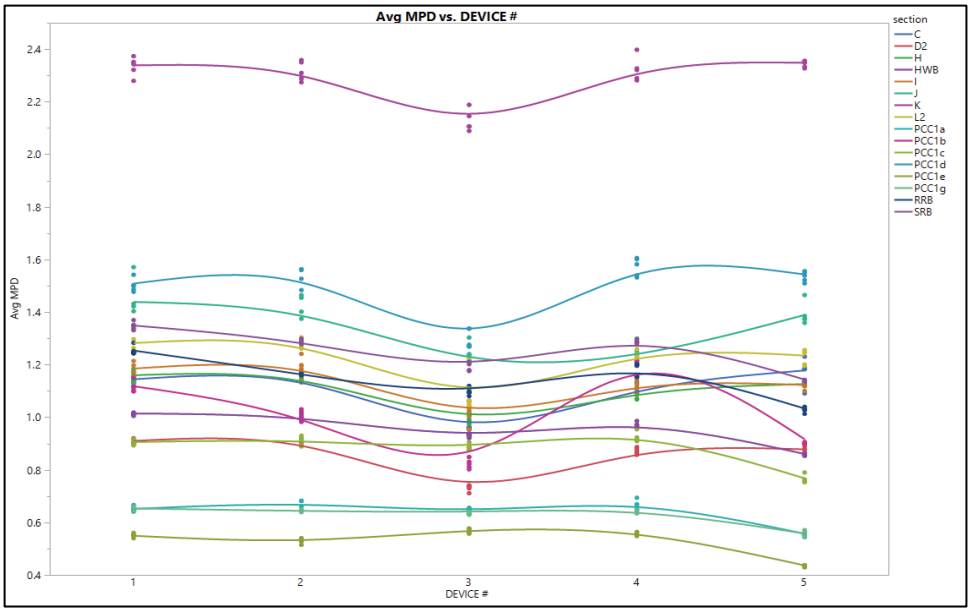
Avg MPD vs. DEVICE #
section
C
D2
H
HWB
I
J
K
L2
PCC1a
PCC1b
PCC1c
PCC1d
PCC1e
PCC1g
RRB
SRB
Avg MPD
DEVICE #

ANOVA of 55 MPH high speed runs, all devices, transversely grooved sections only

Summary of Fit					
RSquare	0.998491				
RSquare Adj	0.998125				
Root Mean Square Error	0.011404				
Mean of Response	0.859956				
Observations (or Sum Wgts)	175				
Analysis of Variance					
Source	DF	Sum of Squares	Mean Square	F Ratio	Prob > F
Model	34	12.05054	0.354428	2725.409	<.0001
Error	140	0.018206	0.00013		
C. Total	174	12.06874			
Effect Tests					
Source	Nparm	DF	Sum of Squares	F Ratio	Prob > F
DEVICE #	4	4	0.487641	937.4428	<.0001
section	6	6	11.46243	14690.26	<.0001
section*DEVICE #	24	24	0.100468	32.19	<.0001

Normal Quantile Plot demonstrates assumptions for ANOVA are acceptably met.

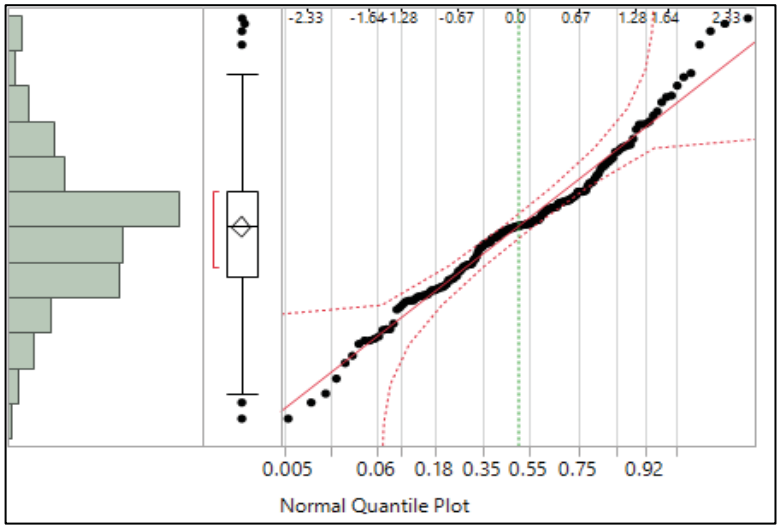

LSMeans Differences Tukey HSD

Alpha= 0.050 Q= 2.76365

LSMean[j]

LSMean[i] Mean[i]-Mean[j] / Std Err Dif / Lower CL Dif / Upper CL Dif	1	2	3	4	5
1	0	0.02322	0.05922	0.021	0.14895
	0	0.00273	0.00273	0.00273	0.00273
	0	0.01569	0.05168	0.01347	0.14141
	0	0.03075	0.06675	0.02853	0.15648
2	-0.0232	0	0.036	-0.0022	0.12573
	0.00273	0	0.00273	0.00273	0.00273
	-0.0308	0	0.02846	-0.0098	0.11819
	-0.0157	0	0.04353	0.00531	0.13326
3	-0.0592	-0.036	0	-0.0382	0.08973
	0.00273	0.00273	0	0.00273	0.00273
	-0.0668	-0.0435	0	-0.0457	0.0822
	-0.0517	-0.0285	0	-0.0307	0.09727
4	-0.021	0.00222	0.03822	0	0.12795
	0.00273	0.00273	0.00273	0	0.00273
	-0.0285	-0.0053	0.03068	0	0.12041
	-0.0135	0.00975	0.04575	0	0.13548
5	-0.1489	-0.1257	-0.0897	-0.1279	0
	0.00273	0.00273	0.00273	0.00273	0
	-0.1565	-0.1333	-0.0973	-0.1355	0
	-0.1414	-0.1182	-0.0822	-0.1204	0

Level					Least Sq Mean
1	A				0.91043316
4		B			0.88943299
2		B			0.88721282
3			C		0.85121683
5				D	0.76148536

Levels not connected by same letter are significantly different.

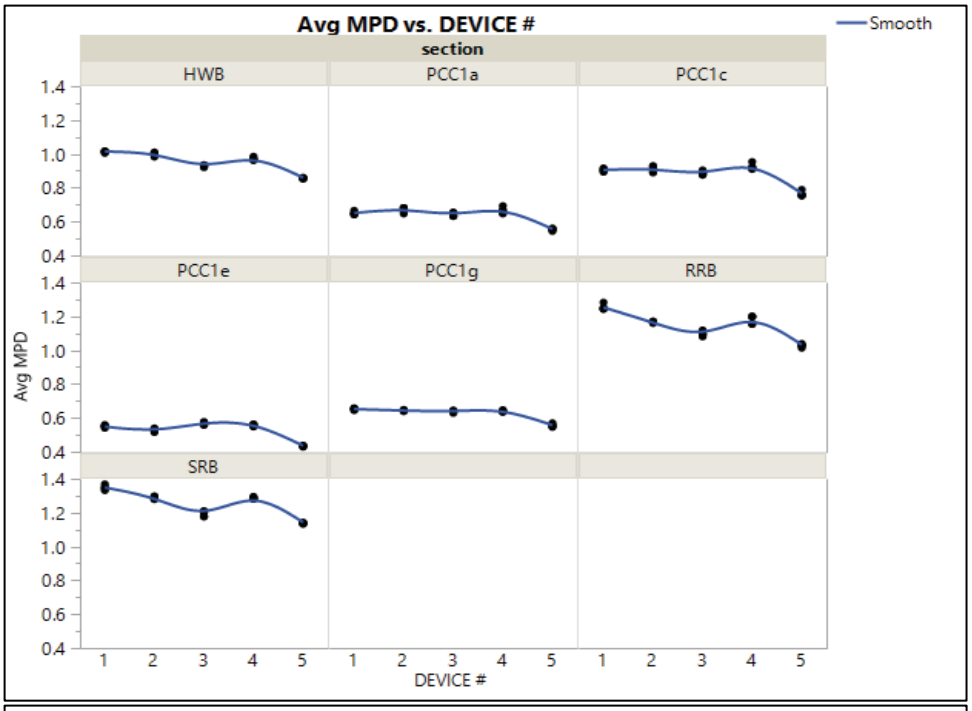
Avg MPD vs. DEVICE #
Smooth
section
HWB
PCC1a
PCC1c
PCC1e
PCC1g
RRB
SRB
Avg MPD
DEVICE #

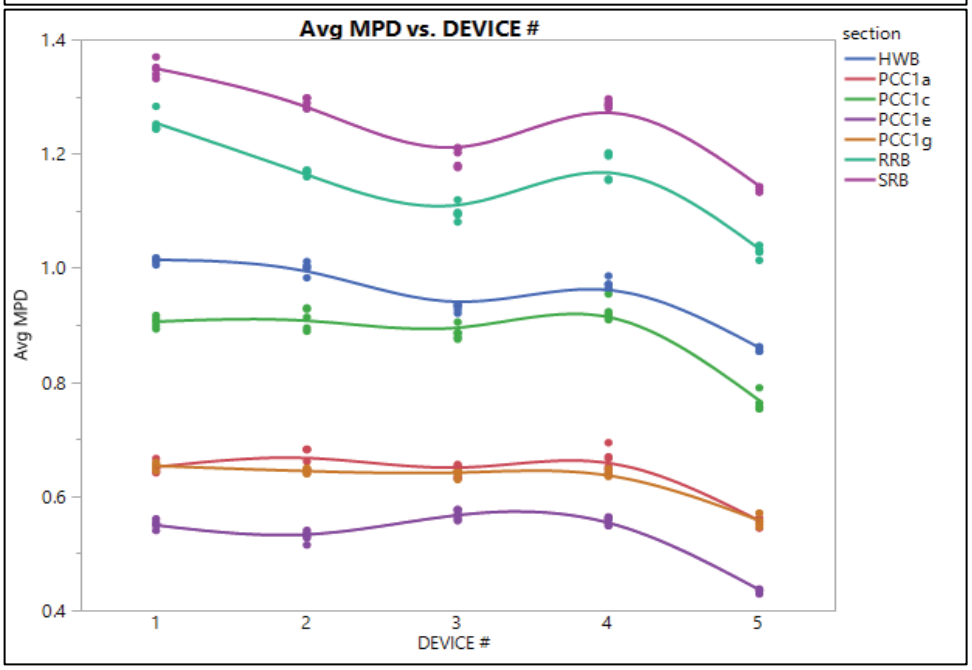
Avg MPD vs. DEVICE #
section
HWB
PCC1a
PCC1c
PCC1e
PCC1g
RRB
SRB
Avg MPD
DEVICE #

ANOVA of 55 MPH high speed runs, all devices, random texture (asphalt like) sections only

Summary of Fit					
RSquare	0.994456				
RSquare Adj	0.993101				
Root Mean Square Error	0.033723				
Mean of Response	1.282526				
Observations (or Sum Wgts)	225				
Analysis of Variance					
Source	DF	Sum of Squares	Mean Square	F Ratio	
Model	44	36.72192	0.834589	733.8583	
Error	180	0.204707	0.001137		Prob > F
C. Total	224	36.92663		<.0001	
Effect Tests					
Source	Nparm	DF	Sum of Squares	F Ratio	Prob > F
DEVICE #	4	4	1.194341	262.5474	<.0001
section	8	8	35.07149	3854.817	<.0001
section*DEVICE #	32	32	0.456088	12.5325	<.0001

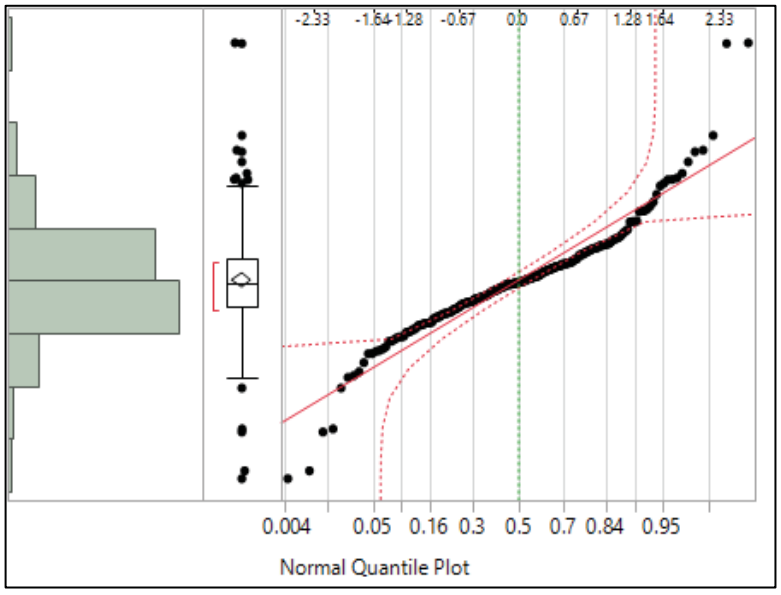

Normal Quantile Plot demonstrates assumptions for ANOVA are acceptably met.

LSMeans Differences Tukey HSD

Alpha= 0.050 Q= 2.75563

LSMean[i]	Mean[i]-Mean[j] Std Err Dif Lower CL Dif Upper CL Dif	LSMean[j] 1	2	3	4	5
1		0	0.01124	0.19879	0.02915	0.03886
		0	0.00711	0.00711	0.00711	0.00711
		0	-0.0083	0.17919	0.00956	0.01927
		0	0.03083	0.21838	0.04874	0.05845
2		-0.0112	0	0.18754	0.01791	0.02761
		0.00711	0	0.00711	0.00711	0.00711
		-0.0308	0	0.16795	-0.0017	0.00802
		0.00835	0	0.20713	0.0375	0.04721
3		-0.1988	-0.1875	0	-0.1696	-0.1599
		0.00711	0.00711	0	0.00711	0.00711
		-0.2184	-0.2071	0	-0.1892	-0.1795
		-0.1792	-0.168	0	-0.15	-0.1403
4		-0.0292	-0.0179	0.16963	0	0.0097
		0.00711	0.00711	0.00711	0	0.00711
		-0.0487	-0.0375	0.15004	0	-0.0099
		-0.0096	0.00168	0.18922	0	0.02929
5		-0.0389	-0.0276	0.15993	-0.0097	0
		0.00711	0.00711	0.00711	0.00711	0
		-0.0584	-0.0472	0.14034	-0.0293	0
		-0.0193	-0.008	0.17952	0.00989	0

Level					Least Sq Mean
1	A				1.3381336
2	A	B			1.3268916
4		B	C		1.3089801
5			C		1.2992773
3				D	1.1393479

Levels not connected by same letter are significantly different.

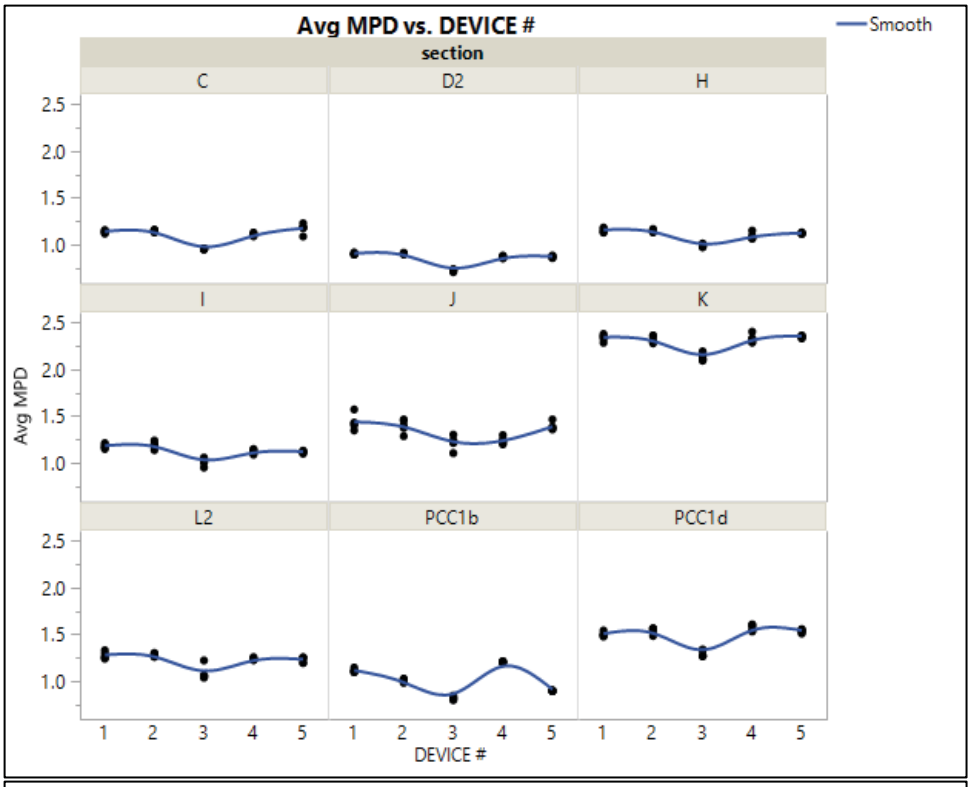
Avg MPD vs. DEVICE #
Smooth
section
C
D2
H
I
J
K
L2
PCC1b
PCC1d
Avg MPD
DEVICE #

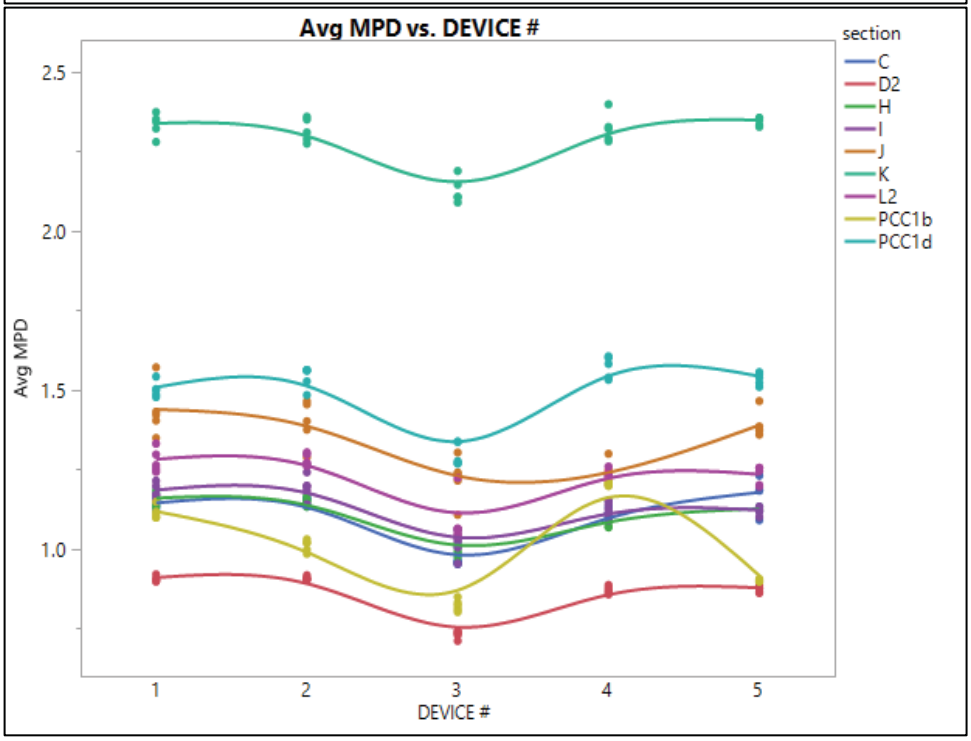
Avg MPD vs. DEVICE #
section
C
D2
H
I
J
K
L2
PCC1b
PCC1d
Avg MPD
DEVICE #

ANOVA of 65 MPH high speed runs, all devices, all sections

Summary of Fit					
RSquare	0.996748				
RSquare Adj	0.995943				
Root Mean Square Error	0.027192				
Mean of Response	1.033221				
Observations (or Sum Wgts)	450				
Analysis of Variance					
Source	DF	Sum of Squares	Mean Square	F Ratio	
Model	89	81.573336	0.916554	1239.621	
Error	360	0.266178	0.000739		Prob > F
C. Total	449	81.839514		<.0001	
Effect Tests					
Source	Nparm	DF	Sum of Squares	F Ratio	Prob > F
DEVICE #	4	4	1.473894	498.3528	<.0001
section	17	17	72.095698	5735.763	<.0001
section*DEVICE #	68	68	8.003744	159.1897	<.0001

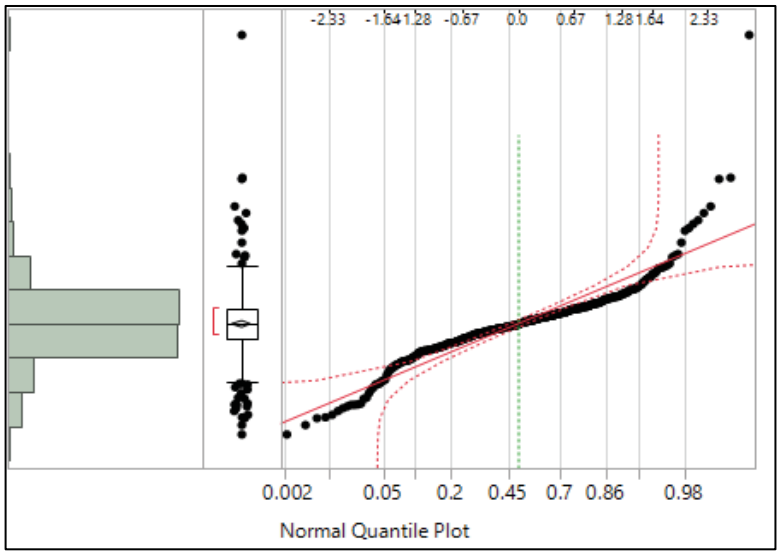

Normal Quantile Plot demonstrates assumptions for ANOVA are acceptably met.

LSMeans Differences Tukey HSD

Alpha= 0.050 Q= 2.74167

LSMean[i]	Mean[i]-Mean[j] Std Err Dif Lower CL Dif Upper CL Dif	1	2	3	4	5
	1	0 0 0 0	0.01924 0.00405 0.00812 0.03035	0.14595 0.00405 0.13483 0.15706	0.01295 0.00405 0.00184 0.02407	-0.011 0.00405 -0.0222 6.49e-5
	2	-0.0192 0.00405 -0.0303 -0.0081	0 0 0 0	0.12671 0.00405 0.1156 0.13782	-0.0063 0.00405 -0.0174 0.00483	-0.0303 0.00405 -0.0414 -0.0192
	3	-0.1459 0.00405 -0.1571 -0.1348	-0.1267 0.00405 -0.1378 -0.1156	0 0 0 0	-0.133 0.00405 -0.1441 -0.1219	-0.157 0.00405 -0.1681 -0.1459
	4	-0.013 0.00405 -0.0241 -0.0018	0.00628 0.00405 -0.0048 0.01739	0.13299 0.00405 0.12188 0.1441	0 0 0 0	-0.024 0.00405 -0.0351 -0.0129
	5	0.01105 0.00405 -0.0001 0.02216	0.03028 0.00405 0.01917 0.0414	0.157 0.00405 0.14588 0.16811	0.024 0.00405 0.01289 0.03512	0 0 0 0

Level				Least Sq Mean
5	A			1.0776875
1	A			1.0666391
4		B		1.0536841
2		B		1.0474038
3			C	0.9206925

Levels not connected by same letter are significantly different.

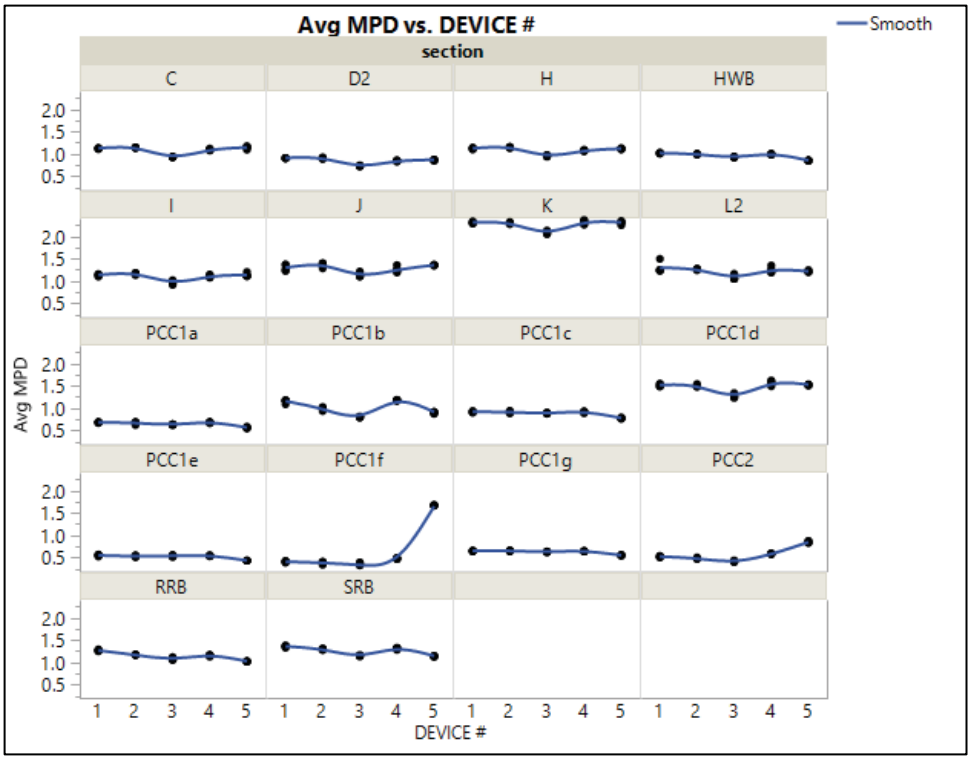
Avg MPD vs. DEVICE #
Smooth
section
C
D2
H
HWB
I
J
K
L2
PCC1a
PCC1b
PCC1c
PCC1d
PCC1e
PCC1f
PCC1g
PCC2
RRB
SRB
Avg MPD
DEVICE #

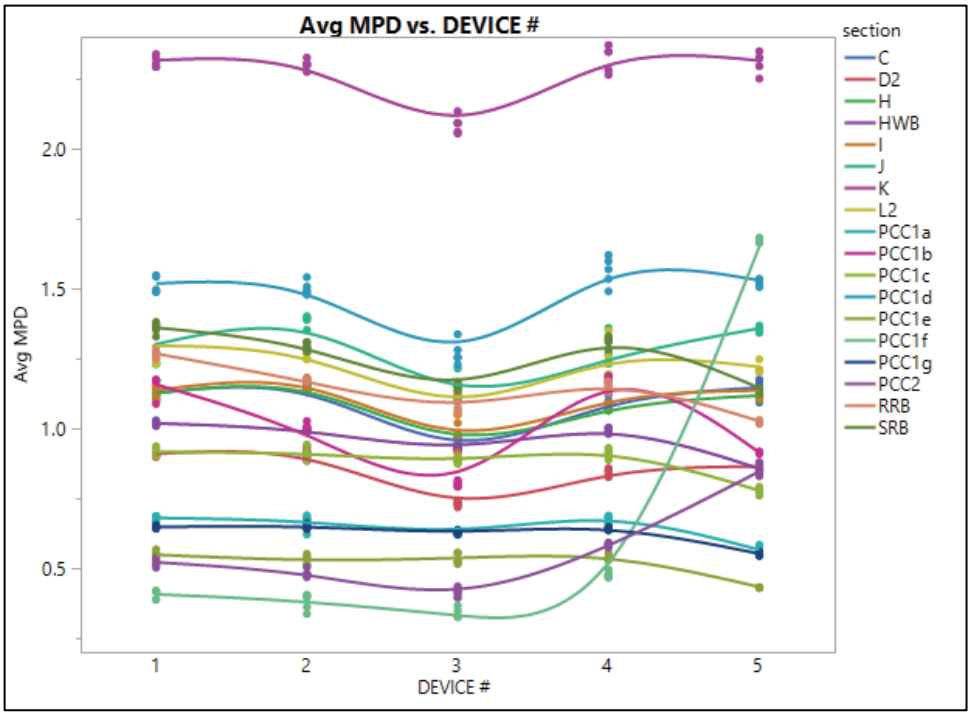
Avg MPD vs. DEVICE #
section
C
D2
H
HWB
I
J
K
L2
PCC1a
PCC1b
PCC1c
PCC1d
PCC1e
PCC1f
PCC1g
PCC2
RRB
SRB
Avg MPD
DEVICE #

Appendix P Chapter 4 Line Laser Orientation

LLT Device

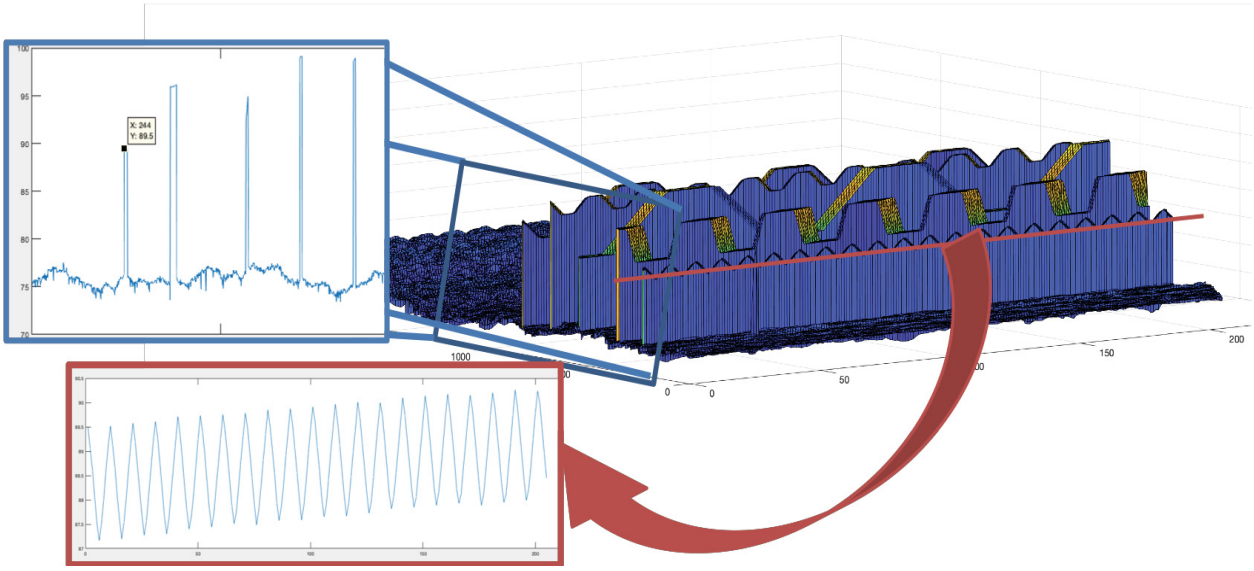

- ✓ Plates have shapes machined in transverse to the plate's long axis
- ✓ Plates were laid transverse to the direction of travel so grooves were parallel to direction of travel (i.e., **simulating longitudinal grooves**)
- ✓ LL laser was mounted with **laser line perpendicular to direction of travel**
  - Results in several (approx. 8) reproductions of the shape

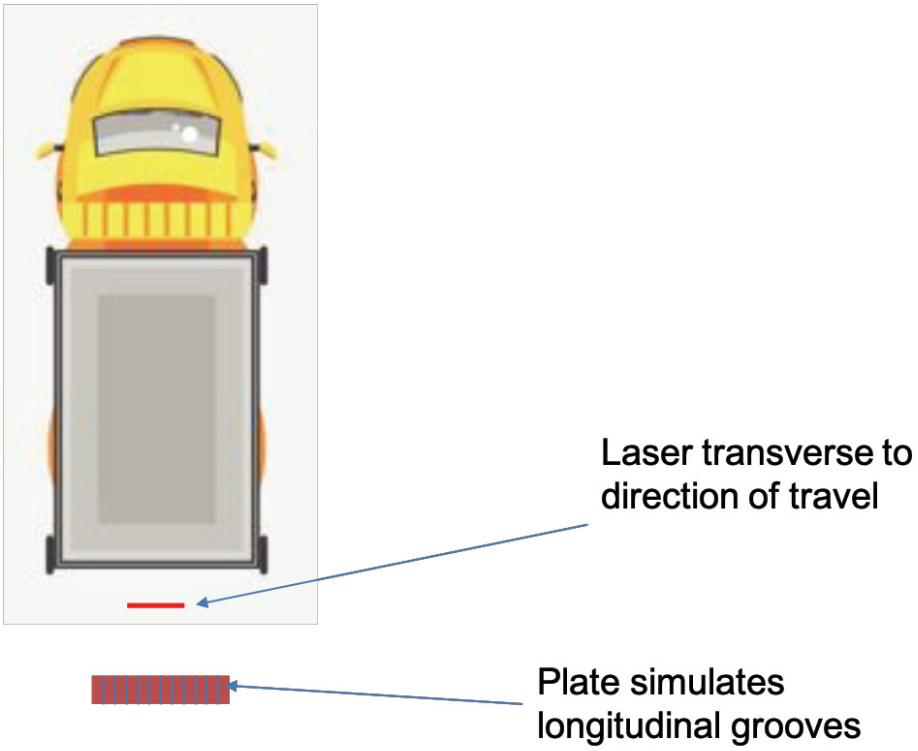

LLL Device

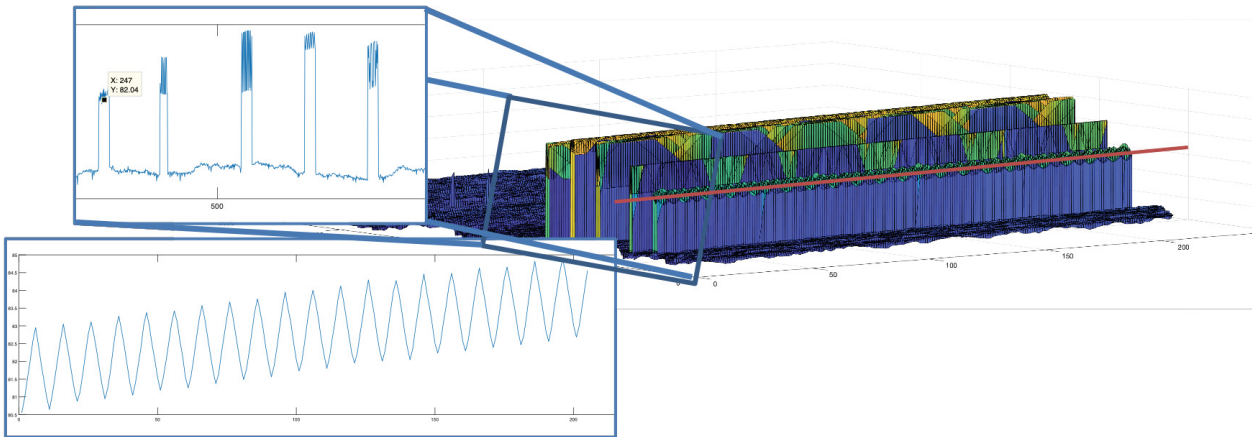

- ✓ Plates have shapes machined in transverse to the plate's long axis
- ✓ Plates were laid parallel to the direction of travel so grooves were perpendicular to direction of travel (i.e., **simulating transverse grooves**)
- ✓ LL laser was mounted with **laser line parallel to direction of travel**
- ✓ Results in many (approx. 20) reproductions of the shape

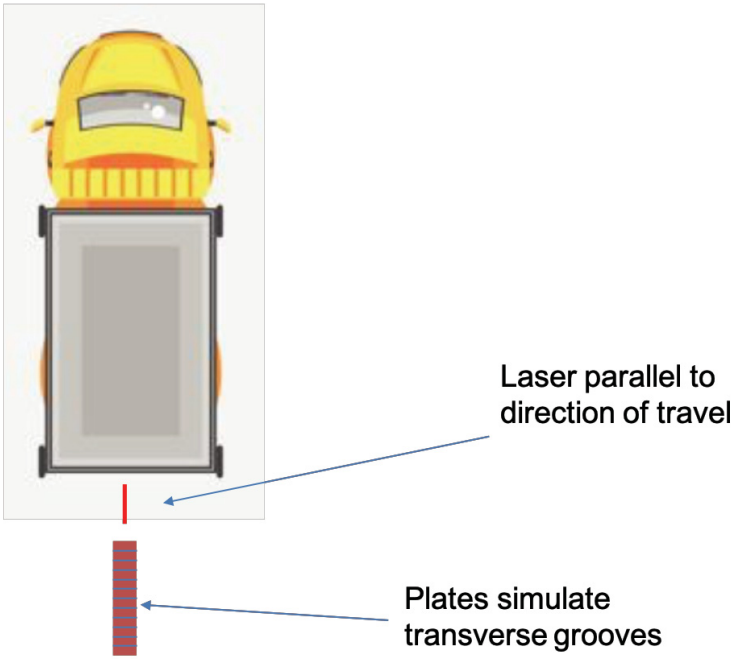

Appendix Q Chapter 4 Speed and Exposure Data Plots

SSL - unfiltered

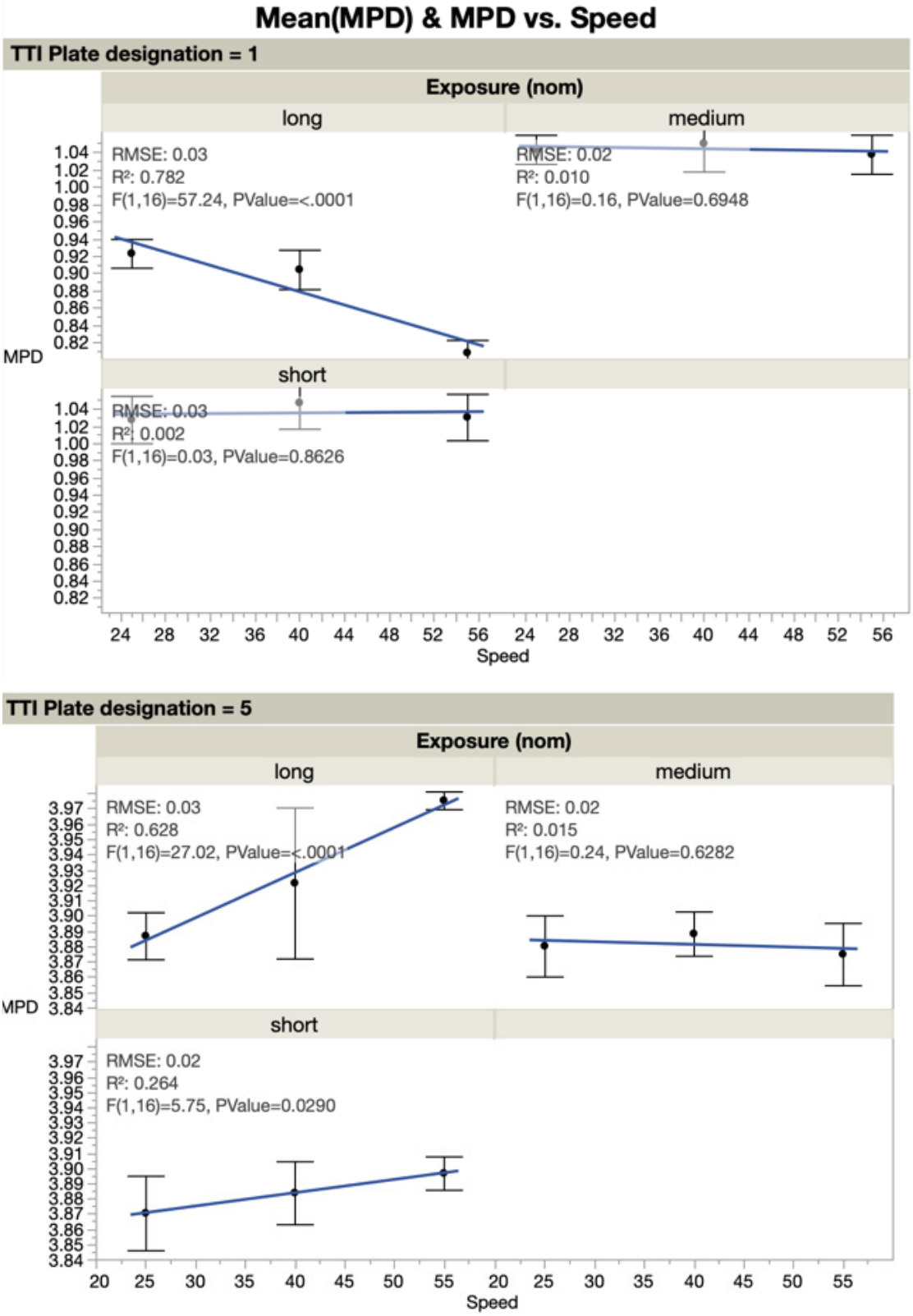

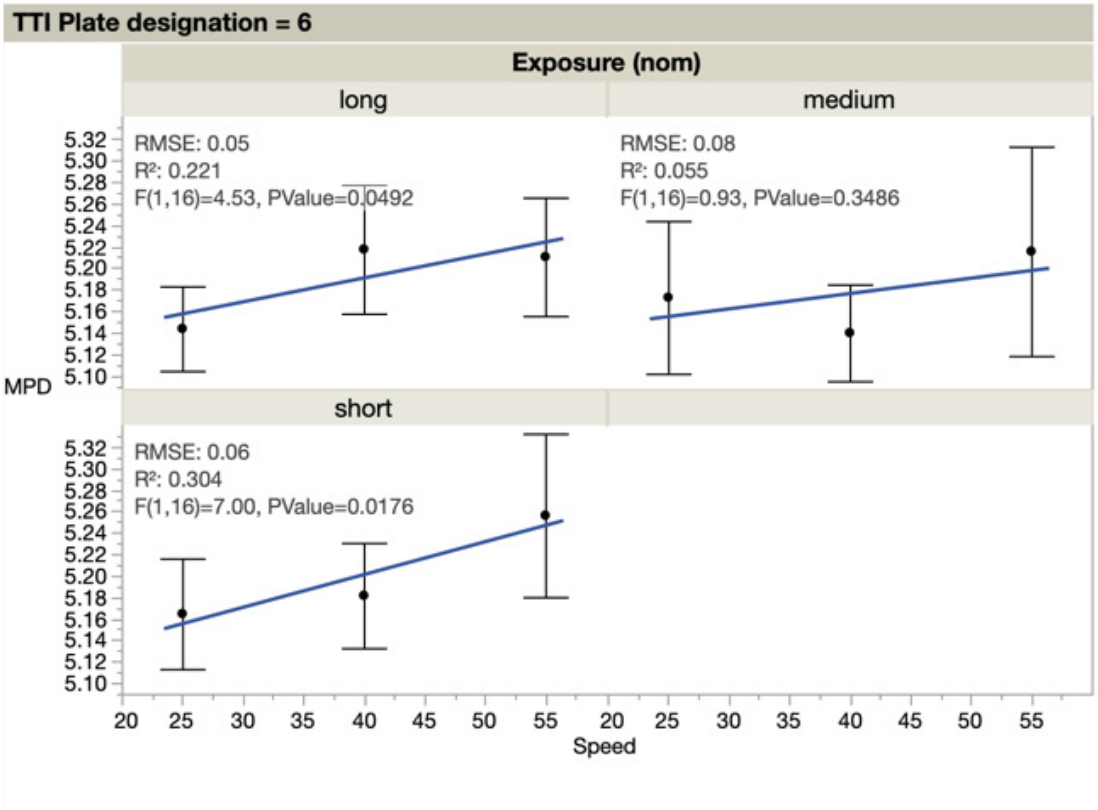
TTI Plate designation = 6
Exposure (nom)
long
medium
short
RMSE: 0.05
R²: 0.221
F(1,16)=4.53, PValue=0.0492
RMSE: 0.08
R²: 0.055
F(1,16)=0.93, PValue=0.3486
RMSE: 0.06
R²: 0.304
F(1,16)=7.00, PValue=0.0176
MPD
5.32
5.30
5.28
5.26
5.24
5.22
5.20
5.18
5.16
5.14
5.12
5.10
20 25 30 35 40 45 50 55
Speed

LLL unfiltered

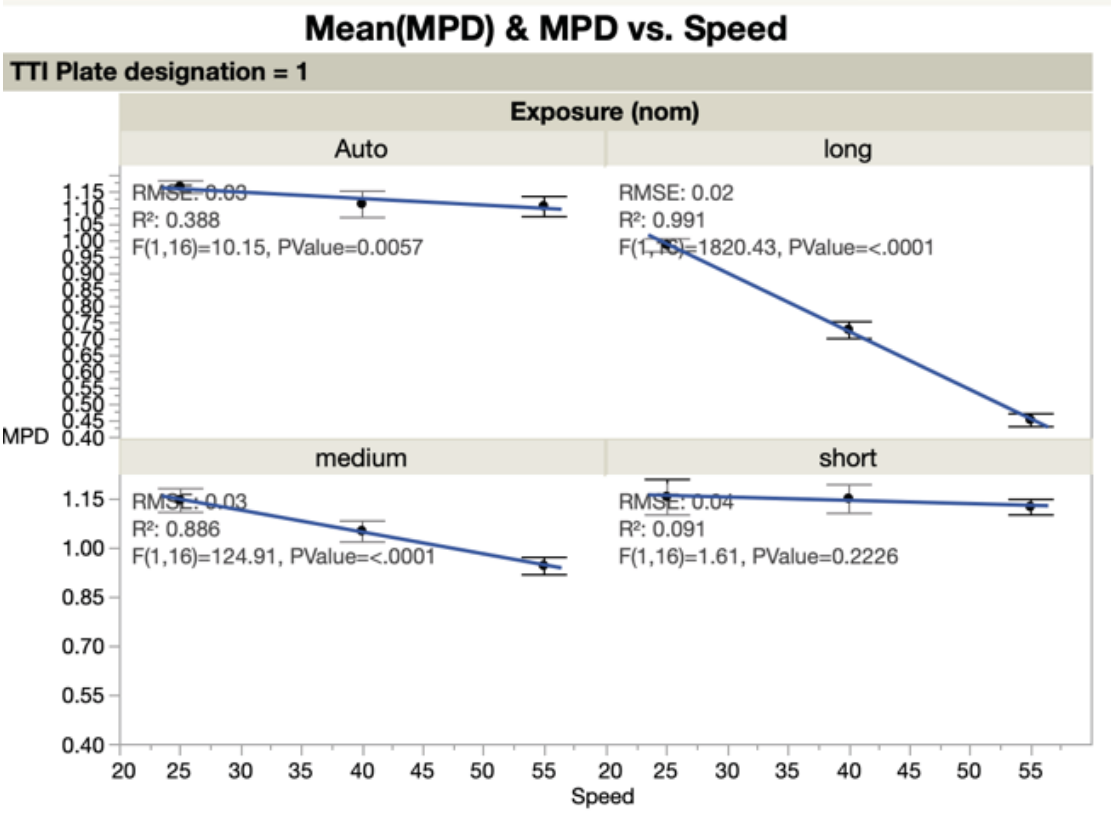

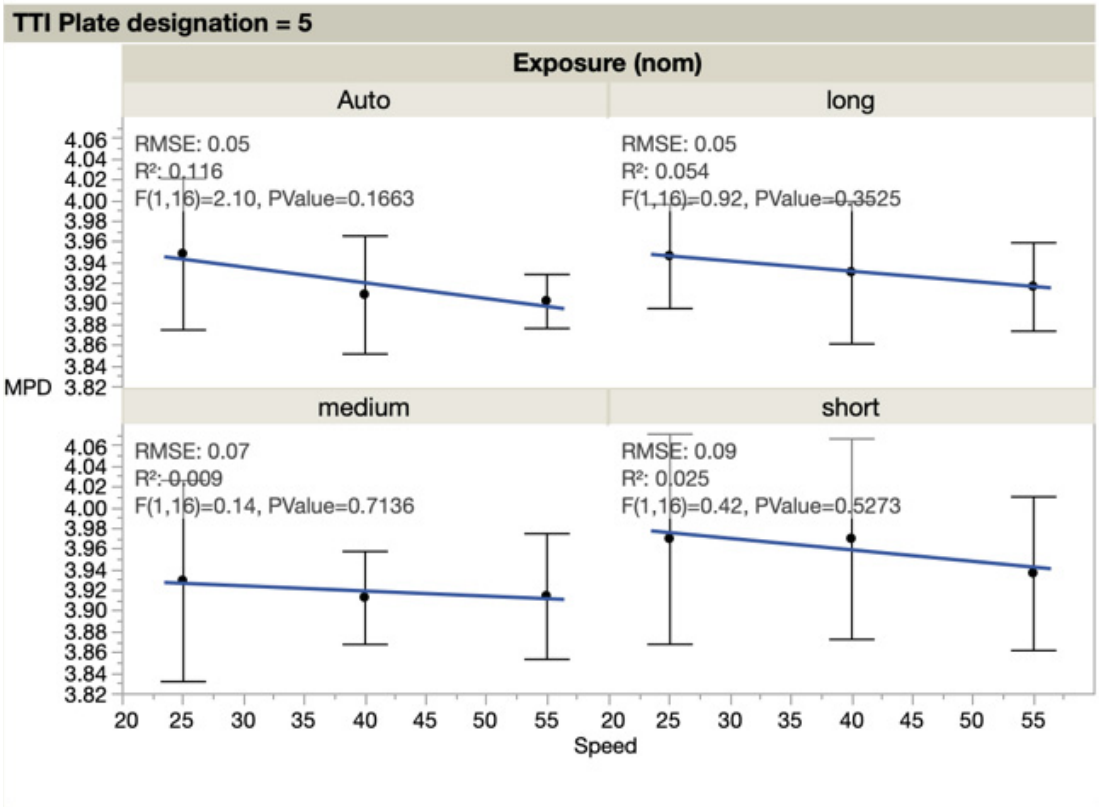

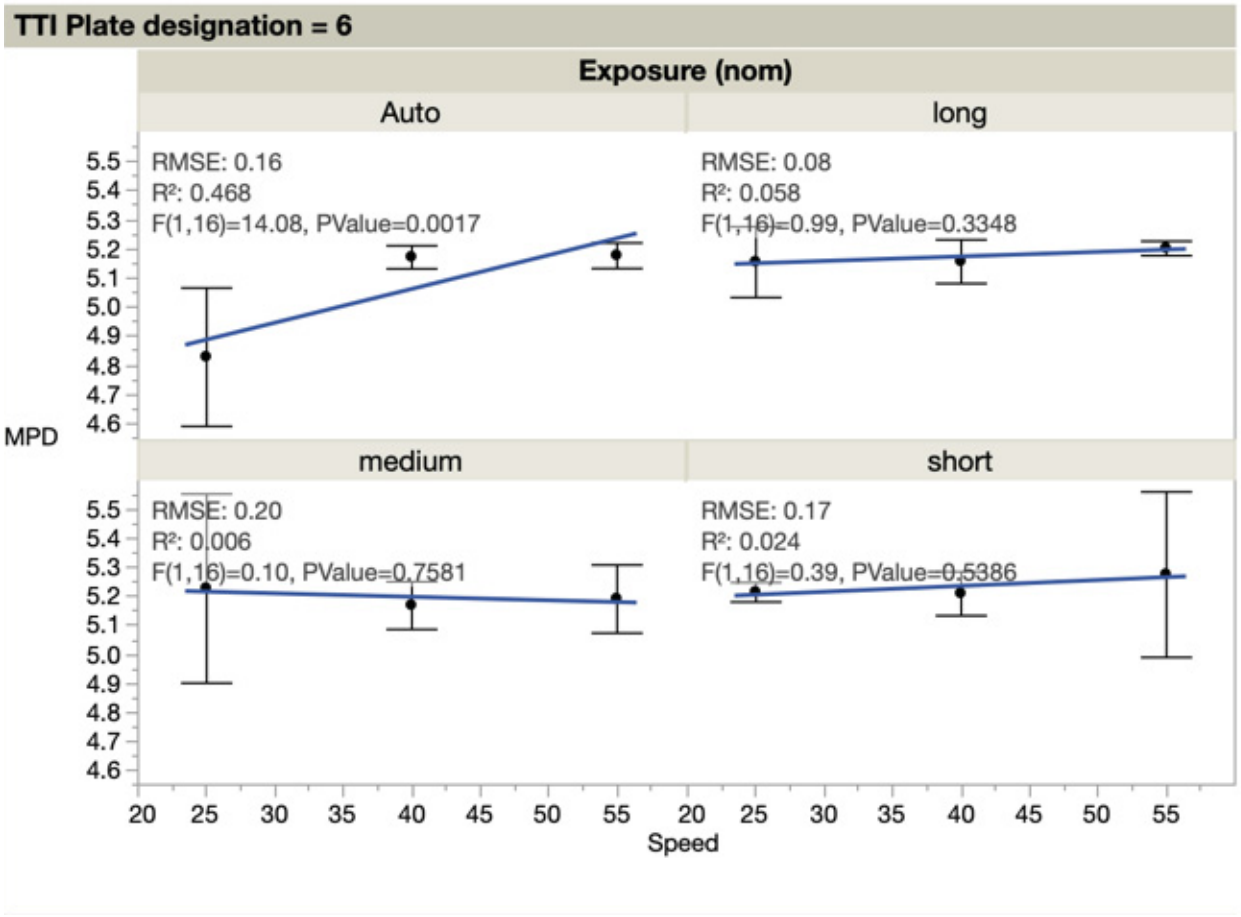
TTI Plate designation = 6
Exposure (nom)
Auto
long
medium
short
RMSE: 0.16
R²: 0.468
F(1,16)=14.08, PValue=0.0017
RMSE: 0.08
R²: 0.058
F(1,16)=0.99, PValue=0.3348
RMSE: 0.20
R²: 0.006
F(1,16)=0.10, PValue=0.7581
RMSE: 0.17
R²: 0.024
F(1,16)=0.39, PValue=0.5386
MPD
Speed
5.5
5.4
5.3
5.2
5.1
5.0
4.9
4.8
4.7
4.6
20
25
30
35
40
45
50
55

LLT unfiltered

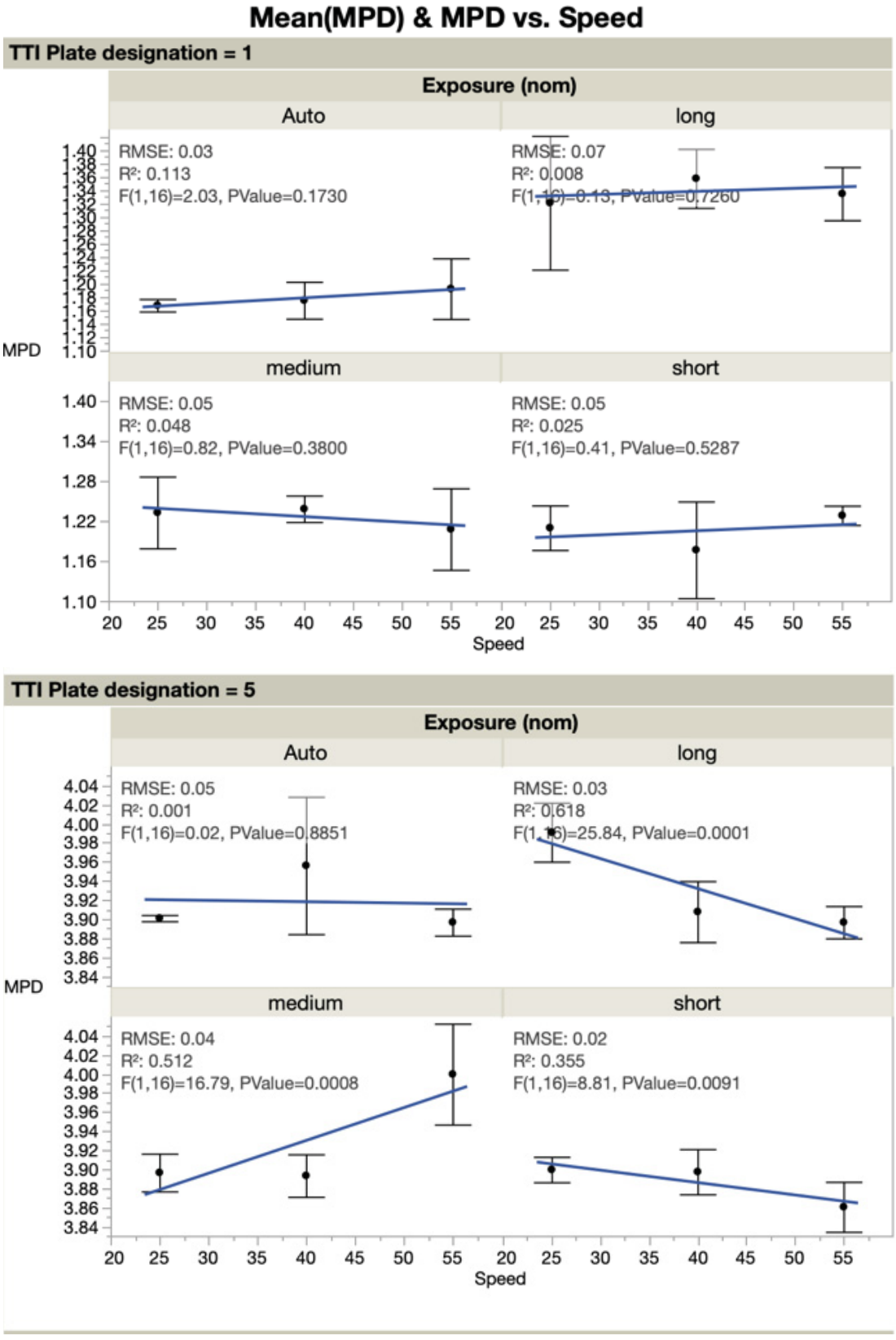

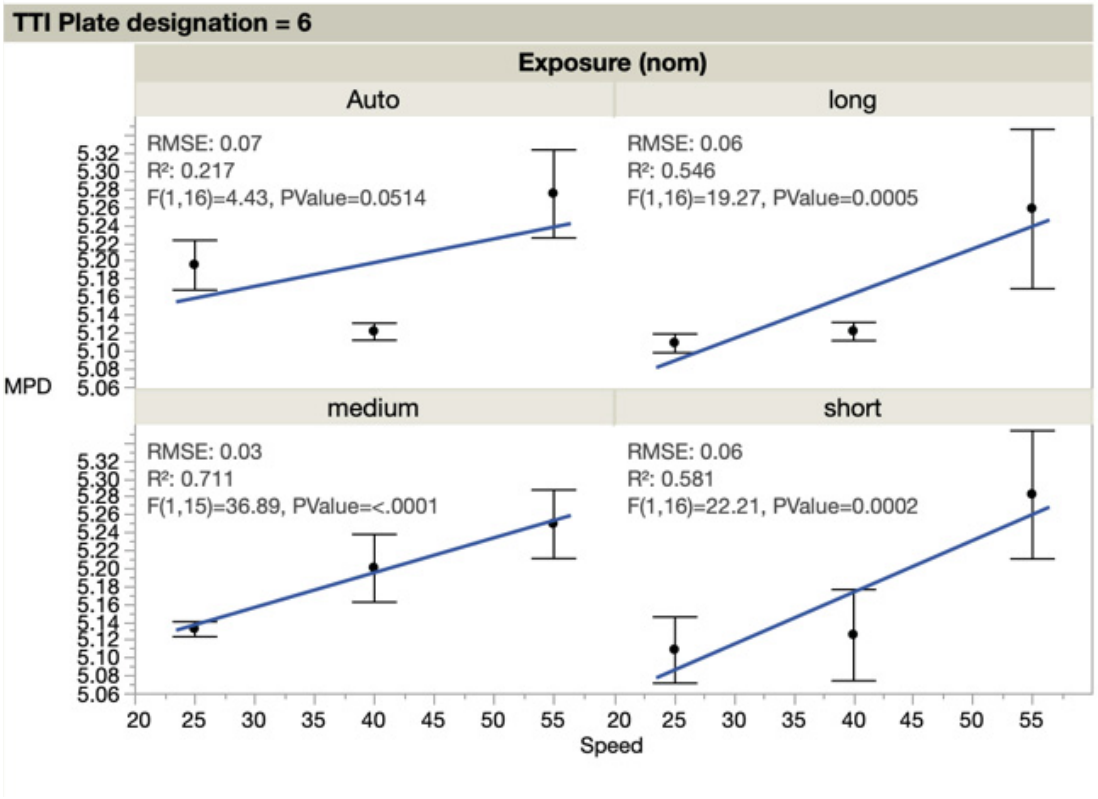
TTI Plate designation = 6
Exposure (nom)
Auto
long
medium
short
RMSE: 0.07
R²: 0.217
F(1,16)=4.43, PValue=0.0514
RMSE: 0.06
R²: 0.546
F(1,16)=19.27, PValue=0.0005
RMSE: 0.03
R²: 0.711
F(1,15)=36.89, PValue=<.0001
RMSE: 0.06
R²: 0.581
F(1,16)=22.21, PValue=0.0002
MPD
Speed

Appendix R Chapter 4 ANOVA Effects and Paired t-tests

- ✓ Response: MPD
- ✓ Model Effects: Speed, Exposure, Speed * Exposure
- ✓ Filtering: None

ANOVA

	P-Value		
	Dev_1	**LL_L**	**LL_T**
Plate 1	<.0001*	<.0001*	<.0001*
Plate 3	<.0001*	<.0001*	<.0001*
DEV_4	<.0001*	0.0009*	<.0001*
Plate 5	<.0001*	0.7961	<.0001*
Plate 6	0.0402*	0.0030*	<.0001*

Effects Test

		P-Value		
		Dev_1	**LL_L**	**LL_T**
Plate 1	**Exposure**	<.0001*	<.0001*	0.8558
	Speed	<.0001*	<.0001*	<.0001*
	Speed * Exposure	<.0001*	<.0001*	0.368
Plate 3	**Exposure**	<.0001*	<.0001*	0.5401
	Speed	<.0001*	0.2004	<.0001*
	Speed * Exposure	0.0007*	<.0001*	0.0110*
DEV_4	**Exposure**	<.0001*	0.2527	0.4795
	Speed	<.0001*	<.0001*	<.0001*
	Speed * Exposure	0.1292	0.194	0.0013*
Plate 5	**Exposure**	0.0001*	0.3163	0.5831
	Speed	<.0001*	0.2952	0.0002*
	Speed * Exposure	0.0003*	0.9917	<.0001*
Plate 6	**Exposure**	0.0076*	0.0708	<.0001*
	Speed	0.503	0.0099*	0.0671
	Speed * Exposure	0.2348	0.0299*	0.0025*

- ✓ Response: MPD
- ✓ Model Effects: Speed, Exposure, Speed * Exposure
- ✓ Filtering: ASTM 1845 Butterworth Filtering

ANOVA

	P-Value		
	Dev_1	**LL_L**	**LL_T**
Plate 1	<.0001*	<.0001*	<.0001*
Plate 3	<.0001*	<.0001*	<.0001*
DEV_4	<.0001*	<.0001*	<.0001*
Plate 5	<.0001*	<.0001*	<.0001*
Plate 6	<.0001*	<.0001*	<.0001*

Effects Test

		P-Value		
		Dev_1	**LL_L**	**LL_T**
Plate 1	**Exposure**	<.0001*	<.0001*	0.2805
	Speed	<.0001*	<.0001*	<.0001*
	Speed * Exposure	<.0001*	<.0001*	0.2627
Plate 3	**Exposure**	<.0001*	<.0001*	0.4458
	Speed	0.1199	<.0001*	<.0001*
	Speed * Exposure	<.0001*	<.0001*	0.0036*
DEV_4	**Exposure**	<.0001*	0.2209	0.5147
	Speed	0.3551	0.0049*	<.0001*
	Speed * Exposure	0.0155*	0.0164*	0.0011*
Plate 5	**Exposure**	0.4216	0.2687	0.8399
	Speed	0.524	0.3132	<.0001*
	Speed * Exposure	0.0195*	0.9943	<.0001*
Plate 6	**Exposure**	0.0503	0.0674	<.0001*
	Speed	0.0934	0.0104*	0.0819
	Speed * Exposure	0.2259	0.0222*	0.0028*

Paired t-tests P-values (LAPS and vendor) – unfiltered

		25 mph			40 mph			55 mph		
	Exposure	Dev_1	LL_L	LL_T	Dev_1	LL_L	LL_T	Dev_1	LL_L	LL_T
Plate 1	Auto	-	0.0019*	0.0003*	-	0.0005*	0.0021*	-	0.0008*	0.051
	Short	<.0001*	0.0166*	0.132	<.0001*	0.0010*	0.110	<.0001*	0.0009*	0.103
	Medium	<.0001*	0.0015*	0.612	<.0001*	0.0001*	0.404	<.0001*	<.0001*	0.253
	Long	<.0001*	<.0001*	0.168	<.0001*	<.0001*	0.0005*	<.0001*	<.0001*	0.0092*
Plate 3	Auto	-	0.198	0.237	-	0.333	0.0017*	-	0.101	0.0052*
	Short	0.659	0.900	0.0310*	0.369	0.290	0.111	0.078	0.435	0.792
	Medium	0.206	0.876	0.557	0.546	0.910	0.0229*	0.0451*	0.062	0.0261*
	Long	0.0024*	0.232	0.058	0.0011*	0.416	0.0027*	0.0004*	0.0010*	0.230
DEV_4	Auto	-	0.529	0.603	-	0.0362*	0.607	-	0.994	0.331
	Short	0.102	0.622	0.500	0.920	0.419	0.224	0.0043*	0.924	0.386
	Medium	0.243	0.671	0.239	0.0341*	0.172	0.387	0.0018*	0.184	0.647
	Long	0.0052*	0.274	0.065	0.0024*	0.143	0.0322*	0.0017*	0.0252*	0.0146*

Observations

- ✓ Plate 1 (2.5mm saw tooth pattern) was difficult to reproduce for the SSL and the LLL
  - LLT measured well (P-values > 5%) for all speeds at short/medium exposure settings
    - Any latency in LLL may result in some profile averaging with transverse grooves. Peaks may be better preserved when laser remains perpendicular
    - LLT should reproduce accurate profiles of even low longitudinal groove and tine marks
    - LLL was closest to reference at shortest exposure & slowest speed
- ✓ For Plate 3, LLL measured accurately for all speeds & exposures except longest exposure time/highest speed
  - LLT had difficulty reproducing the reference measurements accurately at speeds >25 mph for all but shortest exposure
  - SSL was able to accurately reproduce the plate at all speeds using the short and medium exposure settings

- ✓ Both LL accurately reproduced the reference measurements of the DEV_4 plate (deep grooves) at all speeds and exposure settings
  - The SSL had difficulty reproducing the shape at long exposure settings, made worse by increasing speed. The reference measurement was not reproduced satisfactorily at 55 mph for any exposure setting of the SSL
    - This is likely due to the sharp drop-off of the deep groove walls paired with laser dispersal at the corners
    - LLs faired better as dispersed light could be offset by surrounding points of the laser line

Appendix S Chapter 6 Equivalent Circle Distribution of HVS

The following is an analysis in which the fraction of the traffic load that was applied at the transverse positions was used as the independent variable instead of the total load, however, this analysis method produced no significant improvement to the overall model and is therefore excluded from this study to reduce complexity.

This analysis sought to determine the percent distribution of the cumulative ESALs at each of the CT meter measurement locations such that the effect of traffic load on macrotexture is independent of the wander, in that is accounted for in the magnitude of the cumulative load. To simplify the determination of the distribution of the load, the dual wheel configuration is simplified to an equivalent circle by equation where the radius of the contact area a, is defined by the below equation.

Equation 1 – Radius of contact area for equivalent circle

$$a = \sqrt{\frac{0.8521P_d}{q\pi} + \frac{S_d}{\pi}\left(\frac{p_d}{0.5227q}\right)^{\frac{1}{2}}}$$

(Huang 2004b)
Where: a = theoretical radius of equivalent circle
P_d = load on one tire (lb) = increased over time
S_d = center to center space between tires (in) = 13.78 inches (constant for experiment)
q = tire contact pressure (psi) = 110 psi (constant for experiment)

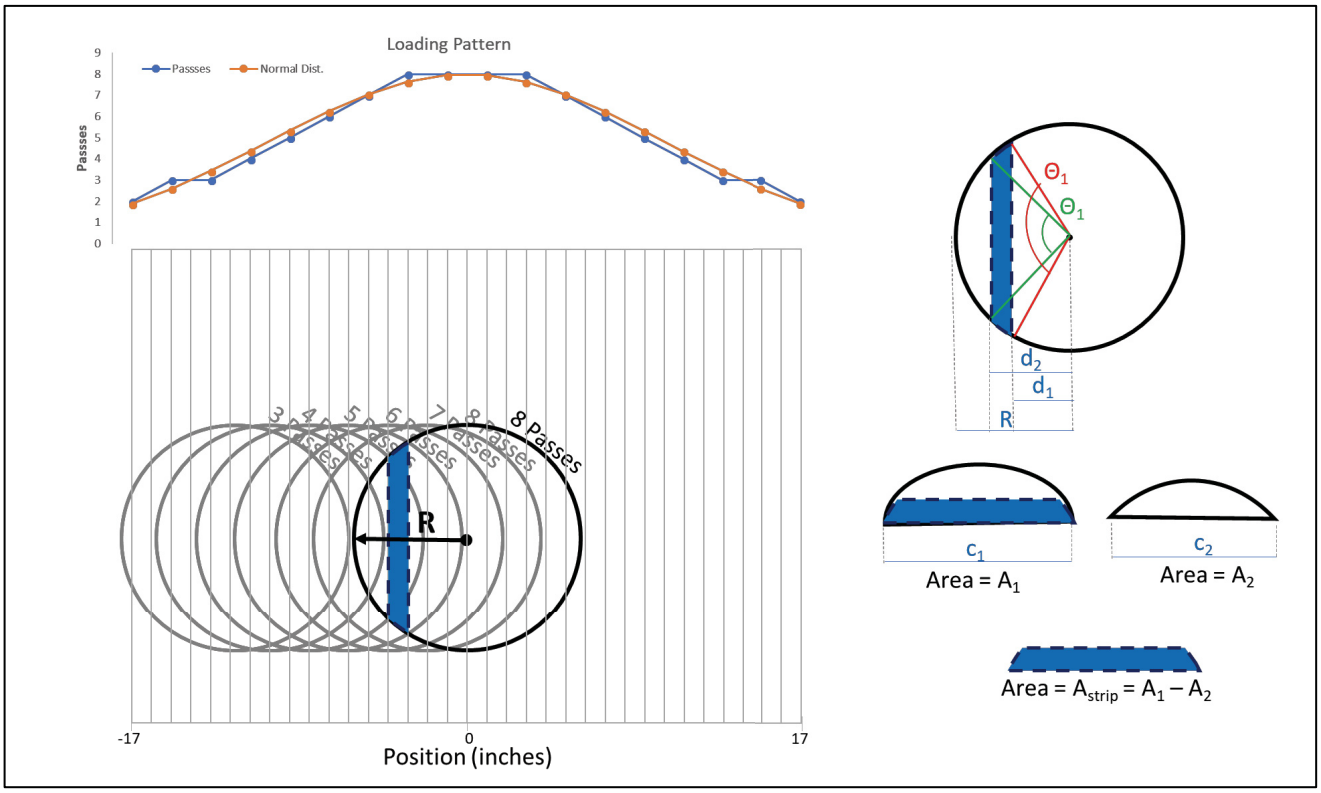

Figure 1 - Equivalent Circle inputs

Using geometric properties of a circle among variables R, θ, d, and C as indicated in Figure 1, the percent of the theoretical circle that passes over 1-inch wide sections of the pavement for each loading position can be calculated.
The relevant equations derived from Figure 1 are:

Equations 6 & 7 – Height of triangular portion of circle segment

$$d_1 = LP - x - 1$$
$$d_2 = LP - x$$

Where; LP = Load position and x = position of 1-inch lane, based on distance from a common reference point

Equations 8 & 9 – Cord length

$$C_1 = 2R \cdot \sqrt{1 - \left(\frac{d_1}{R}\right)^2}$$
$$C_2 = 2R \cdot \sqrt{1 - \left(\frac{d_2}{R}\right)^2}$$

Equations 10 & 11 – Central Angle in radians

$$\theta_1 = 2 \arcsin\left(\frac{c_1}{2R}\right)$$
$$\theta_2 = 2 \arcsin\left(\frac{c_2}{2R}\right)$$

Equations 12 & 13 – Circular segment areas

$$A_1 = \frac{R^2}{2}(\theta_1 - \sin\theta_1)$$
$$A_2 = \frac{R^2}{2}(\theta_2 - \sin\theta_2)$$

These equations were combined to determine the percent of the circular area distributed to each 1-inch lane:

Equation 14 – Area of circle covering 1-inch strip

$$A_s = \frac{R^2}{2}\left[2 \arcsin\sqrt{1 - \left(\frac{LP - x - 1}{R}\right)^2} - \sin\left(2 \arcsin\sqrt{1 - \left(\frac{LP - x - 1}{R}\right)^2}\right]\right.$$
$$\left. - \frac{R^2}{2}\left[2 \arcsin\sqrt{1 - \left(\frac{LP - x}{R}\right)^2} - \sin\left(2 \arcsin\sqrt{1 - \left(\frac{LP - x}{R}\right)^2}\right]\right.$$

An excel algorithm was developed in which the variables d_1 and d_2 were defined based on the location of the center of the theoretical circle and the 1-inch lane for which the percent area was being determined from a common reference point. This was repeated for each load position and each 1-inch lane effected by the load. These percent areas were then multiplied based on the number of passes that occur for each loading position. Finally, the percent of

overall load applied from each full cycle of the normal distribution of load positions was calculated for each 1-inch strip.

Figure 2 below shows the traffic distribution of the equivalent circles for a radius of 5.74 in and 8.78 in which correspond to HVS loads of 4500 lb and 18000 lb respectively (the range used in this experiment). Table 1 summarizes the percent of the load distribution that passes over the footprint of the CT Meter at each of the measurement positions. The distribution is not symmetrical to the measurement locations because the measurement locations are aligned along the right edge of the trafficked surface.

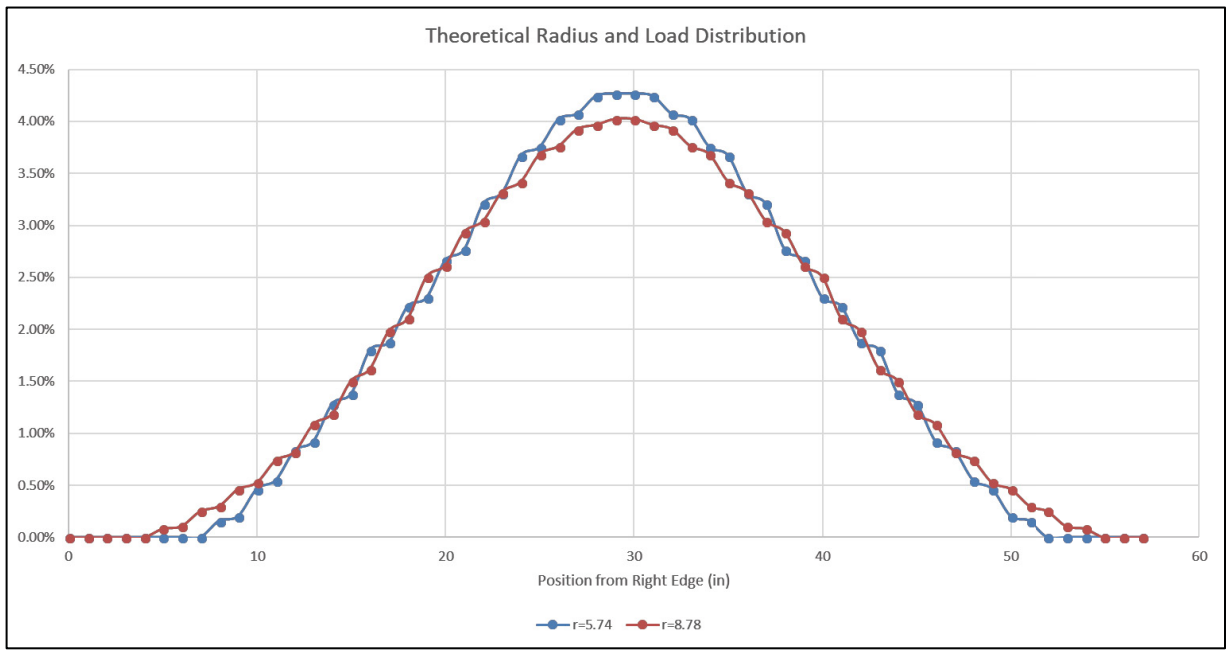

Figure 2 - Traffic Distribution

Table 1 - Percent of passes per position

	Radius	**5.75"**	**6.25"**	**6.68"**	**7.06"**	**7.41"**	**7.72"**	**8.01"**	**8.28"**	**8.54"**	**8.78"**
	HVS Load	**4500 lb**	**6000 lb**	**7500 lb**	**9000 lb**	**10500 lb**	**12000 lb**	**13500 lb**	**15000 lb**	**16500 lb**	**18000 lb**
CT Meter Position	**R**	3.13%	3.48%	3.55%	3.79%	3.86%	3.90%	4.21%	4.30%	4.36%	4.40%
	RC	18.61%	18.80%	18.83%	18.86%	18.87%	18.88%	19.04%	19.08%	19.10%	19.12%
	C	41.85%	41.45%	41.36%	40.91%	40.78%	40.71%	40.31%	40.20%	40.12%	40.06%
	LC	38.31%	38.10%	38.05%	37.73%	37.64%	37.59%	37.35%	37.28%	37.23%	37.19%
	L	16.30%	16.33%	16.34%	16.53%	16.57%	16.60%	16.66%	16.68%	16.70%	16.71%

Figure 3 below shows the difference between the total ESALS and distributed ESALs when plotted against the MPD and RMS for the entire data set.

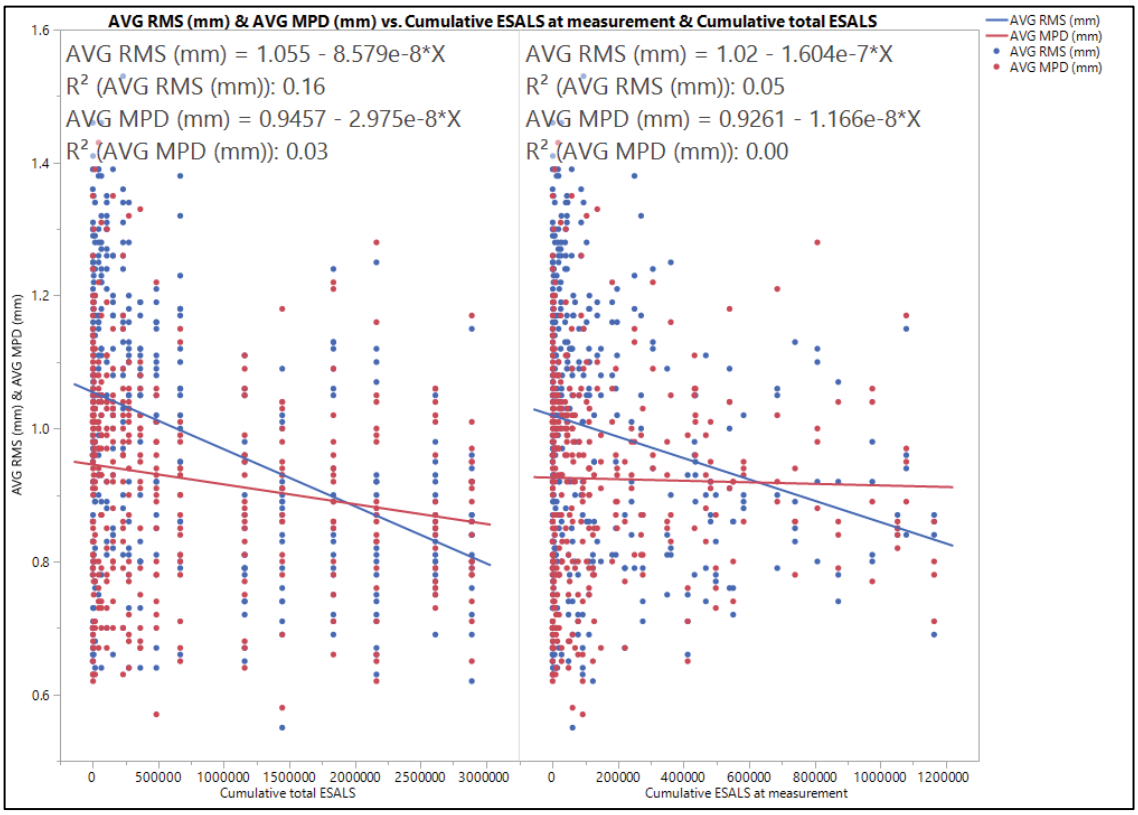

Figure 3 - Effect of distriuting EASALs

Overall with ESALs at measurement 2nd degree factorial ANOVA

Analysis of Variance

Source	DF	Sum of Squares	Mean Square	F Ratio
Model	27	11.174804	0.413882	30.7478
Error	371	4.993856	0.013461	**Prob > F**
C. Total	398	16.168659		<.0001*

Effect Tests

Source	Nparm	DF	Sum of Squares	F Ratio	Prob > F
Cumulative ESALS at measurement	1	1	0.4971077	36.9308	<.0001*
Station	3	3	0.0127627	0.3161	0.8138
Reading	4	4	2.9789378	55.3273	<.0001*
Cumulative ESALS at measurement*Station	3	3	0.0301066	0.7456	0.5255
Cumulative ESALS at measurement*Reading	4	4	0.1556076	2.8901	0.0223*
Station*Reading	12	12	2.1069817	13.0442	<.0001*

In a comparison to determine effect of equivalent circle distribution analysis, ESALS-reading interaction was reduced in significance from <.001 p-value to 0.0223, however not enough to call it effective, furthermore the reading blocking factor effect on RMS remained significant with a p-value of less than .0001. Based on these results, distributing the normal load across the pavement to determine the ESALs applied at specific positions transversely due to wander is not an effective technique for analysis.

The interactions between the initial conditions of differing macrotextures across the width of the lane, and the overlapping effects of the bleeding distresses made this analysis ineffective. Therefore, the overall cumulative total ESALs is the preferred model input over the ESALs applied at the measurement locations.

Appendix T Chapter 6 Binder Content of surface mix in HVS

VIRGINIA DEPARTMENT OF TRANSPORTATION
MATERIALS DIVISION
STATEMENT OF ASPHALT CONCRETE JOB-MIX FORMULA

Submit to the District Administrator, Virginia Department of Transportation. Approval must be received by the contractor from the Materials Division before work is begun. The job-mix design is approved for all projects of the Department for the type of mix and the calendar year shown below.

Contractor:	Adams Construction Company, Inc.	Design Mix No.:	SMA 12.5	Design Lab:	Roanoke
Job Mix ID:	**2024-2017-113**	Production Year:	**2017**	TSR Test No.:	
Design Type:	Stone Matrix Asphalt	Type Mix / Size Aggregate:	**SMA-12.5 (64E-22)**		
Plant Location:	**Roanoke**	Plant Phone:	540-362-0915		

Materials			Kind		Source
Approval Phase	A	B*	Type	Size	
Aggregate	12 %		Limestone	Filler	Boxley Materials Company - Blue Ridge Stone Corp.
Aggregate	63 %		Quartzite	#7	Salem Stone Corp. - Sylvatus
Aggregate	10 %		Quartzite	#8	Salem Stone Corp. - Sylvatus
RAP	15 %		Recycled Asphalt Pavement	Recycled-1/2 inch	Adams Construction Company, Inc. - Roanoke
Asphalt Cement			PG 64E-22		
Additives	0.30 %		Cellulose Fiber		
Additives	0.50 %		Ad-here HP Plus		

SIEVE		Total % Passing		TOLERANCE	Acceptance Range Average of 8 Test(s)				Design / Spec. Range	
Approval Phase		A	B		A		B			
ENGLISH	METRIC	Lab JMF	Production JMF	% + or -	Min	Max	Min	Max	Min	Max
3/4in	19mm	100 %		0 %	100 %	100 %			100 %	
1/2in	12.5mm	92 %		2.8 %	89.2 %	94.8 %			83 %	93 %
3/8in	9.5mm	69 %		2.8 %	66.2 %	71.8 %				80 %
#4	4.75mm	28 %		2.1 %	25.9 %	30.1 %			22 %	28 %
#8	2.36mm	22 %		2.1 %	19.9 %	24.1 %			16.0 %	24.0 %
#30	0.6mm	18 %		2.1 %	15.9 %	20.1 %			15 %	20 %
#200	0.075mm	10.0 %		1.4 %	8.6 %	11.4 %			9.0 %	11.0 %
Asphalt	A.C.	6.80 %		0.21 %	6.59 %	7.01 %				

Lay Down Temperatures	Min: 290	Max: 350	°F	Muffle Furnace Correction Factor:	**1.13**
Lab Compaction Temperatures	Min: 320	Max: 330	°F	Field Correction Factor (G_{se}-G_{sb}):	0.005
				Pill Weight:	**4650**

Submission:	Type: Part A	Submitter: Marty Wallace	Date: 5/22/2017 12:11:11 PM	SMA Mixes	VCA_{DRC}: 42.0 %
					G_{CA}: 2.667

Producer Remarks: VCAmix: 40.71 , Draindown: 0.0%

MATERIALS DIVISION ONLY

VDOT Remarks: Gse = 2.696; Pba = 6.73; VCAmix = 40.83

Nominal Max. Size Aggregate:		Application Rates:		Min:		Max:		lb/yd²
Mix Properties at the Job-Mix Asphalt Content:	Compacted Unit Weight	JMF A: 147.1	lb/ft³	VTM:	JMF A: 2.9 %	G_{mm}:	JMF A:	**2.429**
		JMF B:	lb/ft³		JMF B:		JMF B:	

Approved tentatively subject to the production of material meeting all other applicable requirements of the specification.

* Note: Part B 'Production JMF' and corresponding Material percentages will be filled out by the DME upon receipt of the additional requirements of the HMA producer within the first three lots under Section 502.01(b).

Copies:	State Materials Engineer District Materials Engineer Project Inspector Sub-Contractor and/or Producer	Approval:	Type: Part A	Status: Approved	Approver: Clyde Landreth on behalf of David T. Lee, P.E.	Date: 5/23/2017

Appendix U Chapter 7 LASSO, SLR and MLR

SCRIM_Random_Lasso

Generalized Regression for SCRIM Tex Direction=Random, Train / Validate=Train

Adaptive Lasso with BIC Validation

Model Summary

Response	SCRIM
Distribution	Normal
Estimation Method	Adaptive Lasso
Validation Method	BIC
Mean Model Link	Identity
Scale Model Link	Identity

Measure	
Number of rows	825
Sum of Frequencies	825
-LogLikelihood	2240.0884
Number of Parameters	26
BIC	4654.7768
AICc	4533.9362
ERIC	4593.5711
RSquare	0.7080602
RMSE	3.6558189
Lambda Penalty	97.83291

Estimation Details

Number of Grid Points	150
Minimum Penalty Fraction	0
Grid Scale	Square Root

Solution Path

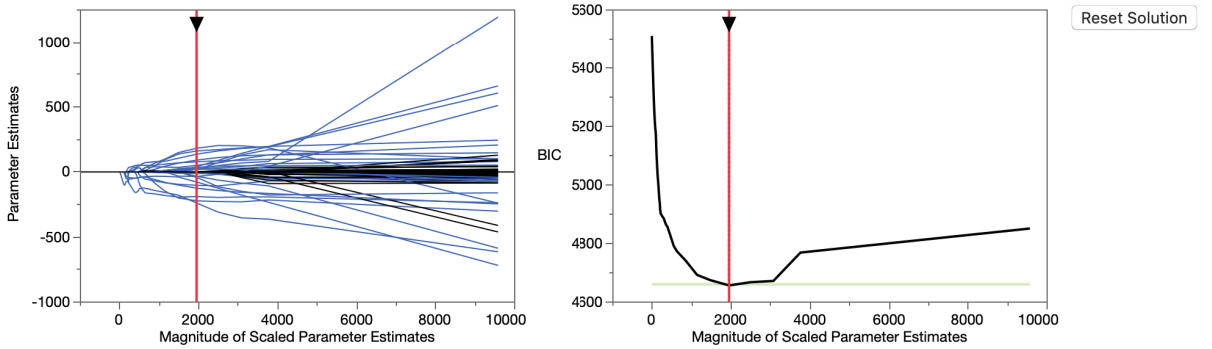

Effect Tests

Source	Nparm	DF	Wald ChiSquare	Prob > ChiSquare	
Gradient	1	1	59.2691	<.0001*	
contact_nfilt_0_1tol_d0_001	1	1	43.935246	<.0001*	
EAWE_d1eneg4	1	1	24.342162	<.0001*	
MDE	1	1	23.689836	<.0001*	
EAWE_butfilt_d1eneg5	1	1	17.858763	<.0001*	
Curvature	1	1	15.162869	<.0001*	
contact_yfilt_0_1tol_d0_00001	1	1	13.942432	0.0002*	
MPWR_filty_p0_1	1	1	12.859463	0.0003*	
MWMSR_filty_p0_1	1	1	11.361257	0.0007*	
MWMSR_filty_p0_25	1	1	5.8318322	0.0157*	
MWIDTHSGZ_filty_p0_25	1	1	5.2382558	0.0221*	
Kurtosis	1	1	4.0516187	0.0441*	
wd_filt_n_RMS_Level_5	1	1	2.3281737	0.1271	
wd_filt_n_RMS_Level_2	1	1	1.0305578	0.3100	
env_dneg0_02_MPD	1	1	0.6652181	0.4147	
wd_filt_n_KURT_Level_3	1	1	0.4738831	0.4912	
MPD_97	1	1	0.4564782	0.4993	
MPROMGZ_filty_p0_25	1	1	0.4554317	0.4998	
MPROMGZ_filty_p0_1	1	1	0.423184	0.5154	
MPMSR_T_filty_p0_25	1	1	0.196842	0.6573	
Max_Height	1	1	0.1866617	0.6657	
MPMSR_filty_p0_1	1	1	0.0595371	0.8072	
wd_filt_n_RMS_Level_4	1	1	0.0054639	0.9411	
N_Peaks_gz_filty_p0_25	1	1	0.004995	0.9437	
MPD	1	0	0	1.0000	Removed

SCRIM_Random_SLR_VIF<10

Response SCRIM Tex Direction=Random, Train / Validate=Train

Effect Summary

Source	LogWorth	PValue
MPMSR_filty_p0_1	45.107	0.00000
Gradient	19.999	0.00000
MWMSR_filty_p0_1	14.163	0.00000
wd_filt_n_KURT_Level_3	6.417	0.00000
N_Peaks_gz_filty_p0_25	5.550	0.00000
Curvature	4.529	0.00003
Kurtosis	0.669	0.21409
MWIDTHSGZ_filty_p0_25	0.471	0.33790
contact_yfilt_0_1tol_d0_00001	0.328	0.46975
contact_nfilt_0_1tol_d0_001	0.065	0.86181

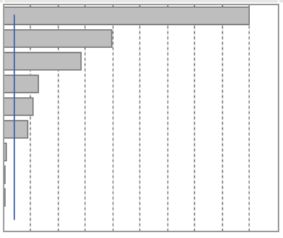

Remove Add Edit FDR

Summary of Fit

RSquare	0.567899
RSquare Adj	0.56259
Root Mean Square Error	4.477603
Mean of Response	79.09639
Observations (or Sum Wgts)	825

Analysis of Variance

Source	DF	Sum of Squares	Mean Square	F Ratio
Model	10	21448.691	2144.87	106.9817
Error	814	16319.826	20.05	Prob > F
C. Total	824	37768.517		<.0001*

Parameter Estimates

Term	Estimate	Std Error	t Ratio	Prob>|t|
Intercept	144.82169	5.497593	26.34	<.0001*
Kurtosis	-0.755219	0.607394	-1.24	0.2141
contact_nfilt_0_1tol_d0_001	-1.396471	8.020013	-0.17	0.8618
contact_yfilt_0_1tol_d0_00001	6.7126715	9.28167	0.72	0.4698
wd_filt_n_KURT_Level_3	-1.785015	0.348673	-5.12	<.0001*
MWIDTHSGZ_filty_p0_25	-0.387076	0.403671	-0.96	0.3379
N_Peaks_gz_filty_p0_25	-2.039548	0.432381	-4.72	<.0001*
MPMSR_filty_p0_1	-184.0491	12.15245	-15.15	<.0001*
MWMSR_filty_p0_1	-54.61208	6.881114	-7.94	<.0001*
Gradient	3.4392213	0.358462	9.59	<.0001*
Curvature	1773.5163	422.2027	4.20	<.0001*

SCRIM_Random_MLR_1-20m_VIF<4

Response SCRIM aggregation=1m, Tex Direction=Random

Whole Model

Actual by Predicted Plot

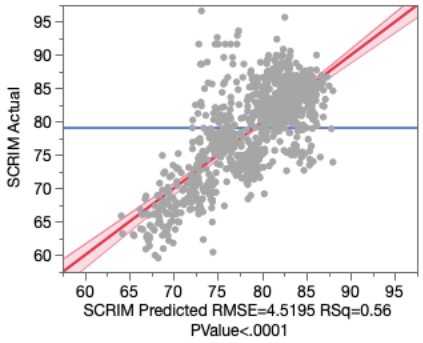

Effect Summary

Source	LogWorth	PValue
MPMSR_filty_p0_1	102.401	0.00000
Gradient	31.766	0.00000
MWMSR_filty_p0_1	27.726	0.00000
wd_filt_n_KURT_Level_3	13.033	0.00000
N_Peaks_gz_filty_p0_25	9.415	0.00000

Remove Add Edit FDR

Residual by Predicted Plot

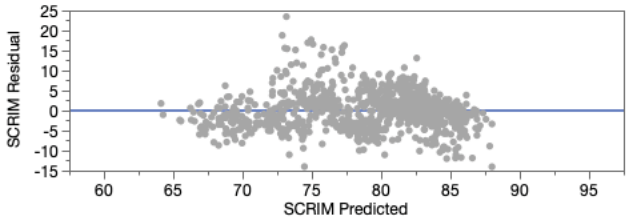

Summary of Fit

RSquare	0.555446
RSquare Adj	0.553267
Root Mean Square Error	4.519506
Mean of Response	79.09061
Observations (or Sum Wgts)	1026

Analysis of Variance

Source	DF	Sum of Squares	Mean Square	F Ratio
Model	5	26031.490	5206.30	254.8866
Error	1020	20834.457	20.43	Prob > F
C. Total	1025	46865.947		<.0001*

Parameter Estimates

Term	Estimate	Std Error	t Ratio	Prob>|t|
Intercept	147.28108	3.166266	46.52	<.0001*
wd_filt_n_KURT_Level_3	-1.960417	0.259478	-7.56	<.0001*
N_Peaks_gz_filty_p0_25	-1.61442	0.255353	-6.32	<.0001*
MPMSR_filty_p0_1	-178.2887	7.343628	-24.28	<.0001*
MWMSR_filty_p0_1	-63.17103	5.537835	-11.41	<.0001*
Gradient	2.1350261	0.173662	12.29	<.0001*

Response SCRIM aggregation=3m, Tex Direction=Random

Whole Model

Actual by Predicted Plot

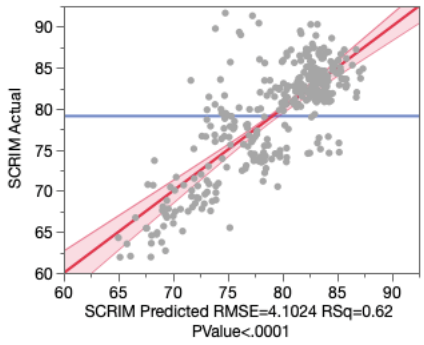

Effect Summary

Source	LogWorth	PValue
MPMSR_filty_p0_1	35.502	0.00000
Gradient	14.738	0.00000
wd_filt_n_KURT_Level_3	9.364	0.00000
MWMSR_filty_p0_1	6.355	0.00000
N_Peaks_gz_filty_p0_25	5.760	0.00000

Remove Add Edit FDR

Residual by Predicted Plot

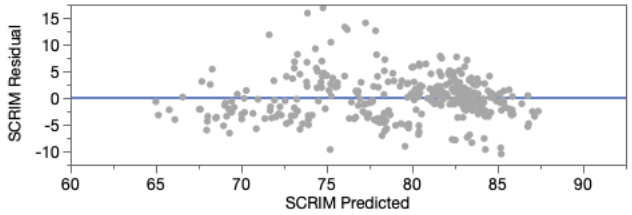

Summary of Fit

RSquare	0.616514
RSquare Adj	0.610773
Root Mean Square Error	4.102386
Mean of Response	79.10649
Observations (or Sum Wgts)	340

Analysis of Variance

Source	DF	Sum of Squares	Mean Square	F Ratio
Model	5	9036.761	1807.35	107.3915
Error	334	5621.077	16.83	Prob > F
C. Total	339	14657.837		<.0001*

Parameter Estimates

Term	Estimate	Std Error	t Ratio	Prob>|t|
Intercept	150.31105	5.174216	29.05	<.0001*
wd_filt_n_KURT_Level_3	-3.465191	0.538623	-6.43	<.0001*
N_Peaks_gz_filty_p0_25	-2.342375	0.481145	-4.87	<.0001*
MPMSR_filty_p0_1	-170.2629	11.96946	-14.22	<.0001*
MWMSR_filty_p0_1	-48.66091	9.444619	-5.15	<.0001*
Gradient	2.3144611	0.277146	8.35	<.0001*

Response SCRIM aggregation=10m, Tex Direction=Random

Whole Model

Actual by Predicted Plot

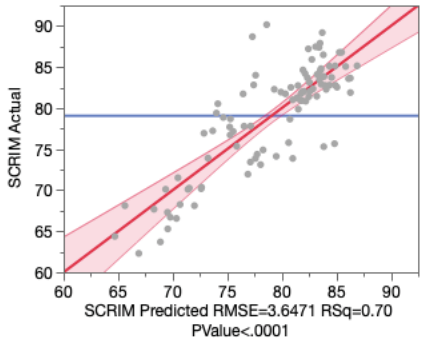

Effect Summary

Source	LogWorth	PValue
MPMSR_filty_p0_1	9.381	0.00000
Gradient	7.005	0.00000
wd_filt_n_KURT_Level_3	6.251	0.00000
N_Peaks_gz_filty_p0_25	2.619	0.00240
MWMSR_filty_p0_1	0.765	0.17186

Remove Add Edit FDR

Residual by Predicted Plot

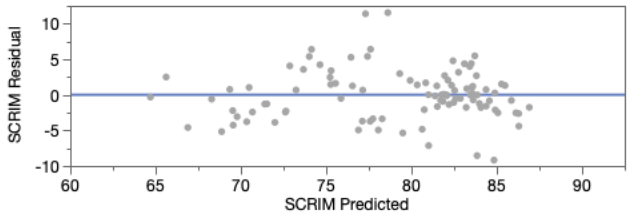

Summary of Fit

RSquare	0.704919
RSquare Adj	0.689054
Root Mean Square Error	3.647077
Mean of Response	79.0591
Observations (or Sum Wgts)	99

Analysis of Variance

Source	DF	Sum of Squares	Mean Square	F Ratio
Model	5	2955.0900	591.018	44.4335
Error	93	1237.0088	13.301	Prob > F
C. Total	98	4192.0988		<.0001*

Parameter Estimates

Term	Estimate	Std Error	t Ratio	Prob>|t|
Intercept	153.15454	8.957006	17.10	<.0001*
wd_filt_n_KURT_Level_3	-6.817602	1.267921	-5.38	<.0001*
N_Peaks_gz_filty_p0_25	-2.985937	0.956806	-3.12	0.0024*
MPMSR_filty_p0_1	-149.1937	21.35289	-6.99	<.0001*
MWMSR_filty_p0_1	-24.30873	17.65495	-1.38	0.1719
Gradient	2.7095646	0.468767	5.78	<.0001*

Response SCRIM aggregation=20m, Tex Direction=Random

Whole Model

Actual by Predicted Plot

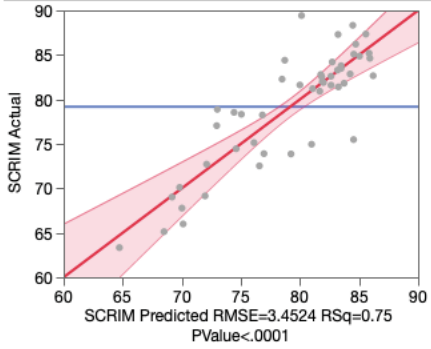

Effect Summary

Source	LogWorth	PValue
Gradient	4.818	0.00002
wd_filt_n_KURT_Level_3	4.641	0.00002
MPMSR_filty_p0_1	3.912	0.00012
N_Peaks_gz_filty_p0_25	2.033	0.00926
MWMSR_filty_p0_1	0.124	0.75199

Remove Add Edit FDR

Residual by Predicted Plot

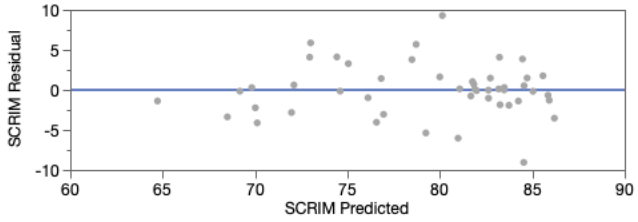

Summary of Fit

RSquare	0.748132
RSquare Adj	0.718148
Root Mean Square Error	3.452442
Mean of Response	79.16973
Observations (or Sum Wgts)	48

Analysis of Variance

Source	DF	Sum of Squares	Mean Square	F Ratio
Model	5	1486.9859	297.397	24.9508
Error	42	500.6128	11.919	Prob > F
C. Total	47	1987.5987		<.0001*

Parameter Estimates

Term	Estimate	Std Error	t Ratio	Prob>|t|
Intercept	152.92462	12.37896	12.35	<.0001*
wd_filt_n_KURT_Level_3	-10.46007	2.195917	-4.76	<.0001*
N_Peaks_gz_filty_p0_25	-3.786734	1.388141	-2.73	0.0093*
MPMSR_filty_p0_1	-129.3511	30.55299	-4.23	0.0001*
MWMSR_filty_p0_1	8.663641	27.23601	0.32	0.7520
Gradient	3.2980814	0.674501	4.89	<.0001*

Generalized Regression for SCRIM Tex Direction=Transverse

Model Launch

Standard Least Squares

Model Summary

Response	SCRIM
Distribution	Normal
Estimation Method	Standard Least Squares
Validation Method	None
Mean Model Link	Identity
Scale Model Link	Identity

Measure	
Number of rows	1318
Sum of Frequencies	1298
-LogLikelihood	2993.8031
Number of Parameters	83
BIC	6582.5984
AICc	6165.0922
RSquare	0.2276218
RSquare Adj	0.1761723
RMSE	2.4291353

Parameter Estimates for Original Predictors

Effect Tests

Adaptive Lasso with BIC Validation

Model Summary

Response	SCRIM
Distribution	Normal
Estimation Method	Adaptive Lasso
Validation Method	BIC
Mean Model Link	Identity
Scale Model Link	Identity

Measure	
Number of rows	1318
Sum of Frequencies	1298
-LogLikelihood	3050.4321
Number of Parameters	20
BIC	6244.2357
AICc	6141.5219
ERIC	6200.2657
RSquare	0.1571997
RMSE	2.5374591
Lambda Penalty	29.55166

Estimation Details

Number of Grid Points	150
Minimum Penalty Fraction	0
Grid Scale	Square Root

Solution Path

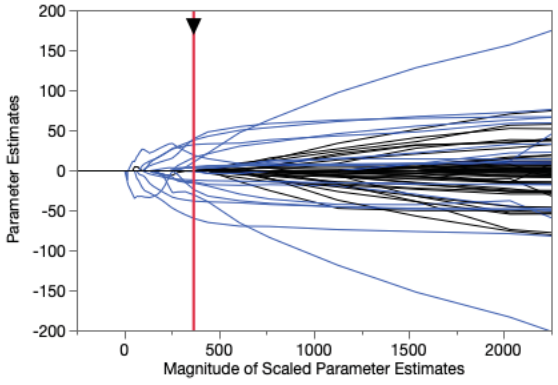

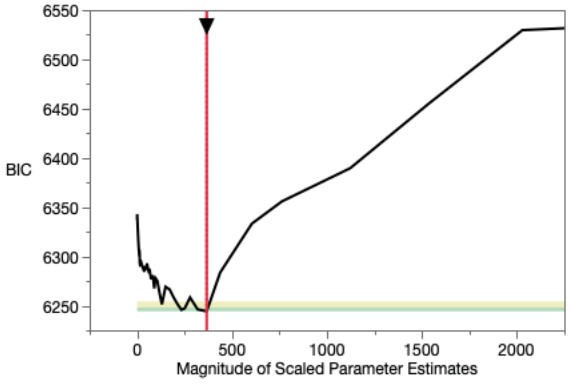

Response SCRIM Tex Direction=Transverse, Train / Validate=Train

Effect Summary

Source	LogWorth	PValue
wd_filt_n_SKEW_Level_1	10.282	0.00000
wd_filt_n_SKEW_Level_3	7.538	0.00000
MWIDTHSGZ_filty_p0_1	5.362	0.00000
Gradient	4.315	0.00005
wd_filt_n_KURT_Level_10	2.774	0.00168
Curvature	1.652	0.02228
wd_filt_n_KURT_Level_4	1.376	0.04208

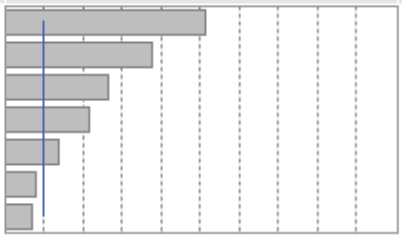

Remove Add Edit ☐ FDR

Summary of Fit

RSquare	0.121888
RSquare Adj	0.116045
Root Mean Square Error	2.60311
Mean of Response	80.97499
Observations (or Sum Wgts)	1060

Analysis of Variance

Source	DF	Sum of Squares	Mean Square	F Ratio
Model	7	989.4890	141.356	20.8607
Error	1052	7128.5418	6.776	Prob > F
C. Total	1059	8118.0308		<.0001*

Parameter Estimates

Term	Estimate	Std Error	t Ratio	Prob>|t|
Intercept	72.63886	1.261678	57.57	<.0001*
wd_filt_n_KURT_Level_4	0.4342953	0.213392	2.04	0.0421*
wd_filt_n_KURT_Level_10	1.5990919	0.507713	3.15	0.0017*
wd_filt_n_SKEW_Level_1	-6.157551	0.928187	-6.63	<.0001*
wd_filt_n_SKEW_Level_3	7.7489477	1.386286	5.59	<.0001*
MWIDTHSGZ_filty_p0_1	0.4384375	0.094932	4.62	<.0001*
Gradient	-0.293309	0.071889	-4.08	<.0001*
Curvature	543.09602	237.274	2.29	0.0223*

Response SCRIM aggregation=1m, Tex Direction=Transverse

Whole Model

Actual by Predicted Plot

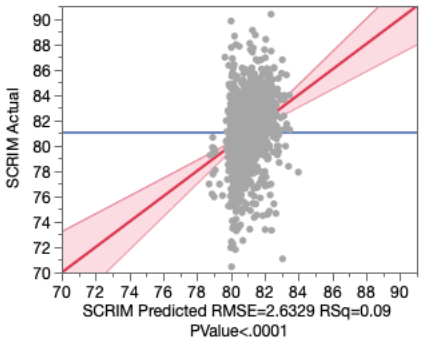

Effect Summary

Source	LogWorth	PValue
Gradient	8.912	0.00000
MWMSR_filty_p0_1	6.228	0.00000
wd_filt_n_KURT_Level_3	5.507	0.00000
MPMSR_filty_p0_1	0.452	0.35303
N_Peaks_gz_filty_p0_25	0.142	0.72055

Remove Add Edit FDR

Residual by Predicted Plot

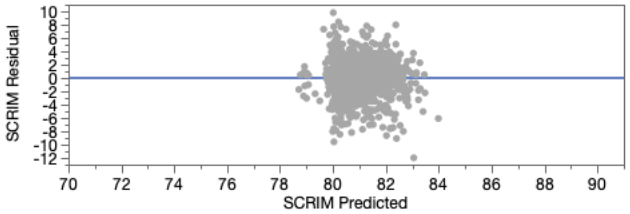

Summary of Fit

RSquare	0.086539
RSquare Adj	0.083058
Root Mean Square Error	2.632892
Mean of Response	81.01855
Observations (or Sum Wgts)	1318

Analysis of Variance

Source	DF	Sum of Squares	Mean Square	F Ratio
Model	5	861.6296	172.326	24.8591
Error	1312	9094.9385	6.932	Prob > F
C. Total	1317	9956.5681		<.0001*

Parameter Estimates

Term	Estimate	Std Error	t Ratio	Prob>|t|
Intercept	95.002271	2.862971	33.18	<.0001*
wd_filt_n_KURT_Level_3	0.5147716	0.109905	4.68	<.0001*
N_Peaks_gz_filty_p0_25	-0.043327	0.121095	-0.36	0.7206
MPMSR_filty_p0_1	4.3819559	4.716525	0.93	0.3530
MWMSR_filty_p0_1	-19.24913	3.835314	-5.02	<.0001*
Gradient	-0.410264	0.067023	-6.12	<.0001*

Response SCRIM aggregation=3m, Tex Direction=Transverse

Whole Model

Actual by Predicted Plot

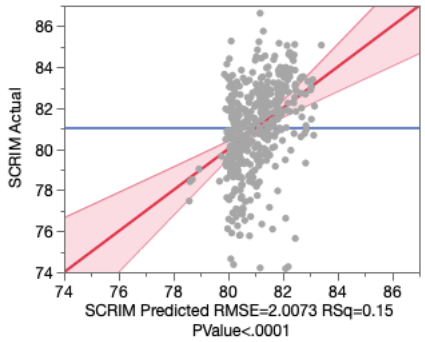

Effect Summary

Source	LogWorth	PValue
Gradient	6.116	0.00000
MWMSR_filty_p0_1	4.784	0.00002
wd_filt_n_KURT_Level_3	3.764	0.00017
MPMSR_filty_p0_1	0.943	0.11411
N_Peaks_gz_filty_p0_25	0.594	0.25448

Remove Add Edit FDR

Residual by Predicted Plot

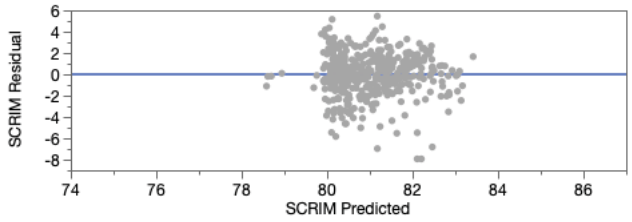

Summary of Fit

RSquare	0.149975
RSquare Adj	0.140114
Root Mean Square Error	2.007342
Mean of Response	81.02258
Observations (or Sum Wgts)	437

Analysis of Variance

Source	DF	Sum of Squares	Mean Square	F Ratio
Model	5	306.4121	61.2824	15.2087
Error	431	1736.6815	4.0294	Prob > F
C. Total	436	2043.0936		<.0001*

Parameter Estimates

Term	Estimate	Std Error	t Ratio	Prob>|t|
Intercept	97.720713	3.960784	24.67	<.0001*
wd_filt_n_KURT_Level_3	0.6203924	0.16369	3.79	0.0002*
N_Peaks_gz_filty_p0_25	-0.232742	0.203969	-1.14	0.2545
MPMSR_filty_p0_1	11.543333	7.291085	1.58	0.1141
MWMSR_filty_p0_1	-22.75277	5.220906	-4.36	<.0001*
Gradient	-0.458369	0.091349	-5.02	<.0001*

Response SCRIM aggregation=10m, Tex Direction=Transvers

Whole Model

Actual by Predicted Plot

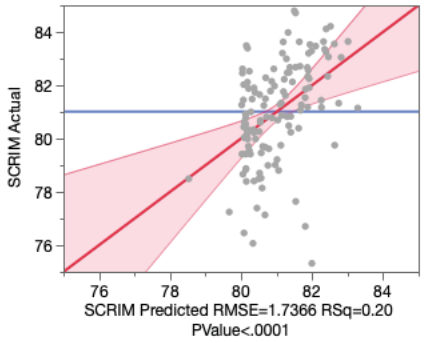

Effect Summary

Source	LogWorth	PValue
Gradient	2.937	0.00116
MWMSR_filty_p0_1	2.214	0.00611
wd_filt_n_KURT_Level_3	1.893	0.01280
MPMSR_filty_p0_1	0.641	0.22881
N_Peaks_gz_filty_p0_25	0.473	0.33676

Remove Add Edit FDR

Residual by Predicted Plot

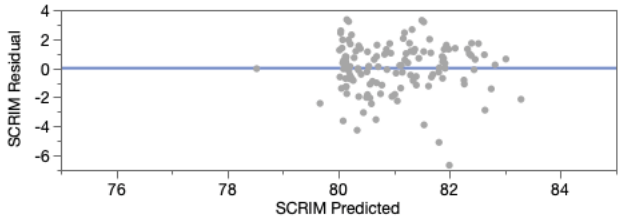

Summary of Fit

RSquare	0.202581
RSquare Adj	0.1699
Root Mean Square Error	1.73655
Mean of Response	81.0118
Observations (or Sum Wgts)	128

Analysis of Variance

Source	DF	Sum of Squares	Mean Square	F Ratio
Model	5	93.46463	18.6929	6.1987
Error	122	367.90399	3.0156	Prob > F
C. Total	127	461.36863		<.0001*

Parameter Estimates

Term	Estimate	Std Error	t Ratio	Prob>|t|
Intercept	99.102142	6.933279	14.29	<.0001*
wd_filt_n_KURT_Level_3	0.7840478	0.31031	2.53	0.0128*
N_Peaks_gz_filty_p0_25	-0.435578	0.451662	-0.96	0.3368
MPMSR_filty_p0_1	18.080978	14.949	1.21	0.2288
MWMSR_filty_p0_1	-24.65573	8.835775	-2.79	0.0061*
Gradient	-0.522904	0.157119	-3.33	0.0012*

Response SCRIM aggregation=20m, Tex Direction=Transvers

Whole Model

Actual by Predicted Plot

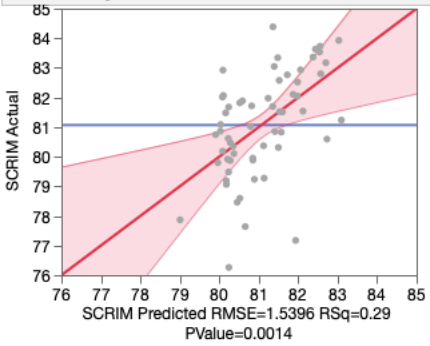

Effect Summary

Source	LogWorth	PValue
Gradient	1.794	0.01607
MWMSR_filty_p0_1	1.764	0.01720
wd_filt_n_KURT_Level_3	0.912	0.12237
MPMSR_filty_p0_1	0.282	0.52262
N_Peaks_gz_filty_p0_25	0.102	0.78979

Remove Add Edit FDR

Residual by Predicted Plot

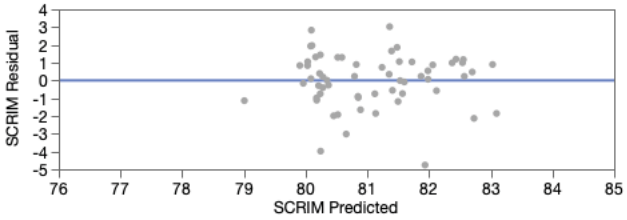

Summary of Fit

RSquare	0.294672
RSquare Adj	0.230552
Root Mean Square Error	1.539576
Mean of Response	81.06893
Observations (or Sum Wgts)	61

Analysis of Variance

Source	DF	Sum of Squares	Mean Square	F Ratio
Model	5	54.46446	10.8929	4.5956
Error	55	130.36617	2.3703	Prob > F
C. Total	60	184.83062		0.0014*

Parameter Estimates

Term	Estimate	Std Error	t Ratio	Prob>|t|
Intercept	101.83141	9.416464	10.81	<.0001*
wd_filt_n_KURT_Level_3	0.7092779	0.452035	1.57	0.1224
N_Peaks_gz_filty_p0_25	-0.176334	0.658241	-0.27	0.7898
MPMSR_filty_p0_1	13.736641	21.34906	0.64	0.5226
MWMSR_filty_p0_1	-29.04441	11.82183	-2.46	0.0172*
Gradient	-0.521796	0.210069	-2.48	0.0161*

Effect Tests

GT50_Random_Lasso

Generalized Regression for GT_20180828_31MPH_0_009INWFT_CC_1_AVE_trimmed Tex Directio

Model Launch

Standard Least Squares

Model Summary

Response	GT_20180828_31MPH_0_009INWFT_CC_1_AVE_trimmed
Distribution	Normal
Estimation Method	Standard Least Squares
Validation Method	None
Mean Model Link	Identity
Scale Model Link	Identity

Measure	
Number of rows	1026
Sum of Frequencies	1026
-LogLikelihood	-1956.41
Number of Parameters	83
BIC	-3337.345
AICc	-3732.017
RSquare	0.769837
RSquare Adj	0.7500878
RMSE	0.0359448

Parameter Estimates for Original Predictors

Effect Tests

Adaptive Lasso with BIC Validation

Model Summary

Response	GT_20180828_31MPH_0_009INWFT_CC_1_AVE_trimmed
Distribution	Normal
Estimation Method	Adaptive Lasso
Validation Method	BIC
Mean Model Link	Identity
Scale Model Link	Identity

Measure	
Number of rows	1026
Sum of Frequencies	1026
-LogLikelihood	-1880.914
Number of Parameters	32
BIC	-3539.958
AICc	-3695.7
ERIC	-3605.078
RSquare	0.7333455
RMSE	0.0386895
Lambda Penalty	0.0082635

Estimation Details

Number of Grid Points	150
Minimum Penalty Fraction	0
Grid Scale	Square Root

Solution Path

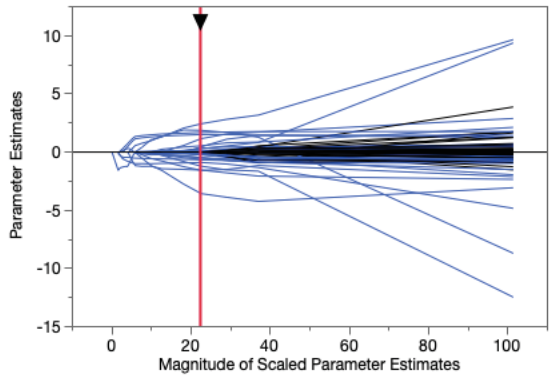

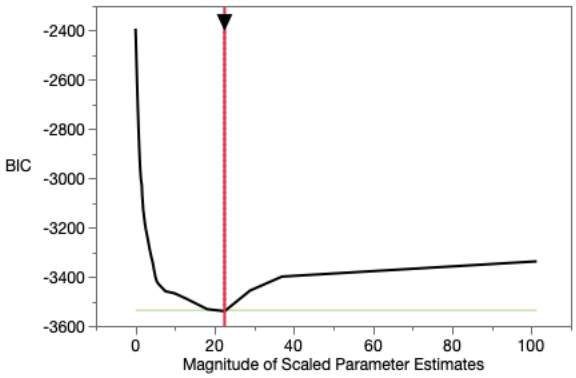

GT50_Random_SLR_VIF_under_4

Response GT_20180828_31MPH_0_009INWFT_CC_1_AVE_trimmed
Tex Direction=Random, Train / Validate=Train

Effect Summary

Source	LogWorth	PValue
MPMSR_T_filty_p0_25	70.173	0.00000
MWMSR_filty_p0_1	21.596	0.00000
Gradient	11.362	0.00000
wd_filt_n_KURT_Level_3	9.797	0.00000
Skewness	4.306	0.00005
N_Peaks_gz_filty_p0_25	3.989	0.00010
wd_filt_n_SKEW_Level_3	3.919	0.00012
wd_filt_n_SKEW_Level_7	1.911	0.01227
contact_yfilt_0_1tol_d0_00001	0.443	0.36055

Remove Add Edit FDR

Summary of Fit

RSquare	0.585763
RSquare Adj	0.581189
Root Mean Square Error	0.048078
Mean of Response	0.736855
Observations (or Sum Wgts)	825

Analysis of Variance

Source	DF	Sum of Squares	Mean Square	F Ratio
Model	9	2.6639570	0.295995	128.0527
Error	815	1.8838815	0.002312	Prob > F
C. Total	824	4.5478385		<.0001*

Parameter Estimates

Term	Estimate	Std Error	t Ratio	Prob>|t|	VIF
Intercept	1.4756052	0.042954	34.35	<.0001*	.
Skewness	-0.052957	0.01298	-4.08	<.0001*	2.1341414
contact_yfilt_0_1tol_d0_00001	-0.079201	0.086574	-0.91	0.3605	1.3948345
wd_filt_n_KURT_Level_3	-0.023141	0.003572	-6.48	<.0001*	1.8082962
wd_filt_n_SKEW_Level_3	0.0470334	0.012172	3.86	0.0001*	1.018846
wd_filt_n_SKEW_Level_7	0.0355942	0.014181	2.51	0.0123*	1.0297085
MPMSR_T_filty_p0_25	-1.936809	0.098368	-19.69	<.0001*	1.9779641
N_Peaks_gz_filty_p0_25	-0.012184	0.003121	-3.90	0.0001*	1.2451621
MWMSR_filty_p0_1	-0.72808	0.072741	-10.01	<.0001*	1.6212591
Gradient	0.0148071	0.002106	7.03	<.0001*	1.4137413

GT50_Random_MLR_1-20m_VIF_under_4

Response GT_20180828_31MPH_0_009INWFT_CC_1_AVE_trimr

Whole Model

Actual by Predicted Plot

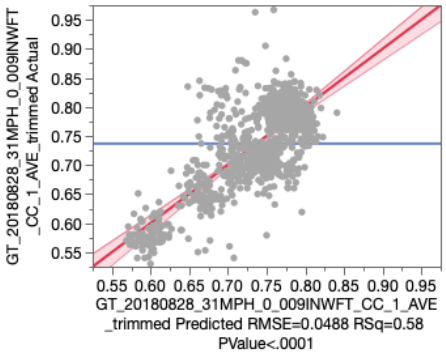

Effect Summary

Source	LogWorth	PValue
MPMSR_T_filty_p0_25	89.679	0.00000
MWMSR_filty_p0_1	27.257	0.00000
Gradient	12.614	0.00000
wd_filt_n_KURT_Level_3	8.824	0.00000
wd_filt_n_SKEW_Level_3	4.120	0.00008
Skewness	3.690	0.00020
N_Peaks_gz_filty_p0_25	3.608	0.00025
wd_filt_n_SKEW_Level_7	1.091	0.08116
contact_yfilt_0_1tol_d0_00001	0.107	0.78238

Remove Add Edit FDR

Residual by Predicted Plot

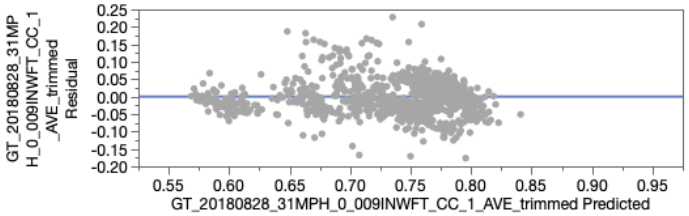

Summary of Fit

RSquare	0.579744
RSquare Adj	0.576021
Root Mean Square Error	0.048809
Mean of Response	0.736786
Observations (or Sum Wgts)	1026

Analysis of Variance

Source	DF	Sum of Squares	Mean Square	F Ratio
Model	9	3.3390299	0.371003	155.7303
Error	1016	2.4204630	0.002382	Prob > F
C. Total	1025	5.7594928		<.0001*

Parameter Estimates

Term	Estimate	Std Error	t Ratio	Prob>|t|
Intercept	1.4704703	0.039364	37.36	<.0001*
Skewness	-0.044352	0.0119	-3.73	0.0002*
contact_yfilt_0_1tol_d0_00001	-0.021822	0.078982	-0.28	0.7824
wd_filt_n_KURT_Level_3	-0.018607	0.00305	-6.10	<.0001*
wd_filt_n_SKEW_Level_3	0.0437676	0.011015	3.97	<.0001*
wd_filt_n_SKEW_Level_7	0.0229947	0.013172	1.75	0.0812
MPMSR_T_filty_p0_25	-1.986074	0.088805	-22.36	<.0001*
N_Peaks_gz_filty_p0_25	-0.010489	0.002851	-3.68	0.0002*
MWMSR_filty_p0_1	-0.766809	0.067846	-11.30	<.0001*
Gradient	0.0142988	0.001926	7.42	<.0001*

Response GT_20180828_31MPH_0_009INWFT_CC_1_AVE_trimr

Whole Model

Actual by Predicted Plot

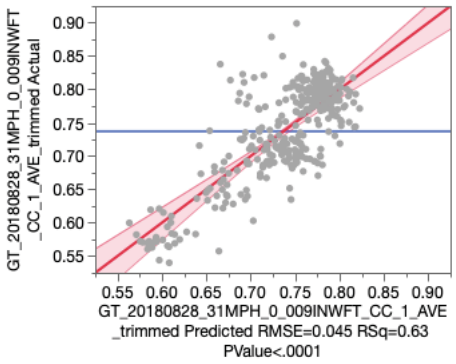

Effect Summary

Source	LogWorth	PValue
MPMSR_T_filty_p0_25	25.361	0.00000
MWMSR_filty_p0_1	9.377	0.00000
wd_filt_n_KURT_Level_3	6.652	0.00000
Gradient	6.482	0.00000
Skewness	3.365	0.00043
wd_filt_n_SKEW_Level_3	3.289	0.00051
N_Peaks_gz_filty_p0_25	3.060	0.00087
wd_filt_n_SKEW_Level_7	0.995	0.10127
contact_yfilt_0_1tol_d0_00001	0.213	0.61256

Remove Add Edit FDR

Residual by Predicted Plot

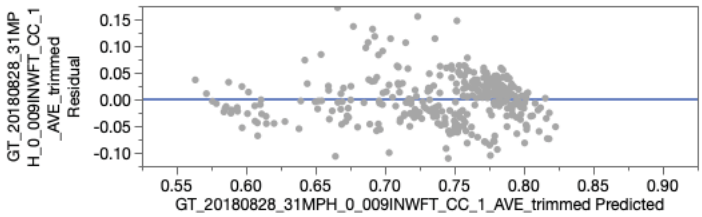

Summary of Fit

RSquare	0.631732
RSquare Adj	0.621688
Root Mean Square Error	0.044961
Mean of Response	0.73717
Observations (or Sum Wgts)	340

Analysis of Variance

Source	DF	Sum of Squares	Mean Square	F Ratio
Model	9	1.1443406	0.127149	62.8985
Error	330	0.6670927	0.002021	Prob > F
C. Total	339	1.8114333		<.0001*

Parameter Estimates

Term	Estimate	Std Error	t Ratio	Prob>|t|
Intercept	1.5660215	0.069274	22.61	<.0001*
Skewness	-0.086545	0.024339	-3.56	0.0004*
contact_yfilt_0_1tol_d0_00001	-0.074696	0.147356	-0.51	0.6126
wd_filt_n_KURT_Level_3	-0.035256	0.006664	-5.29	<.0001*
wd_filt_n_SKEW_Level_3	0.0913317	0.026034	3.51	0.0005*
wd_filt_n_SKEW_Level_7	0.0478709	0.029131	1.64	0.1013
MPMSR_T_filty_p0_25	-1.798904	0.155966	-11.53	<.0001*
N_Peaks_gz_filty_p0_25	-0.018596	0.005534	-3.36	0.0009*
MWMSR_filty_p0_1	-0.76857	0.119325	-6.44	<.0001*
Gradient	0.0164753	0.003161	5.21	<.0001*

Response GT_20180828_31MPH_0_009INWFT_CC_1_AVE_trimr

Whole Model

Actual by Predicted Plot

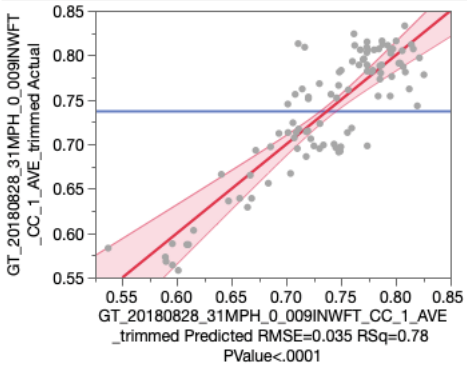

Effect Summary

Source	LogWorth	PValue
wd_filt_n_KURT_Level_3	6.697	0.00000
Gradient	5.431	0.00000
MPMSR_T_filty_p0_25	4.018	0.00010
MWMSR_filty_p0_1	3.258	0.00055
Skewness	2.760	0.00174
N_Peaks_gz_filty_p0_25	2.539	0.00289
wd_filt_n_SKEW_Level_3	2.211	0.00615
wd_filt_n_SKEW_Level_7	0.696	0.20129
contact_yfilt_0_1tol_d0_00001	0.094	0.80570

Remove Add Edit FDR

Residual by Predicted Plot

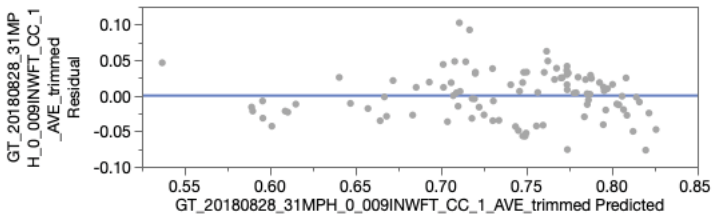

Summary of Fit

RSquare	0.780312
RSquare Adj	0.758097
Root Mean Square Error	0.034986
Mean of Response	0.736798
Observations (or Sum Wgts)	99

Analysis of Variance

Source	DF	Sum of Squares	Mean Square	F Ratio
Model	9	0.38693974	0.042993	35.1245
Error	89	0.10893822	0.001224	Prob > F
C. Total	98	0.49587796		<.0001*

Parameter Estimates

Term	Estimate	Std Error	t Ratio	Prob>|t|
Intercept	1.7205789	0.11662	14.75	<.0001*
Skewness	-0.169127	0.052371	-3.23	0.0017*
contact_yfilt_0_1tol_d0_00001	0.0771283	0.312627	0.25	0.8057
wd_filt_n_KURT_Level_3	-0.087826	0.01558	-5.64	<.0001*
wd_filt_n_SKEW_Level_3	0.1801597	0.064186	2.81	0.0061*
wd_filt_n_SKEW_Level_7	0.0954646	0.074152	1.29	0.2013
MPMSR_T_filty_p0_25	-1.181198	0.289093	-4.09	<.0001*
N_Peaks_gz_filty_p0_25	-0.030618	0.009993	-3.06	0.0029*
MWMSR_filty_p0_1	-0.722562	0.201623	-3.58	0.0006*
Gradient	0.0240178	0.004867	4.94	<.0001*

20m

Response GT_20180828_31MPH_0_009INWFT_CC_1_AVE_trimr

Whole Model

Actual by Predicted Plot

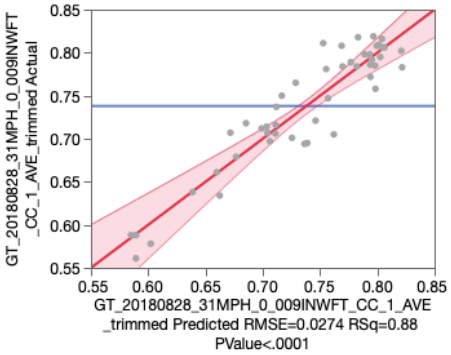

Effect Summary

Source	LogWorth	PValue
wd_filt_n_KURT_Level_3	7.583	0.00000
Gradient	5.583	0.00000
Skewness	3.969	0.00011
N_Peaks_gz_filty_p0_25	2.937	0.00116
MWMSR_filty_p0_1	2.002	0.00995
wd_filt_n_SKEW_Level_3	0.864	0.13669
wd_filt_n_SKEW_Level_7	0.344	0.45269
MPMSR_T_filty_p0_25	0.193	0.64059
contact_yfilt_0_1tol_d0_00001	0.109	0.77860

Remove Add Edit ☐ FDR

Residual by Predicted Plot

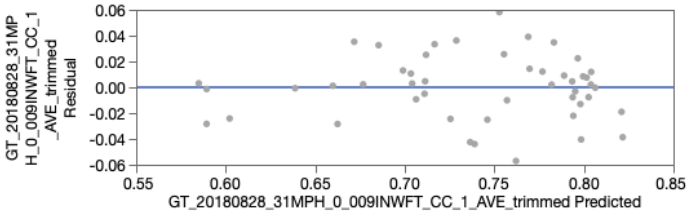

Summary of Fit

RSquare	0.875042
RSquare Adj	0.845446
Root Mean Square Error	0.027448
Mean of Response	0.738063
Observations (or Sum Wgts)	48

Analysis of Variance

Source	DF	Sum of Squares	Mean Square	F Ratio
Model	9	0.20047623	0.022275	29.5668
Error	38	0.02862858	0.000753	Prob > F
C. Total	47	0.22910481		<.0001*

Parameter Estimates

Term	Estimate	Std Error	t Ratio	Prob>|t|
Intercept	1.9782752	0.16847	11.74	<.0001*
Skewness	-0.368063	0.085158	-4.32	0.0001*
contact_yfilt_0_1tol_d0_00001	-0.229925	0.812048	-0.28	0.7786
wd_filt_n_KURT_Level_3	-0.177352	0.025406	-6.98	<.0001*
wd_filt_n_SKEW_Level_3	0.1601062	0.105306	1.52	0.1367
wd_filt_n_SKEW_Level_7	0.0898829	0.118464	0.76	0.4527
MPMSR_T_filty_p0_25	-0.197396	0.419421	-0.47	0.6406
N_Peaks_gz_filty_p0_25	-0.04273	0.012159	-3.51	0.0012*
MWMSR_filty_p0_1	-0.702872	0.259027	-2.71	0.0100*
Gradient	0.0355289	0.006439	5.52	<.0001*

GT50_Transverse_Lasso

Generalized Regression for GT_20180828_31MPH_0_009INWFT_CC_1_AVE_trimmed Tex Directi

Model Launch

Standard Least Squares

Model Summary

Response	GT_20180828_31MPH_0_009INWFT_CC_1_AVE_trimmed
Distribution	Normal
Estimation Method	Standard Least Squares
Validation Method	None
Mean Model Link	Identity
Scale Model Link	Identity

Measure	
Number of rows	1318
Sum of Frequencies	1298
-LogLikelihood	-2758.542
Number of Parameters	83
BIC	-4922.092
AICc	-5339.598
RSquare	0.5625151
RSquare Adj	0.5333734
RMSE	0.0288928

Parameter Estimates for Original Predictors

Effect Tests

Adaptive Lasso with BIC Validation

Model Summary

Response	GT_20180828_31MPH_0_009INWFT_CC_1_AVE_trimmed
Distribution	Normal
Estimation Method	Adaptive Lasso
Validation Method	BIC
Mean Model Link	Identity
Scale Model Link	Identity

Measure	
Number of rows	1318
Sum of Frequencies	1298
-LogLikelihood	-2698.982
Number of Parameters	22
BIC	-5240.255
AICc	-5353.17
ERIC	-5290.024
RSquare	0.5204662
RMSE	0.0302494
Lambda Penalty	0.0053806

Estimation Details

Number of Grid Points	150
Minimum Penalty Fraction	0
Grid Scale	Square Root

Solution Path

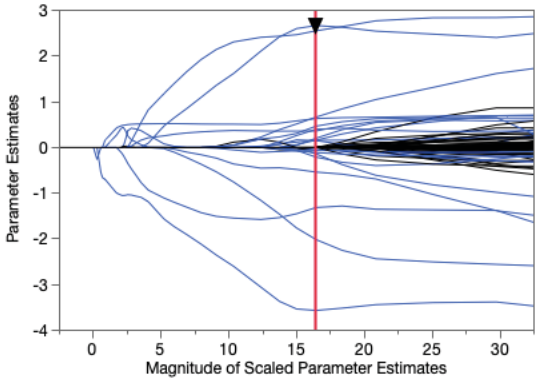

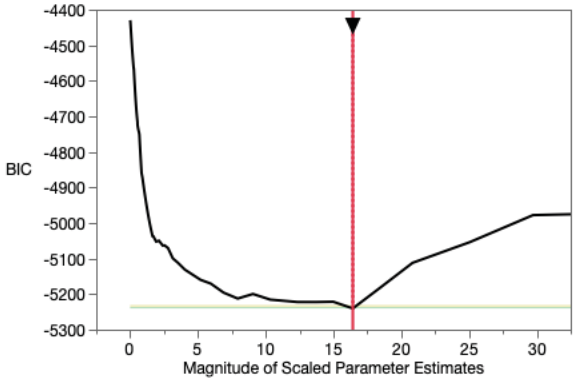

GT50_Random_SLR_VIF_under_4

Response GT_20180828_31MPH_0_009INWFT_CC_1_AVE_trimmed
Tex Direction=Random, Train / Validate=Train

Effect Summary

Source	LogWorth	PValue
MPMSR_T_filty_p0_25	70.173	0.00000
MWMSR_filty_p0_1	21.596	0.00000
Gradient	11.362	0.00000
wd_filt_n_KURT_Level_3	9.797	0.00000
Skewness	4.306	0.00005
N_Peaks_gz_filty_p0_25	3.989	0.00010
wd_filt_n_SKEW_Level_3	3.919	0.00012
wd_filt_n_SKEW_Level_7	1.911	0.01227
contact_yfilt_0_1tol_d0_00001	0.443	0.36055

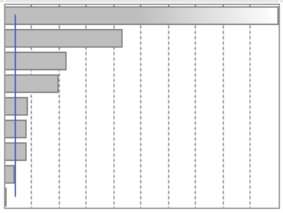

Remove Add Edit FDR

Summary of Fit

RSquare	0.585763
RSquare Adj	0.581189
Root Mean Square Error	0.048078
Mean of Response	0.736855
Observations (or Sum Wgts)	825

Analysis of Variance

Source	DF	Sum of Squares	Mean Square	F Ratio
Model	9	2.6639570	0.295995	128.0527
Error	815	1.8838815	0.002312	Prob > F
C. Total	824	4.5478385		<.0001*

Parameter Estimates

Term	Estimate	Std Error	t Ratio	Prob>|t|	VIF
Intercept	1.4756052	0.042954	34.35	<.0001*	.
Skewness	-0.052957	0.01298	-4.08	<.0001*	2.1341414
contact_yfilt_0_1tol_d0_00001	-0.079201	0.086574	-0.91	0.3605	1.3948345
wd_filt_n_KURT_Level_3	-0.023141	0.003572	-6.48	<.0001*	1.8082962
wd_filt_n_SKEW_Level_3	0.0470334	0.012172	3.86	0.0001*	1.018846
wd_filt_n_SKEW_Level_7	0.0355942	0.014181	2.51	0.0123*	1.0297085
MPMSR_T_filty_p0_25	-1.936809	0.098368	-19.69	<.0001*	1.9779641
N_Peaks_gz_filty_p0_25	-0.012184	0.003121	-3.90	0.0001*	1.2451621
MWMSR_filty_p0_1	-0.72808	0.072741	-10.01	<.0001*	1.6212591
Gradient	0.0148071	0.002106	7.03	<.0001*	1.4137413

Effect Tests

Effect Details

GT50_Random_MLR_1-20m_VIF_under_4

Response GT_20180828_31MPH_0_009INWFT_CC_1_AVE_trimm

Whole Model

Actual by Predicted Plot

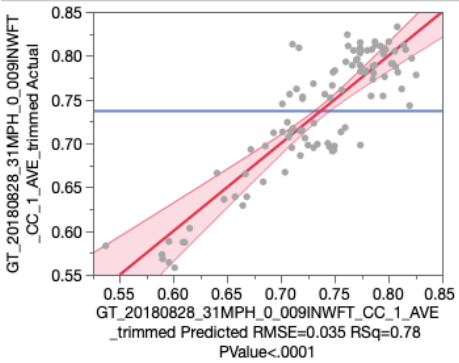

Effect Summary

Source	LogWorth	PValue
wd_filt_n_KURT_Level_3	6.697	0.00000
Gradient	5.431	0.00000
MPMSR_T_filty_p0_25	4.018	0.00010
MWMSR_filty_p0_1	3.258	0.00055
Skewness	2.760	0.00174
N_Peaks_gz_filty_p0_25	2.539	0.00289
wd_filt_n_SKEW_Level_3	2.211	0.00615
wd_filt_n_SKEW_Level_7	0.696	0.20129
contact_yfilt_0_1tol_d0_00001	0.094	0.80570

Remove Add Edit FDR

Residual by Predicted Plot

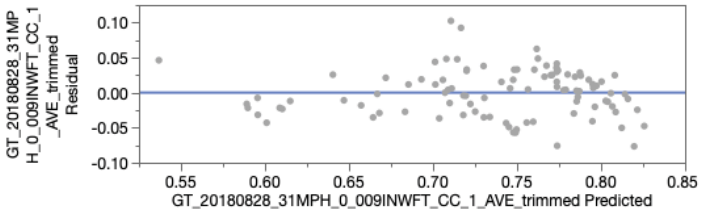

Summary of Fit

RSquare	0.780312
RSquare Adj	0.758097
Root Mean Square Error	0.034986
Mean of Response	0.736798
Observations (or Sum Wgts)	99

Analysis of Variance

Source	DF	Sum of Squares	Mean Square	F Ratio
Model	9	0.38693974	0.042993	35.1245
Error	89	0.10893822	0.001224	Prob > F
C. Total	98	0.49587796		<.0001*

Parameter Estimates

Term	Estimate	Std Error	t Ratio	Prob>|t|
Intercept	1.7205789	0.11662	14.75	<.0001*
Skewness	-0.169127	0.052371	-3.23	0.0017*
contact_yfilt_0_1tol_d0_00001	0.0771283	0.312627	0.25	0.8057
wd_filt_n_KURT_Level_3	-0.087826	0.01558	-5.64	<.0001*
wd_filt_n_SKEW_Level_3	0.1801597	0.064186	2.81	0.0061*
wd_filt_n_SKEW_Level_7	0.0954646	0.074152	1.29	0.2013
MPMSR_T_filty_p0_25	-1.181198	0.289093	-4.09	<.0001*
N_Peaks_gz_filty_p0_25	-0.030618	0.009993	-3.06	0.0029*
MWMSR_filty_p0_1	-0.722562	0.201623	-3.58	0.0006*
Gradient	0.0240178	0.004867	4.94	<.0001*

GT50_Transverse_Lasso

Generalized Regression for GT_20180828_31MPH_0_009INWFT_CC_1_AVE_trimmed Tex Direct

Model Launch

Standard Least Squares

Model Summary

Response	GT_20180828_31MPH_0_009INWFT_CC_1_AVE_trimmed
Distribution	Normal
Estimation Method	Standard Least Squares
Validation Method	None
Mean Model Link	Identity
Scale Model Link	Identity

Measure	
Number of rows	1318
Sum of Frequencies	1298
-LogLikelihood	-2758.542
Number of Parameters	83
BIC	-4922.092
AICc	-5339.598
RSquare	0.5625151
RSquare Adj	0.5333734
RMSE	0.0288928

Parameter Estimates for Original Predictors

Effect Tests

Adaptive Lasso with BIC Validation

Model Summary

Response	GT_20180828_31MPH_0_009INWFT_CC_1_AVE_trimmed
Distribution	Normal
Estimation Method	Adaptive Lasso
Validation Method	BIC
Mean Model Link	Identity
Scale Model Link	Identity

Measure	
Number of rows	1318
Sum of Frequencies	1298
-LogLikelihood	-2698.982
Number of Parameters	22
BIC	-5240.255
AICc	-5353.17
ERIC	-5290.024
RSquare	0.5204662
RMSE	0.0302494
Lambda Penalty	0.0053806

Estimation Details

Number of Grid Points	150
Minimum Penalty Fraction	0
Grid Scale	Square Root

Solution Path

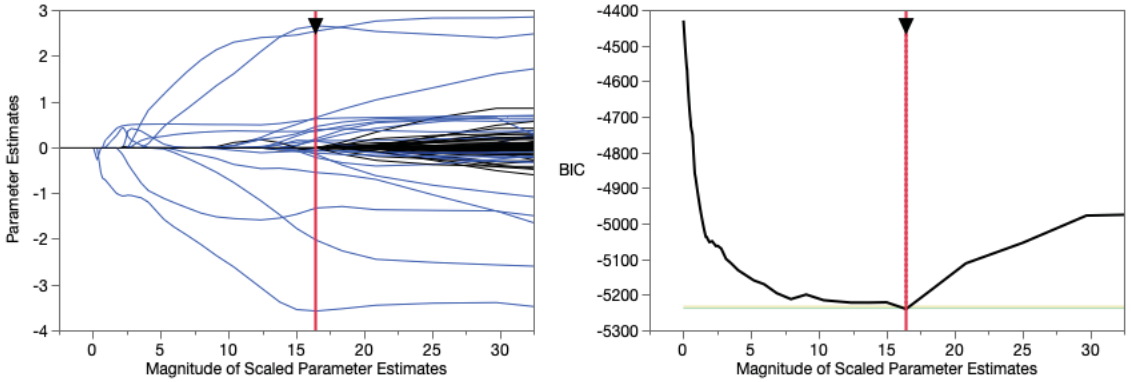

GT50_Transverse_SLR_VIF_under_4

Response GT_20180828_31MPH_0_009INWFT_CC_1_AVE_trimmed

Effect Summary

Source	LogWorth	PValue
Crossfall	39.424	0.00000
MWMSR_filty_p0_25	35.998	0.00000
contact_yfilt_0_1tol_d0_00001	3.300	0.00050
MWIDTHSGZ_filty_p0_25	2.734	0.00184
Curvature	1.919	0.01206
EAWE_butfilt_d1eneg2	1.851	0.01411

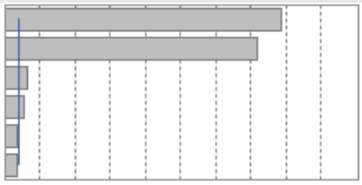

Remove Add Edit Undo FDR

Summary of Fit

RSquare	0.431126
RSquare Adj	0.427834
Root Mean Square Error	0.032859
Mean of Response	0.740453
Observations (or Sum Wgts)	1044

Analysis of Variance

Source	DF	Sum of Squares	Mean Square	F Ratio
Model	6	0.8485624	0.141427	130.9830
Error	1037	1.1196863	0.001080	Prob > F
C. Total	1043	1.9682487		<.0001*

Parameter Estimates

Term	Estimate	Std Error	t Ratio	Prob>|t|
Intercept	1.0585592	0.031848	33.24	<.0001*
contact_yfilt_0_1tol_d0_00001	0.0927501	0.026567	3.49	0.0005*
EAWE_butfilt_d1eneg2	0.0002751	0.000112	2.46	0.0141*
MWIDTHSGZ_filty_p0_25	0.0036148	0.001158	3.12	0.0018*
MWMSR_filty_p0_25	-0.470796	0.035756	-13.17	<.0001*
Crossfall	0.0108755	0.000785	13.85	<.0001*
Curvature	-10.72244	4.263591	-2.51	0.0121*

GT50_Transverse_MLR_1-20_VIF_under_4 - 1m

Response GT_20180828_31MPH_0_009INWFT_CC_1_AVE_trimm

Whole Model

Actual by Predicted Plot

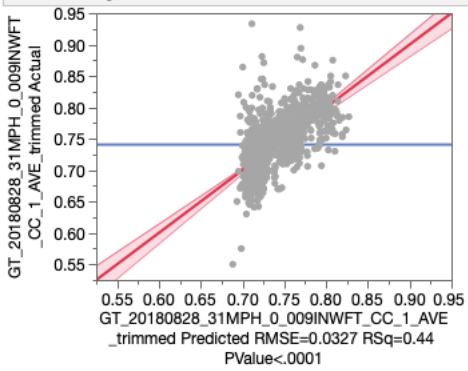

Effect Summary

Source	LogWorth	PValue
MWMSR_filty_p0_25	53.207	0.00000
Crossfall	51.642	0.00000
SCRIM_CALC_RMSTD	11.642	0.00000
contact_yfilt_0_1tol_d0_00001	7.940	0.00000
MWIDTHSGZ_filty_p0_25	4.389	0.00004
Curvature	3.362	0.00043

Remove Add Edit FDR

Residual by Predicted Plot

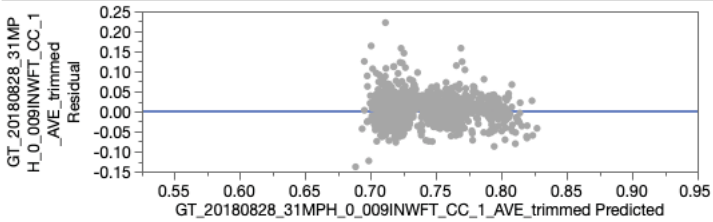

Summary of Fit

RSquare	0.442196
RSquare Adj	0.439603
Root Mean Square Error	0.032713
Mean of Response	0.740539
Observations (or Sum Wgts)	1298

Analysis of Variance

Source	DF	Sum of Squares	Mean Square	F Ratio
Model	6	1.0952284	0.182538	170.5718
Error	1291	1.3815682	0.001070	Prob > F
C. Total	1297	2.4767966		<.0001*

Parameter Estimates

Term	Estimate	Std Error	t Ratio	Prob>|t|
Intercept	1.0793343	0.028767	37.52	<.0001*
contact_yfilt_0_1tol_d0_00001	0.145365	0.025305	5.74	<.0001*
MWIDTHSGZ_filty_p0_25	0.0037502	0.000911	4.12	<.0001*
MWMSR_filty_p0_25	-0.544159	0.033569	-16.21	<.0001*
SCRIM_CALC_RMSTD	0.0320178	0.004519	7.09	<.0001*
Crossfall	0.0111385	0.000699	15.94	<.0001*
Curvature	-13.46869	3.818519	-3.53	0.0004*

GT50_Transverse_MLR_1-20_VIF_under_4 - 3m

Response GT_20180828_31MPH_0_009INWFT_CC_1_AVE_trimm

Whole Model

Actual by Predicted Plot

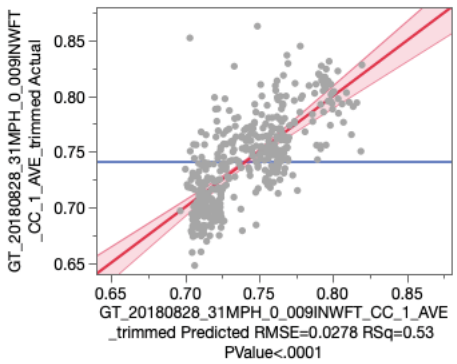

Effect Summary

Source	LogWorth	PValue
MWMSR_filty_p0_25	23.502	0.00000
Crossfall	23.063	0.00000
SCRIM_CALC_RMSTD	5.712	0.00000
contact_yfilt_0_1tol_d0_00001	3.542	0.00029
MWIDTHSGZ_filty_p0_25	2.300	0.00502
Curvature	1.806	0.01563

Remove Add Edit FDR

Residual by Predicted Plot

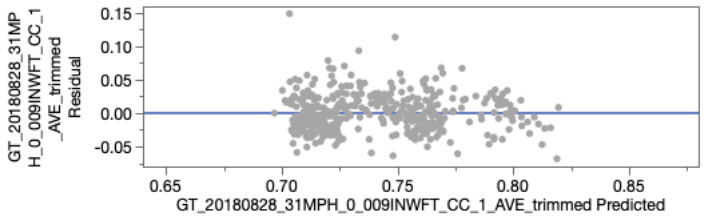

Summary of Fit

RSquare	0.526318
RSquare Adj	0.519615
Root Mean Square Error	0.027765
Mean of Response	0.740762
Observations (or Sum Wgts)	431

Analysis of Variance

Source	DF	Sum of Squares	Mean Square	F Ratio
Model	6	0.36317726	0.060530	78.5192
Error	424	0.32685685	0.000771	Prob > F
C. Total	430	0.69003410		<.0001*

Parameter Estimates

Term	Estimate	Std Error	t Ratio	Prob>|t|
Intercept	1.0712622	0.044406	24.12	<.0001*
contact_yfilt_0_1tol_d0_00001	0.1530496	0.041846	3.66	0.0003*
MWIDTHSGZ_filty_p0_25	0.0042297	0.001499	2.82	0.0050*
MWMSR_filty_p0_25	-0.544118	0.050325	-10.81	<.0001*
SCRIM_CALC_RMSTD	0.0339454	0.007033	4.83	<.0001*
Crossfall	0.0110622	0.001034	10.69	<.0001*
Curvature	-13.72596	5.655221	-2.43	0.0156*

GT50_Transverse_MLR_1-20_VIF_under_4 - 10m

Response GT_20180828_31MPH_0_009INWFT_CC_1_AVE_trimm

Whole Model

Actual by Predicted Plot

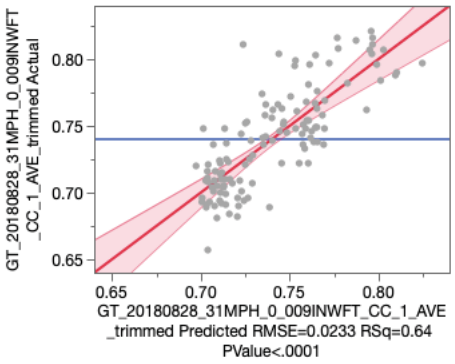

Effect Summary

Source	LogWorth	PValue
Crossfall	9.901	0.00000
MWMSR_filty_p0_25	9.422	0.00000
SCRIM_CALC_RMSTD	3.716	0.00019
contact_yfilt_0_1tol_d0_00001	2.358	0.00438
Curvature	1.119	0.07611
MWIDTHSGZ_filty_p0_25	0.955	0.11088

Remove Add Edit FDR

Residual by Predicted Plot

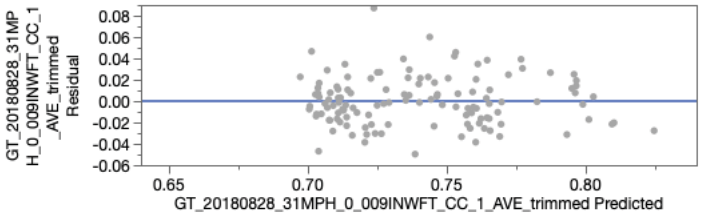

Summary of Fit

RSquare	0.643527
RSquare Adj	0.625553
Root Mean Square Error	0.023322
Mean of Response	0.739992
Observations (or Sum Wgts)	126

Analysis of Variance

Source	DF	Sum of Squares	Mean Square	F Ratio
Model	6	0.11684835	0.019475	35.8043
Error	119	0.06472665	0.000544	Prob > F
C. Total	125	0.18157499		<.0001*

Parameter Estimates

Term	Estimate	Std Error	t Ratio	Prob>|t|
Intercept	1.0747914	0.077453	13.88	<.0001*
contact_yfilt_0_1tol_d0_00001	0.2387905	0.082201	2.90	0.0044*
MWIDTHSGZ_filty_p0_25	0.0042862	0.002669	1.61	0.1109
MWMSR_filty_p0_25	-0.582203	0.085213	-6.83	<.0001*
SCRIM_CALC_RMSTD	0.0470608	0.012227	3.85	0.0002*
Crossfall	0.0117847	0.001671	7.05	<.0001*
Curvature	-16.46932	9.204444	-1.79	0.0761

GT50_Transverse_MLR_1-20_VIF_under_4 – 20m

Response GT_20180828_31MPH_0_009INWFT_CC_1_AVE_trimm

Whole Model

Actual by Predicted Plot

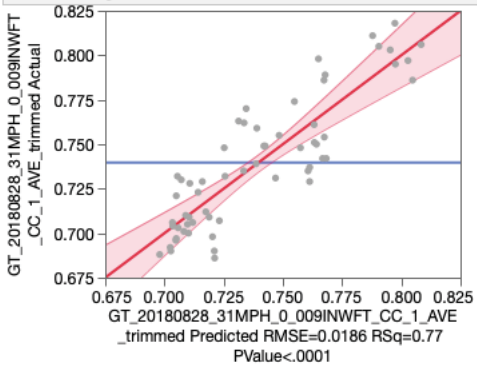

Effect Summary

Source	LogWorth	PValue
MWMSR_filty_p0_25	6.726	0.00000
Crossfall	6.056	0.00000
SCRIM_CALC_RMSTD	2.973	0.00106
contact_yfilt_0_1tol_d0_00001	1.124	0.07521
Curvature	0.646	0.22599
MWIDTHSGZ_filty_p0_25	0.102	0.79059

Remove Add Edit FDR

Residual by Predicted Plot

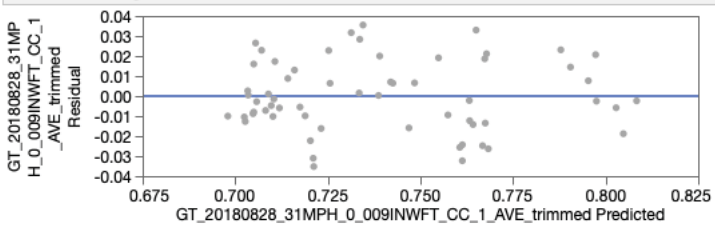

Summary of Fit

RSquare	0.766254
RSquare Adj	0.739792
Root Mean Square Error	0.018624
Mean of Response	0.739683
Observations (or Sum Wgts)	60

Analysis of Variance

Source	DF	Sum of Squares	Mean Square	F Ratio
Model	6	0.06026358	0.010044	28.9570
Error	53	0.01838340	0.000347	Prob > F
C. Total	59	0.07864698		<.0001*

Parameter Estimates

Term	Estimate	Std Error	t Ratio	Prob>|t|
Intercept	1.2142956	0.115166	10.54	<.0001*
contact_yfilt_0_1tol_d0_00001	0.2910399	0.160369	1.81	0.0752
MWIDTHSGZ_filty_p0_25	0.0009819	0.003679	0.27	0.7906
MWMSR_filty_p0_25	-0.742891	0.124023	-5.99	<.0001*
SCRIM_CALC_RMSTD	0.0560429	0.01618	3.46	0.0011*
Crossfall	0.0120928	0.002172	5.57	<.0001*
Curvature	-14.89531	12.15945	-1.22	0.2260

Noise_Random_Lasso

Generalized Regression for Noise Tex Direction=Random

Model Launch

Standard Least Squares

Model Summary

Response	Noise
Distribution	Normal
Estimation Method	Standard Least Squares
Validation Method	None
Mean Model Link	Identity
Scale Model Link	Identity

Measure	
Number of rows	1026
Sum of Frequencies	1026
-LogLikelihood	1153.5582
Number of Parameters	83
BIC	2882.5904
AICc	2487.9189
RSquare	0.3967678
RSquare Adj	0.3450074
RMSE	0.7448199

Parameter Estimates for Original Predictors

Effect Tests

Adaptive Lasso with BIC Validation

Model Summary

Response	Noise
Distribution	Normal
Estimation Method	Adaptive Lasso
Validation Method	BIC
Mean Model Link	Identity
Scale Model Link	Identity

Measure	
Number of rows	1026
Sum of Frequencies	1026
-LogLikelihood	1241.8983
Number of Parameters	13
BIC	2573.9311
AICc	2510.1563
ERIC	2532.5149
RSquare	0.283409
RMSE	0.8117918
Lambda Penalty	8.0644697

Estimation Details

Number of Grid Points	150
Minimum Penalty Fraction	0
Grid Scale	Square Root

Solution Path

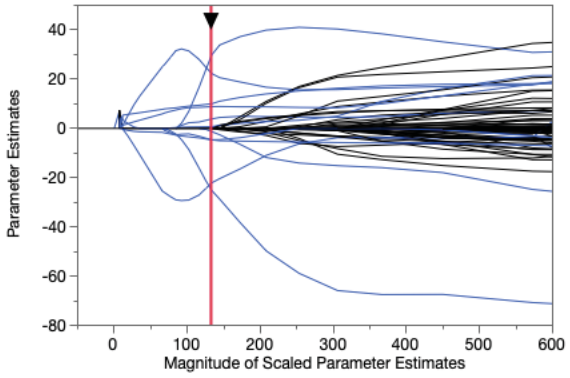

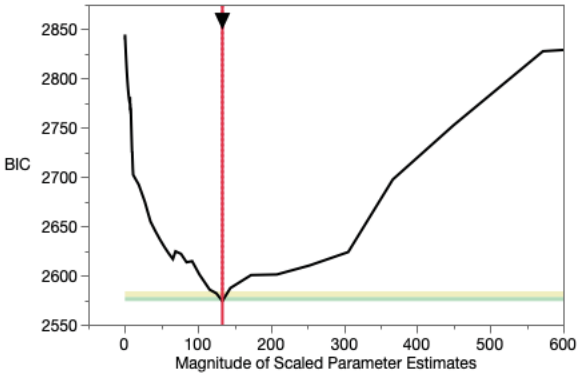

Response Noise Tex Direction=Random, Train / Validate=Train

Effect Summary

Source	LogWorth	PValue
Gradient	23.315	0.00000
MWMSR_filty_p0_1	4.306	0.00005
contact_nfilt_0_1tol_d0_01	0.044	0.90374

Remove Add Edit FDR

Summary of Fit

RSquare	0.170272
RSquare Adj	0.16724
Root Mean Square Error	0.878047
Mean of Response	102.6802
Observations (or Sum Wgts)	825

Analysis of Variance

Source	DF	Sum of Squares	Mean Square	F Ratio
Model	3	129.89307	43.2977	56.1603
Error	821	632.96311	0.7710	Prob > F
C. Total	824	762.85618		<.0001*

Parameter Estimates

Term	Estimate	Std Error	t Ratio	Prob>|t|
Intercept	103.29962	0.859995	120.12	<.0001*
contact_nfilt_0_1tol_d0_01	0.077337	0.639271	0.12	0.9037
MWMSR_filty_p0_1	-4.274394	1.047593	-4.08	<.0001*
Gradient	0.3951695	0.037853	10.44	<.0001*

Noise_Random_MLR_1-20m_VIF_under_4 – 1m

Response Noise aggregation=1m, Tex Direction=Random

Whole Model

Actual by Predicted Plot

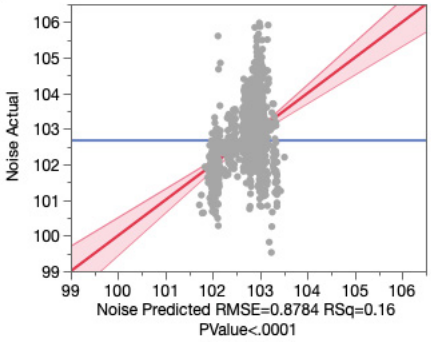

Effect Summary

Source	LogWorth	PValue
Gradient	27.504	0.00000
MWMSR_filty_p0_1	5.602	0.00000
contact_nfilt_0_1tol_d0_01	0.094	0.80508

Remove Add Edit FDR

Residual by Predicted Plot

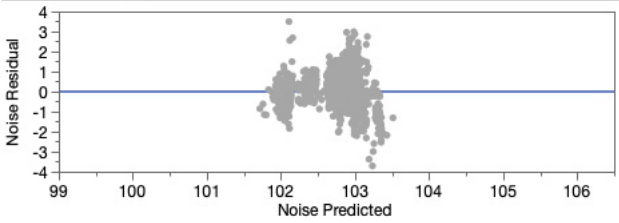

Summary of Fit

RSquare	0.164248
RSquare Adj	0.161795
Root Mean Square Error	0.878407
Mean of Response	102.6717
Observations (or Sum Wgts)	1026

Analysis of Variance

Source	DF	Sum of Squares	Mean Square	F Ratio
Model	3	154.97665	51.6589	66.9504
Error	1022	788.57430	0.7716	Prob > F
C. Total	1025	943.55095		<.0001*

Parameter Estimates

Term	Estimate	Std Error	t Ratio	Prob>|t|
Intercept	103.39608	0.775695	133.29	<.0001*
contact_nfilt_0_1tol_d0_01	0.1415839	0.573568	0.25	0.8051
MWMSR_filty_p0_1	-4.478668	0.945921	-4.73	<.0001*
Gradient	0.3868474	0.034065	11.36	<.0001*

Noise_Random_MLR_1-20m_VIF_under_4 – 3m

Response Noise aggregation=3m, Tex Direction=Random

Whole Model

Actual by Predicted Plot

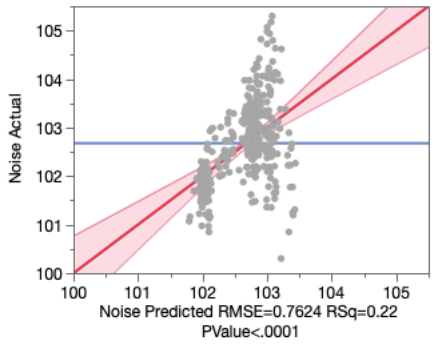

Effect Summary

Source	LogWorth	PValue
Gradient	11.814	0.00000
MWMSR_filty_p0_1	2.970	0.00107
contact_nfilt_0_1tol_d0_01	0.182	0.65725

Remove Add Edit FDR

Residual by Predicted Plot

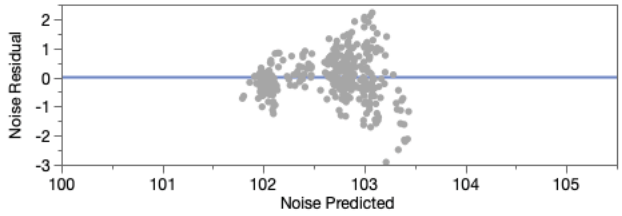

Summary of Fit

RSquare	0.216592
RSquare Adj	0.209598
Root Mean Square Error	0.762412
Mean of Response	102.6764
Observations (or Sum Wgts)	340

Analysis of Variance

Source	DF	Sum of Squares	Mean Square	F Ratio
Model	3	53.99747	17.9992	30.9651
Error	336	195.30721	0.5813	Prob > F
C. Total	339	249.30468		<.0001*

Parameter Estimates

Term	Estimate	Std Error	t Ratio	Prob>|t|
Intercept	103.97256	1.197818	86.80	<.0001*
contact_nfilt_0_1tol_d0_01	-0.399165	0.898808	-0.44	0.6573
MWMSR_filty_p0_1	-4.730179	1.433553	-3.30	0.0011*
Gradient	0.3801988	0.051737	7.35	<.0001*

Noise_Random_MLR_1-20m_VIF_under_4 - 10m

Response Noise aggregation=10m, Tex Direction=Random

Whole Model

Actual by Predicted Plot

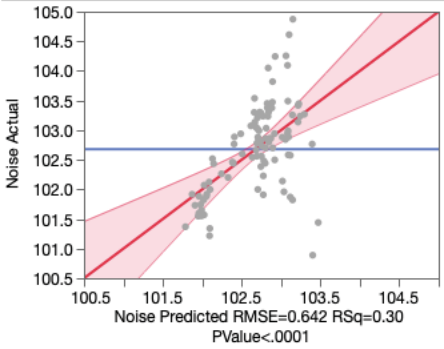

Effect Summary

Source	LogWorth	PValue
Gradient	4.985	0.00001
MWMSR_filty_p0_1	1.738	0.01827
contact_nfilt_0_1tol_d0_01	0.289	0.51382

Remove Add Edit FDR

Residual by Predicted Plot

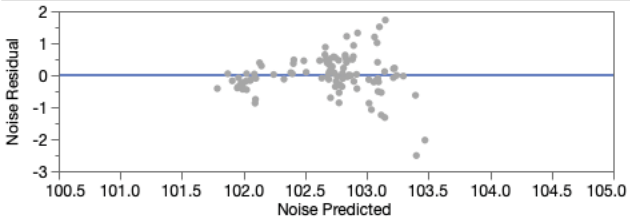

Summary of Fit

RSquare	0.303537
RSquare Adj	0.281543
Root Mean Square Error	0.642038
Mean of Response	102.6782
Observations (or Sum Wgts)	99

Analysis of Variance

Source	DF	Sum of Squares	Mean Square	F Ratio
Model	3	17.067031	5.68901	13.8011
Error	95	39.160243	0.41221	Prob > F
C. Total	98	56.227274		<.0001*

Parameter Estimates

Term	Estimate	Std Error	t Ratio	Prob>|t|
Intercept	104.82699	1.935725	54.15	<.0001*
contact_nfilt_0_1tol_d0_01	-0.963124	1.469619	-0.66	0.5138
MWMSR_filty_p0_1	-5.483261	2.283189	-2.40	0.0183*
Gradient	0.3791862	0.081393	4.66	<.0001*

Noise_Random_MLR_1-20m_VIF_under_4 – 20m

Response Noise aggregation=20m, Tex Direction=Random

Whole Model

Actual by Predicted Plot

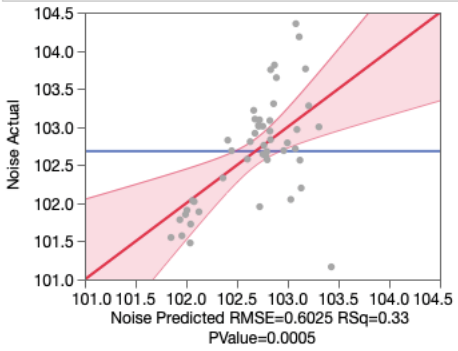

Effect Summary

Source	LogWorth	PValue
Gradient	2.791	0.00162
MWMSR_filty_p0_1	1.102	0.07912
contact_nfilt_0_1tol_d0_01	0.179	0.66204

Remove Add Edit FDR

Residual by Predicted Plot

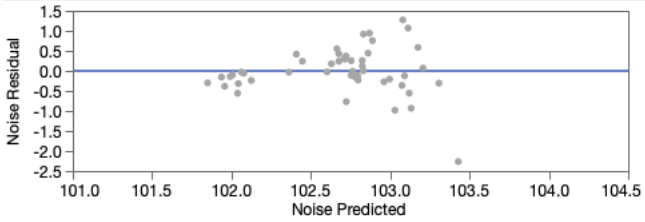

Summary of Fit

RSquare	0.33112
RSquare Adj	0.285515
Root Mean Square Error	0.602546
Mean of Response	102.6816
Observations (or Sum Wgts)	48

Analysis of Variance

Source	DF	Sum of Squares	Mean Square	F Ratio
Model	3	7.908065	2.63602	7.2605
Error	44	15.974699	0.36306	Prob > F
C. Total	47	23.882763		0.0005*

Parameter Estimates

Term	Estimate	Std Error	t Ratio	Prob>|t|
Intercept	104.87095	2.72019	38.55	<.0001*
contact_nfilt_0_1tol_d0_01	-0.918846	2.087962	-0.44	0.6620
MWMSR_filty_p0_1	-5.592774	3.111364	-1.80	0.0791
Gradient	0.3753564	0.111697	3.36	0.0016*

Noise_Transverse_Lasso

Generalized Regression for Noise Tex Direction=Transverse

Model Launch

Standard Least Squares

Model Summary

Response	Noise
Distribution	Normal
Estimation Method	Standard Least Squares
Validation Method	None
Mean Model Link	Identity
Scale Model Link	Identity

Measure	
Number of rows	1318
Sum of Frequencies	1298
-LogLikelihood	1674.8847
Number of Parameters	83
BIC	3944.7615
AICc	3527.2554
RSquare	0.3773877
RSquare Adj	0.3359143
RMSE	0.8793428

Parameter Estimates for Original Predictors

Effect Tests

Adaptive Lasso with BIC Validation

Model Summary

Response	Noise
Distribution	Normal
Estimation Method	Adaptive Lasso
Validation Method	BIC
Mean Model Link	Identity
Scale Model Link	Identity

Measure	
Number of rows	1318
Sum of Frequencies	1298
-LogLikelihood	1750.7496
Number of Parameters	14
BIC	3601.8593
AICc	3529.8266
ERIC	3560.8277
RSquare	0.3001828
RMSE	0.9322698
Lambda Penalty	8.0387485

Estimation Details

Number of Grid Points	150
Minimum Penalty Fraction	0
Grid Scale	Square Root

Solution Path

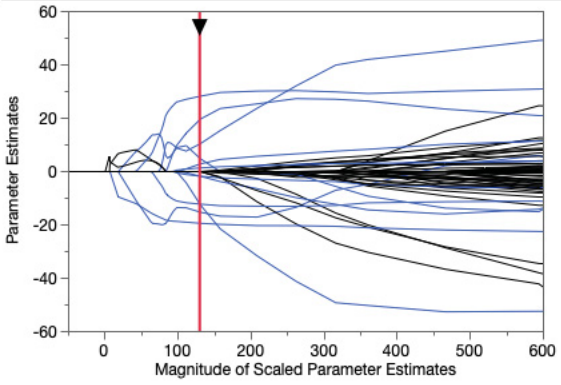

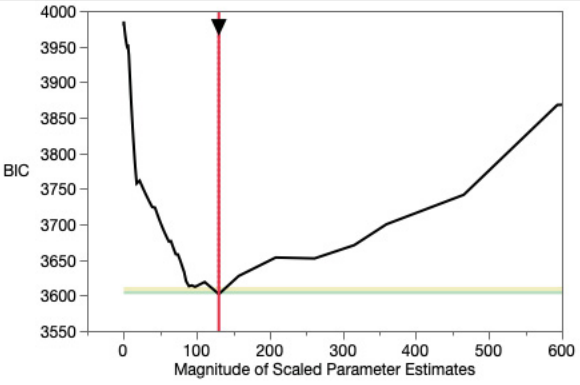

Response Noise Tex Direction=Transverse, Train / Validate=Train

Effect Summary

Source	LogWorth	PValue
Crossfall	45.489	0.00000
MWMSR_filty_p0_1	31.148	0.00000
MWMSR_filty_p0_25	10.645	0.00000
contact_yfilt_0_1tol_d0_001	8.567	0.00000
wd_filt_n_SKEW_Level_41	3.924	0.00012
wd_filt_n_RMS_Level_9	2.893	0.00128
Gradient	0.725	0.18819

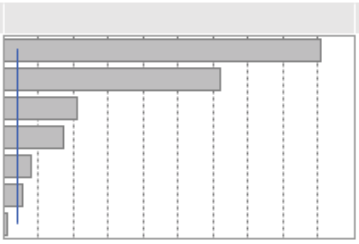

Remove Add Edit FDR

Summary of Fit

RSquare	0.278192
RSquare Adj	0.273315
Root Mean Square Error	0.936465
Mean of Response	104.1248
Observations (or Sum Wgts)	1044

Analysis of Variance

Source	DF	Sum of Squares	Mean Square	F Ratio
Model	7	350.1592	50.0227	57.0406
Error	1036	908.5378	0.8770	Prob > F
C. Total	1043	1258.6969		<.0001*

Parameter Estimates

Term	Estimate	Std Error	t Ratio	Prob>|t|
Intercept	91.766351	1.339461	68.51	<.0001*
contact_yfilt_0_1tol_d0_001	4.570955	0.761729	6.00	<.0001*
wd_filt_n_RMS_Level_9	0.3678605	0.113911	3.23	0.0013*
wd_filt_n_SKEW_Level_41	-1.27137	0.329166	-3.86	0.0001*
MWMSR_filty_p0_25	-11.25776	1.664747	-6.76	<.0001*
MWMSR_filty_p0_1	21.447941	1.764549	12.15	<.0001*
Gradient	0.036518	0.027732	1.32	0.1882
Crossfall	-0.237762	0.015843	-15.01	<.0001*

Noise_Transverse_MLR_1-20m_VIF_under_4 – 1m

Response Noise aggregation=1m, Tex Direction=Transverse

Whole Model

Actual by Predicted Plot

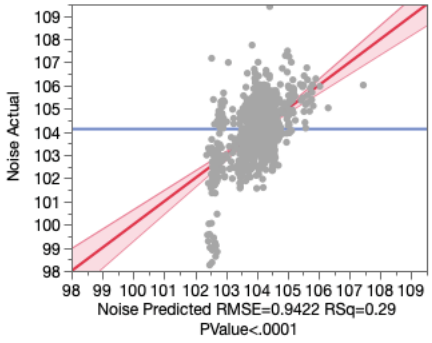

Effect Summary

Source	LogWorth	PValue
Crossfall	60.402	0.00000
MWMSR_filty_p0_1	38.136	0.00000
MWMSR_filty_p0_25	13.052	0.00000
contact_yfilt_0_1tol_d0_001	9.698	0.00000
wd_filt_n_SKEW_Level_41	4.122	0.00008
wd_filt_n_RMS_Level_9	3.282	0.00052
Gradient	1.145	0.07159

Remove Add Edit FDR

Residual by Predicted Plot

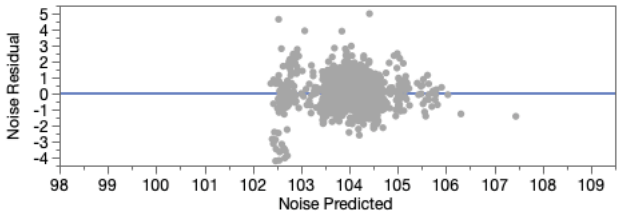

Summary of Fit

RSquare	0.289586
RSquare Adj	0.285731
Root Mean Square Error	0.94221
Mean of Response	104.1196
Observations (or Sum Wgts)	1298

Analysis of Variance

Source	DF	Sum of Squares	Mean Square	F Ratio
Model	7	466.8212	66.6887	75.1203
Error	1290	1145.2097	0.8878	Prob > F
C. Total	1297	1612.0309		<.0001*

Parameter Estimates

Term	Estimate	Std Error	t Ratio	Prob>|t|
Intercept	91.660429	1.225736	74.78	<.0001*
contact_yfilt_0_1tol_d0_001	4.4099787	0.687711	6.41	<.0001*
wd_filt_n_RMS_Level_9	0.352717	0.101416	3.48	0.0005*
wd_filt_n_SKEW_Level_41	-1.187053	0.298945	-3.97	<.0001*
MWMSR_filty_p0_25	-11.52881	1.529147	-7.54	<.0001*
MWMSR_filty_p0_1	21.905961	1.62462	13.48	<.0001*
Gradient	0.045072	0.024995	1.80	0.0716
Crossfall	-0.24892	0.014299	-17.41	<.0001*

Noise_Transverse_MLR_1-20m_VIF_under_4 – 3m

Response Noise aggregation=3m, Tex Direction=Transverse

Whole Model

Actual by Predicted Plot

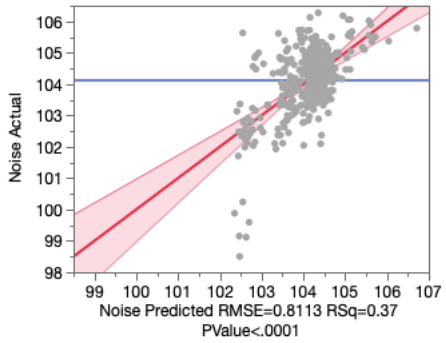

Effect Summary

Source	LogWorth	PValue
Crossfall	26.756	0.00000
MWMSR_filty_p0_1	17.897	0.00000
MWMSR_filty_p0_25	6.049	0.00000
contact_yfilt_0_1tol_d0_001	6.035	0.00000
wd_filt_n_RMS_Level_9	2.804	0.00157
wd_filt_n_SKEW_Level_41	2.356	0.00441
Gradient	0.453	0.35274

Remove Add Edit FDR

Residual by Predicted Plot

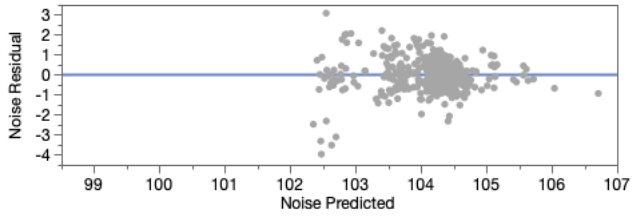

Summary of Fit

RSquare	0.365532
RSquare Adj	0.355033
Root Mean Square Error	0.811336
Mean of Response	104.1161
Observations (or Sum Wgts)	431

Analysis of Variance

Source	DF	Sum of Squares	Mean Square	F Ratio
Model	7	160.41965	22.9171	34.8143
Error	423	278.44646	0.6583	Prob > F
C. Total	430	438.86611		<.0001*

Parameter Estimates

Term	Estimate	Std Error	t Ratio	Prob>|t|
Intercept	89.088596	2.071911	43.00	<.0001*
contact_yfilt_0_1tol_d0_001	6.2437715	1.253432	4.98	<.0001*
wd_filt_n_RMS_Level_9	0.616308	0.193683	3.18	0.0016*
wd_filt_n_SKEW_Level_41	-1.675721	0.585343	-2.86	0.0044*
MWMSR_filty_p0_25	-11.44278	2.294261	-4.99	<.0001*
MWMSR_filty_p0_1	23.208099	2.513302	9.23	<.0001*
Gradient	0.0351782	0.037814	0.93	0.3527
Crossfall	-0.25267	0.021646	-11.67	<.0001*

Noise_Transverse_MLR_1-20m_VIF_under_4 – 10m

Response Noise aggregation=10m, Tex Direction=Transverse

Whole Model

Actual by Predicted Plot

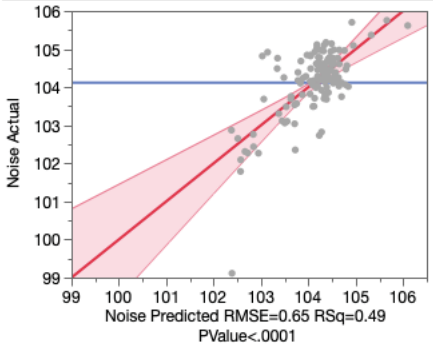

Effect Summary

Source	LogWorth	PValue
Crossfall	11.828	0.00000
MWMSR_filty_p0_1	8.517	0.00000
contact_yfilt_0_1tol_d0_001	3.851	0.00014
MWMSR_filty_p0_25	2.219	0.00605
wd_filt_n_RMS_Level_9	2.096	0.00801
wd_filt_n_SKEW_Level_41	1.765	0.01717
Gradient	0.078	0.83648

Remove Add Edit FDR

Residual by Predicted Plot

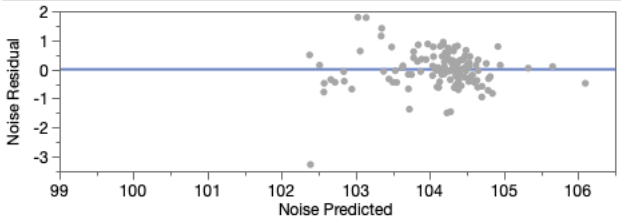

Summary of Fit

RSquare	0.493418
RSquare Adj	0.463367
Root Mean Square Error	0.649979
Mean of Response	104.1176
Observations (or Sum Wgts)	126

Analysis of Variance

Source	DF	Sum of Squares	Mean Square	F Ratio
Model	7	48.556354	6.93662	16.4191
Error	118	49.851800	0.42247	Prob > F
C. Total	125	98.408155		<.0001*

Parameter Estimates

Term	Estimate	Std Error	t Ratio	Prob>|t|
Intercept	83.553418	3.800871	21.98	<.0001*
contact_yfilt_0_1tol_d0_001	9.9147888	2.51937	3.94	0.0001*
wd_filt_n_RMS_Level_9	1.1076492	0.410629	2.70	0.0080*
wd_filt_n_SKEW_Level_41	-2.86049	1.183421	-2.42	0.0172*
MWMSR_filty_p0_25	-10.13123	3.623694	-2.80	0.0060*
MWMSR_filty_p0_1	25.313522	3.946028	6.41	<.0001*
Gradient	0.0118017	0.057052	0.21	0.8365
Crossfall	-0.262427	0.033147	-7.92	<.0001*

Noise_Transverse_MLR_1-20m_VIF_under_4 – 20m

Response Noise aggregation=20m, Tex Direction=Transverse

Whole Model

Actual by Predicted Plot

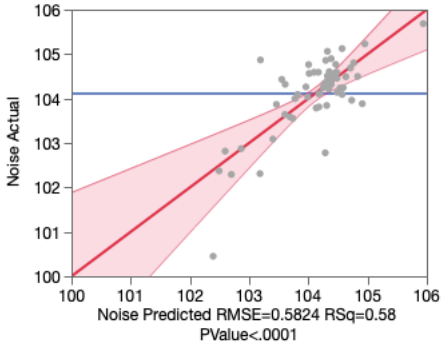

Effect Summary

Source	LogWorth	PValue
Crossfall	7.178	0.00000
MWMSR_filty_p0_1	5.117	0.00001
contact_yfilt_0_1tol_d0_001	2.981	0.00105
wd_filt_n_RMS_Level_9	1.846	0.01425
wd_filt_n_SKEW_Level_41	1.143	0.07199
MWMSR_filty_p0_25	0.829	0.14812
Gradient	0.075	0.84221

Remove Add Edit FDR

Residual by Predicted Plot

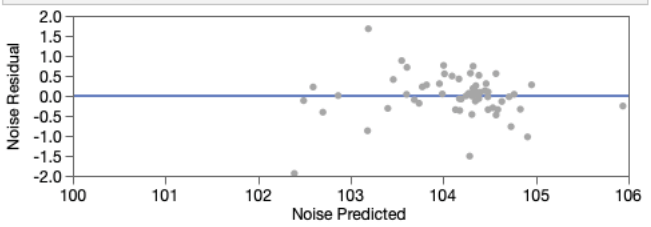

Summary of Fit

RSquare	0.581064
RSquare Adj	0.524668
Root Mean Square Error	0.582384
Mean of Response	104.1115
Observations (or Sum Wgts)	60

Analysis of Variance

Source	DF	Sum of Squares	Mean Square	F Ratio
Model	7	24.462326	3.49462	10.3034
Error	52	17.636901	0.33917	Prob > F
C. Total	59	42.099227		<.0001*

Parameter Estimates

Term	Estimate	Std Error	t Ratio	Prob>|t|
Intercept	77.189493	6.106902	12.64	<.0001*
contact_yfilt_0_1tol_d0_001	14.303512	4.118447	3.47	0.0010*
wd_filt_n_RMS_Level_9	1.685387	0.664545	2.54	0.0143*
wd_filt_n_SKEW_Level_41	-3.469759	1.889269	-1.84	0.0720
MWMSR_filty_p0_25	-8.216395	5.59685	-1.47	0.1481
MWMSR_filty_p0_1	27.238874	5.480149	4.97	<.0001*
Gradient	-0.015001	0.074984	-0.20	0.8422
Crossfall	-0.272336	0.043284	-6.29	<.0001*